TECHNICAL MEMORANDUM
Chehalis Water Quality and Hydrodynamic Modeling
Model Setup, Calibration and Scenario Analysis

Water Quality Research Group
Department of Civil and Environmental Engineering
Maseeh College of Engineering and Computer Science

Prepared for Washington Department of Ecology

April 2017

Portland State UNIVERSITY

Technical Memorandum
Chehalis Water Quality and Hydrodynamic Modeling: Model Setup, Calibration, and Scenario Analysis

by

Sarah Van Glubt, Chris Berger, and Scott Wells

Water Quality Research Group
Department of Civil and Environmental Engineering
Maseeh College of Engineering and Computer Science

Portland State University
Portland, Oregon 97201-0751

Prepared for Washington Department of Ecology

April 2017

Table of Contents

List of Figures

List of Tables

Introduction

Basin Background

The Chehalis River Basin is located in southwest Washington State (see Figure 1). The drainage area to the Chehalis River is over 2000 square miles, with area existing within five counties: Lewis, Thurston, Grays Harbor, Pacific, and Cowlitz (WADOE, 2001). The Chehalis River originates in Coast Range east of Willapa Bay, and also drains the western foothills of the Cascades and the southern Olympic Mountains. It ultimately flows into Grays Harbor and the Pacific Ocean, totaling over 125 miles in length.

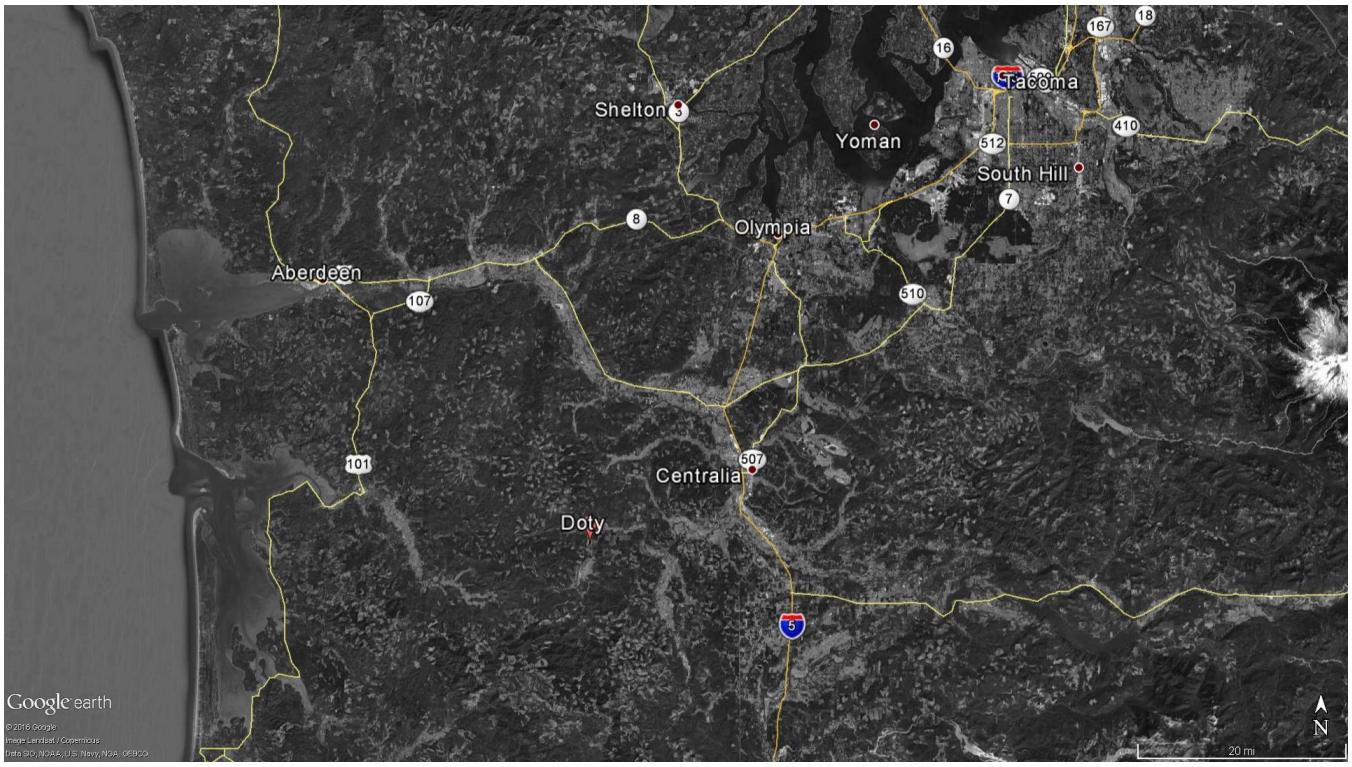

Figure 1. Chehalis River study area from near Doty, through Centralia to Aberdeen in southwestern Washington State (Google earth, 2017).

The State of Washington has designated the Chehalis River basin as Water Resource Inventory Areas 22 and 23. This study focuses on WRIA 23, which is the upper river above the U.S. Geological Survey flow gage at Porter. In this report, "Chehalis River" refers to the river in the WRIA 23 study area, unless otherwise noted.

The larger tributaries to the Chehalis River include the South Fork Chehalis River, Newaukum River, Skookumchuck River, and Black River (see Figure 2). The smaller tributaries include many creeks, such as Elk, Bunker, Mill, Stearns, Salzer, China, Scammon, Lincoln, Prairie, Scatter, Independence, Garrard, Cedar, Rock, Gibson, and Porter. Near the downstream end between Rochester and Oakville the river flows through the Chehalis Tribal Reservation (Pickett, 1994).

The mainstem Chehalis River in the study area has three distinct reaches based on their unique physical characteristics of slope and depth. The upper reach, beginning upstream of Pe Ell and extending to Chehalis, WA, has steep gradients with riffles and pools (Pickett, 1994). The middle reach, beginning just below the Newaukum River near Chehalis, WA and extending to the just above the Skookumchuck River, has slow, deep, lake-like

conditions that at times exhibit stratification (Pickett, 1994). The lower reach, beginning near the Skookumchuck River and extending to Porter, WA, is similar to the upper reach, with faster velocities and riffles and pools (Pickett, 1994). Figure 3, Figure 4, and Figure 5 show examples of the different physical characteristics seen on the Chehalis River.

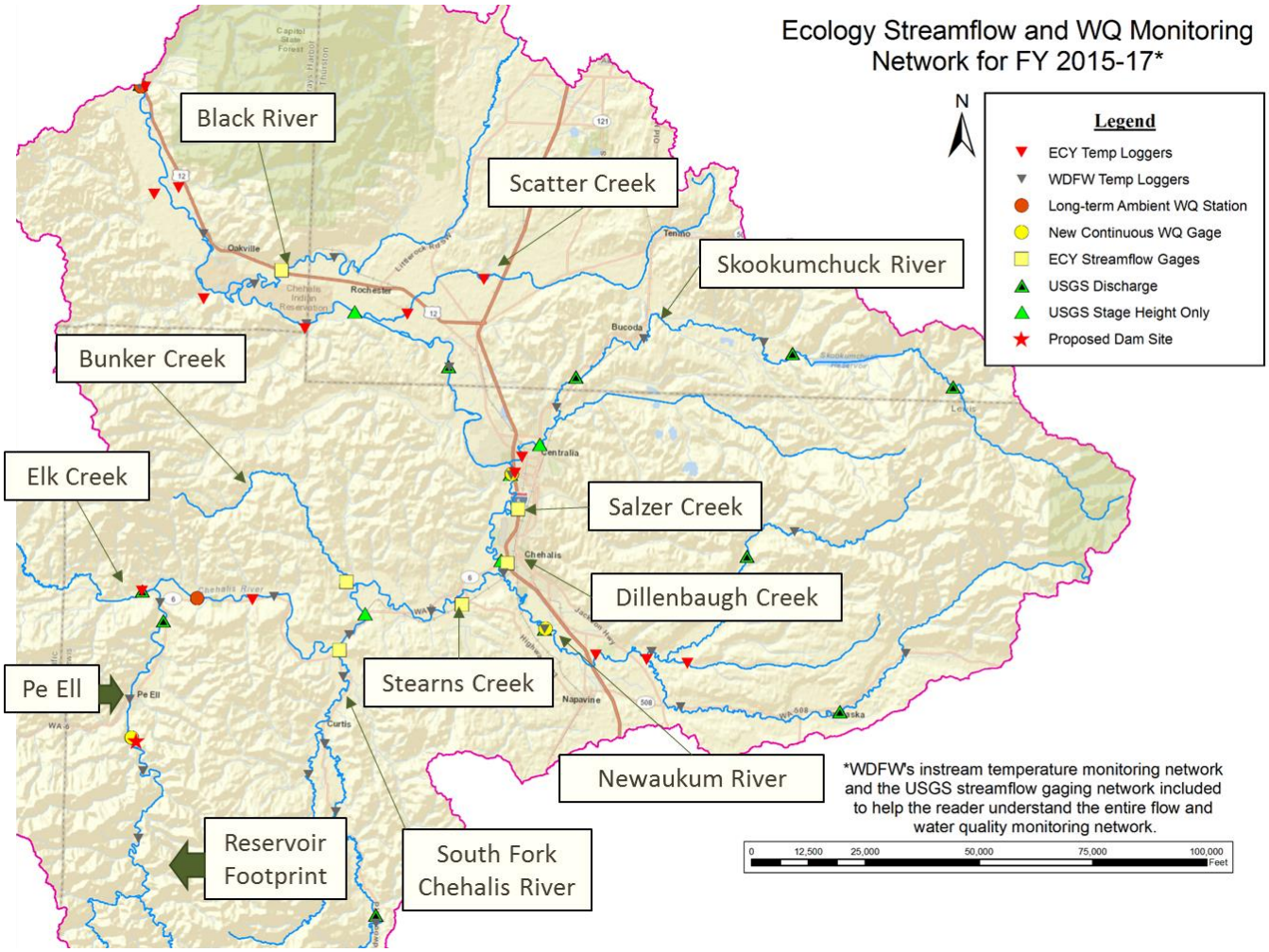

Figure 2. Chehalis River basin and associated tributaries (adapted from Dustin Bilhimer, 2015)

The land uses in the Chehalis river basin are diverse, including residential, agricultural, industrial, and logging and forest (WADOE, 2001). The river passes through urban areas, including the cities Centralia and Chehalis. In the study area, four municipal wastewater treatment plants (Pe Ell, Chehalis, Centralia, and Grand Mound) and one industrial wastewater treatment plant (Darigold) discharge to the river. Wastewater land application is required as an alternative for the Chehalis and Darigold wastewater treatment plant during periods of low river flows. National Frozen Foods has a state waste discharge permit to land apply wastewater in fields bordering the river between Chehalis and Centralia.

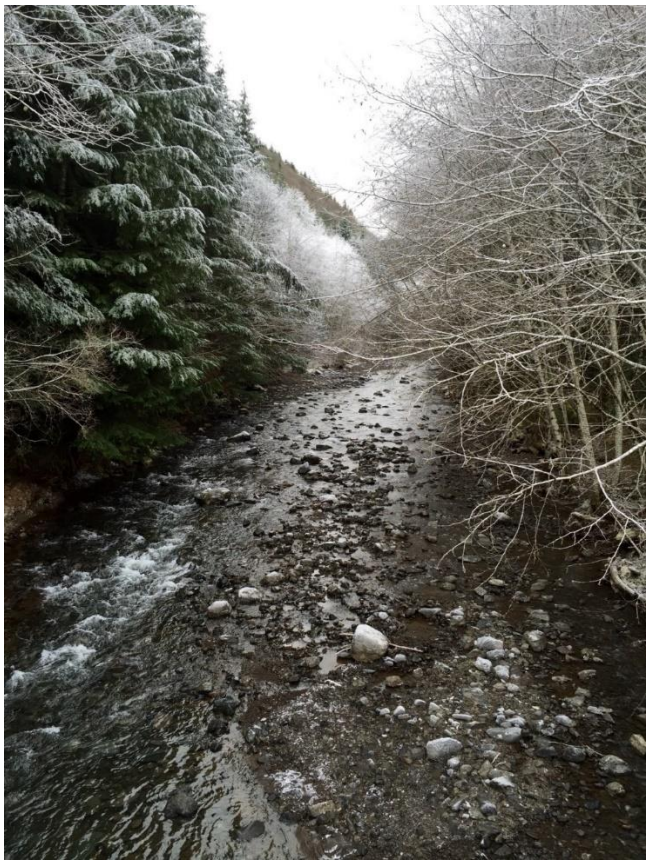

Figure 3. Upstream portion of the Chehalis River exhibiting steep gradients with riffles and pools

Figure 4. Middle portion of the Chehalis River near Centralia exhibiting slow, deep, lake-like conditions

Figure 5. Lower portion of the Chehalis River near Porter exhibiting steeper gradients than the middle portion, with swift-moving water

Project Background

The Washington State Department of Ecology is a part of the "Chehalis Basin Strategy", a project of flood hazard reduction and aquatic species restoration and enhancement in the Chehalis River Basin in the state of Washington. As part of that project, Portland State University developed a water quality model of the mainstem Chehalis River. This report outlines the modeling approach, model set-up, model calibration and model scenarios. The model was set-up to simulate the years 2013 and 2014. The mainstem model extends from the proposed water retention structure upstream of Pe Ell, WA (near Doty in Figure 6) to the USGS gage at Porter, WA. In addition, this report provides results from PSU's model of the uninundated stream network in the proposed water retention structure footprint (upstream of "Proposed Dam Site" in Figure 2 near "Reservoir Footprint"), corresponding to a reservoir model of the proposed water retention structure that Anchor QEA has developed.

Washington State Department of Ecology has established Total Maximum Daily Loads (TMDLs) to protect temperature and dissolved oxygen in the Chehalis River. The river was modeled for dissolved oxygen and temperature in the 1990s. A key feature of the river is the slow reach between the Newaukum and Skookumchuck Rivers with a summer travel time of up to 7 days and areas of thermal stratification.

The project goals include:

- Assess the water quality impacts of the proposed retention structure
- Determine the water quality impacts of aquatic restoration and enhancement, such as riparian and floodplain restoration.
- Integration of Chehalis flood hazard reduction activities with any future permitting under state and federal water quality laws and regulations, and with implementation and effectiveness monitoring of the existing Total Maximum Daily Loads for temperature and dissolved oxygen

These goals will be accomplished by applying the hydrodynamic and water quality model CE-QUAL-W2 (http://www.cee.pdx.edu/w2) to the Chehalis River and the proposed reservoir footprint. CE-QUAL-W2 is a two dimensional model (longitudinal and vertical) that describes and simulates dissolved oxygen-nutrients-sediment interactions, algae and zooplankton, selective withdrawal from stratified reservoirs, and flow over submerged hydraulic structures. The Water Quality Research Group at Portland State University maintains and provides enhancements for the public domain model.

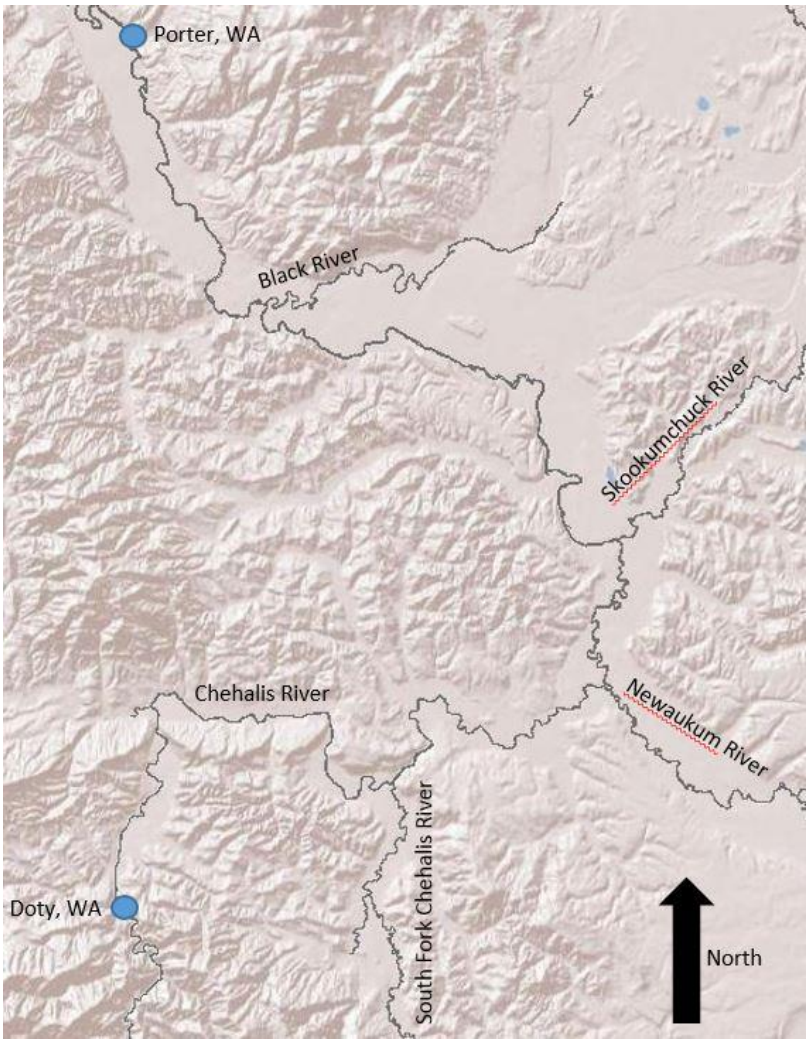

Figure 6. Study area with major tributaries near Doty to Porter.

Model Capabilities

CE-QUAL-W2 is a two-dimensional, longitudinal/vertical, hydrodynamic and water quality model developed by the US Army Corps of Engineers and the Water Quality Research Group at Portland State University. It has been applied to over a thousand systems, including rivers, lakes, reservoirs, estuaries, and combinations thereof. Because the model assumes lateral homogeneity, it is best suited for relatively long and narrow water bodies that exhibit longitudinal and vertical water quality gradients. CE-QUAL-W2 consists of directly coupled hydrodynamic and water quality transport models. CE-QUAL-W2 simulates parameters such as temperature, algae concentration, dissolved oxygen concentration, pH, nutrient concentrations, organic matter and detention time.

CE-QUAL-W2 has been under continuous development since 1975. The original model was known as LARM (**L**aterally **A**veraged **R**eservoir **M**odel) developed by Edinger and Buchak (1975). The first LARM application was on a reservoir with no branches. Subsequent modifications to allow for multiple branches and estuarine boundary conditions resulted in the code known as GLVHT (**G**eneralized **L**ongitudinal-**V**ertical **H**ydrodynamics and **T**ransport Model). Addition of the water quality algorithms by the Water Quality Modeling Group at the US Army Engineer Waterways Experiment Station (WES) resulted in CE-QUAL-W2 Version 1.0. Version 2.0 was a result of major modifications to the code to improve the mathematical description of the prototype and increase computational accuracy and efficiency. The current version (version 4.0) includes additional improvements to the numerical solution scheme and water quality algorithms, as well as extending the utility of the model to provide state-of-the-art capabilities for modeling entire water basins in two-dimensions (Cole and Wells, 2016).

Model capabilities are summarized below:

Hydrodynamics: The model predicts water surface elevations, velocities, and temperatures. Temperature is included in the hydrodynamic calculations because of its effect on water density and cannot be turned off.

Water Quality: Any combination of constituents can be included/excluded from a simulation. The effects of salinity or total dissolved solids/salinity on density and thus hydrodynamics are included only if they are simulated in the water quality module. The water quality algorithm is modular allowing constituents to be easily added as additional subroutines. The current version includes the following water quality state variables in addition to temperature:

1. any number of generic constituents defined by a 0 and/or a 1st order decay rate and/or a settling velocity and/or an Arrhenius temperature rate multiplier that can be used to define any number of the following:
    a. conservative tracer(s)
    b. water age or hydraulic residence time
    c. N_2 gas and %Total Dissolved Gas
    d. coliform bacteria(s)
    e. contaminant(s)
2. any number of inorganic suspended solids groups
3. any number of phytoplankton groups
4. any number of periphyton/epiphyton groups
5. any number of CBOD groups
6. any number of submerged macrophyte groups
7. ammonium
8. nitrate+nitrite
9. bioavailable phosphorus (commonly represented by orthophosphate or soluble reactive phosphorus)
10. silica (dissolved and particulate)
11. labile dissolved organic matter
12. refractory dissolved organic matter
13. labile particulate organic matter
14. refractory particulate organic matter
15. total inorganic carbon
16. alkalinity
17. iron and manganese
18. dissolved oxygen
19. organic sediments
20. gas entrainment
21. any number of macrophyte groups
22. any number of zooplankton groups
23. labile dissolved organic matter-P

24. refractory dissolved organic matter-P
25. labile particulate organic matter-P
26. refractory particulate organic matter-P
27. labile dissolved organic matter-N
28. refractory dissolved organic matter-N
29. labile particulate organic matter-N
30. refractory particulate organic matter-N
31. Sediment and water column CH4
32. Sediment and water column H2S
33. Sediment and water column SO4
34. Sediment and water column Sulfide
35. Sediment and water column FeOOH(s)
36. Sediment and water column Fe+2
37. Sediment and water column MnO2(s)
38. Sediment and water column Mn+2
39. Sediment organic P, sediment PO4
40. Sediment organic N, sediment NO3, sediment NH4
41. Sediment Temperature
42. Sediment pH
43. Sediment alkalinity
44. Sediment Total inorganic C
45. Sediment organic C
46. Turbidity correlation to Suspended solids

Additionally, over 60 derived variables including pH, TOC, DOC, TON, TOP, DOP, TN, TP, and TSS can be computed internally from the state variables and output for comparison to measured data.

Sediment Diagenesis Compartment: The model includes full sediment diagenesis including organic matter and metals transformations in the sediments. There is variable pH and alkalinity and bubble formation from the sediments included.

Long-term simulations: The water surface elevation is solved implicitly, which eliminates the surface gravity wave restriction on the time step. This permits larger time steps during a simulation resulting in decreased computational time. As a result, the model can easily simulate long-term water quality responses.

Head boundary conditions: The model can be applied to estuaries, rivers, or portions of a waterbody by specifying upstream or downstream head boundary conditions.

Multiple branches: The branching algorithm allows application to geometrically complex waterbodies such as dendritic reservoirs or estuaries.

Multiple waterbodies: The model can be applied to any number of rivers, reservoirs, lakes, and estuaries linked in series.

Variable grid spacing: Variable segment lengths and layer thicknesses can be used allowing specification of higher resolution where needed. Vertical grid spacing can vary in thickness between waterbodies.

Water quality independent of hydrodynamics: Water quality can be updated less frequently than hydrodynamics thus reducing computational requirements. However, water quality is ***not*** decoupled from the hydrodynamics (i.e., separate, standalone code for hydrodynamics and water quality where output from the hydrodynamic model

is stored on disk and then used to specify advective fluxes for the water quality computations). Storage requirements for long-term hydrodynamic output to drive the water quality model are prohibitive for anything except very small grids. Additionally, reduction in computer time is minimal when hydrodynamic data used to drive water quality are input every time step.

Auto-stepping: The model includes a variable time step algorithm that attempts to help ensure stability requirements for the hydrodynamics imposed by the numerical solution scheme are not violated.

Restart provision: The user can output results during a simulation that can subsequently be used as input. Execution can then be resumed at that point. Note that this feature has not been updated for the latest version but will be included in the next release.

Layer/segment addition and subtraction: The model will adjust surface layer and upstream segment locations for a rising or falling water surface during a simulation.

Multiple inflows and outflows: Provisions are made for inflows and inflow loadings from point/nonpoint sources, branches, and precipitation. Outflows are specified either as releases at a branch's downstream segment or as lateral withdrawals. Although evaporation is not considered an outflow in the strictest sense, it can be included in the water budget.

Ice cover calculations: The model can calculate onset, growth, and breakup of ice cover.

Selective withdrawal calculations: The model can calculate the vertical extent of the withdrawal zone based on outlet geometry, outflow, and density.

Time-varying boundary conditions: The model accepts a given set of time-varying inputs at the frequency they occur independent of other sets of time-varying inputs.

Outputs: The model allows the user considerable flexibility in the type and frequency of outputs. Output is available for the screen, hard copy, plotting, and restarts. The user can specify model predictions both the starting time period and the frequency of output.

Model Setup

Chehalis River Downstream Model

Bathymetry

The Chehalis River was modeled from upstream of Pe Ell at the proposed dam site (river mile 108) to Porter, WA (river mile 33.3). Only the mainstem Chehalis River was modeled and was discretized into 10 model branches and 9 waterbodies. The physical characteristics of the river varied widely, and multiple branches allowed for separate characteristics (such as branch slope) unique to each branch to be implemented in the model. The upstream reaches had steep gradients with riffles and pools (see Figure 7), while the middle portion near Centralia had slow and deep lake-like conditions (see Figure 8). These varying slopes along the Chehalis River and the model branches and waterbodies can be seen in Figure 9, showing the longitudinal profile of the river thalweg. Figure 10 shows the bottom elevation of the model grid compared to the longitudinal profile of the river thalweg. The model grid follows the contour of the river profile well even though some of the individual pools have not been characterized. This will continue to be evaluated as we improve the model grid (see section on Model Improvements).

Figure 7. Step gradient river section with pools and riffles

Figure 8 Lake like region of Chehalis River

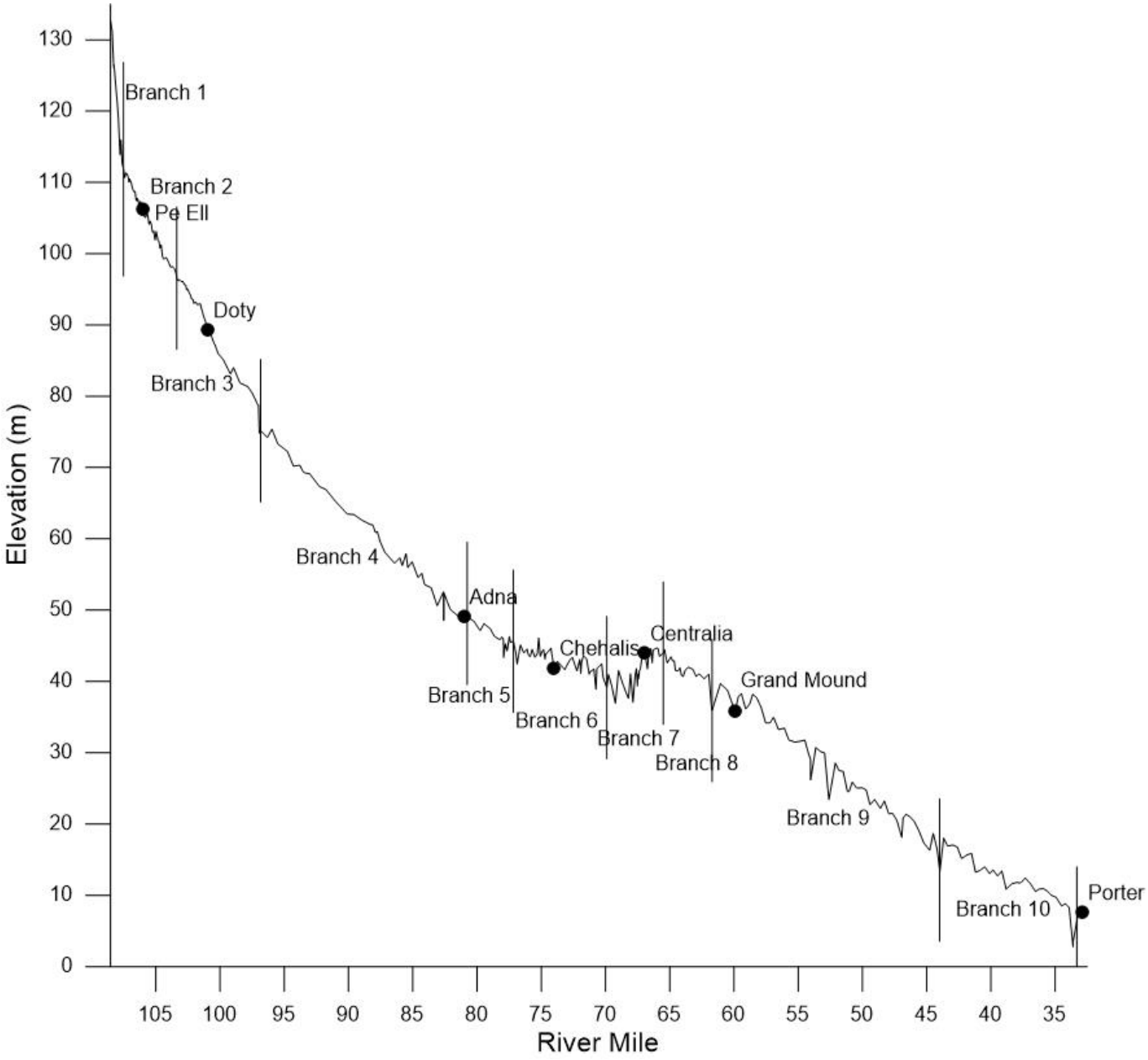

Figure 9. Longitudinal profile of the Chehalis River thalweg (vertical lines show model branch breaks)

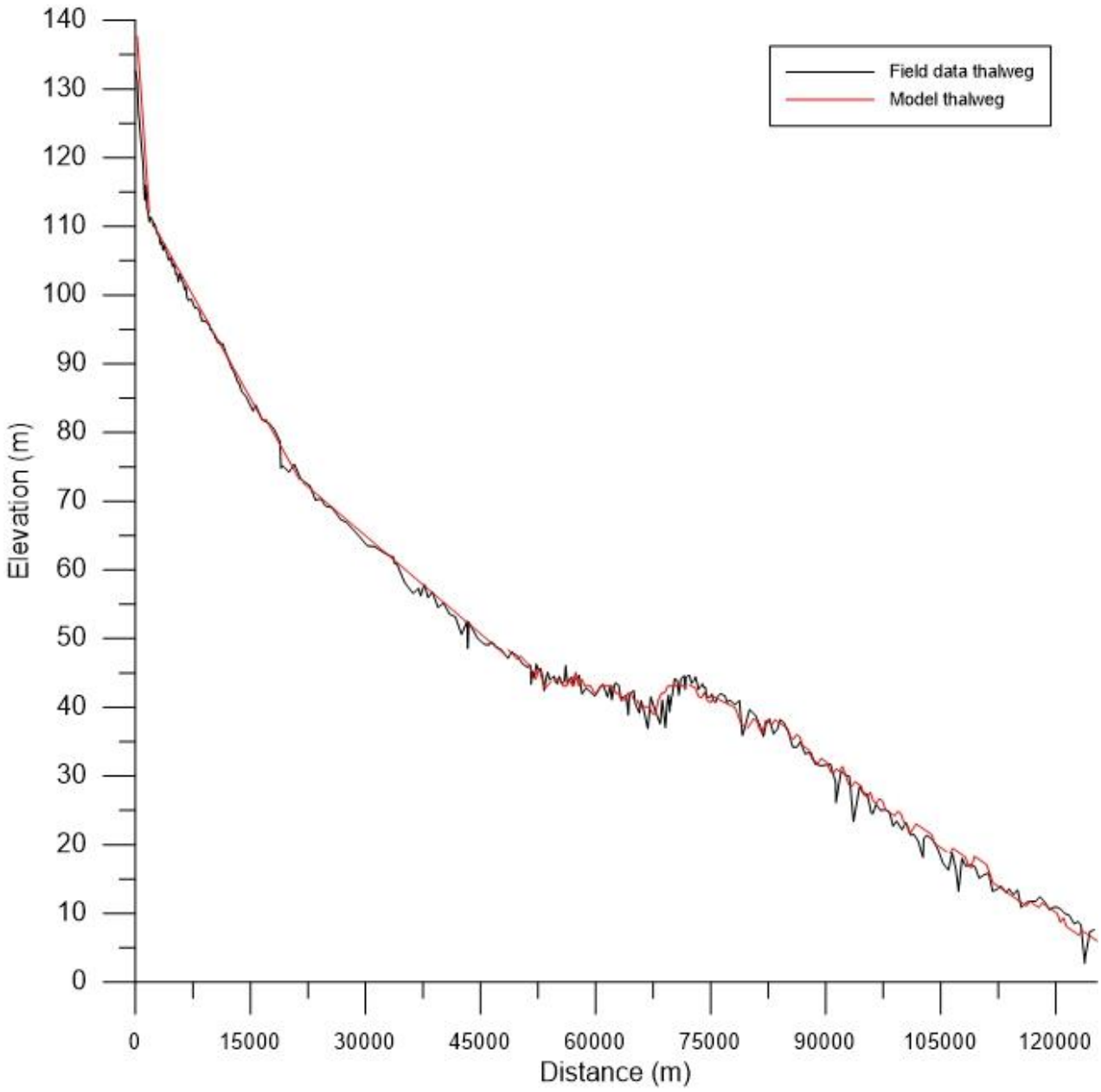

Figure 10. Longitudinal profile of the model grid and field data bottom elevation of the Chehalis River.

The model grid was developed based on river cross section data provided by Anchor QEA (2011). This included elevation and station data for over 350 cross sections along the Chehalis River. The model grid consisted of 334 longitudinal segments of 400 m length, each with 20 vertical layers of 1 m thickness. Field cross section data were interpolated to determine layer widths in each model segment. Examples of field cross section data used to calculate model segment layer widths can be seen in Figure 11 for model segment 140 at river mile 77.92, and Figure 12 for model segment 151 at river mile 76. Figure 13 shows an aerial view of all active model segments along the mainstem Chehalis River.

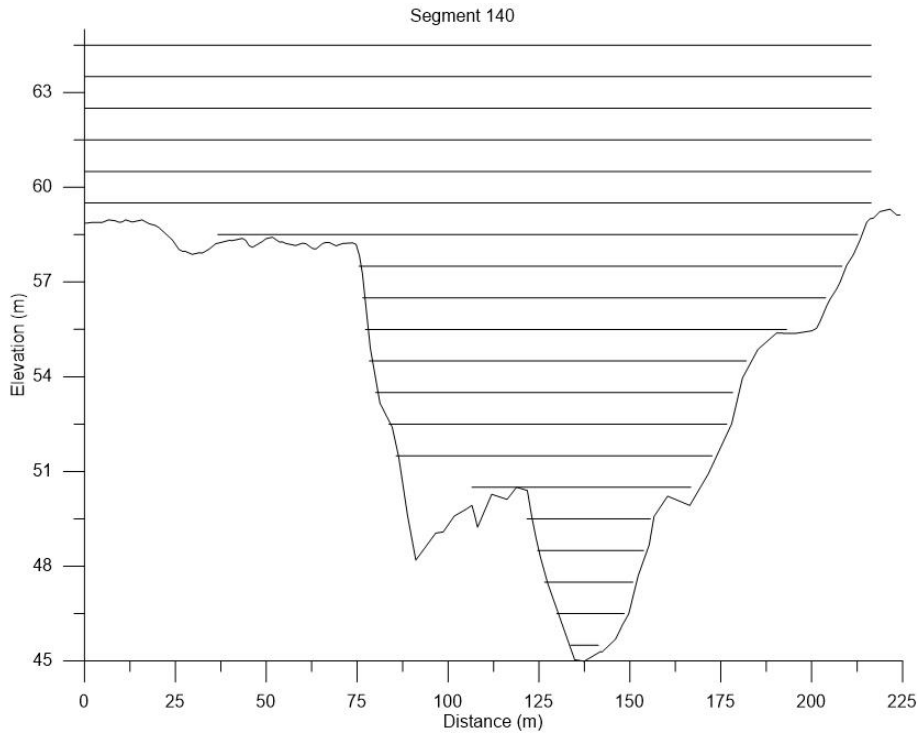

Figure 11. Example Chehalis River field cross section at river mile 77.92 used to calculate layer widths for model segment 140. The CE-QUAL-W2 model widths are represented by the straight lines for each vertical layer.

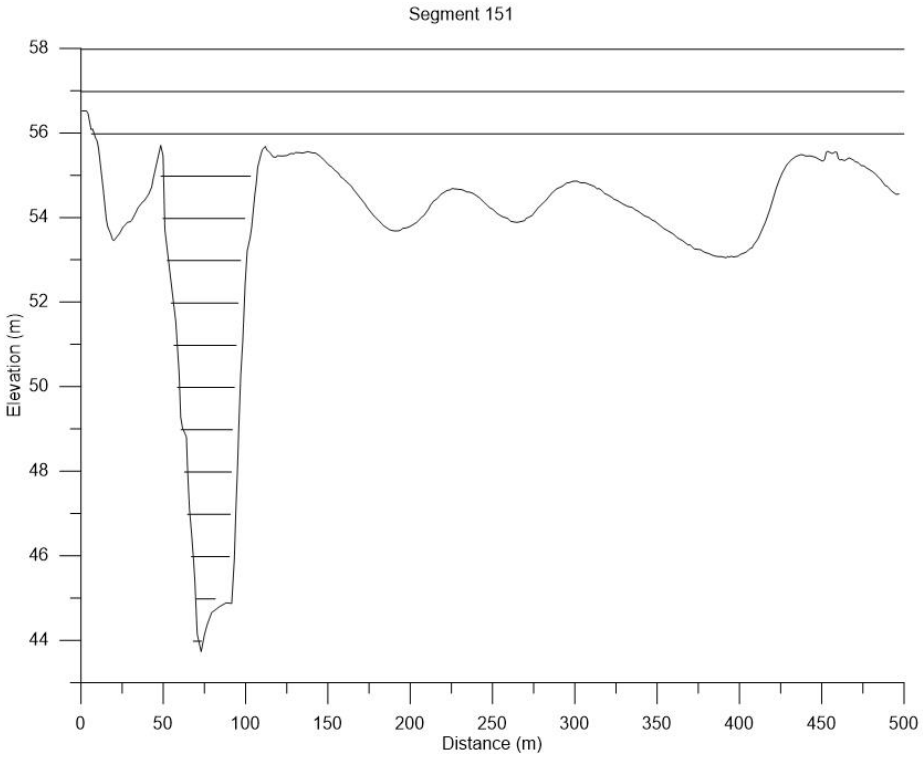

Figure 12. Example Chehalis River field cross section at river mile 76 used to calculate layer widths for model segment 151. The CE-QUAL-W2 model widths are represented by the straight lines for each vertical layer.

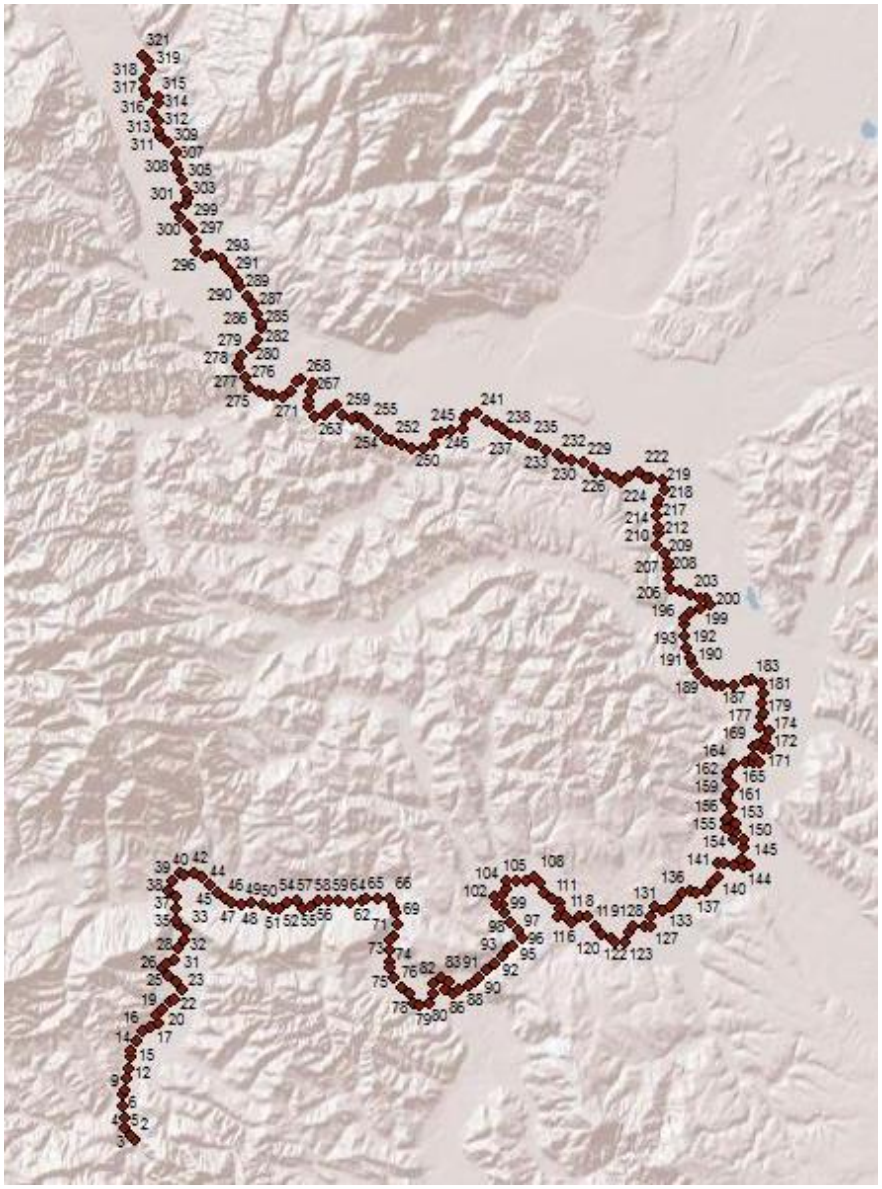

Figure 13. Aerial view of the entire model grid, showing active model segments along the mainstem Chehalis River

Cross sectional data were also used to identify active layers of each model segment and calculate channel slope. Elevation data entered to the model were referenced to the NAVD88 datum. Initial water surface depths were set to 2 meters (6.6 feet) for each segment.

Table 1 gives a summary of the waterbody and branch segments and layer dimensions. Figure 14, Figure 15, Figure 16, Figure 17, Figure 18, Figure 19, Figure 20, Figure 21, Figure 22, and Figure 23 show the model side profile for branch 1, branch 2, branch 3, branch 4, branch 5, branch 6, branch 7, branch 8, branch 9, and branch 10, respectively.

Table 1. Summary of waterbody and branch segments and layers

Waterbody	Branch	Starting Active Segment	Ending Active Segment	Number of Segments	Branch Length (m)	Number of layers	Vertical layer Thickness (m)	SLOPE	SLOPEC
1	1	2	6	5	2000	20	1	0.01600	0.003
2	2	9	28	20	8000	20	1	0.00200	0.0004
3	3	31	59	29	11600	20	1	0.00200	0.0006
4	4	62	128	66	26400	20	1	.000950	0.00095
5	5	131	145	15	6000	20	1	.001182	0.00055
6	6	148	174	27	10800	20	1	.000001	0.000001
	7	177	193	17	6800	20	1	.000001	0.000001
7	8	196	214	18	7200	20	1	.000550	0.00055
8	9	217	282	65	26000	20	1	.000769	0.000769
9	10	285	321	48	19200	20	1	0.00077	0.00077

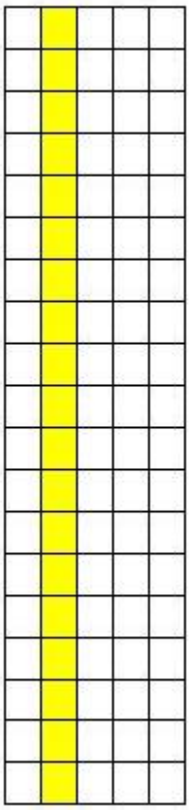

Figure 14. Model branch 1 side profile view, including all segments and layers

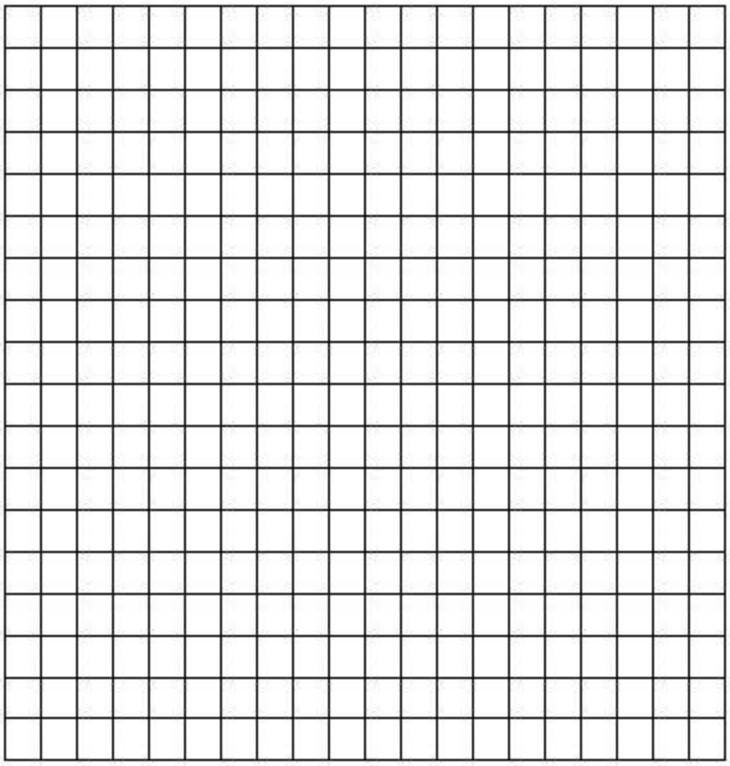

Figure 15. Model branch 2 side profile view, including all segments and layers

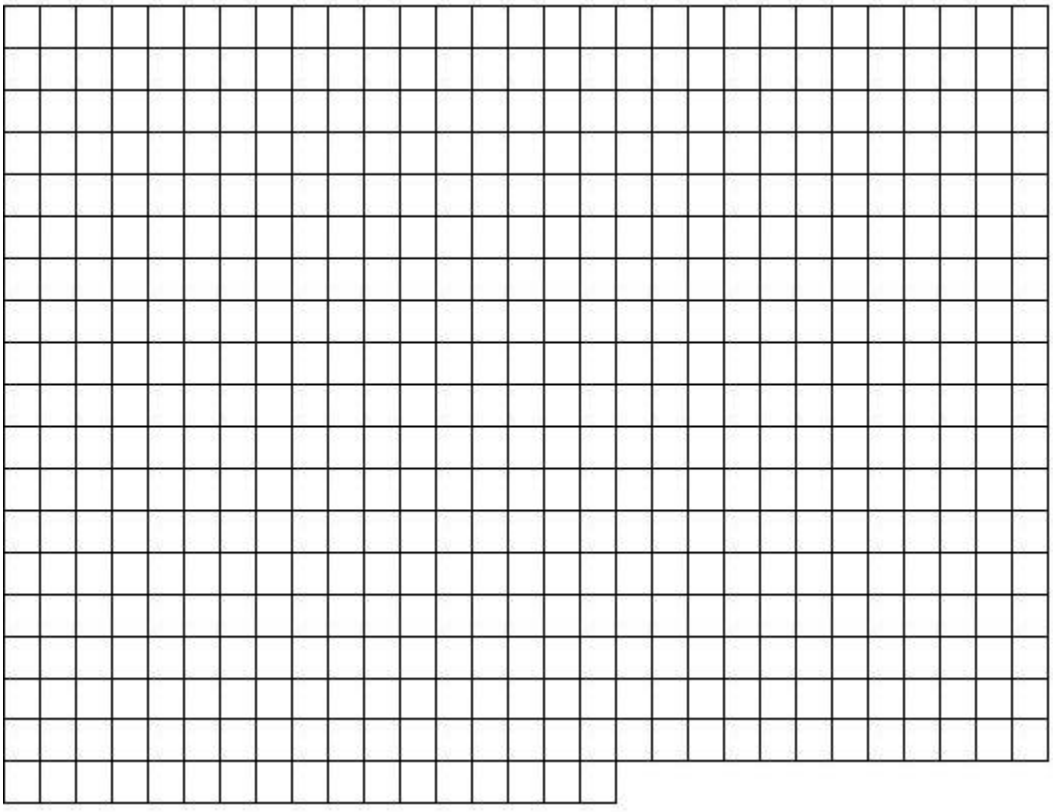

Figure 16. Model branch 3 side profile view, including all segments and layers

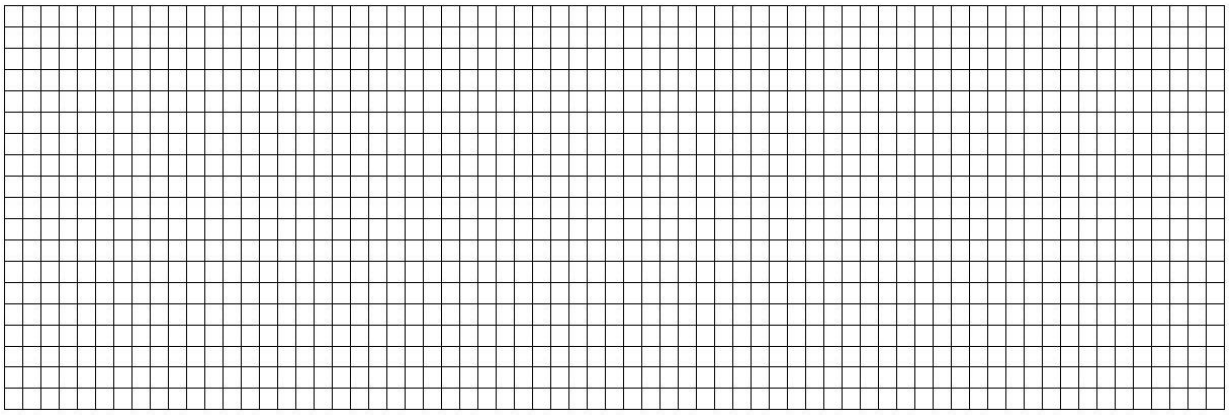

Figure 17. Model branch 4 side profile view, including all segments and layers

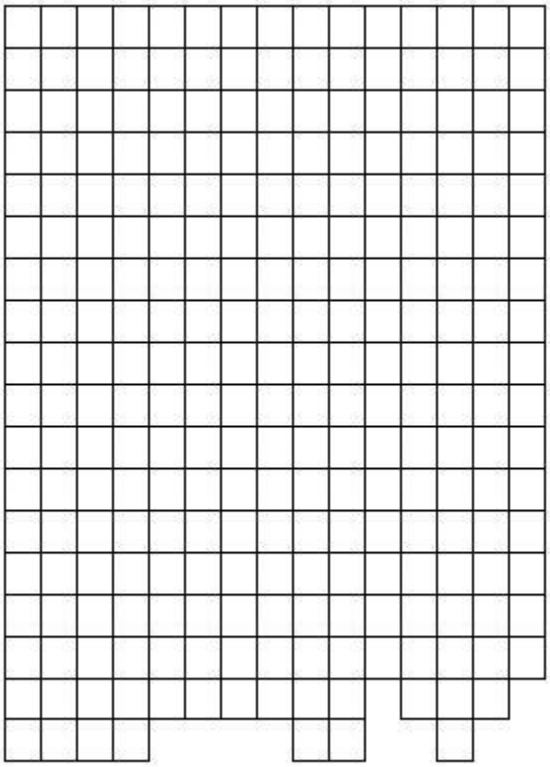

Figure 18. Model branch 5 side profile view, including all segments and layers

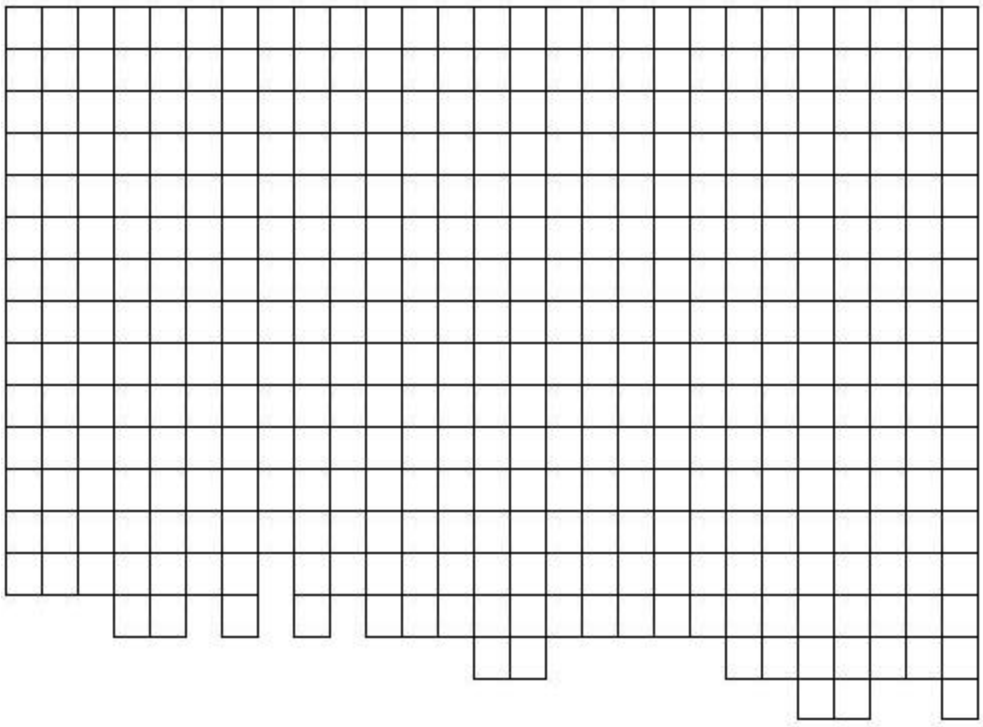

Figure 19. Model branch 6 side profile view, including all segments and layers

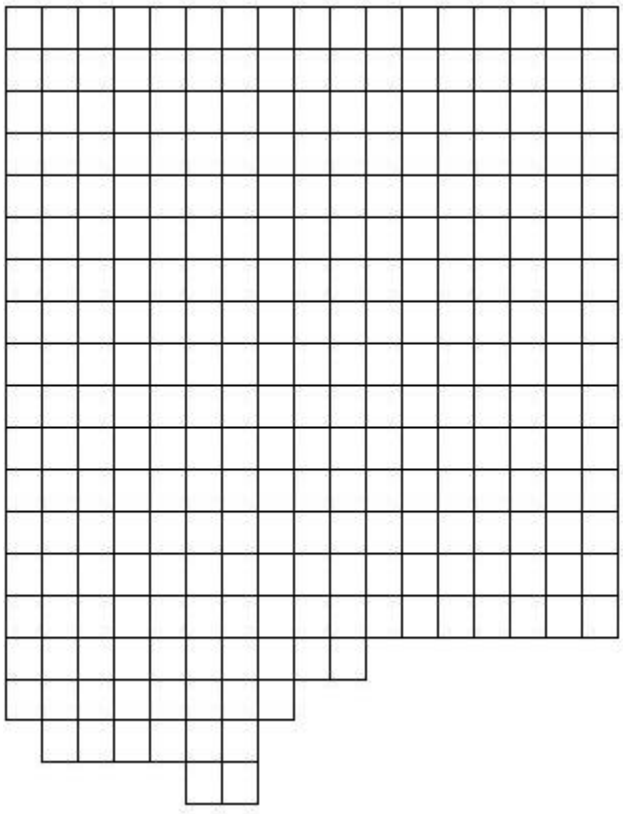

Figure 20. Model branch 7 side profile view, including all segments and layers

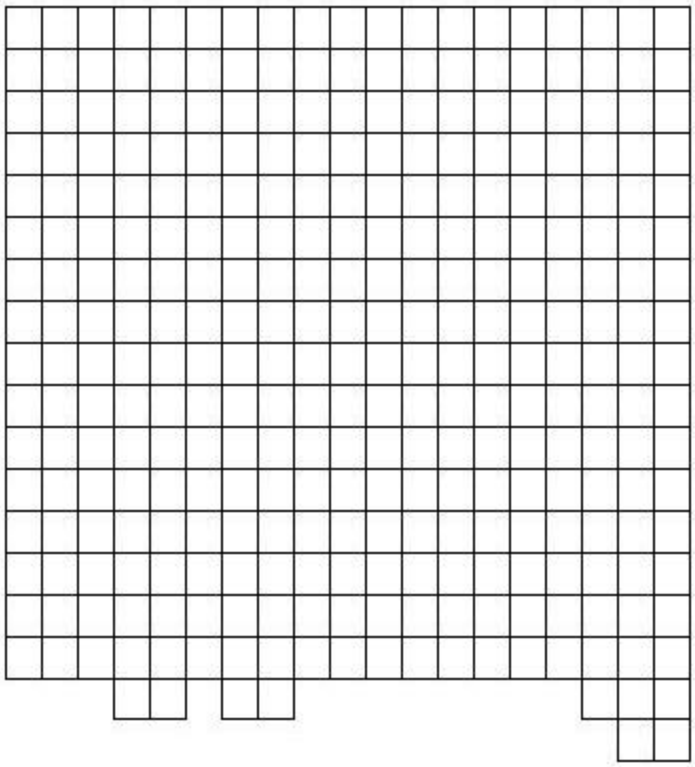

Figure 21. Model branch 8 side profile view, including all segments and layers

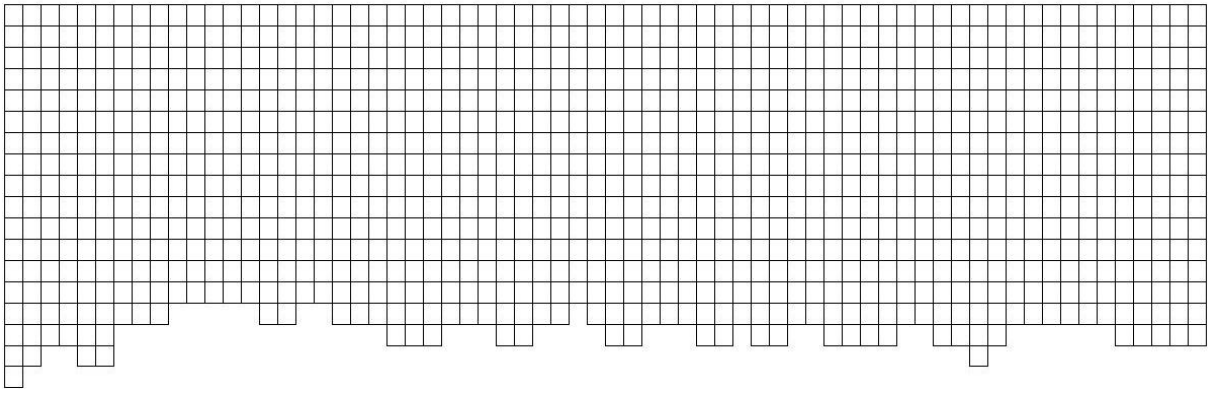

Figure 22. Model branch 9 side profile view, including all segments and layers

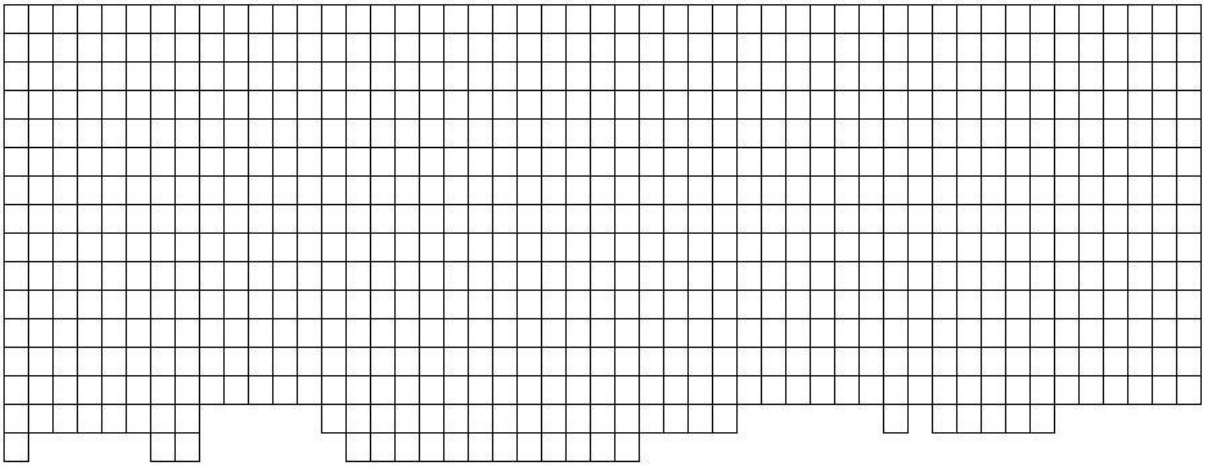

Figure 23. Model branch 10 side profile view, including all segments and layers

Meteorological Inputs

Meteorological parameters used in this study included air temperature, dew temperature, wind speed, wind direction, cloud cover, and solar radiation. CE-QUAL-W2 has the capability to internally calculate solar radiation based on cloud cover data and latitude and longitude.

One source of meteorological data was the Remote Automatic Weather Stations (RAWS, 2014) database, with hourly data available (Bowman, 2016 and Breckner, 2016). Another source of meteorological data was Chehalis River Basin Flood Authority (CRBFA, 2016) at Thrash Creek near the proposed dam site, with 15-minute frequency. Lastly, the National Oceanic and Atmospheric Administration (NOAA, 2015) provided data from the Chehalis-Centralia meteorological station. Table 2 lists the stations used to create input meteorological files.

Table 2. Monitoring stations that provided meteorological data

Organization	Station ID	Description	Location	Dates with data	Waterbodies applied to in model	River Miles applied to in model
CRBFA	Thrash Creek	Thrash Creek	Near Pe Ell	1/1/13 – 12/31/15	1, 2, & 3	108 – 96.9
RAWS	HKFW1	Huckleberry Ridge	Near Pe Ell	4/2/13 – 12/31/15	-	-
RAWS	CLSW1	Chehalis	Near Chehalis	1/1/13 – 12/31/15	4, 5, 6, & 7	96.9 – 61.7
NOAA	KCLS	Chehalis-Centralia Airport	Chehalis, WA	1/1/13 – 12/31/15	-	-
RAWS	MIPW1	Minot Peak	Near Porter	4/9/13 – 12/31/15	8 & 9	61.7 – 33.3

The CRBFA Thrash Creek gage data were applied to model waterbodies 1, 2, and 3; the RAWS Chehalis gage data were applied to waterbodies 4, 5, 6, and 7; and the RAWS Minot Peak gage data were applied to waterbodies 8 and 9. While the HKFW1 RAWS station and Chehalis-Centralia Airport station data were not used in model input files, they were used to evaluate and compare to the other meteorological stations. Both RAWS and CRBFA had a meteorological data site near Pe Ell. The CRBFA site was used to be consistent with other modeling projects of the Chehalis River as well as because of its proximity to the upstream boundary. The CLSW1 station data were used

rather than the airport because CLSW1 collected data at shorter time intervals. Figure 24 shows the locations of the meteorological stations in relation to the model grid.

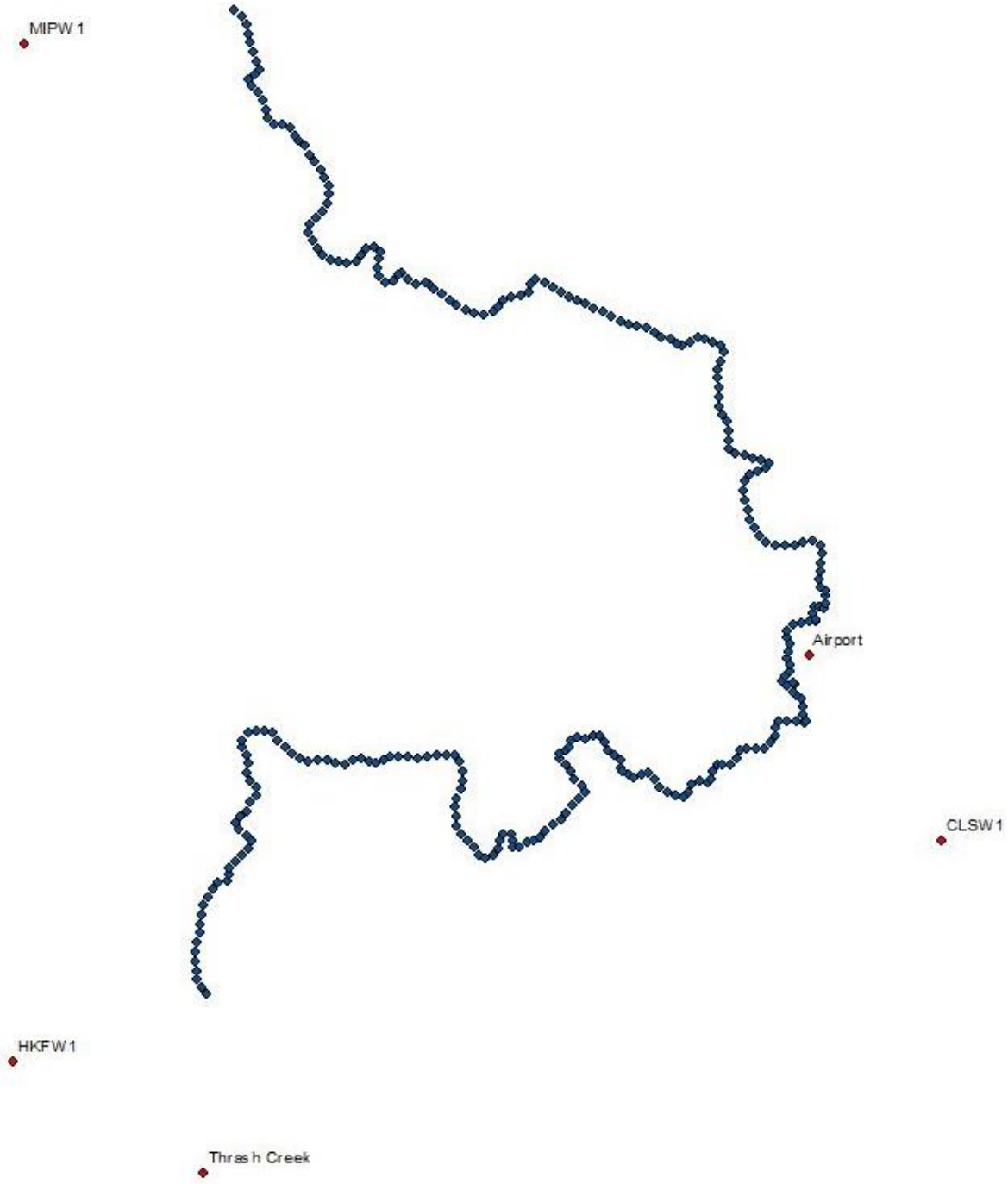

Figure 24. Meteorological stations near to the model grid that provided data, including Thrash Creek, HKFW1, CLSW1, Centralia-Chehalis Airport, and MIPW1.

Since data were required for the entire model time period of January 1, 2013 to December 31, 2014, there were many data gaps that needed to be filled. Linear interpolation was employed to fill in missing data for short time gaps, on the order of hours. For some longer temporal gaps data from another station were used. For example, the first months of the MIPW data set were unavailable, so values from the CLSW data set were used. For other

longer time gaps, linear correlation relationships with another station's data were created and used to estimate missing data:

1. For times when both stations had data available, a linear regression equation was created between a station with missing data and the closest station with a full data set.
2. This relationship was used to estimate values for the station with missing data during times when data were unavailable.

Regression relationships were created for air and dew point temperature between the MIPW and CLSW monitoring stations. These regression equations can be viewed in Table 3 and plots of the regression relationships are shown in Figure 25 and Figure 26 for air and dew point temperature, respectively.

Table 3. Air and Dew Temperature Regression Relationships for Minot Peak (MIPW1) Station Data to Chehalis (CLSW1) Station Data

Station with missing data	Regression Equation	R^2 Value
Minot Peak (MIPW1)	$Tair_{MIPW1} = 0.6559 * Tair_{CLSW1} + 1.7891$	0.6562
Minot Peak (MIPW1)	$Tdew_{MIPW1} = 0.6265 * Tdew_{CLSW1} + 1.8753$	0.4879

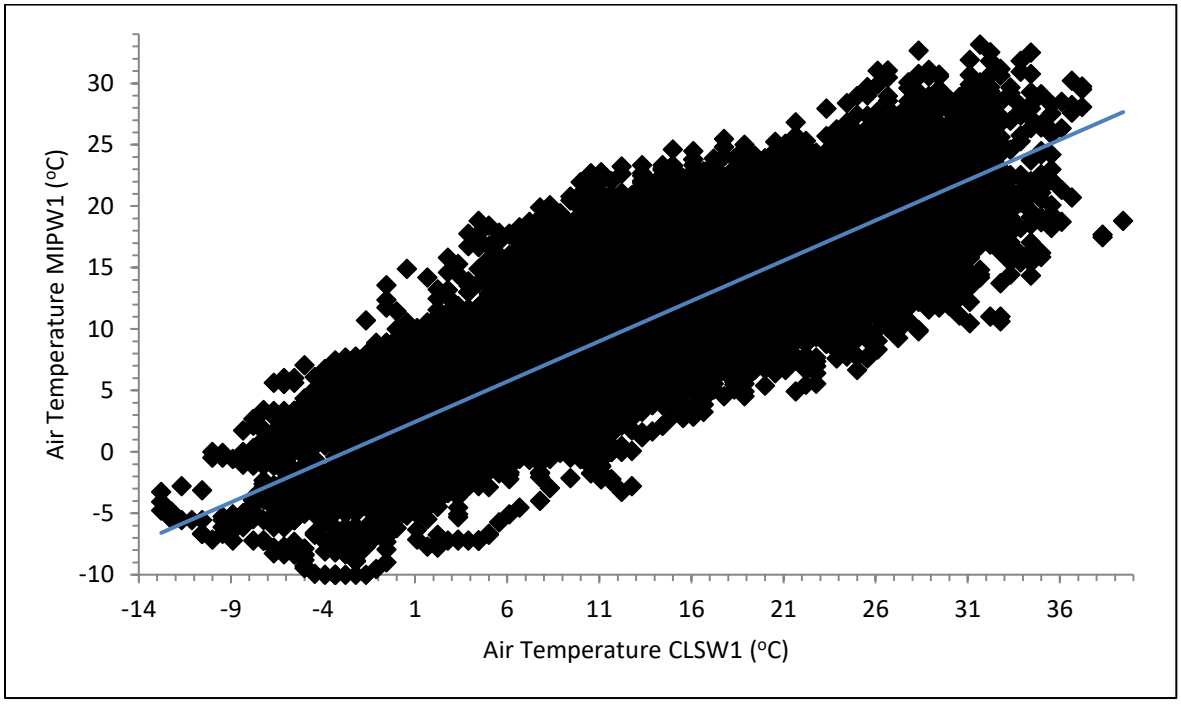

Figure 25. Air temperature relationship between Minot Peak (MIPW1) and Chehalis (CLSW1) RAWS stations when both had data available

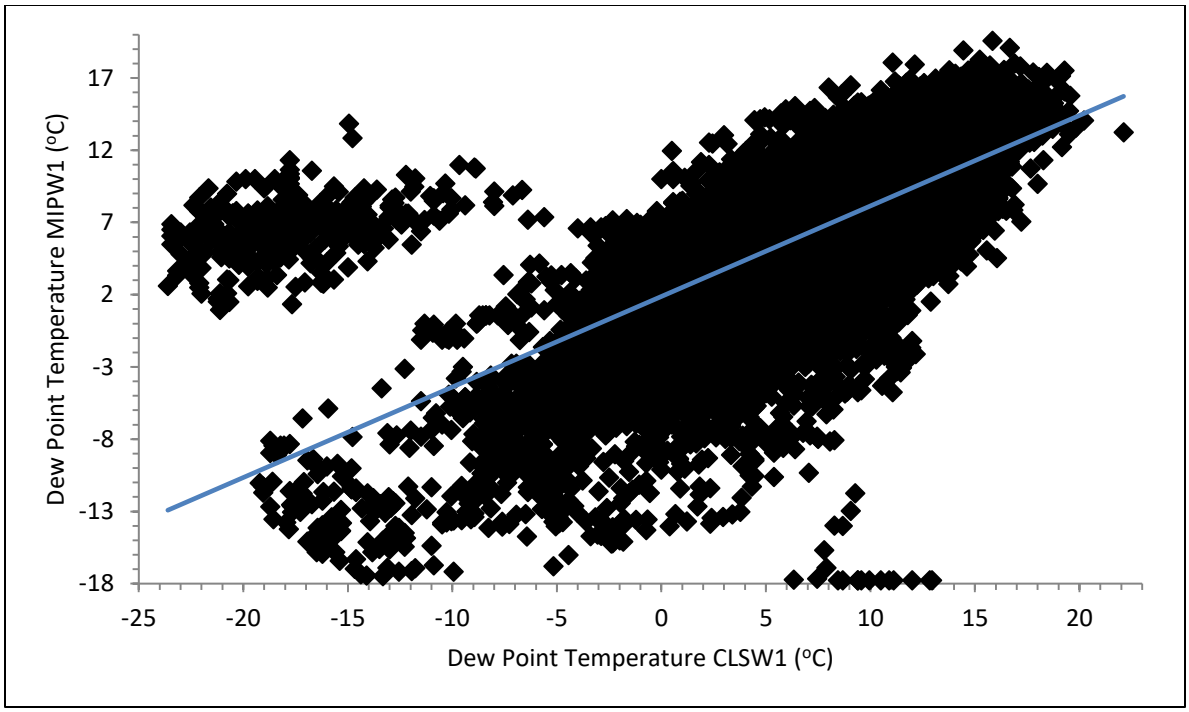

Figure 26. Dew Point temperature relationship between Minot Peak (MIPW1) and Chehalis (CLSW1) RAWS stations when both had data available

Cloud cover values were missing for the RAWS stations. These were estimated using solar radiation data. First, theoretical clear sky solar radiation based on latitude and longitude were calculated using code from CE-QUAL-W2 (Cole and Wells, 2016). Then, cloud cover was calculated by comparing solar radiation data with theoretical clear sky solar radiation using (Cole and Wells, 2016):

$$\varphi_{s\_data} = \varphi_{s\_clearsky}(1 - 0.65C^2)$$

Where

ϕ_{s_data} is the real short wave solar radiation
$\phi_{s\_clearsky}$ is the theoretical clear sky short wave solar radiation
C is the fraction of cloud cover between 0 and 1

Meteorological data including air temperature, dew temperature, wind speed, wind direction, cloud cover, and solar radiation, for the Thrash Creek, HKFW1, CLSW1, and MIPW1 stations are shown in Figure 27, Figure 28, Figure 29, and Figure 30, respectively.

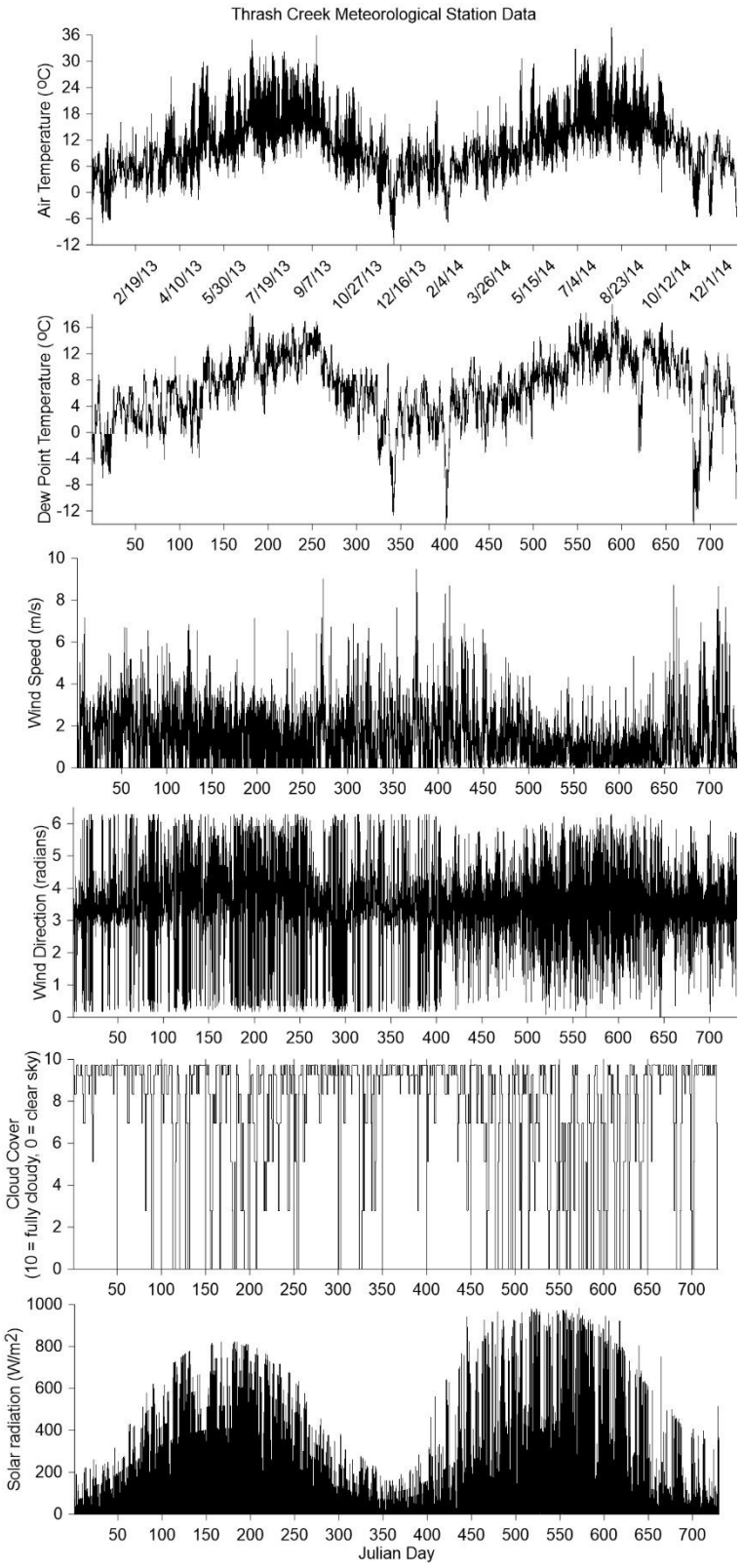

Figure 27. Meteorological data from Thrash Creek (filled in with interpolation and regression when necessary)

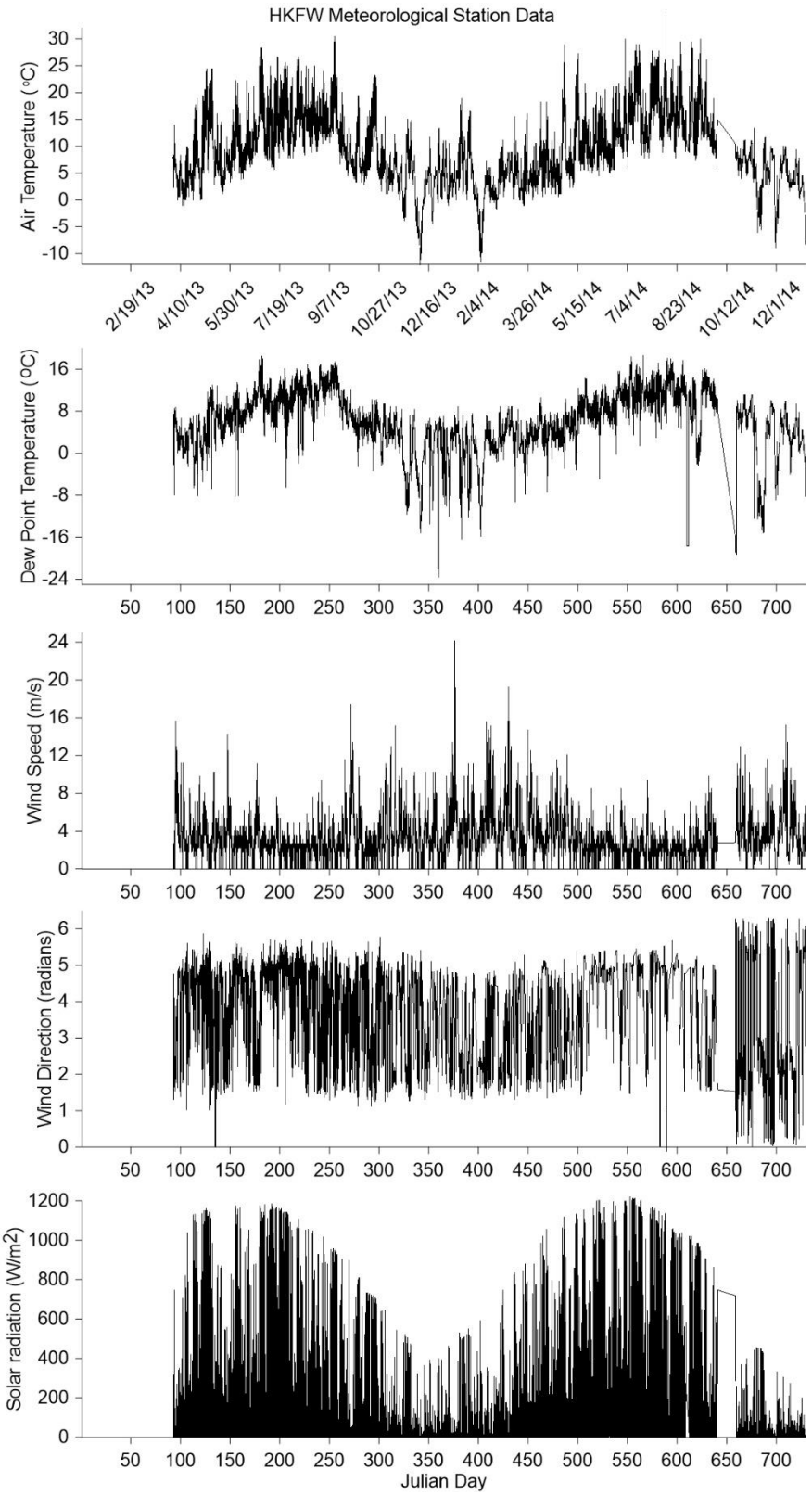

Figure 28. Raw meteorological data from HKFW station (raw values only)

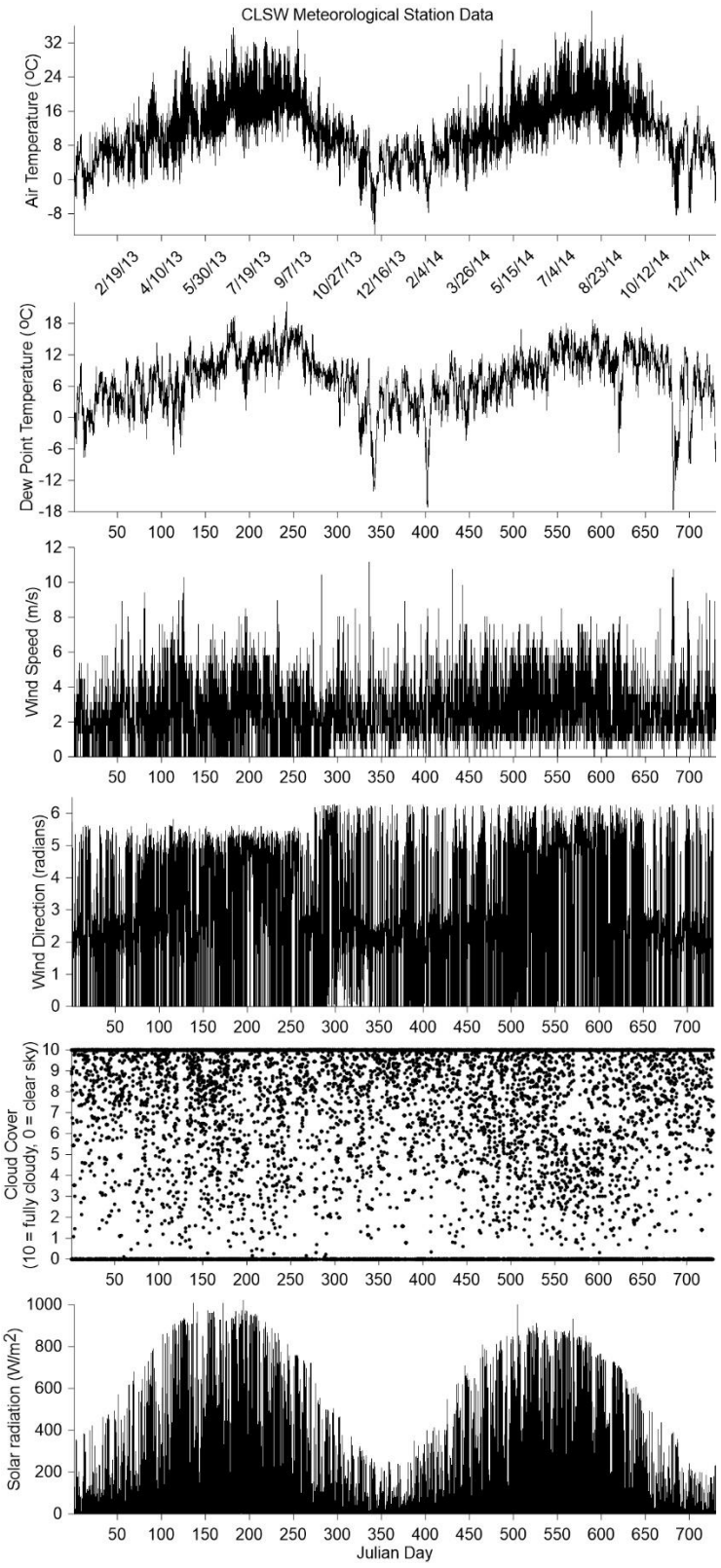

Figure 29. Meteorological data from CLSW station (including estimated values)

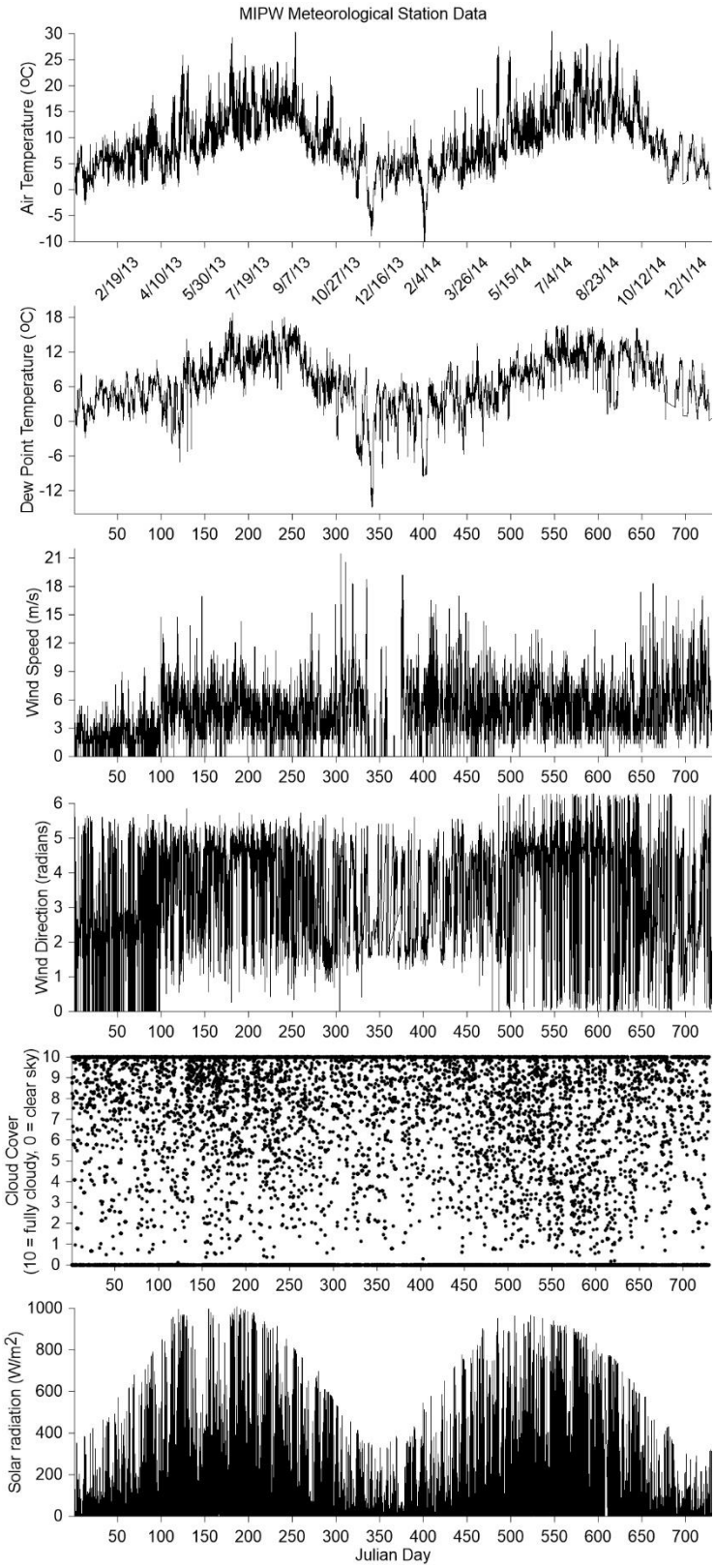

Figure 30. Meteorological data from MIPW station (including estimated values)

Flow Inputs

Many tributaries discharge to the mainstem Chehalis River within the model reach. The larger tributaries include the Newaukum River, Skookumchuck River, South Fork Chehalis River and Black River. The smaller tributaries include Bunker, Mill, Stearns, Dillenbaugh, Salzer, China, Scammon, Prairie, Lincoln, Scatter, Independence, Garrard, Rock, Cedar, Gibson, and Porter creeks. Five wastewater treatment plants (WWTP) discharge to the river. Four are municipal (Pe Ell, Centralia, Chehalis, and Grand Mound), while the other is industrial (Darigold, Inc.). Groundwater inputs also occur along the Chehalis River, starting upstream of Elk Creek and continuing until the downstream boundary at Porter. The river mile and model segment locations of the tributaries, dischargers, and groundwater inputs is shown in Table 4. A schematic of the tributaries and dischargers entering the Chehalis River is shown in Figure 31.

Table 4. River mile and segment locations for tributaries, dischargers, and groundwater inputs to the Chehalis River

Description	Model Segment	River Mile
Pe Ell WWTP	15	107
Elk Creek	38	100
South Fork Chehalis River	89	88
Bunker Creek	105	85
Stearns Creek	134	78.1
Mill Creek	135	78
Newaukum River	145	75.2
Darigold WWTP	150	75
Dillenbaugh Creek	150	74.4
Chehalis WWTP	150	74.3
Salzer Creek	171	69.2
China Creek	181	67.5
Skookumchuck River	182	66.8
Scammon Creek	187	65.5
Lincoln Creek	205	61.8
Centralia WWTP	207	61.25
Grand Mound WWTP	218	59.17
Prairie Creek	222	58.2
Scatter Creek	236	55.2
Independence Creek	250	50
Black River	267	47
Garrard Creek	275	44.9
Rock Creek	300	39.3
Cedar Creek	302	38.7
Gibson Creek	308	37.3
Porter Creek	321	33.3
Groundwater – Upstream of Elk Creek to downstream Boundary at Porter	35 – 321	101.9 – 33.3

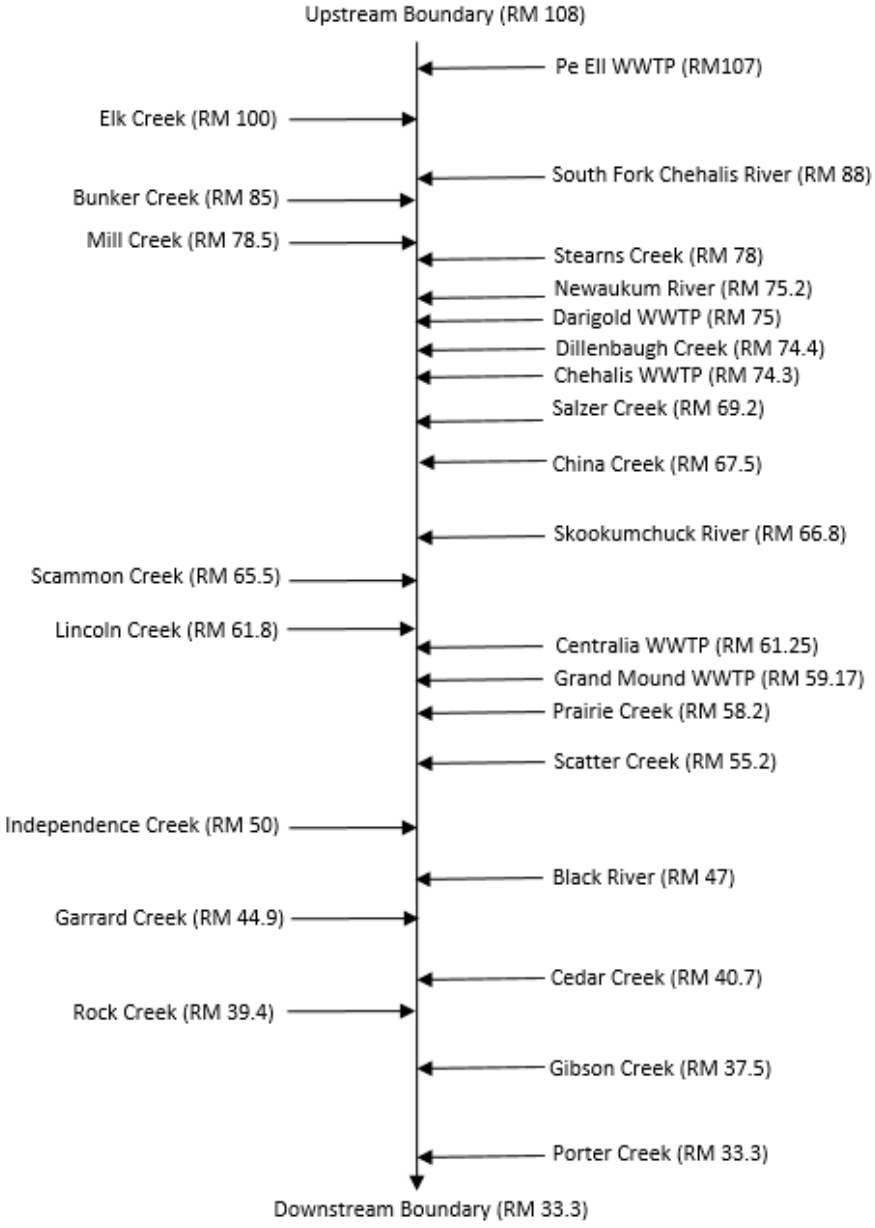

Figure 31. Schematic of tributaries to the model reach of the Chehalis River and their corresponding river miles (WEST Consultants, 2011 and WADOE, 2001). Note: figure is not to scale.

Flow and stage data were available from multiple monitoring stations along the mainstem Chehalis River, and for some of the tributaries. Flow data were made available by USGS (2014), WADOE (2014), and Thurston County (2014). WWTP data were provided by the WADOE National Pollutant Discharge Elimination System (NPDES) permit database and directly from the wastewater treatment plant managers (NPDES, 2016; Phelps, 2016; Hillock, 2016; Bilhimer, 2016; Zentner, 2016; and Patching, 2016).

Groundwater is generally a flow source to the river and varies at different locations along the channel. Multiple studies have been conducted that give average groundwater flow values for various locations along the Chehalis River. These include a TMDL study (Erickson, 1993), an aquifer characterization study (Garrigues, et al., 1998), a Centralia-Chehalis area groundwater study (Pitz et al., 2005), a seepage investigation in the Chehalis River basin (Ely, et al., 2008), and a groundwater/surface water study in the Chehalis River basin (Gendaszek, 2011). Flow data from these studies were generally given as gains and losses of flow for various reaches along the Chehalis River.

The most recent data were used from the Gendaszek (2011) report when possible, and then from the Ely, et al. (2008) report for reaches of the Chehalis River to fill in data gaps. Due to the approximate estimate of the groundwater flow, these flow values were assumed constant over time. These flows were allocated to each applicable segment, acting as many individual point tributaries. Table 5 lists the stations that provided flow data for tributaries, dischargers, and groundwater inputs.

Table 5. Flow monitoring stations with measured or estimated flow data

Organization	Station ID	Description
USGS	12019310	Chehalis River above Mahaffey Creek
USGS	12020000	Chehalis River near Doty, WA
USGS	12020525	Elk Creek below Deer Creek near Doty, WA
USGS	12020800	South Fork Chehalis River near Wildwood,
USGS	12025000	Newaukum River near Chehalis, WA
USGS	12026400	Skookumchuck River near Bucoda, WA
USGS	12027500	Chehalis River near Grand Mound, WA
USGS	12031000	Chehalis River at Porter, WA
Thurston County	55a	Scatter Creek at James Road
WADOE	23E060	Black River at Hwy 12
WADOE	23H060	Salzer Creek at Airport Road
WADOE NPDES	WA0020192	Pe Ell WWTP
WADOE NPDES	WA0037478	Darigold WWTP
WADOE NPDES	WA0021105	Chehalis WWTP
WADOE NPDES	WA0020982	Centralia WWTP
WADOE NPDES	WA0042099	Grand Mound WWTP
USGS	Reach T (Ely, et al.)	Groundwater river mile 101.9 – 100.5
USGS	Reach S (Ely, et al.)	Groundwater river mile 100.5 – 97.9
USGS	Reach R (Ely, et al.)	Groundwater river mile 97.9 – 93.8
USGS	Reach Q (Ely, et al.)	Groundwater river mile 93.8 – 90.2
USGS	Reach P (Ely, et al.)	Groundwater river mile 90.2 – 86
USGS	Reach O (Ely, et al.)	Groundwater river mile 86 – 79.9
USGS	Reach N (Ely, et al.)	Groundwater river mile 79.9 – 75.1
USGS	Reach A	Groundwater river mile 75.1 – 66.7
USGS	Reach B	Groundwater river mile 66.7 – 64.2
USGS	Reach C	Groundwater river mile 64.2 – 61.4
USGS	Reach D	Groundwater river mile 61.4 – 59.9
USGS	Reach E (Gendaszek)	Groundwater river mile 59.9 – 58.8
USGS	Reach F (Gendaszek)	Groundwater river mile 58.8 – 57.1
USGS	Reach G	Groundwater river mile 57.1 – 55.7
USGS	Reach H	Groundwater river mile 55.7 – 54.2
USGS	Reach I (Gendaszek)	Groundwater river mile 54.2 – 52.5
USGS	Reach J (Gendaszek)	Groundwater river mile 52.5 – 51.5
USGS	Reach K (Gendaszek)	Groundwater river mile 51.5 – 50.2
USGS	Reach L (Gendaszek)	Groundwater river mile 50.2 – 49.1
USGS	Reach M	Groundwater river mile 49.1 – 47.9
USGS	Reach N	Groundwater river mile 47.9 – 47.1
USGS	Reach O	Groundwater river mile 47.1 – 46.1
USGS	Reach P (Gendaszek)	Groundwater river mile 46.1 – 45
USGS	Reach Q	Groundwater river mile 45 – 44
USGS	Reach R	Groundwater river mile 44 – 42.3

Organization	Station ID	Description
USGS	Reach E (Ely, et al.)	Groundwater river mile 42.3 – 34
USGS	Reach D (Ely, et al.)	Groundwater river mile 34 – 33.3

Flow data were required for the entire model time period of January 1, 2013 to December 31, 2014, and gaps needed to be filled when necessary. The nearest mainstem flow monitoring station to the upstream boundary was located on the Chehalis River near Mahaffey Creek (USGS 12019310), with 15-minute frequency flow values. The Chehalis River at Mahaffey Creek, South Fork Chehalis River, Black River, and Elk Creek had flow records available, though sometimes with sizable data gaps on the order of months. Correlations were developed in order to fill in these gaps, following the same procedure as the meteorological data. The flow regression equations for Chehalis River near Mahaffey Creek, Elk Creek, South Fork Chehalis River, and Black River are shown in Table 6. Plots of the regression relationships can be seen in Figure 32, Figure 33, Figure 34, and Figure 35 for Chehalis River near Mahaffey Creek, Elk Creek, South Fork Chehalis River, and Black River, respectively.

Table 6. Flow Regression Relationships for South Fork Chehalis River, Black River, and Elk Creek to Chehalis River at Doty or Grand Mound

Tributary	Regression Equation	R^2 Value
Upstream boundary (Chehalis River at Mahaffey Creek)	$Q_{Ch\,R.\ Mahaffey} = 0.8262 * Q_{Chehalis@Doty} - 0.3337$	0.98
Elk Creek	$Q_{Elk\ Creek} = 0.3254 * Q_{Chehalis@Doty}$	0.7654
South Fork Chehalis River	$Q_{SF\ Chehalis} = 0.1818 * Q_{Chehalis@Doty}$	0.8453
Black River	$Q_{Black} = 0.0956 * Q_{Chehalis@Grand\ Mound}$	0.4688

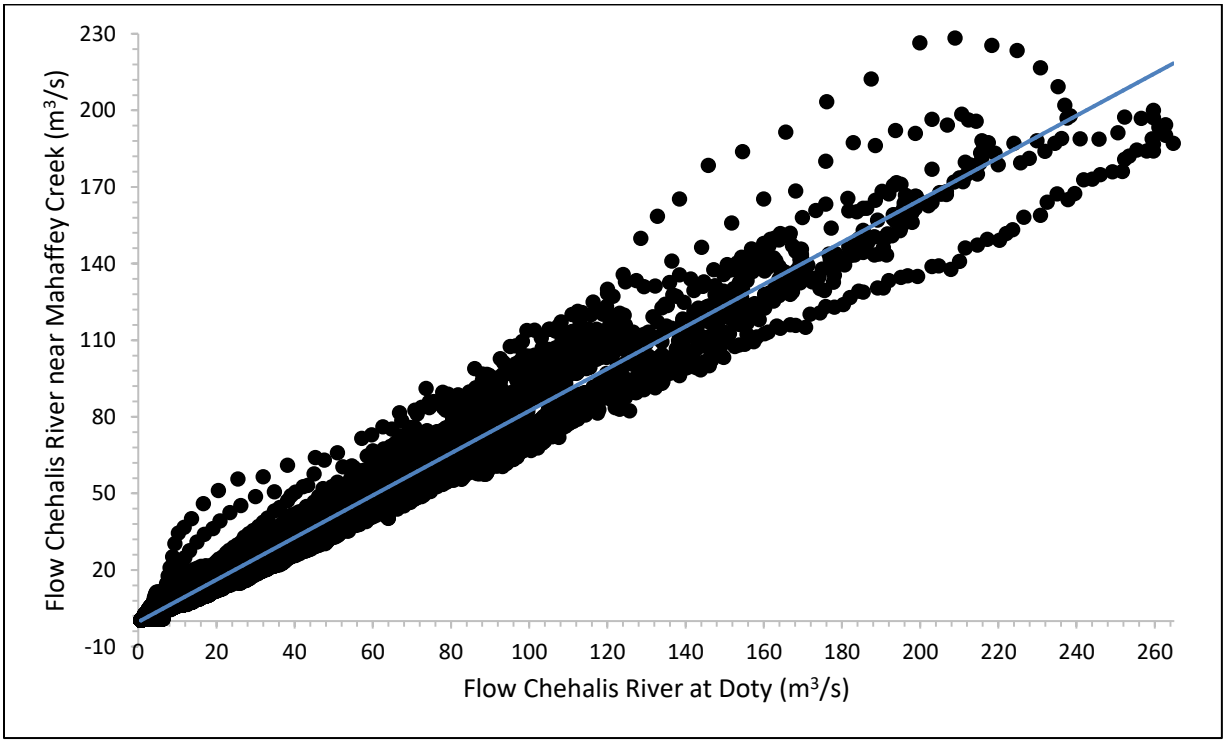

Figure 32. Flow relationship between Chehalis River near Mahaffey Creek and Chehalis River at Doty when both gaging stations had data available

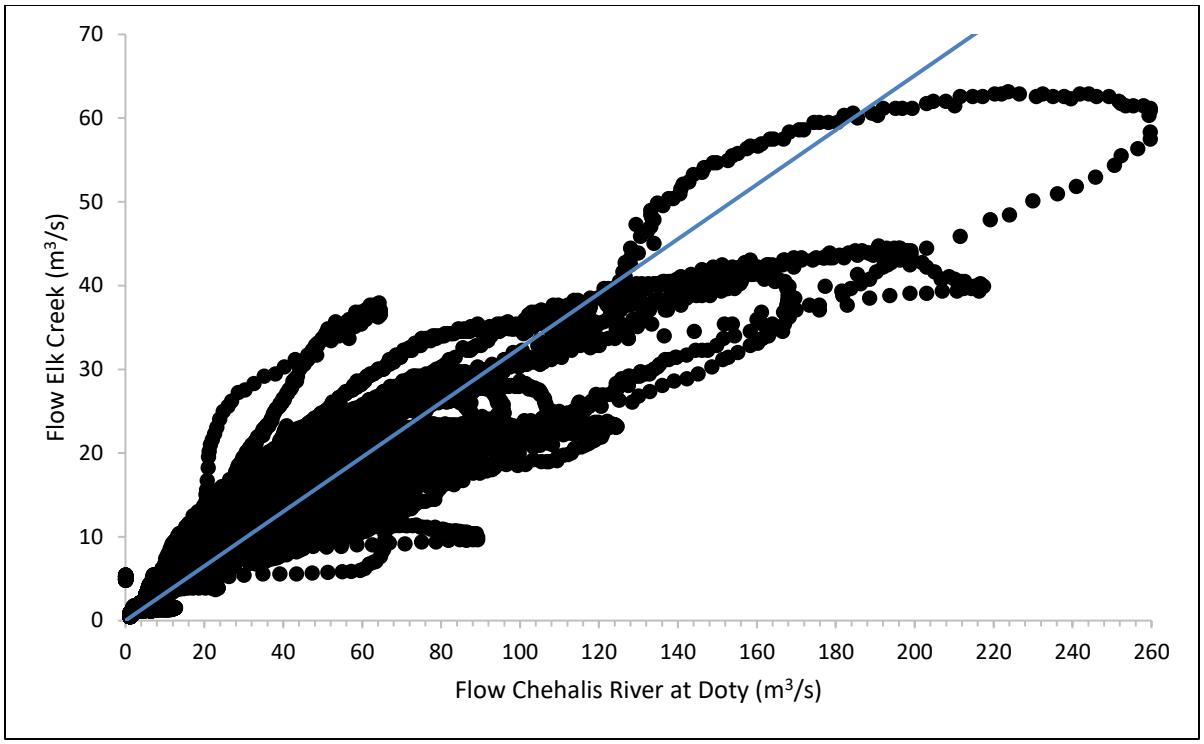

Figure 33. Flow relationship between Elk Creek and Chehalis River at Doty when both gaging stations had data available

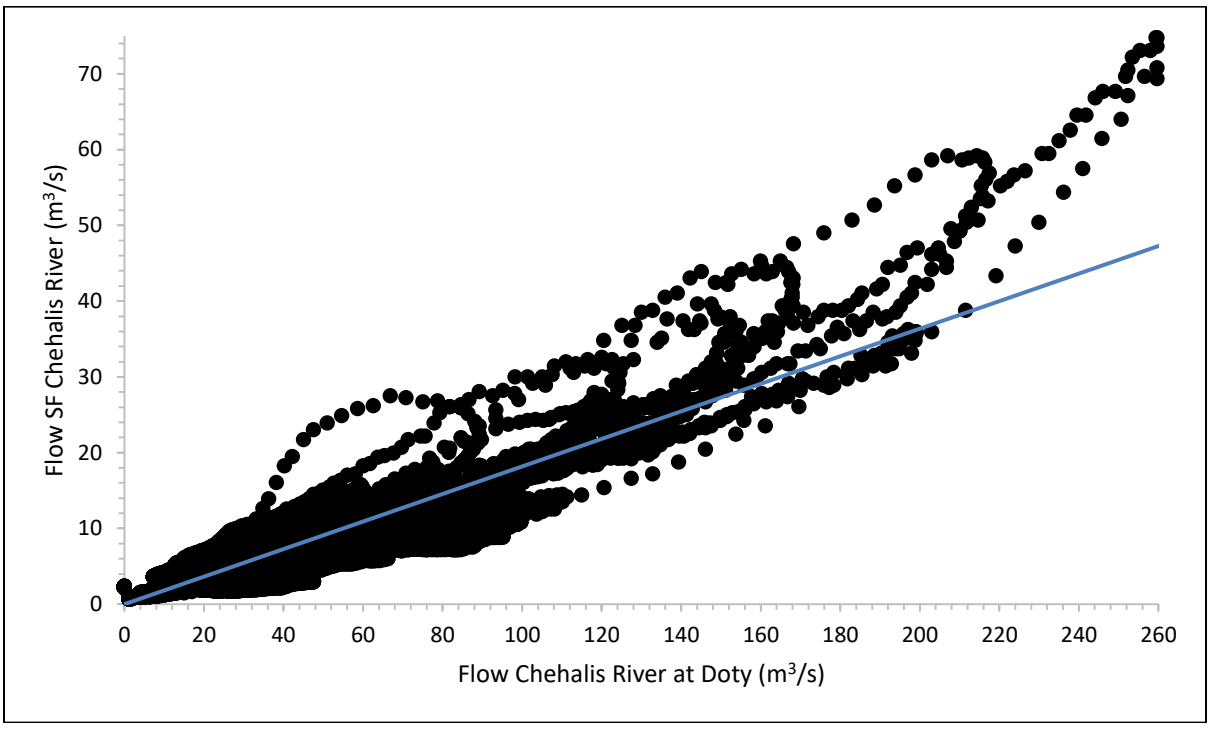

Figure 34. Flow relationship between South Fork Chehalis River and Chehalis River at Doty when both gaging stations had data available

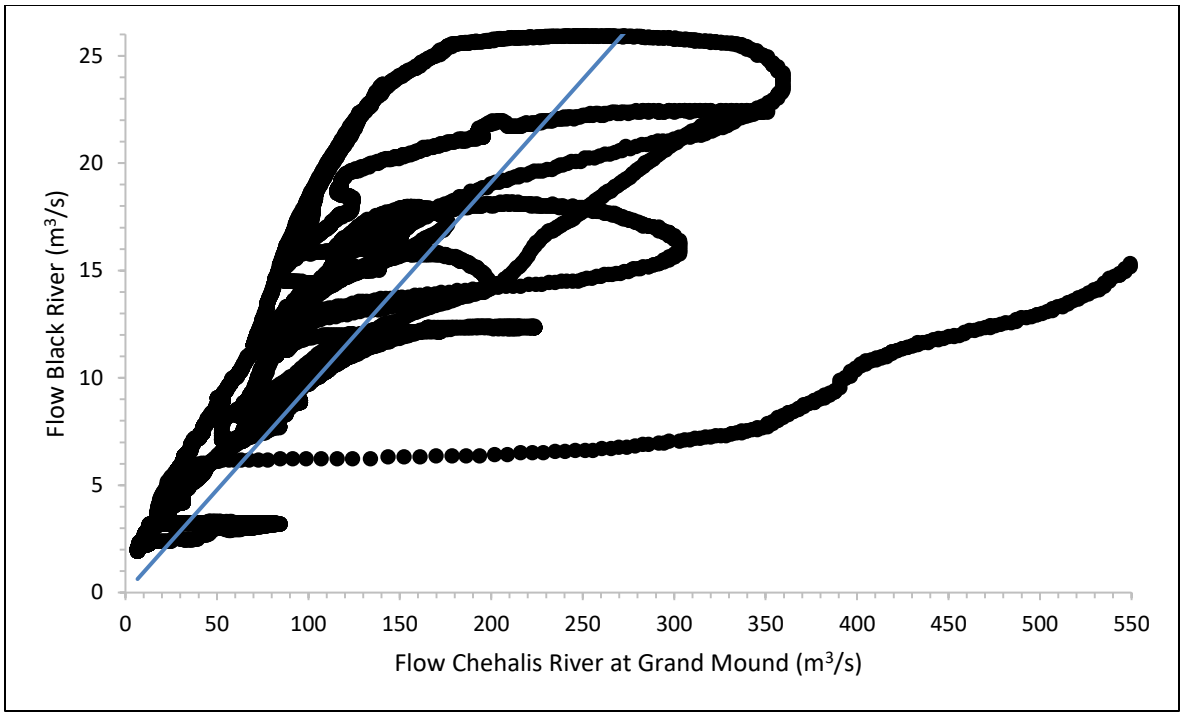

Figure 35. Flow relationship between Black River and Chehalis River at Grand Mound when both gaging stations had data available

Many of the smaller tributaries – including Bunker, Mill, Stearns, Dillenbaugh, Salzer, China, Scammon, Prairie, Lincoln, Scatter, Independence, Garrard, Rock, Cedar, Gibson, and Porter creeks – had little to no flow data available during the model time period, and hence it was not possible to create a regression relationship. In this case, gaged flow data from a mainstem monitoring station and a ratio of drainage area of the ungaged station to the drainage area of the gaged station was employed to estimate the missing tributary flow following the equation below (Anchor QEA, 2012 and WEST Consultants, 2011). The monitoring stations on the mainstem Chehalis River at Doty, Grand Mound, or Porter were used as the gaged data set depending which was closest since these stations had data available for the entire model time period. The drainage area values were provided by USGS (2016). Table 7 shows the tributary gaging stations and corresponding drainage areas used to employ this method.

Table 7. Drainage area values used to calculate flow for tributaries with missing data

Station ID	Station Name	Drainage Area (mi^2)
USGS 12019310	Chehalis River above Mahaffey Creek near Pe Ell, WA	68.9
USGS 12010000	Chehalis River at Doty, WA	113
USGS 12025000	Newaukum River	155
USGS 12022010	Bunker Creek above Deep Creek near Bunker, WA	20.7
USGS 12023400	Mill Creek at Littell, WA	6.17
USGS 12022500	Stearns Creek near Napavine, WA	14.1
USGS 12025075	Dillenbaugh Creek below Berwick Creek near Chehalis, WA	12.4
USGS 12025330	Salzer Creek	16.5
USGS 12025530	China creek near Centralia, WA	1.58
USGS 12026670	Scammon creek at Cooks Hill Road near Centralia, WA	5.13
LNC-CRK	Lincoln Creek	19.3
USGS 12027200	Lincoln creek at RM 1.6 near Galvin, WA	37.1

Station ID	Station Name	Drainage Area (mi^2)
USGS 12027540	Prairie creek near Grand Mound, WA	3.76
	Scatter Creek	40.01
USGS 12028150	Independence Creek	13.2
USGS 12029325	Garrard Creek	11
USGS 12030500	Cedar Creek	38.2
USGS 12030000	Rock Creek	24.8
USGS 12030550	Gibson Creek	6.96
USGS 12030950	Porter Creek	39.8

Figure 36 shows the input flow to the model for tributaries with data available, including those where regression estimation techniques were employed. Figure 37, Figure 38, and Figure 39 show the input flow for tributaries where flow values were estimated from drainage areas and mainstem river data. Figure 40 shows the input flows from the WWTP dischargers, and Figure 41 shows the input flows for groundwater sources to the Chehalis River.

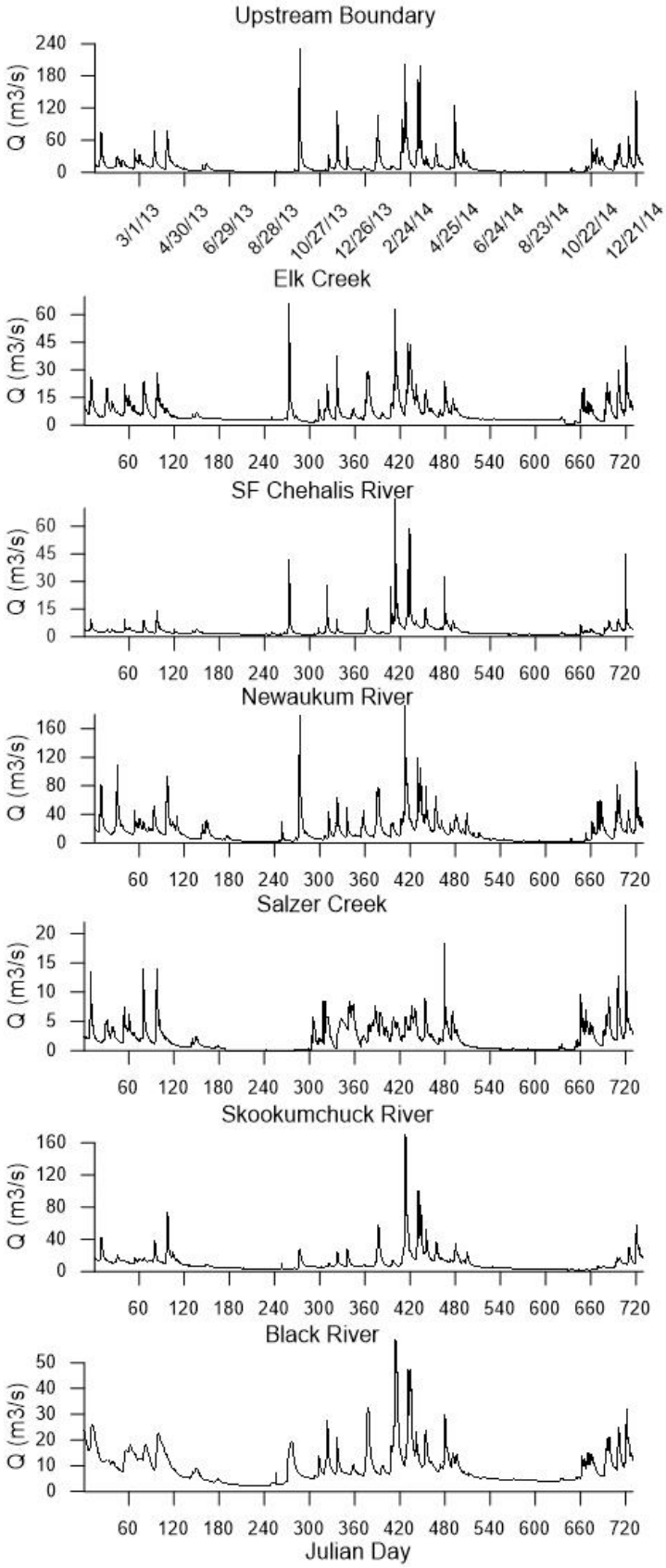

Figure 36. Input flow data where field data were available for Chehalis River at Mahaffey Creek (upstream boundary), Elk Creek, South Fork Chehalis River, Newaukum River, Salzer Creek, Skookumchuck River, and Black River

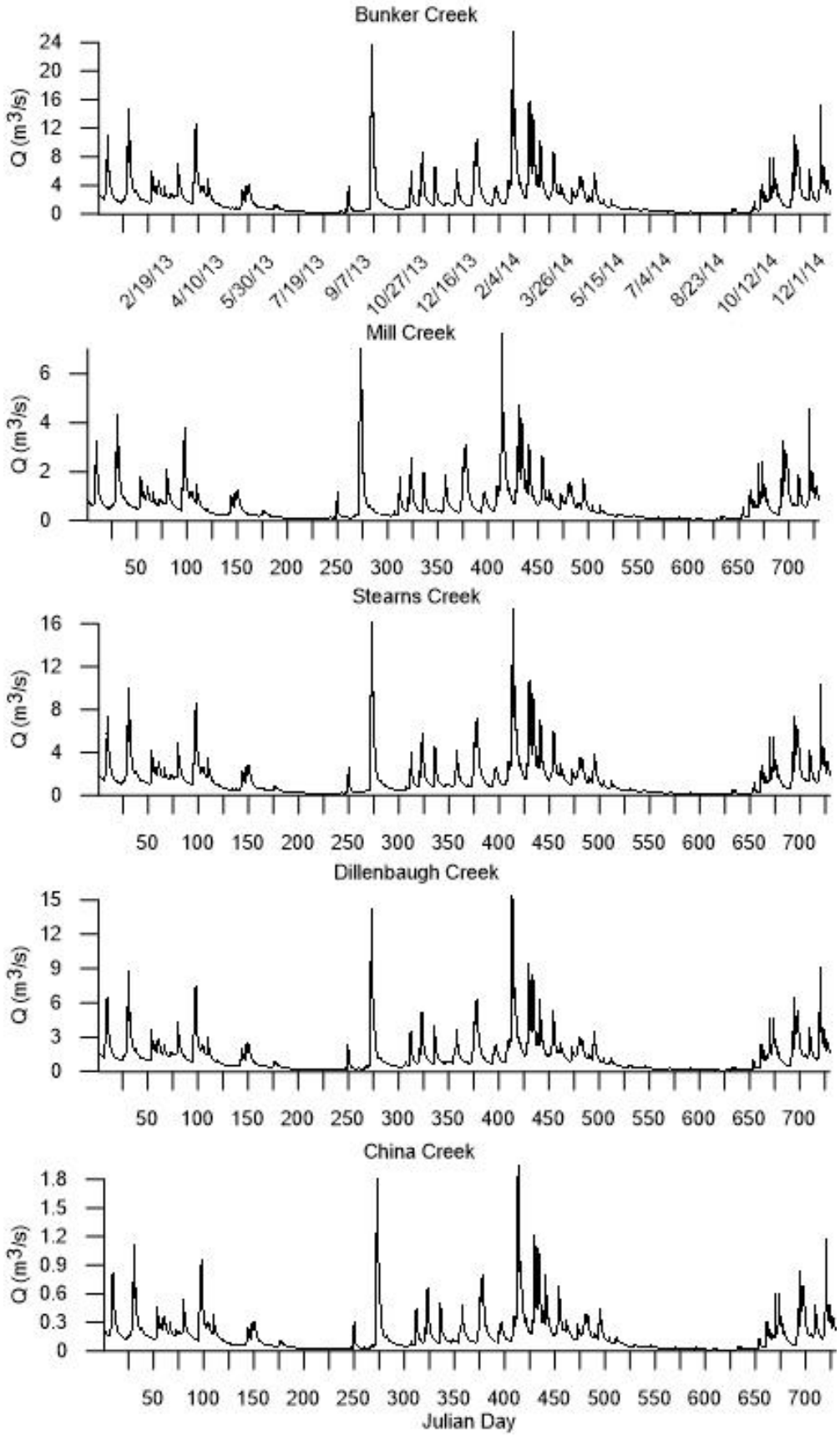

Figure 37. Input flow based on drainage area ratios to Chehalis River data for Bunker Creek, Mill Creek, Stearns Creek, Dillenbaugh Creek, and China Creek

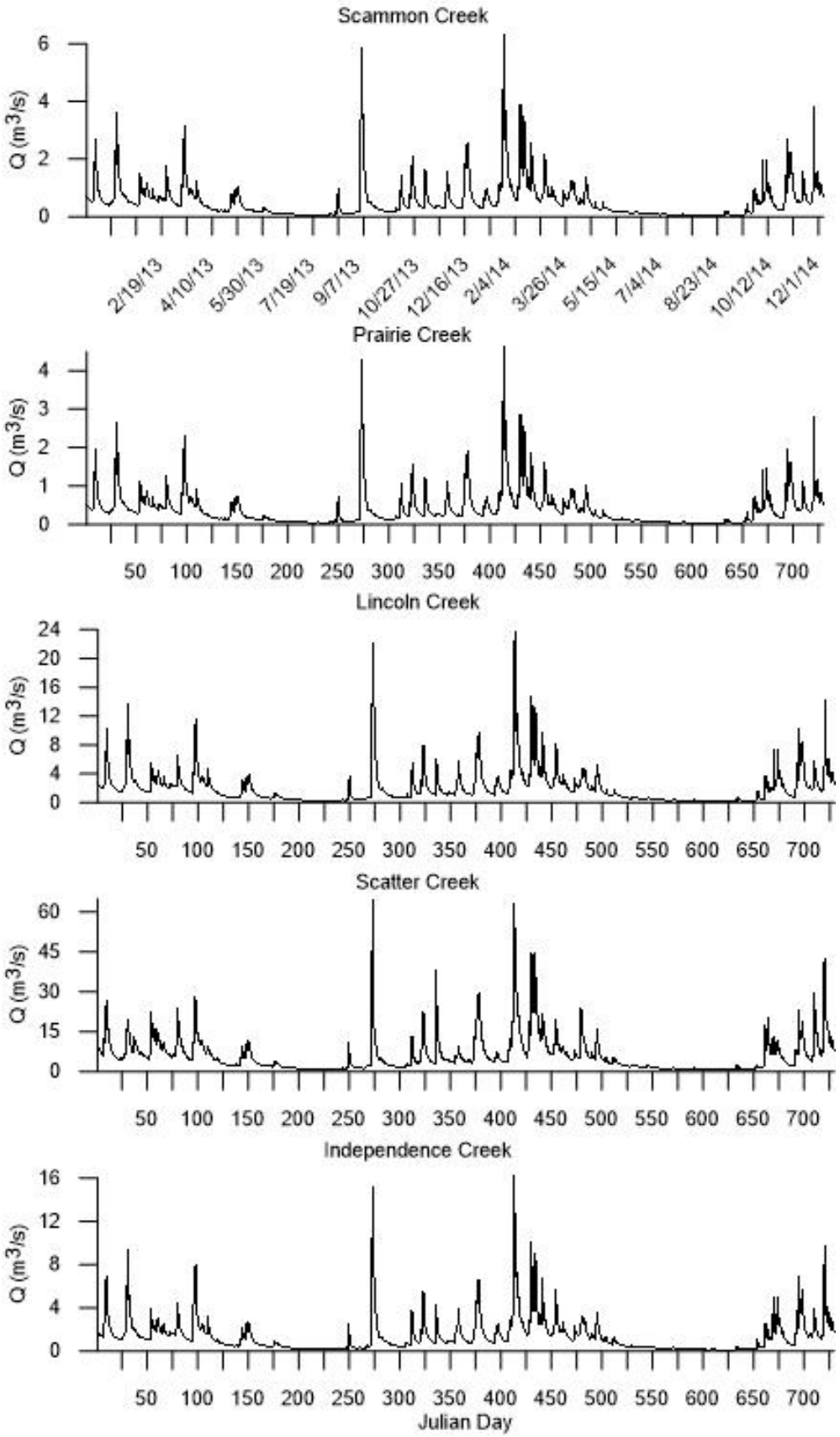

Figure 38. Input flow based on drainage area ratios to Chehalis River data for Scammon Creek, Prairie Creek, Lincoln Creek, Scatter Creek, and Independence Creek

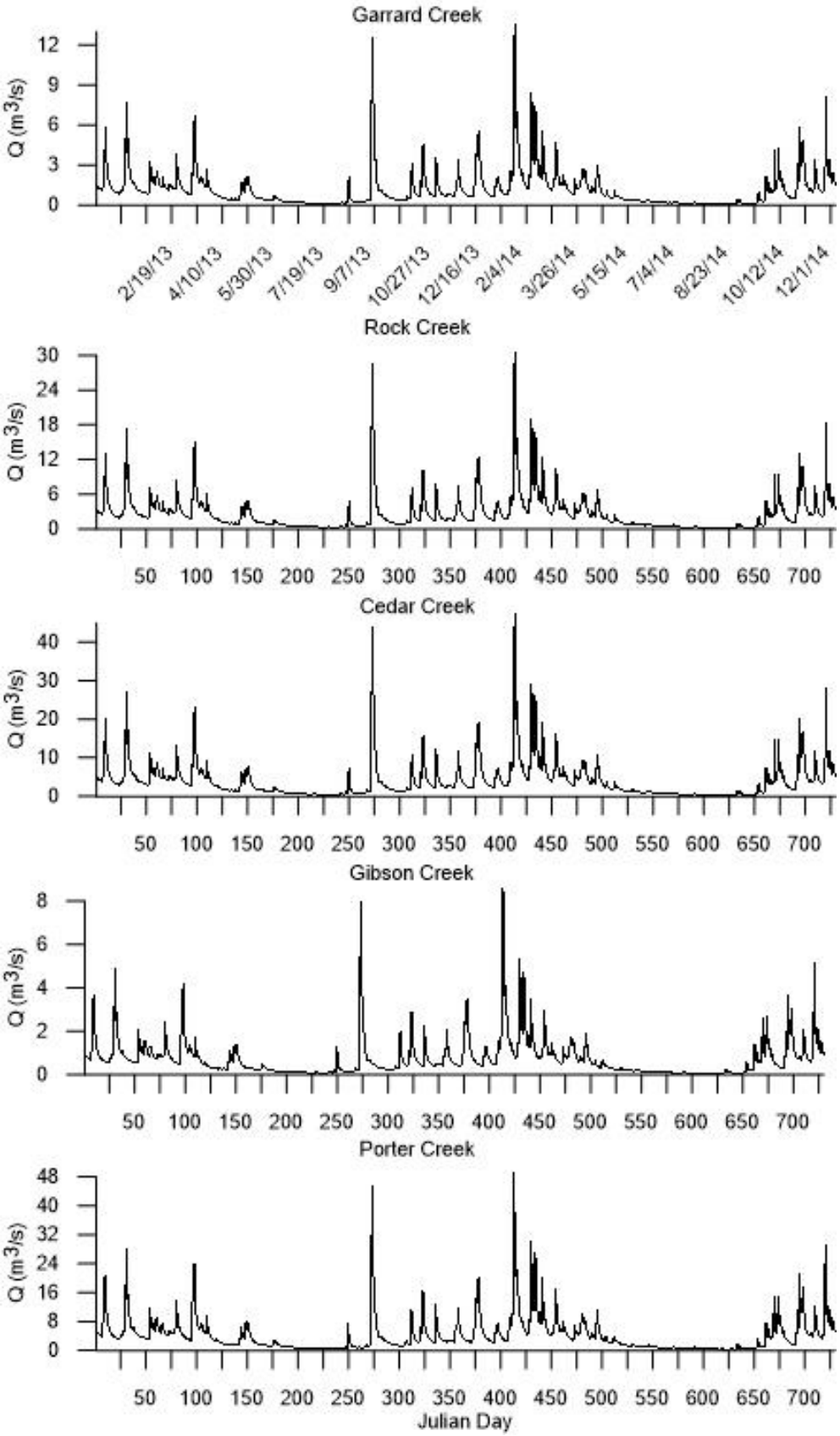

Figure 39. Input flow based on drainage area ratios to Chehalis River data for Garrard Creek, Rock Creek, Cedar Creek, Gibson Creek, and Porter Creek

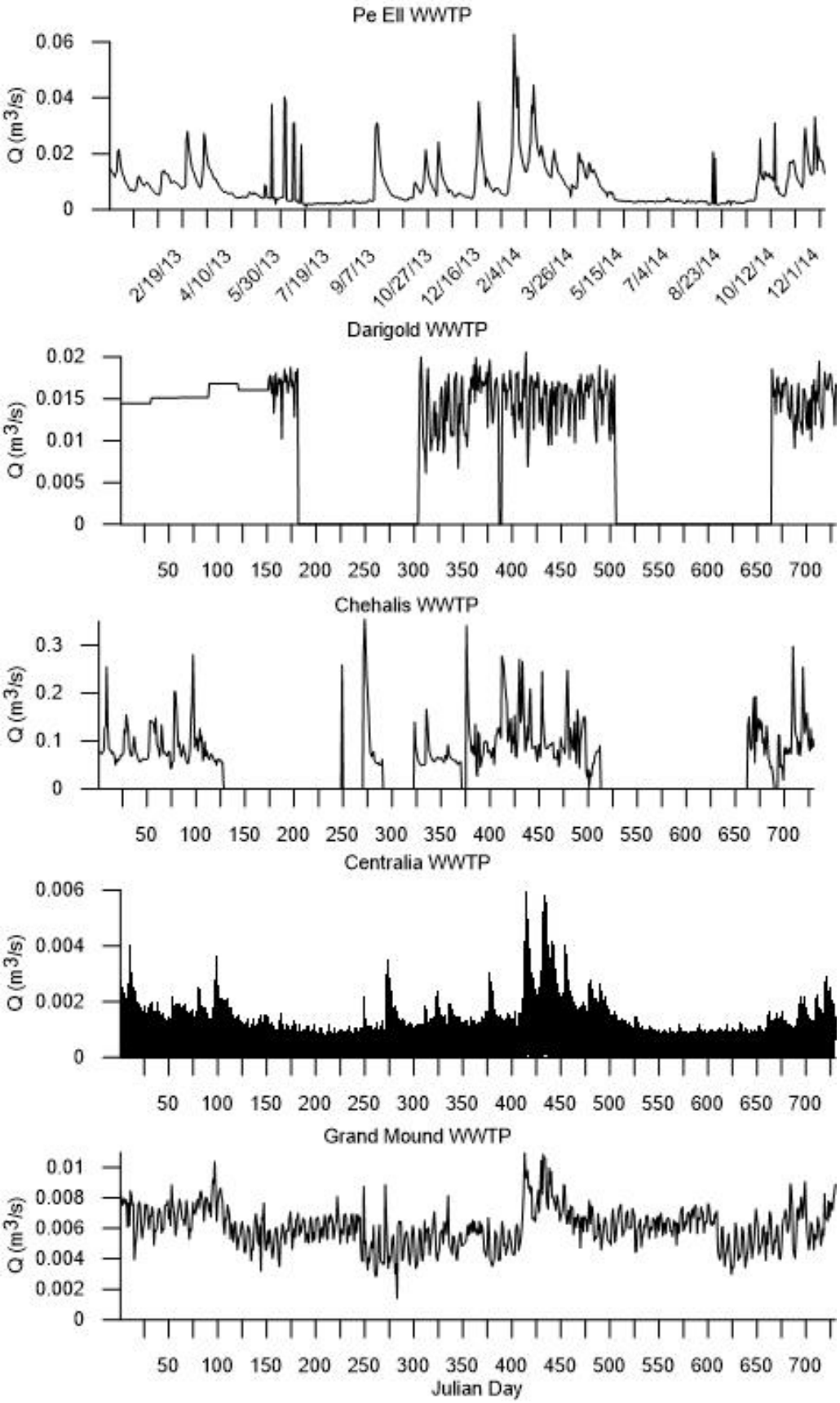

Figure 40. Input flow for the Pe Ell, Darigold, Chehalis, Centralia, and Grand Mound wastewater treatment plants

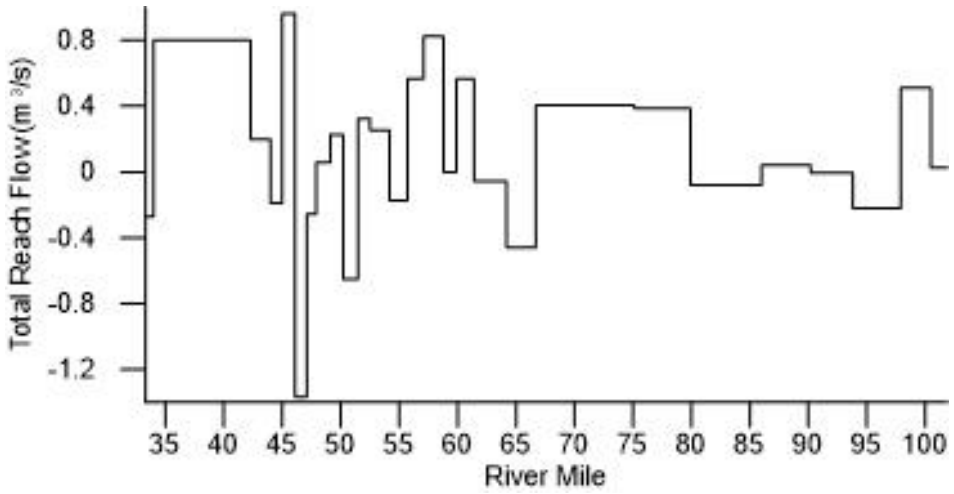

Figure 41. Input flow for groundwater inflows

Temperature Inputs

Temperature data were also required for the entire model time period for all input flows. Temperature data were available from measurement locations along the mainstem Chehalis River as well as for some of the tributaries. Temperature data were made available by WADOE (2014), Anchor QEA (2014), Washington Department of Fish and Wildlife (WDFW, 2014), and Thurston County (2014). WWTP data were provided by the WADOE NPDES permit data base as well as directly from some plant managers (NPDES 2003a, 2003b, 2010, 2011, 2012; Phelps, 2016; Hillock, 2016; Bilhimer, 2016; Zentner, 2016; and Patching, 2016). Groundwater temperature data were provided from the Chehalis River TMDL study (Erickson, 1993) and an Engineering Report conducted by Brown and Caldwell for National Frozen Foods (2016). Average groundwater temperatures were estimated for the various reaches along the Chehalis River. Temperature groundwater data from the wells closest to the river for each reach were used. Table 8 lists the gaging stations that were used for the model temperature for tributaries, dischargers, and groundwater inputs.

Table 8. Monitoring stations used to develop model temperature inputs

Organization	Station ID	Description	Dates with data
Anchor QEA	CHL-PEL-US	Chehalis Upstream of Pe Ell	7/31/13 - 3/26/14
Anchor QEA	CHL-PEL-DS	Chehalis Downstream of Pe Ell	7/31/13 - 7/30/14
Anchor QEA	CHL-WOODSTEAD	Chehalis at Woodstead Farm 01	7/2/13 - 10/28/13
Anchor QEA	CHL-DOTY	Chehalis at Doty	7/3/13 - 10/16/13
Anchor QEA	ELK-CRK	Elk Creek	7/31/13 - 3/26/14
Anchor QEA	CHL-RAINBOW-FALLS	Chehalis at Rainbow Falls	7/2/13 - 10/16/13
Anchor QEA	CHL-CERES-HILLS	Chehalis at Ceres Hill Road	7/3/13 - 10/16/13
Anchor QEA	SF-CHL-MOUTH	South Fork Mouth	7/31/13 - 3/26/14
Anchor QEA	CHL-ADNA	Chehalis Near Adna	7/31/13 - 7/21/14
Anchor QEA	CHL-US-NWK	Chehalis Upstream of Newaukum Confluence	7/31/13 - 3/26/14
Anchor QEA	NWK-MOUTH	Newaukum Mouth	9/18/13 - 7/21/14
Anchor QEA	SKM-MOUTH	Skookumchuck Mouth	9/5/13 - 10/15/13
Anchor QEA	CHL-GLV	Chehalis at Galvin Bridge	7/30/13 - 7/21/14
Anchor QEA	CHL-US-BLK	Chehalis Upstream of Black River	7/30/13 - 7/22/14
Anchor QEA	BLK-RT12	Black River Mouth	9/5/13 - 7/22/14
Anchor QEA	CHL-OAK	Chehalis at Oakville	7/30/13 - 7/22/14

Organization	Station ID	Description	Dates with data
WDFW	11-UCH	Upper Chehalis	6/9/14 - 9/15/15
WDFW	3-UCH	Upper Chehalis	5/15/14 - 9/15/15
WDFW	13-CH	Chehalis mainstem	6/10/14 - 9/15/15
WDFW	4-UCH	Upper Chehalis	5/15/14 - 9/15/15
WDFW	15-CH	Chehalis mainstem	6/10/14 - 10/14/14
WDFW	19-CH	Chehalis mainstem	6/18/14 - 9/2/15
WDFW	21-CH	Upper Chehalis	6/11/14 - 9/2/15
WDFW	NEW-1	Newaukum	7/15/14 - 9/4/15
WDFW	22-CH	Upper Chehalis	6/11/14 - 8/5/15
WDFW	16-CH	Chehalis mainstem	6/10/14 - 9/3/15
WDFW	17-CH	Chehalis mainstem	6/10/14 - 9/1/15
WDFW	18-CH	Chehalis mainstem	6/10/14 - 8/26/15
WDFW	23-CH	Chehalis mainstem	7/15/14 - 8/17/15
Thurston	55a	Scatter Creek at James Road	1/1/13 – 5/19/15
WADOE	23A160	Chehalis River at Dryad	7/1/13 - 9/18/13, 6/24/14 - 9/23/14, & 5/19/15 - 9/15/15
WADOE	23A070	Chehalis River at Porter	10/23/12 - 6/25/13 & 9/18/13 - 5/26/15
WADOE NPDES	WA0020192	Pe Ell WWTP	1/1/13 - 12/31/14
WADOE NPDES	WA0037478	Darigold WWTP	1/1/13 - 9/30/13, & 11/1/13 - 12/31/14
WADOE NPDES	WA0021105	Chehalis WWTP	1/1/13 - 12/31/14
WADOE NPDES	WA0020982	Centralia WWTP	1/1/13 - 12/31/14
WADOE NPDES	WA0042099	Grand Mound WWTP	1/1/13 - 12/31/14
Darigold WWTP	41	Chehalis River Upstream Darigold WWTP	1/1/13 - 11/30/15
Darigold WWTP	40	Chehalis River Downstream Darigold WWTP	1/1/13 - 11/30/15
WADOE	DW03	GW – Bunker Creek to Adna reach	1993
WADOE	DW08	GW – Adna to Claquato reach	1993
WADOE	DW07	GW – Claquato to Golf Course reach	1993
WADOE	DW15	GW – Golf Course to Mellen Street reach	1993
WADOE	DW18	GW – Centralia/Fords Prairie reach	1993
WADOE	DW27	GW – Grand Mound to Oakville reach	1993
NFF	Fields 7, 4-5, and 2	GW – Chehalis-Centralia Reach	1/1/13 – 12/8/13

Temperature data gaps were filled using the same regression procedure as for meteorological data by creating correlations between stations with missing data and stations with complete data sets. The Chehalis River downstream of Darigold WWTP and the Chehalis River upstream of Darigold WWTP gages had data for the entire model time period and hence were used for correlations with other incomplete data series. However, the regression relationships using the Chehalis River downstream of Darigold WWTP gage to fill in missing data had

higher coefficient of determination (R^2) values than when using data from the upstream site. For this reason, the downstream site was used rather than the upstream to fill missing data. The exceptions to this were when closer temperature gages had data available. For Elk Creek this was 4-UCH and for Black River this was 18-CH. When these closer gages did not have data, the downstream of Darigold gage was used.

The closest temperature measurement station to the upstream boundary was 11-UCH. When possible, data from 11-UCH was used. The next closest stations were CHL-PEL-US and 3-UCH, which were close together and were located in the same model segment (length 400 m). A data set including temperature data from CHL-PEL-US from 1/1/13 to 5/14/14 and 3-UCH from 5/15/15 to 9/15/15 was created. One regression relationship was formed between 11-UCH and the CHL-PEL-US and 3-UCH data set. This relationship was used to estimate upstream boundary temperatures when CHL-PEL-US and 3-UCH had data. A second regression relationship was created between 11-UCH and Chehalis River Downstream of Darigold WWTP and was used to estimate upstream boundary temperatures for the remainder of the model time period.

The temperature linear regression relationships for Chehalis River near the upstream boundary (station 11-UCH), Elk Creek, South Fork Chehalis River, Newaukum River, Skookumchuck River, and Black River are shown in Table 9. Example plots of the temperature regression relationships are shown for the Chehalis River upstream boundary and South Fork Chehalis River in Figure 42 and Figure 43, respectively.

Table 9. Temperature Regression Relationships for Upstream Boundary, Elk Creek, South Fork Chehalis River, Newaukum River, Skookumchuck River, and Black River

Tributary	Regression Equation	R^2 Value
Chehalis River Downstream of Darigold	$T_{Ch\ R.DS\ Darigold} = 1.0488 * T_{Ch\ R.Porter} - 1.135$	0.988
Upstream boundary (station 11-UCH)	$T_{Ch\ R.(\ 11-UCH)} = 1.0191 * T_{CHL-PEL-US\ \&\ 3-UCH} - 0.5085$ $T_{Ch\ R.(\ 11-UCH)} = 0.8186 * T_{Ch\ R.DS\ Darigold} + 1.0174$	0.9778 0.954
Elk Creek	$T_{Elk\ Creek} = 0.7681 * T_{Ch\ R.(\ 4-UCH)} + 1.7319$ $T_{Elk\ Creek} = 0.7383 * T_{Ch\ R.DS\ Darigold} + 1.6909$	0.9742 0.9789
South Fork Chehalis River	$T_{SF\ Chehalis} = 0.9627 * T_{Ch\ R.DS\ Darigold} + 0.583$	0.9883
Newaukum River	$T_{Newaukum\ R.} = 0.9521 * T_{Ch\ R.DS\ Darigold} + 0.5257$	0.9778
Skookumchuck River	$T_{Skookumchuck\ R.} = 0.67 * T_{Ch\ R.DS\ Darigold} + 4.7899$	0.9693
Black River	$T_{Black} = 0.7406 * T_{Ch\ R.(18-CH)} + 3.2796$ $T_{Black} = 0.8222 * T_{Ch\ R.DS\ Darigold} + 2.3484$	0.8358 0.9672

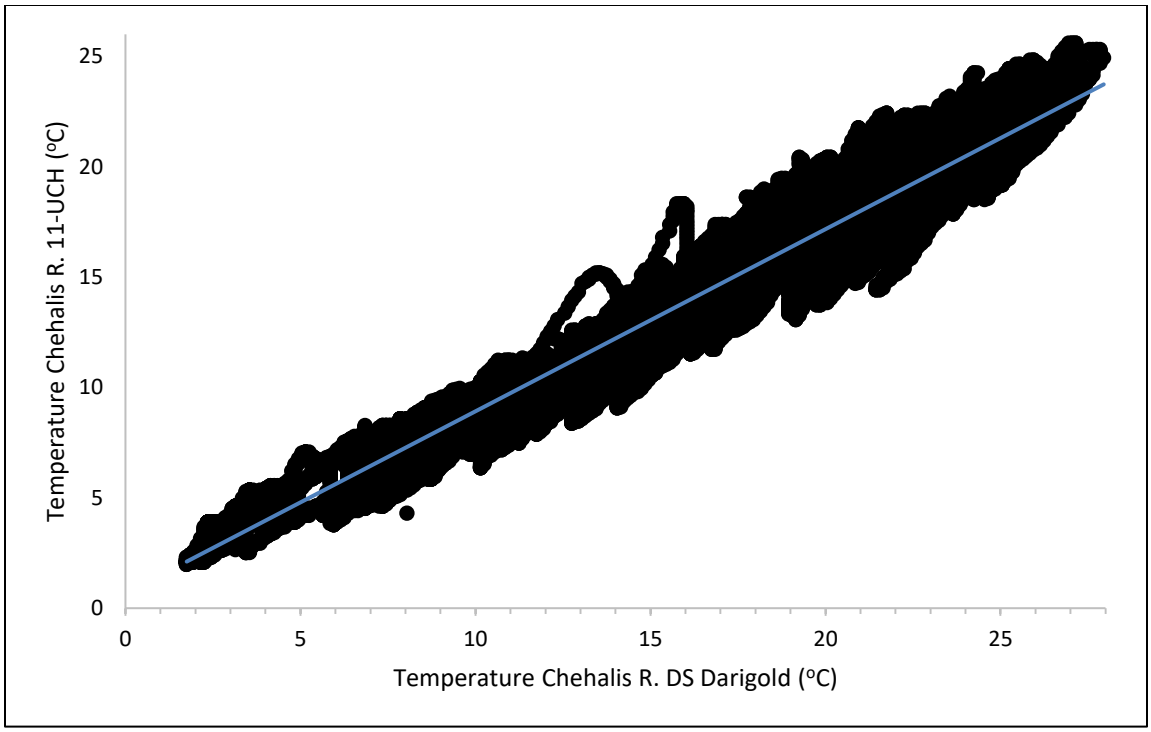

Figure 42. Temperature relationship between Chehalis River at upstream boundary station 11-UCH and Chehalis River Downstream of Darigold when both gaging stations had data available

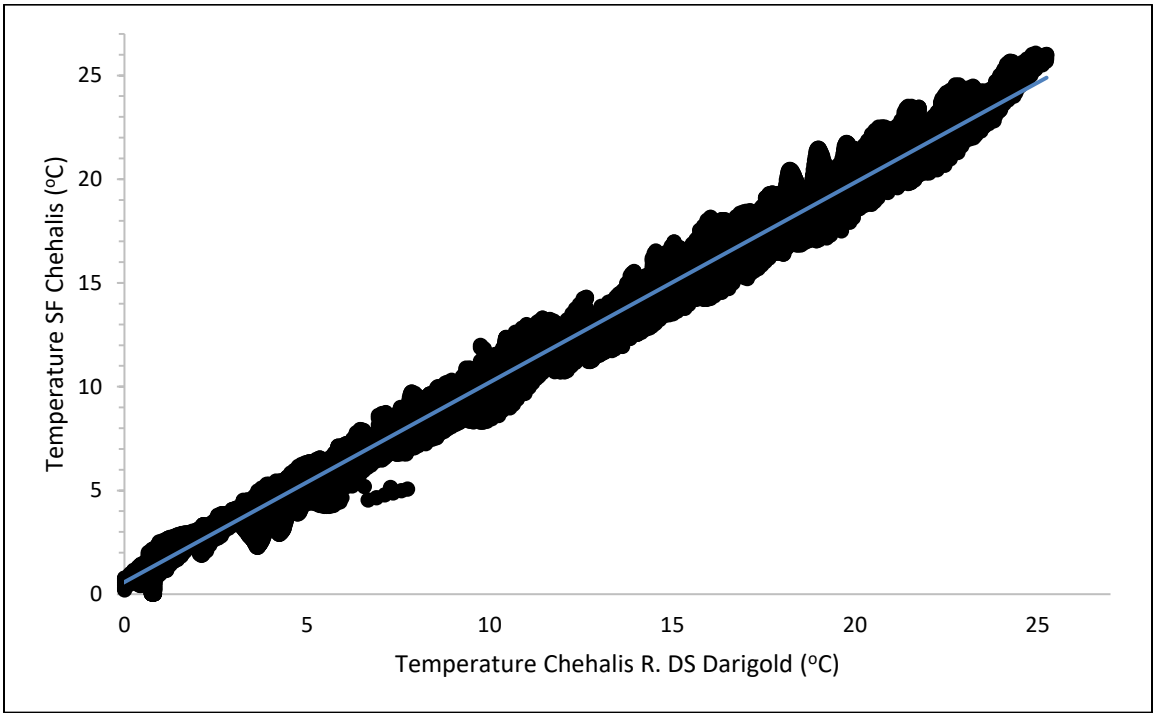

Figure 43. Temperature relationship between South Fork Chehalis River and Chehalis River Downstream of Darigold when both gaging stations had data available

For tributaries where no data were available, it was not possible to create a regression relationship to estimate temperature values. In these cases, the input temperature file from another tributary with similar flow magnitudes was used instead.

Groundwater reaches typically had one data value for temperature available, and sometimes no data. In order to estimate seasonal variation in groundwater temperature, 2 ^{o}C was added to the groundwater temperature data during the summer months. Additional data in the Chehalis-Centralia Reach gave general seasonal trends in groundwater temperature for the year 2013. The general trends were estimated to be the same for the year 2014.

Additional groundwater data from Brown and Caldwell was available for the Chehalis-Centralia reach of the river for 2013. By using some values from 2013, the same general temperature trend from 2013 was used to estimate temperatures for 2014 in this reach.

Figure 44 shows input temperature to the model for tributaries with data available, including those where regression estimation techniques were employed. Figure 45 shows the input temperature for the wastewater treatment plants. Figure 46 and Figure 47 show the temperature input data for the groundwater sources.

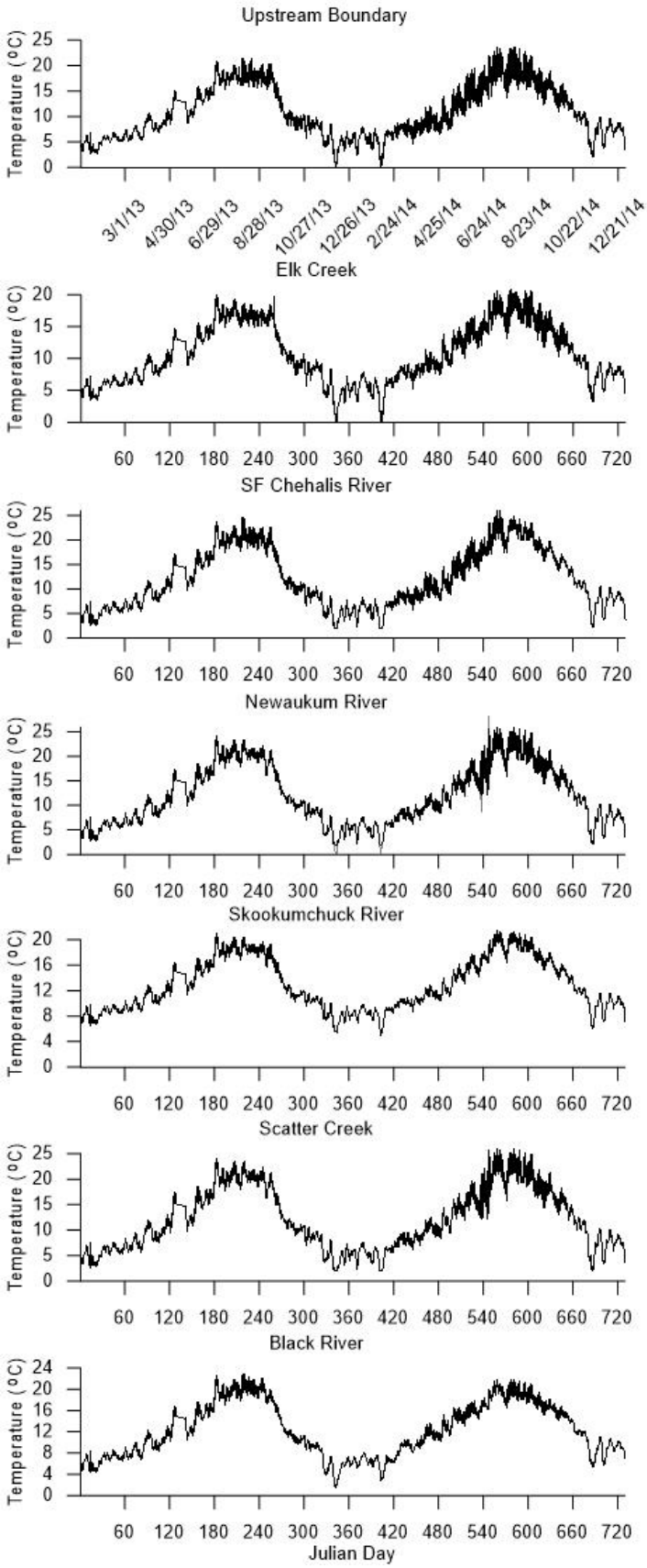

Figure 44. Input temperature data where field data were available for station 11-UCH (upstream boundary), Elk Creek, South Fork Chehalis River, Newaukum River, Skookumchuck River, Scatter Creek, and Black River

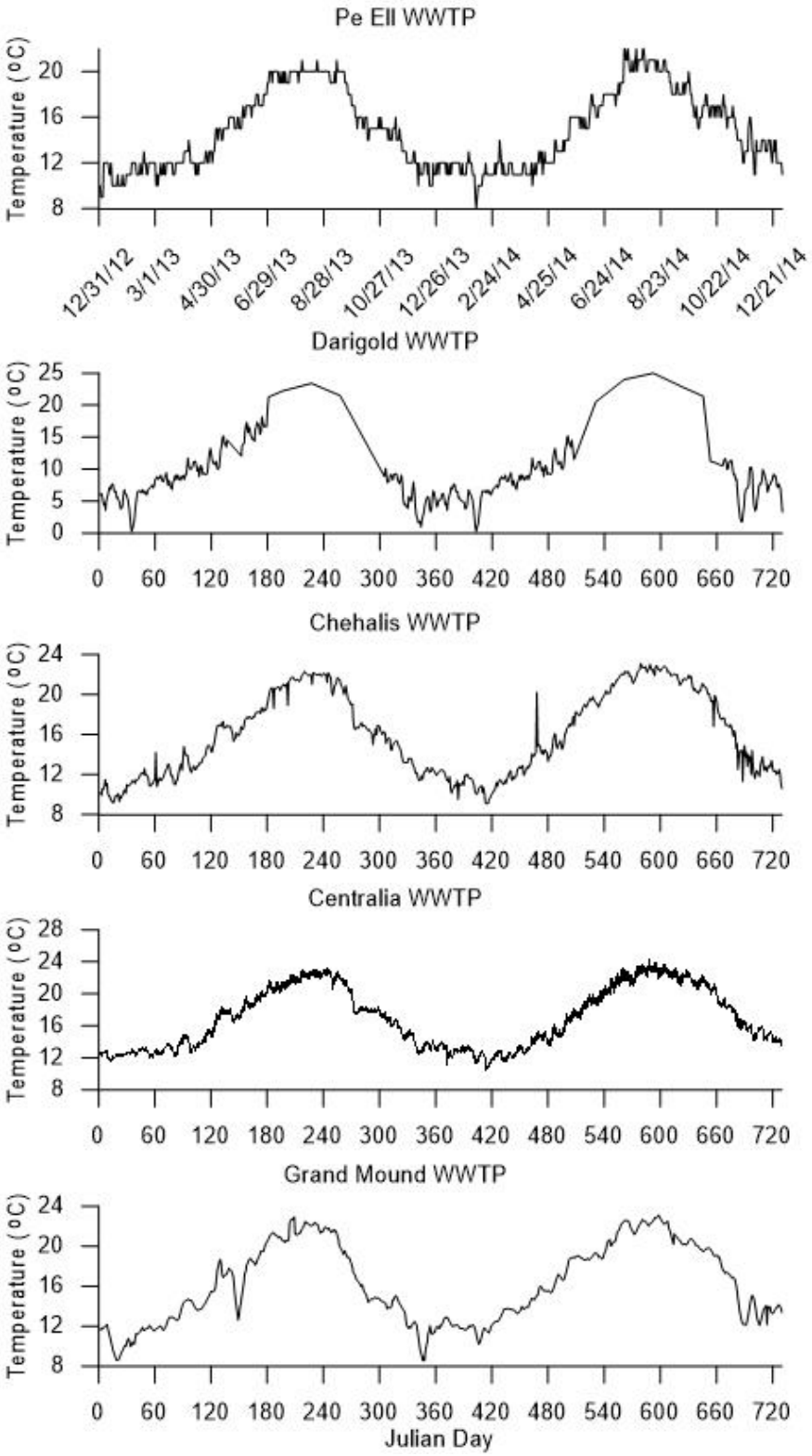

Figure 45. Input temperature for the Pe Ell, Darigold, Centralia, Chehalis, and Grand Mound wastewater treatment plants

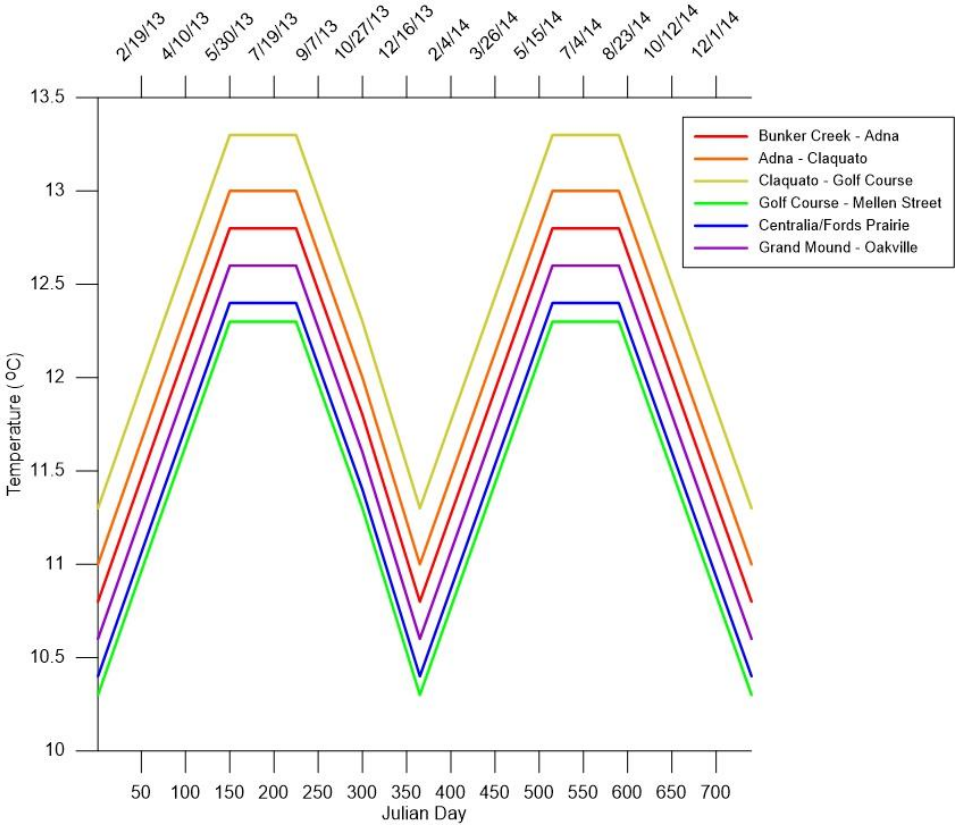

Figure 46. Input temperature for groundwater inflows

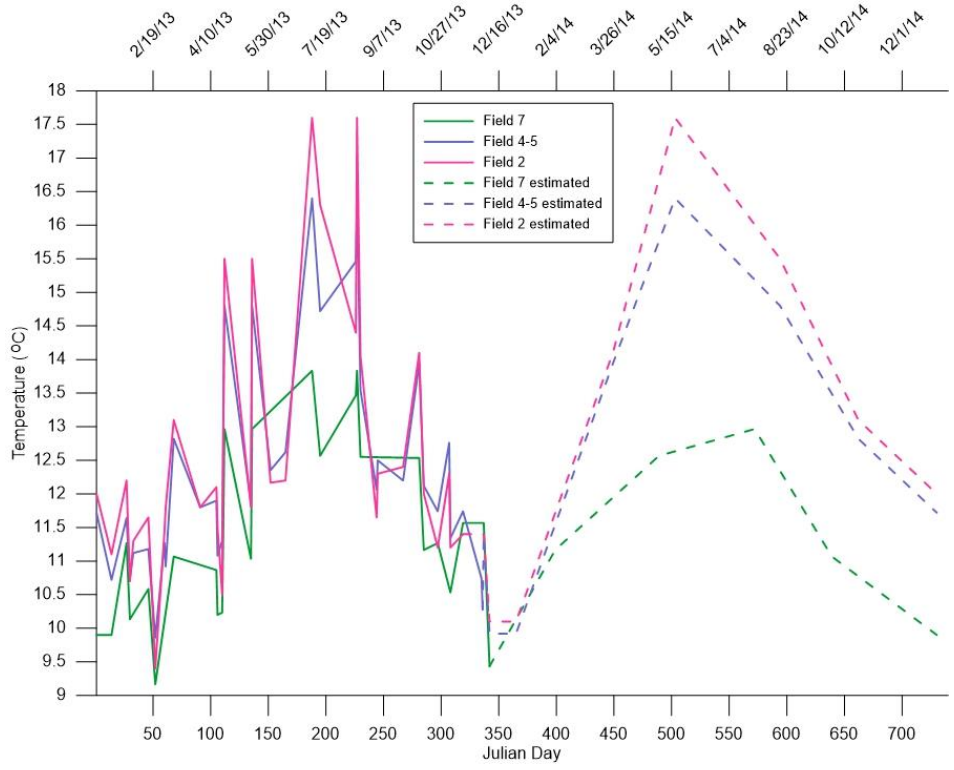

Figure 47. Input temperature for groundwater inflows in the Chehalis-Centralia reach using 2013 data from the Engineering Report prepared by Brown and Caldwell for National Frozen Foods (2016)

Constituent Inputs

The water quality state variables modeled included:

- Total dissolved solids (TDS)
- Fecal coliform (FC)
- Inorganic suspended solids (ISS)
- Phosphate (PO4)
- Ammonia (NH3)
- Nitrates (NOx)
- Labile dissolved organic matter (LDOM)
- Refractory dissolved organic matter (RDOM)
- Labile particulate organic matter (LPOM)
- Refractory particulate organic matter (RPOM)
- Biochemical oxygen demand (BOD)
- Biochemical oxygen demand as phosphorus (BOD-P)
- Biochemical oxygen demand as nitrogen (BOD-N)
- Algae
- Dissolved oxygen (DO)
- Alkalinity (alk)
- Zooplankton
- LDOM as phosphorus (LDOM-P)
- RDOM as phosphorus (RDOM-P)
- LPOM as phosphorus (LPOM-P)
- RPOM as phosphorus (RPOM-P)
- LDOM as nitrogen (LDOM-N)
- RDOM as nitrogen (RDOM-N)
- LPOM as nitrogen (LPOM-N)
- RPOM as nitrogen (RPOM-N).

Data were needed for the entire model time period for all flow inputs for all water quality state variables. Some water quality data for various locations along the Chehalis mainstem were available from WADOE (2014) and Anchor QEA (2014). Some of the tributaries had data available from Anchor QEA (2014), including the Newaukum River, Skookumchuck River, South Fork Chehalis River, Black River, Elk creek, and Lincoln Creek. Water quality data for the mainstem Chehalis River and the tributaries were generally point data collected during the summer months, often with only two or three samples collected for a given constituent over the course of the years 2013 and 2014. Some water quality data were available for the wastewater treatment plants and were made available by the WADOE NPDES permit database (2014) and directly from the wastewater treatment plant managers, as either daily point data or monthly averages (Phelps, 2016; Hillock, 2016; Bilhimer, 2016; Zentner, 2016; and Patching, 2016). Groundwater water quality data were provided from the Chehalis River TMDL (Erickson, 1993) and an Engineering Report conducted by Brown and Caldwell for National Frozen Foods. Table 10 lists the stations that provided water quality data.

Table 10. Monitoring stations that provided water quality data

Organization	Station ID	Description	Dates with data
Anchor QEA	CHL-PEL-US	Chehalis Upstream of Pe Ell	8/6/13, 9/17/13, 1/27/14, & 7/22/14
Anchor QEA	ELK-CRK	Elk Creek	8/6/13, 9/17/13, 7/22/14, & 7/30/14
Anchor QEA	SF-CHL-MOUTH	South Fork Mouth	8/6/13, 9/17/13, & 7/22/14
Anchor QEA	NWK-MOUTH	Newaukum Mouth	8/6/13, 9/17/13, & 7/22/14
Anchor QEA	SKM-MOUTH	Skookumchuck Mouth	8/6/13, 9/17/13, & 7/22/14
Anchor QEA	LNC-CRK	Lincoln Creek	8/6/13, 9/17/13, 7/22/14, & 7/30/14
Anchor QEA	BLK-RT12	Black River Mouth	8/6/13, 9/17/13, & 7/22/14
WADOE	WA0020192	Pe Ell WWTP	1/1/13 - 12/31/14
WADOE	WA0037478	Darigold WWTP	1/1/13 - 9/30/13, & 11/1/13 - 12/31/14
WADOE	WA0021105	Chehalis WWTP	1/1/13 - 12/31/14
WADOE	WA0020982	Centralia WWTP	1/1/13 - 12/31/14
WADOE	WA0042099	Grand Mound WWTP	1/1/13 - 12/31/14
WADOE	DW03	GW Bunker Creek to Adna reach	11/17/92, 11/18/92, 12/1/92, 12/2/92, & 12/8/92
WADOE	DW08	GW Adna to Claquato reach	11/17/92, 11/18/92, 12/1/92, 12/2/92, & 12/8/92
WADOE	DW07	GW Claquato to Golf Course reach	11/17/92, 11/18/92, 12/1/92, 12/2/92, & 12/8/92
WADOE	DW15	GW Golf Course to Mellen Street reach	11/17/92, 11/18/92, 12/1/92, 12/2/92, & 12/8/92
WADOE	DW18	GW Centralia/Fords Prairie reach	11/17/92, 11/18/92, 12/1/92, 12/2/92, & 12/8/92
WADOE	DW27	GW Grand Mound to Oakville	11/17/92, 11/18/92, 12/1/92, 12/2/92, & 12/8/92
WADOE	AHL145	GW Chehalis R. at Pranther Rd.	10/05, 5/10/04, 6/7/04, 7/6/04, 8/4/04, 8/31/04, & 10/4/04
WADOE	AHL144	GW Chehalis R. above WWTP outfall	5/10/04, 6/7/04, 7/6/04, 8/4/04, 8/31/04, & 10/4/04
WADOE	AHL143	GW Chehalis R.	5/10/04, 6/7/04, 7/6/04, & 10/4/04
WADOE	AHL142	GW Chehalis R. at Galvin Rd.	5/11/04
WADOE	ABK199	GW Chehalis R. at Mellen St.	5/11/04, 6/15/04, 7/8/04, 8/3/04, 9/2/04, & 10/6/04
WADOE	ABK198	GW Chehalis R. nr. Airport Rd.	5/12/04 & 6/9/04
WADOE	AHL146	GW Chehalis R. nr. Airport Rd.	6/9/04, 7/8/04, 8/3/04, 9/2/04, 10/6/04, & 10/6/04
WADOE	ABK197	GW Chehalis R. at State Rte. 6	5/12/04, 6/9/04, 7/7/04, 8/3/04, 9/1/04, & 10/5/04
NFF	Fields 7, 4-5, and 2	GW Chehalis-Centralia Reach	1/1/13 – 12/8/13

In order to estimate the state variables of the CE-QUAL-W2 model, many conversions were made from measured to field data. When field data were not available, reasonable estimates were made for a given constituent. The assumptions and estimations employed for the input model constituents are outlined below, including the equations used for making calculations.

- TDS, FC, and BOD were assumed zero for tributaries with no data available.

- To convert 5-day BOD (BOD_5) field data to ultimate BOD (BOD_U), the following typical relationship was used (Cole and Wells, 2016) assuming a BOD dcay rate of 0.1 day^{-1}:

$$BOD_u = 2.54 * BOD_5$$

BOD_U was assumed to be 50% dissolved ($BOD_{U\ dissolved}$) and 50% particulate ($BOD_{U\ particulate}$).

- Organic matter (OM) was calculated by (Cole and Wells, 2016):

$$OM = \frac{BOD_u}{1.4}$$

- PO4 was assumed to equal 1% of the OM concentration when no data were available.

- When NO3 data were not available for the wastewater treatment plants, values between 0.5 and 1 mg/L were used.

- Algae concentrations (dry weight biomass concentration) were calculated by:

$$Algae = 0.1 * Chlorophyll\ a$$

- Algae concentrations were assumed to be 1% phosphorus (AlgaeP) and 8% nitrogen (AlgaeN).

- Chlorophyll a concentrations for groundwater were assumed to be zero, and so algae, algaeP, and algaeN concentrations were also assumed to be zero.

- ISS were calculated by (Cole and Wells, 2016):

$$ISS = TSS - \frac{BOD_{U\ particulate}}{1.4} - algae$$

- TSS was assumed zero for groundwater flows, and hence ISS was also assumed zero.

- Dissolved organic matter (DOM) was calculated by (Cole and Wells, 2016):

$$DOM = \frac{BOD_{U\ dissolved}}{1.4}$$

- Particulate organic matter (POM) was calculated by (Cole and Wells, 2016):

$$POM = \frac{BOD_{U\ particulate}}{1.4}$$

- DOM was assumed to be 50% labile (LDOM) and 50% refractory (RDOM), and POM was also assumed to be 50% labile (LPOM) and refractory (RPOM). However, for groundwater inflows, POM was zero, implying all OM was dissolved.

- Organic matter as phosphorus (OMP) was calculated by:

$$OMP = TP - PO4 - AlgaeP$$

Where TP is total phosphorus.

- OMP was assumed to be equally portioned as labile dissolved LDOM-P, RDOM-P, LPOM-P, RPOM-P. LDOM, RDOM, LPOM, and RPOM concentrations were assumed to be 8% nitrogen.

- Total nitrogen (TN) was calculated by:

$$TN = TKN + NO3$$

Where TKN is total Kjeldahl nitrogen, and equals the sum of ammonia and organic matter as nitrogen.

- Organic matter as nitrogen (OMN) was calculated by:

$$OMN = TN - NH3 - NO3 - AlgaeN$$

- OMN was assumed to be equally portioned as labile dissolved LDOM-N, RDOM-N, LPOM-N, RPOM-N. LDOM, RDOM, LPOM, and RPOM concentrations were assumed to be 1% phosphorus.

- Some of the fact sheets for the wastewater treatment plants included alkalinity for the Chehalis River near to the plats. Alkalinity for tributaries were assumed to be an average of these values when no data were available.

- No zooplankton data were available. Zooplankton concentrations were estimated as 0.01 mg/L for tributaries. Zooplankton was assumed to have zero concentration for groundwater inflows.

- Techniques for computing pH, alkalinity, or total inorganic carbon are outlined below (Wells, 2016):

Alkalinity [ALK] is usually given in units of mg/L as $CaCO_3$. By dividing by 50,000 the units are converted to moles/L. The model uses units of mg/L as C for total inorganic C [C_T] and can be converted to moles/L by dividing by 12,000. C_T (in moles/L) is defined as:

$$C_T = [H_2CO_3] + [HCO_3^-] + [CO_3^{-2}]$$

Following equilibrium chemistry (see Stumm and Morgan, 1986), the alkalinity is then defined as:

$$[ALK] = C_T(\alpha_1 + 2\alpha_2) + \frac{K_w}{[H^+]} - [H^+]$$

Where

$$\alpha_1 = \left(\frac{[H^+]}{K_1} + 1 + \frac{K_2}{[H^+]} \right)^{-1}$$

$$\alpha_2 = \left(\frac{[H^+]^2}{K_1 K_2} + 1 + \frac{[H^+]}{K_2} \right)^{-1}$$

$K_w = 10^{-14}$ mol^2/L^2 at 25 °C

$$K_w = 10^{\left[\frac{-5242.39}{T} + 35.3944 - 0.00835T + 11.8261 \log_{10}(T)\right]}$$

$K_1 = 10^{-6.419}$ mol/L at 15°C

$$K_1 = 10^{(-3404.71/T + 14.8435 - 0.032786*T)}$$

$K_2 = 10^{-10.430}$ mol/L at 15 °C

$$K_2 = 10^{(-2902.39/T + 6.498 - 0.02379*T)}$$

T = temperature (°C)
$[H^+]$ = hydrogen ion concentration
pH = -log$[H^+]$

These equations assume the activity corrections for the species concentrations are unity, implying that the inflowing water has a low TDS. By knowing any 2 of the 3 components – pH, alkalinity, or total inorganic carbon – the above equations allow for the computation of the other.

For times when data for a constituent were not available for a tributary or groundwater inflow, averages or medians of the other values were used as an estimate. Tributaries that did not have any water quality data available used an input water quality constituent file from the nearest tributary with data available. For wastewater treatment plants with no data for a constituent, reasonable or typical values were used as an estimate. For reaches of the river with no groundwater data available, data from the closest reach were used.

Input constituent data for ISS, PO4, NH3, and NO3 are shown in Figure 48. Input constituent data for TIC, alkalinity, algae, and DO are shown in Figure 49. Input constituent data for LDOM, RDOM, LPOM, and RPOM are shown in Figure 50. Input constituent data for LDOM-P, RDOM-P, LPOM-P, and RPOM-P are shown in Figure 51. Input constituent data for LDOM-N, RDOM-N, LPOM-N, and RPOM-N are shown in Figure 52. Figure 53 shows tributary field data for pH, BOD5, and TSS while Figure 54 shows tributary field data for chlorophyll a, TKN, and TP that were used to calculate constituents with the equations outlined above.

Figure 55 shows model input data for the wastewater treatment plants for FC, ISS, PO4, and NH3, while Figure 56 shows NO3, DO, TIC, and alkalinity. Figure 57 shows the wastewater treatment plant BOD species, including dissolved, particulate, phosphorus, and nitrogen.

Figure 58 shows input constituent data for TDS, PO4, NH3, NO3, BOD and DO for the groundwater inflows. Figure 59 shows data for TIC, alkalinity, and the DOM and POM species (labile, refractory, phosphorus, and nitrogen) for the groundwater inflows. Figure 60 shows field data for pH, BOD5, and TP used to calculate groundwater constituent concentrations with the equations described above.

Figure 61 shows concentrations for phosphate, ammonia, nitrates, alkalinity, and DO for groundwater in the Chehalis-Centralia reach. Figure 62 shows concentrations for the DOM and POM species (labile, refractory, phosphorus, and nitrogen) for groundwater in the Chehalis-Centralia reach. Figure 63 shows concentrations for pH, BOD, and TKN for groundwater in the Chehalis-Centralia reach used to calculate input constituent concentrations.

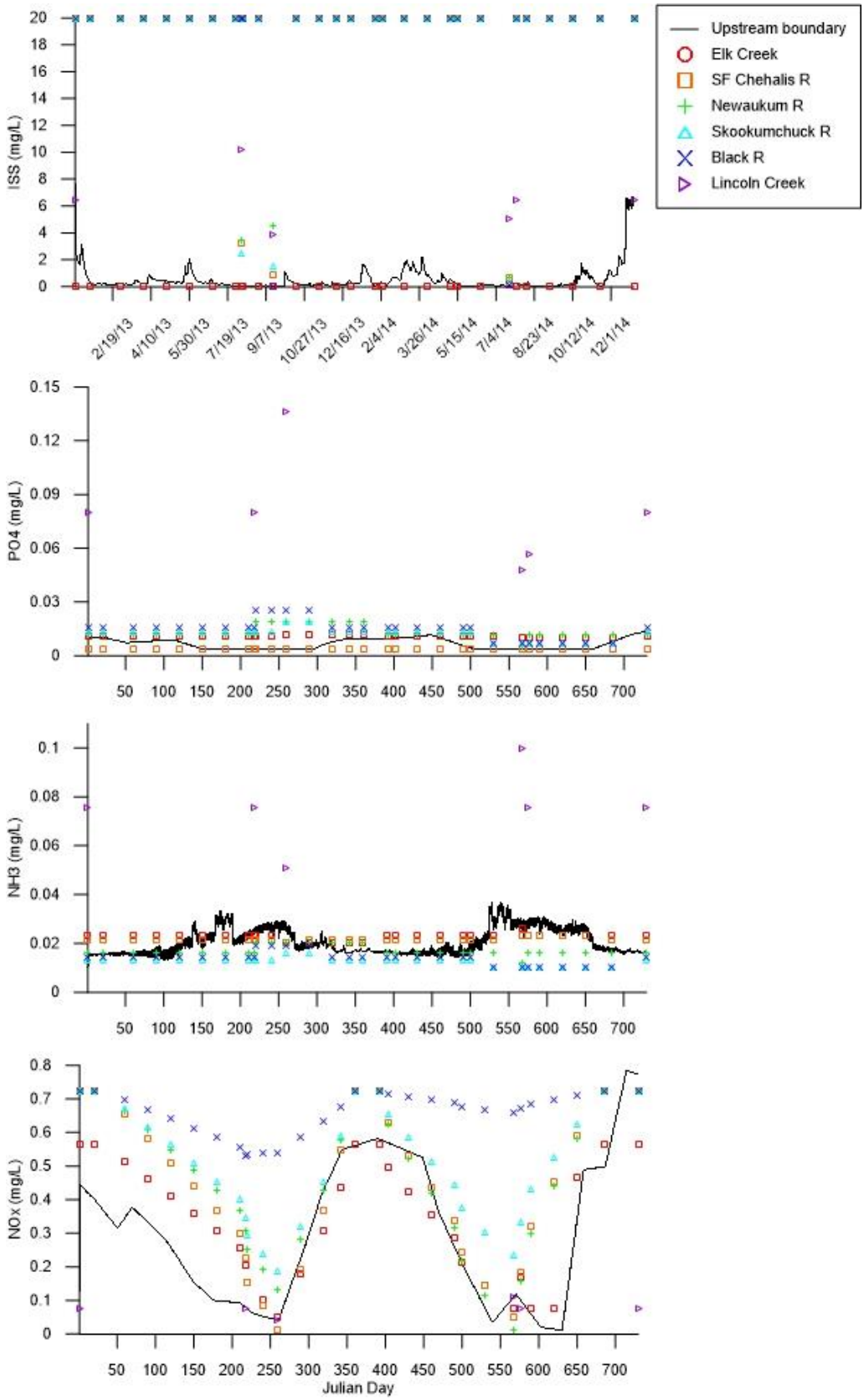

Figure 48. Input concentrations for ISS, PO4, NH3, and NO3 for tributaries with data available, including the upstream boundary, Elk Creek, South Fork Chehalis River, Newaukum River, Skookumchuck River, Black River, and Lincoln Creek.

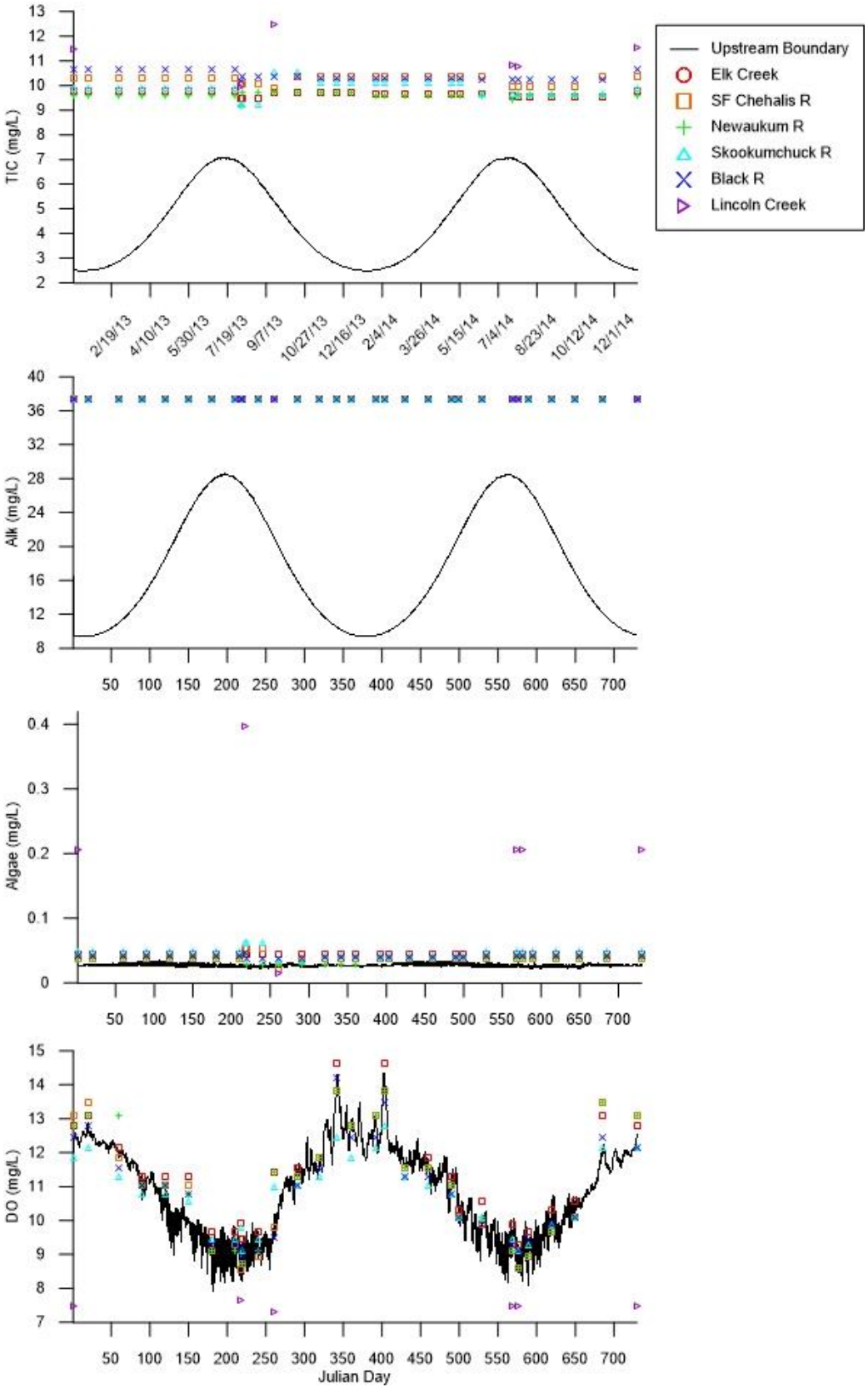

Figure 49. Input concentrations for TIC, alkalinity, algae, and DO for tributaries with data available, including the upstream boundary, Elk Creek, South Fork Chehalis River, Newaukum River, Skookumchuck River, Black River, and Lincoln Creek

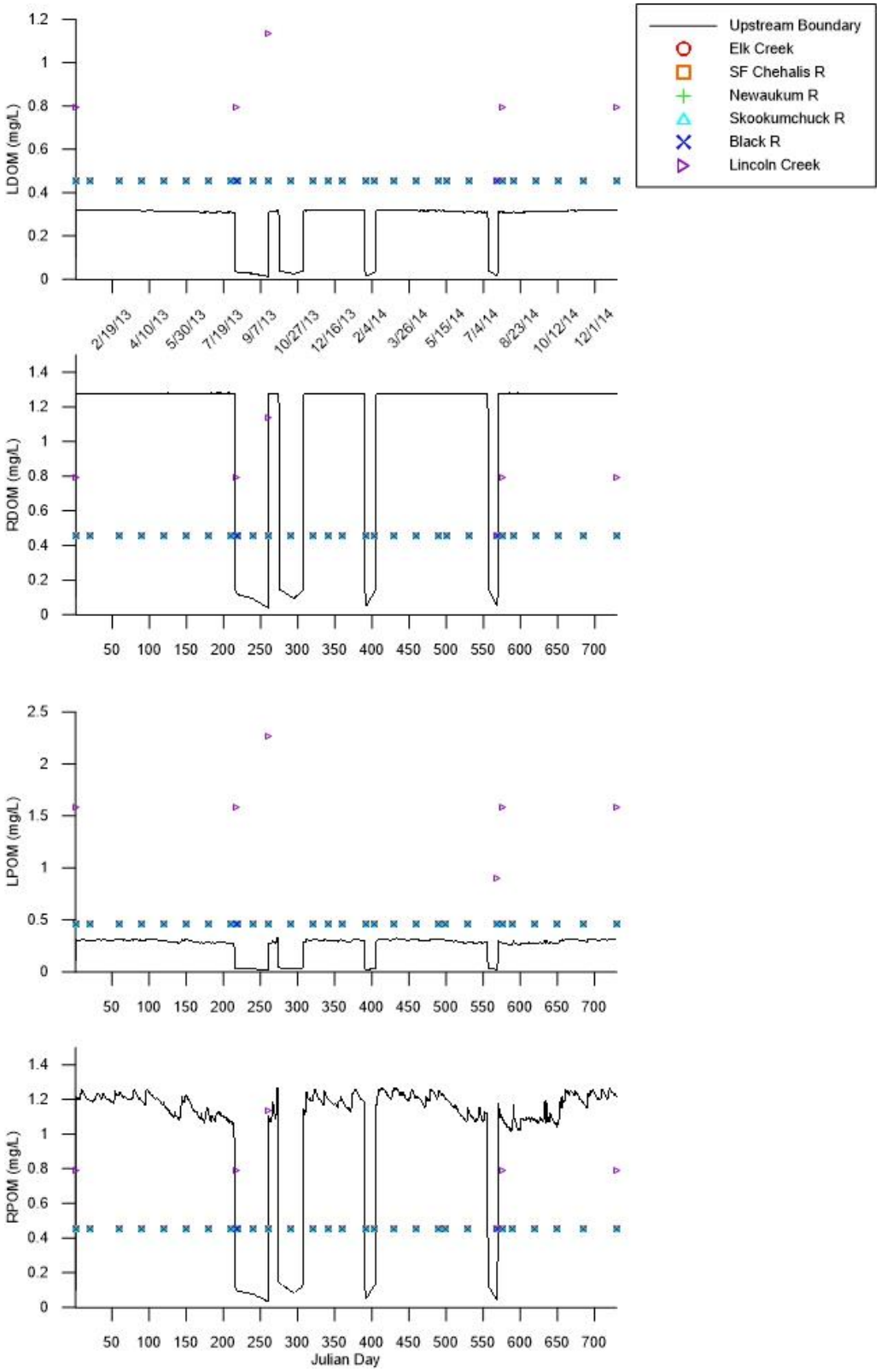

Figure 50. Input concentrations for LDOM, RDOM, LPOM, and RPOM for tributaries with data available, including the upstream boundary, Elk Creek, South Fork Chehalis River, Newaukum River, Skookumchuck River, Black River, and Lincoln Creek

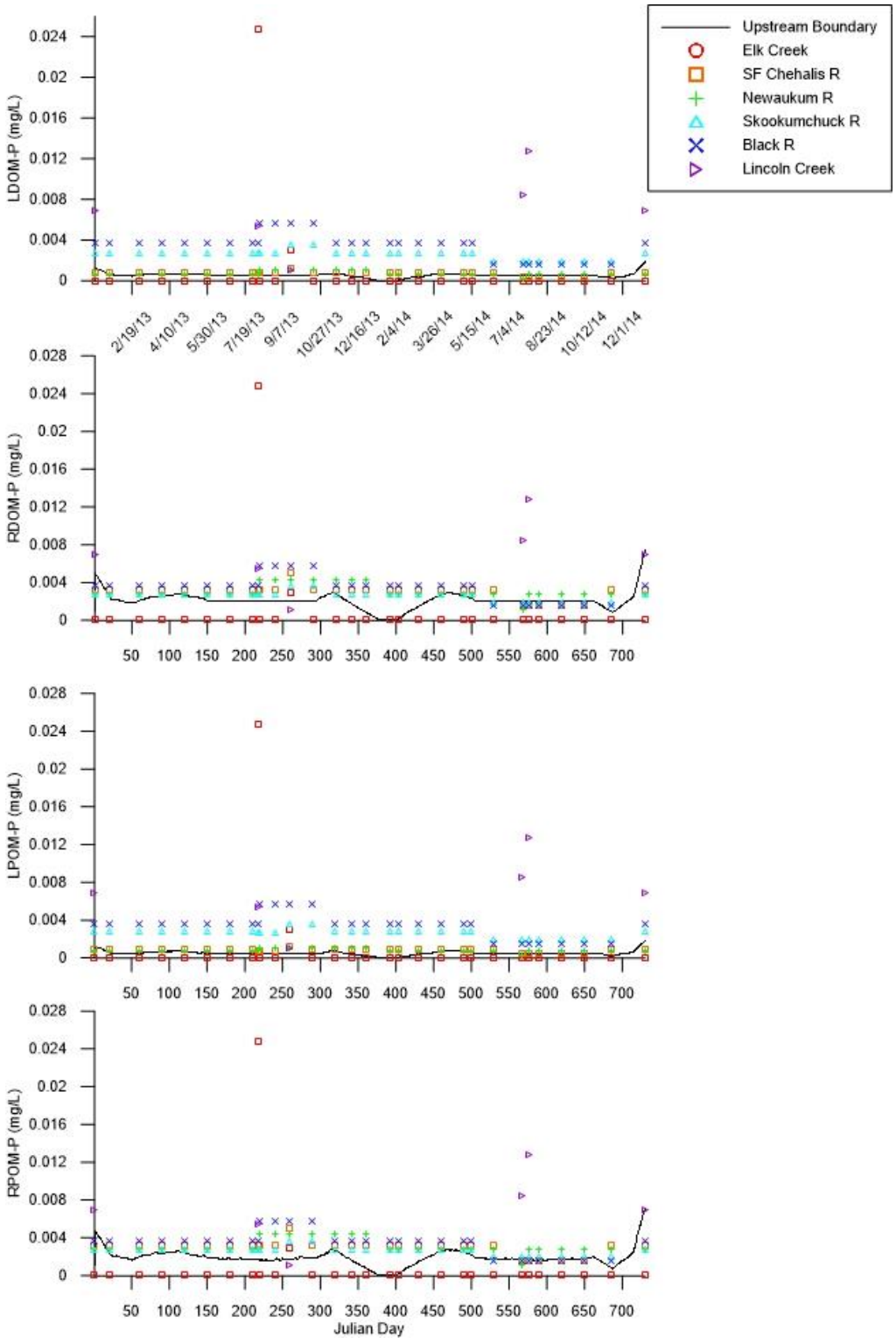

Figure 51. Input concentrations for LDOM-P, RDOM-P. LPOM-P, and RPOM-P for tributaries with data available, including the upstream boundary, Elk Creek, South Fork Chehalis River, Newaukum River, Skookumchuck River, Black River, and Lincoln Creek

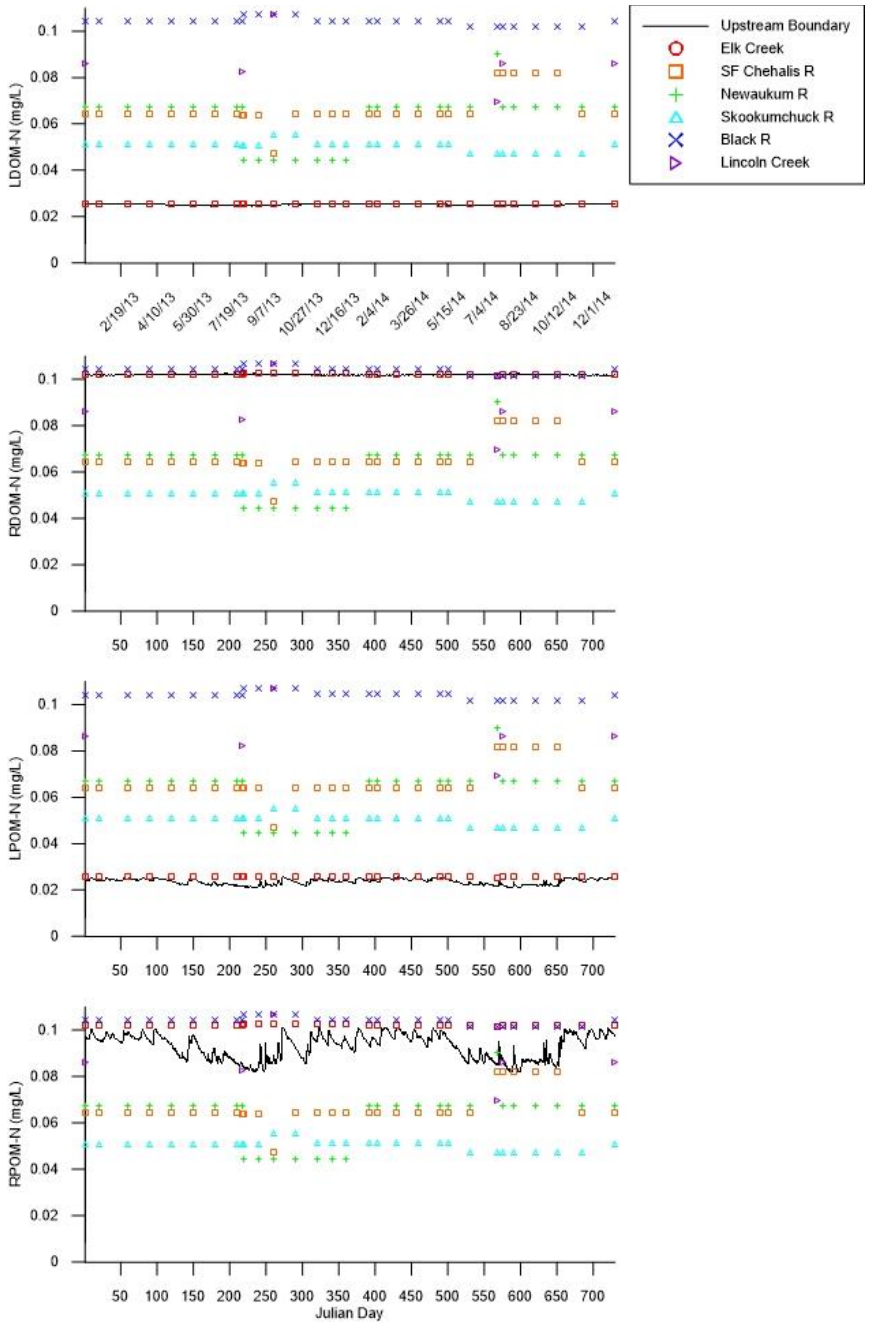

Figure 52. Input concentrations for LDOM-N, RDOM-N. LPOM-N, and RPOM-N for tributaries with data available, including the upstream boundary, Elk Creek, South Fork Chehalis River, Newaukum River, Skookumchuck River, Black River, and Lincoln Creek

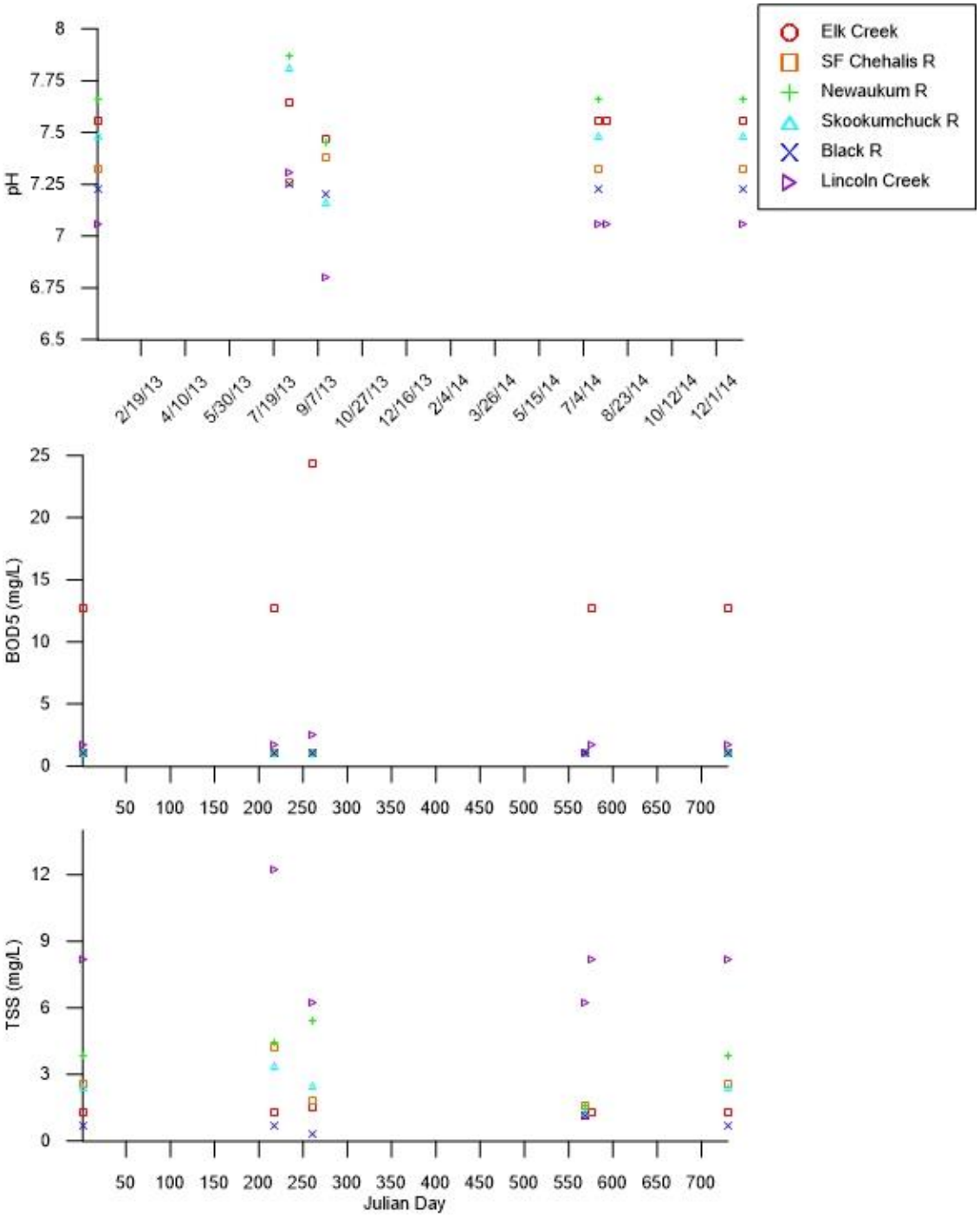

Figure 53. Field data concentrations for pH, BOD5, and TSS used to calculate input water quality concentrations for Elk Creek, South Fork Chehalis River, Newaukum River, Skookumchuck River, Black River, and Lincoln Creek

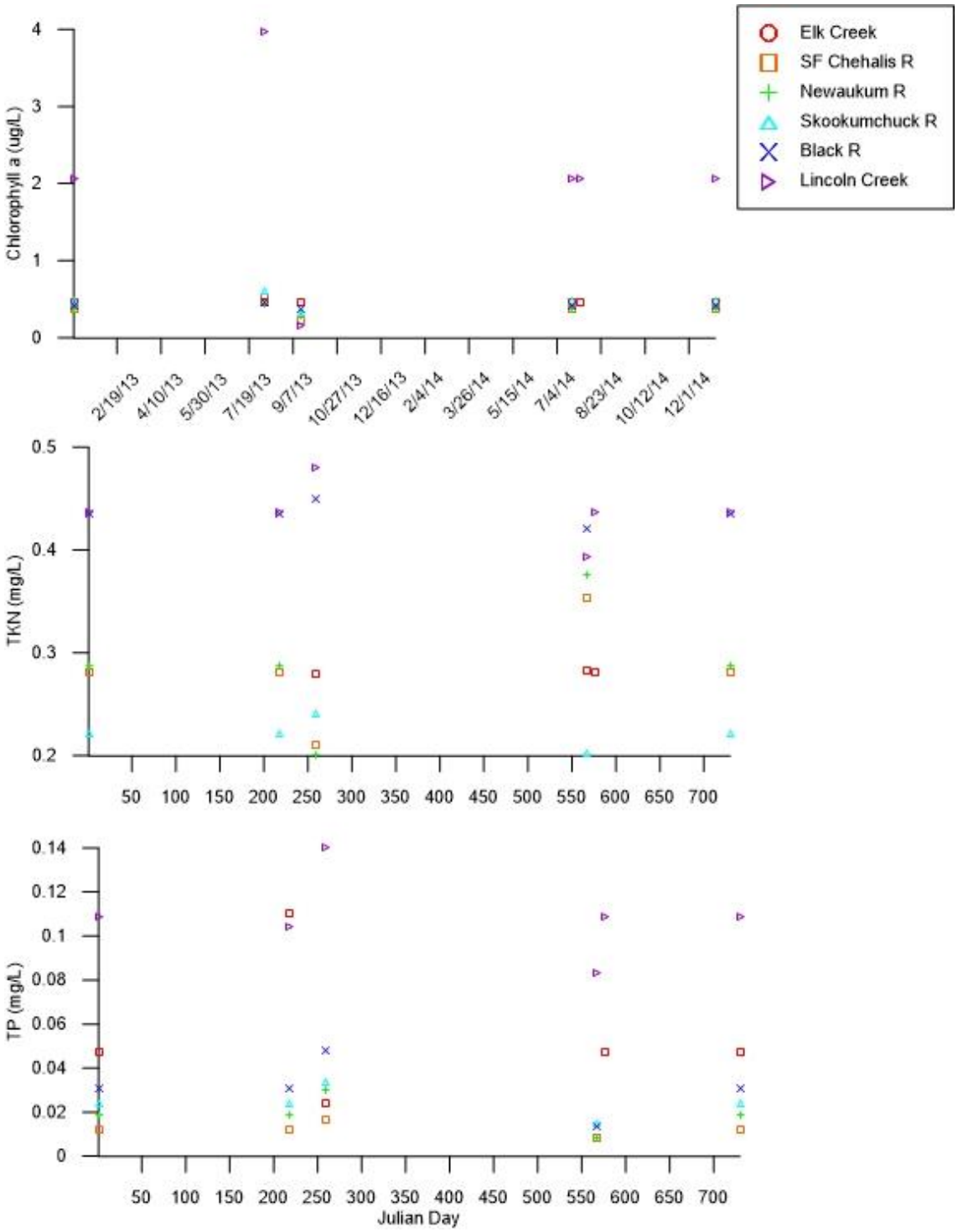

Figure 54. Field data concentrations for chlorophyll a, TKN, and TP used to calculate input water quality concentrations for Elk Creek, South Fork Chehalis River, Newaukum River, Skookumchuck River, Black River, and Lincoln Creek

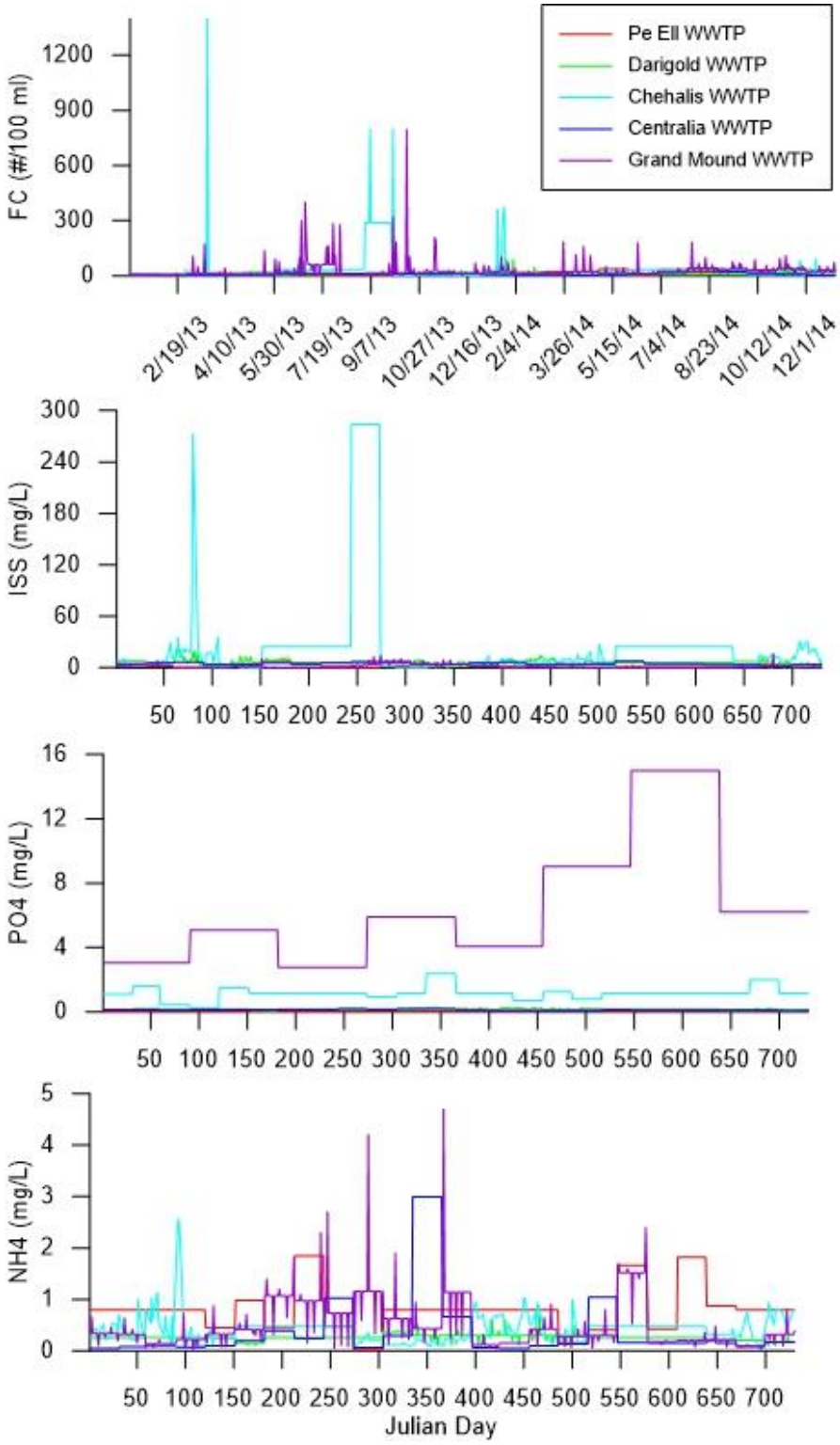

Figure 55. Model input concentrations for FC, ISS, PO4, and NH3 for the Pe Ell, Darigold, Centralia, Chehalis, and Grand Mound wastewater treatment plants

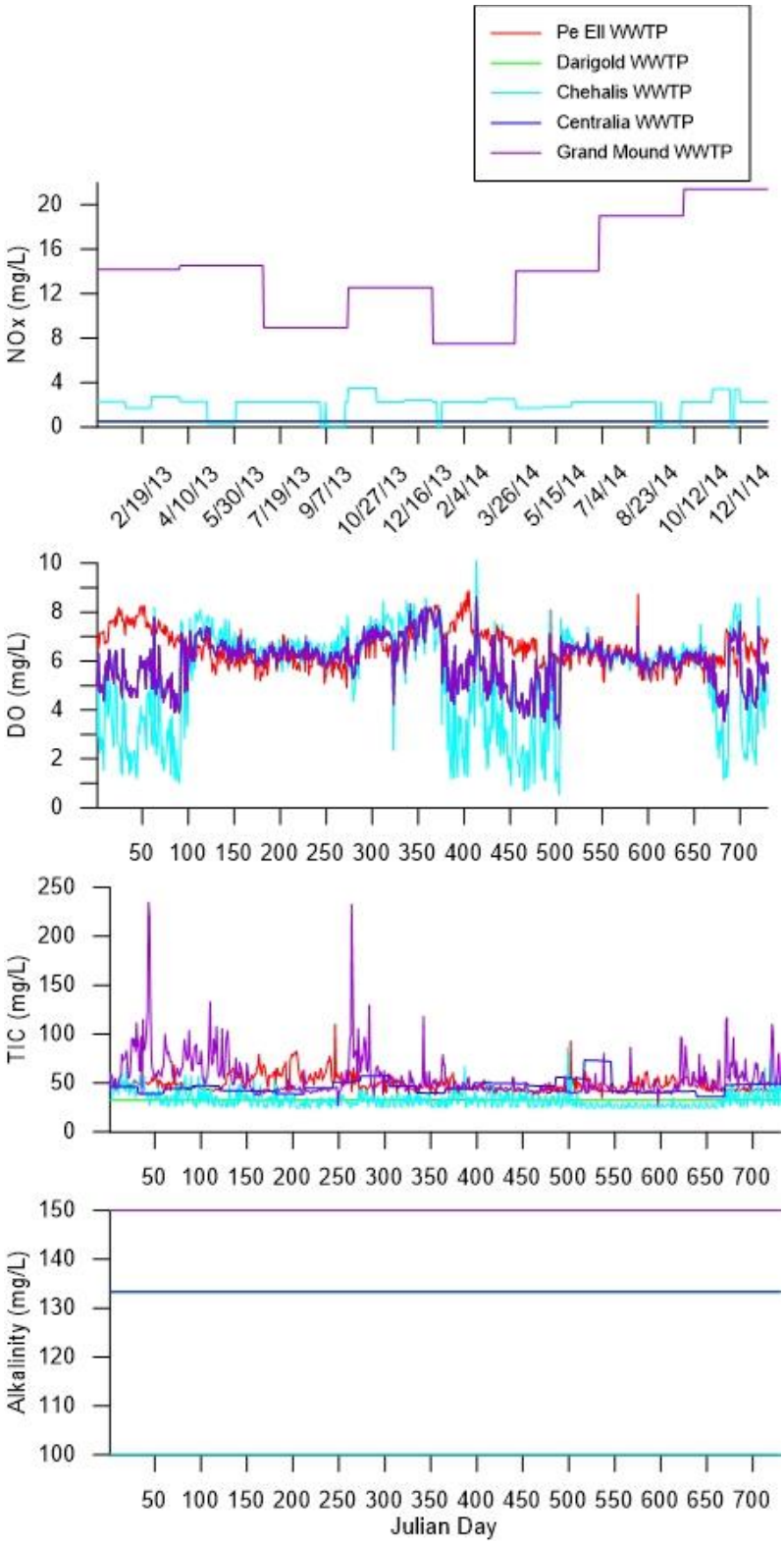

Figure 56. Model input concentrations for NO3, DO, TIC, and alkalinity for the Pe Ell, Darigold, Centralia, Chehalis, and Grand Mound wastewater treatment plants

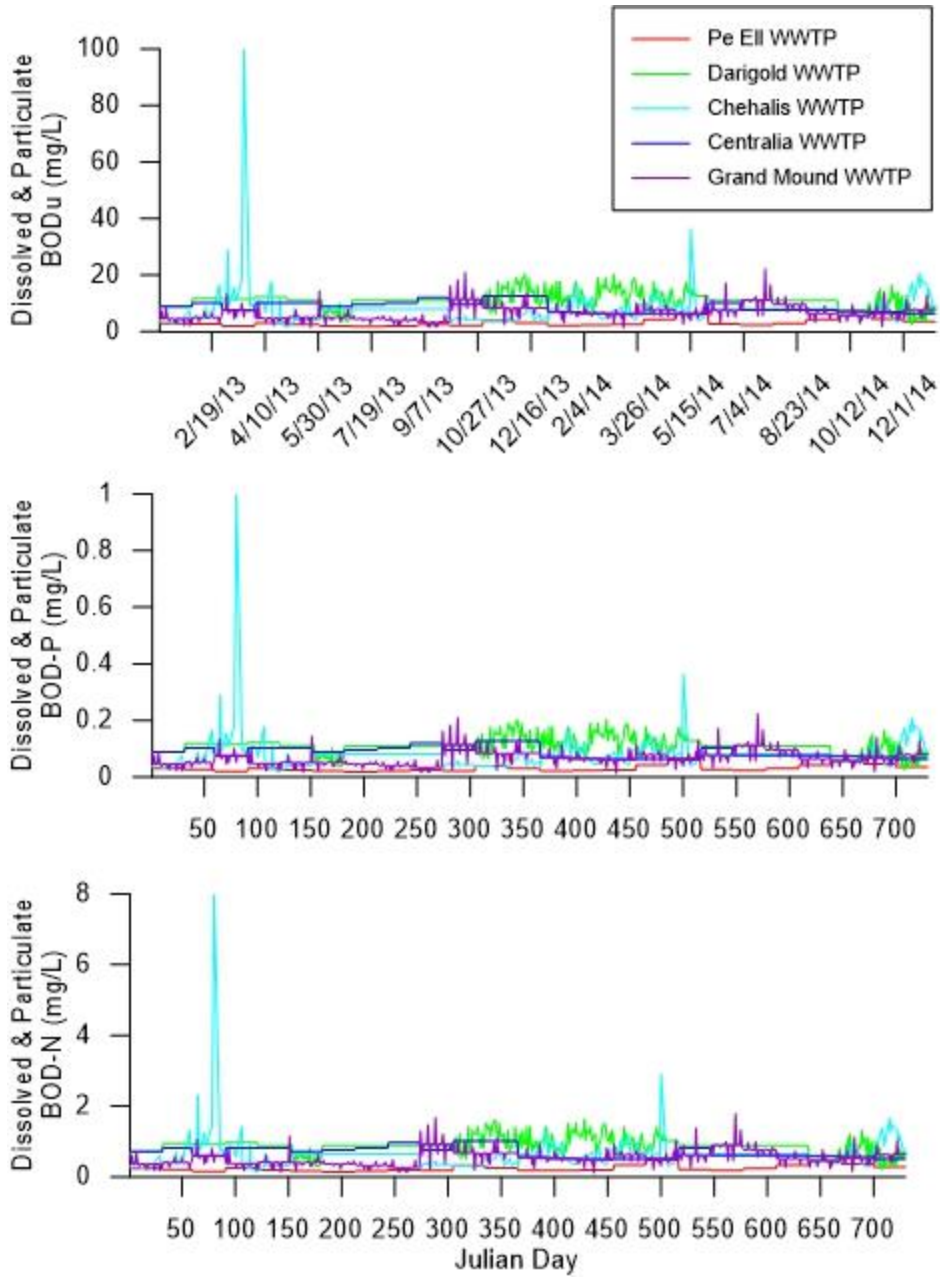

Figure 57. Model input concentrations for dissolved, particulate, phosphorus, and nitrogen BOD for the Pe Ell, Darigold, Centralia, Chehalis, and Grand Mound wastewater treatment plants

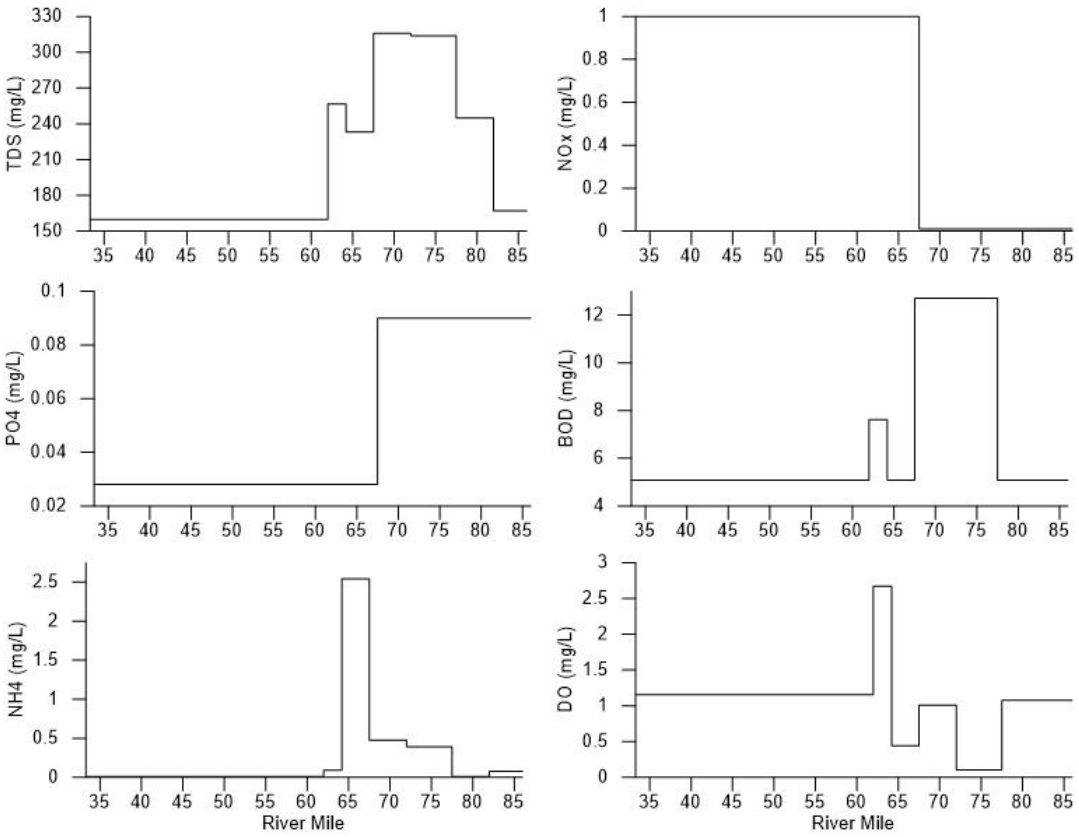

Figure 58. Model input concentrations for groundwater reaches with data for TDS, PO4, NH3, NO3, BOD, and DO

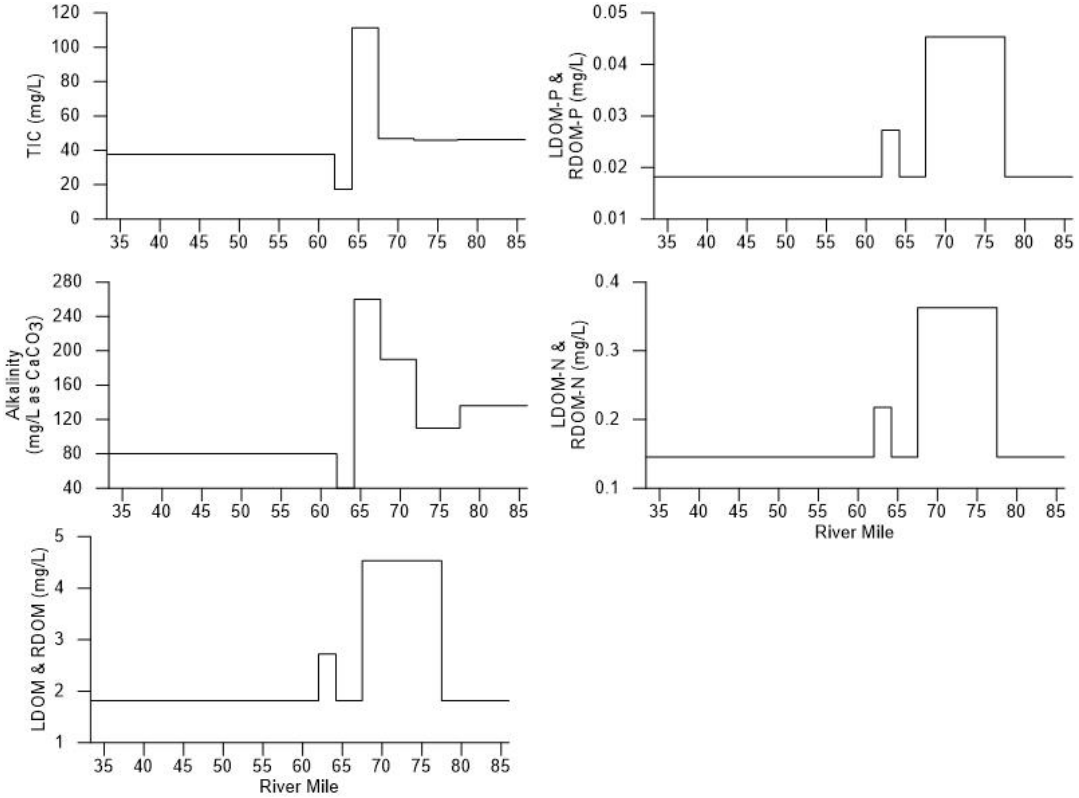

Figure 59. Model input concentrations for groundwater reaches with data for TIC, alkalinity, and the DOM and POM species (labile, refractory, phosphorus, and nitrogen)

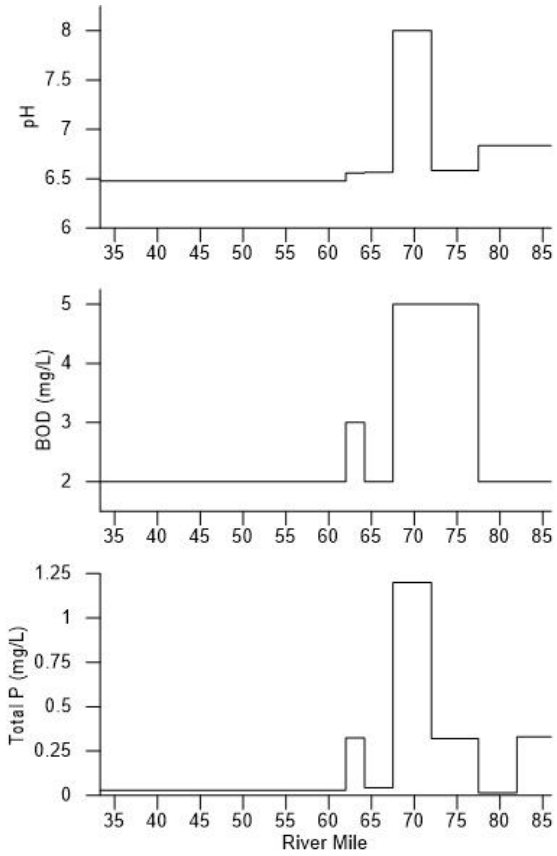

Figure 60. Field groundwater data for pH, BOD5, and TP used to calculate input water quality concentrations

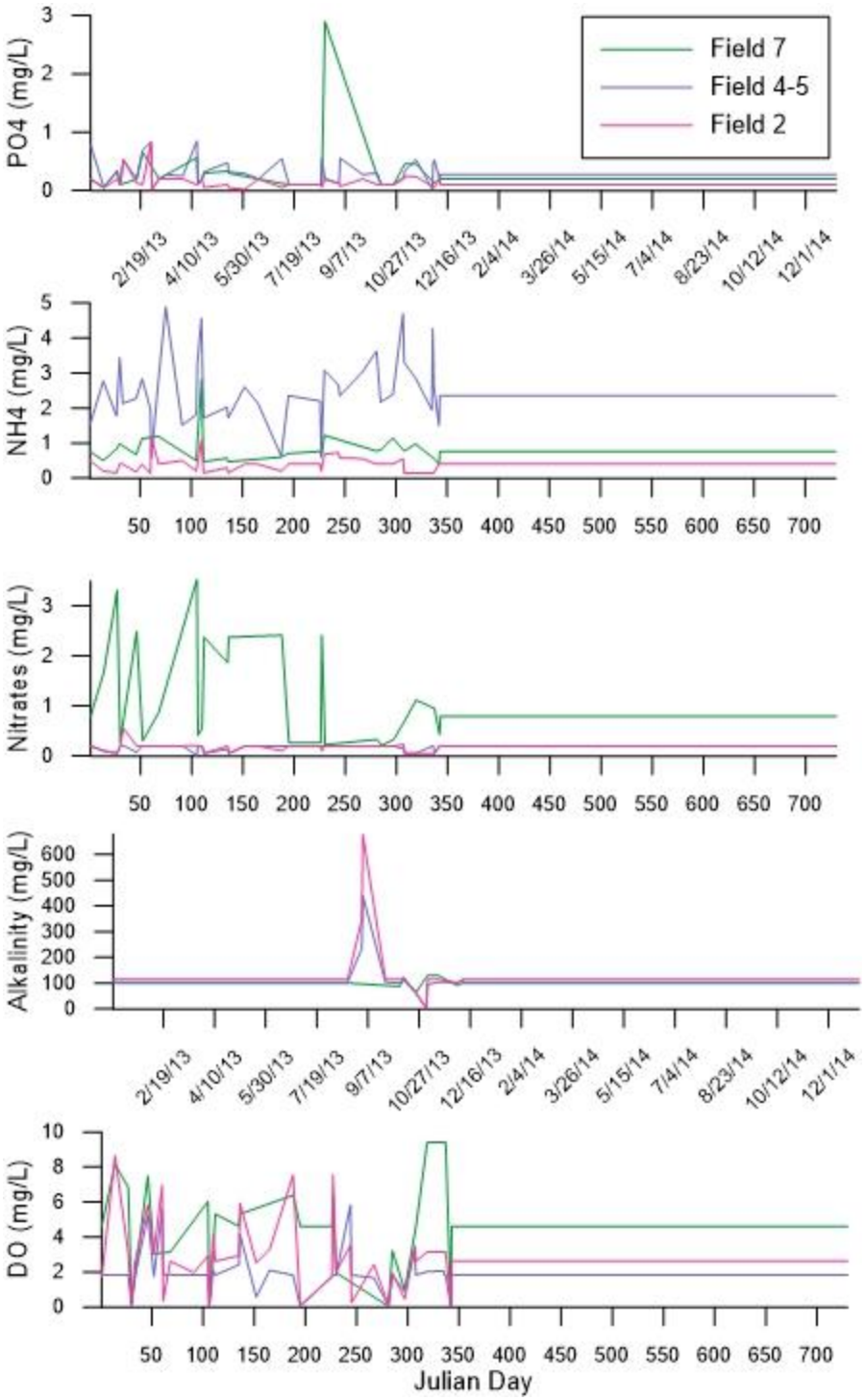

Figure 61. Model input concentrations for phosphate, ammonia, nitrates, alkalinity, and DO for groundwater in the Chehalis-Centralia reach

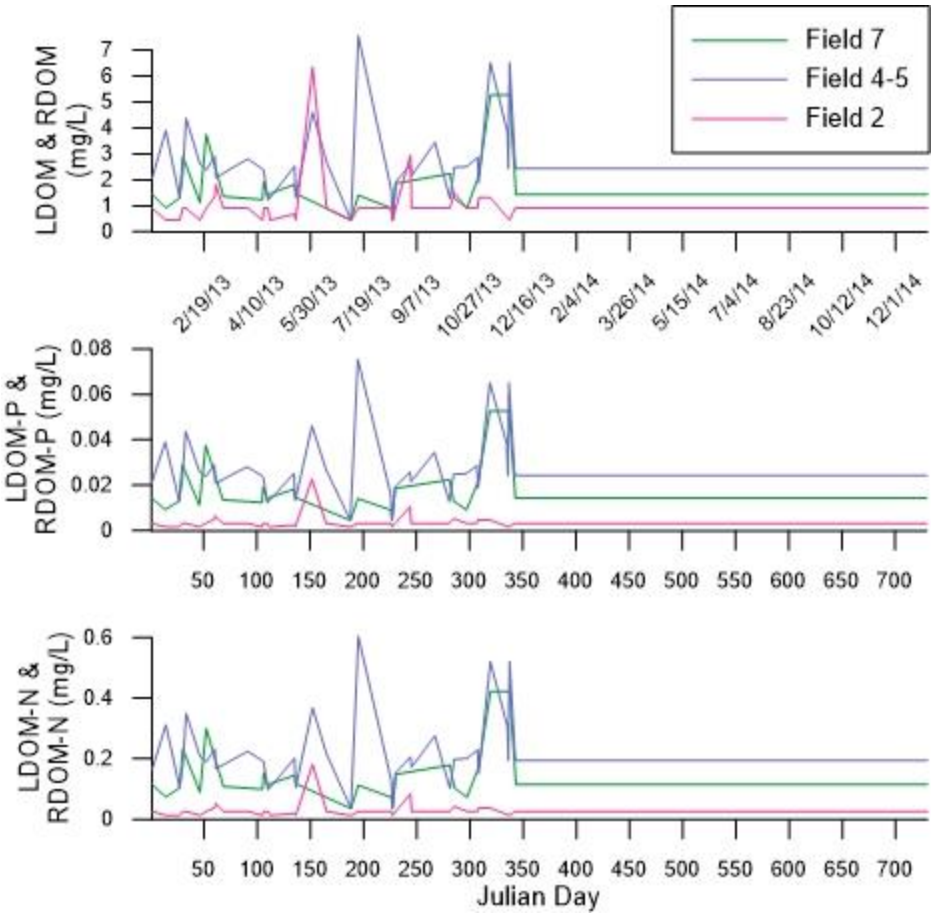

Figure 62. Model input concentrations for the DOM and POM species (labile, refractory, phosphorus, and nitrogen) for groundwater in the Chehalis-Centralia reach

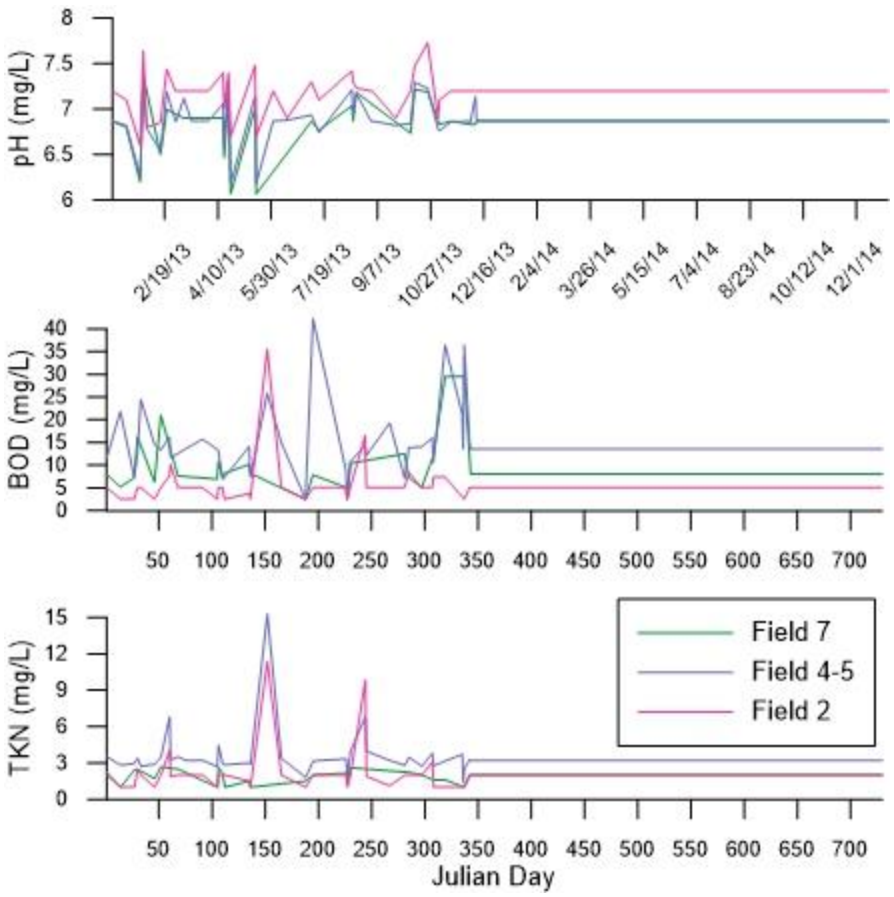

Figure 63. Concentrations for pH, BOD, and TKN for groundwater in the Chehalis-Centralia reach used to calculated input constituent concentrations

Shading

CE-QUAL-W2 requires shading information for each model segment, including left and right bank vegetation elevation, distance to left and right bank vegetation, left and right bank shade reduction factors for leaf on and leaf off conditions, and Julian days when the shade reduction factors apply. The shade reduction factors specified the opacity of the vegetation.

A shading study conducted by Stillwater Sciences for Anchor QEA provided all shading data along the Chehalis River (Merrill, 2014). The data collected in this study were interpolated to the locations of the model segments. Increased shading had a cooling effect on river temperature, while the opposite was true for decreased shading. The upstream, steep gradient portion was especially shaded. Figure 64 and Figure 65 show the elevations of vegetation on the left and right banks of the channel along the thalweg of the Chehalis River, respectively.

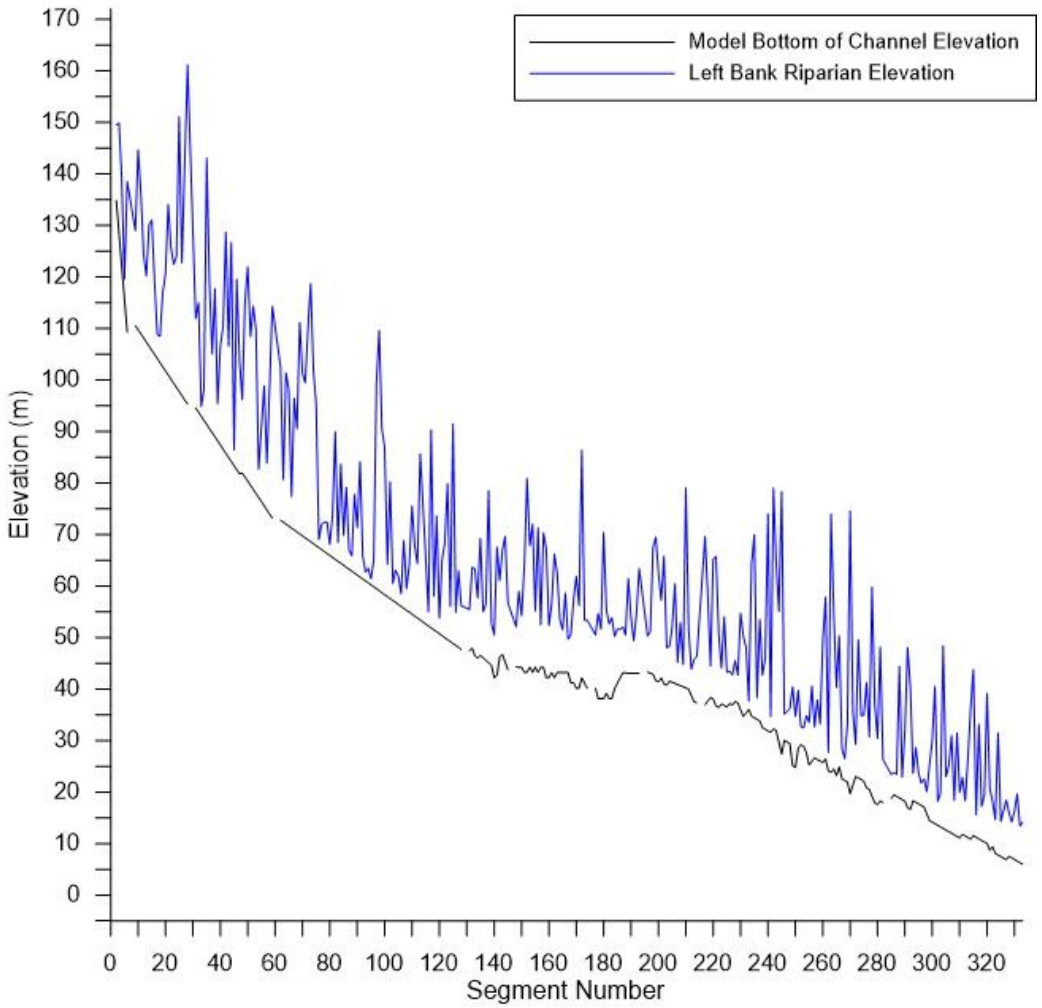

Figure 64. Left bank vegetation elevation for each segment input to the model in the shade file

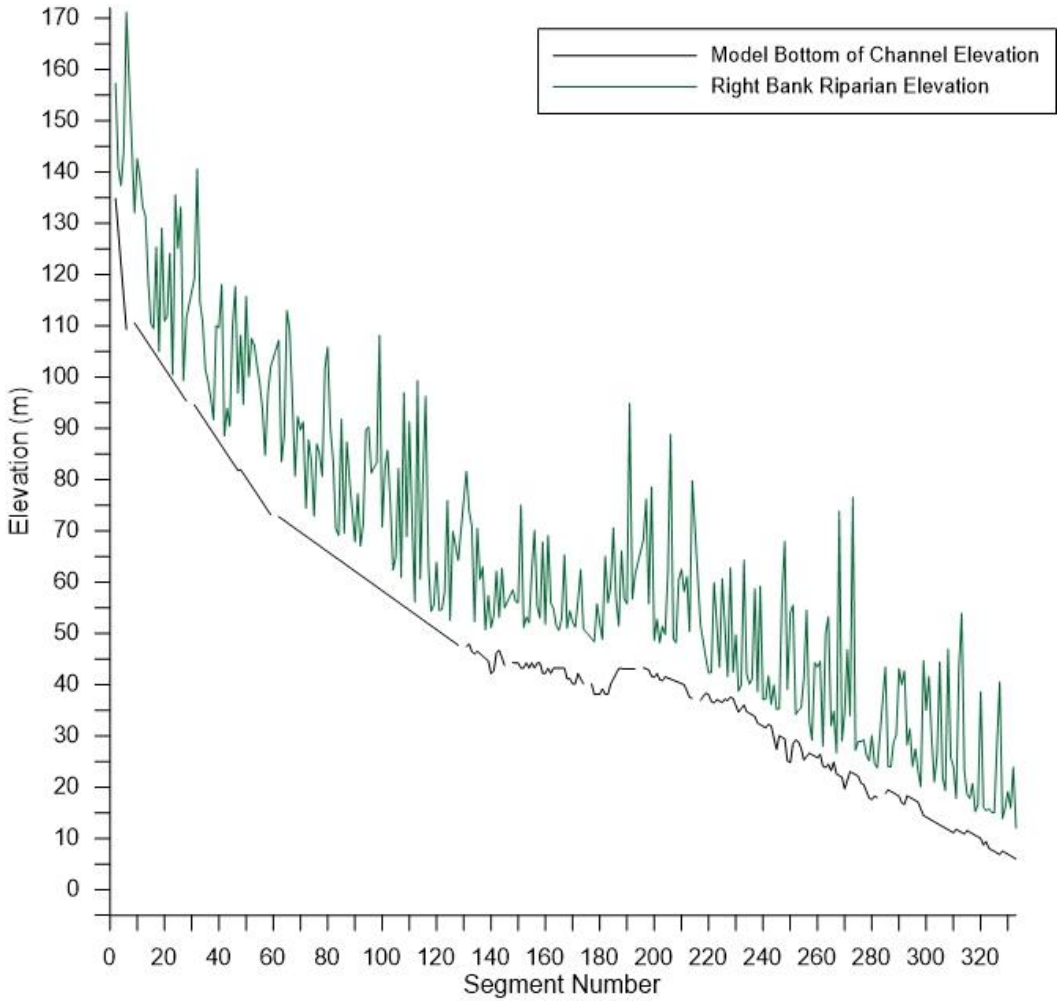

Figure 65. Right bank vegetation elevation for each segment input to the model in the shade file

Chehalis Reservoir Footprint Model

Bathymetry

The footprint model grid included the mainstem Chehalis River, Crim Creek, Lester Creek, Big Creek, and Roger Creek. Bathymetry inputs were developed using HECRAS cross-sectional data provided by Anchor QEA.

Segment locations of the footprint model are shown in Figure 66. The model grid included 185 active segments, each 150 m or 152.4 m long. Layer thickness is 0.5 m. Model grid details are summarized in Table 11. The footprint model actually extends below the dam site, which is near model segment 111 at the end of branch 5. For the scenarios output from model segment 111 were used as inputs to the downstream model

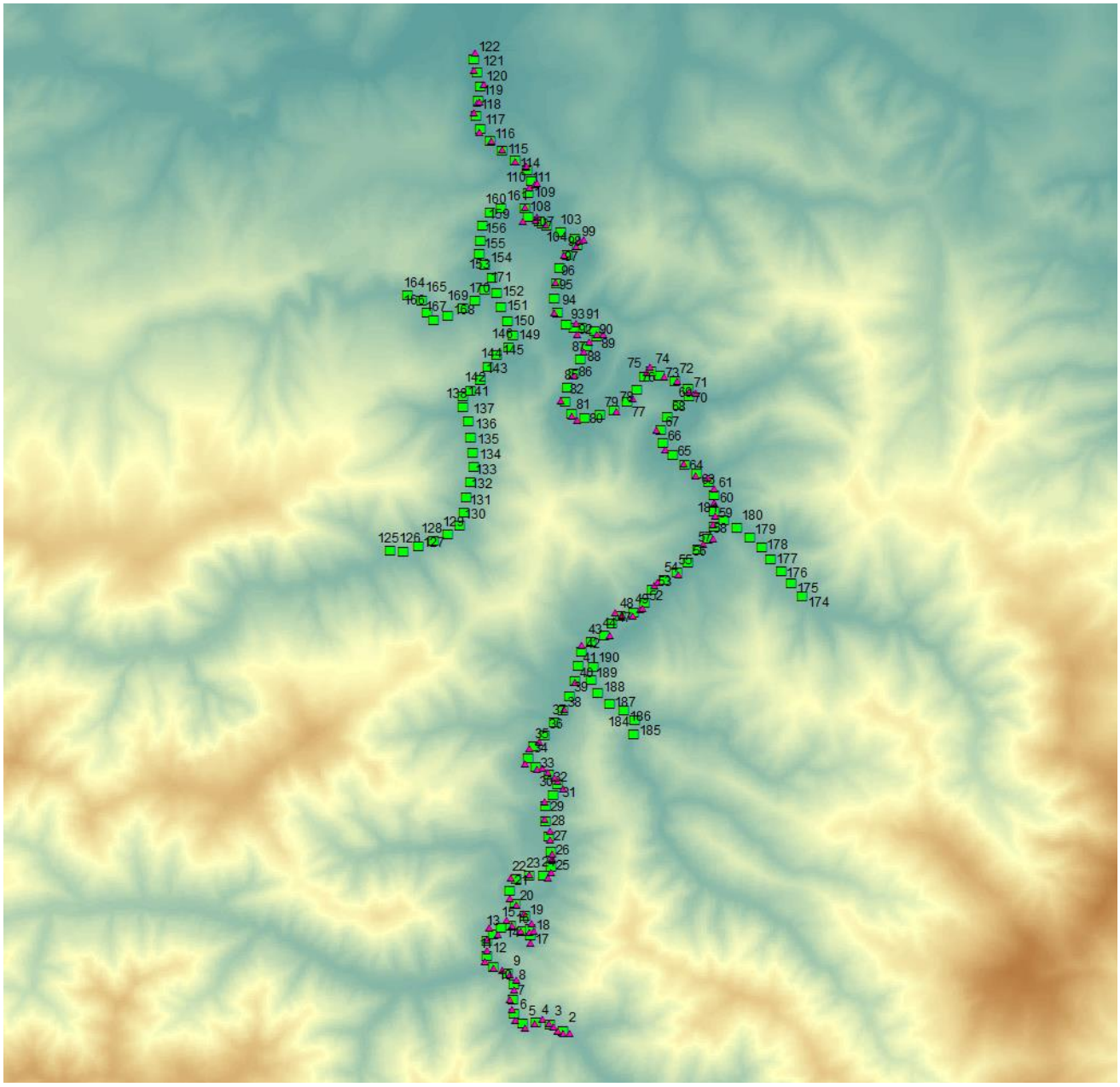

Figure 66. Location of footprint model segments (green squares). The HECRAS cross-section locations are marked by the red triangles.

Table 11. Summary of Chehalis footprint model grid details.

Number of water bodies	13
Number of branches	13
Number of segments	191
Minimum grid elevation	115.58 m
Maximum grid elevation	231.51 m
Number of layers	22
Layer thickness	0.5 m
Latitude	46.5°
Longitude	-123.3 °

Meteorological Inputs

Meteorological inputs for the footprint model were identical to those in waterbodies 1, 2 and 3 and also used by Anchor QEA for the reservoir model (Anchor QEA, 2016). These data were measured at the Thrash Creek site near the proposed dam site.

Flow Inputs

Flow inputs were developed using the total reservoir inflows developed by Anchor QEA. Flows for each watershed above the dam site were divided given the ratio of watershed area divided by total reservoir area (Table 12). Inflows for the tributaries and distributed tributaries are plotted in Figure 67 and Figure 68, respectively.

Table 12. Watershed areas above dam.

Watershed	Watershed Area (km^2)	Fraction of Reservoir Watershed Area	Type of Model Inflow
Lester Creek	10.39	0.058	Branch 11 inflow
Crim Creek (not including Lester Creek area)	21.66	0.121	Branch 7 inflow
Big Creek	9.02	0.051	Branch 12 inflow
Roger Creek	13.18	0.074	Branch 13 inflow
Chehalis River Watershed upstream of reservoir	104.25	0.585	Branch 1 inflow
Distributed inflows for mainstem branch 1	8.35	0.0468	Branch 1 distributed inflow
Distributed inflows for mainstem branch 2	0.58	0.0033	Branch 2 distributed Inflow
Distributed inflows for mainstem branch 3	6.02	0.0338	Branch 3 distributed Inflow
Distributed inflows for mainstem branch 4	2.91	0.0163	Branch 4 distributed Inflow
Distributed inflows for mainstem branch 5	1.94	0.0109	Branch 5 distributed Inflow
Total Watershed Area above Dam	178.30	1.000	

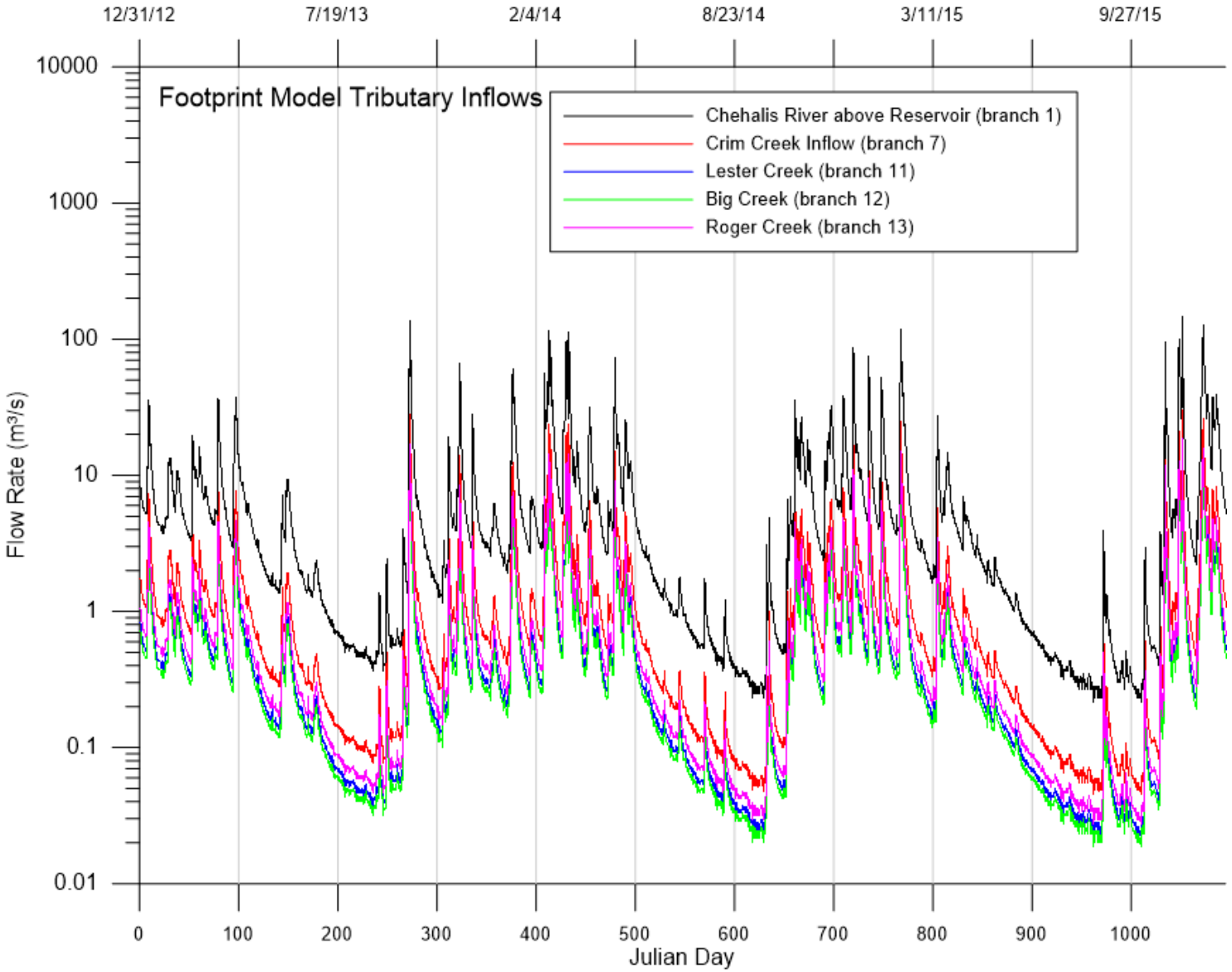

Figure 67. Footprint model tributary flow rates.

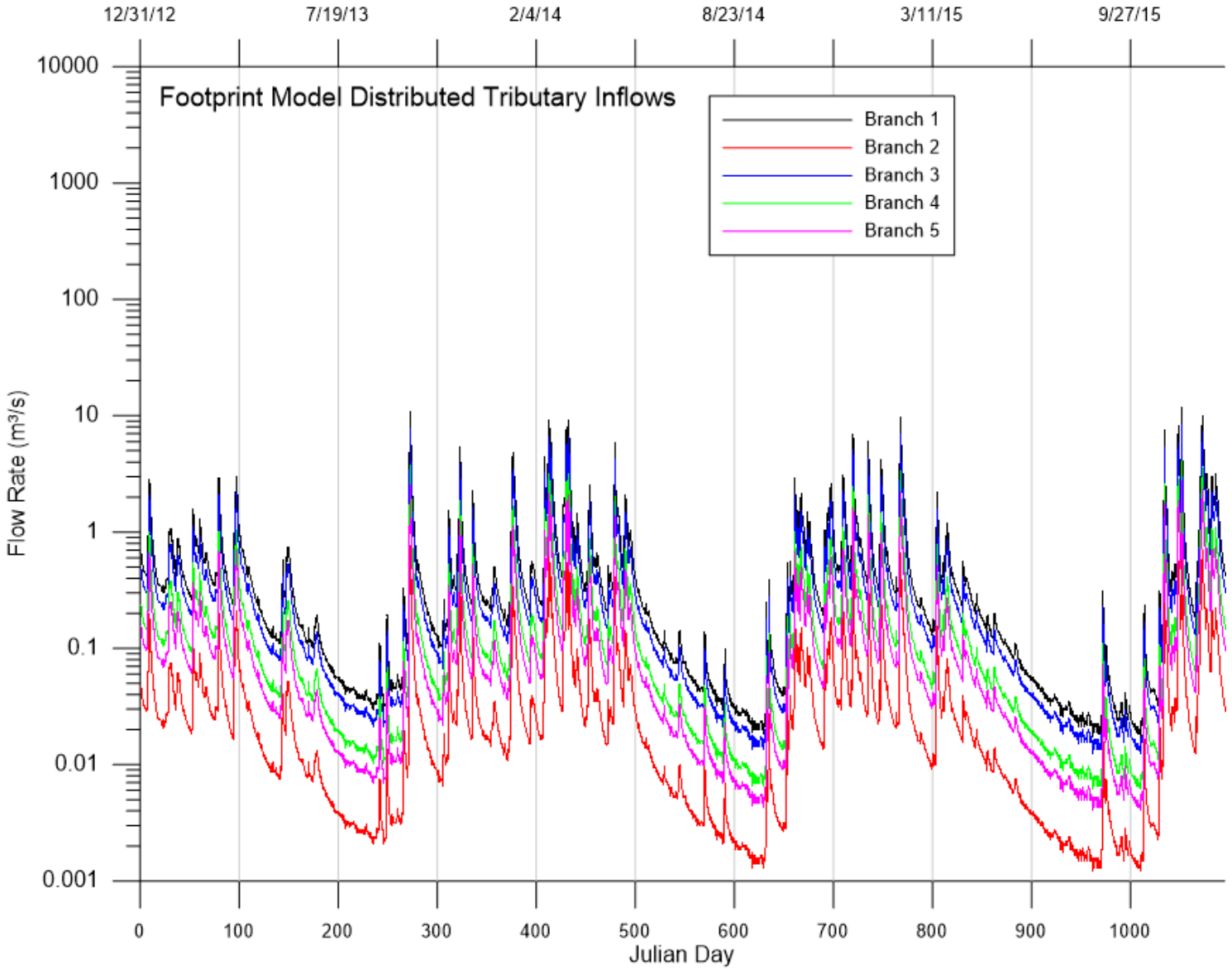

Figure 68. Footprint model distributed tributary flow rates.

Temperature Inputs

Temperature inflows of the footprint model are plotted in Figure 69. Anchor QEA developed upstream inflow temperatures for the Chehalis River and these were applied to the distributed tributaries in main stem branches 1 through 5. Lester Creek, Crim Creek, Roger Creek, and Big Creek inflow temperatures were developed using temperatures measured at site CRIM. CRIM data were available on and after Julian day 538 (6/22/2014). Before Julian day 538, a regression equation correlating temperatures measured at Crim Creek site CRIM and the Chehalis River site upstream of Darigold was used to estimate tributary inflow temperatures (Figure 70).

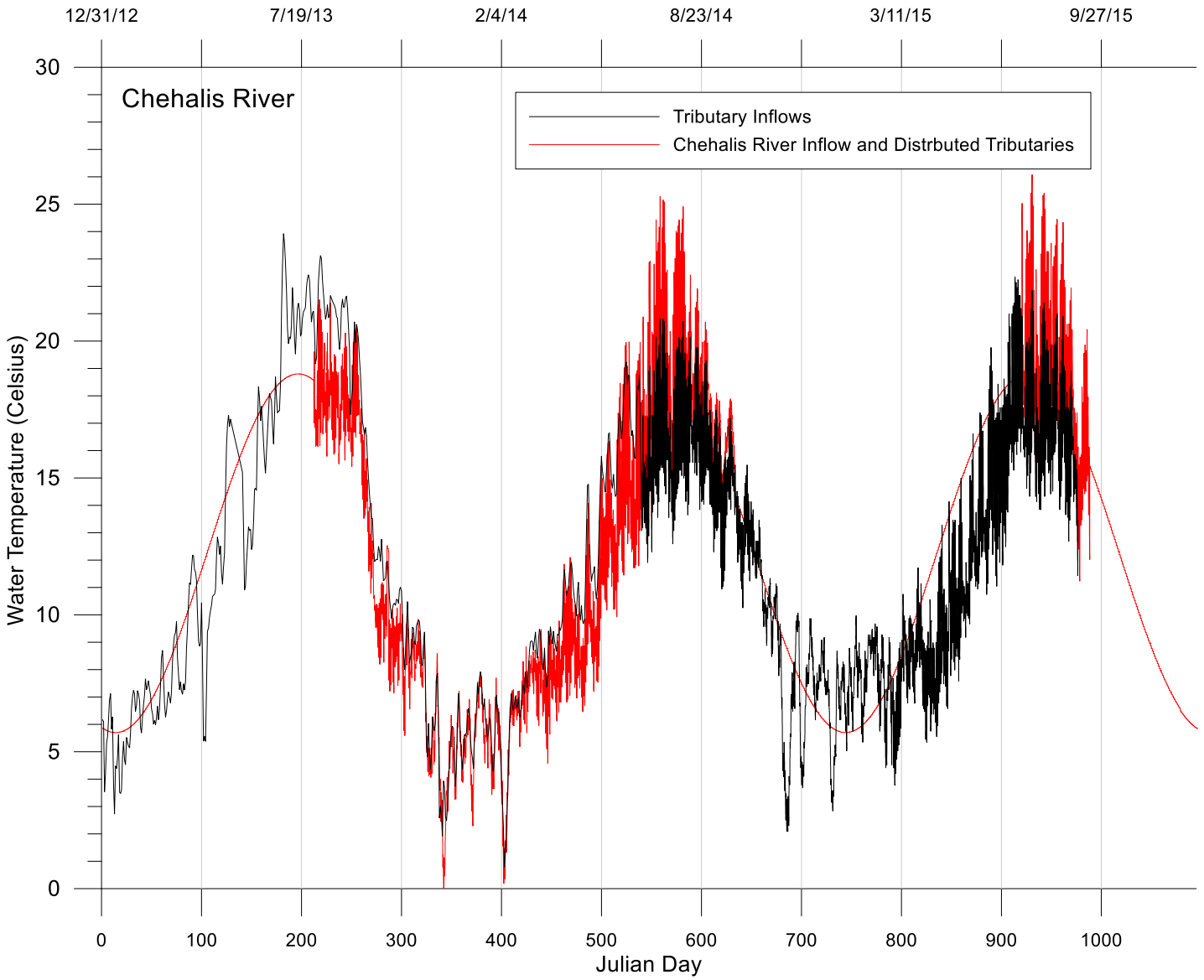

Figure 69. Temperature inflows of the footprint model.

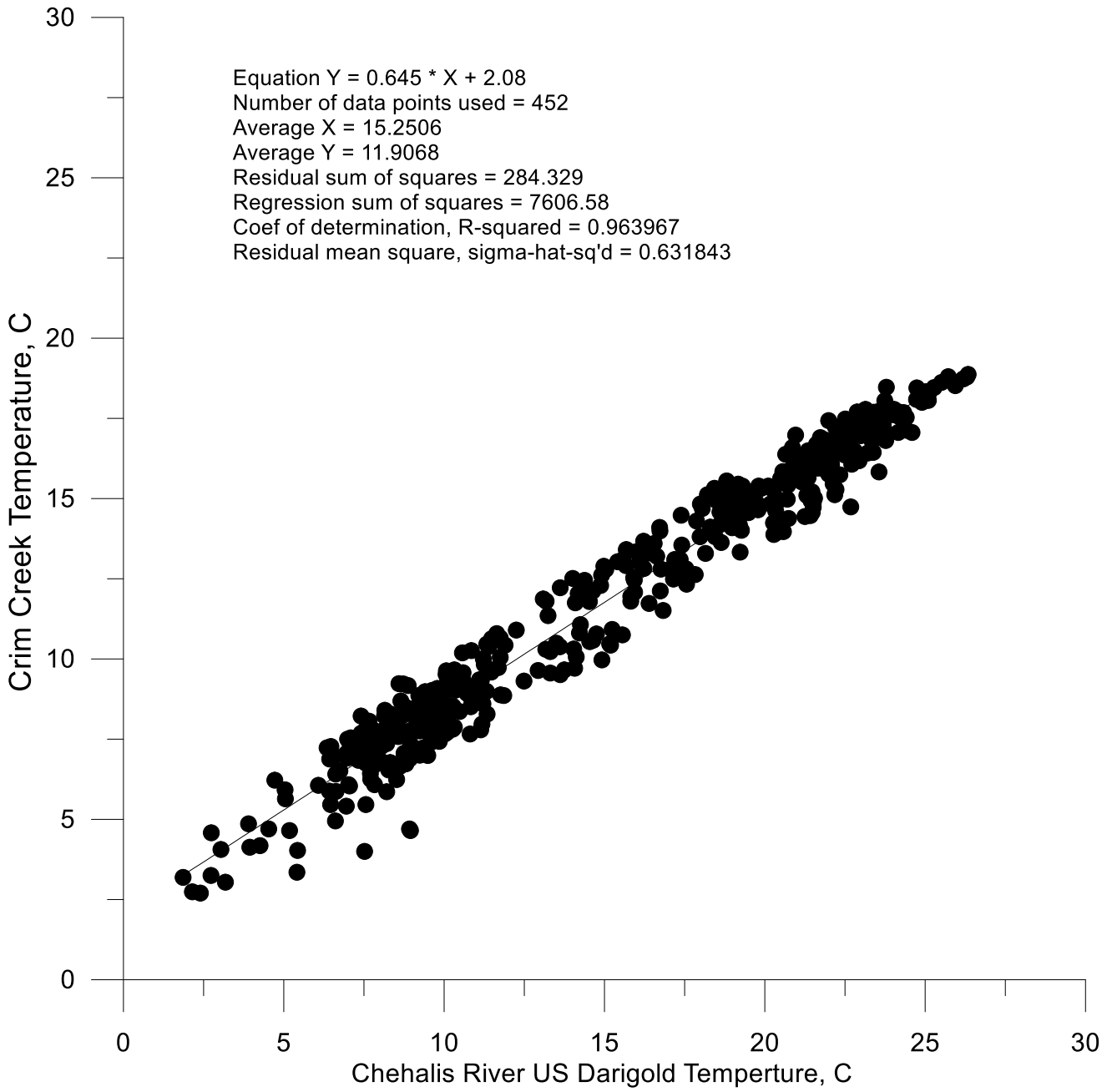

Figure 70. Plot and regression equation showing correlation of daily average temperatures measured at Crim Creek site CRIM and at the Chehalis River upstream of Darigold.

Constituent Inputs

Constituent input files for the footprint model were provided by Anchor QEQ and identical to the reservoir model constituent inputs. Figure 71 through Figure 74 show plots of the constituent concentrations.

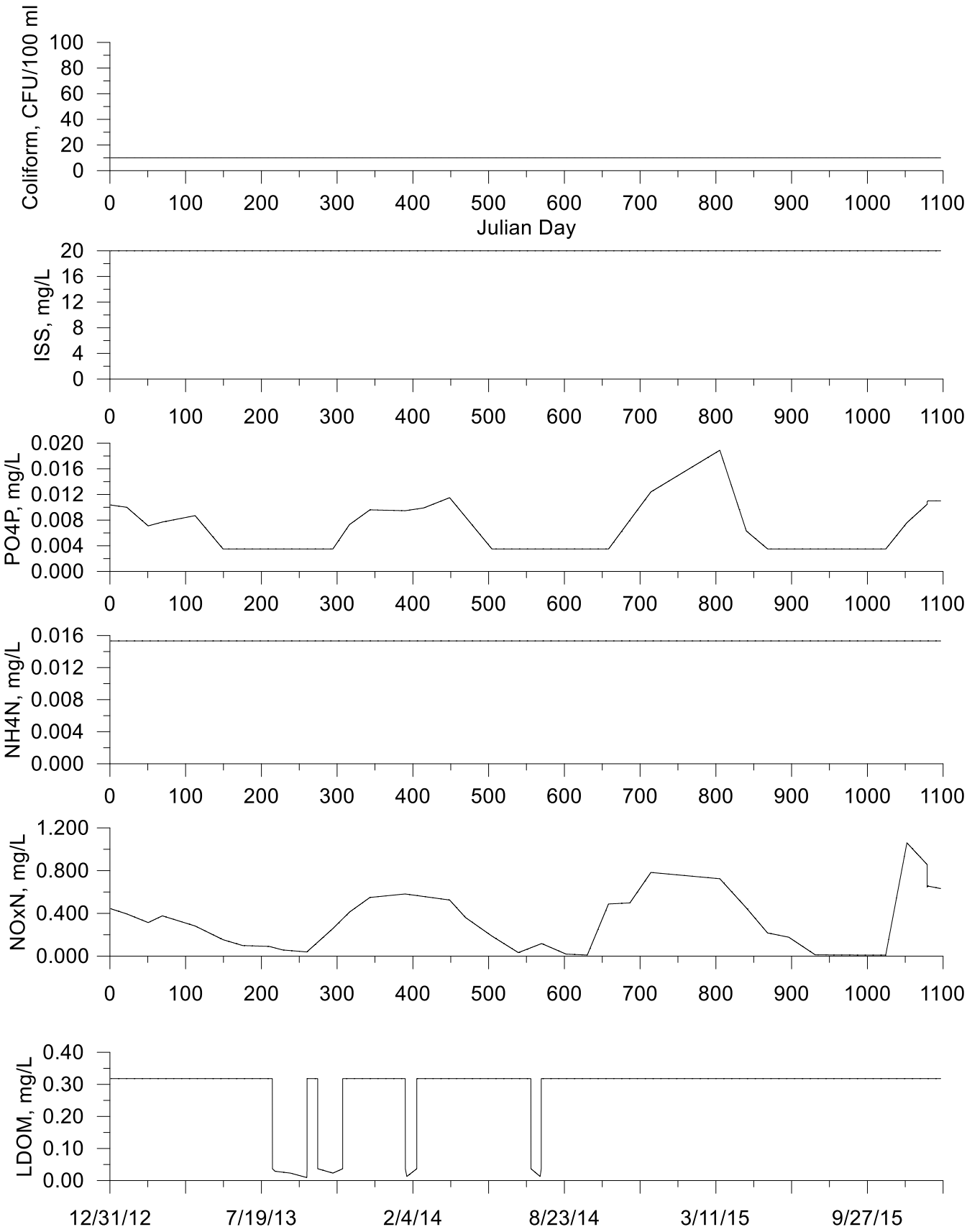

Figure 71. Inflow constituent concentrations for footprint model (1).

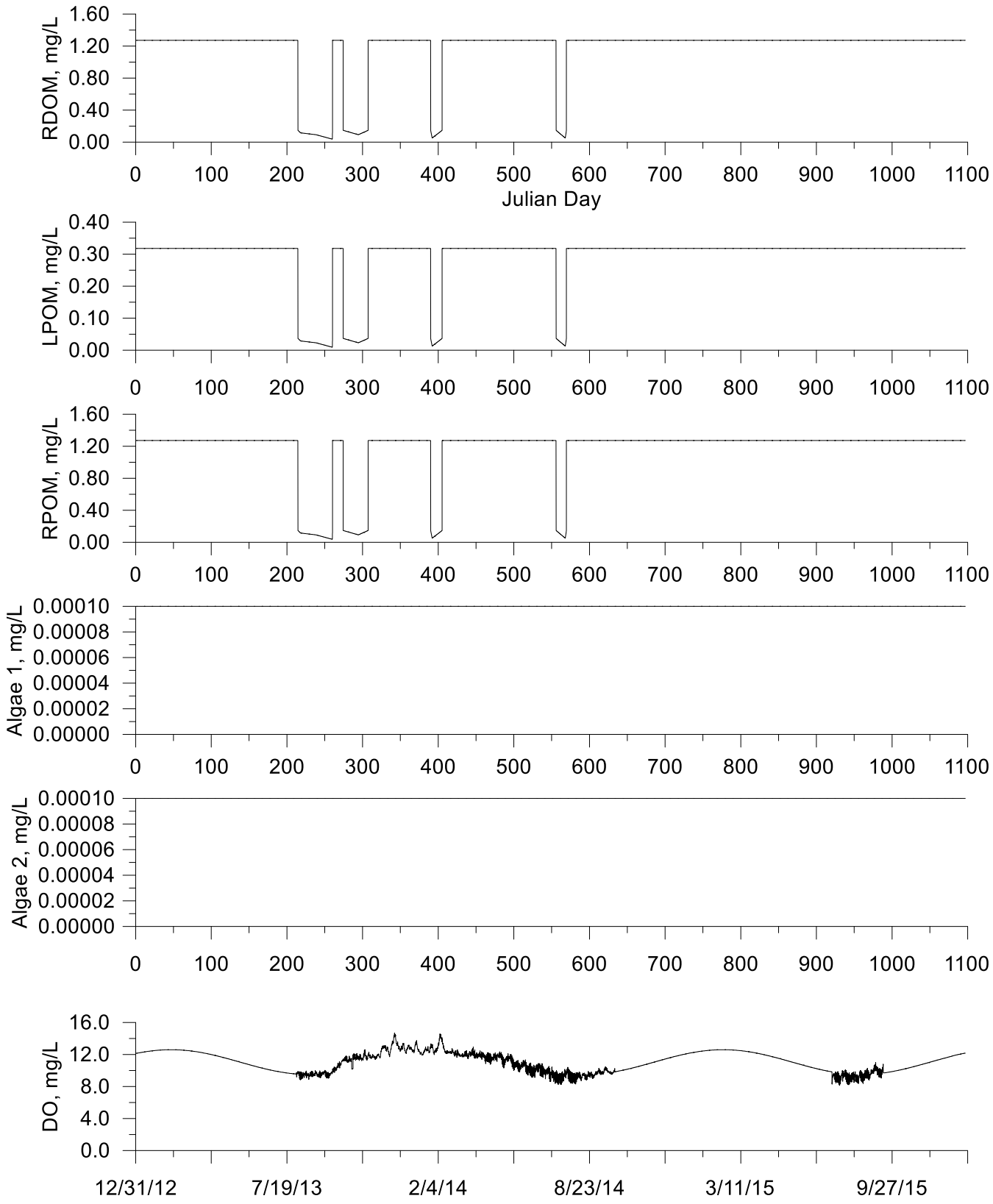

Figure 72. Inflow constituent concentrations for footprint model (2).

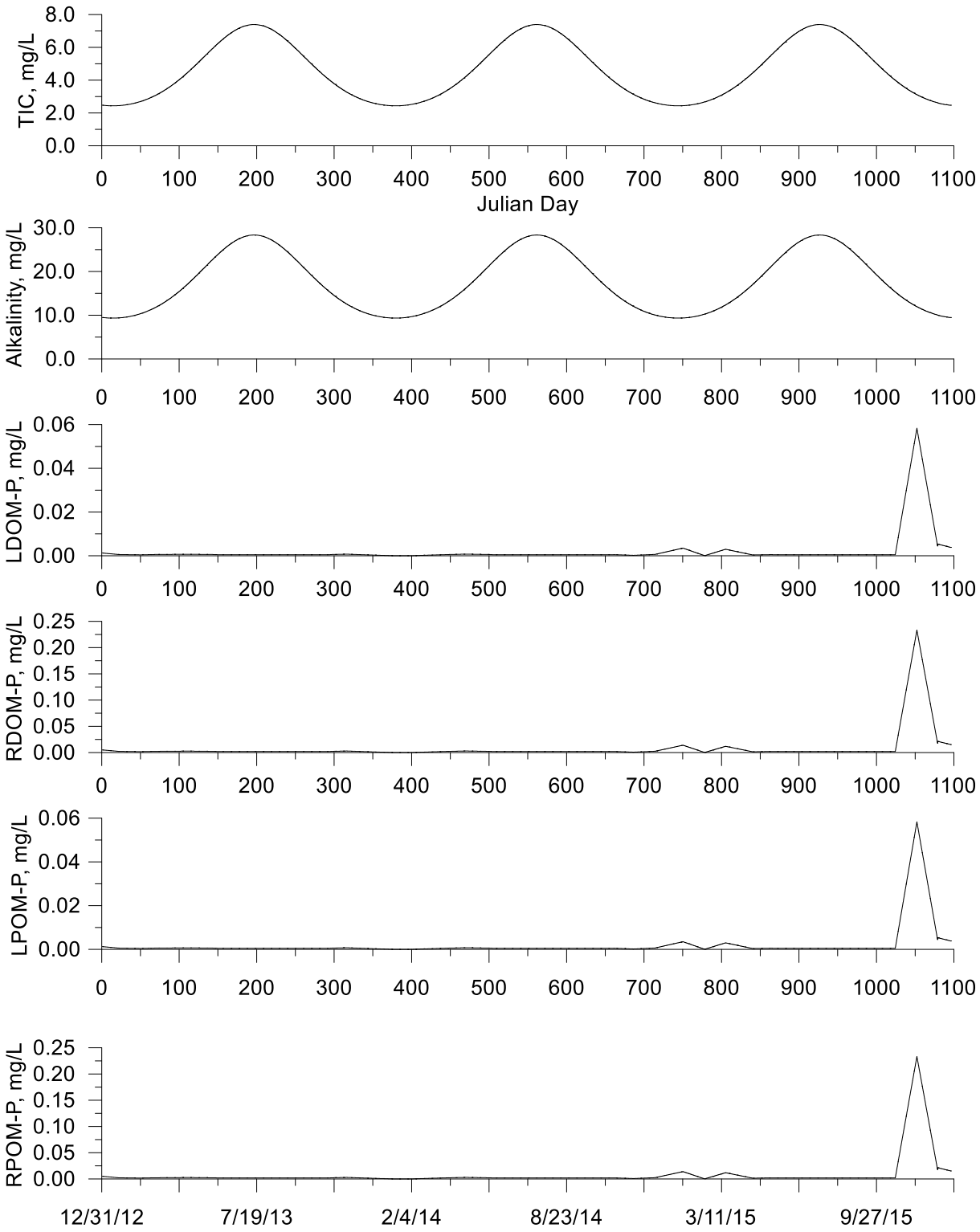

Figure 73. Inflow constituent concentrations for footprint model (3).

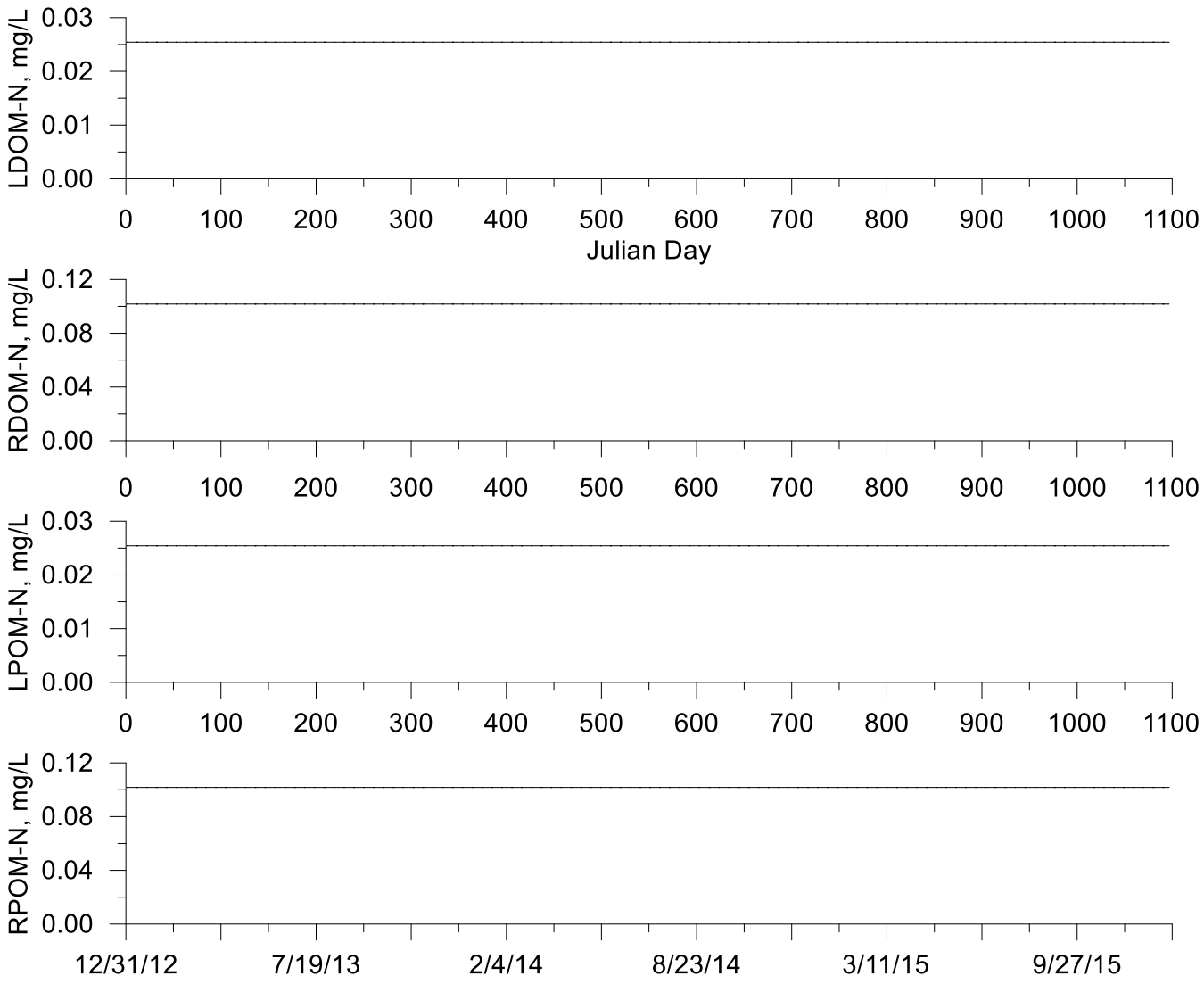

Figure 74. Inflow constituent concentrations for footprint model (4).

Shading

Topographic and vegetative shading was simulated in the footprint model (Figure 75). Topographic shading was determined using a digital elevation map of the reservoir area (Figure 76). The shade algorithm uses 18 topographic inclination angles surrounding each segment center-point. Figure 77 shows these angles for each model segment.

Unlike the downstream model, vegetative shading data did not exist in the footprint model area. Vegetative shading was assumed to be equivalent to vegetative shade in branch 1 of the downstream model, which is the river reach extending for 2 km directly downstream of the dam location.

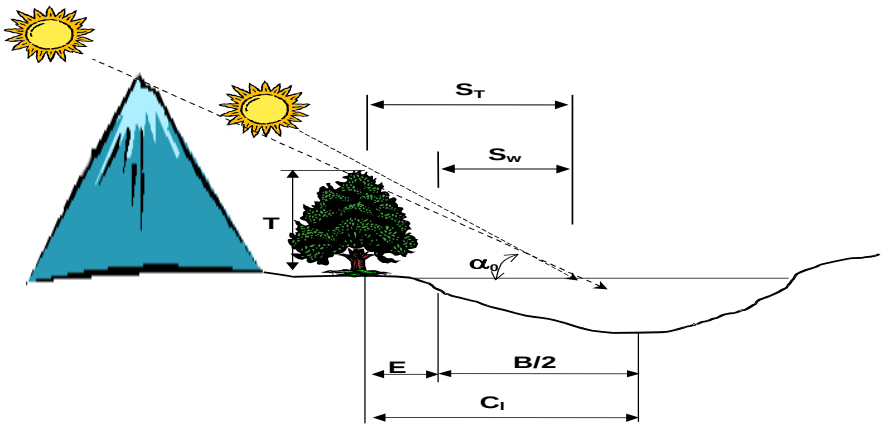

Figure 75. Schematic of topographic and vegetative shading, solar altitude (α_0), and vegetation height (T) and their effect on shadow length.

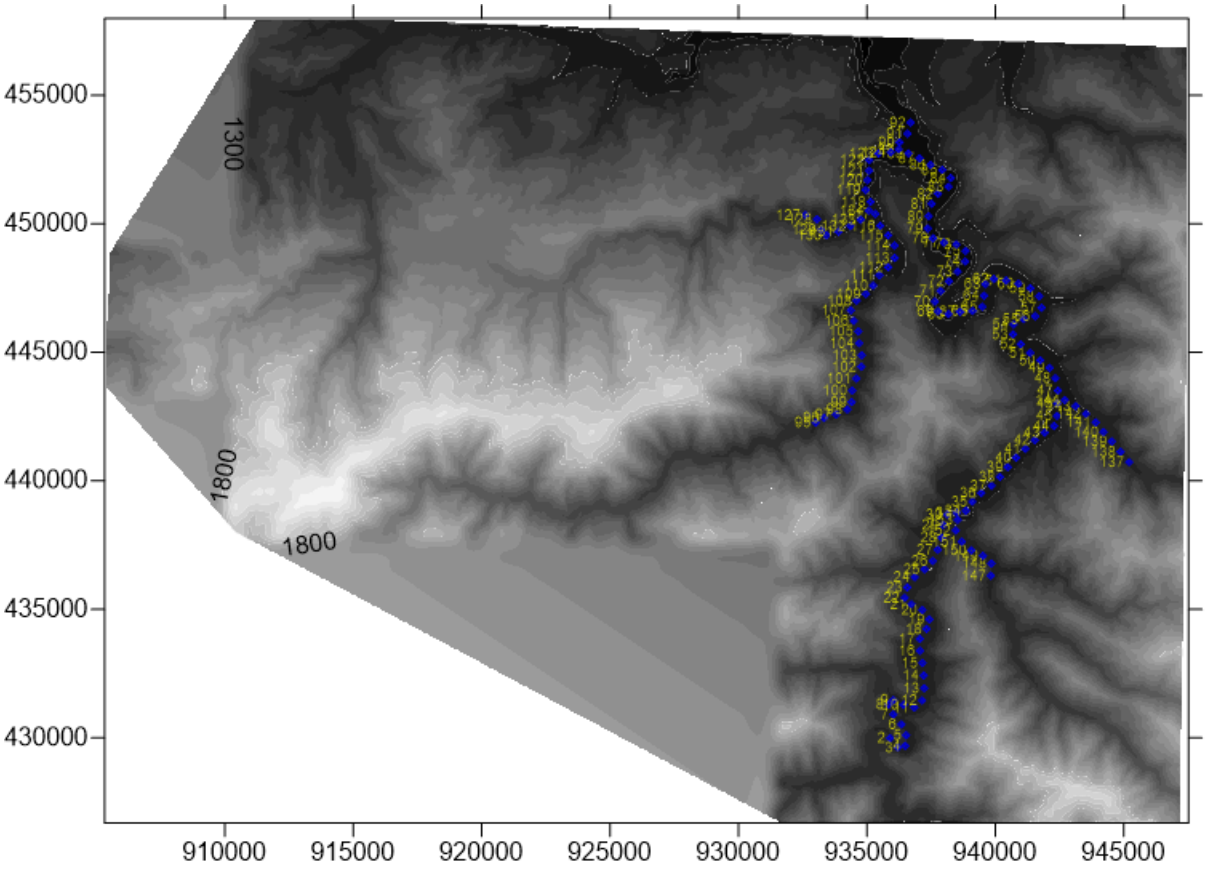

Figure 76. Digital elevation map used to develop topographic shading for the footprint model.

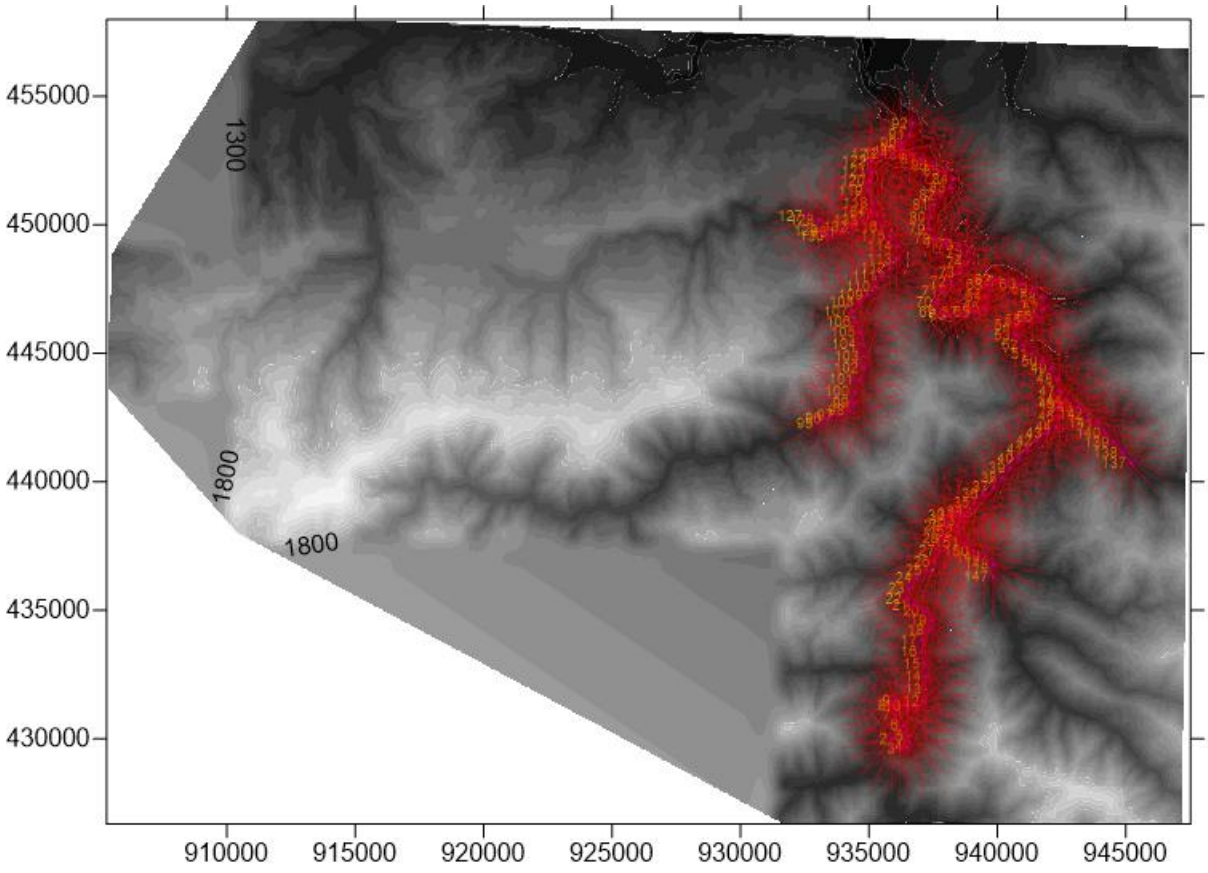

Figure 77. Shading angle directions for each model segment in the footprint model.

Model Calibration: Flow Rate

Chehalis River Downstream Model

The model calibration of flow rate began with upstream portions of the model and moved downstream. By comparing model flow predictions to field flow data along the mainstem of the Chehalis River, locations of excesses and deficiencies of flow were determined. Flow and water level data from the mainstem Chehalis River collected by USGS (2016a, 2016b, 2016c, 2016d, 2016e, 2016h, 2016i) were used for model-data comparisons during the model simulations years of 2013 and 2014. Table 13 lists these flow gaging stations. All of these stations had data available for the entire model time period. Figure 78 gives a longitudinal view of the locations of the flow calibration gaging stations along the Chehalis River.

Table 13. Flow and water surface elevation gaging stations on the mainstem Chehalis River used to compare model predictions to field data

Organization	Station ID	Description	Data Type Provided	Model Segment
USGS	12020000	Chehalis River near Doty, WA	Flow & water level	32
USGS	12021800	Chehalis River near Adna, WA	Water level	97
USGS	12025100	Chehalis River at Chehalis	Water level	150
USGS	12025500	Chehalis River at Centralia, WA	Water level	181

USGS	12027500	Chehalis River near Grand Mound, WA	Flow & water level	213
USGS	12028060	Chehalis River near Rochester,	Water level	238
USGS	12031000	Chehalis River at Porter, WA	Flow & water level	321

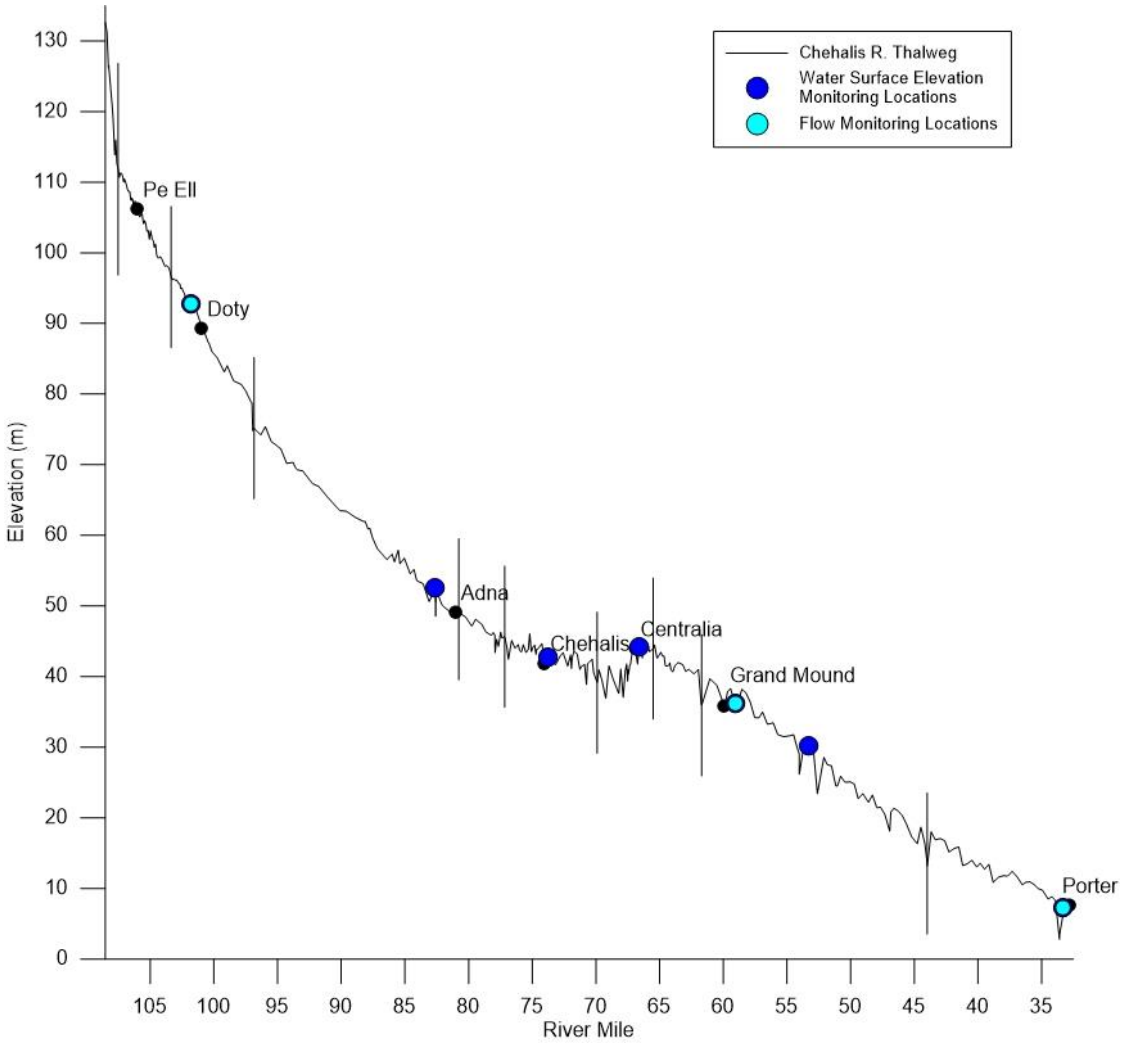

Figure 78. Longitudinal view of the mainstem Chehalis River flow and water surface elevation gaging stations used for flow calibration (vertical lines show model branch breaks)

Figure 79 shows model predictions of flow compared to field data collected at Doty, Grand Mound, and Porter, WA. Figure 80 shows the model water surface elevation predictions compared to field data for gaging stations at Doty, Adna, Chehalis WWTP, and Centralia. Figure 81 shows these comparisons at Grand Mound, Rochester, and Porter. The water level data were adjusted with the mean errors calculated with model predictions in order to account for datum discrepancies. This is discussed in further detail below.

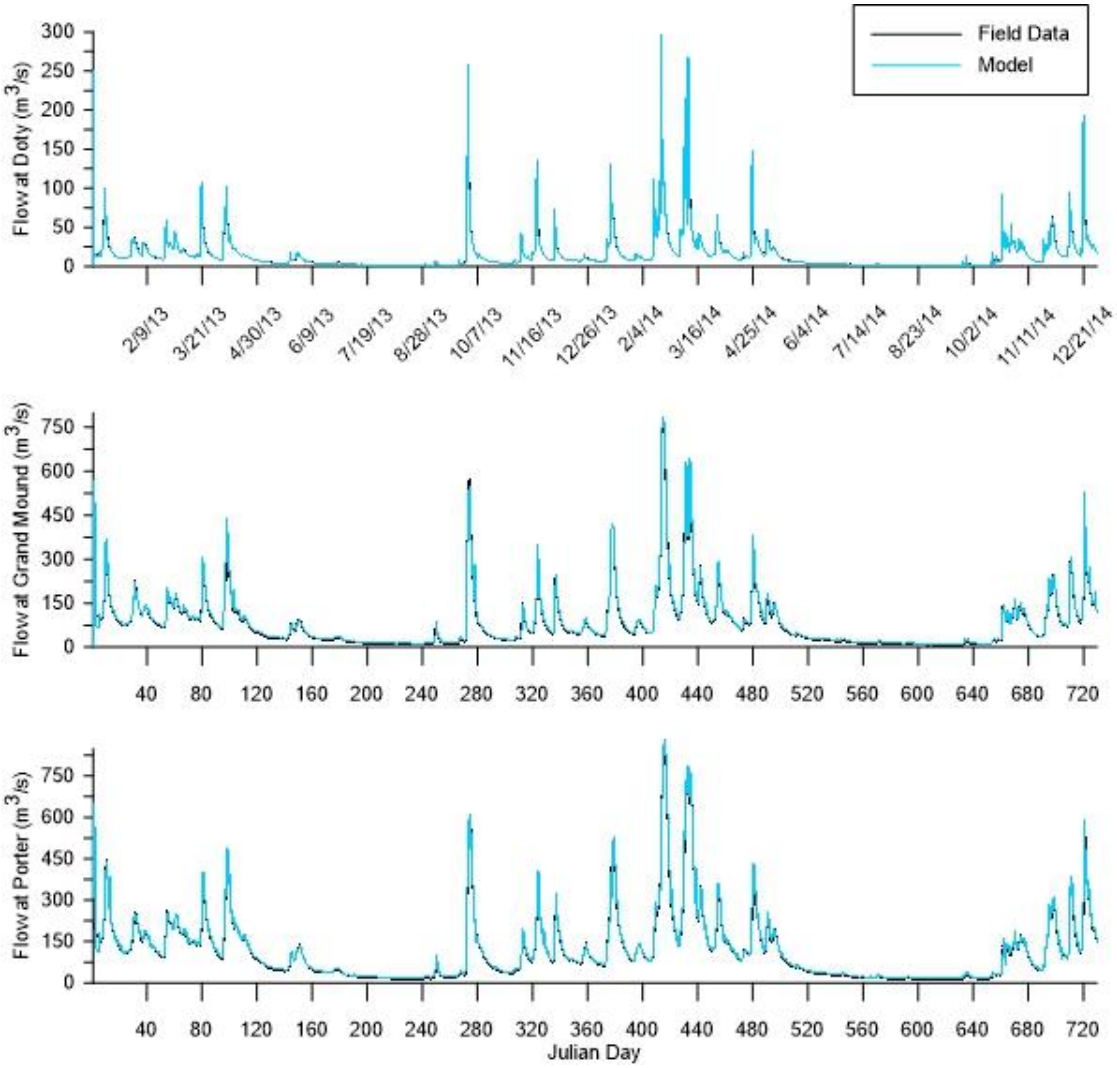

Figure 79. Model flow predictions compared to field data at Doty, Grand Mound, and Porter

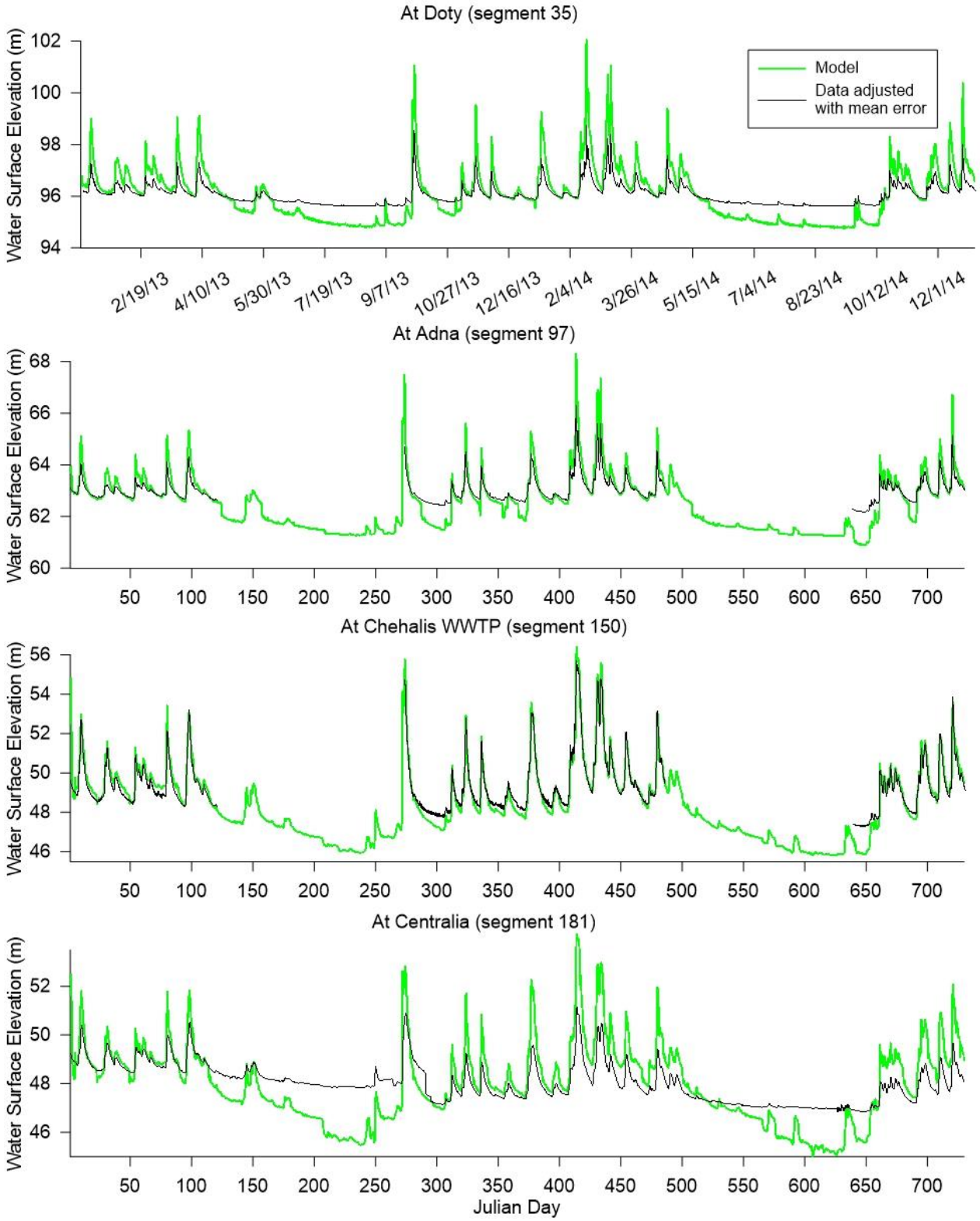

Figure 80. Model water surface elevation predictions compared to mean-error-adjusted field data collected at Doty, Adna, Chehalis WWTP, and Centralia mainstem Chehalis River gaging stations.

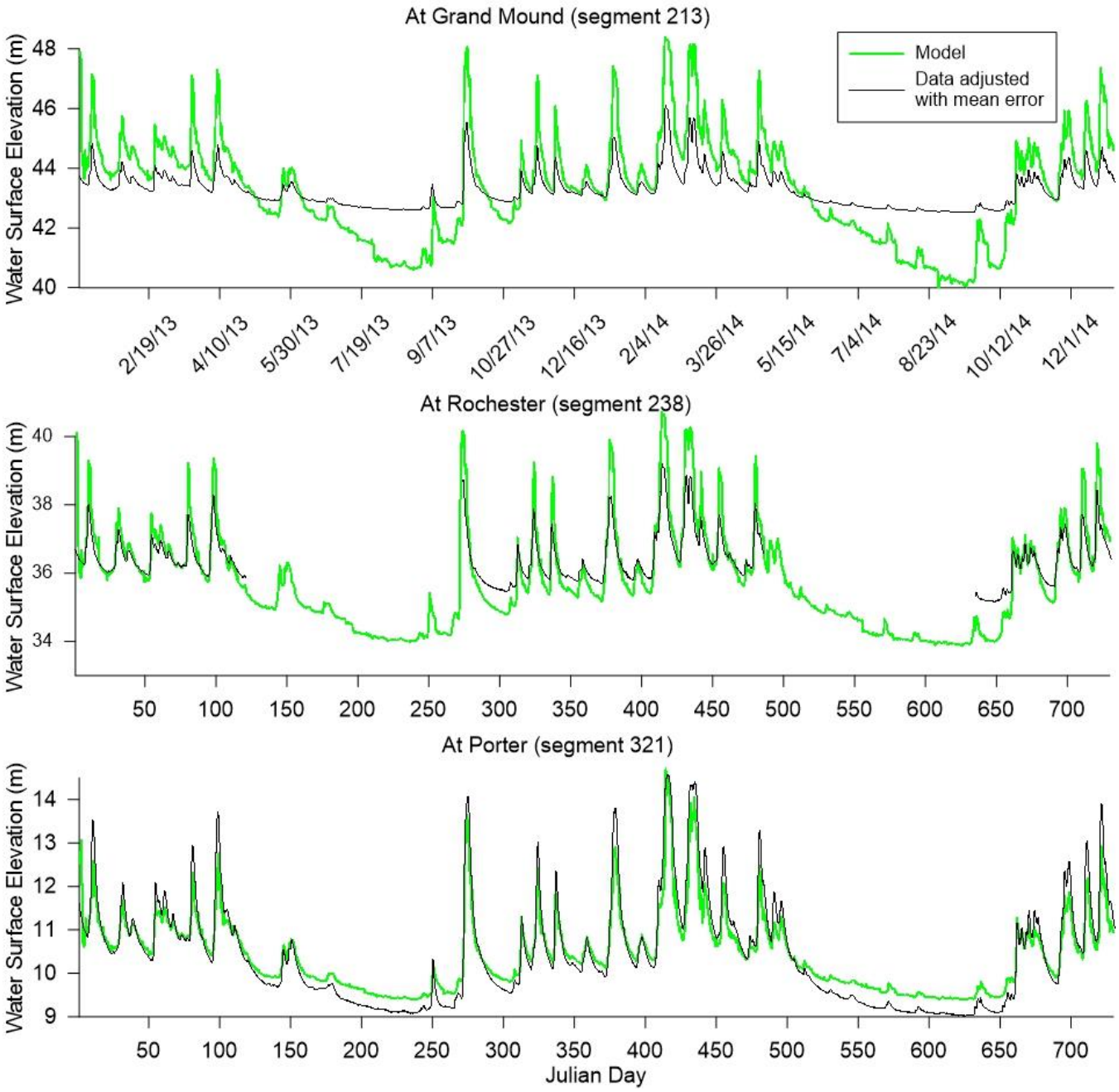

Figure 81. Model water surface elevation predictions compared to mean-error-adjusted field data collected at Grand Mound, Rochester, and Porter Chehalis River mainstem gaging stations

Error Statistics

The closeness of model predicted flow to field data was evaluated through error statistics, including mean error (ME), absolute mean error (AME), and root mean square error (RMSE). These were calculated using the equations described below.

$$ME = \frac{1}{N}\Sigma(Q_{model} - Q_{field\ data})$$

Where N is the number of model-field data comparisons, Q_{model} is the model flow output value, and $Q_{field\ data}$ is the field flow data value.

$$AME = \frac{1}{N}\Sigma|(Q_{model} - Q_{field\ data})|$$

$$RMS = \sqrt{\frac{1}{N}\Sigma(Q_{model} - Q_{field\ data})^2}$$

Error statistics for model flow predictions compared to field data at Doty, Grand Mound, and Porter are shown in Table 14. Error statistics for flow predictions at these same locations during the months of May through October can be seen in Table 15. Error statistics for flow predictions at these same locations during the months of November through April can be seen in Table 16.

Error statics for model predicted water surface elevation compared to field data at Doty, Adna, Chehalis WWTP, Centralia, Grand Mound, Rochester, and Porter mainstem Chehalis River stations are shown in Table 17. These error statistics were calculated with water level data that were adjusted with mean errors in order to account for datum discrepancies. This is discussed in further detail below.

Table 14. Error statistics for model comparisons to field data for flow at Doty, Grand Mound, and Porter.

Location	Number of Model-Data Comparisons	Mean Error (m^3/s)	Absolute Mean Error (m^3/s)	Root Mean Square Error (m^3/s)
Doty	69880	0.042	0.574	2.37
Grand Mound	68732	0.50	3.77	16.3
Porter	68839	2.00	7.54	22.0

Table 15. Error statistics for model comparisons to field data for flow at Doty, Grand Mound, and Porter during the months of May through October

Location	Number of Model-Data Comparisons	Mean Error (m^3/s)	Absolute Mean Error (m^3/s)	Root Mean Square Error (m^3/s)
Doty	35328	-0.079	0.339	1.97
Grand Mound	35136	0.275	1.41	4.73
Porter	34266	0.482	4.48	10.1

Table 16. Error statistics for model comparisons to field data for flow at Doty, Grand Mound, and Porter during the months of November through April

Location	Number of Model-Data Comparisons	Mean Error (m^3/s)	Absolute Mean Error (m^3/s)	Root Mean Square Error (m^3/s)
Doty	34369	0.004	0.815	2.71
Grand Mound	33504	2.76	7.78	23.7
Porter	34581	-5.44	16.9	34.8

Table 17. Error statistics for model comparisons to water level data at Doty, Adna, Chehalis WWTP, Centralia, Grand Mound, Rochester, and Porter mainstem Chehalis River stations

Location	Number of Model-Data Comparisons	Mean Error (m)	Absolute Mean Error (m)	Root Mean Square Error (m)
Doty	69793	0.00	0.488	0.623
Adna	40608	0.00	0.327	0.541
Chehalis WWTP	40608	0.00	0.342	0.520
Centralia	32187	0.00	0.806	1.03
Grand Mound	68640	0.00	0.933	1.15
Rochester	40608	0.00	0.433	0.604
Porter	68847	0.00	0.290	0.376

Model Calibrated Distributed Flows

The process of adding or subtracting flow was based on comparisons of model predictions to field data at the 3 gages: Doty, Grand Mound, and Porter. The flow error was calculated as field data minus model predicted flow rate for every time field data were available. While all tributaries, dischargers, and groundwater inflows were taken into account with input flow files, not all flow dynamics could be captured this way. For example, there may have been flow inputs to the river in the form of storm events and overland flow. Alternatively, there may have been ungaged agricultural withdrawals from the river. In addition to a lack of data for the magnitude of these flow sources and sinks, the precise locations are also unknown. For this reason, the flow error was added or subtracted to the model as distributed flow along the model branch upstream of the gage location of comparison.

Distributed flows helped to keep the model hydrated, particularly during the summer months when flow in the river became very low and the model was prone to dry up. This was a multiple-iteration process until model predicted flows were in agreement with field data at Doty. First, flow calibration with distributed flows was conducted at Doty, the most upstream flow gage station. Once the Doty location was properly calibrated, the same method was employed for the Grand Mound location. Then, once the Grand Mound location was properly calibrated, the same method was repeated for the Porter gage at the downstream model boundary. Figure 82 shows the distributed tributary flows added to the branches upstream of the flow monitoring locations as part of the calibration process.

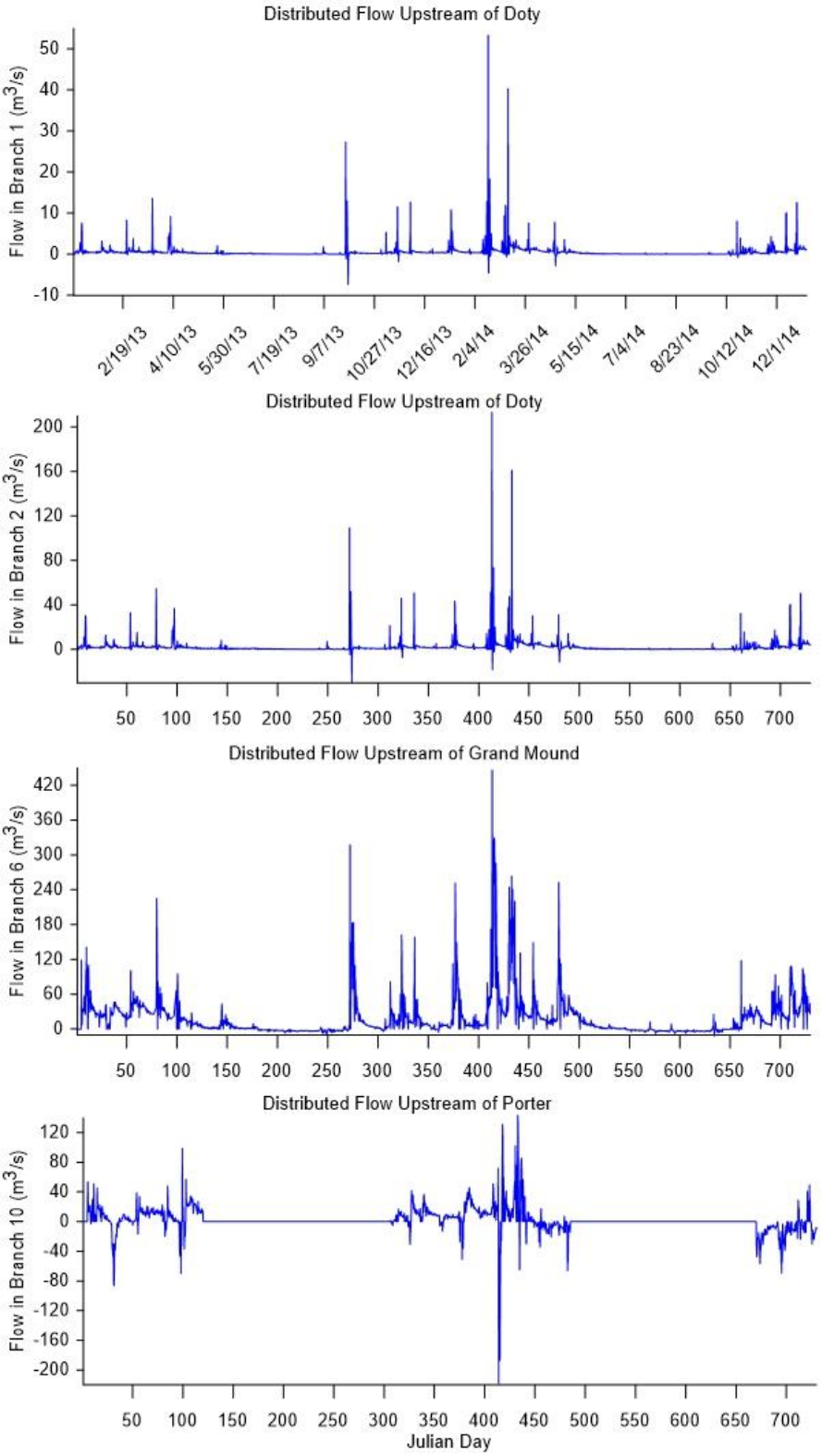

Figure 82. Distributed tributary flows input upstream of flow monitoring Doty, Grand Mound, and Porter locations for model calibration.

In general, the distributed flows represented ungaged inflows during storm events. At multiple times the distributed flows for the branch upstream of Porter had large negative magnitudes. There were no clear indications that these large withdrawals were as a result of irrigation. The timing of the large distributed flows in

branch 10 happened at times near to when peak water surface elevation occurred at Porter, generally during winter months. Figure 83 shows how water surface elevation varies with distributed flows in branch 10. This figure shows that generally, larger magnitudes of distributed flows correspond to peak water surface elevations.

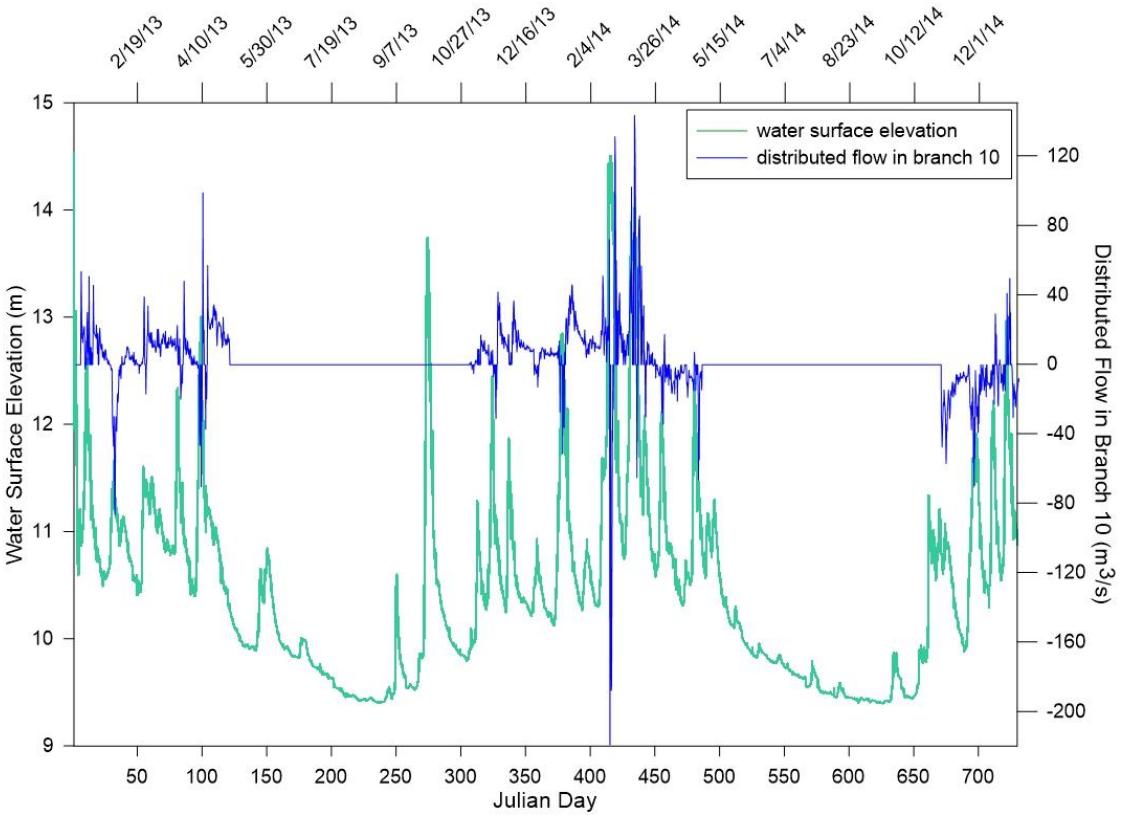

Figure 83. Water surface elevation at Porter versus distributed flow in branch 10 upstream of Porter

It is thought that storm events resulting in large volumes of overland flow account for the large positive distributed flow values, raising the water surface elevations. Once the water reaches bank-full levels, the water spills out of the river channel flooding the surrounding land, accounting for the large negative distributed flow values. The water spilling out of the river could be draining to natural storage, such as nearby ponds or oxbows. Figure 84 shows examples of many such features located near the Chehalis River.

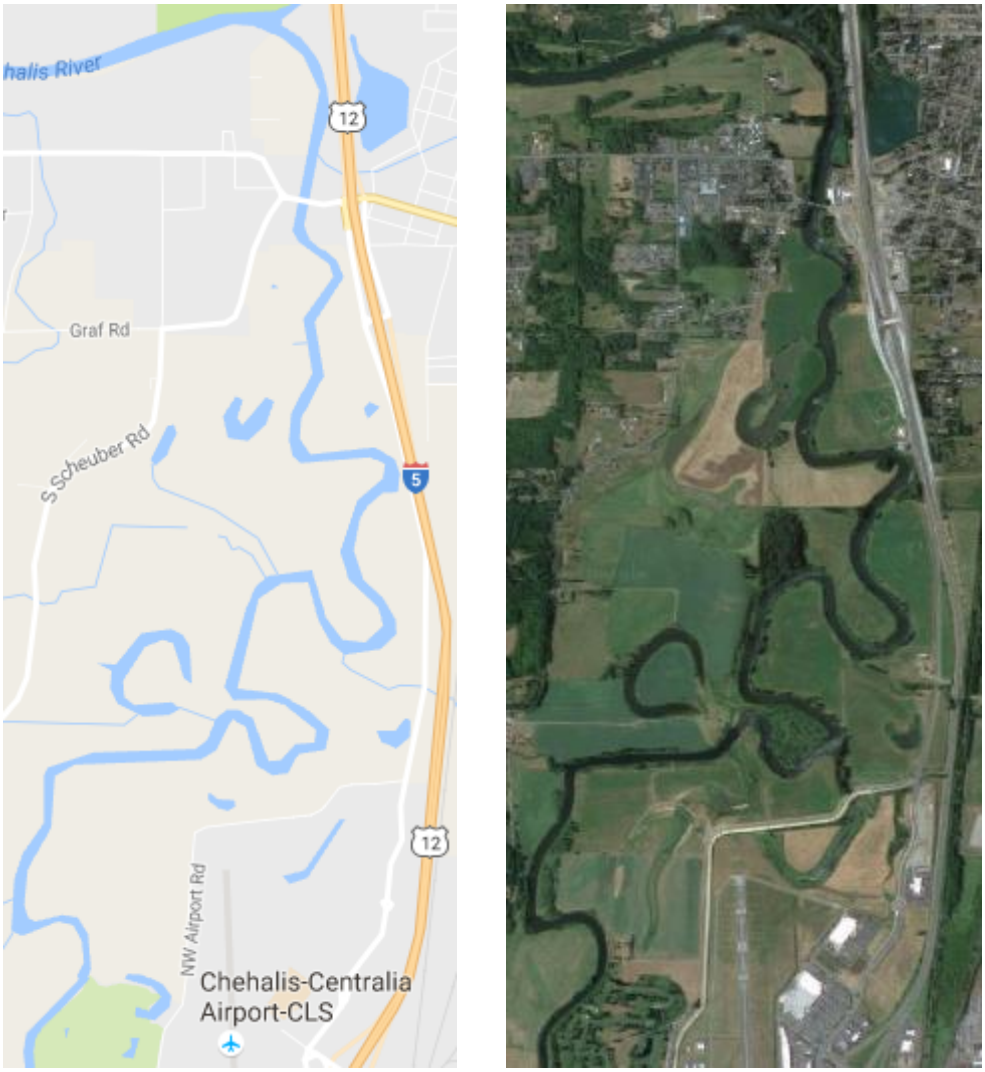

Figure 84. Map and earth aerial views of ponds and oxbows adjacent to the Chehalis River near Chehalis and Centralia, WA where flooded water may be stored

It is important to note that while the distributed flow was implemented in the branch upstream of Porter, the flow could actually be occurring anywhere between the next upstream calibration station at Grand Mound and the station at Porter, in branches 7 to 10. With a more detailed description of the basin, the distributed flows could be more accurately placed. This is true for all flow calibration locations.

Additional distributed flows were added to branches 3, 4, and 9 during calibration, The original regression relationships for Elk Creek, South Fork Chehalis River, and Black River were not forced through the origin, and thus allowed for tributary flows to be much higher than the mainstem flows when the mainstem flows were very low. In reality this was unrealistic. By updating the regression relationships so that they were forced through zero meant that the tributary flows would be very low when mainstem flows were also very low. In order to maintain the flow balance of the system, the flow reduced from the tributaries by making regression updates was added back as distributed flow in the branch the tributary resided in. Elk Creek was in branch 3, South Fork Chehalis River was in branch 4, and Black River was in branch 9. Distributed flows in branches 3, 4, and 9 are shown in Figure 85.

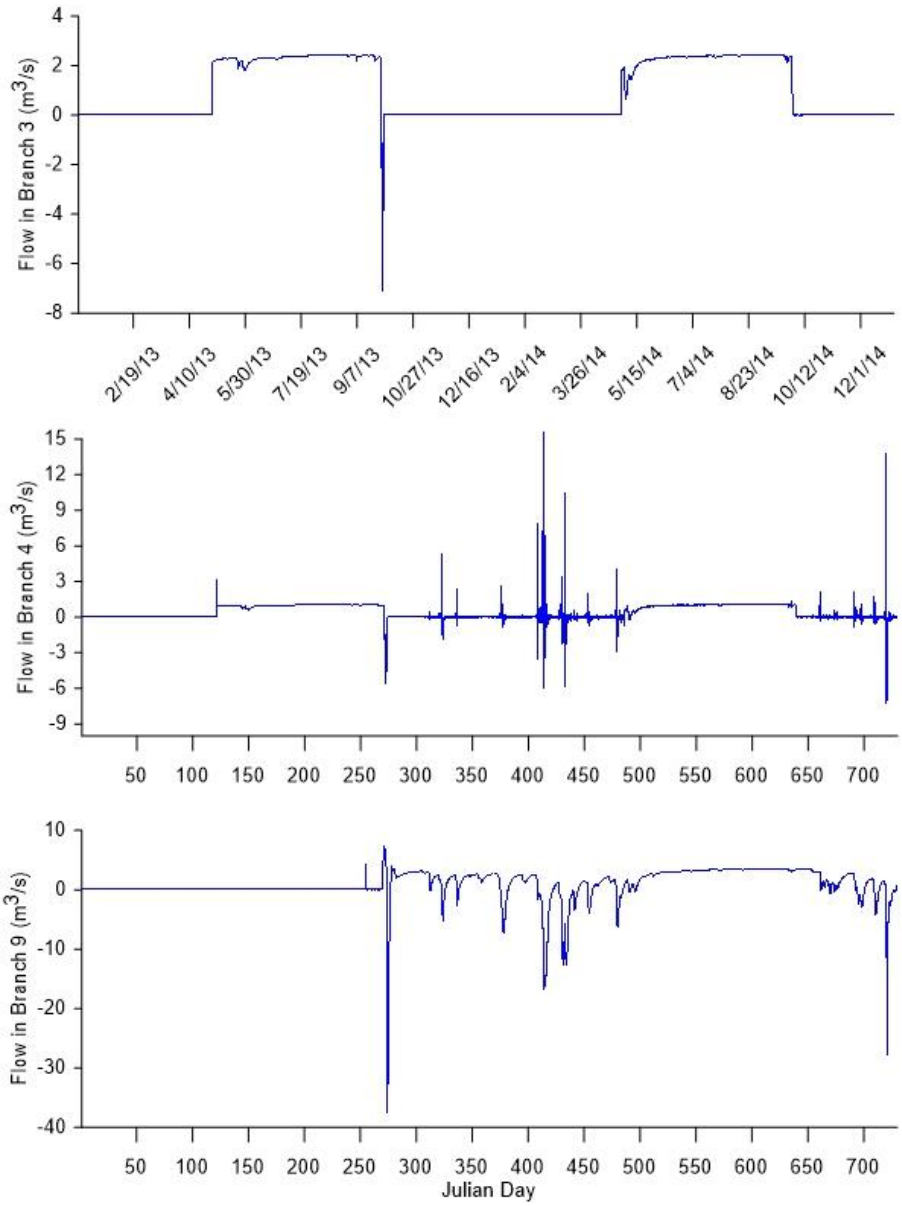

Figure 85. Distributed tributary flows input to branches 3, 4, and 9

Water Level Datums

Many water level data sets had datums that were not clearly defined or were not tied to a national standard datum. This made it difficult to know whether the water surface elevations predicted by the model and field data were all referenced to the same datum. As the model flow values and bathymetry closely matched field data, large water level discrepancies between model and measured data were likely due to unresolved datums. In order to correct this, the initial mean error between the model predictions of water level and measured data was calculated. Then, the mean error was added to the field data water level values to adjust the datum. This adjustment accounts for the near zero mean error shown in Table 17. The error statistics before the datums were adjusted with mean errors can be seen in

Table 18. Figure 86 shows how water level values between model predictions and field data compare before and after the mean error adjusted datum at Doty.

Table 18. Error statistics for model comparisons to water level data at Doty, Adna, Chehalis WWTP, Centralia, Grand Mound, Rochester, and Porter mainstem Chehalis River stations

Location	Number of Model-Data Comparisons	Mean Error (m)	Absolute Mean Error (m)	Root Mean Square Error (m)
Doty	69793	2.38	2.38	2.46
Adna	40608	3.33	3.33	3.37
Chehalis WWTP	40608	1.11	1.12	1.23
Centralia	32187	0.570	0.972	1.18
Grand Mound	68640	2.76	2.76	2.99
Rochester	40608	3.49	3.49	3.54
Porter	68847	-0.254	0.311	0.454

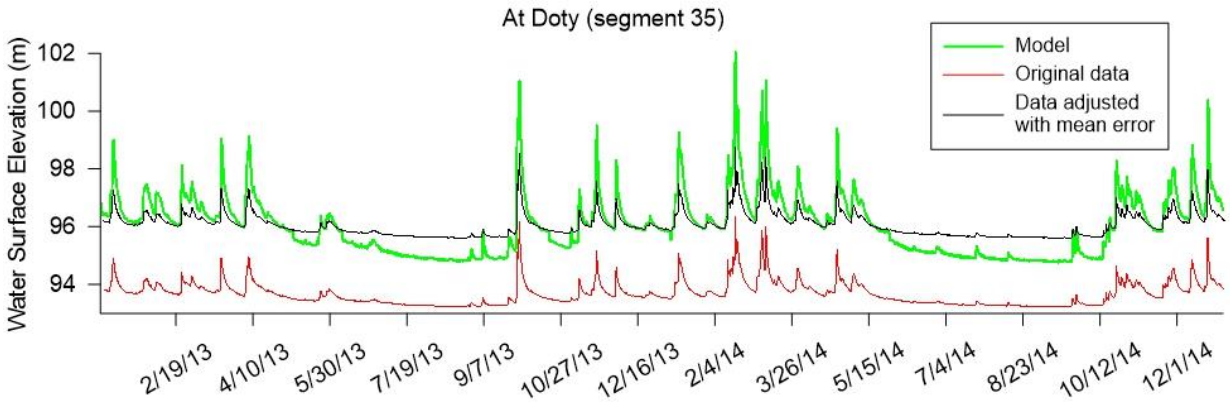

Figure 86. Model water surface elevation predictions compared to original field data and mean-error-adjusted field data collected at the Chehalis River at Doty mainstem gaging stations

Bathymetry

The bathymetry, including channel friction, channel slope, and segment depths and widths, all impacted the flow calibration.

Channel Friction

A manning's friction coefficient was specified for every model segment. Increasing friction slowed the travel time of water through the system and increased water depths, keeping the system hydrated during the low flow summer months. This was especially important for the upstream locations where gradients were very steep and water flushed through quickly. Similarly, decreasing friction had the opposite effect of causing water level to decrease and move more quickly through the system. Matching magnitudes as well as timing of flow peaks was important to accurately describe the system. Altering friction helped to match timing of peak flows to field data.

Channel Slope

Each branch in the model had a specified channel slope. This gave the general slope of the branch, for all segments it included. However, the slope may not accurately capture the hydraulic gradient slope due to real channel characteristics, such as falls, riffles, or other features (Cole and Wells, 2016). Because of this, a separate variable, SLOPEC, was specified for each branch and represented the hydraulic equivalent slope. This variable was used to calculate fluid acceleration in the momentum equations (Cole and Wells, 2016).

Similar to friction, increasing or decreasing SLOPEC either quickened or slowed water moving through the system. This affected timing of flow peaks, water surface levels, and keeping the model hydrated during low flow summer months. In the Centralia reach where the river is slow and deep, the model slope was essentially zero.

Segment Widths and Depths

Model instabilities were more likely to occur when segment depths changed rapidly from one segment to the next. For example, when water moved through segments that were very wide and deep to segments that were suddenly narrow and shallow, water backed up behind this constriction which may not have been the case in reality. Conversely, when water moved through segments that were very narrow and shallow to segments that were suddenly very wide and deep, sometimes the model could dry up under some flow conditions. Scenarios such as these made it necessary to smooth some widths and depths in the bathymetry files so that transitions between wide, narrow, deep, and shallow segments were not abrupt. Additionally, very small widths in segments, such as 5 m or less, required the model to use a smaller time step because of numerical stability considerations. By removing some very small bottom layers in the bathymetry files, shorter model run times were achieved.

Spillways

Weirs were added at the end of some branches. These had crest elevations that could be raised slightly so that water backed up behind them, allowing the upstream locations to remain more hydrated. The spillways also had a set of user-defined coefficients that affected the way water moved over the spillway and between branches, giving either a retaining or a flushing effect. In general, most of the spillways between branches were set so that the spillway crest was on the bottom elevation of the channel.

The spillways had the following power function describing behavior for free flowing conditions and submerged conditions (Cole and Wells, 2016):

$$Q = \alpha_1 \Delta h^{\beta_1}$$ Free flowing conditions

where α_1 and β_1 are empirical coefficients and Δh is the difference between the upstream head and spillway crest elevation

$$Q = \alpha_2 \Delta h^{\beta_2}$$ Submerged conditions

where α_2 and β_2 are empirical coefficients and Δh is the difference between the upstream head and downstream head

First, α_1 was calculated by using the equation for a broad crested weir:

$$\alpha_1 = C_D C_v \frac{2}{3}\sqrt{2g}W$$

where C_D is a discharge coefficient (0.84 to 1.06), C_v is a velocity coefficient (1.0 to 1.2), g is gravitational acceleration, and W is channel width

Figure 87 shows a schematic describing the water and weir heights used in the previous equations. The coefficients C_D and C_v were assumed to equal 1. Width W was calculated as the average bottom three layer widths of the segment where the spillway was located, since these layers were the most commonly occupied by water.

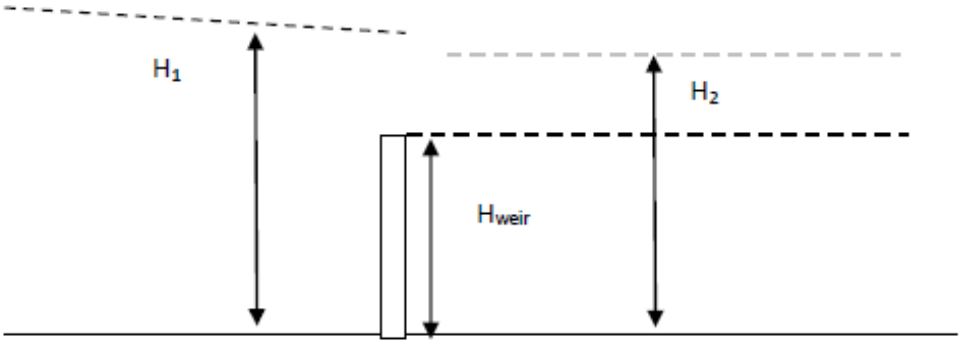

Figure 87. Schematic of water and weir heights for a free flowing submerged weir used with the spillway equations (Cole and Wells, 2016).

Following the methodology outlined in the CE-QUAL-W2 user manual (Cole and Wells, 2016), at a given flow value Q, the previous equations can be combined to give:

$$\alpha_2 = \frac{\alpha_1 (H_1 - H_{weir})^{\beta_1 - \beta_2}}{0.33^{\beta_2}}$$

Both β_1 and β_2 were set equal to each other. This implied:

$$\alpha_2 = \frac{\alpha_1}{0.33^{\beta_2}}$$

By using this process, the spillway or weir coefficients for free flowing and submerged flow were set.

Groundwater Flow Influences

Groundwater flow magnitudes varied by location. The influence of these flows were assessed by determining how they compared to flow along the mainstem channel. Model-predicted flow values were viewed within each groundwater reach. Then, the percent of the mainstem Chehalis River flow attributed to groundwater was computed. Groundwater flows accounted for a larger portion of the mainstem river during the summer seasons than during the winter seasons. Table 19 shows how the percent of mainstem Chehalis River flow attributed to groundwater varied by season, and for the entire model duration. Negative values are indicative of groundwater losses, or flow moving from the river to an aquifer.

Table 19. Percent of mainstem Chehalis River flow attributed to groundwater throughout the model

		% of Mainstem Chehalis River Flow				
Groundwater Reach Segment Range	Groundwater Reach Gain/Loss (m3/s)	Winter	Spring	Summer	Fall	Overall
35-37	0.025	0.17	0.36	2.03	0.47	0.77
38-47	0.510	0.02	0.04	0.11	0.06	0.06
48-66	-0.221	-0.95	-1.66	-4.73	-2.31	-2.43
67-80	-0.003	-0.01	-0.02	-0.06	-0.03	-0.03
81-97	0.040	0.15	0.25	0.67	0.34	0.36
98-122	-0.082	-0.28	-0.47	-1.32	-0.66	-0.69
123-143	0.388	1.34	2.28	6.10	2.93	3.19
144-181	0.404	0.62	1.17	5.41	1.84	2.28
182-191	-0.460	-0.50	-0.96	-5.33	-1.63	-2.13
192-204	-0.056	-0.06	-0.12	-0.66	-0.20	-0.05
205-210	0.565	0.59	1.12	6.13	1.91	2.46
211-214	0.823	0.84	1.60	8.17	2.64	3.35

		% of Mainstem Chehalis River Flow				
Groundwater Reach Segment Range	Groundwater Reach Gain/Loss (m3/s)	Winter	Spring	Summer	Fall	Overall
224-229	0.567	0.56	1.08	5.31	1.75	2.20
230-235	-0.174	-0.17	-0.33	-1.66	-0.54	-0.68
236-242	0.255	0.23	0.45	2.26	0.74	0.93
243-246	0.326	0.29	0.57	2.85	0.94	1.17
247-251	-0.652	-0.57	-1.16	-5.88	-1.91	-2.41
252-255	0.227	0.20	0.40	2.09	0.67	0.85
256-260	0.058	0.05	0.10	0.53	0.17	0.22
261-264	-0.256	-0.22	-0.46	-2.52	-0.79	-1.01
265-268	-1.368	-1.06	-2.16	-10.52	-3.41	-4.34
269-272	0.962	0.74	1.50	7.07	2.34	2.94
273-276	-0.190	-0.14	-0.29	-1.38	-0.46	-0.57
277-285	0.197	0.15	0.30	1.45	0.48	0.60
286-318	0.799	0.56	1.14	5.36	1.78	2.23
319-321	-0.272	-0.19	-0.39	-1.84	-0.61	-0.76
	Average:	0.09	0.17	0.76	0.25	0.33

Travel time, Age, and Dispersion

The time it took for a parcel of water to travel through the entire length of the model reach was evaluated by using a tracer. Tracer inputs of 100 mg/L were added over 2.4 hours to the upstream boundary every 30 days. Then the time for each tracer pulse peak to reach various downstream segments was found. The difference between the time a pulse peak appeared at a downstream location and the time it was originally input to the upstream boundary was the travel time. Figure 88 shows examples of how the tracer peak magnitudes decreased and time of peak occurrence became later moving downstream. Table 20 gives example values of travel time for various locations in the model and Figure 89 shows how travel time increases moving downstream for various initial upstream input pulse times.

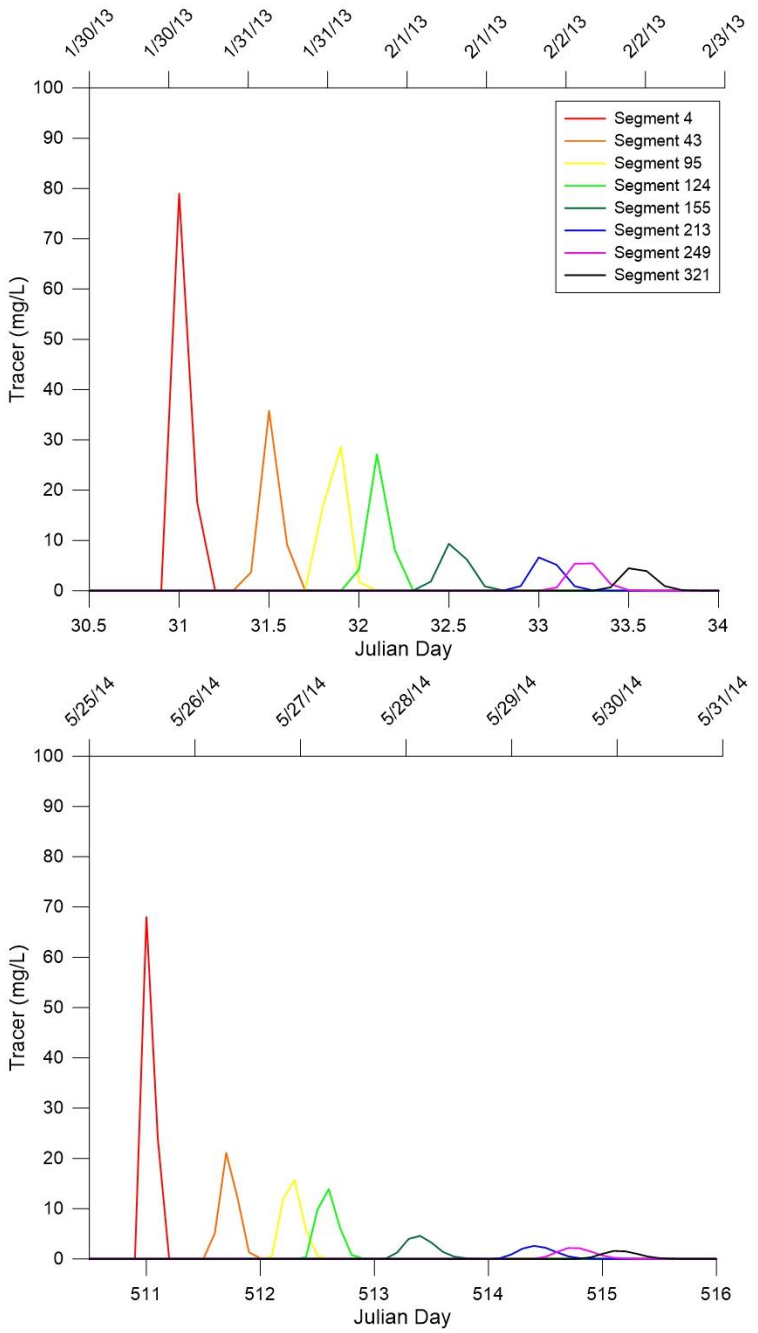

Figure 88. Resulting tracer magnitudes and timing along the river channel for tracer pulses input to the upstream boundary at Julian days 31 and 511

Table 20. Travel times for upstream pulse inputs to reach various downstream locations for various input pulse times

	Travel Time (days)				
Initial Upstream Pulse Julian Day	Segment 43	Segment 124	Segment 193	Segment 249	Segment 321
1	0.7	1.2	2.1	2.6	2.9
31	0.5	1.1	1.9	2.3	2.5
61	0.5	1.1	1.9	2.3	2.6
91	0.7	1.5	2.9	3.3	3.7

121	0.7	1.6	3.2	3.7	4.1
151	0.5	1.3	2.5	3	3.3
181	0.7	1.7	3.9	4.6	5.1
211	1	2	5	5.6	6.1
241	0.9	1.8	4.9	5.5	5.9
271	0.5	1	1.6	2	2.3
301	0.7	1.7	4.2	4.8	5.3
331	0.6	1.5	2.9	3.4	3.8
361	0.7	1.5	2.9	3.4	3.7
391	0.7	1.6	3.2	3.7	4
421	0.5	1.15	2	2.4	2.7
451	0.6	1.3	2.2	2.6	2.8
481	0.4	1	1.7	2.1	2.4
511	0.7	1.6	3.2	3.7	4.1
541	0.8	1.8	4.1	4.7	5.1
571	0.8	1.7	4.7	5.3	5.8
601	1.2	2.2	5.5	6.2	6.75
631	1.2	2.1	4.7	5.2	5.6
661	0.4	0.9	1.6	1.9	2.2
691	0.5	1.2	2.1	2.4	2.7
721	0.4	0.9	1.5	2	2.3

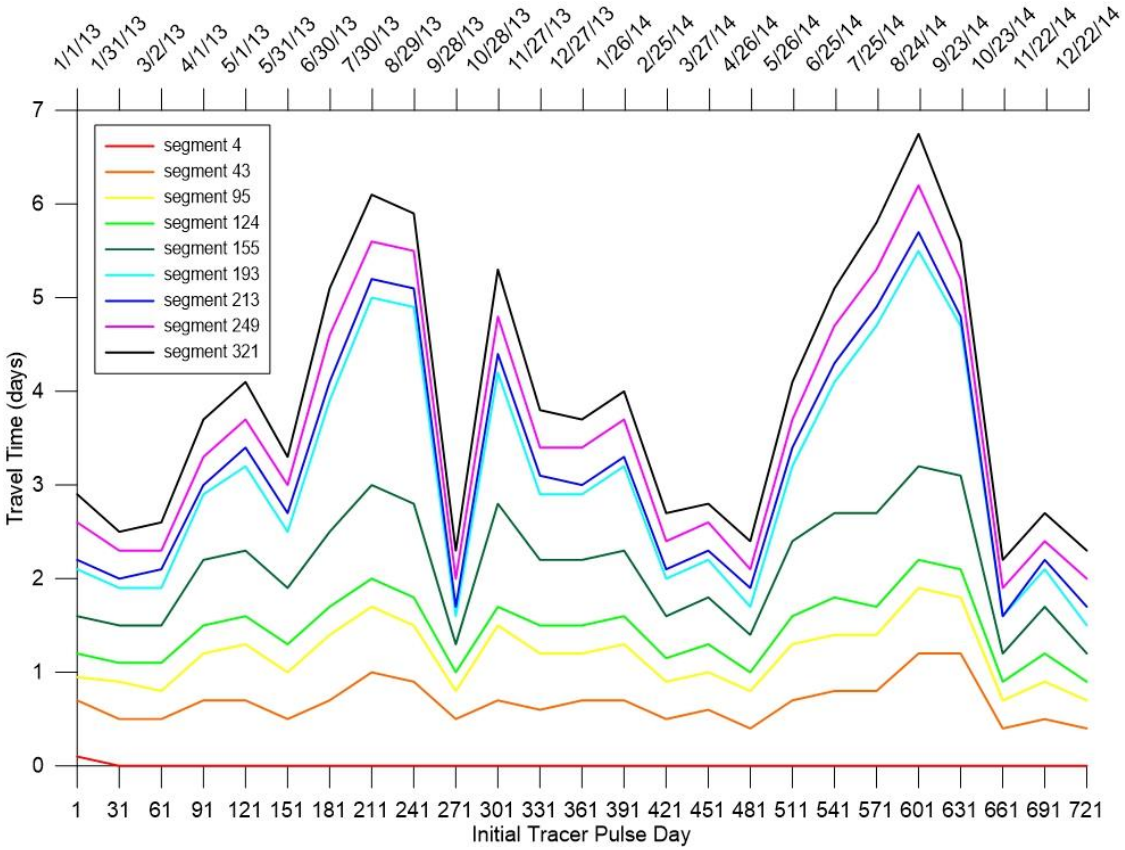

Figure 89. Travel times for tracer pulse peaks at various downstream locations

Water age is a measure of how long water has been in the system, and is similar to travel time in that it is a function of how quickly water moves through the system. However, flow inputs from tributaries or groundwater are set to "new" water or zero water age when they enter the river. For example, the water age may be lower for

a segment just downstream of a major tributary than for a segment just upstream of a major tributary. This is because the new flow coming in from the major tributary mixes with the flow already in the mainstem river and reduces the water age. This implies water age will generally be less than travel time. Figure 90 shows how water age generally increases moving downstream, though it is influenced by boundary flows.

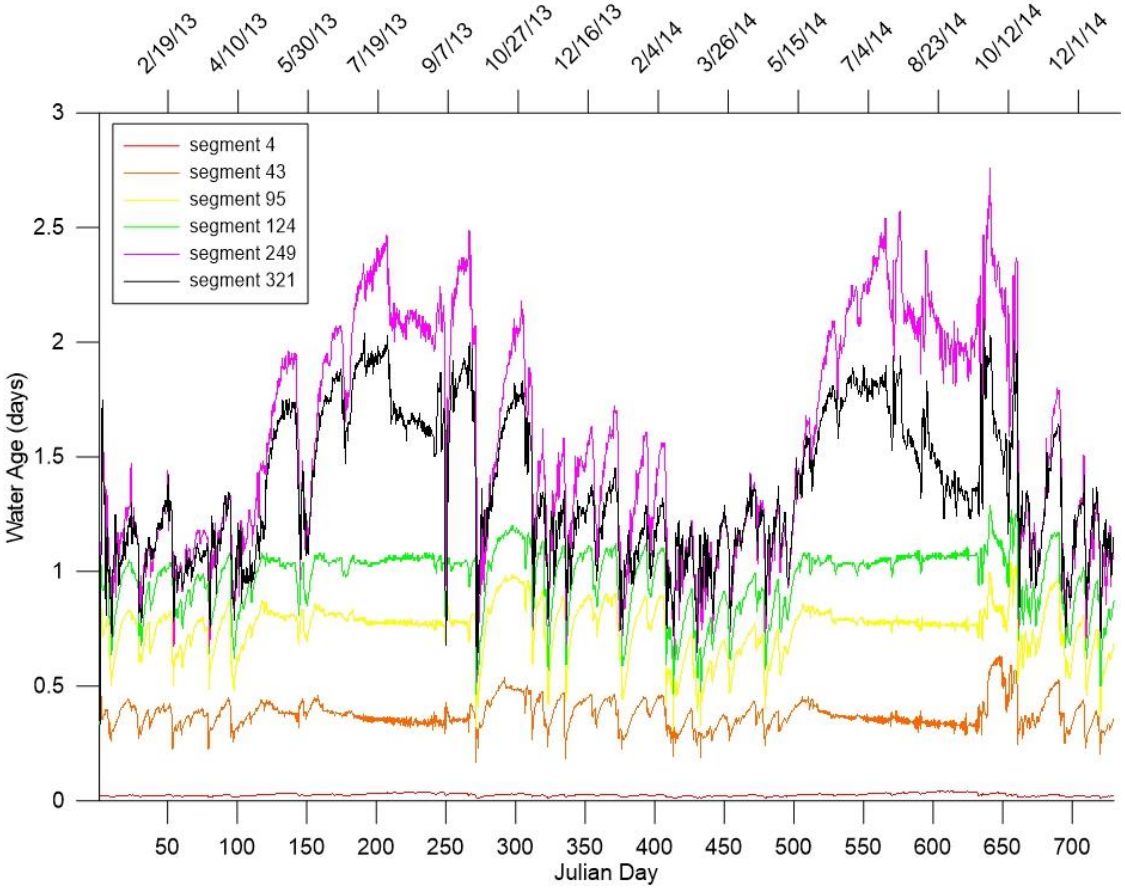

Figure 90. Model-predicted water age throughout the model reach

The mount of mixing taking place in the system was evaluated using TDS. TDS is conservative, so any decrease in concentration can be attributed to dilution. All input TDS values were set to zero except for the upstream boundary, which was set to a constant 100 mg/L throughout the entire model time period. The amount that TDS decreased moving downstream was how much dilution was taking place. Table 21 gives example values of percent mixing at various downstream locations at various times throughout the model simulation. Percent mixing was evaluated as the percent of the difference between the remaining TDS concentration compared to the initial 100 mg/L input at the upstream boundary. Figure 91 shows how TDS and mixing change moving downstream. Generally, mixing increased and TDS concentration decreased moving downstream as more mixing and dilution processes occurred along the channel.

Table 21. Percent mixing at various segments throughout the model at various times during the model simulation

	% Mixing				
Julian Day	Segment 43	Segment 124	Segment 193	Segment 249	Segment 321
1	43	43	43	43	43
31	50.3	60.3	86.9	90.6	94.7

	% Mixing				
Julian Day	Segment 43	Segment 124	Segment 193	Segment 249	Segment 321
61	33.4	61	87.2	88	91.6
91	46.6	57.6	86.2	88.2	90.5
121	49.5	58.9	85.8	90	91.5
151	32.5	51.1	84	87.4	91.4
181	59	68.4	88.1	91.4	93.7
211	77.7	84.6	94.3	95.9	97.5
241	82.2	84.2	94.9	97.1	98.1
271	59.3	69.4	82.3	85.8	91.6
301	50.2	63.9	87.4	90.3	93.1
331	45.8	56.4	86.1	85.9	88.9
361	51.7	61.3	85.9	87.8	92.4
391	52.8	62.4	88.2	88.5	92.9
421	47.8	58	85.8	87.8	91.1
451	62.9	75	91.5	92.5	93.8
481	27.5	38.1	77.3	75.9	83.9
511	54.4	63.9	87.6	90.0	92.2
541	71.7	80.6	90.4	93.5	95.3
571	57.1	74.2	93.3	94.9	97.6
601	81.5	87.6	94.6	96.7	98.1
631	89.4	91.3	96	97.8	99.0
661	24.8	53.1	80.1	84.3	87
691	60.9	57.8	87	88.4	91.8
721	26.3	44.8	77.8	89.5	91.9

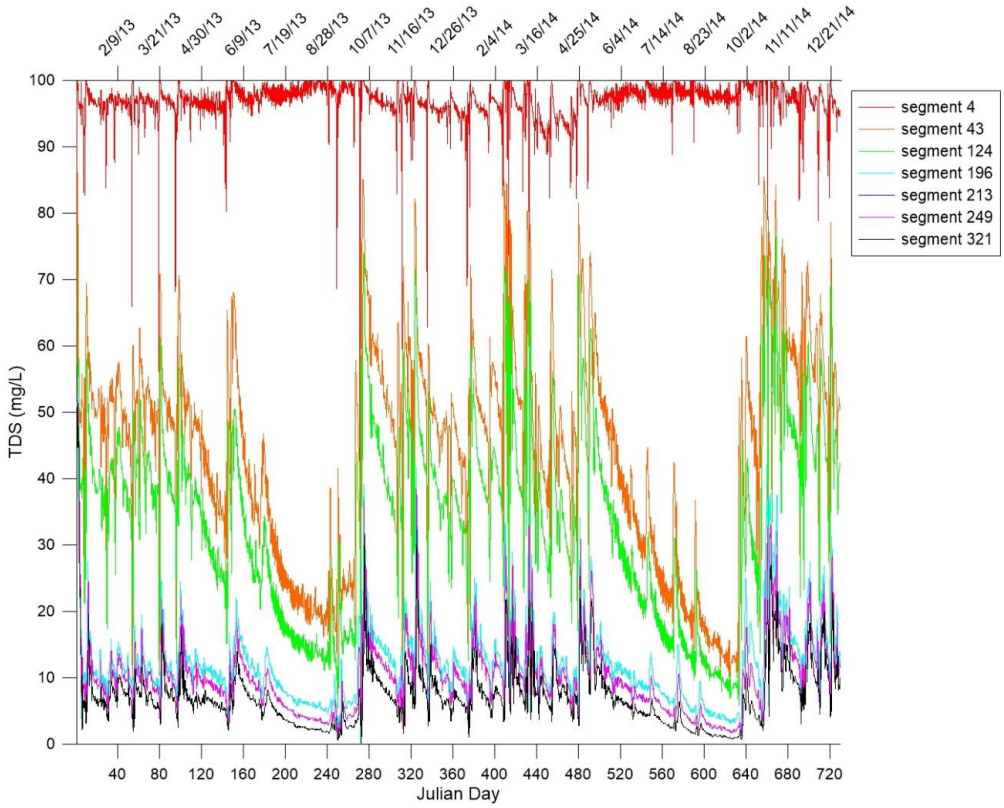

Figure 91. Model-predicted TDS concentrations at various downstream locations after a constant input of 100 mg/L was applied to the upstream boundary

Chehalis Reservoir Footprint Model

Model flow predictions of the footprint model were compared with data measured at USGS Station 2019310 Chehalis River above Mahaffey Creek near Pe Ell, WA. This station is located immediately downstream of the proposed dam site and data were available beginning 5/23/2013. Mean absolute error for flow rate was 2.54 m^3/s (Table 22). For the critical July through September period, mean error was -0.41 m^3/s and the mean absolute error was 0.64 m^3/s (Table 23). Model predictions and data are plotted in Figure 92.

Table 22. Flow rate error statistics for footprint model.

Site	Segment #	# of Data	Mean Error, m^3/s	Mean Absolute Error, m^3/s	Root Mean Square Error, m^3/s
USGS 2019310	112	55467	0.00	2.54	8.61

Table 23. Flow rate error statistics for footprint model during July to September period.

Site	Segment #	# of Data	Mean Error, m^3/s	Mean Absolute Error, m^3/s	Root Mean Square Error, m^3/s
USGS 2019310	112	16822	-0.41	0.64	5.57

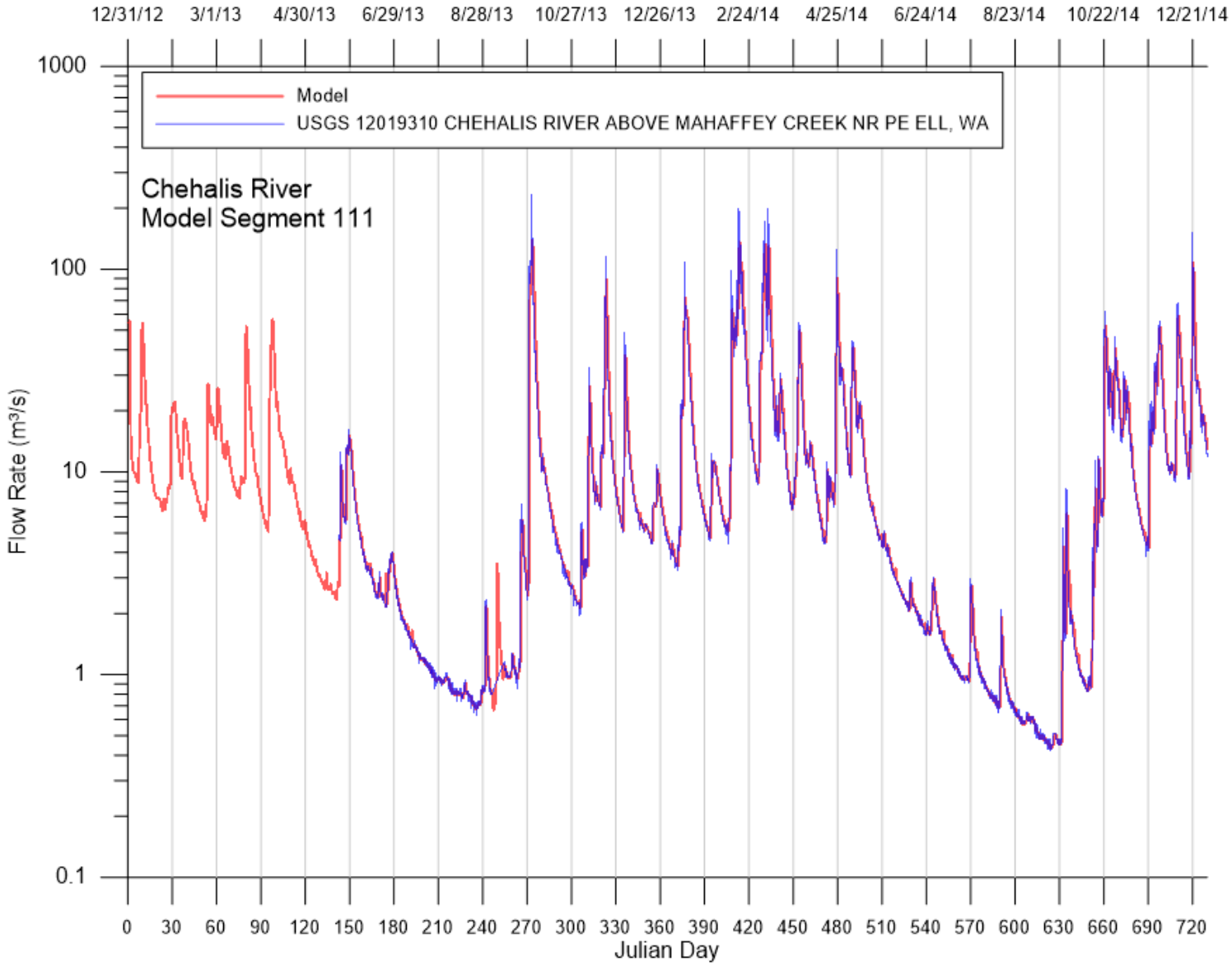

Figure 92. Comparison of model flow predictions and data measure at USGS station 12019310 Chehalis River above Mahaffey Creek near Pe Ell, WA.

Model Calibration: Temperature

Chehalis River Downstream Model

Temperature was highly dependent on water depths and travel time, and hence was calibrated after the flow rate calibration was finalized. Many water quality state variables were temperature dependent, so it was also important to calibrate temperature before water quality. Similar to flow calibration, field temperature data along the mainstem of the Chehalis River were compared to model predictions moving from upstream to downstream. Table 24 lists the continuous temperature stations on the mainstem Chehalis River that were used to compare to model predictions.

Vertical temperature profile data were provided by Anchor QEA (2014). These data were collected at specific dates in the deeper lake-like region of the river near Chehalis and Centralia, WA. Table 25 lists the vertical temperature stations, locations, and dates when data were collected on the Chehalis River.

Figure 93 shows a longitudinal view of the locations of the mainstem continuous and vertical temperature gaging stations and vertical temperature data collection locations along the Chehalis River.

Table 24. Temperature stations on the mainstem Chehalis River used to compare to model predictions

Organization	Station ID	Description	Dates with data	Model Segment	River Mile
WDFW	11-UCH	Upper Chehalis	6/9/14 - 9/15/15	4	108
WDFW	3-UCH	Upper Chehalis Chehalis mainstem	5/15/14 - 9/15/15	12	108
Anchor QEA	CHL-PEL-US	Chehalis Upstream of Pe Ell	7/31/13 - 3/26/14	12	107
Anchor QEA	CHL-PEL-DS	Chehalis Downstream of Pe Ell	7/31/13 - 7/30/14	15	106
WDFW	13-CH	Chehalis mainstem	6/10/14 - 9/15/15	19	105
Anchor QEA	CHL-WOODSTEAD	Chehalis at Woodstead farm 01	7/2/13 - 10/28/13	24	103
WDFW	4-UCH	Upper Chehalis	5/15/14 - 9/15/15	36	102
Anchor QEA	CHL-DOTY	Chehalis at Doty	7/3/13 - 10/16/13	36	101
WADOE	23A160	Chehalis River at Dryad	7/1/13 - 9/18/13, 6/24/14 - 9/23/14, & 5/19/15 - 9/15/15	48	99.5
WDFW	15-CH	Chehalis mainstem	6/10/14 - 10/14/14	47	99
Anchor QEA	CHL-RAINBOW-FALLS	Chehalis at Rainbow Falls	7/2/13 - 10/16/13	50	97.1
WDFW	19-CH	Chehalis mainstem	6/18/14 - 9/2/15	64	95.5
Anchor QEA	CHL-CERES-HILLS	Chehalis at Ceres Hill Road	7/3/13 - 10/16/13	81	90.1
Anchor QEA	CHL-ADNA	Chehalis Near Adna	7/31/13 - 7/21/14	119	81
WDFW	21-CH	Upper Chehalis	6/11/14 – 9/2/15	124	80.6

Organization	Station ID	Description	Dates with data	Model Segment	River Mile
Anchor QEA	CHL-US-NWK	Chehalis Upstream of Newaukum Confluence	7/31/13 - 3/26/14	144	75.4
WDFW	22-CH	Upper Chehalis	6/11/14 - 8/5/15	145	75.3
Darigold WWTP	41	Chehalis River Upstream Darigold WWTP	1/1/13 - 11/30/15	149	74.7
Darigold WWTP	40	Chehalis River Downstream Darigold WWTP	1/1/13 - 11/30/15	150	74.65
WDFW	16-CH	Chehalis mainstem	6/10/14 - 9/3/15	180	66.7
Anchor QEA	CHL-GLV	Chehalis at Galvin Bridge	7/30/13 - 7/21/14	196	64.1
WDFW	17-CH	Chehalis mainstem	6/10/14 – 9/1/15	213	60.1
Anchor QEA	CHL-US-BLK	Chehalis Upstream of Black River	7/30/13 - 7/22/14	238	54.2
WDFW	18-CH	Chehalis mainstem	6/10/14 - 8/26/15	249	50.5
Anchor QEA	CHL-OAK	Chehalis at Oakville	7/30/13 - 7/22/14	287	42.3
WDFW	23-CH	Chehalis mainstem	7/15/14 - 8/17/15	287	41.3
WADOE	23A070	Chehalis River at Porter	10/23/12 - 6/25/13 & 9/18/13 - 5/26/15	321	33.3

Table 25. Mainstem Chehalis River vertical temperature profile collection locations and dates used in temperature calibration

Organization	Station ID	Description	Dates with data	Model Segment
Anchor QEA	CHL-RT6-BR	Chehalis R. at RT6 Bridge at RM 75.31	8/7/13, 9/18/13, & 7/23/14	149
Anchor QEA	HL-14	Chehalis R. at RM	7/31/14	150
Anchor QEA	HL-13	Chehalis R. at RM	7/31/14	153
Anchor QEA	HL-12	Chehalis R. at RM	7/31/14	157
Anchor QEA	HL-11	Chehalis R. at RM	7/31/14	158
Anchor QEA	HL-10	Chehalis R. at RM	7/31/14	160
Anchor QEA	HL-9	Chehalis R. at RM	7/31/14	162
Anchor QEA	HL-8	Chehalis R. at RM	7/31/14	164
Anchor QEA	HL-7	Chehalis R. at RM	7/31/14	166
Anchor QEA	HL-6	Chehalis R. at RM	7/31/14	168
Anchor QEA	HL-5	Chehalis R. at RM	7/31/14	171
Anchor QEA	HL-4	Chehalis R. at RM	7/31/14	173
Anchor QEA	HL-3	Chehalis R. at RM	7/31/14	177
Anchor QEA	HL-2	Chehalis R. at RM	7/31/14	179
Anchor QEA	CHL-US-SKM	Chehalis R. at Mellen Road Bridge	8/7/13, 9/18/13, & 7/23/14	180
Anchor QEA	HL-1	Chehalis R. at RM	7/31/14	181

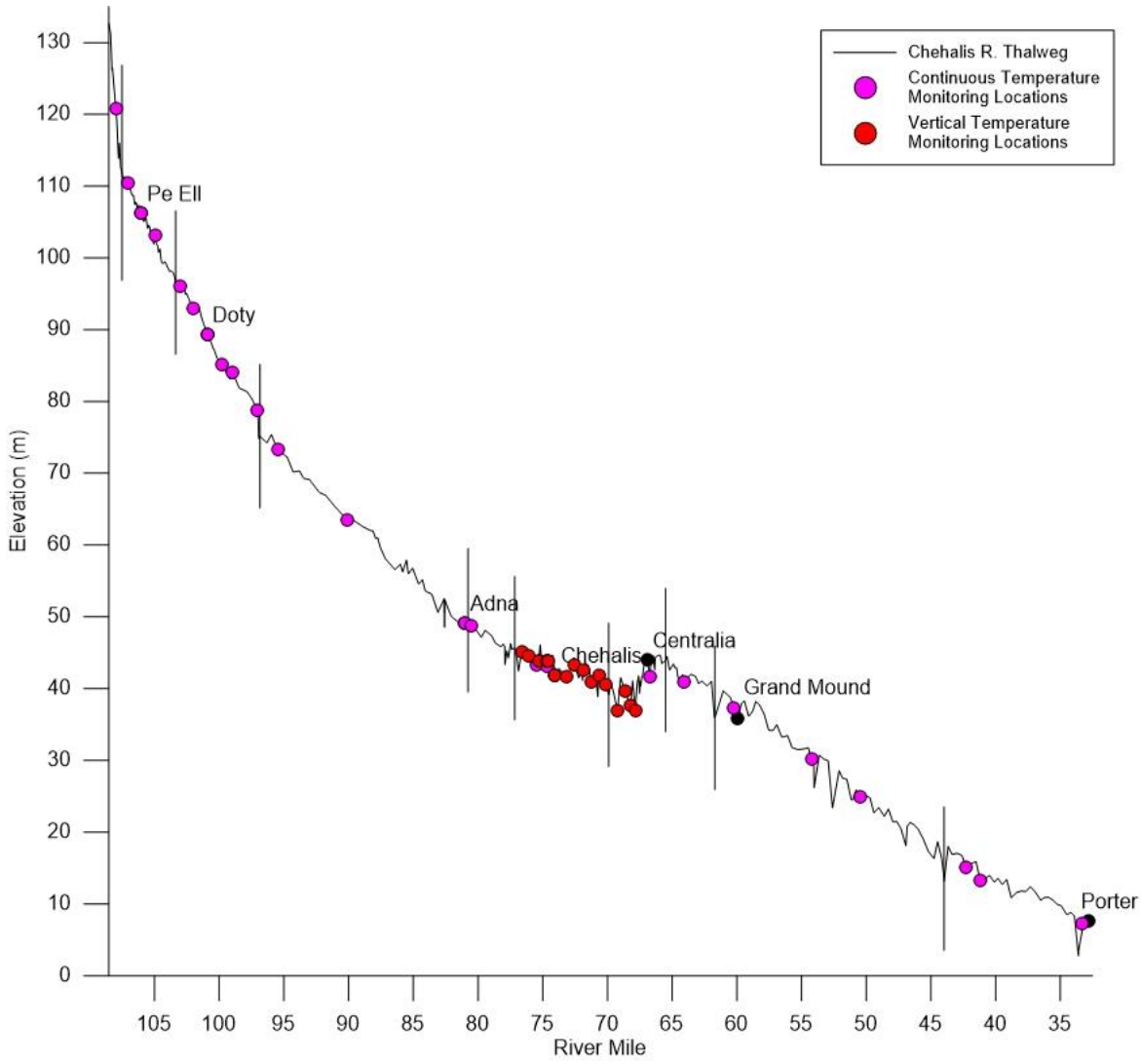

Figure 93. Longitudinal view of the mainstem Chehalis River continuous and vertical temperature gaging stations used for temperature calibration (vertical lines show model branch breaks)

Figure 94 shows model predicted temperature versus field data along the mainstem Chehalis River at the stations: 11-UCH, upstream of Pe Ell, downstream of Pe Ell, station 13-CH, at Woodstead, upstream of Elk Creek, and at Doty mainstem Chehalis River stations. Figure 95 shows model predicted temperature versus field data along the mainstem Chehalis River at the stations: 15-CH, at Dryad, at Rainbow Falls, at station 19-CH, at Ceres Hills Road, and at Adna. Figure 96 shows model predicted temperature versus field data along the mainstem Chehalis River at the stations: 21-CH, near Newaukum Confluence, station 22-CH, upstream of Darigold, downstream of Darigold, upstream of Skookumchuck, and at Galvin Bridge. Figure 97 shows model predicted temperature versus field data along the mainstem Chehalis River at the stations: 17-CH, upstream of Black River, station 18-CH, at Oakville, station 23-CH, and at Porter.

Since daily maximum temperatures are critical for fish habitat, the model predicted daily maximum was compared to daily maximum temperatures at several monitoring locations. Figure 98 shows model predicted daily maximum temperature versus field data along the mainstem Chehalis River at the stations: 11-UCH, upstream of Pe Ell, downstream of Pe Ell, 13-CH, at Woodstead, upstream of Elk Creek, and at Doty. Figure 99 shows model predicted daily maximum temperature versus field data along the mainstem Chehalis River at the stations: 15-CH, at Dryad,

at Rainbow Falls, 19-CH, at Ceres Hills Road, and at Adna. Figure 100 shows model predicted daily maximum temperature versus field data along the mainstem Chehalis River at the stations: 21-CH, near Newaukum Confluence, 22-CH, upstream of Darigold, downstream of Darigold, and upstream of Skookumchuck. Figure 101 shows model predicted daily maximum temperature versus field data along the mainstem Chehalis River at the stations: at Galvin Bridge, 17-CH, upstream of Black River, 18-CH, at Oakville, 23-CH, and at Porter.

Figure 102 shows the model predicted vertical temperature profiles versus field data at the stations: at Route 6 Bridge, HL-14, and HL-13. Figure 103 shows the model predicted vertical temperature profiles versus field data at the stations: HL-12, HL-11, HL-10, HL-9, and HL-8. Figure 104 shows the model predicted vertical temperature profiles versus field data at the stations: HL-7, HL-6, HL-5, HL-4, and HL-3. Figure 105 shows the model predicted vertical temperature profiles versus field data at the stations: HL-2, Mellen Road Bridge, and HL-1.

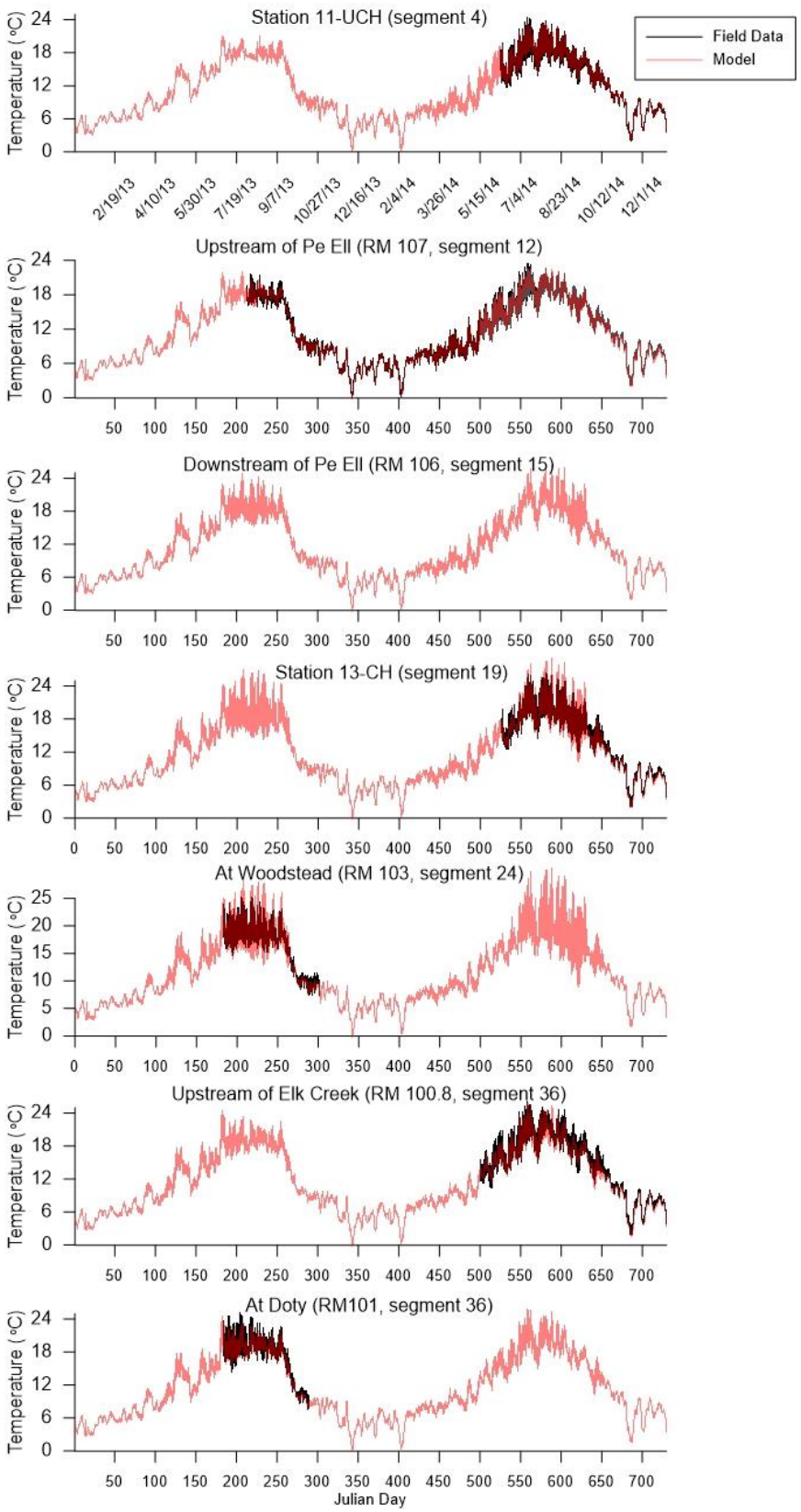

Figure 94. Model temperature predictions compared to field data at the mainstem Chehalis River stations: 11-UCH, upstream of Pe Ell, downstream of Pe Ell, station 13-CH, at Woodstead, upstream of Elk Creek, and at Doty.

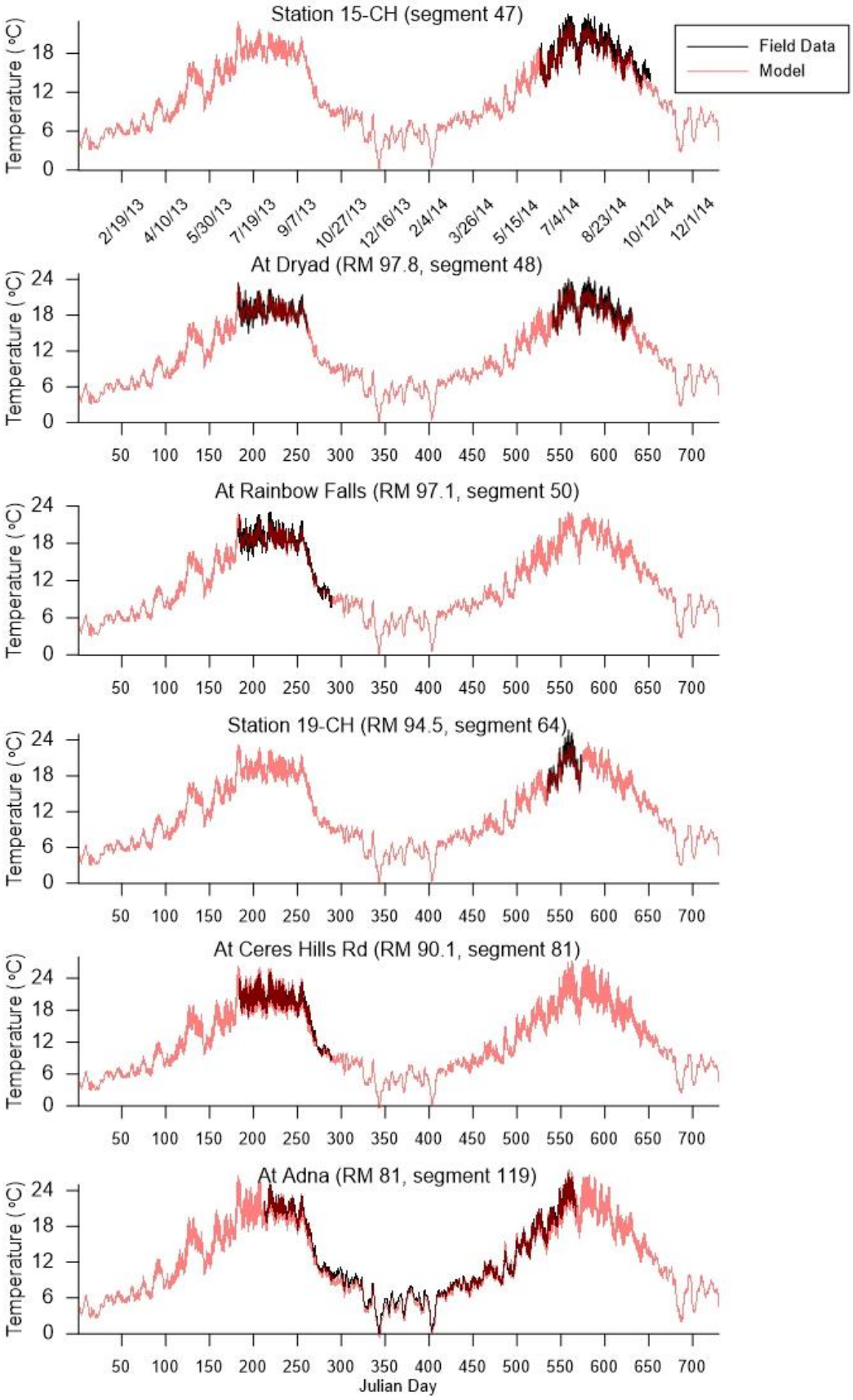

Figure 95. Model temperature predictions compared to field data at the mainstem Chehalis River stations: 15-CH, at Dryad, at Rainbow Falls, at station 19-CH, at Ceres Hills Road, and at Adna.

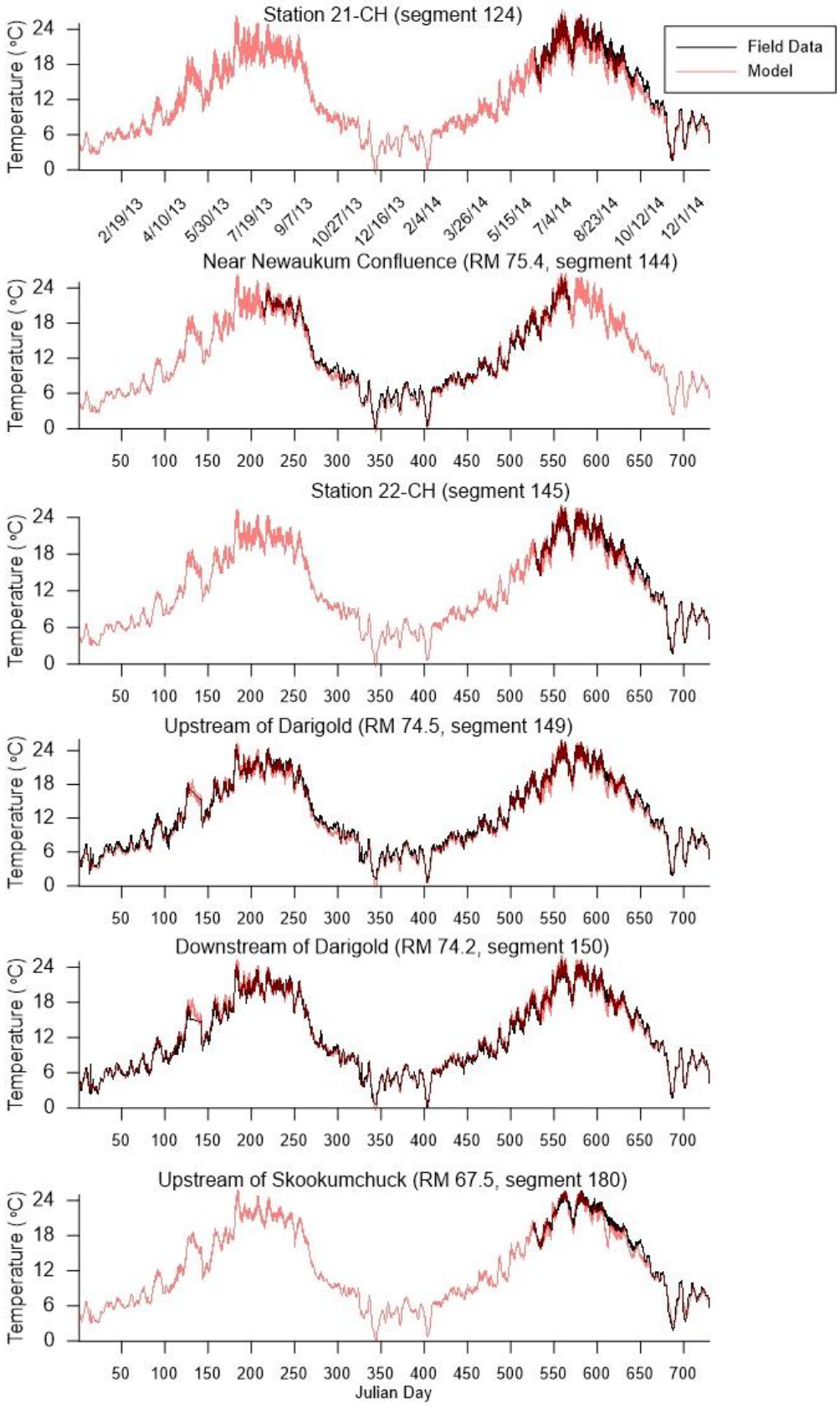

Figure 96. Model temperature predictions compared to field data at the mainstem Chehalis River stations: 21-CH, near Newaukum Confluence, station 22-CH, upstream of Darigold, downstream of Darigold, upstream of Skookumchuck, and at Galvin Bridge.

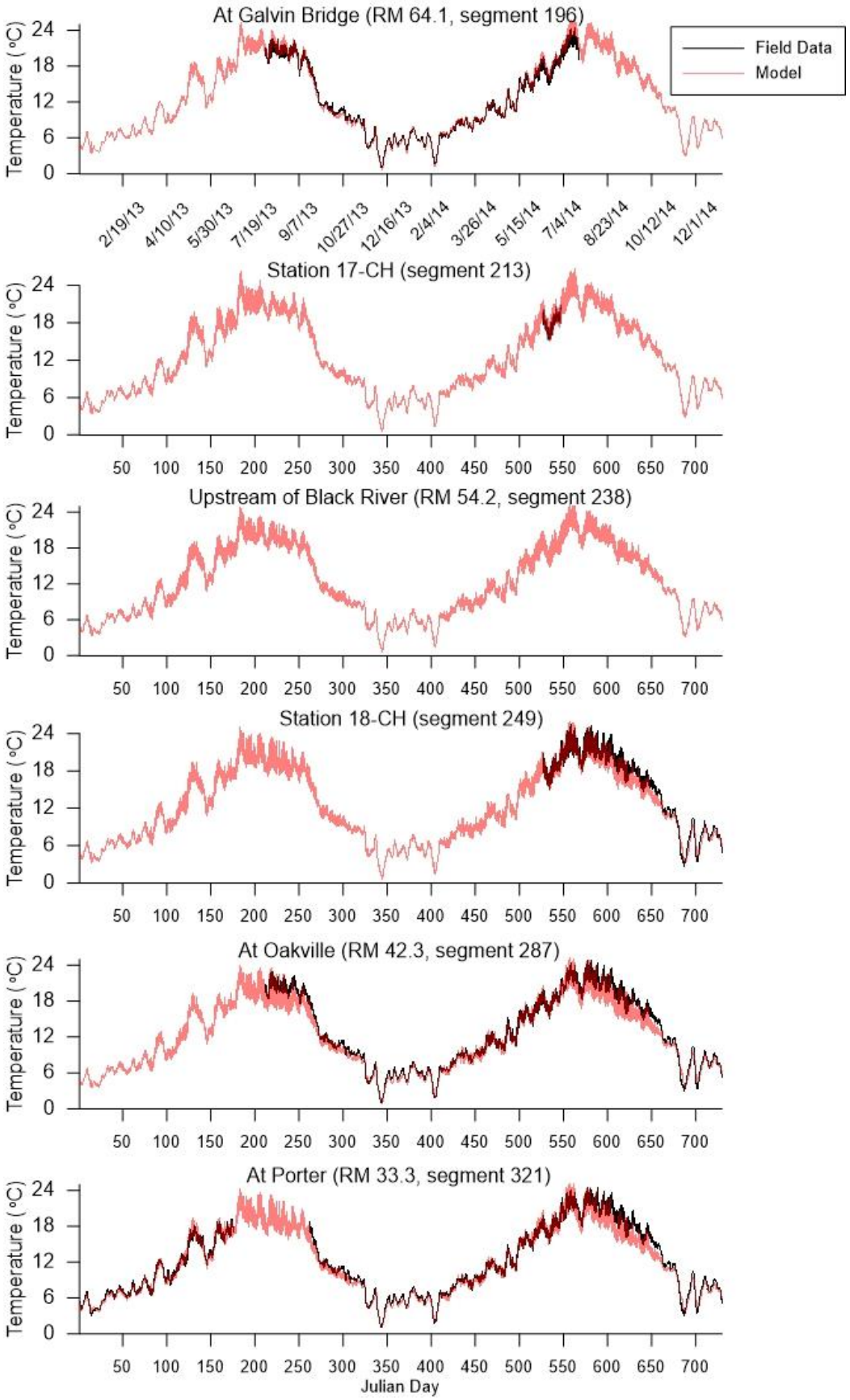

Figure 97. Model temperature outputs versus field data collected at the mainstem Chehalis River stations: 17-CH, upstream of Black River, station 18-CH, at Oakville, station 23-CH, and at Porter.

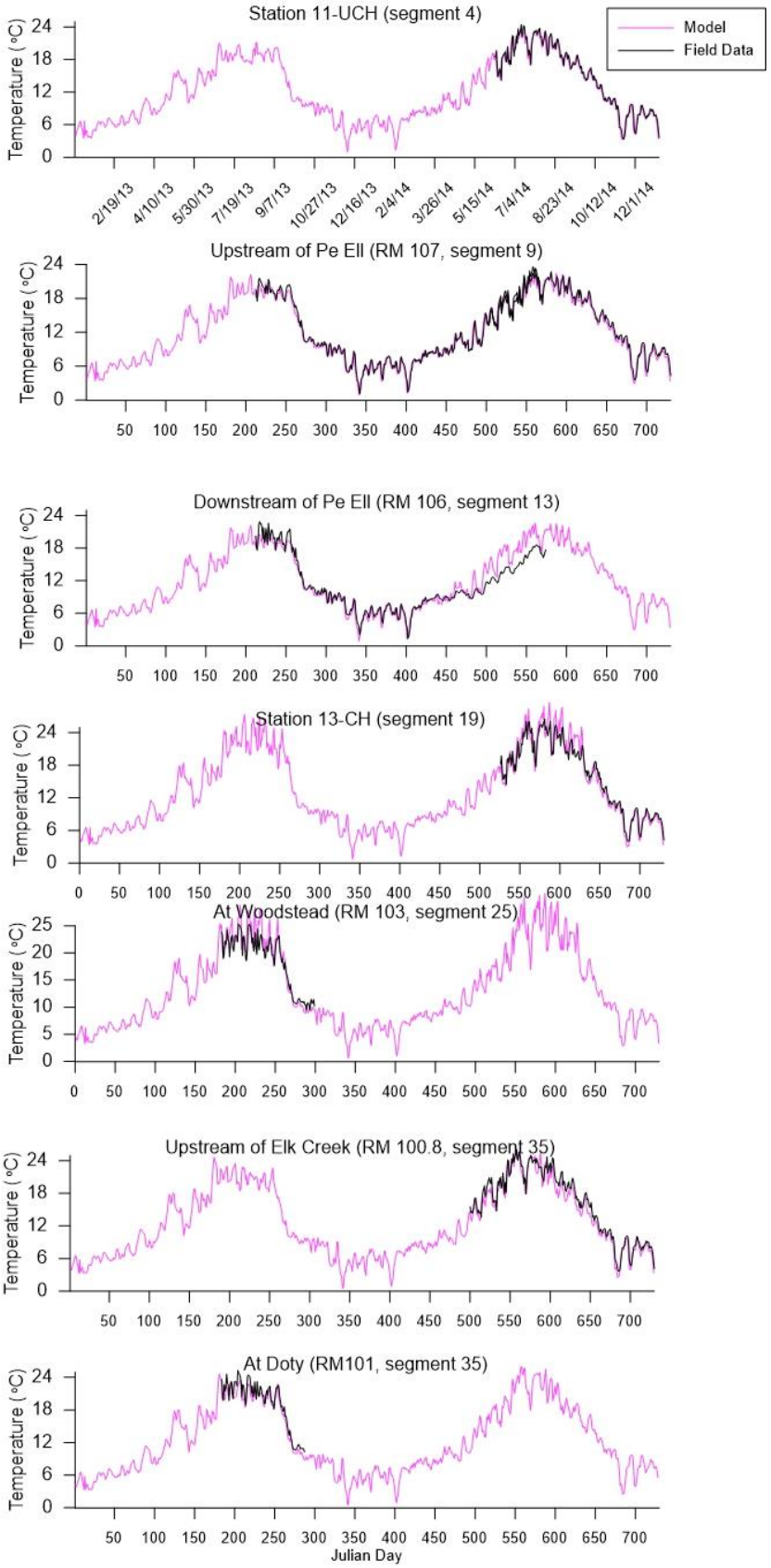

Figure 98. Model predictions of daily maximum temperatures compared to field data at the mainstem Chehalis River stations: 11-UCH, upstream of Pe Ell, downstream of Pe Ell, 13-CH, at Woodstead, upstream of Elk Creek, and at Doty

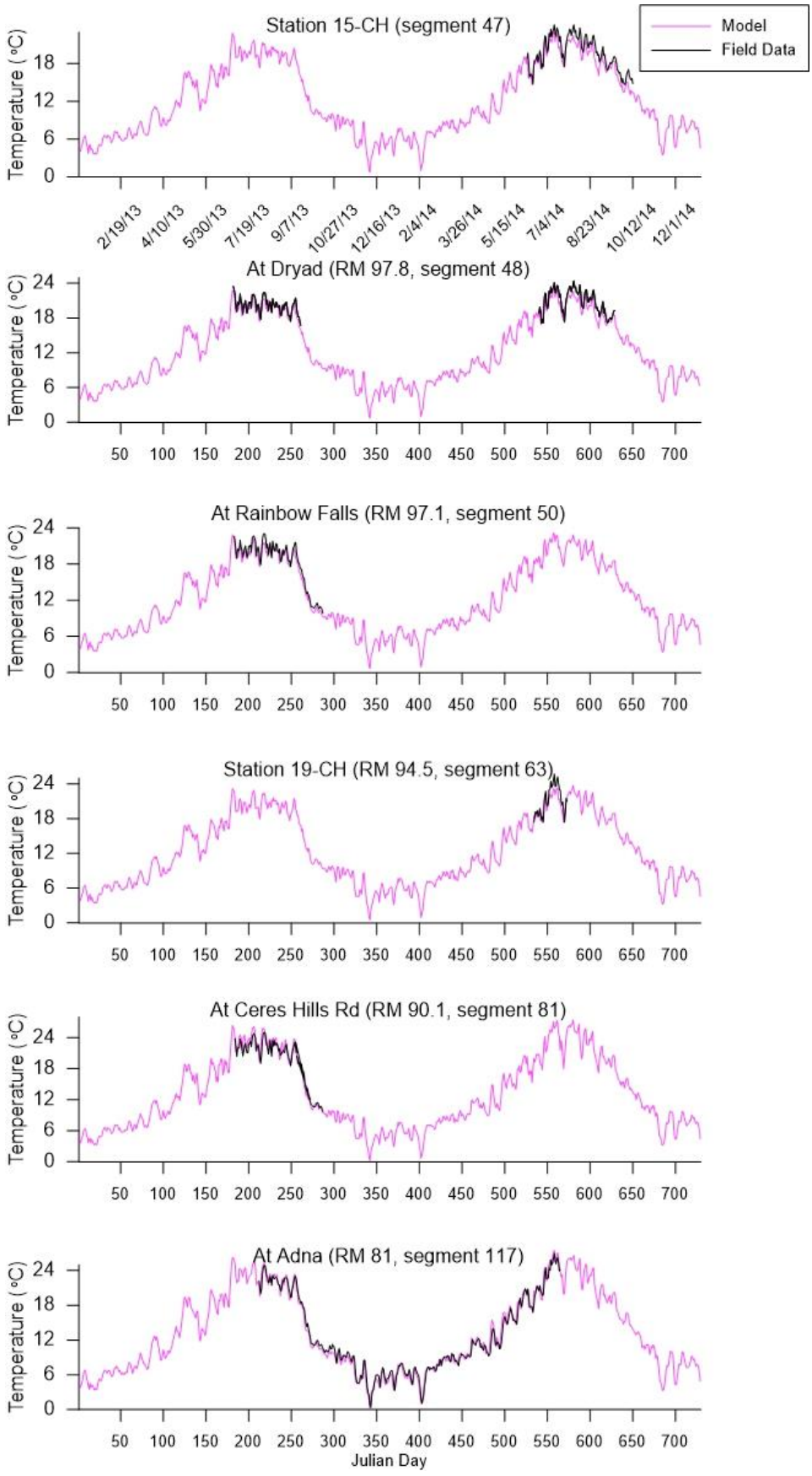

Figure 99. Model predictions of daily maximum temperatures compared to field data at the mainstem Chehalis River stations: 15-CH, at Dryad, at Rainbow Falls, 19-CH, at Ceres Hills Road, and at Adna

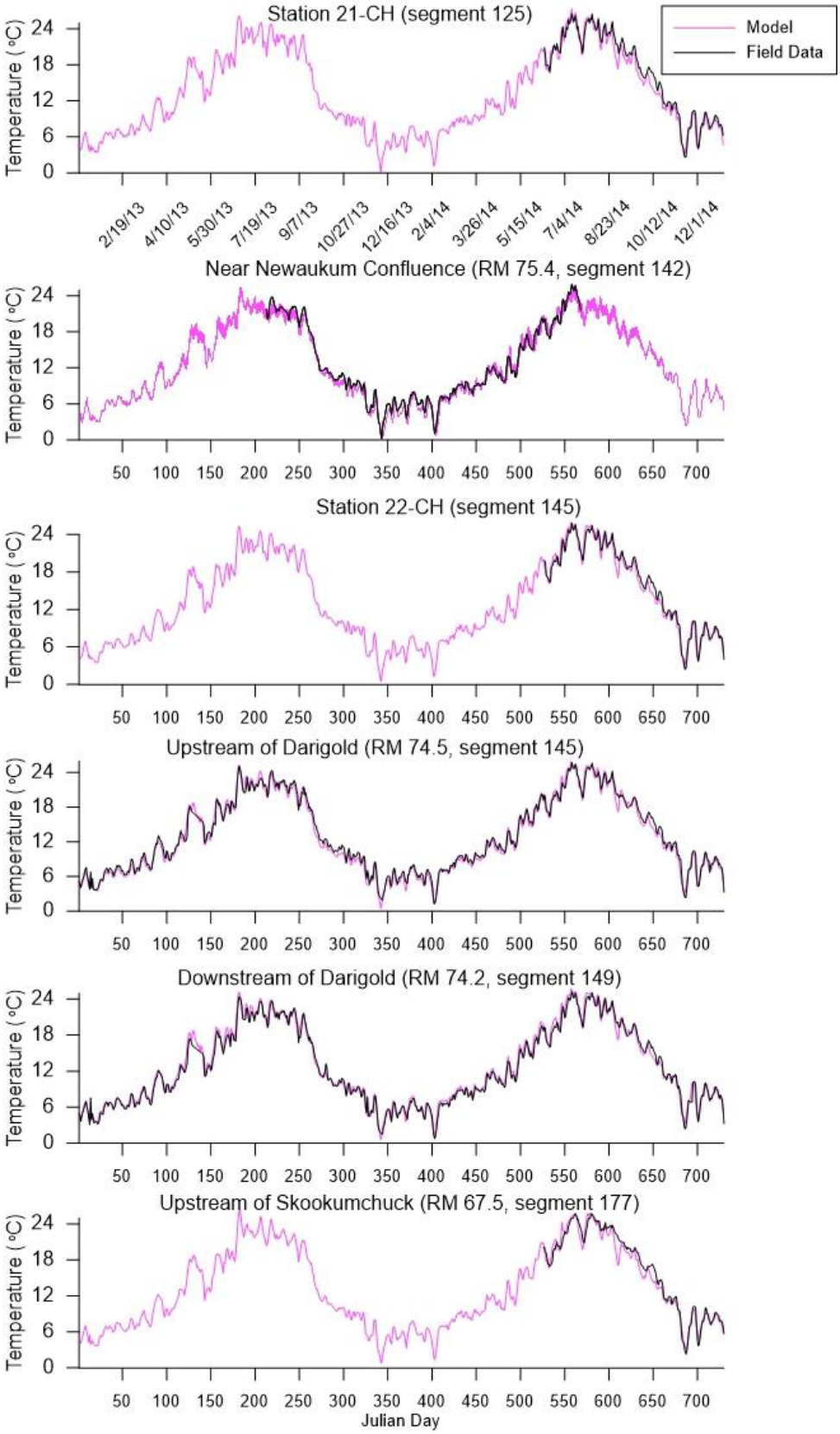

Figure 100. Model predictions of daily maximum temperatures compared to field data at the mainstem Chehalis River stations: 21-CH, near Newaukum Confluence, 22-CH, upstream of Darigold, downstream of Darigold, and upstream of Skookumchuck

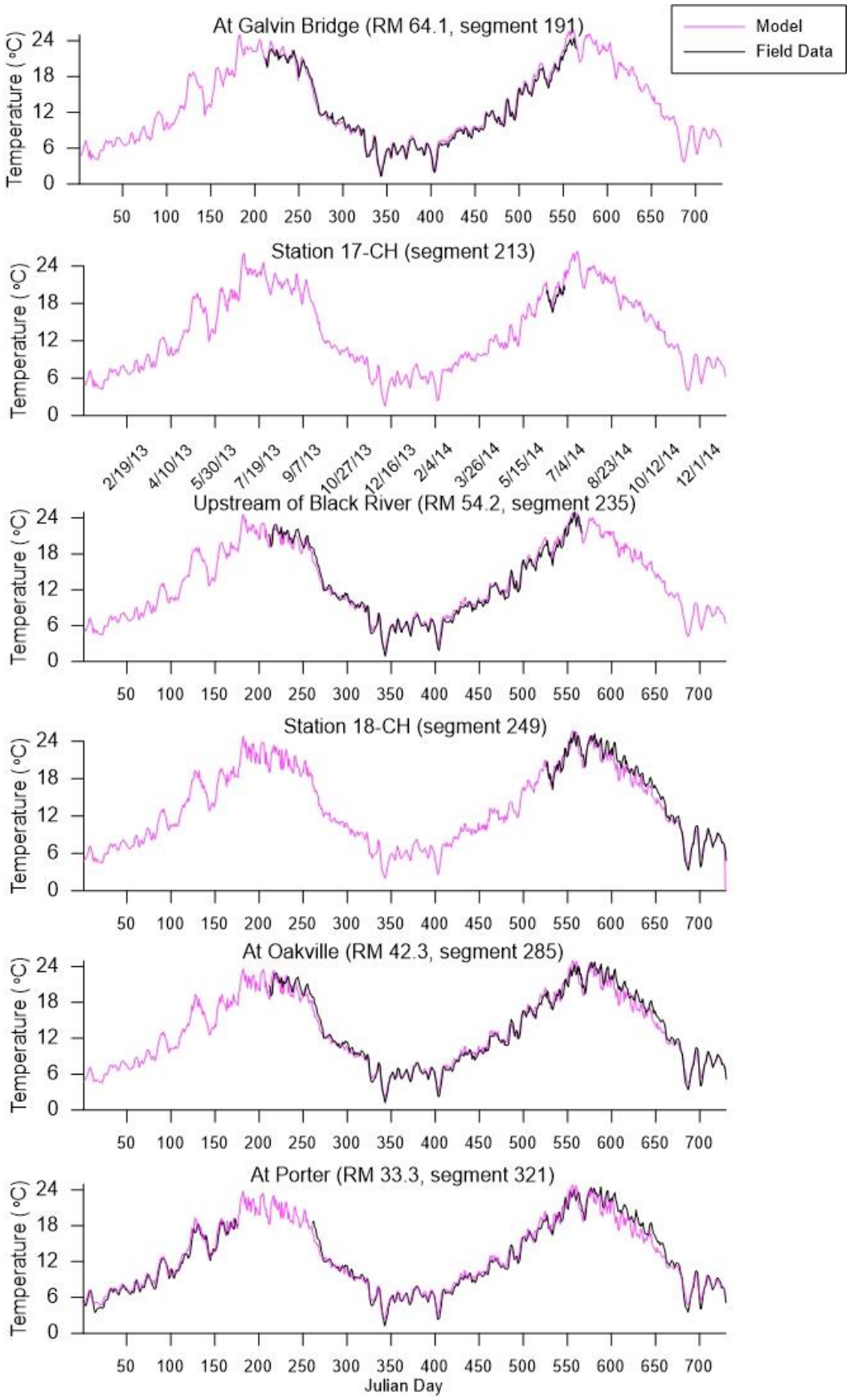

Figure 101. Model predictions of daily maximum temperatures compared to field data at the mainstem Chehalis River stations: at Galvin Bridge, 17-CH, upstream of Black River, 18-CH, at Oakville, and at Porter

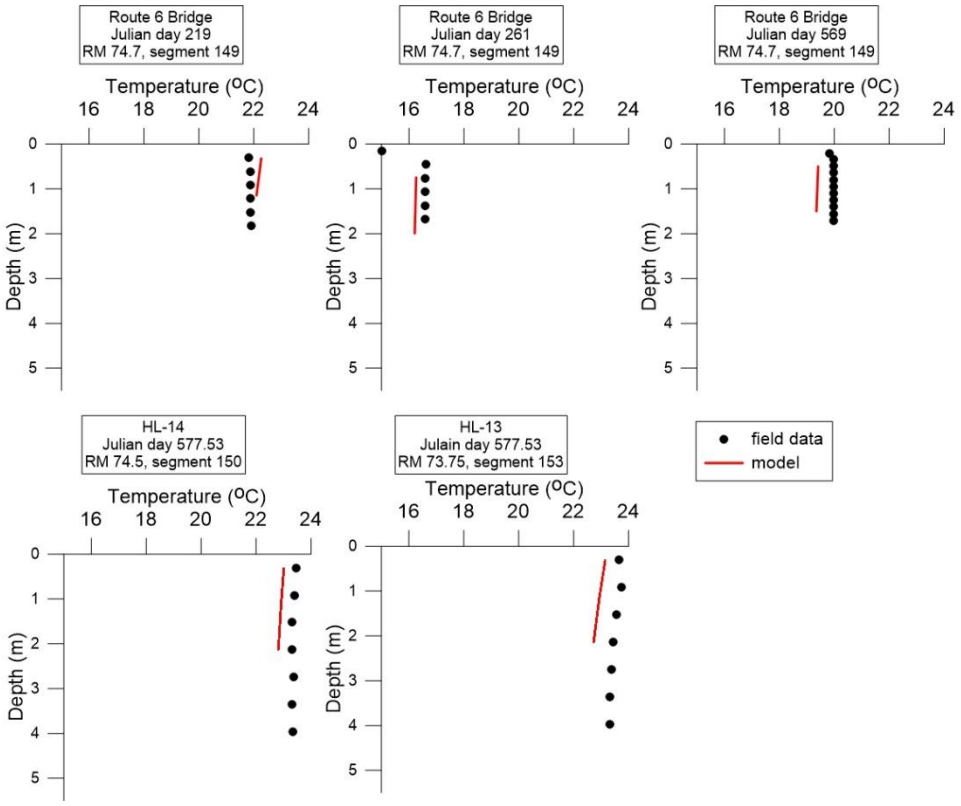

Figure 102. Model versus field data vertical temperature profiles at the mainstem Chehalis River stations: at Route 6 Bridge, HL-14, and HL-13

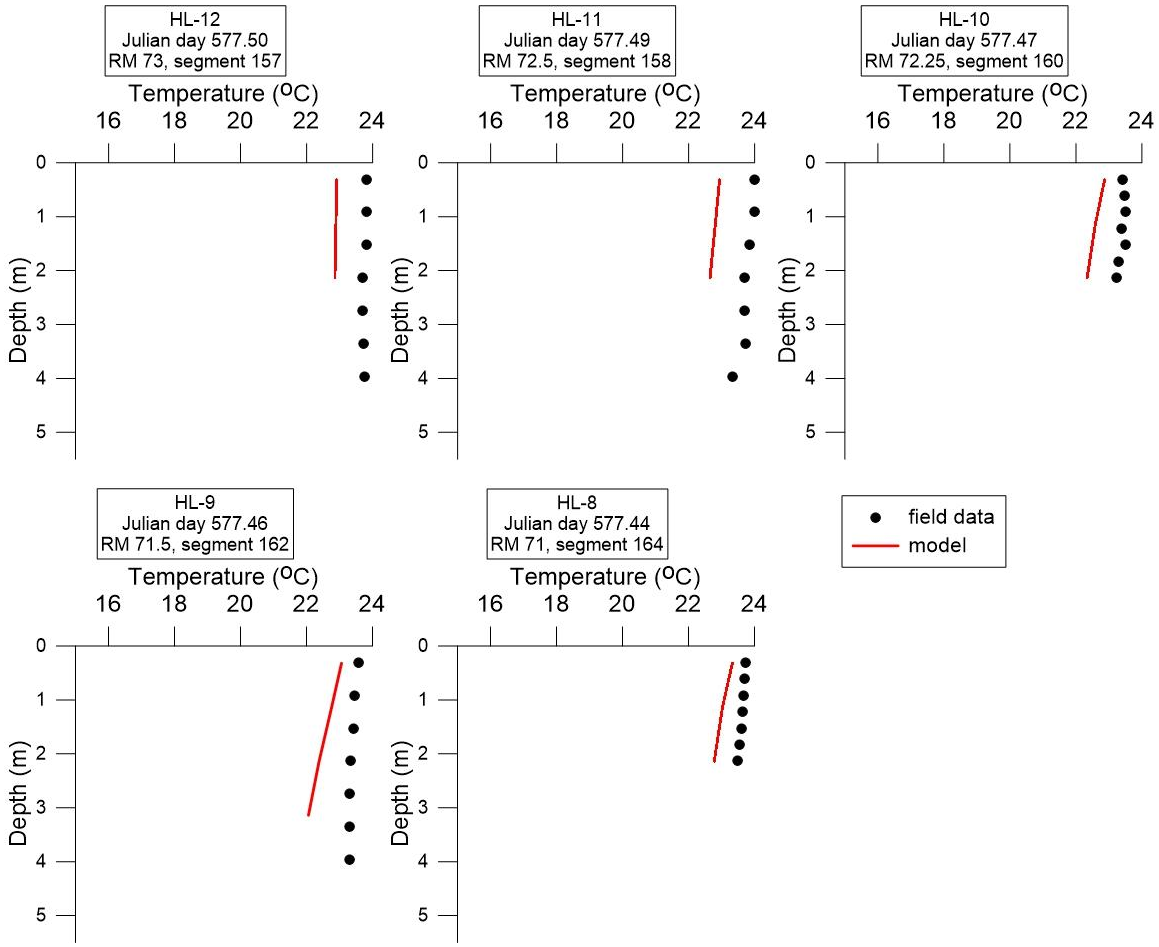

Figure 103. Model versus field data vertical temperature profiles at the mainstem Chehalis River stations: HL-12, HL-11, HL-10, HL-9, and HL-8

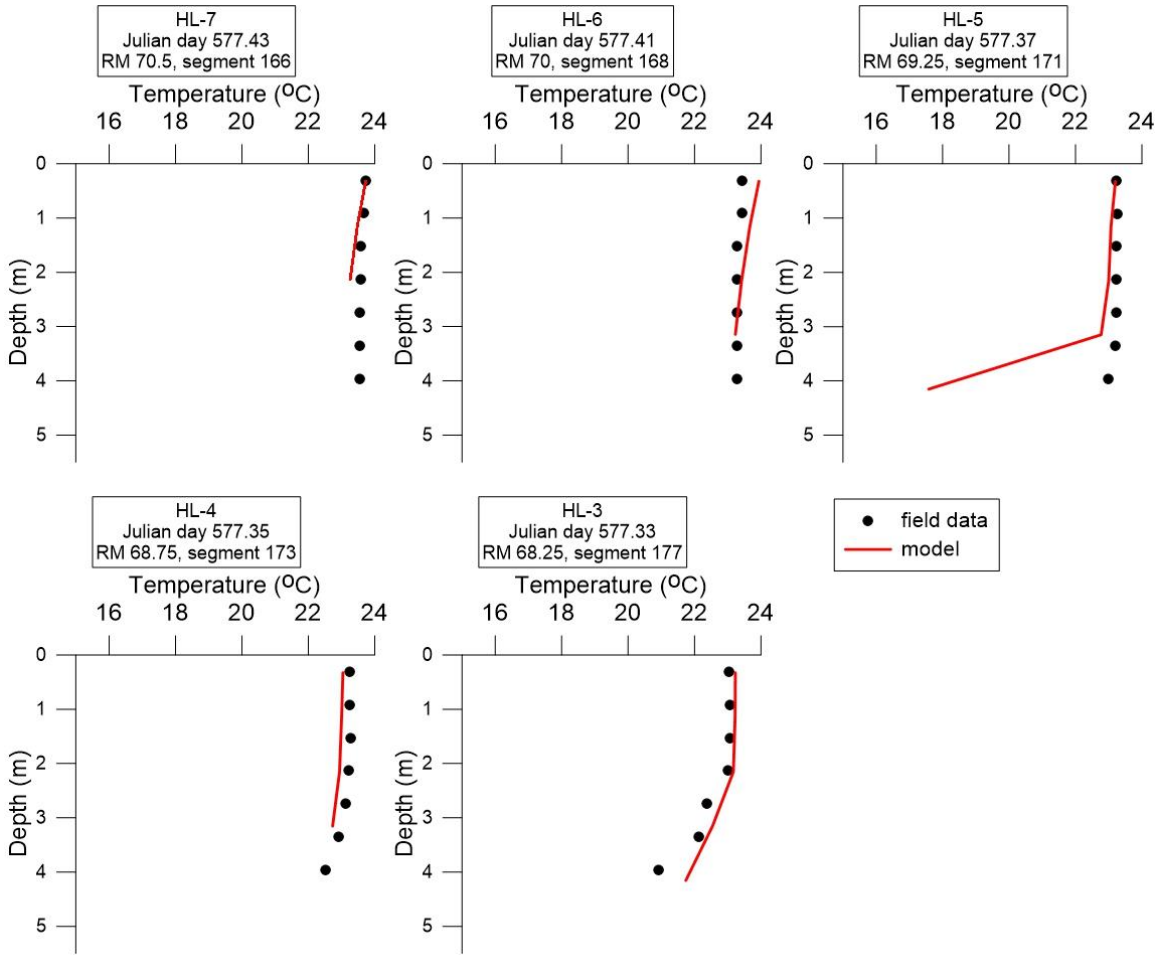

Figure 104. Model versus field data vertical temperature profiles at the mainstem Chehalis River stations: HL-7, HL-6, HL-5, HL-4, and HL-3

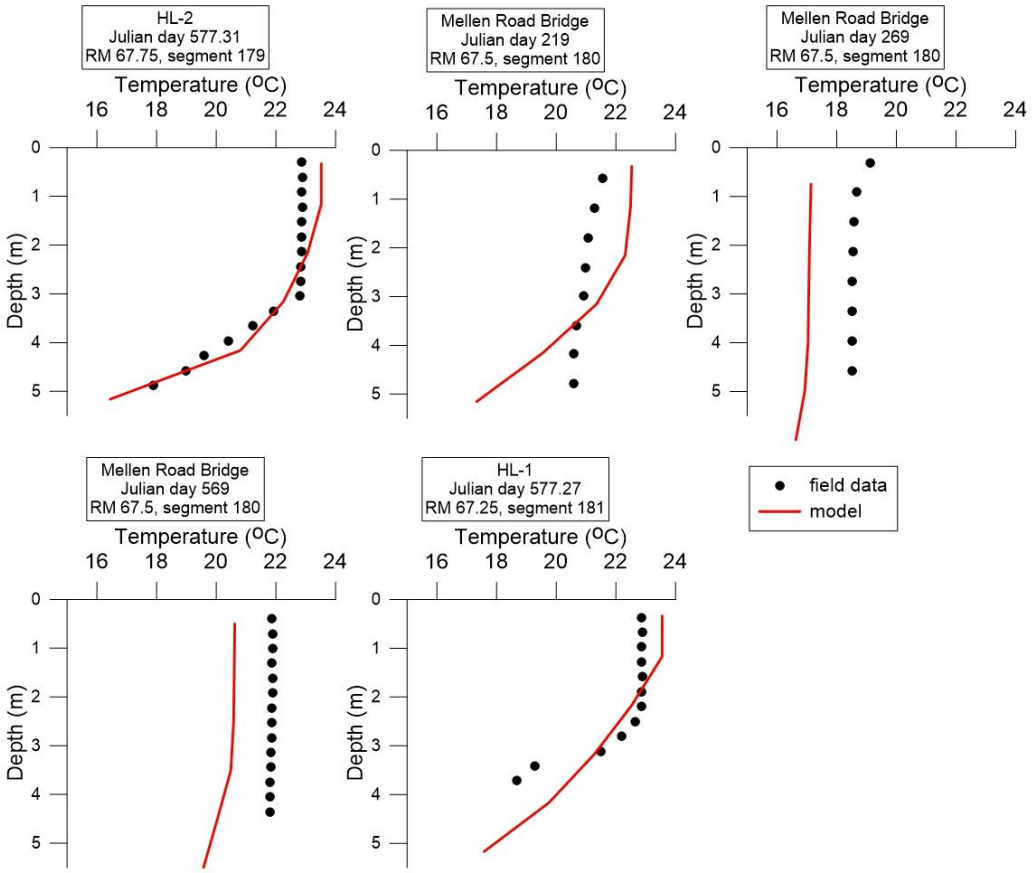

Figure 105. Model versus field data vertical temperature profiles at the mainstem Chehalis River stations: HL-2, Mellen Road Bridge, and HL-1

Error Statistics

The closeness of model predicted temperature to field data was evaluated with error statistics, following the same procedure as with flow. Weighted average mean error, absolute mean error, and root mean square error values were computed using

$$ME_{weighted} = \frac{\Sigma(ME \times N)}{\Sigma N}$$

$$AME_{weighted} = \frac{\Sigma(AME \times N)}{\Sigma N}$$

$$RMSE_{weighted} = \frac{\Sigma(RMSE \times N)}{\Sigma N}$$

Table 26 shows error statistics for model predicted temperature values compared to field data at stations along the mainstem Chehalis River ranging between upstream of Pe Ell and Porter, WA. The error statistics for comparisons of model predicted daily maximum temperatures to field data is shown in Table 27. The model is continuously improving, and as such these results are current, though not final. The current results show the model was generally too cold at most locations, especially during the summer months.

Table 26. Error statistics for temperature comparisons between model predictions and field data along the mainstem Chehalis River ranging between upstream of Pe Ell and Porter, WA

Location	Number of Model-Data Comparisons	Mean Error (°C)	Absolute Mean Error (°C)	Root Mean Square Error (°C)
11-UCH	9814	0.094	0.264	0.449
Upstream Pe Ell	17051	0.010	0.420	0.677
Upstream of Pe Ell as well	11011	-0.058	0.538	0.663
Downstream Pe Ell	17486	0.158	0.857	1.26
Station 13-CH	9769	-0.319	1.04	1.48
At Woodstead	11372	-0.099	1.12	1.49
At Doty	10107	-0.179	0.846	1.14
Upstream Elk Creek	11009	-0.382	0.762	0.988
Station 15-CH	6036	-0.725	0.818	0.994
At Dryad	8166	-0.354	0.643	0.793
At Rainbow Falls	30619	-0.179	0.555	0.682
Between Rainbow Falls and Ceres Hills Road	1876	-0.390	0.588	0.781
At Ceres Hills Road	10113	-0.377	0.736	0.870
At Adna	17043	-0.347	0.584	0.731
Station 21-CH	13430	-0.691	0.936	1.16
Upstream of Newaukum	17082	-0.232	0.601	0.750
Station 22-CH	9713	-0.430	0.667	0.849
Upstream of Darigold	60920	-0.321	0.533	0.666
Downstream of Darigold	64513	0.196	0.480	0.606
Upstream Skookumchuck	9769	-0.425	0.825	1.01
At Galvin Bridge	17090	0.203	0.407	0.548
Station 17-CH	984	0.260	0.659	0.809
Upstream Black River	17142	-0.072	0.542	0.725
Station 18-CH	9762	-0.664	1.07	1.33
At Oakville	16894	-0.305	0.682	0.977
Near Oakville	8084	-0.874	1.21	1.52
At Porter	30909	-0.140	0.693	0.998
Weighted Average Error statistics:		-0.177	0.641	0.841

Table 27. Error statistics for daily maximum temperature comparisons between model predictions and field data along the mainstem Chehalis River ranging between upstream of Pe Ell and Porter, WA

Location	Number of Model-Data Comparisons	Mean Error (°C)	Absolute Mean Error (°C)	Root Mean Square Error (°C)
11-UCH	204	-0.199	0.742	0.988
Upstream Pe Ell	354	-0.239	0.692	0.872

Location	Number of Model-Data Comparisons	Mean Error (°C)	Absolute Mean Error (°C)	Root Mean Square Error (°C)
Upstream of Pe Ell as well	229	-0.281	0.748	0.966
Downstream Pe Ell	362	0.733	1.31	1.94
Station 13-CH	202	0.079	1.37	1.74
At Woodstead	116	0.673	1.63	2.09
At Doty	103	-0.940	1.08	1.32
Upstream Elk Creek	229	-0.882	1.13	1.35
Station 15-CH	124	-1.07	1.22	1.46
At Dryad	169	-0.767	0.987	1.22
At Rainbow Falls	104	-0.697	0.877	1.07
Between Rainbow Falls and Ceres Hills Road	40	-0.799	1.24	1.43
At Ceres Hills Road	107	0.267	1.01	1.27
At Adna	353	-0.039	0.664	0.851
Station 21-CH	202	-0.567	0.924	1.17
Upstream of Newaukum	356	-0.147	0.596	0.737
Station 22-CH	202	-0.277	0.769	0.967
Upstream of Darigold	707	-0.306	0.643	0.804
Downstream of Darigold	704	0.195	0.572	0.771
Upstream Skookumchuck	203	-0.418	0.900	1.19
At Galvin Bridge	354	0.221	0.627	0.782
Station 17-CH	22	0.916	1.19	1.40
Upstream Black River	355	0.130	0.686	0.875
Station 18-CH	203	-0.548	1.00	1.30
At Oakville	351	-0.021	0.730	0.957
Near Oakville	168	-0.645	1.07	1.37
At Porter	644	0.002	0.769	1.056
Weighted Average Error statistics:		-0.132	0.823	1.07

Flow and Water Level

Flow volumes, depth, and timing were important to temperature calibration, so it was important that flow and water level calibration was as accurate as possible. Areas that were too shallow were often too warm and areas that were too deep were often too cool. Accurate depth predictions were necessary for capturing stratification dynamics. Travel time through the system was important, as water that moved slowly had more time to heat up, while water that moved through the system more quickly had less time to absorb solar radiation.

Updates to regression relationships decreased the amount of flow input from tributaries to the system during low flow periods. Often the tributary flows were very cold. By reducing these flows the temperature increased during the summer season.

Bathymetry

Channel Friction and Slope

Similarly to flow calibration, channel friction and slope impacted the timing of peak temperature values. The timing and magnitude of temperature was important for calibration in order to describe the temperature variation.

Segment Widths and Depths

Ensuring the widths of the segment layers were realistic was also important for temperature calibration. Since widths were calculated through interpolation and averaging of field data to model segment locations, it was important to hand check many cross sections and ensure that field data and model estimates of segment geometry were similar. Unrealistic layer widths impacted water depths and temperature. This was especially important for the vertical temperature profiles and continuous monitoring stations during the low flow summer months. Sometimes narrow segment widths caused the water to be deep, so that diurnal temperature swings were not as large as seen in field data. Or conversely, sometimes wide segment widths resulted in shallow water that had diurnal swings in temperature greater than field data showed. Figure 106 shows how widening the lower layers in the bathymetry around the stations at Dryad and Rainbow Falls decreased water depths and resulted in temperature values closer to field data during the summer of 2013.

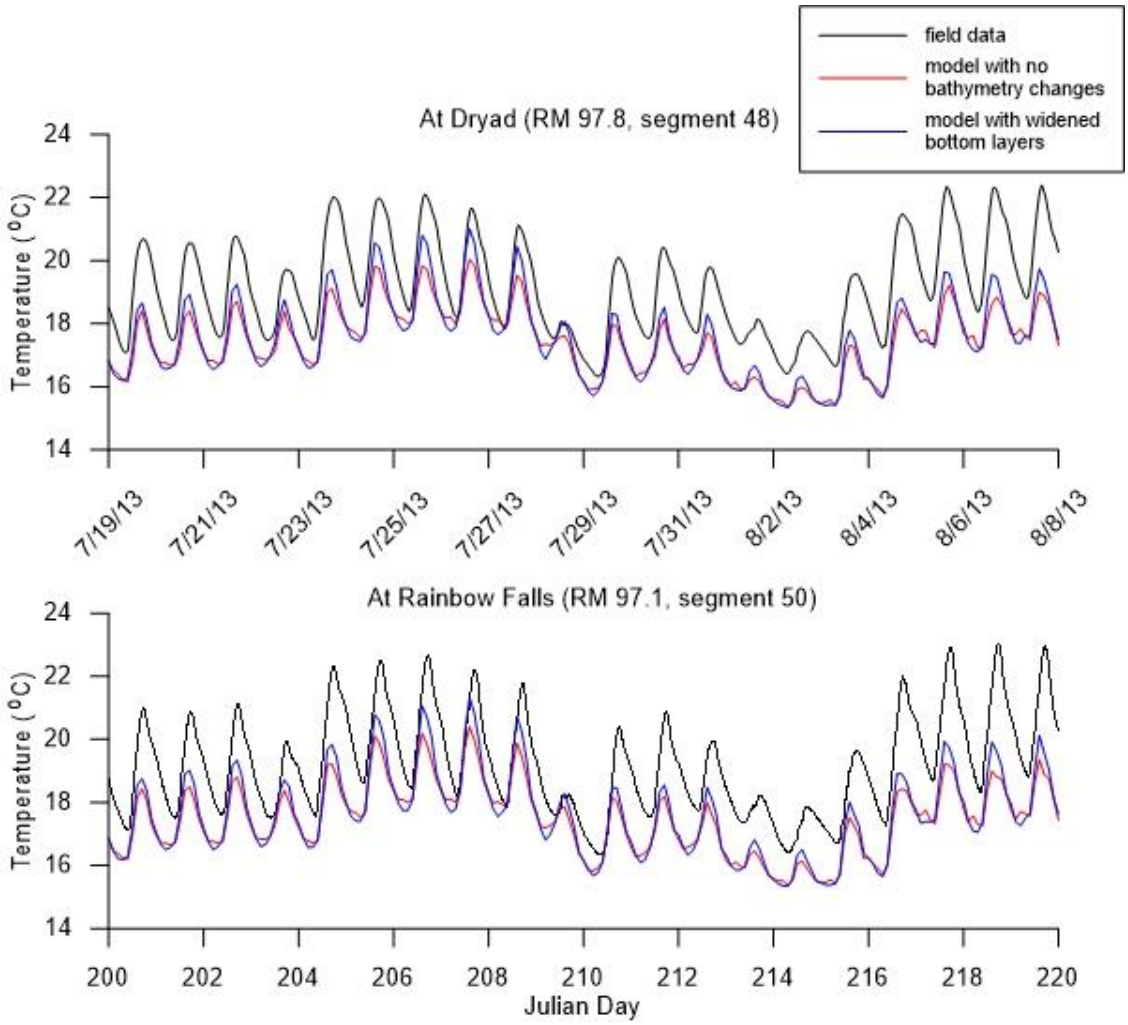

Figure 106. Comparison of model versus field data at Dryad and Rainbow Falls before and after bathymetry segment width changes were made

Boundary Condition Temperature

Accurate input temperature values were important for temperature calibration. Ensuring field data quality and using appropriate temperature estimation techniques was important to this process, especially since so many tributaries lacked temperature field data. For example, the Newaukum River was originally used to create regression relationships to estimate missing tributary data. However, this tributary followed different trends than other tributaries with the timing of peak and minimum temperatures. This lead to poor results when comparing model temperature predictions to field data. Choosing a different temperature gage on the mainstem Chehalis River produced a vast improvement to temperature results. Figure 107 shows the sensitivity of the model to boundary tributary temperature inputs, giving very different results when regression to the Newaukum River data set was used to estimate missing tributary temperature data versus regression to the Chehalis River Downstream of Darigold WWTP data set.

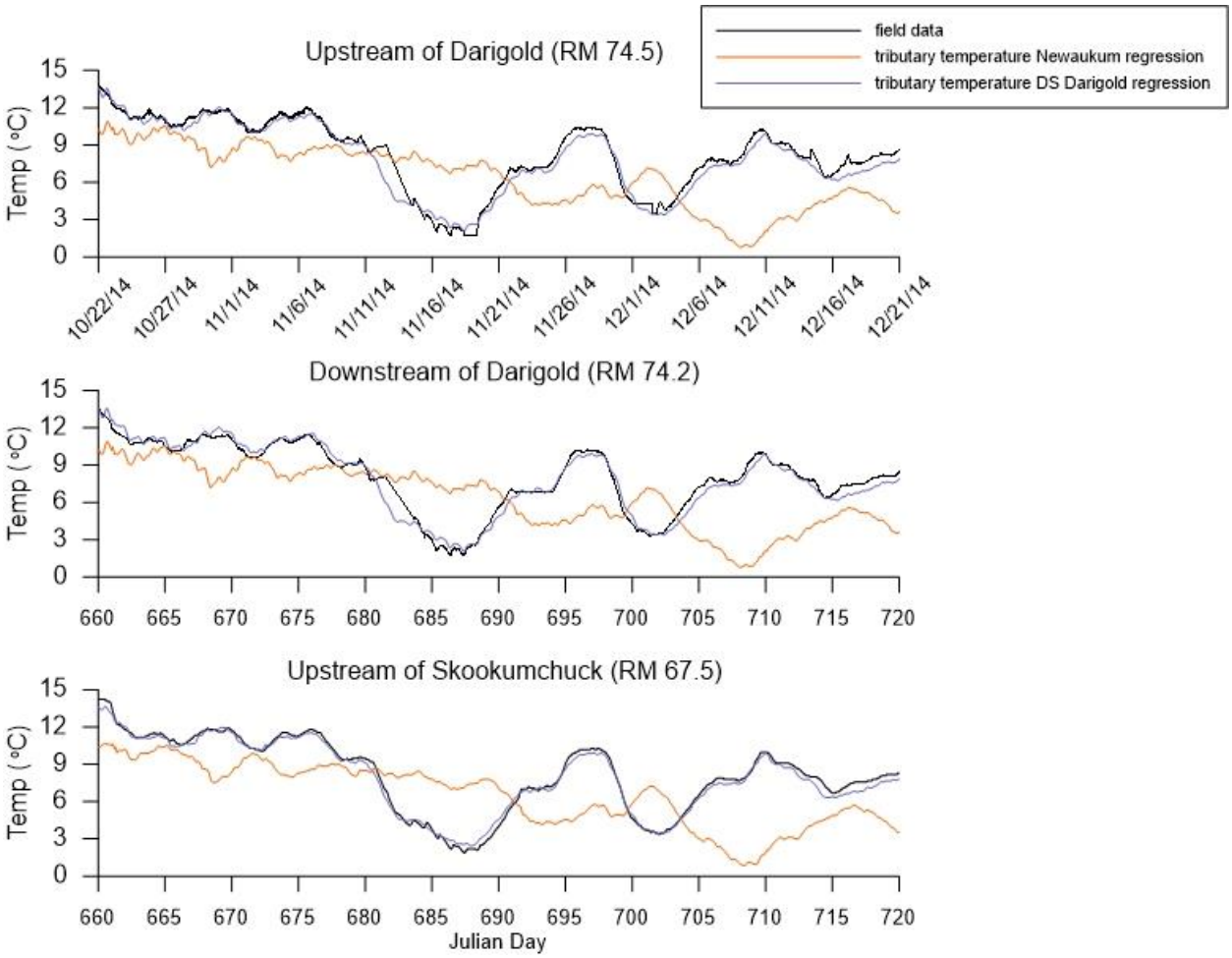

Figure 107. Comparison of model versus field data temperature when boundary tributary temperatures were estimated using Newaukum River versus Chehalis River Downstream of Darigold WWTP data

Input temperature values for groundwater also impacted model temperature predictions, especially during the low flow summer months when the cold groundwater accounted for a larger portion of the mainstem flow. Very little temperature data were available for groundwater, with usually only one value for a given reach or no data at all. Thus, seasonal variations in groundwater temperatures were not known. Originally, a single data value was used for groundwater during the entire model simulation. However, adding 2 ^{o}C to groundwater inputs during the summer months aided the model in staying warm enough during these seasons.

Distributed flows had an important role in river temperatures. Originally, distributed flow temperatures were estimated by implementing the temperatures of a tributary within the same branch. Instead, by using temperature data from mainstem river monitoring stations within each distributed branch, temperatures increased and improved the closeness of model predictions of temperature to field data. When gaps existed in the mainstem data sets in each branch, they were filled using regression to the closest mainstem or tributary station with a complete data set. This change was implemented for all branches with distributed flow except for branch 1, which used the upstream boundary temperature. Table 28 shows the monitoring stations used to estimate distributed flow temperatures.

Table 28. Stations used to estimate temperature for distributed flows in branches 2, 3, 4, 6, 9, and 10

Branch	Mainstem stations used to estimate distributed flow temperature	Stations used to fill gaps in temperature
2	13-CH	CHL-PEL-US & DS Darigold
3	4-UCH	ELK-CRK, 11-UCH, & CHL-PEL-US
4	CHL-ADNA	CHL-CERES-HILLS $ DS Darigold
6	22-CH	DS Darigold
9	18-CH	CHL-US-BLK & DS Darigold
10	23A070	DS Darigold

Meteorological Data

Meteorological data, such as cloud cover, wind speed, and solar radiation impacted resulting temperatures predictions. CE-QUAL-W2 was set to interpolate between meteorological input data values, so having small time intervals between values was important. Hence, meteorological data gaps were often filled to improve the temperature calibration.

Cloud cover was important for temperature calibration. When the Thrash Creek cloud cover data set was implemented for the entire system, resulting water temperatures were much too cold. Thrash Creek is located higher at a higher elevation near the upstream boundary, so is generally cloudier than the lower reaches of the river. Estimating cloud cover based on solar radiation improved model temperature values.

Wind Sheltering

A wind sheltering function was available in the model that either amplified or reduced the input wind speed values by a multiplier. For example, a wind sheltering coefficient of 0.5 meant the model would use only half the input wind speed in calculations of longitudinal momentum and evaporation. This took into account sheltering characteristics of the surroundings, such as topography and wind breaks from trees. This was most important in the slow, deep, lake-like section where the river was more sensitive to wind effects. Reducing wind had a warming effect by decreasing summer evaporation.

Evaporation

Evaporation coefficients were specified for each waterbody, and the amount of evaporation was a function of wind speed. Evaporation was computed from (Cole and Wells, 2016):

$$f(W) = a + bW^C$$

Where f(W) is a wind speed function in W m^{-2} mm Hg^{-1}; a, b, and c are empirical coefficients; and W is the wind speed measured 2 m above the ground

Default model coefficients according to Edinger, et al (1974) as listed in the CE-QUAL-W2 user manual (Cole and Wells, 2016) were initially employed. The a coefficient equaled 9.2 W m^{-2} $mmHg^{-1}$, the b coefficient equaled 0.46 W m^{-2} $mmHg^{-1}$, and the c coefficient equaled 2.0. The a coefficient was then decreased to 4.5 W m^{-2} $mmHg^{-1}$ in order to aid the model in staying warm during the summer months.

Sediments

The loss of short wave solar radiation to the channel bottom can affect water temperature predictions. CE-QUAL-W2 allows the user to specify how much incident solar radiation that makes it to the sediments is reradiated back into the water column or absorbed by the sediments. This was adjusted by altering the TSEDF coefficient, which can range from 0 to 1. When TSEDF equals 1 all incident solar radiation that hits the bottom of the channel is reflected back and available for absorption in the water column. When TSEDF equals 0 all short-wave solar radiation that reaches the bottom of the channel is lost to the sediments (Cole and Wells, 2016). A high TSEDF had a warming effect, while a low TSEDF had a cooling effect. Figure 108, Figure 109, and Figure 110 show model sensitivity to changes in TSEDF values when TSEDF equaled 0.3, 0.6, and 0.8 respectively, at the mainstem Chehalis River stations: downstream of Pe Ell, station 13-CH, at Woodstead, and at Doty. Peak temperatures increased as TSEDF increased.

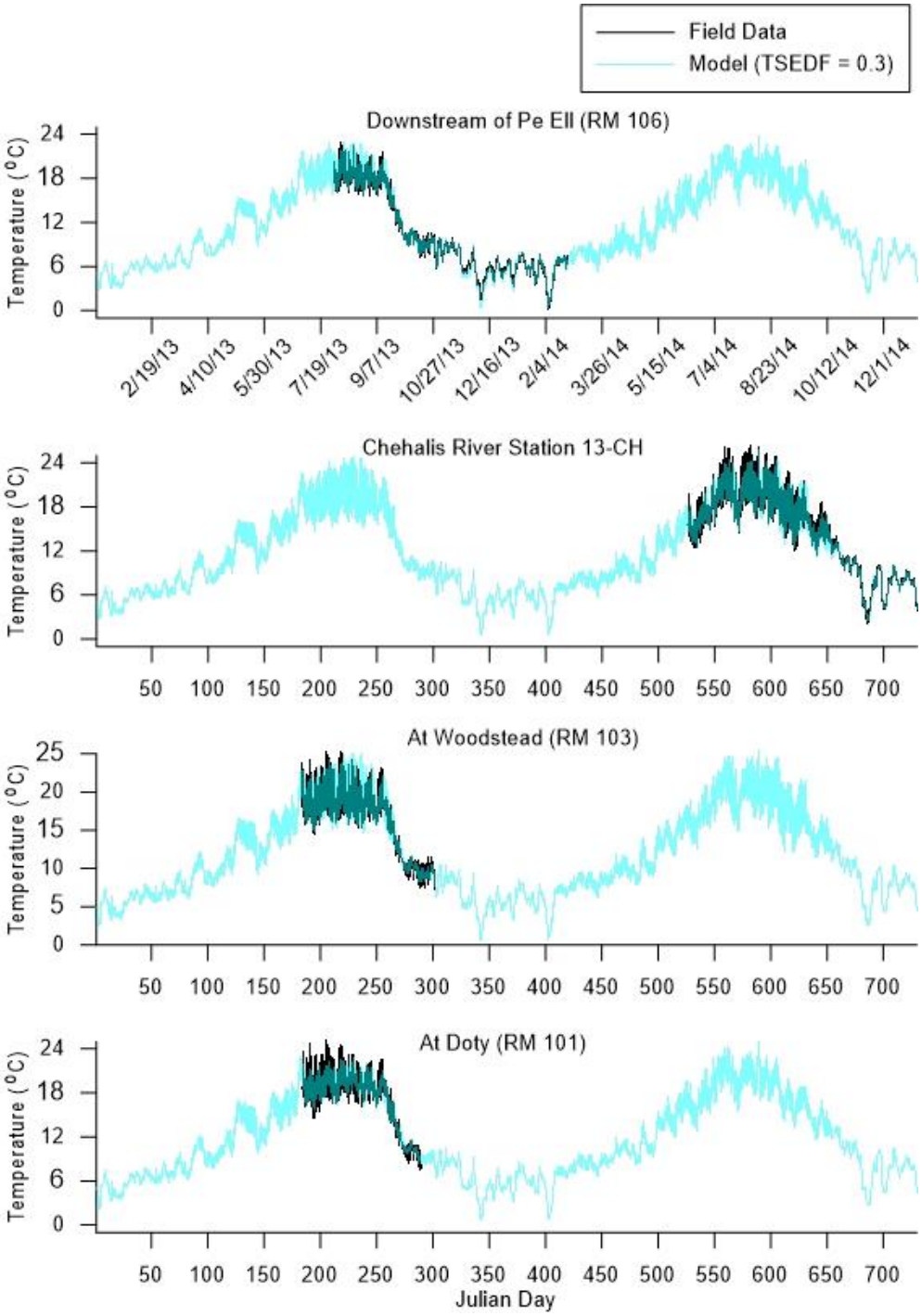

Figure 108. Model temperature versus field data at downstream of Pe Ell, station 13-CH, at Woodstead, and at Doty when TSEDF was set to 0.3

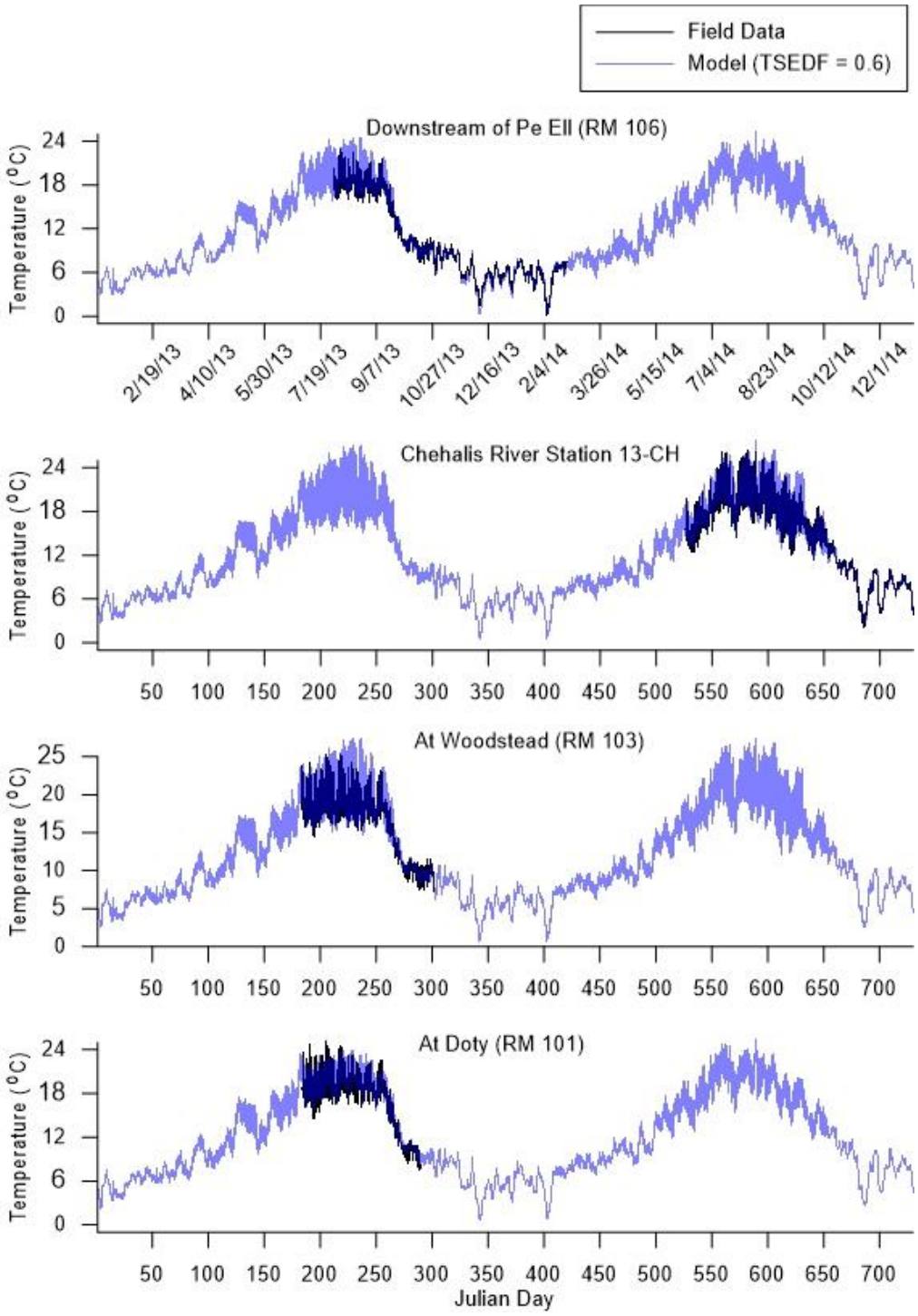

Figure 109. Model temperature versus field data at downstream of Pe Ell, station 13-CH, at Woodstead, and at Doty when TSEDF was set to 0.6

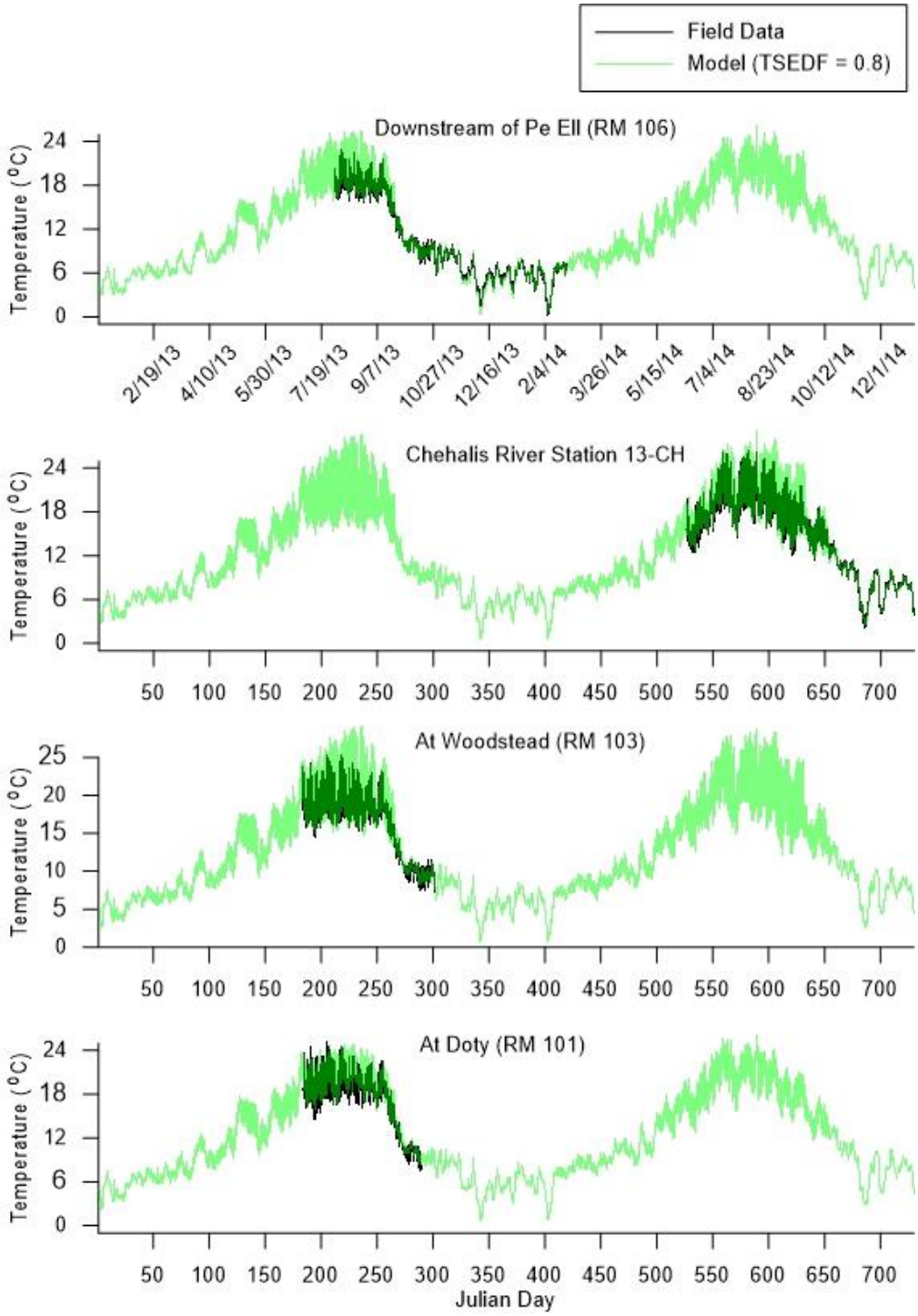

Figure 110. Model temperature versus field data at downstream of Pe Ell, station 13-CH, at Woodstead, and at Doty when TSEDF was set to 0.8

Chehalis Reservoir Footprint Model

Footprint model temperature predictions were calibrated using data collected in 2014. Average mean absolute error for model predictions was 0.91 °C and mean error was 0.16 °C. Error statistics for continuous data and daily maximum temperatures are shown in Table 29 and Table 30. Mean absolute error for the daily maximum temperature was 1.01 °C. .Plots of model-data comparisons are shown in Figure 111 through Figure 115.

Table 29. Temperature error statistics for footprint model.

Site	Segment #	# of Data	Mean Error, C	Mean Absolute Error, C	Root Mean Square Error, C
7-UCH	26	10010	0.34	0.99	1.30
8-UCH	55	17138	0.16	0.82	1.05
2-UCH	86	11011	0.05	0.90	1.15
10-UCH	108	2971	0.46	0.91	1.12
CRIM	161	9136	-0.19	0.92	1.15
Avg./Sum		50266	0.16	0.91	1.15

Table 30. Daily maximum temperature error statistics for footprint model.

Site	Segment #	# of Data	Mean Error, C	Mean Absolute Error, C	Root Mean Square Error, C
7-UCH	26	209	0.65	1.17	1.52
8-UCH	55	209	-0.14	0.78	1.02
2-UCH	86	230	0.05	1.03	1.29
10-UCH	108	63	-0.55	1.05	1.41
CRIM	161	191	-0.63	1.02	1.24
Avg./Sum		902	-0.12	1.01	1.30

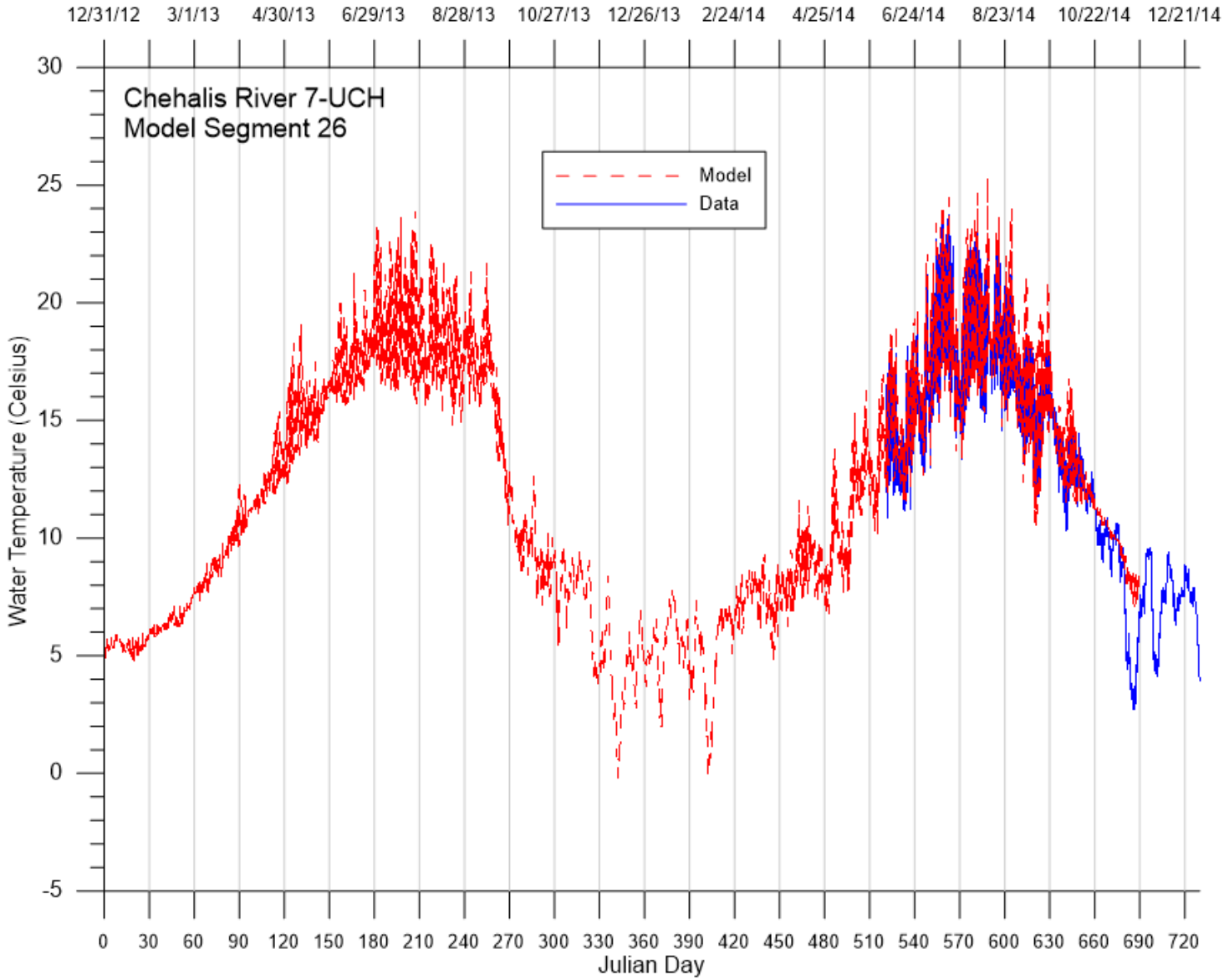

Figure 111. Comparison of model temperature predictions and data at site 7-UCH.

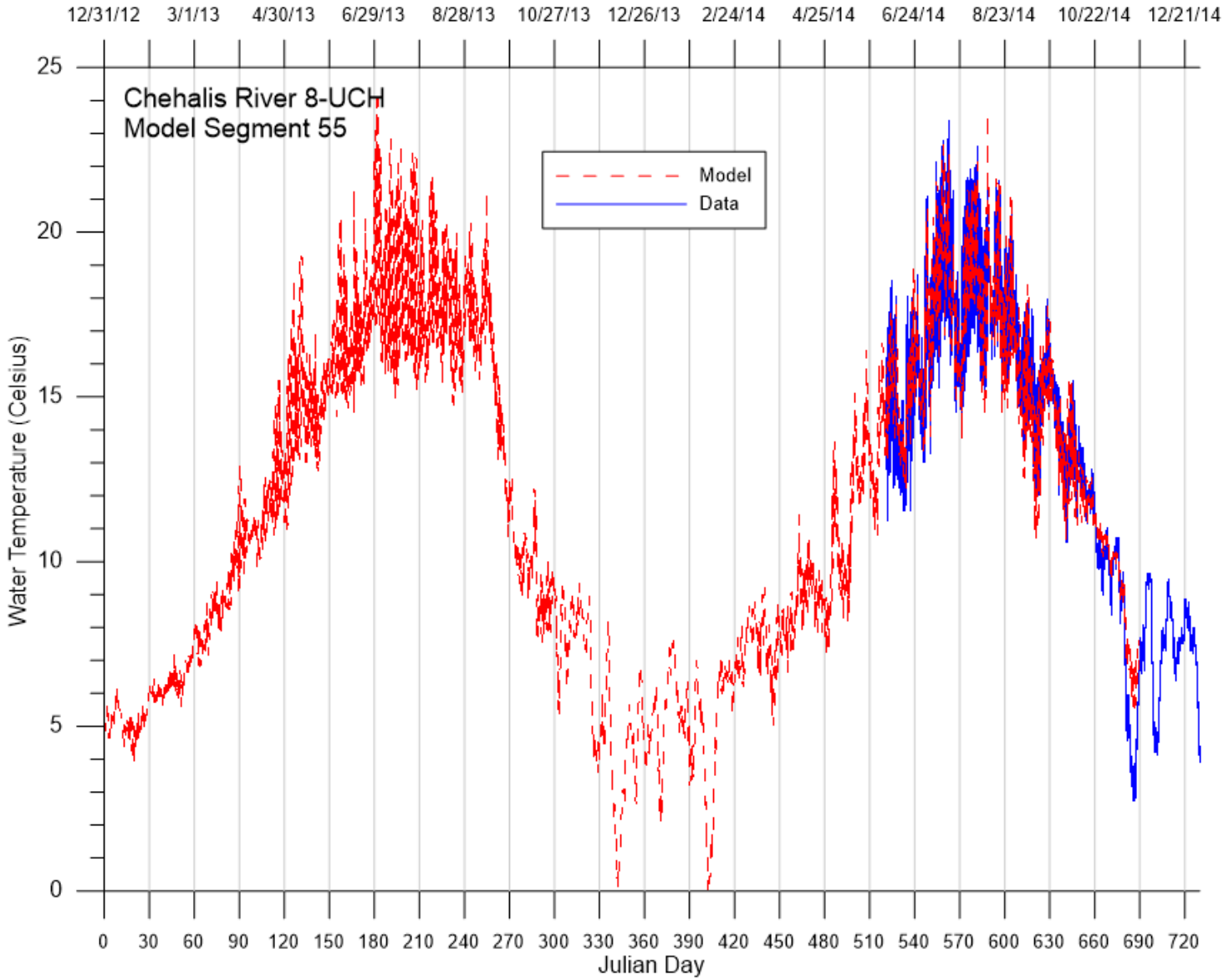

Figure 112. Comparison of model temperature predictions and data at site 8-UCH.

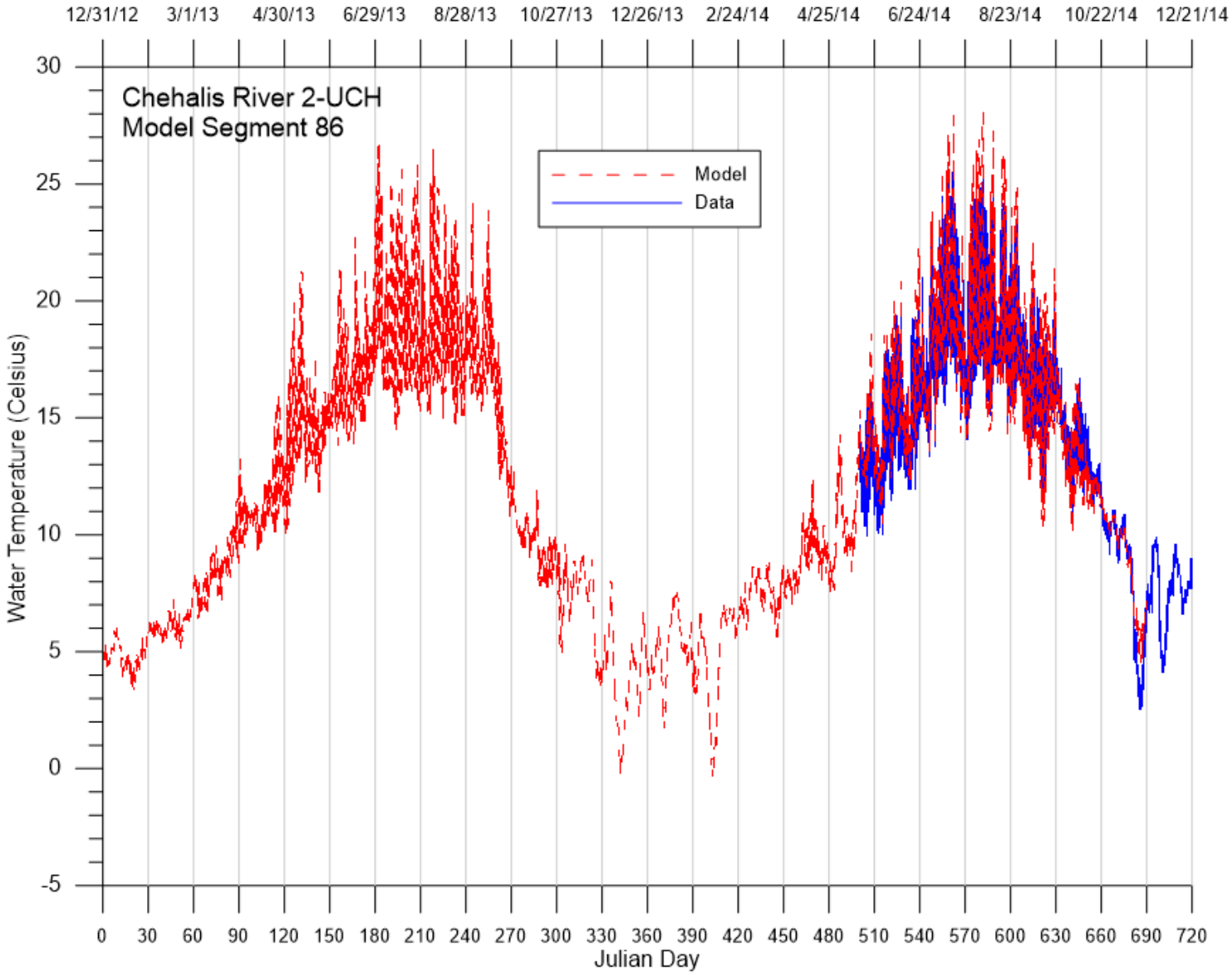

Figure 113. Comparison of model temperature predictions and data at site 2-UCH.

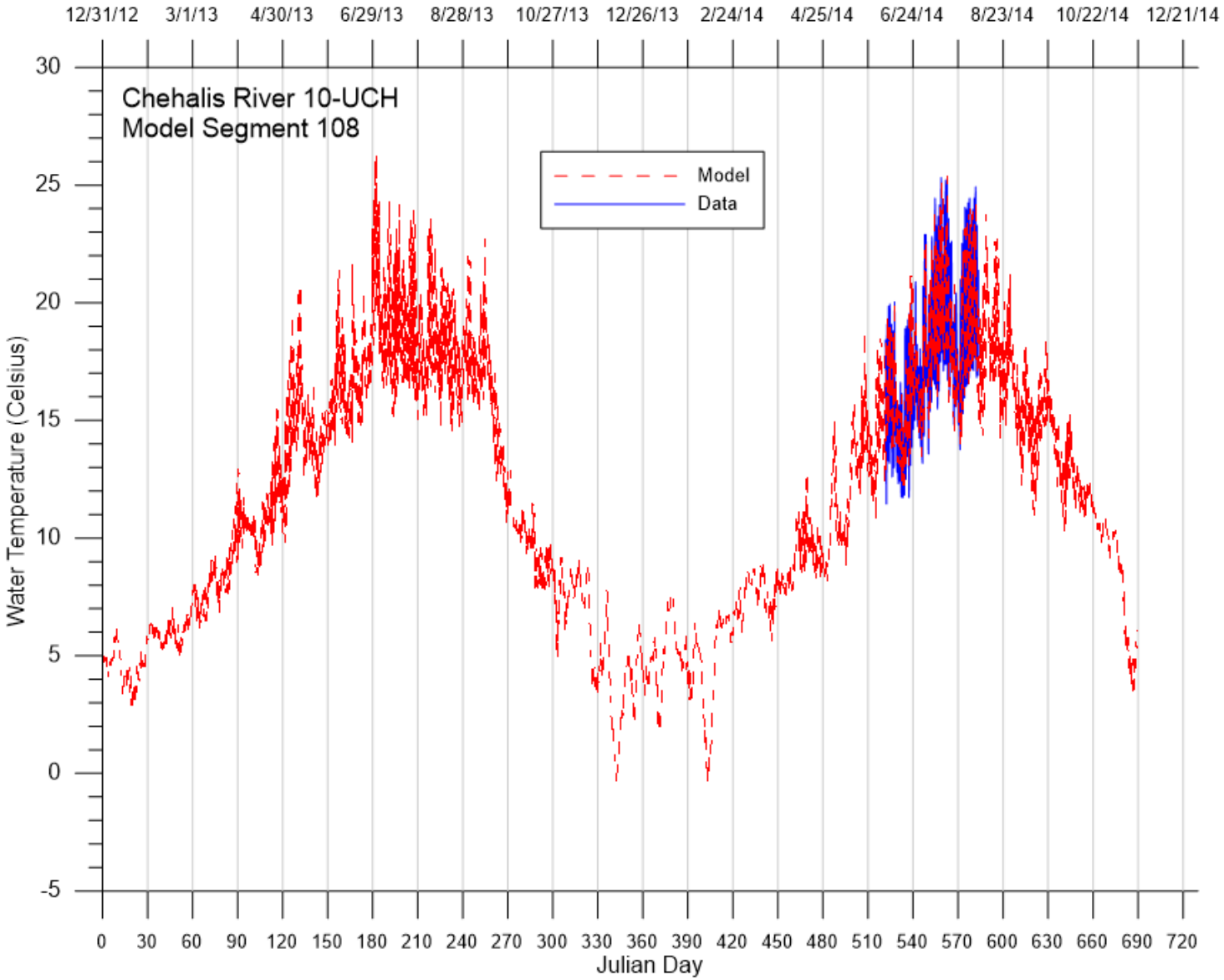

Figure 114. Comparison of model temperature predictions and data at site 10-UCH.

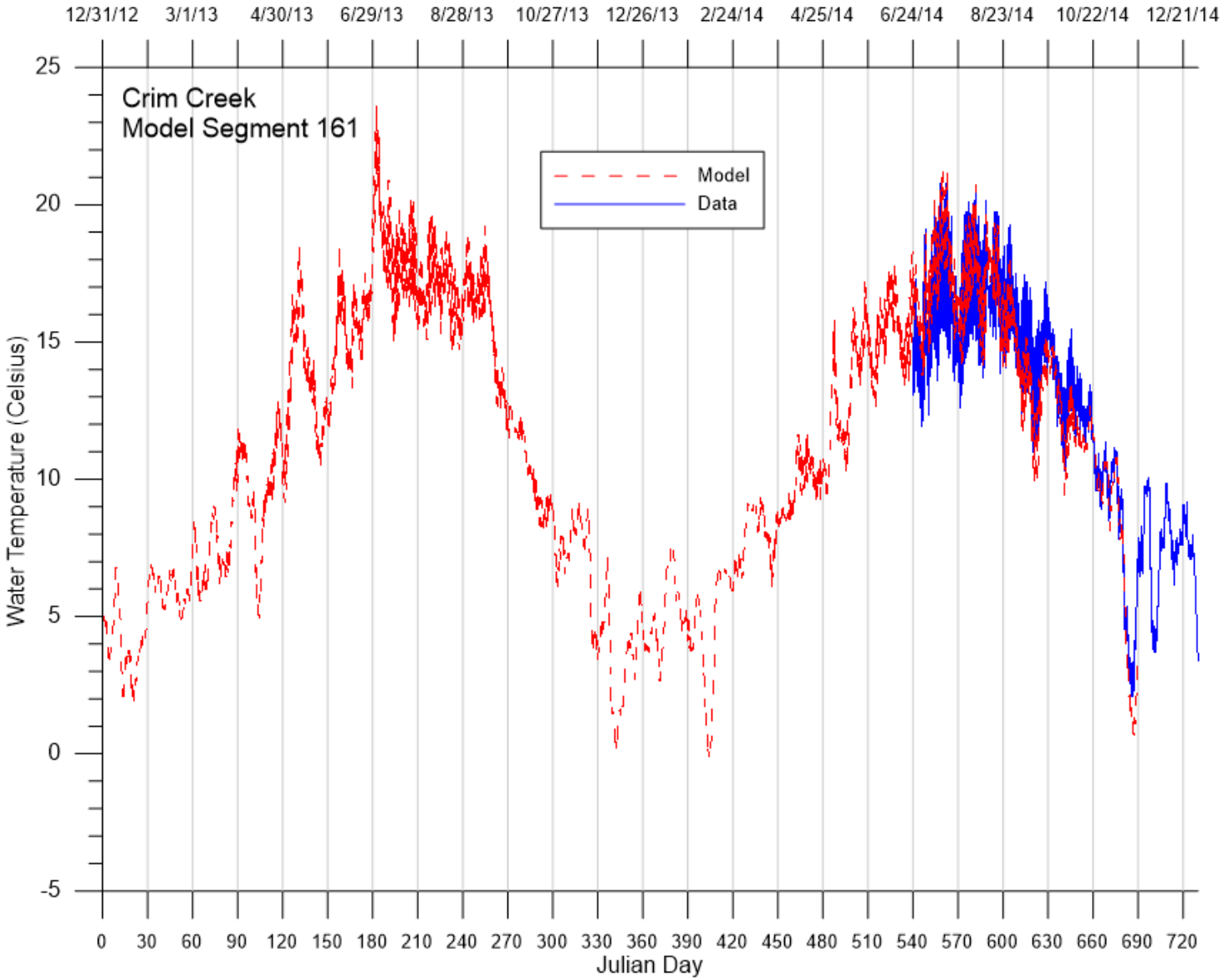

Figure 115. Comparison of model temperature predictions and data at site CRIM.

Model Calibration: Water Quality

Chehalis River Downstream Model

Similar to flow and temperature calibration, model predictions were compared to mainstem Chehalis River field data. Data were provided from Anchor QEA (2014) and WADOE (2016g, 2016h). Table 31 lists the water quality sample sites on the mainstem Chehalis River used for comparisons of model predictions and field data. Table 32 lists the vertical dissolved oxygen stations, locations, and dates when data were collected on the Chehalis River. Figure 116 shows a longitudinal view of water quality sample sites along the river. Water quality coefficients used in the model are shown in Table 33. Many of these coefficients were adjusted during the course of water quality calibration.

Table 31. Water Quality gaging stations on the mainstem Chehalis River used to compare to model outputs for water quality calibration

Organization	Station ID	Description	Data available	Model Segment	River Mile
Anchor QEA	CHL-PEL-DS	Chehalis Downstream of Pe Ell	OrthoP	15	106
WADOE	23A160	Chehalis River at Dryad	DO, FC, NH3, NOx, OrthoP, pH, TP, & TSS	49	98.7
Anchor QEA	CHL-US-SF	Chehalis River Upstream of South Fork	BOD, chl-a, DO, NH3, NOx, OrthoP, pH, TKN, TP, & TSS	88	90
Anchor QEA	CHL-ADNA	Chehalis Near Adna	BOD, chl-a, DO, NH3, NOx, OrthoP, pH, TKN, TP, & TSS	124	81
Anchor QEA	CHL-US-NWK	Chehalis Upstream of Newaukum Confluence	BOD, chl-a, DO, NH3, NOx, OrthoP, pH, TKN, TP, & TSS	152	75.2
Anchor QEA	CHL-RT6-BR	Chehalis at RT6 Bridge	BOD, chl-a, DO, NH3, NOx, OrthoP, pH, TKN, TP, & TSS	156	77.5
Anchor QEA	CHL-US-SKM	Chehalis at Mellen Road Bridge	BOD, chl-a, DO, NH3, NOx, OrthoP, pH, TKN, TP, & TSS	188	67.5
Anchor QEA	CHL-GLV	Chehalis at Galvin Bridge	BOD, chl-a, DO, NH3, NOx, OrthoP, pH, TKN, TP, & TSS	204	64.1
Anchor QEA	CHL-US-BLK	Chehalis Upstream of Black River	BOD, chl-a, DO, NH3, NOx, OrthoP, pH, TKN, TP, & TSS	247	54.2
Anchor QEA	CHL-OAK	Chehalis at Oakville	BOD, chl-a, DO, NH3, NOx, OrthoP, pH, TKN, TP, & TSS	298	42.3
WADOE	23A070	Chehalis River at Porter	DO, FC, NH3, NOx, OrthoP, pH, TP, & TSS	333	33.3

Table 32. Mainstem Chehalis River vertical dissolved oxygen profile collection locations and dates used in water quality calibration

Organization	Station ID	Description	Dates with data	Model Segment
Anchor QEA	CHL-RT6-BR	Chehalis R. at RT6 Bridge at RM 75.31	8/7/13, 9/18/13, &	149

Organization	Station ID	Description	Dates with data	Model Segment
Anchor QEA	HL-14	Chehalis R. at RM	7/31/14	150
Anchor QEA	HL-13	Chehalis R. at RM	7/31/14	153
Anchor QEA	HL-12	Chehalis R. at RM 73	7/31/14	157
Anchor QEA	HL-11	Chehalis R. at RM	7/31/14	158
Anchor QEA	HL-10	Chehalis R. at RM	7/31/14	160
Anchor QEA	HL-9	Chehalis R. at RM	7/31/14	162
Anchor QEA	HL-8	Chehalis R. at RM 71	7/31/14	164
Anchor QEA	HL-7	Chehalis R. at RM	7/31/14	166
Anchor QEA	HL-6	Chehalis R. at RM 70	7/31/14	168
Anchor QEA	HL-5	Chehalis R. at RM	7/31/14	171
Anchor QEA	HL-4	Chehalis R. at RM	7/31/14	173
Anchor QEA	HL-3	Chehalis R. at RM	7/31/14	177
Anchor QEA	HL-2	Chehalis R. at RM	7/31/14	179
Anchor QEA	CHL-US-SKM	Chehalis R. at Mellen Road Bridge at RM	8/7/13, 9/18/13, &	180
Anchor QEA	HL-1	Chehalis R. at RM	7/31/14	181

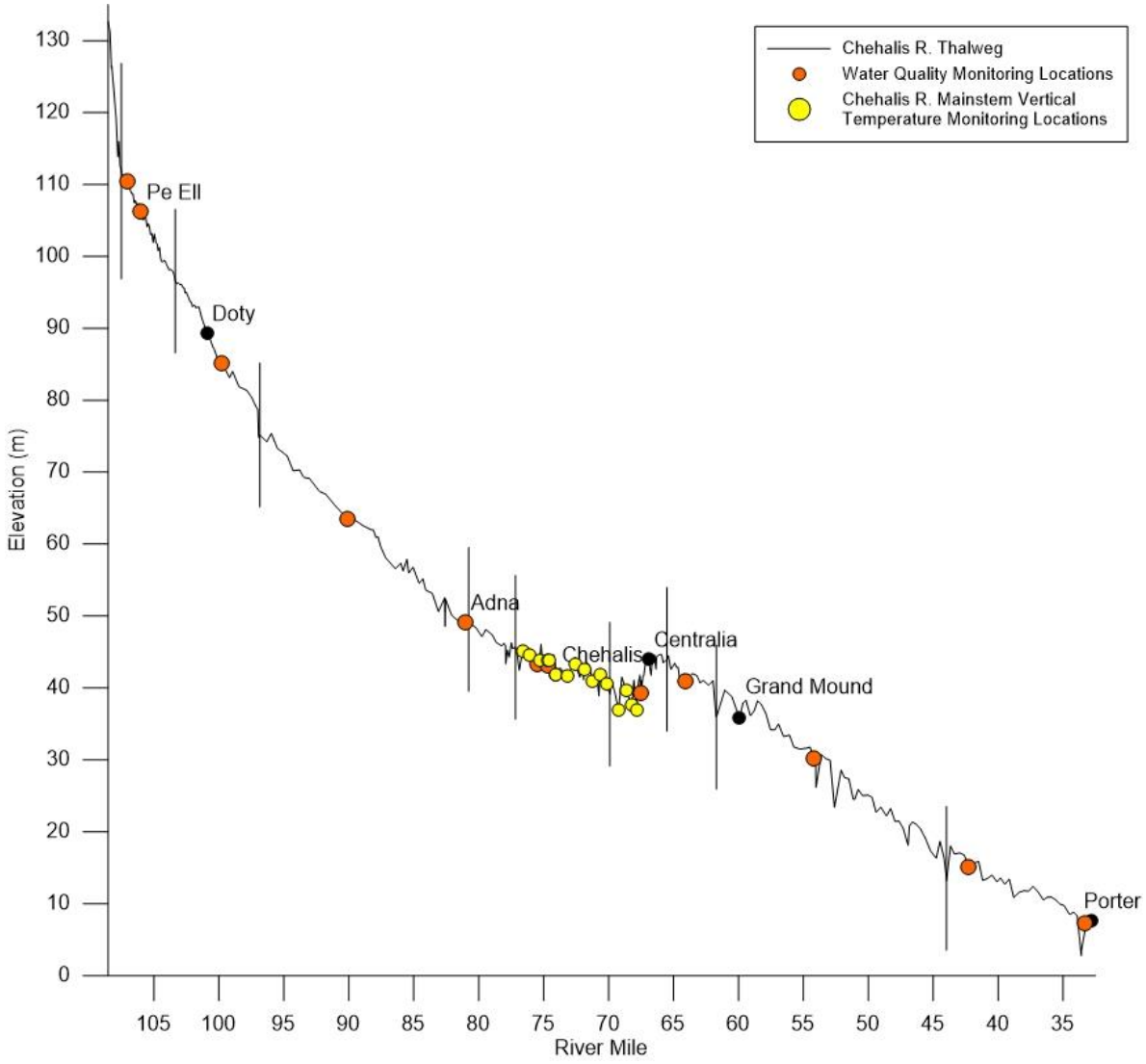

Figure 116. Longitudinal view of the mainstem Chehalis River water quality sample sites (vertical lines show model branch breaks)

Table 33. W2 Model Water Quality Parameters in the Chehalis River Model

Variable	Description	Units	Typical values*	Values
AX	Longitudinal eddy viscosity (for momentum dispersion)	m^2/sec	1	1
DX	Longitudinal eddy diffusivity (for dispersion of heat and constituents)	m^2/sec	1	1
CBHE	Coefficient of bottom heat exchange	Wm^2/sec	0.30	0.30
TSED	Sediment (ground) temperature	^oC		11.5
WSC	Wind sheltering coefficient		0.85	0.25
BETA	Fraction of incident solar radiation absorbed at the water surface		0.45	0.45
EXH20	Extinction for water	/m	0.25-0.45	0.25
AG1	Algal growth rate for group #1	/day	1-3	1.5
AM1	Algal mortality rate for group #1	/day		0.1
AE1	Algal excretion rate for group #1	/day	0.014-0.044	0.04
AR1	Algal dark respiration for group #1	/day	0.01-0.92	0.04
AS1	Algal settling rate for group #1	/day	0.02-1.00	0.1
ASAT1	Algae Saturation intensity at maximum photosynthetic rate for group #1	W/m^2	10-170	150
APOM1	Fraction of algal biomass lost by mortality to detritus for algae for group #1		0.8	0.8
AT1_1	Lower temperature for algal growth for group #1	^oC		3
AT2_1	Lower temperature for maximum algal growth for group #1	^oC		7
AT3_1	Upper temperature for maximum algal growth for group #1	^oC		20
AT4_1	Upper temperature for algal growth for group #1	^oC		30
AK1_1	Fraction of algal growth rate at AT1 for group #1		0.1	0.1
AK2_1	Fraction of maximum algal growth rate at AT2 for group #1		0.99	0.99
AK3_1	Fraction of maximum algal growth rate at AT3 for group #1		0.99	0.99
AK4_1	Fraction of algal growth rate at AT4 for group #1		0.1	0.1
ALGP1	Stoichiometric equivalent between organic matter and phosphorus for algae group #1		0.005	0.01

Variable	Description	Units	Typical values*	Values
ALGN1	Stoichiometric equivalent between organic matter and nitrogen for algae group #1		0.08	0.08
ALGC1	Stoichiometric equivalent between organic matter and carbon for algae group #1		0.4-0.5	0.5
AG2	Algal growth rate for group #2	/day	1-3	2
AM2	Algal mortality rate for group #2	/day		0.1
AE2	Algal excretion rate for group #2	/day	0.014-0.044	0.04
AR2	Algal dark respiration for group #2	/day	0.01-0.92	0.04
AS2	Algal settling rate for group #2	/day	0.02-1.00	0.1
ASAT2	Algae Saturation intensity at maximum photosynthetic rate for group #2	W/m^2	10-170	150
APOM2	Fraction of algal biomass lost by mortality to detritus for algae for group #2		0.8	0.8
AT1_2	Lower temperature for algal growth for group #2	^oC		7
AT2_2	Lower temperature for maximum algal growth for group #2	^oC		15
AT3_2	Upper temperature for maximum algal growth for group #2	^oC		30
AT4_2	Upper temperature for algal growth for group #2	^oC		35
AK1_2	Fraction of algal growth rate at AT1 for group #2		0.1	0.1
AK2_2	Fraction of maximum algal growth rate at AT2 for group #2		0.99	0.99
AK3_2	Fraction of maximum algal growth rate at AT3 for group #2		0.99	0.99
AK4_2	Fraction of algal growth rate at AT4 for group #2		0.1	0.1
ALGP2	Stoichiometric equivalent between organic matter and phosphorus for algae group #2		0.005	0.01
ALGN2	Stoichiometric equivalent between organic matter and nitrogen for algae group #2		0.08	0.08
ALGC2	Stoichiometric equivalent between organic matter and carbon for algae group #2		0.4-0.5	0.5
LDOMDK	Labile DOM decay rate	/day	0.04-0.12	0.08
LRDDK	Labile to refractory decay rate	/day	0.001	0.01
RDOMDK	Maximum refractory decay rate	/day	0.001	0.001
LPOMDK	Labile Detritus decay rate	/day	0.04-0.1	0.06
POMS	Detritus settling rate	m/day	0.2-2	0.75
RPOMDK	Refractory detritus decay rate	/day	0.001	0.001

Variable	Description	Units	Typical values*	Values
OMT1	Lower temperature for organic matter decay	^oC	4	4
OMT2	Lower temperature for maximum organic matter decay	^oC	30	25
OMK1	Fraction of organic matter decay rate at OMT1		0.1	0.1
OMK2	Fraction of organic matter decay rate at OMT2		0.99	0.99
PO4R	Anaerobic sediment release rate of phosphorus as fraction of SOD			0.001
AHSP1	Algal half-saturation constant for phosphorus for group #1	g/m^3	0.002-0.01	0.003
AHSP2	Algal half-saturation constant for phosphorus for group #2	g/m^3	0.002-0.01	0.003
NH4DK	Ammonia decay rate (nitrification rate)	/day	0.001-1.3	0.8
AHSN1	Algal half-saturation constant for nitrogen for group #1	g/m^3	0.014	0.014
AHSN2	Algal half-saturation constant for nitrogen for group #2	g/m^3	0.014	0.014
NH4T1	Lower temperature for ammonia decay	^oC	5	5
NH4T2	Lower temperature for maximum ammonia decay	^oC	20	25
NH4K1	Fraction of nitrification rate at NH4T1		0.1	0.1
NH4K2	Fraction of nitrification rate at NH4T2		0.99	0.99
NO3DK	Nitrate decay rate (denitrification rate)	/day	0.05-0.15	0.03
NO3T1	Lower temperature for nitrate decay	^oC	5	5
NO3T2	Lower temperature for maximum nitrate decay	^oC	20	25
NO3K1	Fraction of denitrification rate at NO3T1		0.1	0.1
NO3K2	Fraction of denitrification rate at NO3T2		0.99	0.99
O2NH4	Oxygen stoichiometric equivalent for ammonia decay		4.57	4.57
O2OM	Oxygen stoichiometric equivalent for organic matter decay		1.4	1.4
O2AR1	Oxygen stoichiometric equivalent for dark respiration for group #1		1.1	1.1
O2AR2	Oxygen stoichiometric equivalent for dark respiration for group #2		1.1	1.1
O2AG1	Oxygen stoichiometric equivalent for algal growth for group #1		1.4	1.6
O2AG2	Oxygen stoichiometric equivalent for algal growth for group #2		1.4	1.6

Variable	Description	Units	Typical values*	Values
O2LIM	Dissolved oxygen concentration at which anaerobic processes begin	g/m^3	0.1	0.07
SEDK	First order sediment compartment decay rate	/day		0.03
SOD	Zeroth order sediment oxygen demand	$g/m^2/day$	0.3-6	0.3-1.9
SEDBR	Sediment burial rate	/day		0.01
* Cole and Wells (2016)				

Figure 117 through Figure 134 show the model results for dissolved oxygen, chlorophyll a, ammonia, nitrates, TKN, phosphate, total phosphorus, pH, and TSS at the Chehalis River stations: upstream of Pe Ell, downstream of Pe Ell, at Dryad, upstream of the South Fork Chehalis River, at Adna, upstream of the Newaukum River, at Route 6 bridge, upstream of Skookumchuck River, at Galvin Road bridge, upstream of Black River, at Oakville, and at Porter.

Model predictions compared to continuous DO field data at the Chehalis River mainstem stations downstream of Pe Ell, at Route 6 Bridge, and at Mellen Road Bridge are shown in Figure 135, Figure 136, and Figure 137 respectively. Model predictions compared to continuous chlorophyll a field data at the mainstem stations downstream of Pe Ell, at Route 6 Bridge, and at Mellen Road Bridge are shown in Figure 138, Figure 139, and Figure 140 respectively. Model predictions compared to continuous pH field data at the mainstem stations downstream of Pe Ell, at Route 6 Bridge, and at Mellen Road Bridge are shown in Figure 141, Figure 142, and Figure 143.

Vertical profile data were available at the same locations as temperature. Comparisons of vertical DO profiles to field data at the mainstem stations at Route 6 Bridge, HL-14, and HL-13 are shown in Figure 144. Comparisons of vertical DO profiles to field data at the mainstem stations at HL-12, HL-11, HL-10, HL-9, and HL-8 are shown in Figure 145. Comparisons of vertical DO profiles to field data at the mainstem stations at HL-7, HL-6, HL-5, HL-4, and HL-3 are shown in Figure 146. Comparisons of vertical DO profiles to field data at the mainstem stations at HL-2, Mellen Road Bridge, and HL-1 are shown in Figure 147.

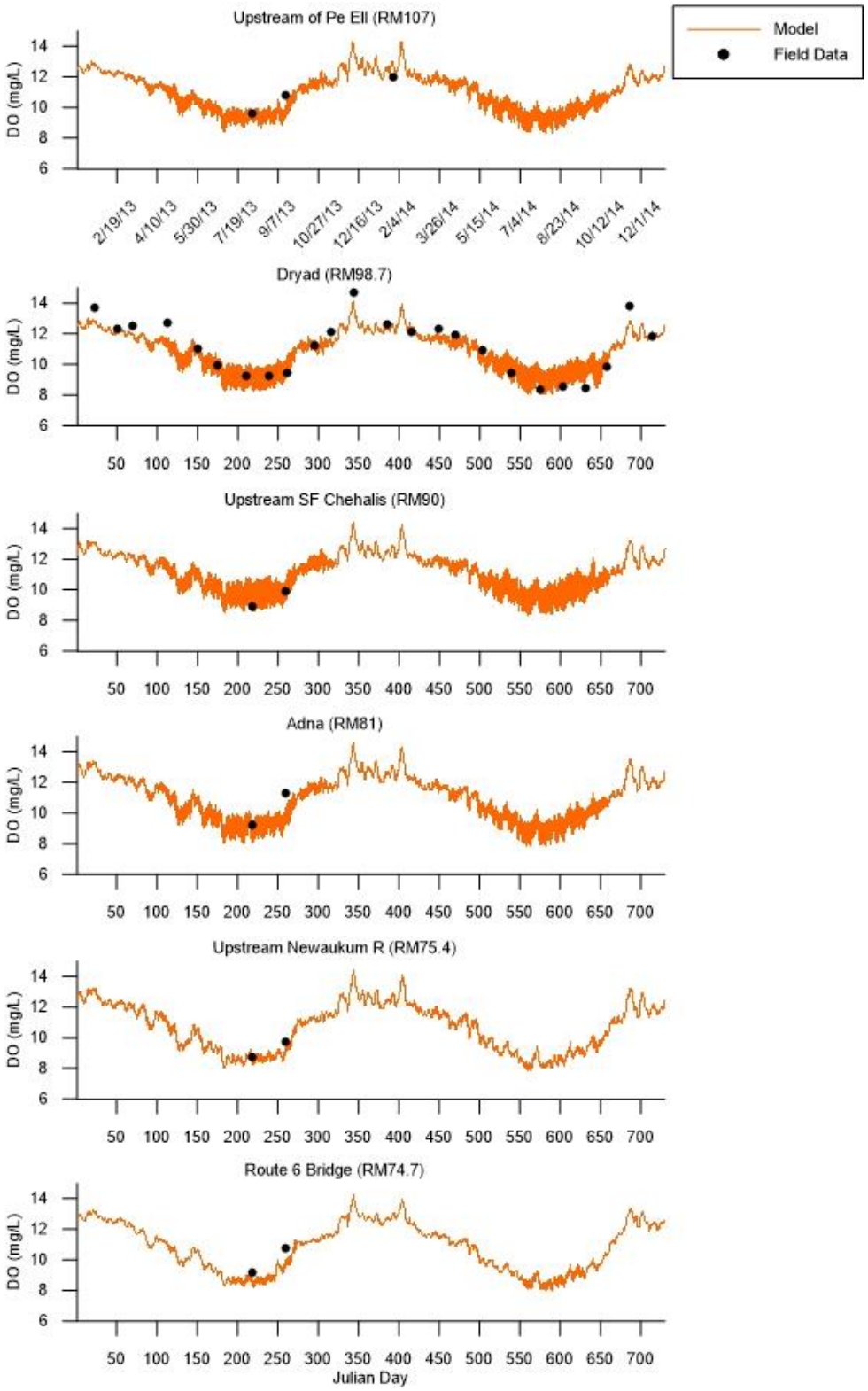

Figure 117. Model dissolved oxygen predictions versus field data at upstream of Pe Ell, Dryad, upstream of South Fork Chehalis River, at Adna, upstream of Newaukum River, and at Route 6 bridge

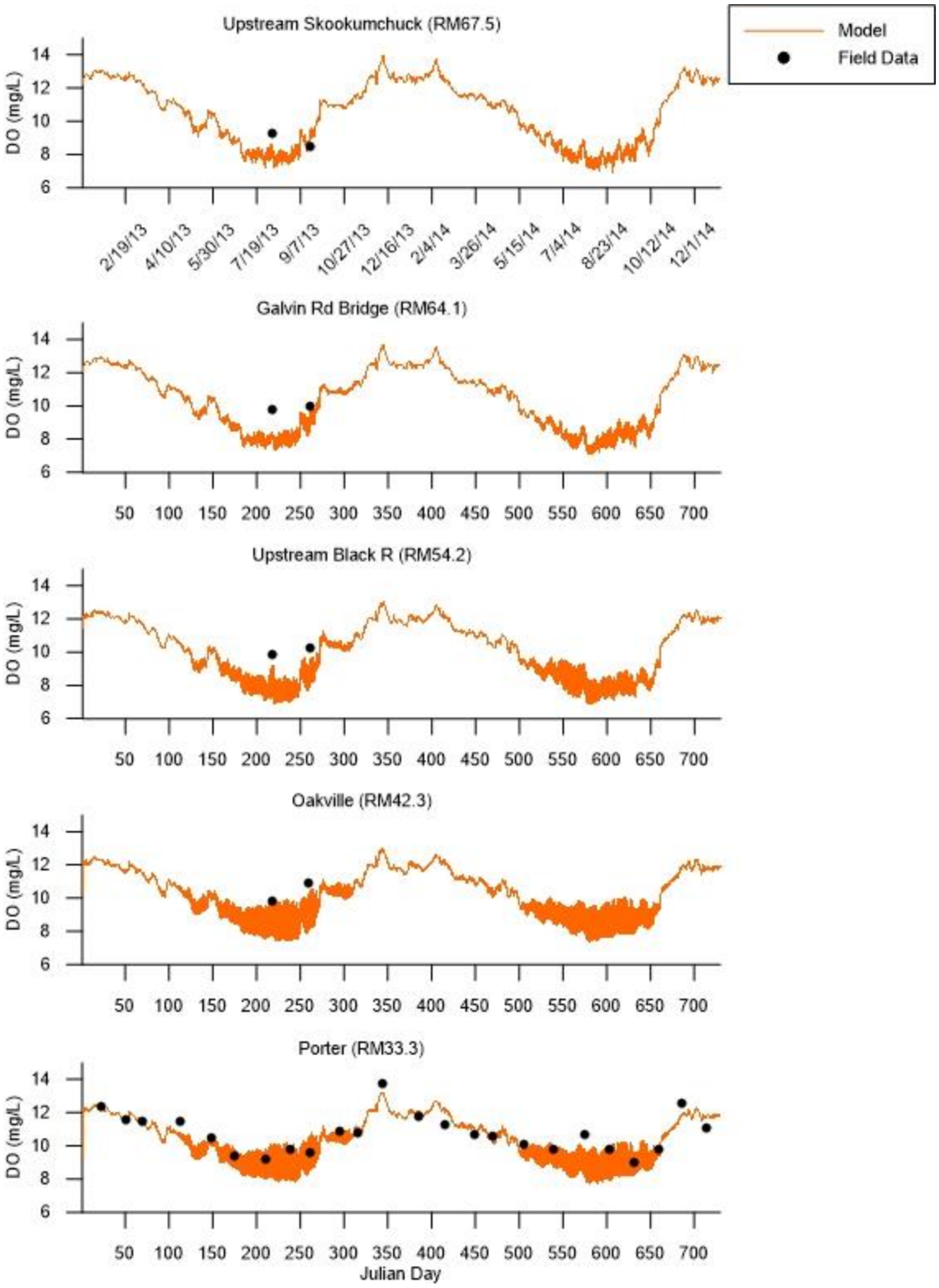

Figure 118. Model dissolved oxygen predictions versus field data at upstream of Skookumchuck River, at Galvin Road bridge, upstream of Black River, at Oakville, and at Porter

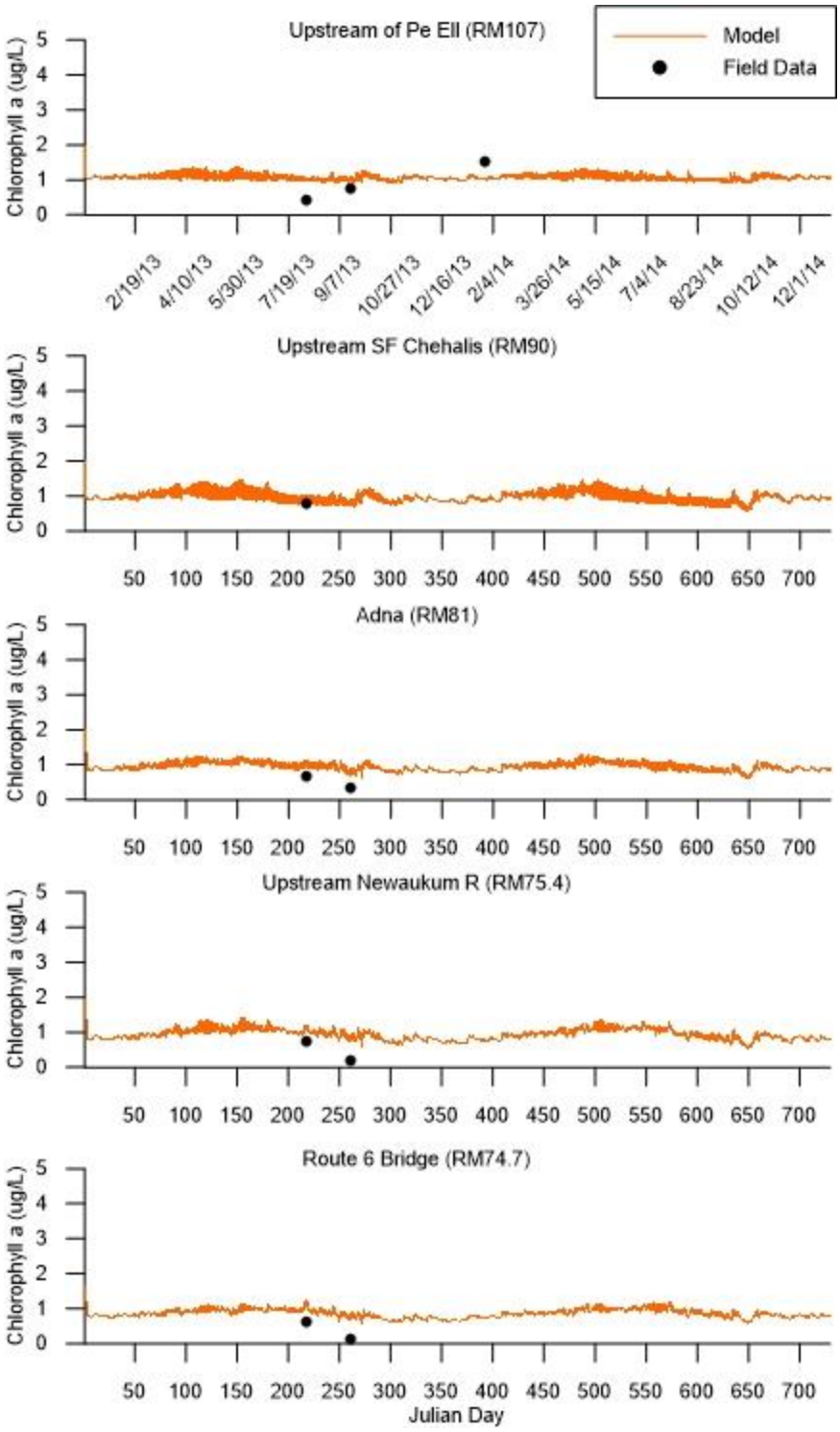

Figure 119. Model Chlorophyll a predictions versus field data at upstream of Pe Ell, Dryad, upstream of South Fork Chehalis River, at Adna, upstream of Newaukum River, and at Route 6 bridge

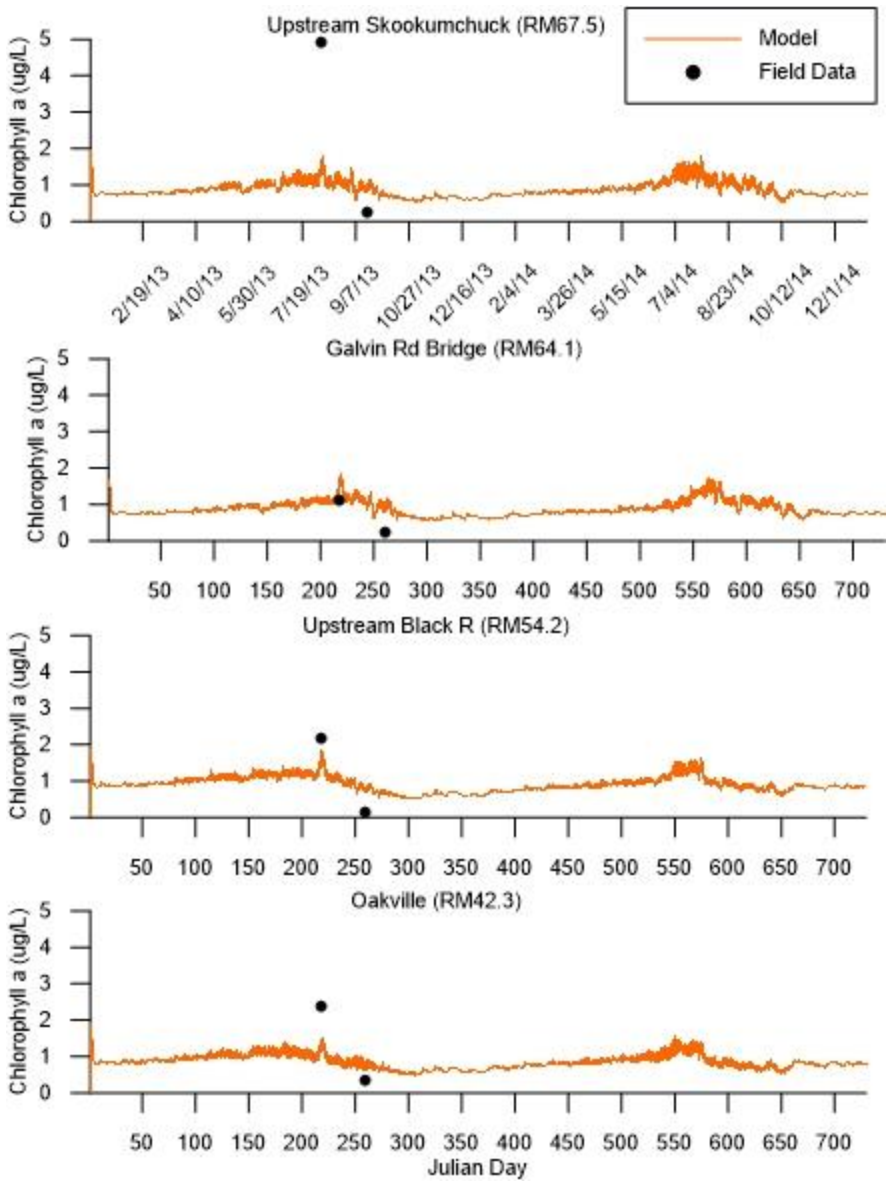

Figure 120. Model Chlorophyll a predictions versus field data at upstream of Skookumchuck River, at Galvin Road bridge, upstream of Black River, and at Oakville

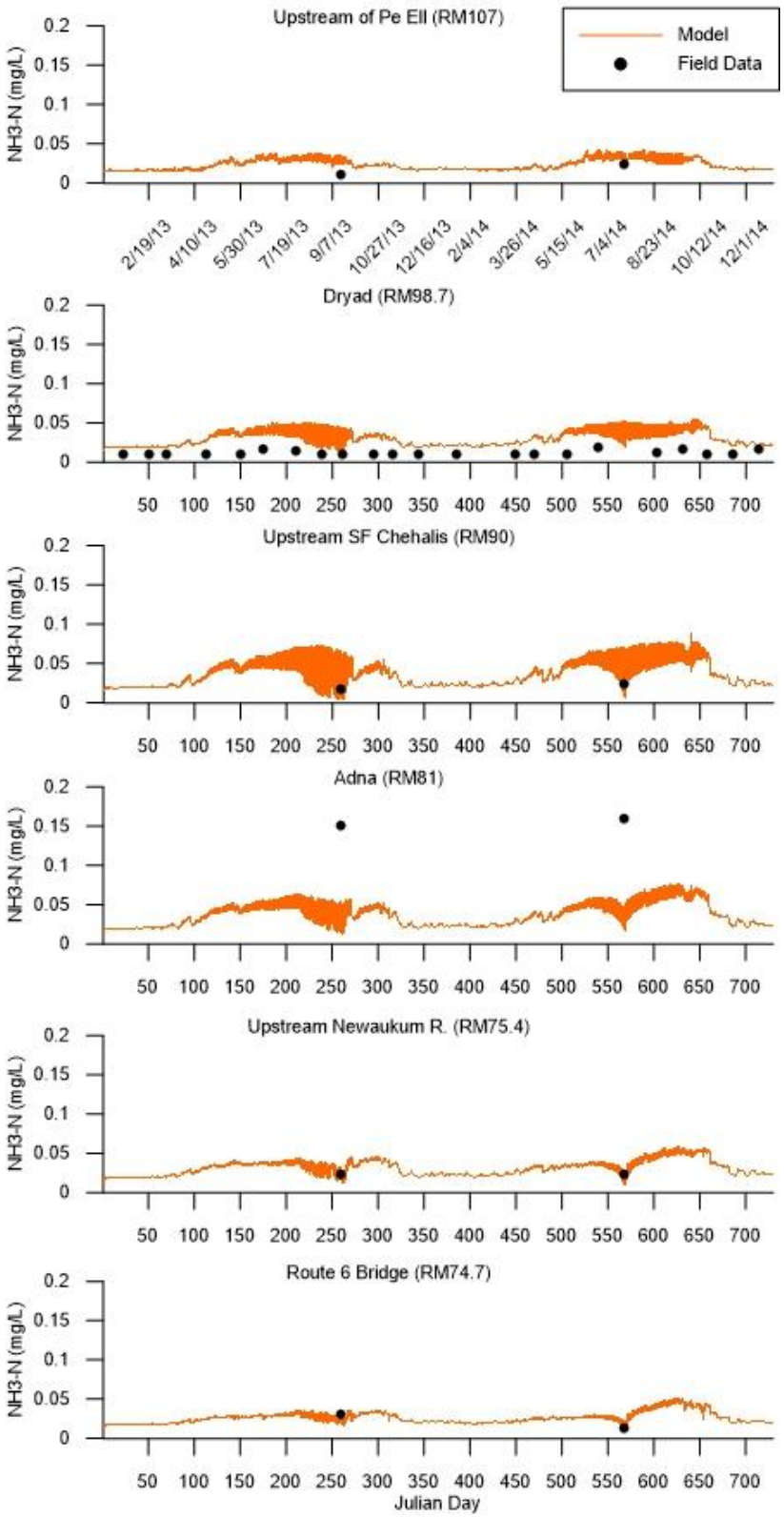

Figure 121. Model NH3 predictions versus field data at upstream of Pe Ell, Dryad, upstream of South Fork Chehalis River, at Adna, upstream of Newaukum River, and at Route 6 bridge

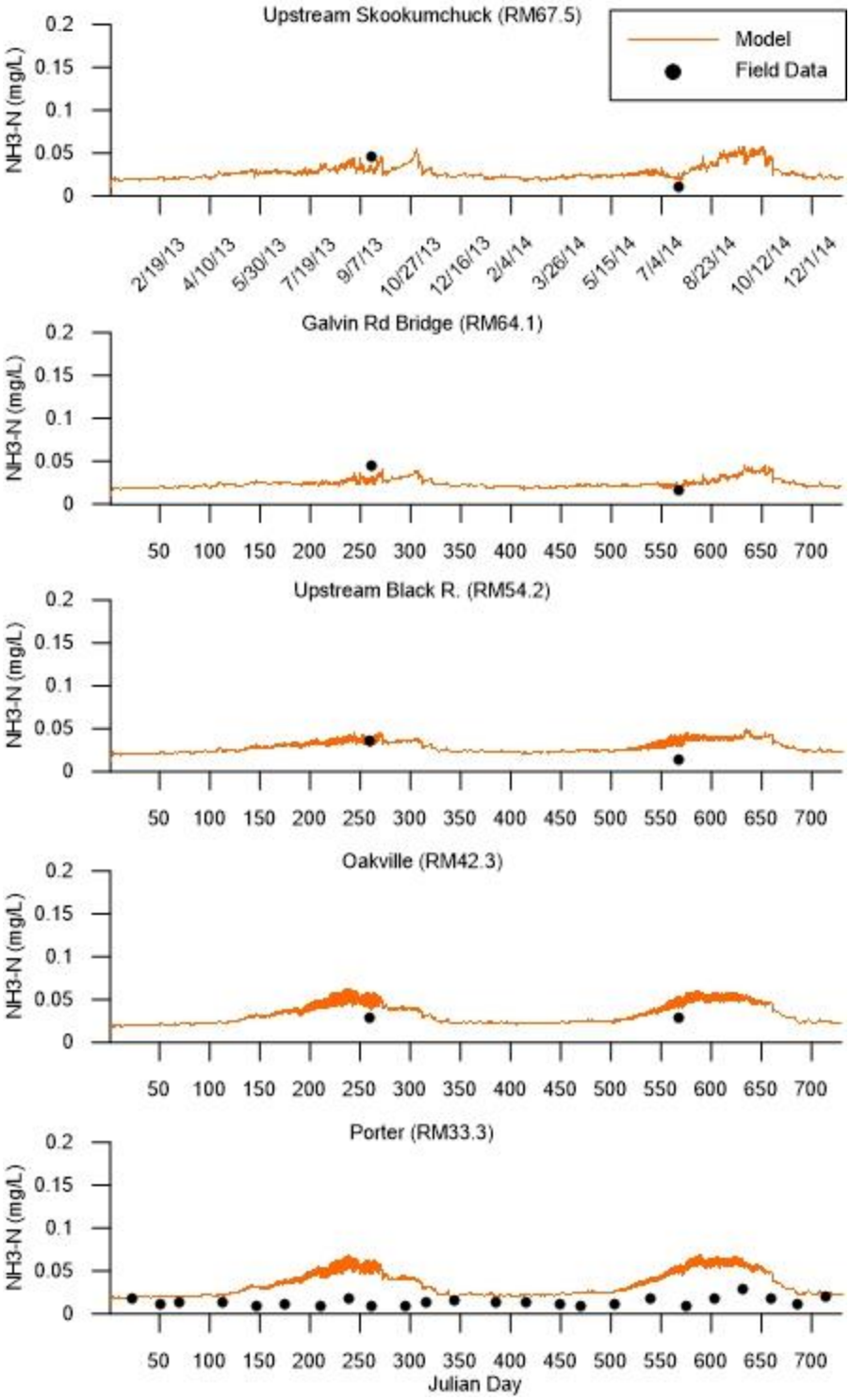

Figure 122. Model NH3 predictions versus field data at upstream of Skookumchuck River, at Galvin Road bridge, upstream of Black River, at Oakville, and at Porter

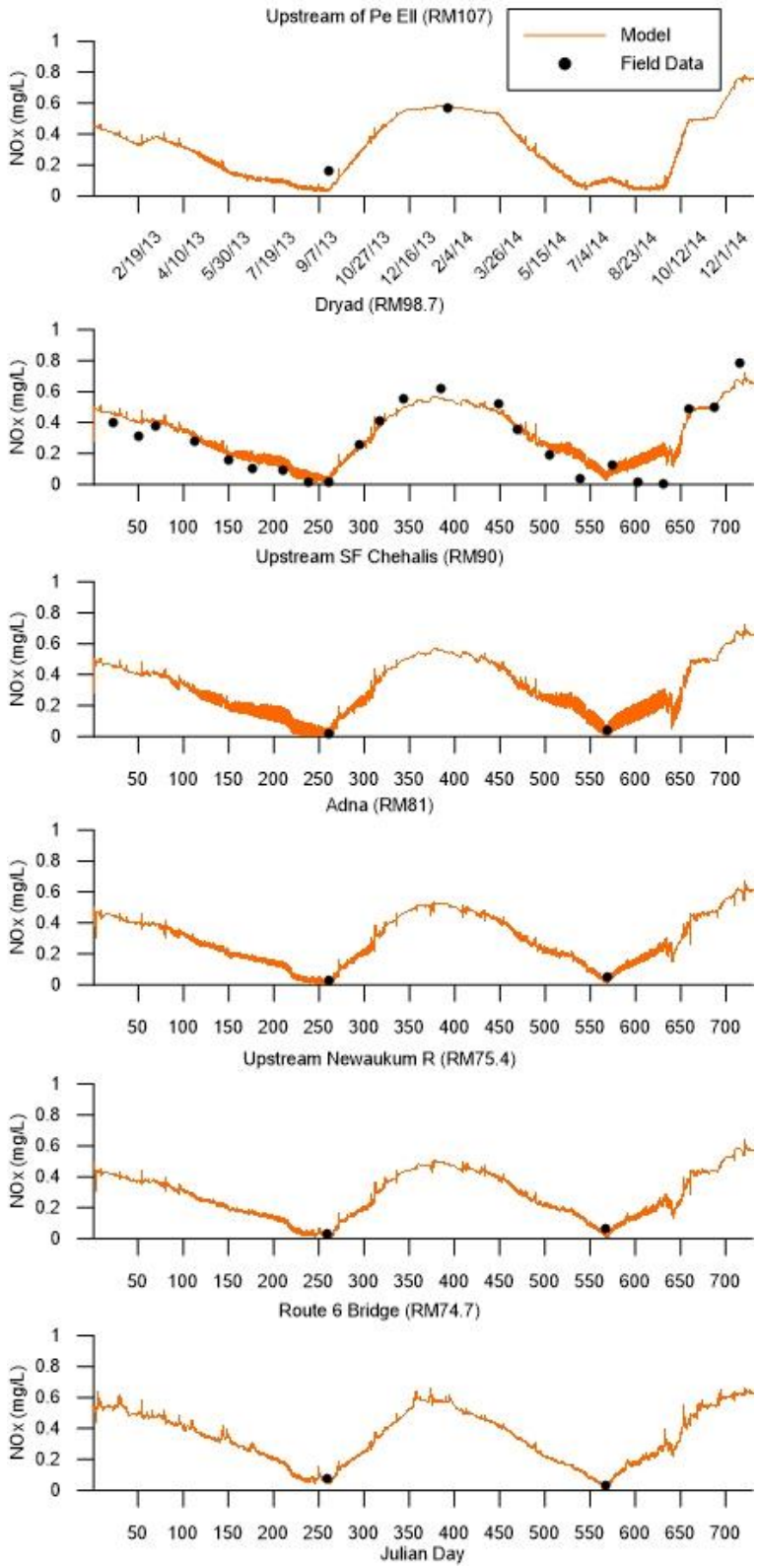

Figure 123. Model NOx predictions versus field data at upstream of Pe Ell, Dryad, upstream of South Fork Chehalis River, at Adna, upstream of Newaukum River, and at Route 6 bridge

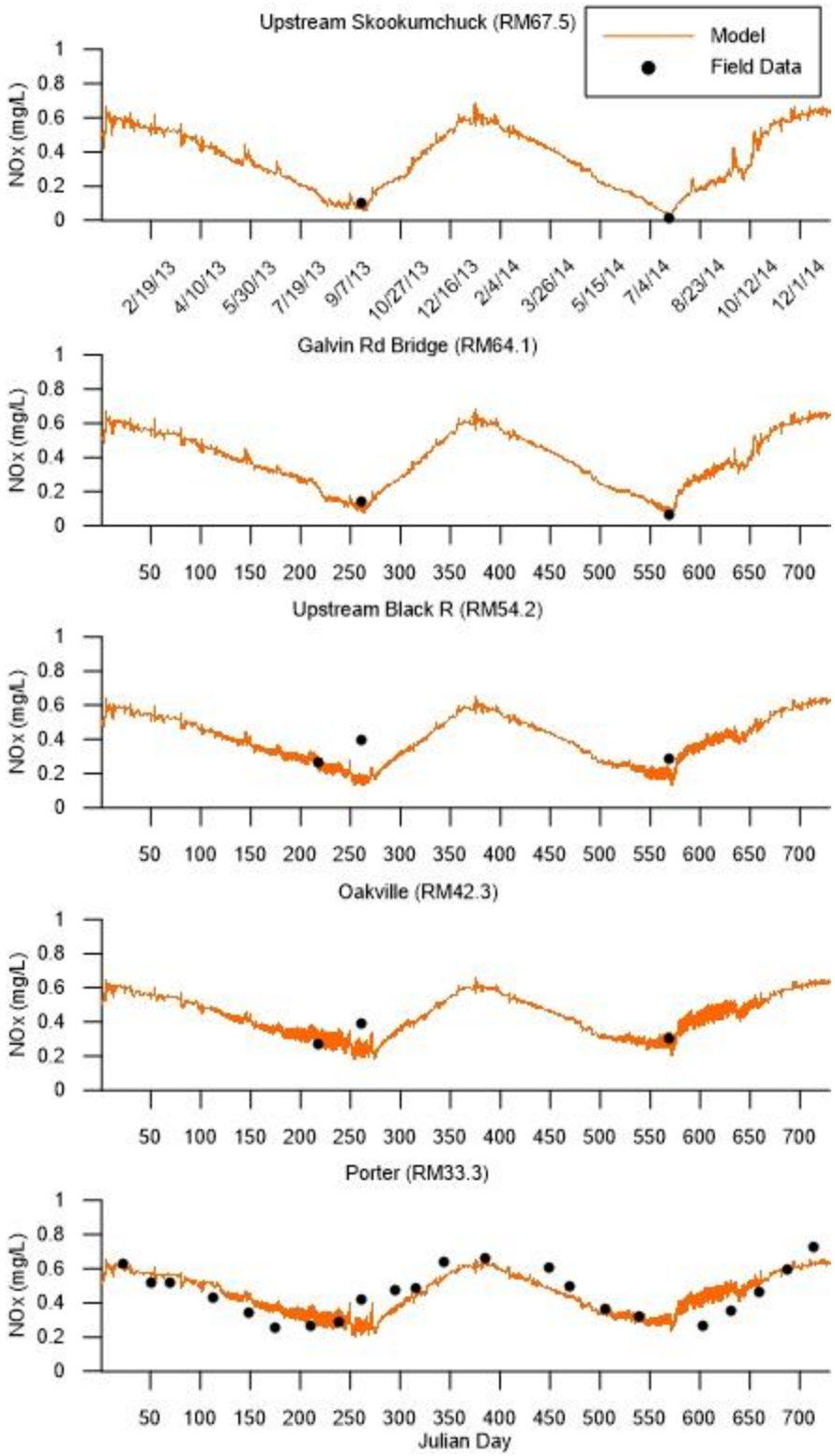

Figure 124. Model NOx predictions versus field data at upstream of Skookumchuck River, at Galvin Road bridge, upstream of Black River, at Oakville, and at Porter

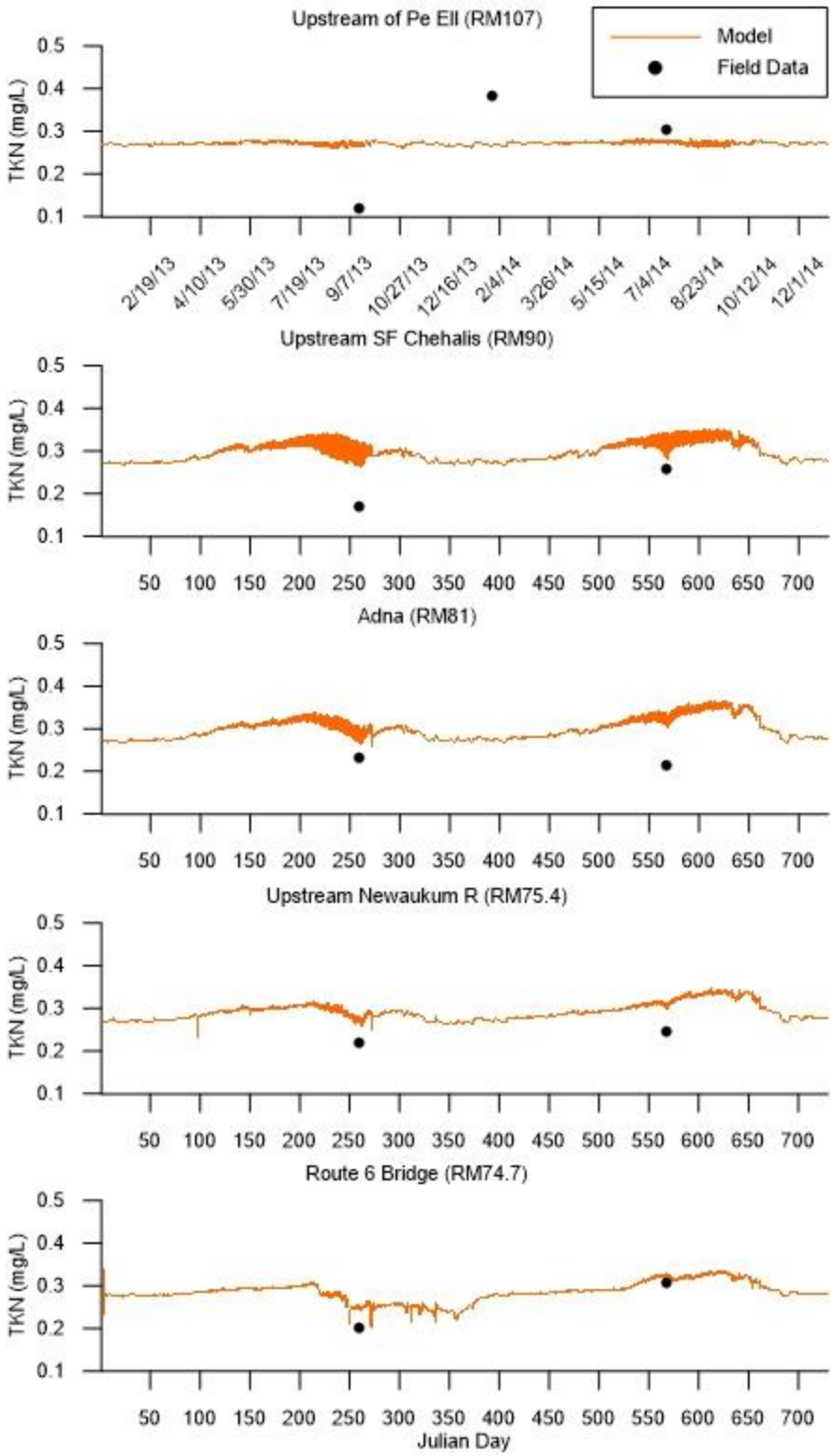

Figure 125. Model TKN predictions versus field data at upstream of Pe Ell, upstream of South Fork Chehalis River, at Adna, upstream of Newaukum River, and at Route 6 bridge

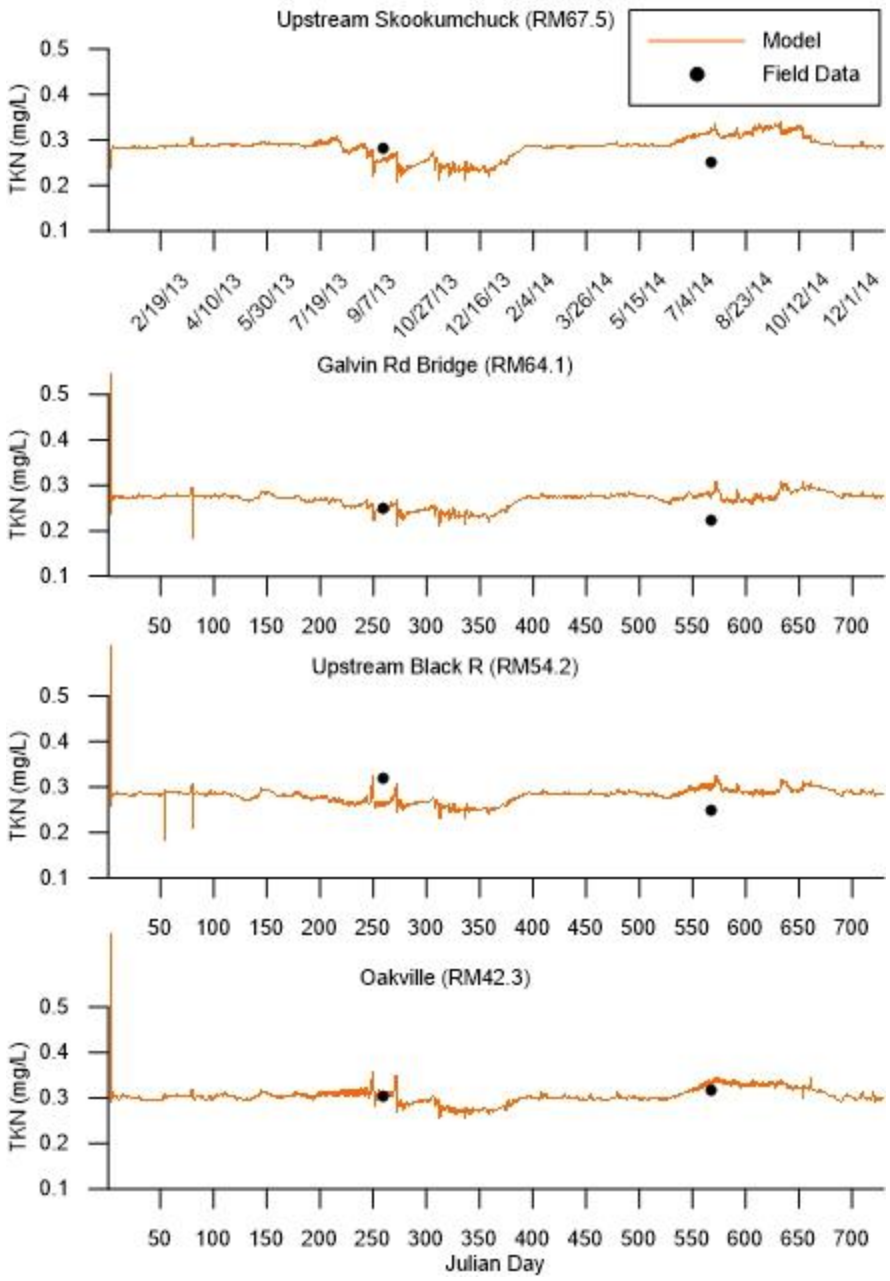

Figure 126. Model TKN predictions versus field data at upstream of Skookumchuck River, at Galvin Road bridge, upstream of Black River, and at Oakville

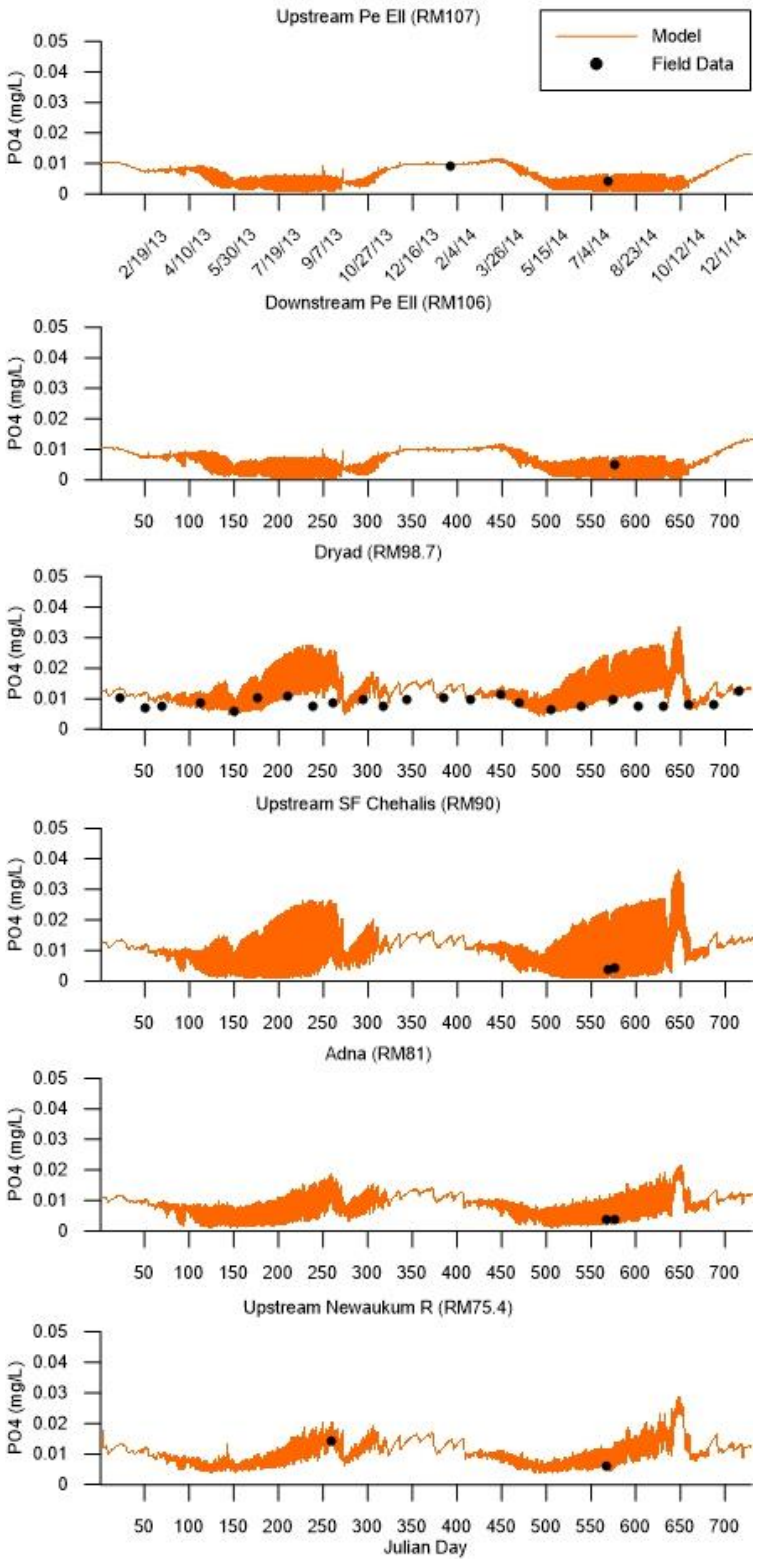

Figure 127. Model PO4 predictions versus field data at upstream of Pe Ell, downstream of Pe Ell, at Dryad, upstream of South Fork Chehalis River, at Adna, and upstream of Newaukum River

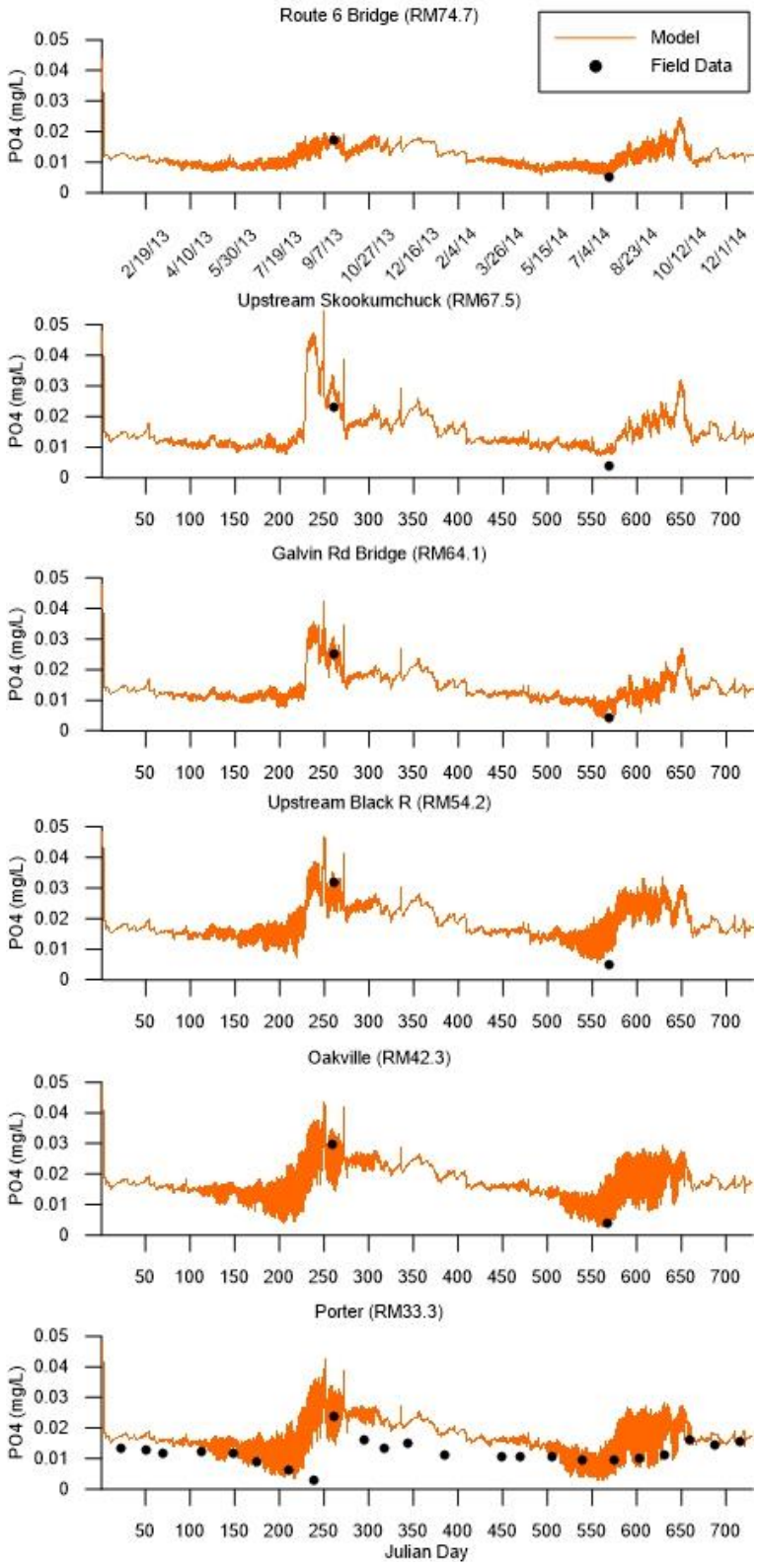

Figure 128. Model PO4 predictions versus field data at Route 6 bridge, upstream of Skookumchuck River, at Galvin Road bridge, upstream of Black River, at Oakville, and at Porter

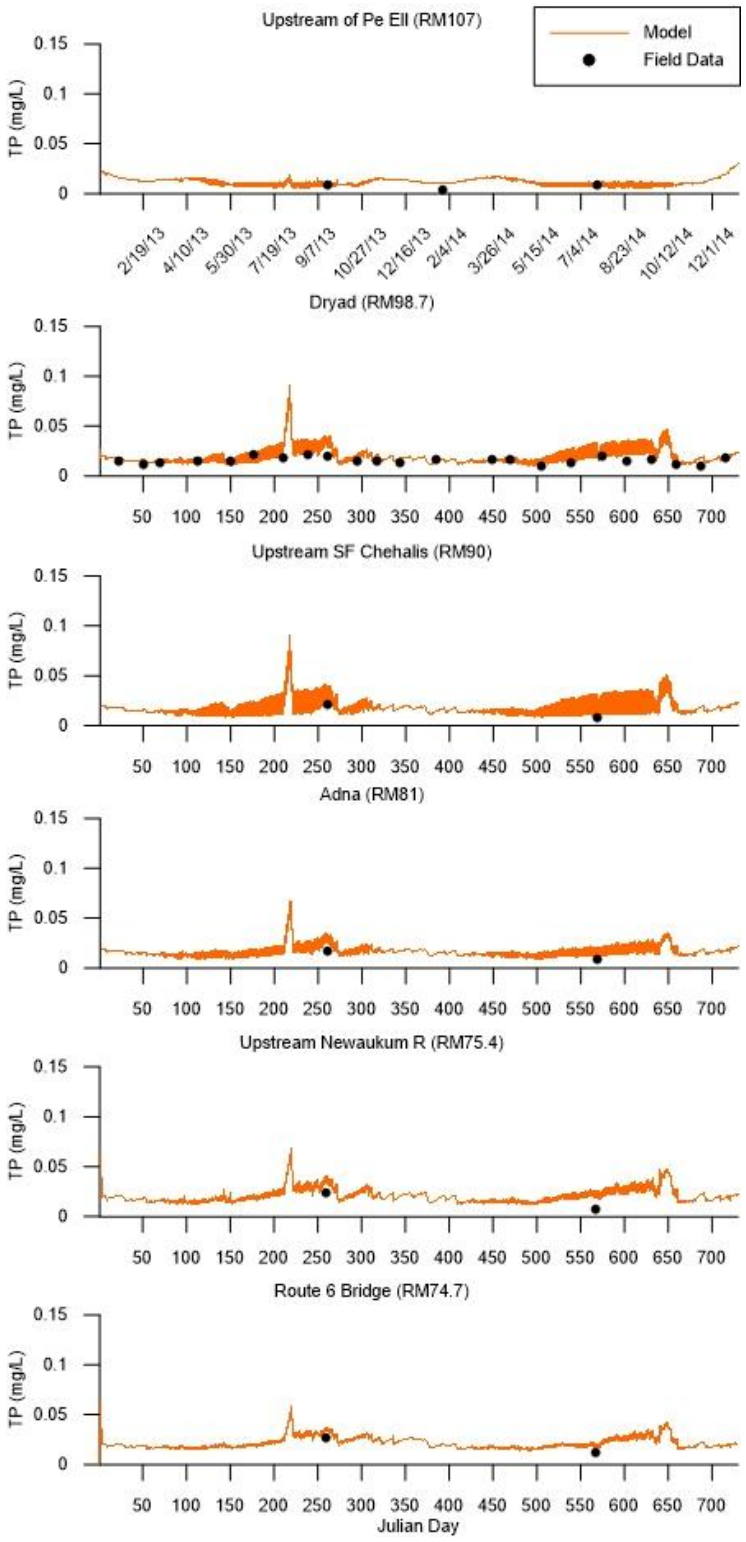

Figure 129. Model total phosphorus predictions versus field data at upstream of Pe Ell, at Dryad, upstream of South Fork Chehalis River, at Adna, upstream of Newaukum River, and at Route 6 bridge

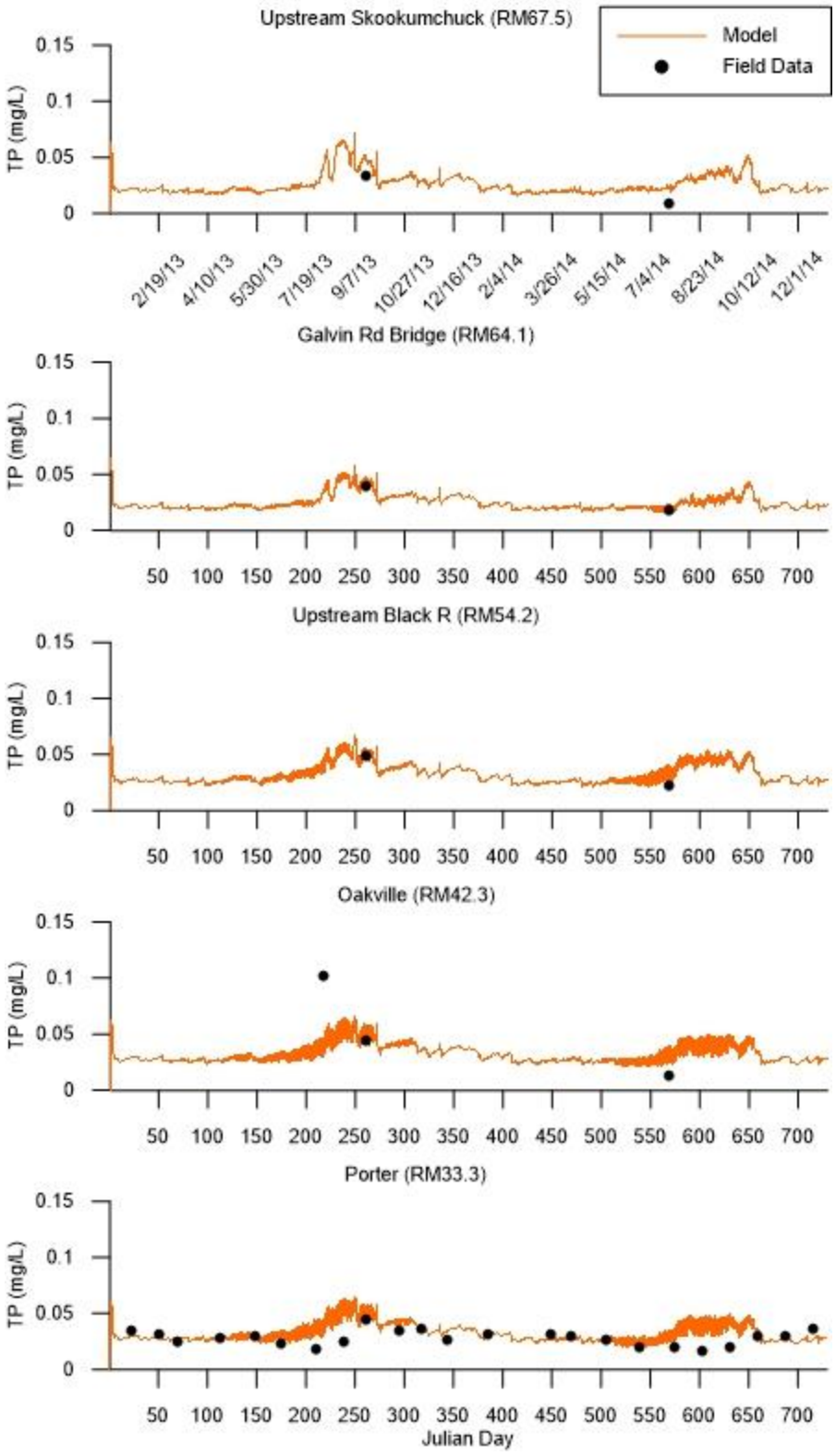

Figure 130. Model total phosphorus predictions versus field data at upstream of Skookumchuck River, at Galvin Road bridge, upstream of Black River, at Oakville, and at Porter

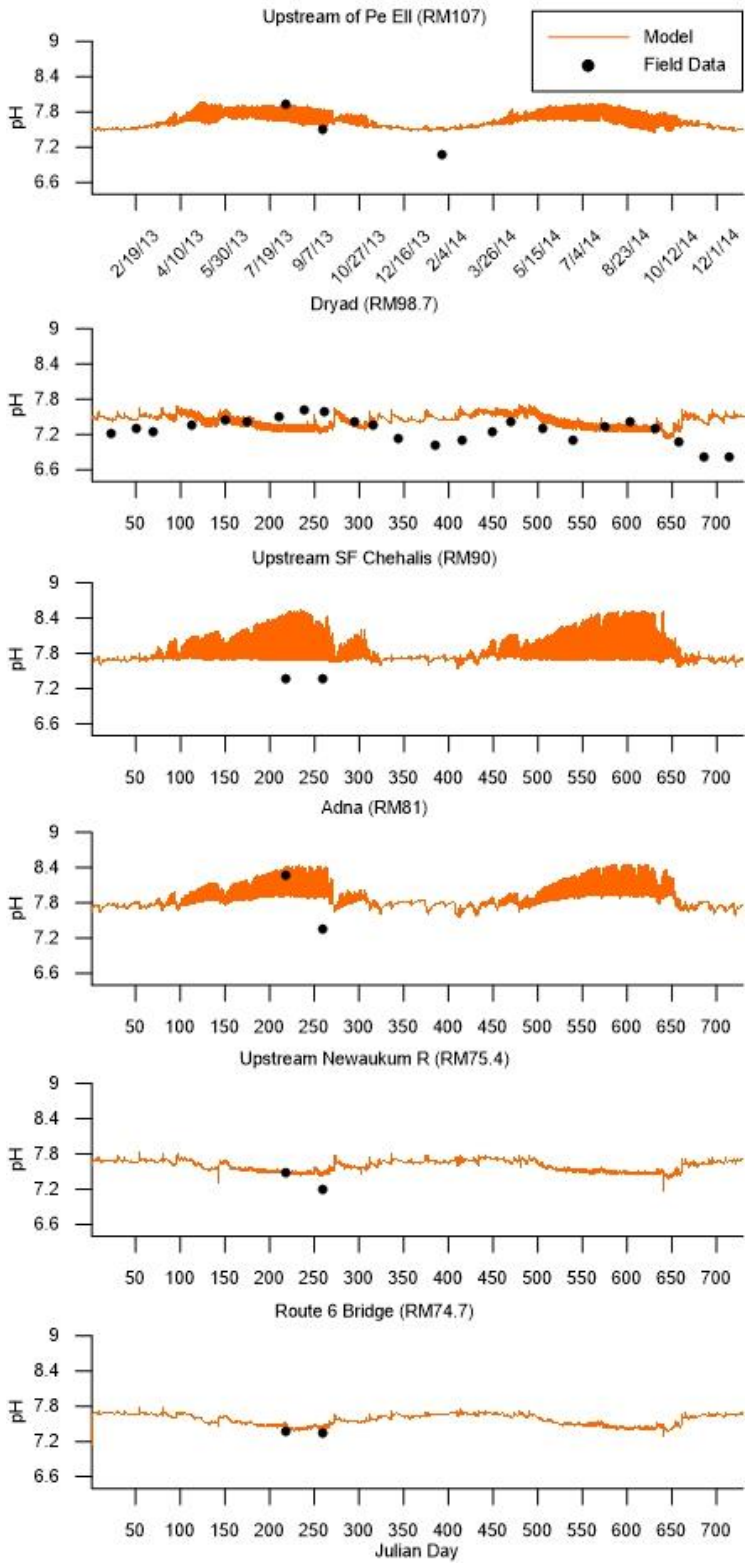

Figure 131. Model pH predictions versus field data at upstream of Pe Ell, at Dryad, upstream of South Fork Chehalis River, at Adna, upstream of Newaukum River, and at Route 6 bridge

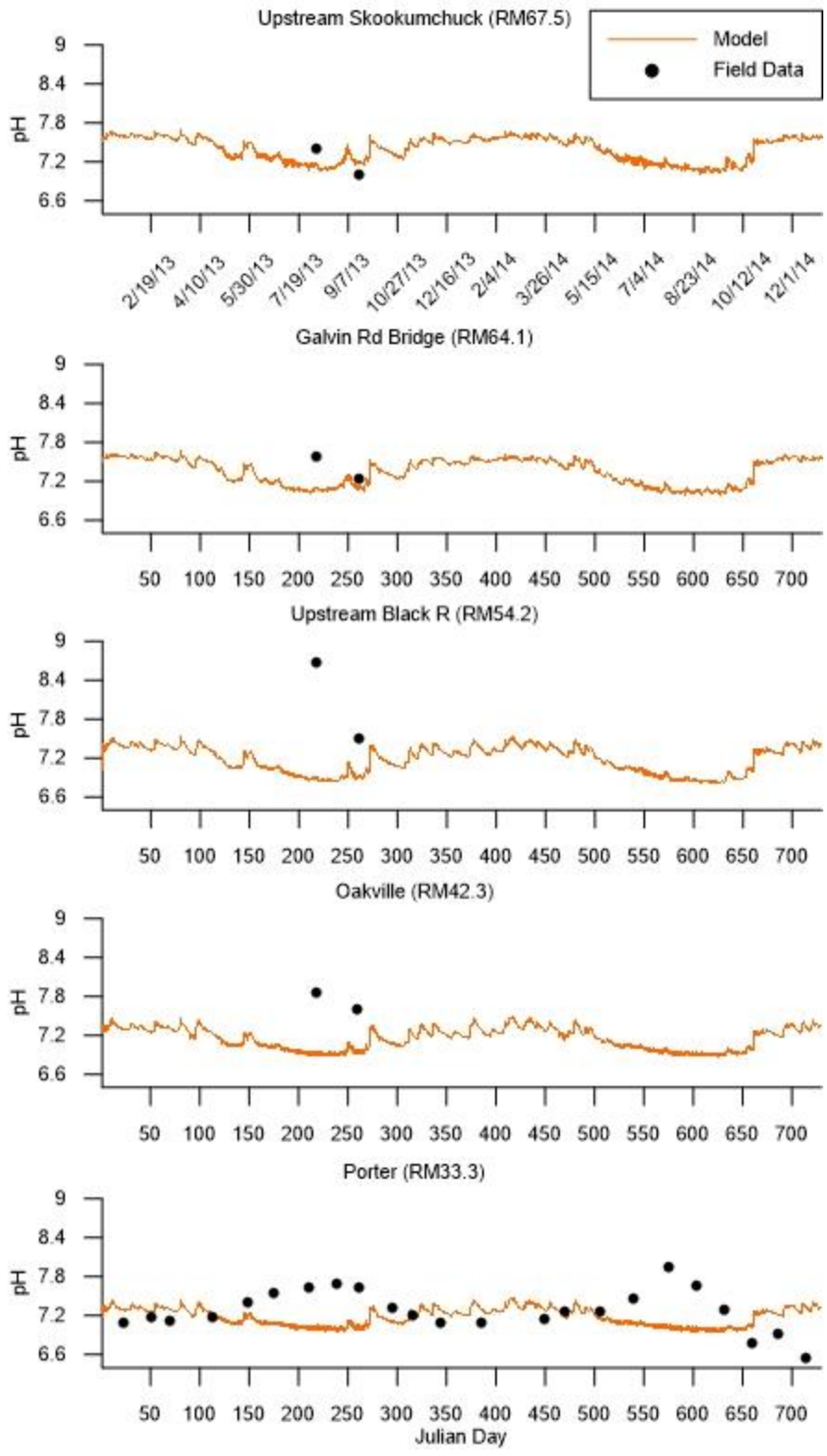

Figure 132. Model pH predictions versus field data at upstream of Skookumchuck River, at Galvin Road bridge, upstream of Black River, at Oakville, and at Porter

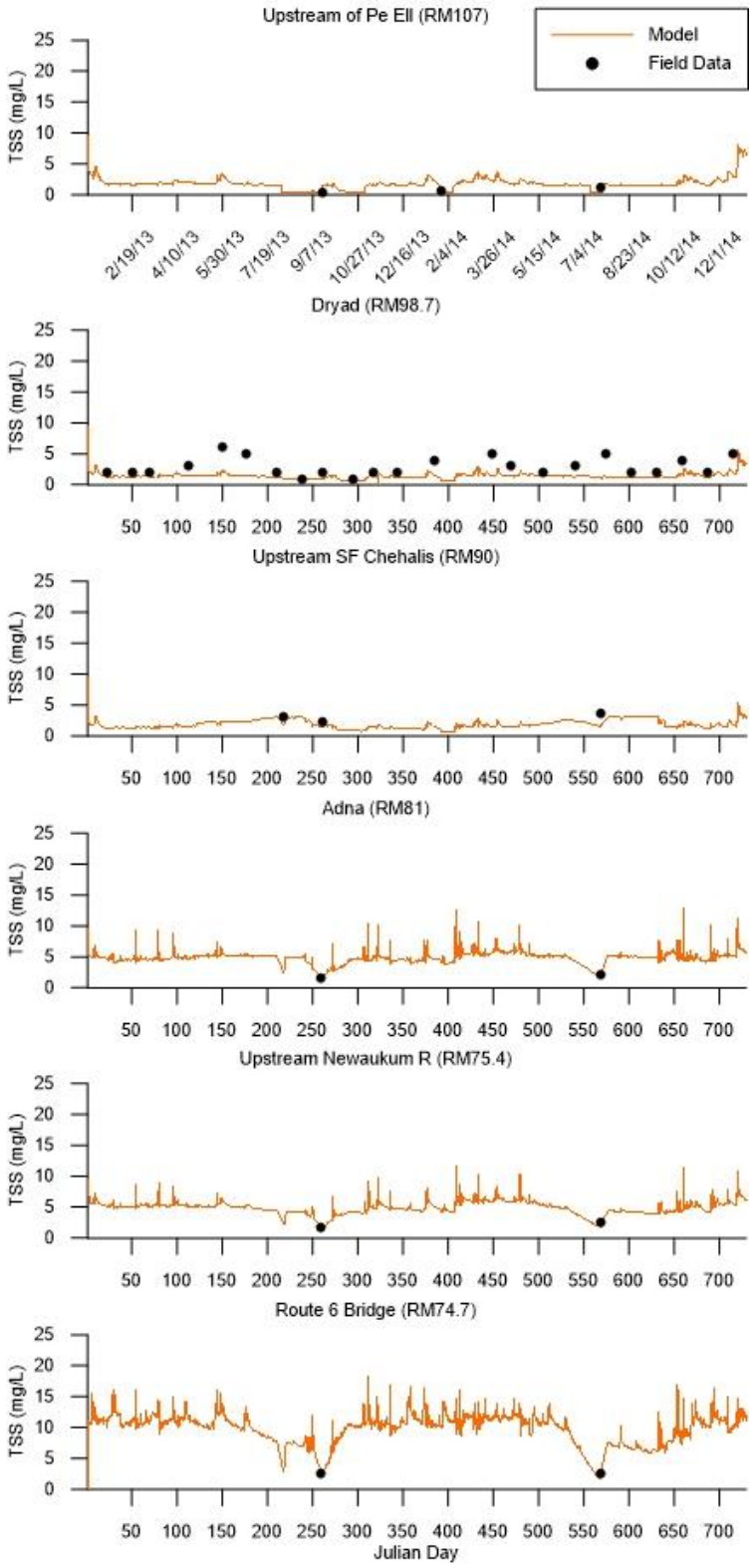

Figure 133. Model TSS predictions versus field data at upstream of Pe Ell, at Dryad, upstream of South Fork Chehalis River, at Adna, upstream of Newaukum River, and at Route 6 bridge

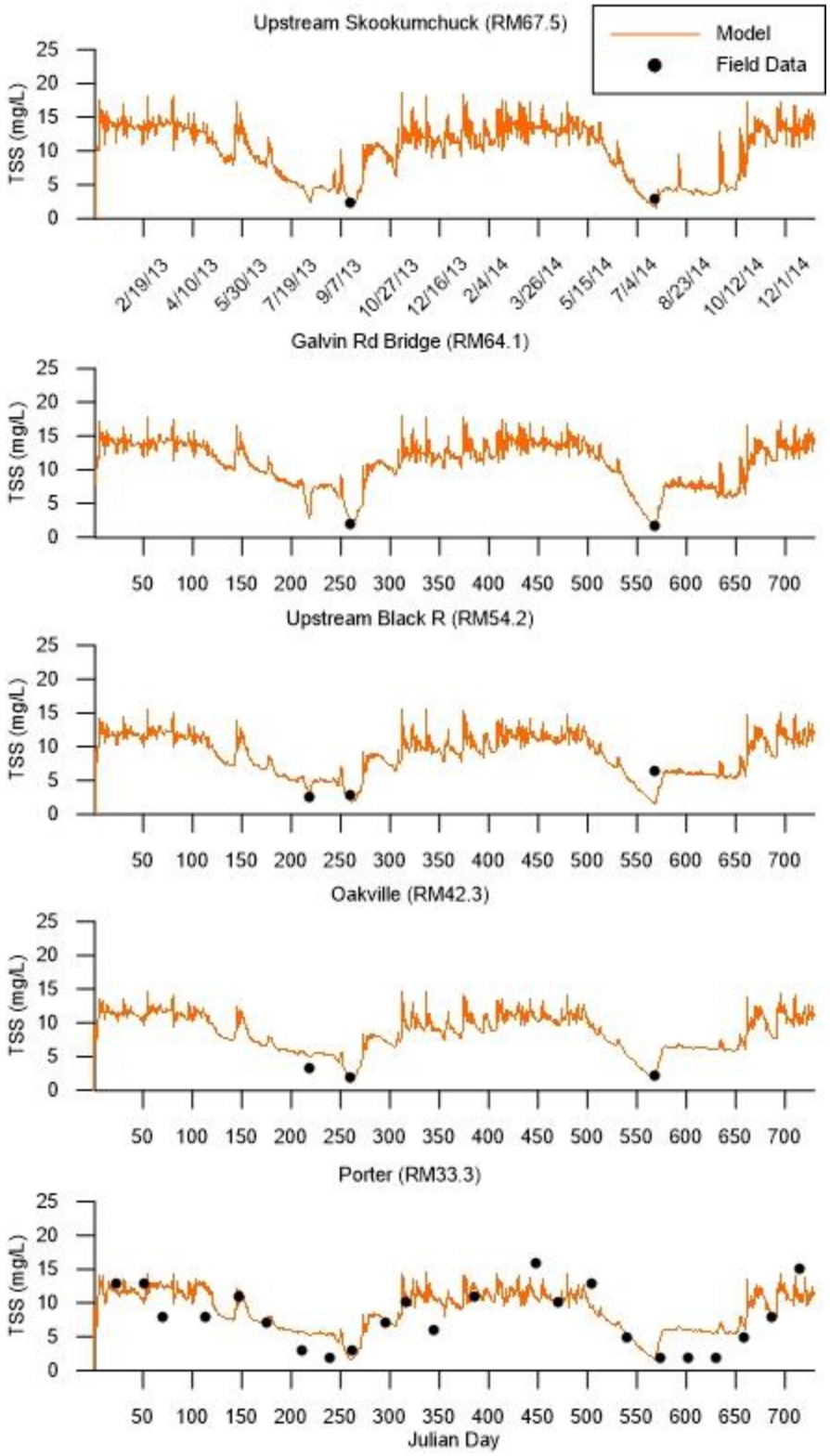

Figure 134. Model TSS predictions versus field data at upstream of Skookumchuck River, at Galvin Road bridge, upstream of Black River, at Oakville, and at Porter

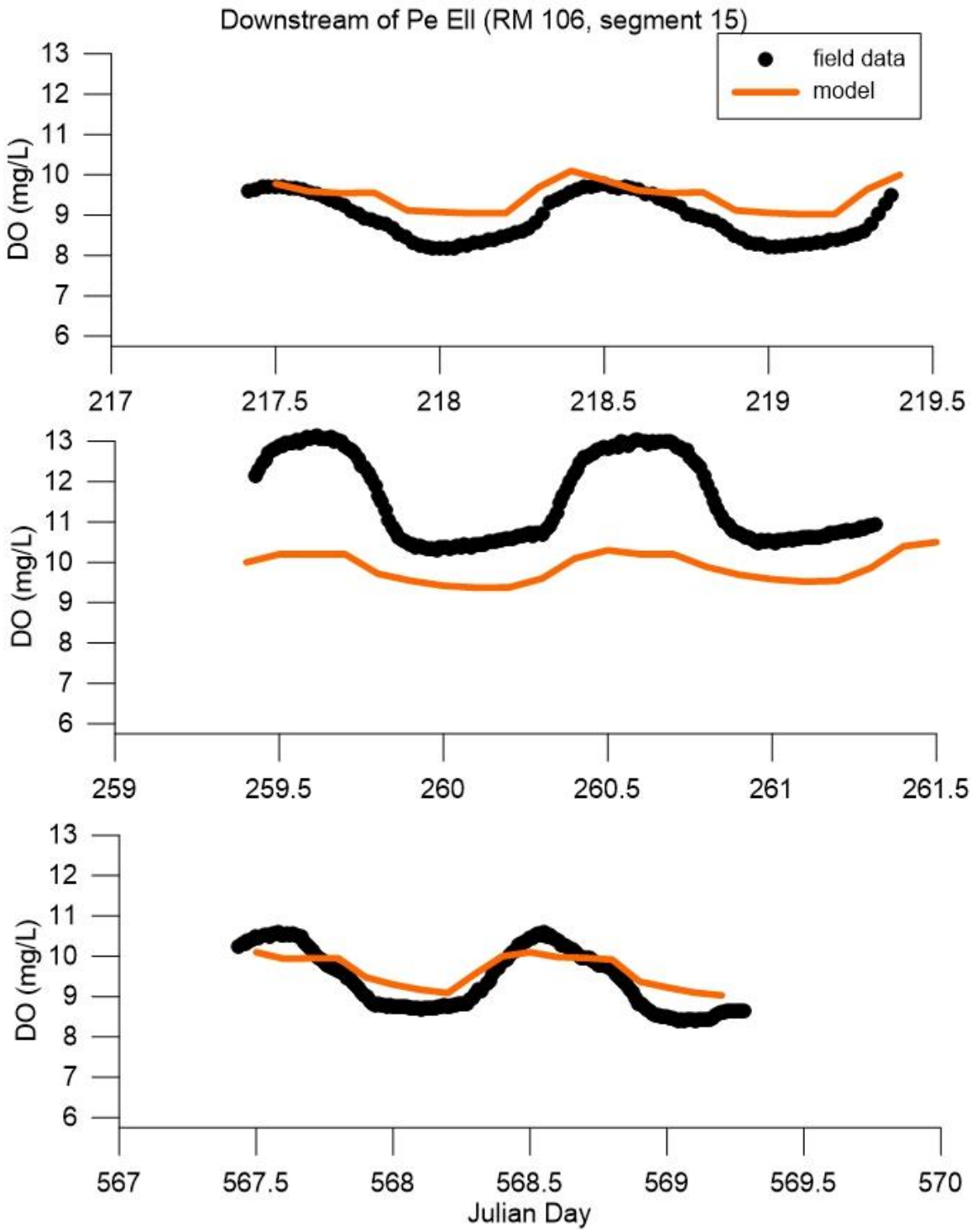

Figure 135. Model dissolved oxygen predictions versus continuous field data at the downstream of Pe Ell monitoring station

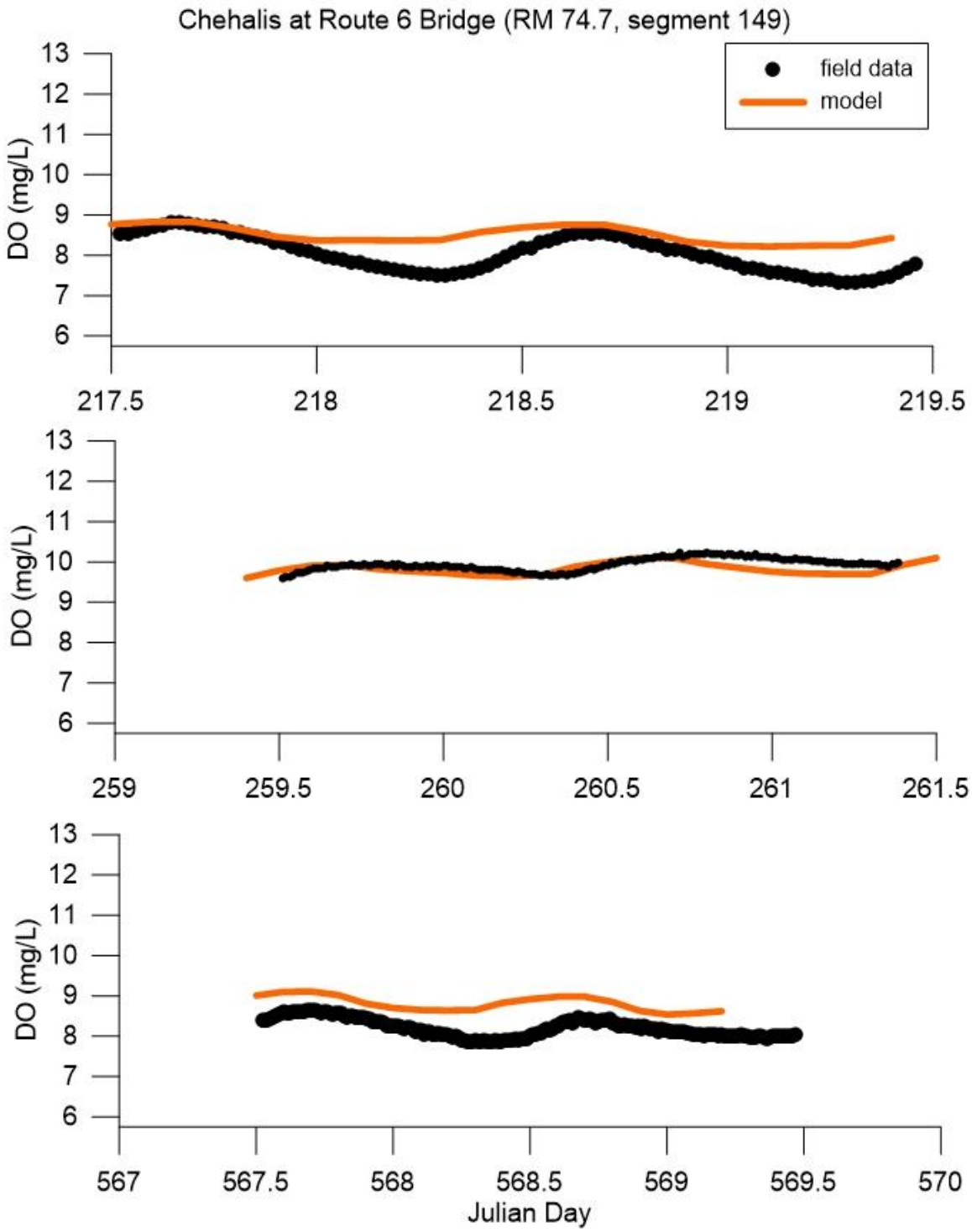

Figure 136. Model dissolved oxygen predictions versus continuous field data at the Route 6 Bridge monitoring station

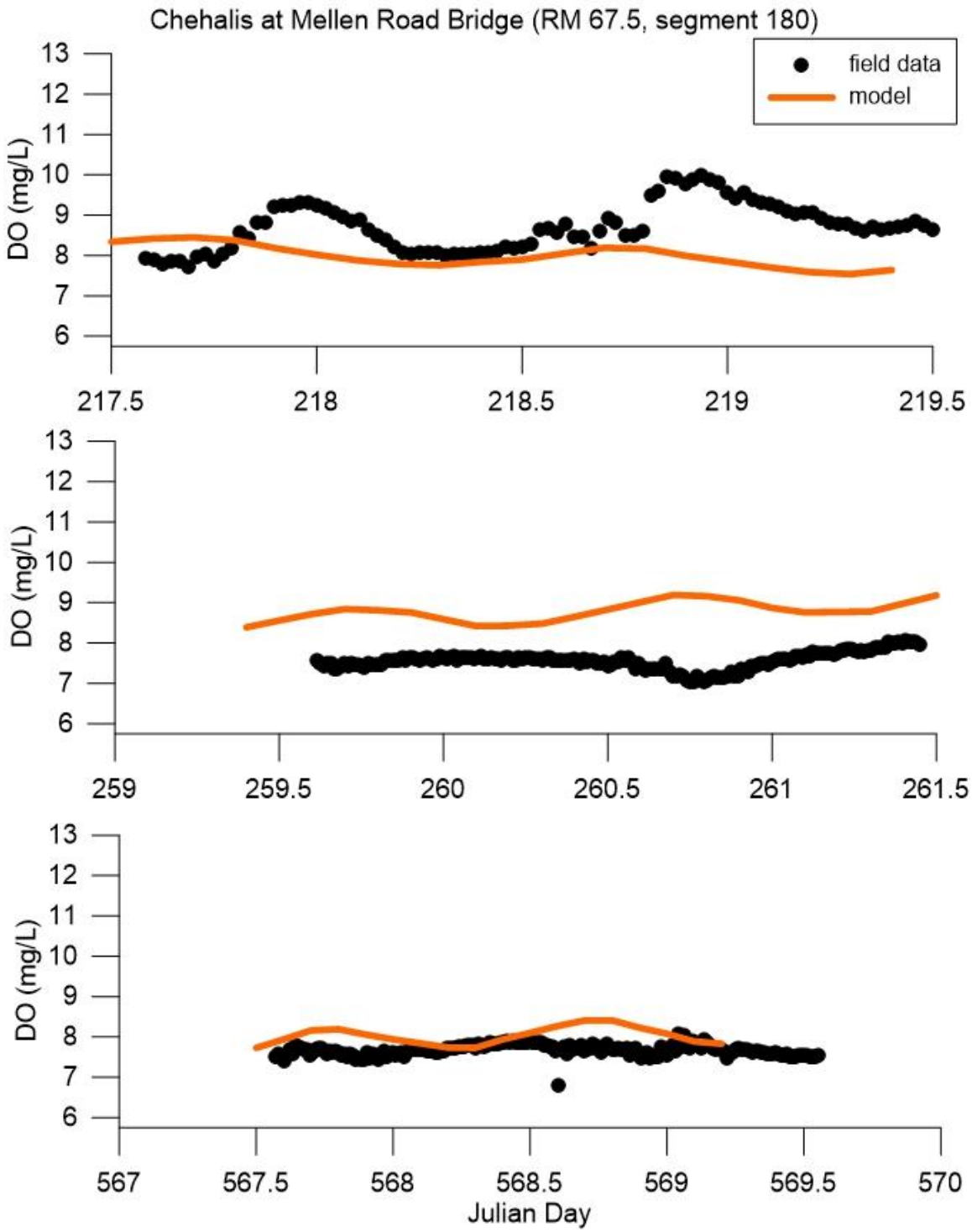

Figure 137. Model dissolved oxygen predictions versus continuous field data at the Mellen Road Bridge monitoring station

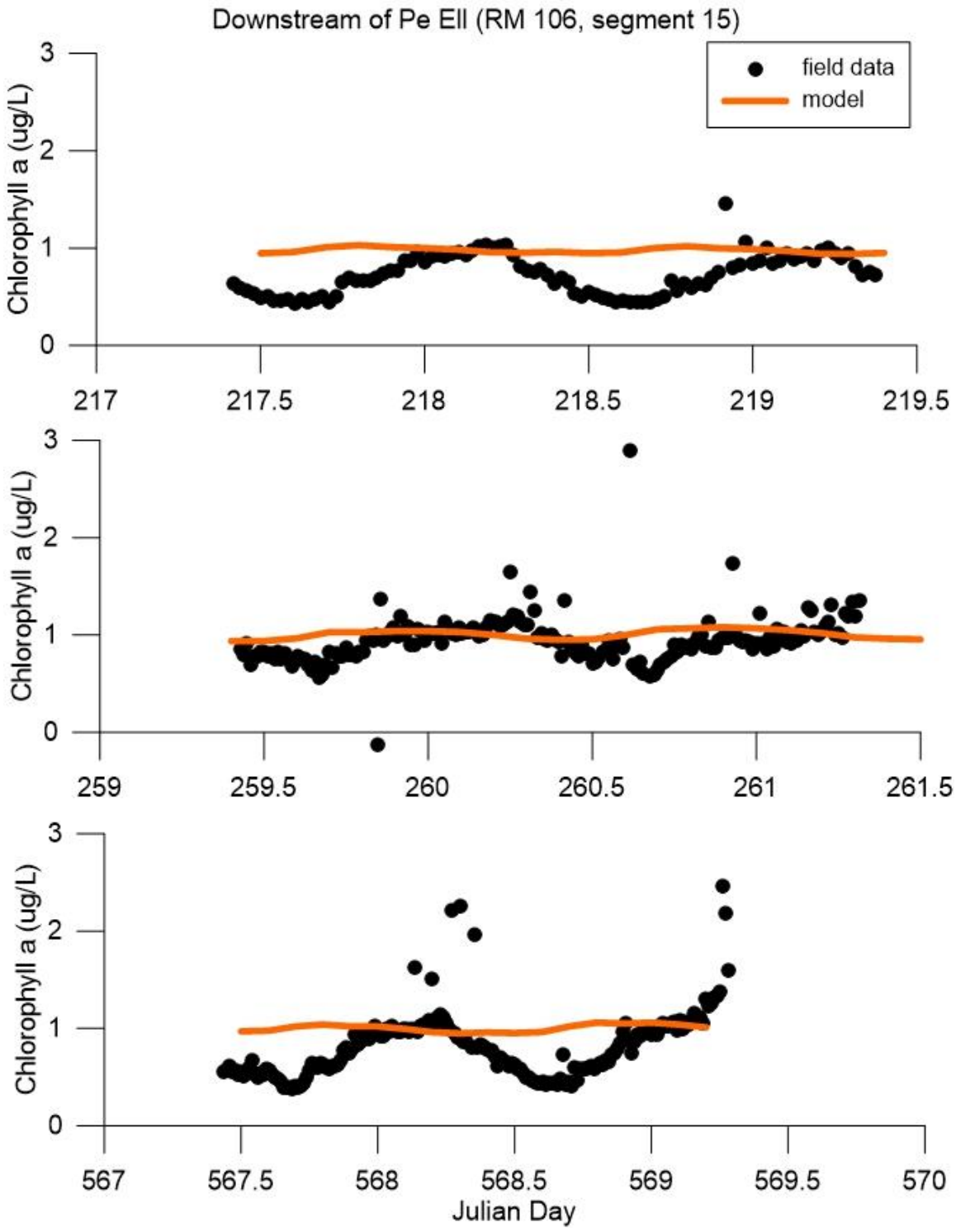

Figure 138. Model chlorophyll a predictions versus continuous field data at the downstream of Pe Ell monitoring station

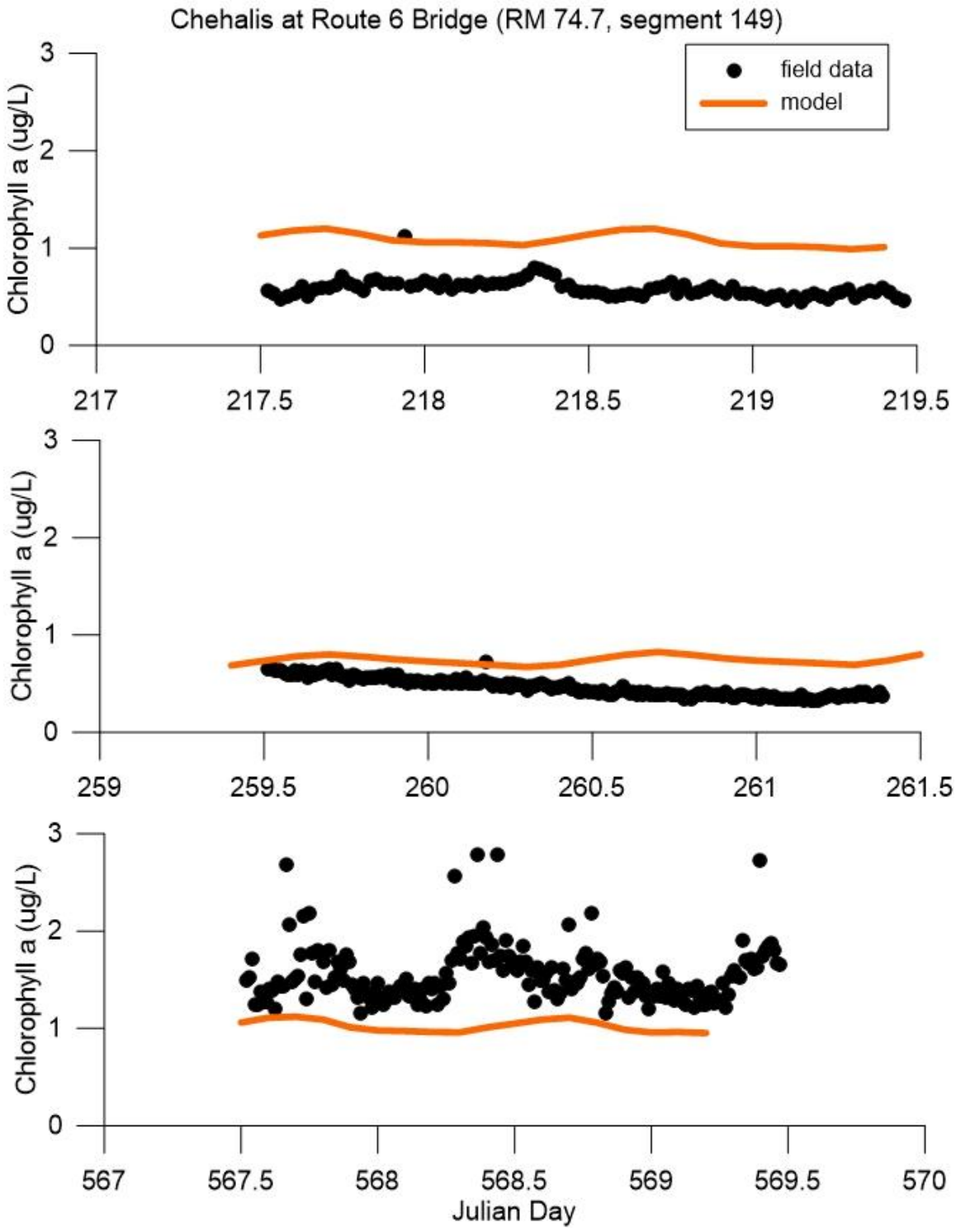

Figure 139. Model chlorophyll a predictions versus continuous field data at the Route 6 Bridge monitoring station

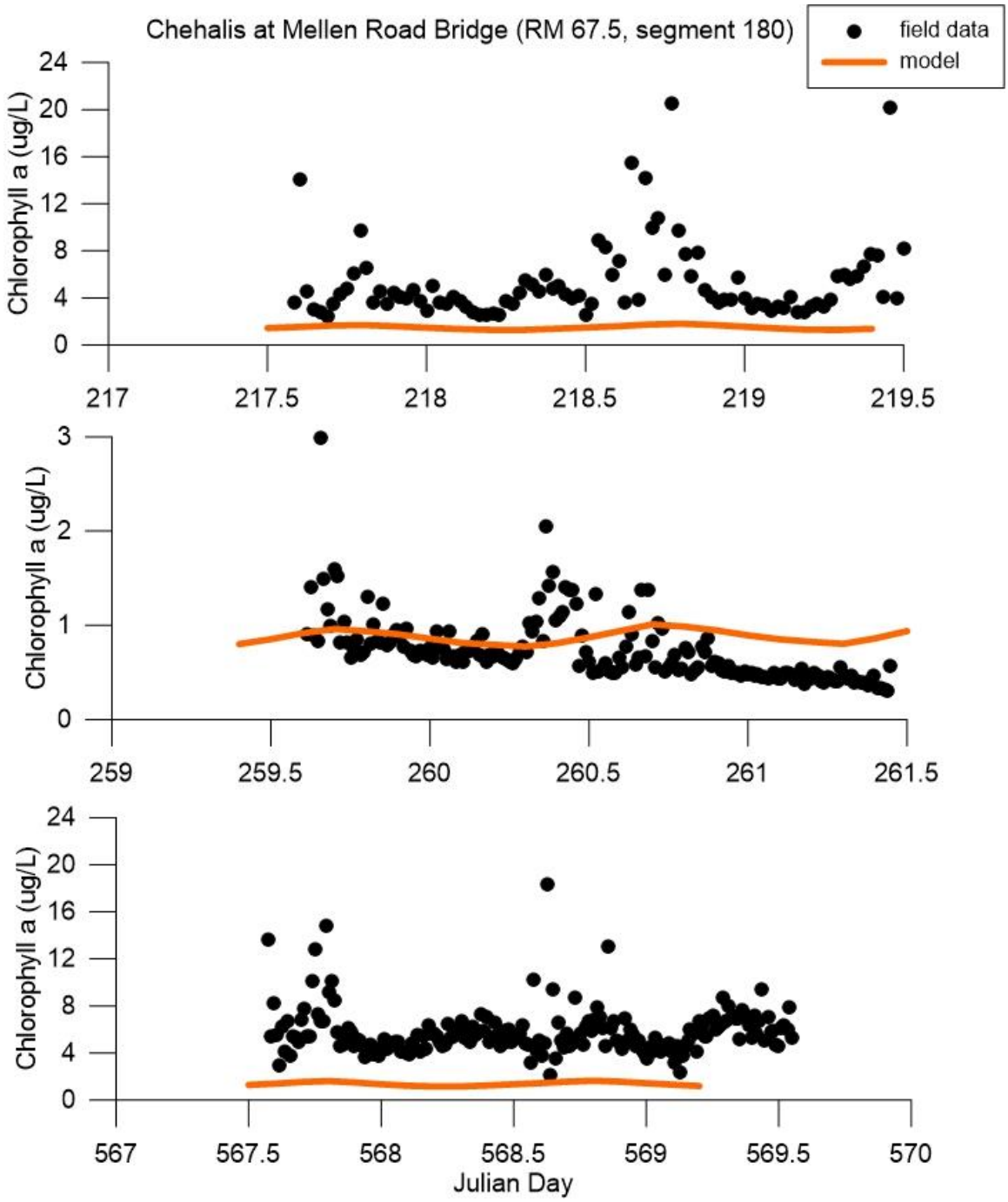

Figure 140. Model chlorophyll a predictions versus continuous field data at the Mellen Road Bridge monitoring station

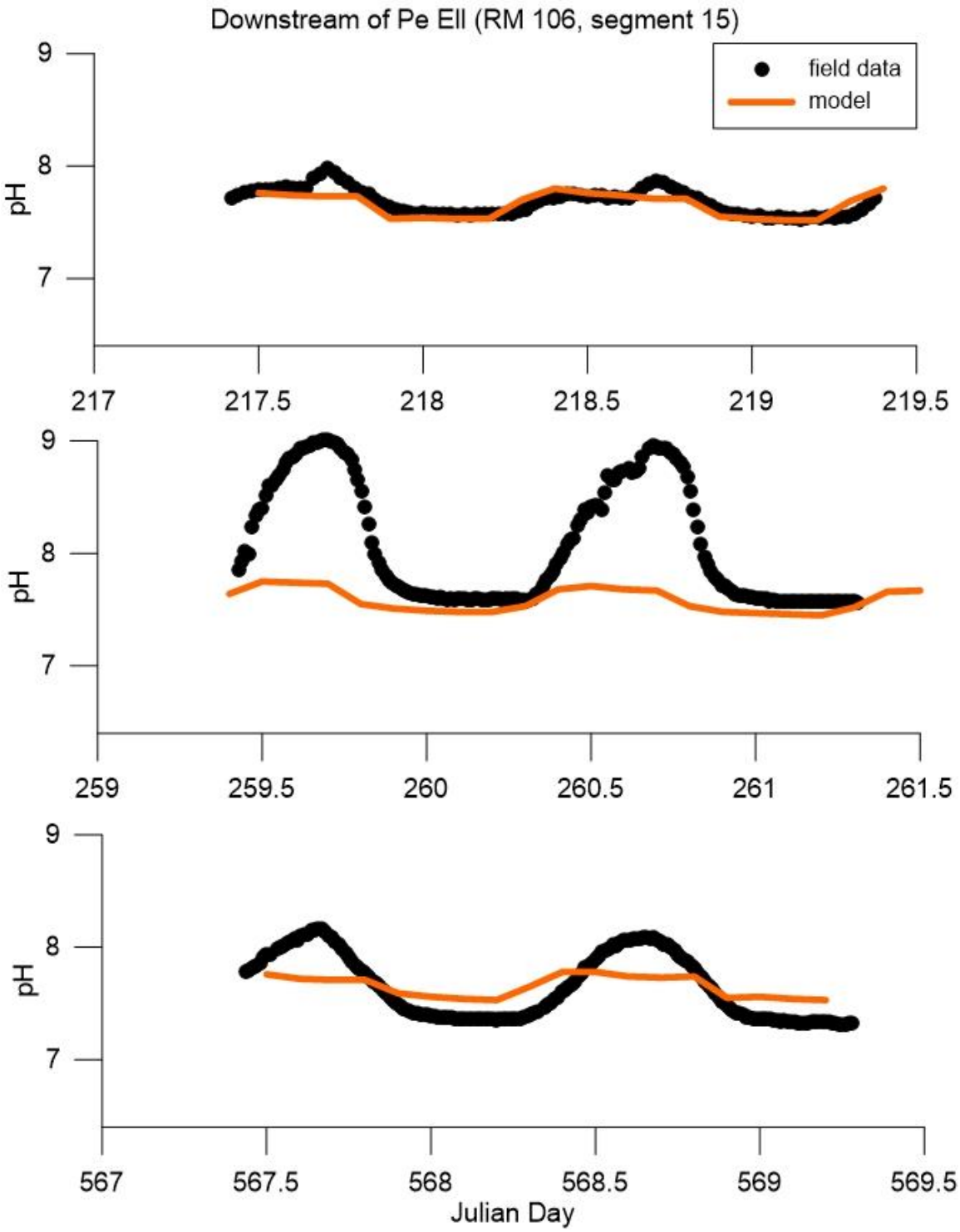

Figure 141. Model pH predictions versus continuous field data at the downstream of Pe Ell monitoring station

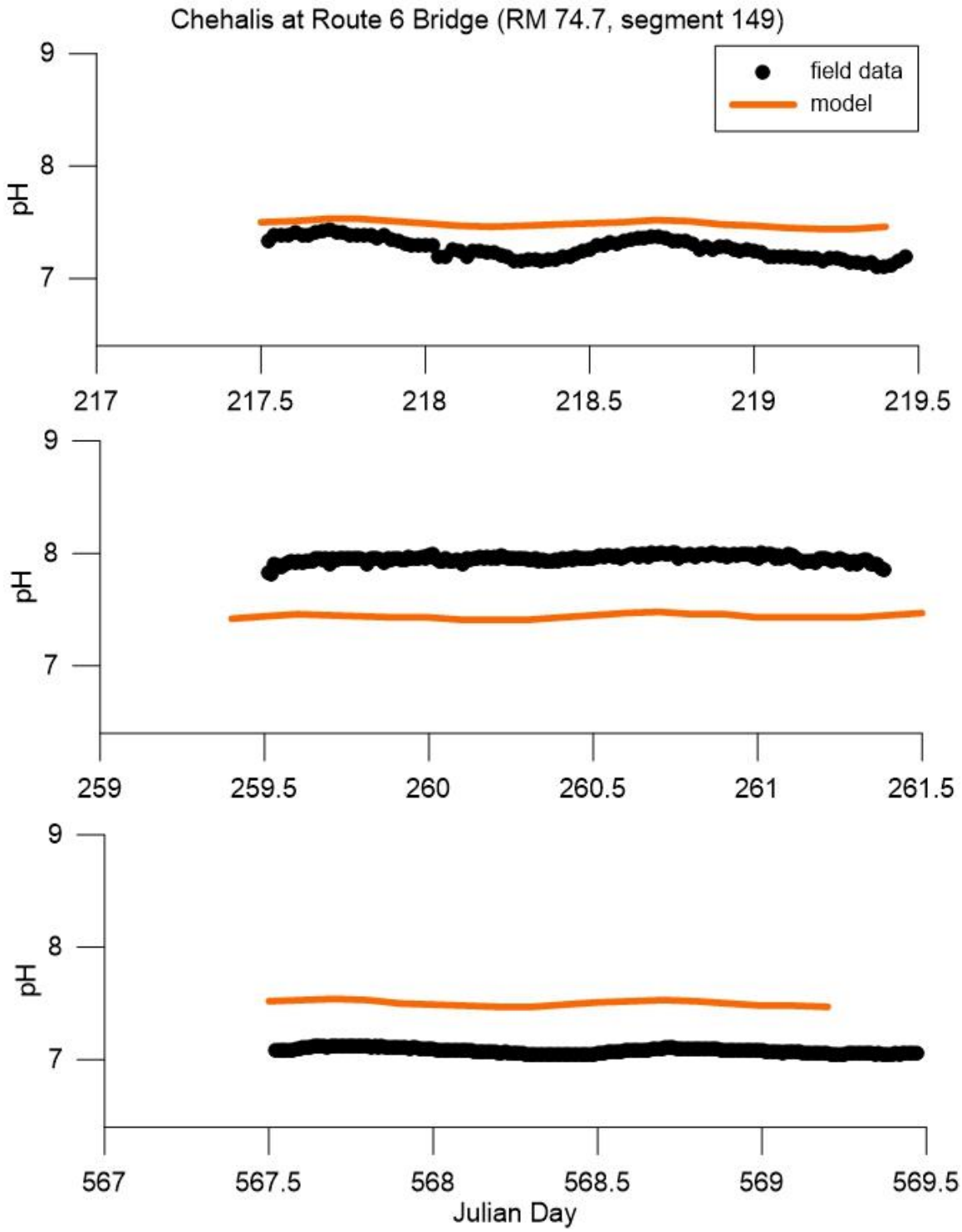

Figure 142. Model pH predictions versus continuous field data at the Route 6 Bridge monitoring station

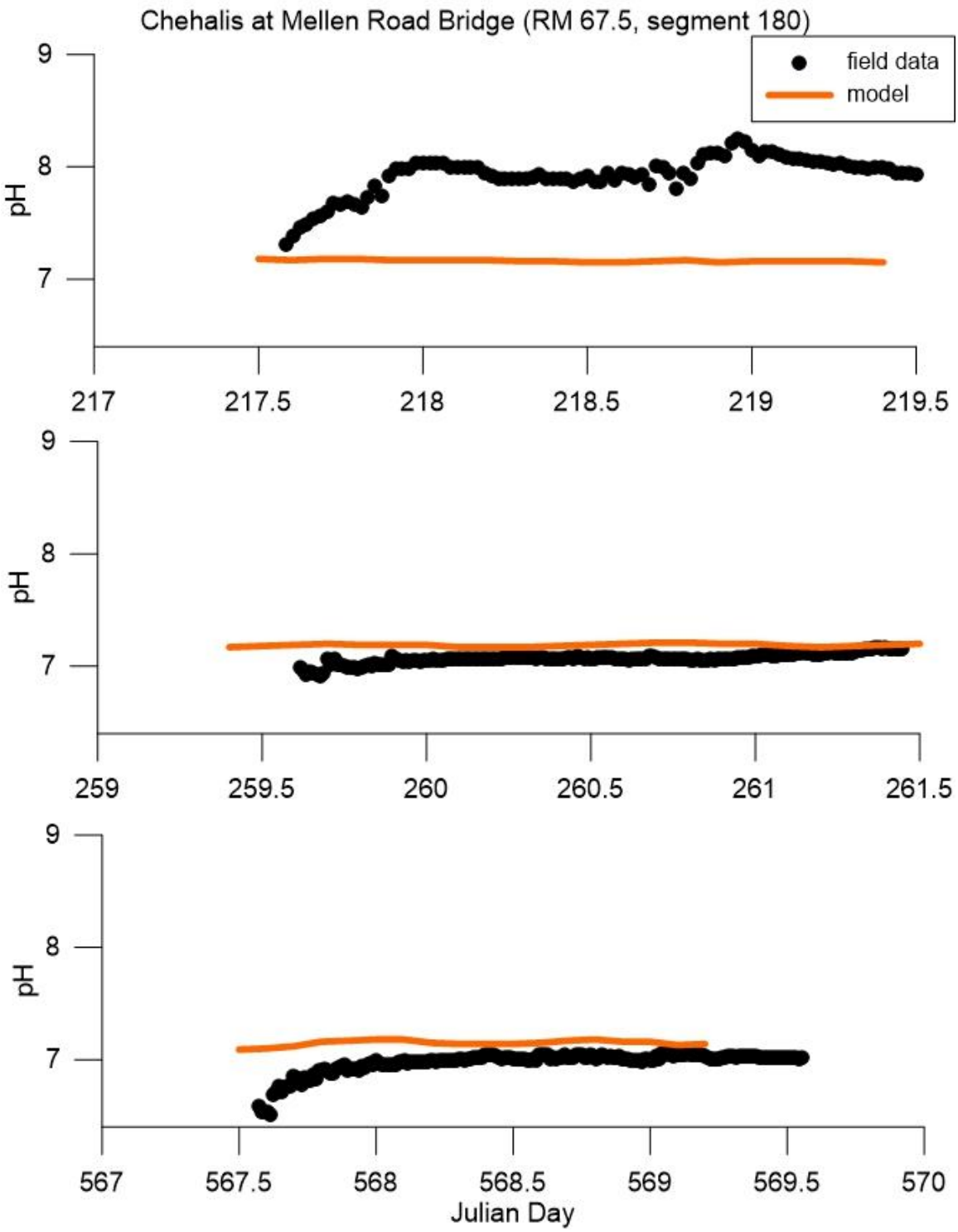

Figure 143. Model pH predictions versus continuous field data at the Mellen Road Bridge monitoring station

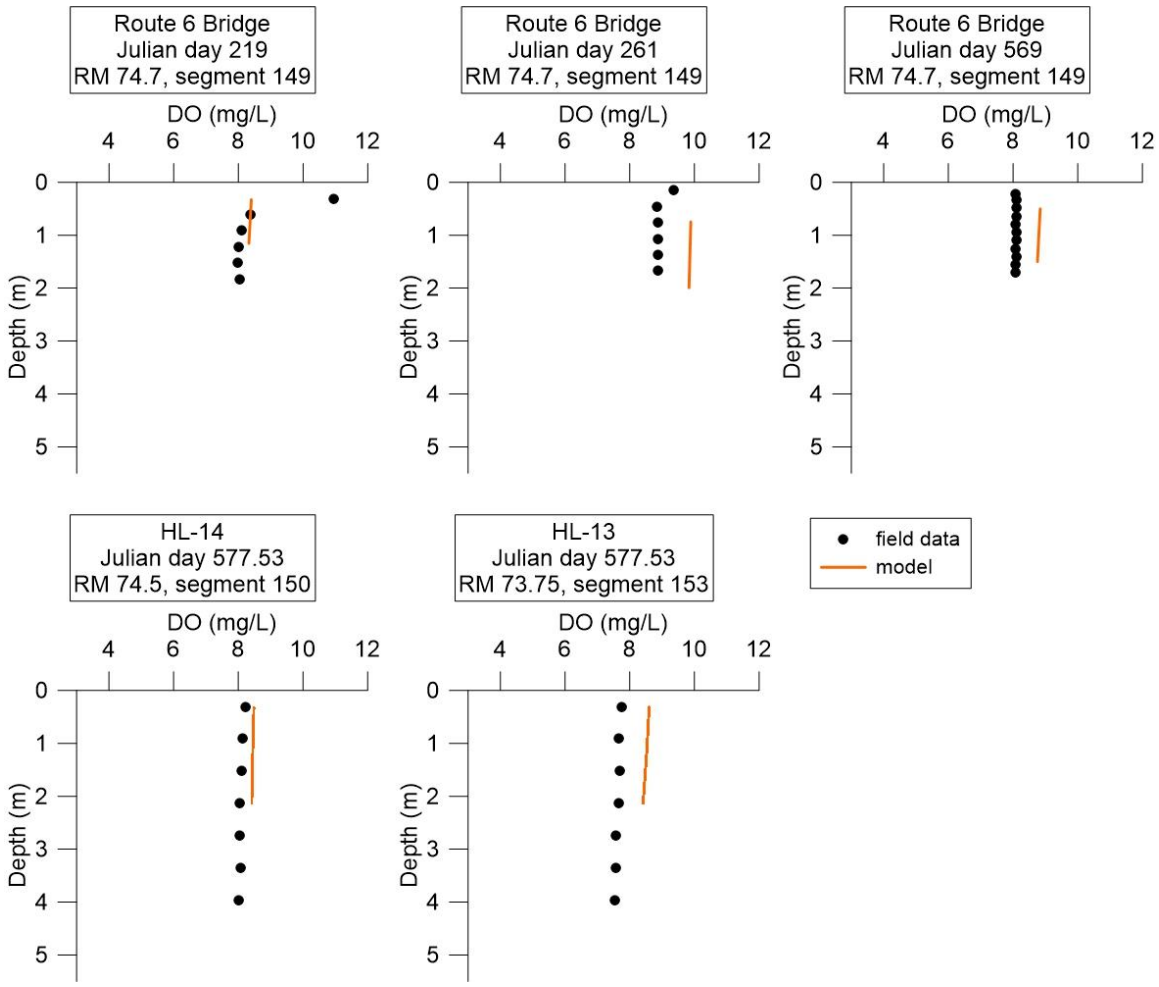

Figure 144. Model-predicted vertical dissolved oxygen profiles compared to field data at the monitoring stations: Route 6 Bridge, HL-14, and HL-13

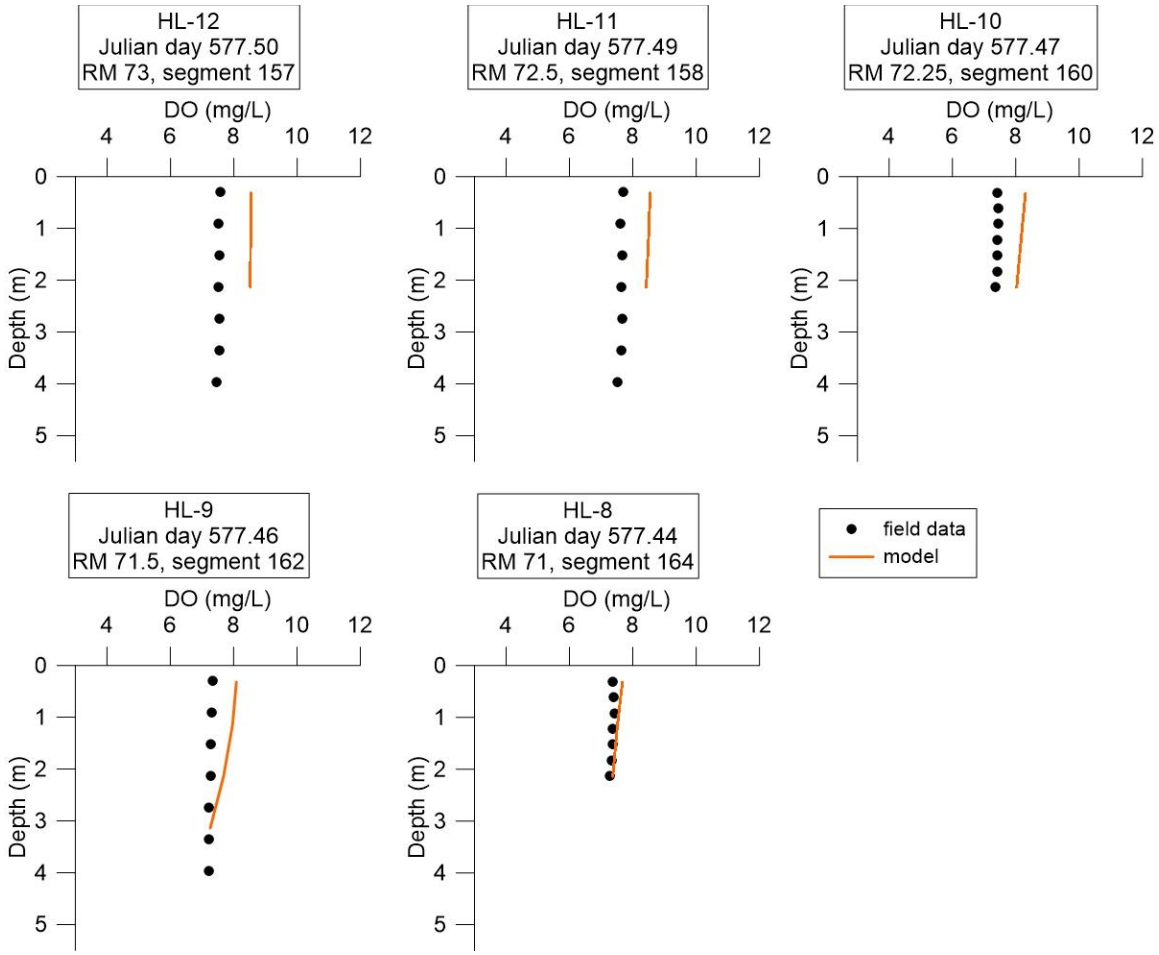

Figure 145. Model-predicted vertical dissolved oxygen profiles compared to field data at the monitoring stations: HL-12, HL-11, HL-10, HL-9 and HL-8

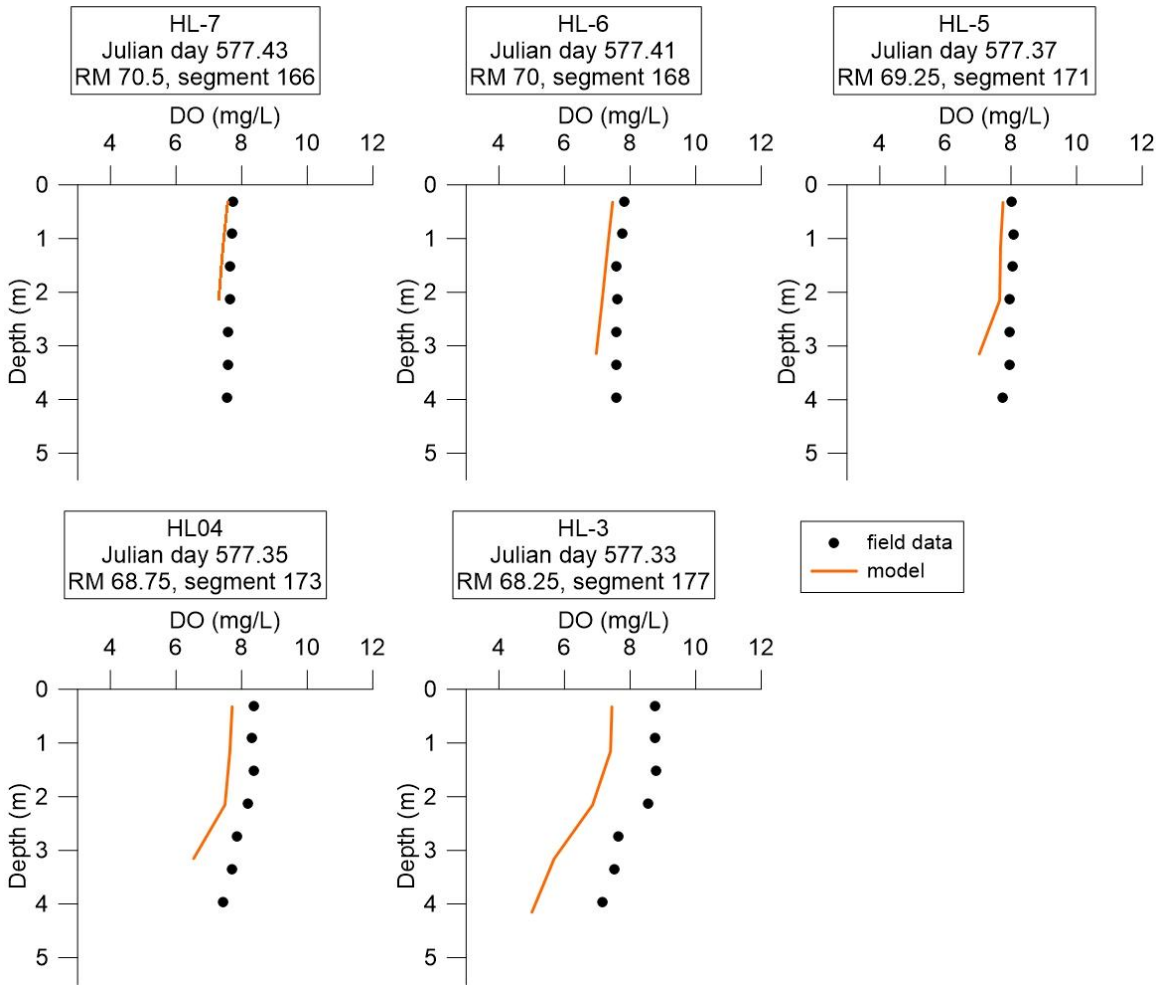

Figure 146. Model-predicted vertical dissolved oxygen profiles compared to field data at the monitoring stations: HL-7, HL-6, HL-5, HL-4 and HL-3

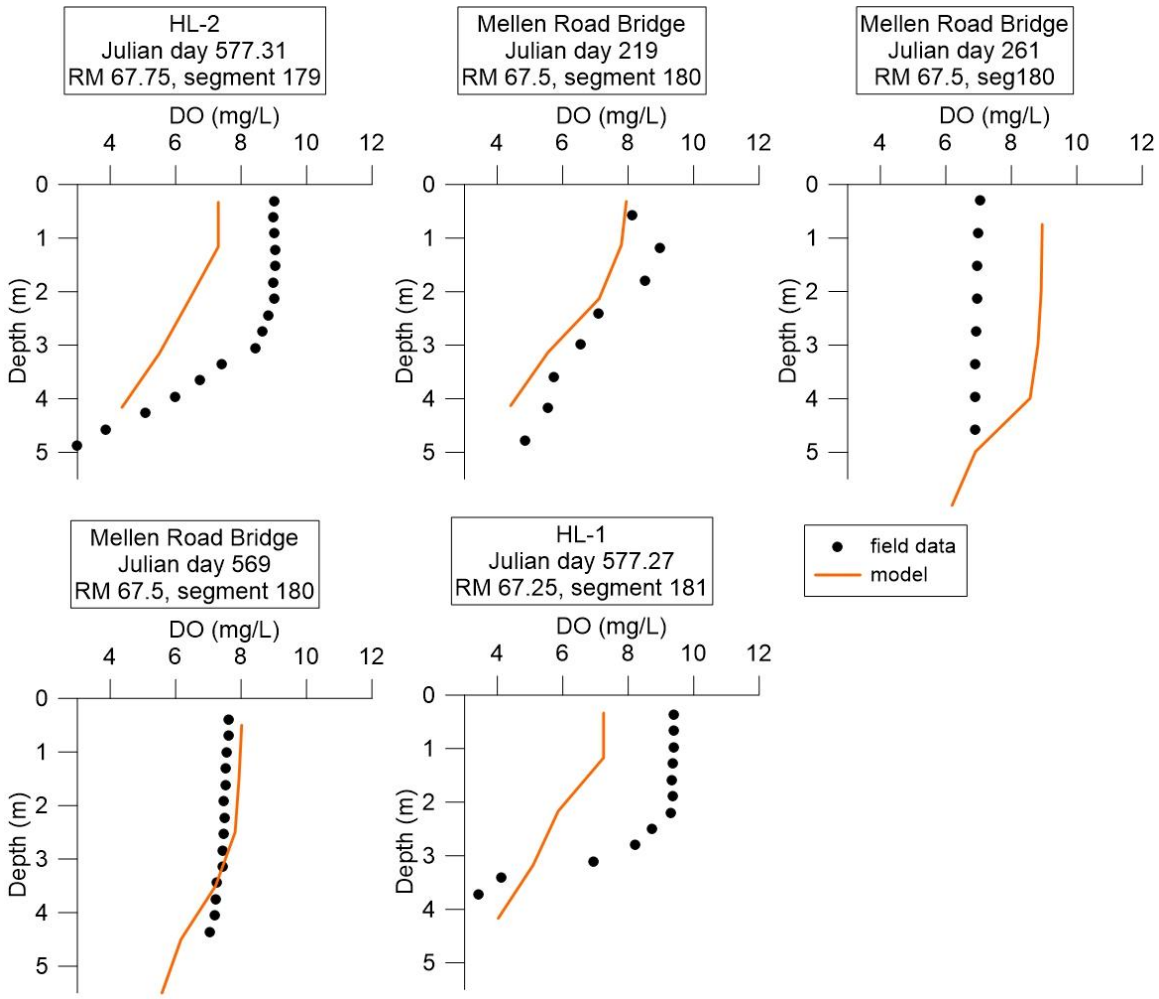

Figure 147. Model-predicted vertical dissolved oxygen profiles compared to field data at the monitoring stations: HL-2, Mellen Road Bridge, and HL-1

Boundary Condition Constituents

The model was very sensitive to boundary inflows for constituents and correctly assessing boundary conditions was perhaps the most important task for water quality calibration. Multiple re-evaluations of estimates used for wastewater treatment plants, tributaries, and groundwater flows were necessary.

Wastewater Treatment Plants

Wastewater treatment plants often significantly impacted the resulting conditions in the river, as their constituent concentrations were often much greater than those from the upstream boundary or inputs from tributaries. This was especially important during the summer months when flow in the river was low. For this reason, careful analysis of wastewater treatment plant data and filling in missing data was an important step for water quality calibration.

Often, constituent data were missing entirely for some wastewater treatment plants. In this case reasonable values were used as an approximation. For example, NO3 data were completely missing for the Pe Ell, Darigold, and Centralia wastewater treatment plants, so typical values between 0.5 mg/L and 1 mg/L were used as estimates. Adjustments were made to concentrations to aid in water quality calibration, as no data were available for confirmation.

Particulate matter settling and decaying in the upper reaches of the model impacted the calibration of dissolved oxygen and nutrient species, particularly ammonia. When the fraction of BOD assumed to be dissolved was low and the fraction assumed particulate was high, large amounts of organic particulates settled to the bottom of the channel and upon degradation in the sediments reseased ammonia back into the water. This raised model concentrations of ammonia above field data values. When BOD was assumed to be equally partitioned between dissolved and particulate, resulting ammonia concentrations more closely matched field data.

Tributary Winter Estimations

Generally, tributary water quality data were only available during the summer months. Using summer values as approximations for winter values proved to be inaccurate in many cases. Field data along the mainstem river showed DO, TSS, and nitrate levels were higher during winter times, while ammonia concentrations were higher during summer times. Presumably, these trends would also be occurring in the tributaries. These seasonal variations were important to include in order to reproduce field data.

When possible, field data collected during winter from the mainstem Chehalis were used as an estimate for tributaries. For example, an NO3 value of 0.724 mg/L was sampled on the mainstem river near the upstream boundary during winter. This value was used for the major tributaries since no other data were available. This value was higher than summer nitrate concentrations, which generally ranged between 0.01 mg/L and 0.5 mg/L. Nitrate concentrations were predicted to be too low when summer values were implemented during winter times. Higher winter nitrate concentrations from runoff from surrounding agricultural land during the winter months may not be captured in data sets containing values only collected during summer.

When it was not possible to use data collected during winter times, reasonable winter values were used as an estimate. For example, TSS data were entirely unavailable during the winter months, so 20 mg/L was used during these times as an approximation. This value was much higher than the summer TSS data, which generally ranged between 1 and 5 mg/L. Higher TSS concentrations are often seen during winter times as rainfall runoff entering the stream often carries additional solids.

Generally, TSS values included particulate BOD. However, one BOD data point collected on September 17, 2013 was excluded for Elk Creek. This value equaled 24.3 mg/L, and was much higher than any other BOD value collected for this tributary, or any of the other tributaries. This data value seemed unreasonable to apply for a long period of time when no other field data were available. Including this data point produced high model predictions for TSS and issues with other mainstem measured concentrations around the date it was collected.

DO values were only available for tributaries during the summer months, when water temperatures were warmer. Warmer water generally has lower DO concentrations than cooler water, so using summer DO values as approximations for winter times was unrealistic. DO values were estimated for the tributaries based on temperature and assuming 100% saturation. This was done using known relationships and assuming zero chloride concentration (Chapra, 1997).

Groundwater

While groundwater flows were very small, the impacts on water quality in the river were still necessary to consider for calibration, particularly during the low flow summer season. Some constituents had much different magnitudes in groundwater than seen in the rivers and creeks entering the system.

When gaps in groundwater constituents existed, they were generally filled in using averages or medians of other available groundwater measurements. Often, using median values to estimate missing data rather than averages was important for groundwater since many averages gave constituent concentrations biased towards higher values. Sometimes groundwater constituents were estimated using a value within the range of data available. For

example, dissolved oxygen for the groundwater reaches ranged between approximately 0.1 mg/L and 2.6 mg/L, so 2 mg/L was assumed reasonable and implemented for much of the groundwater inputs.

Groundwater inputs for nitrates were particularly important for the downstream reaches of the model. When estimates of groundwater nitrate were too high, nitrate built up and steadily increased higher than reflected in mainstem river field data in the downstream reaches. Reducing these concentrations helped to match model predictions to field data. The upstream reaches had a groundwater median nitrate value of 0.01 mg/L implemented (Pitz, 2005). The groundwater nitrate concentrations generally ranged from 0.01 mg/L to 1.3 mg/L, so a value of 0.5 mg/L was assumed reasonable for the downstream reaches for groundwater.

Locating Tributaries that Affected In-Stream Water Quality

Since there were a large number of tributary inputs to the model, determining which inputs were affecting in-stream water quality conditions was an important step in water quality calibration.

Originally, between the locations at river miles 107 and 98.7 a peak in model-predicted TP occurred near Julian day 220 that persisted downstream. This peak was not reflected in mainstem Chehalis River field data. Between these two locations the only inputs to the model were the Pe Ell wastewater treatment plant and Elk Creek. Around this time the Pe Ell wastewater treatment plant TP concentration was approximately 0.08 mg/L, while the model-predicted mainstem TP reached approximately 0.1 mg/L. While wastewater treatment plants often had a major influence on water quality in the Chehalis River, in this case the Pe Ell wastewater treatment plant was not the cause for the peak in TP. Elk Creek, however, had TP concentrations exceeding 0.1 mg/L during this time. This was largely due to its organic matter as phosphorus (OMP) concentration. Elk Creek OMP was initially calculated using an average of its available TP field data, with values of 0.11 mg/L, 0.24 mg/L, and 0.008 mg/L. In order to reduce the OMP concentration in Elk Creek, OMP was re-estimated using the 0.008 mg/L value alone. Figure 148 shows TP values predicted by the model before and after this adjustment was made.

Similar process-of-elimination methods for various constituents and tributaries were conducted in order to determine which inputs to the model were driving water quality in the river. Once the driving influence was located, constituent concentrations were re-evaluated in order to determine whether the original estimation techniques were reasonable or poor.

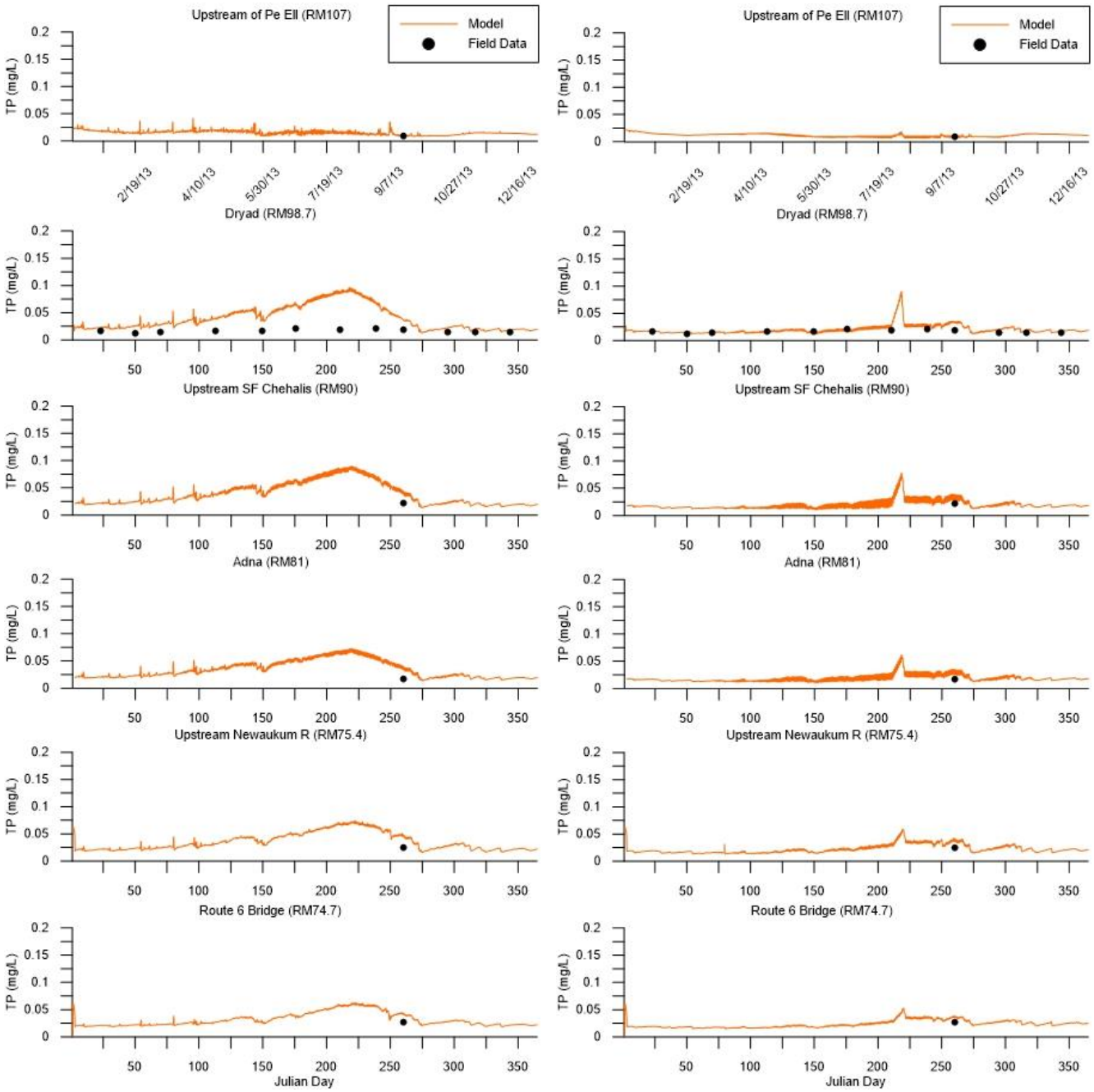

Figure 148. TP model predictions compared to field data when previous (left) and updated (right) technique was used to estimate OMP for Elk Creek

Nitrogen, Phosphorus, & Oxygen Fluxes

The ammonia decay rate (NH4DK) and the nitrate decay rate (NO3DK) were important for calibration for ammonia and nitrates. NH4DK specifies the rate at which ammonia is oxidized to nitrate or nitrite. By increasing these decay rates, the concentration of ammonia or nitrates was decreased as the compound decayed more quickly. Conversely, by decreasing these decay rates, concentrations remained higher.

CE-QUAL-W2 allows the user to view outputs of various fluxes throughout the model simulation, giving a view of what processes are important for various constituents. Viewing these fluxes for nitrogen species, phosphorus species, and dissolved oxygen were used for determining what processes were the largest drivers for river conditions.

Phosphate fluxes included algal respiration, algal growth, algal production, epiphyton respiration, epiphyton growth, epiphyton production, decay of particulate organic matter, decay of dissolved organic matter, 1st order sediment compartment decay, zero-order sediment release, and sorbed phosphate from settling.

Ammonia fluxes included algal respiration, algal growth, algal production, epiphyton respiration, epiphyton growth, epiphyton production, ammonia algal uptake, particulate organic matter decay, dissolved organic matter decay, 1st order sediment compartment decay, and zero-order sediment release.

Nitrates fluxes included denitrification, algal growth, epiphyton growth, and 1st order sediment compartment decay.

Dissolved oxygen fluxes included algal production, algal respiration, epiphyton production, epiphyton respiration, particulate organic matter decay, dissolved organic matter decay, nitrification, carbonaceous BOD decay, reaeration, 1st order sediment compartment decay, and zero-order sediment oxygen demand.

Figure 149, Figure 150, Figure 151, Figure 152, Figure 153, Figure 154, Figure 155, Figure 156, and Figure 157 show the model predictions of the most dominant NH4, NO3, and DO fluxes in waterbody 1, waterbody 2, waterbody 3, waterbody 4, waterbody 5, waterbody 6, waterbody 7, waterbody 8, and waterbody 9 respectively. The largest model-predicted NH4 fluxes were generally attributed to nitrification and periphyton/epiphyton respiration and production. Periphyton/epiphyton growth was generally the dominant model-predicted NO3 flux. The largest model-predicted DO fluxes were generally from algal respiration, periphyton/epiphyton respiration, reaeration, and zero-order sediments.

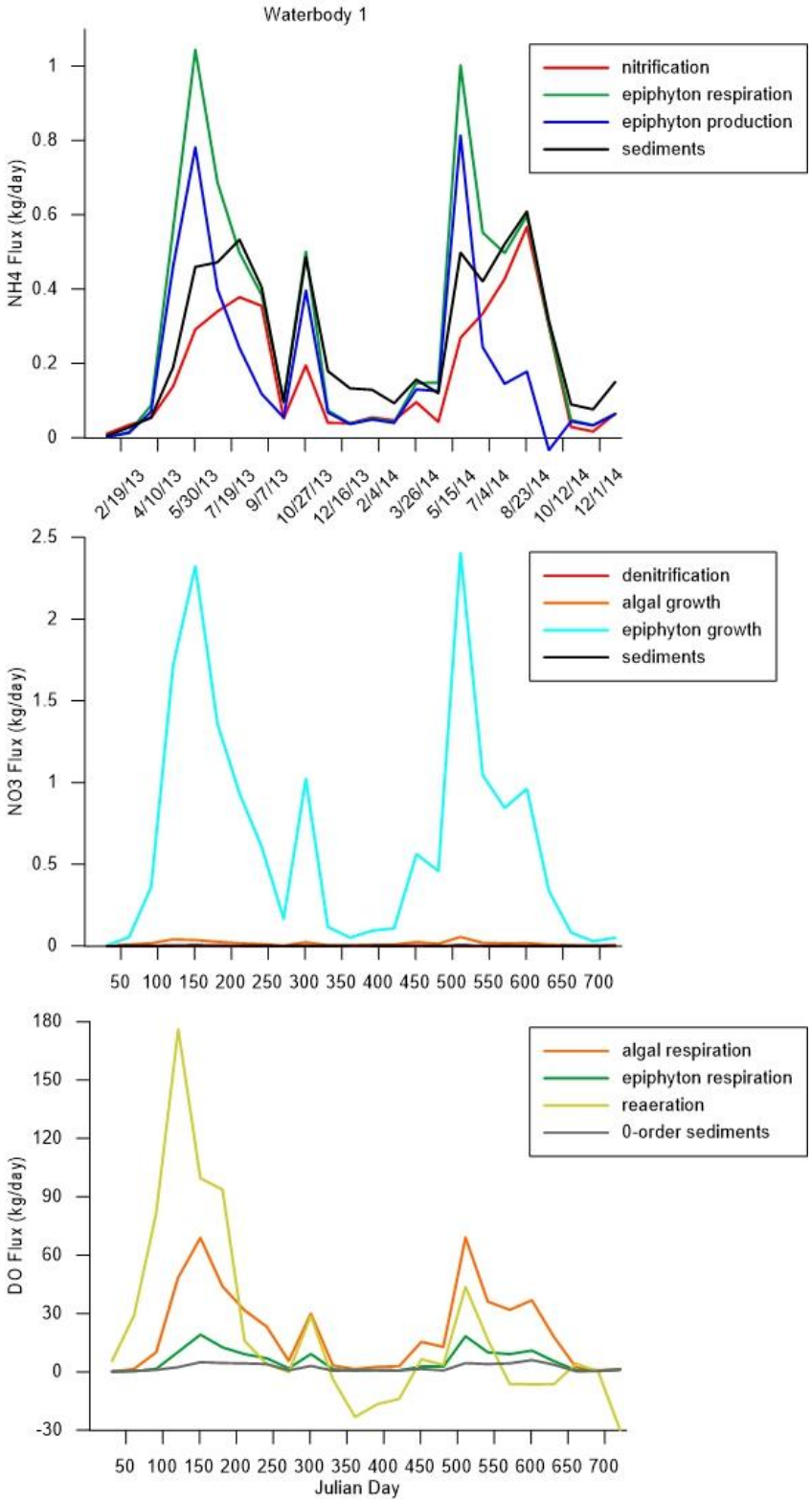

Figure 149. Dominant model-predicted NH4, NO3, and DO fluxes in waterbody 1

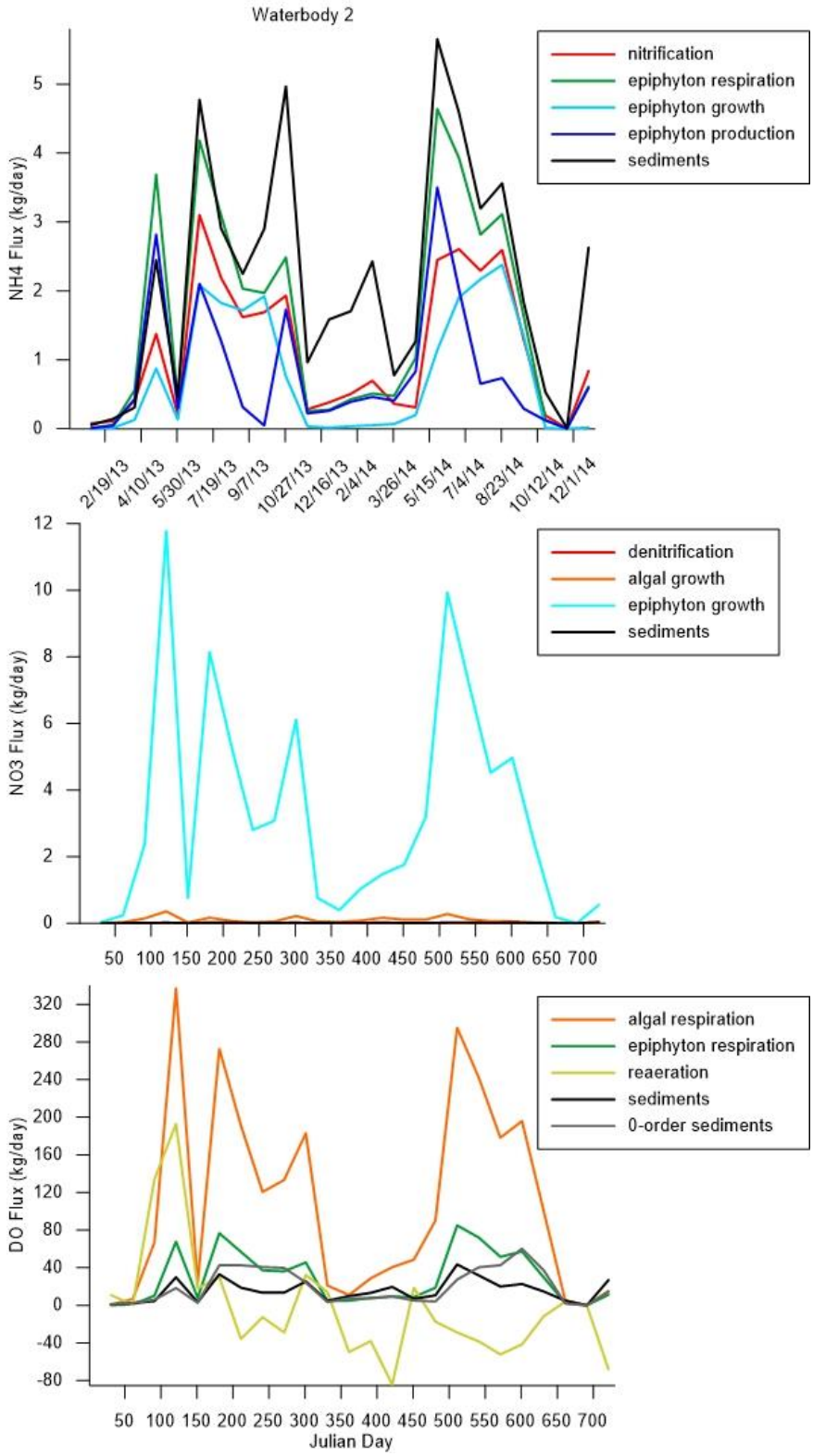

Figure 150. Dominant model-predicted NH4, NO3, and DO fluxes in waterbody 2

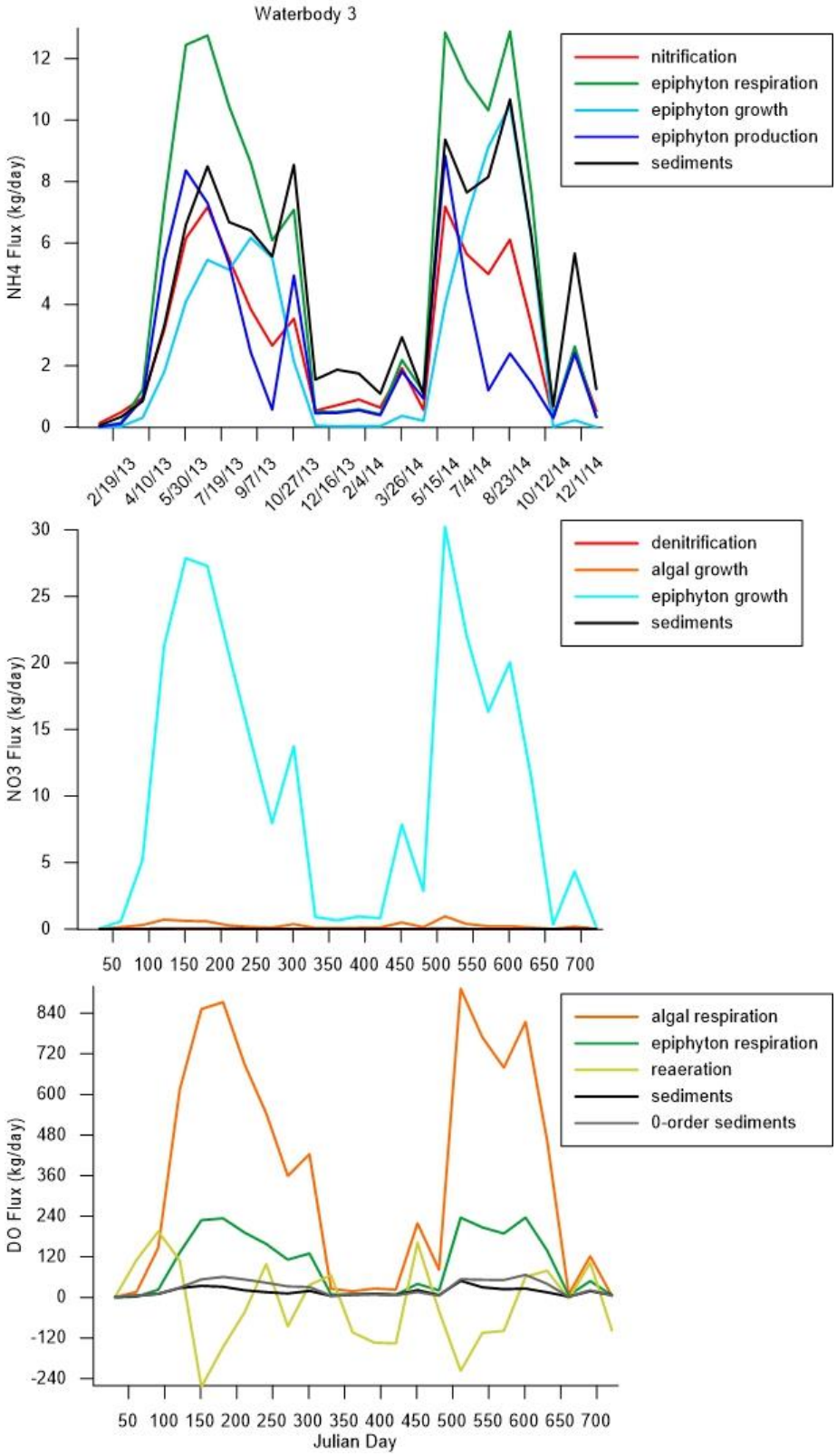

Figure 151. Dominant model-predicted NH4, NO3, and DO fluxes in waterbody 3

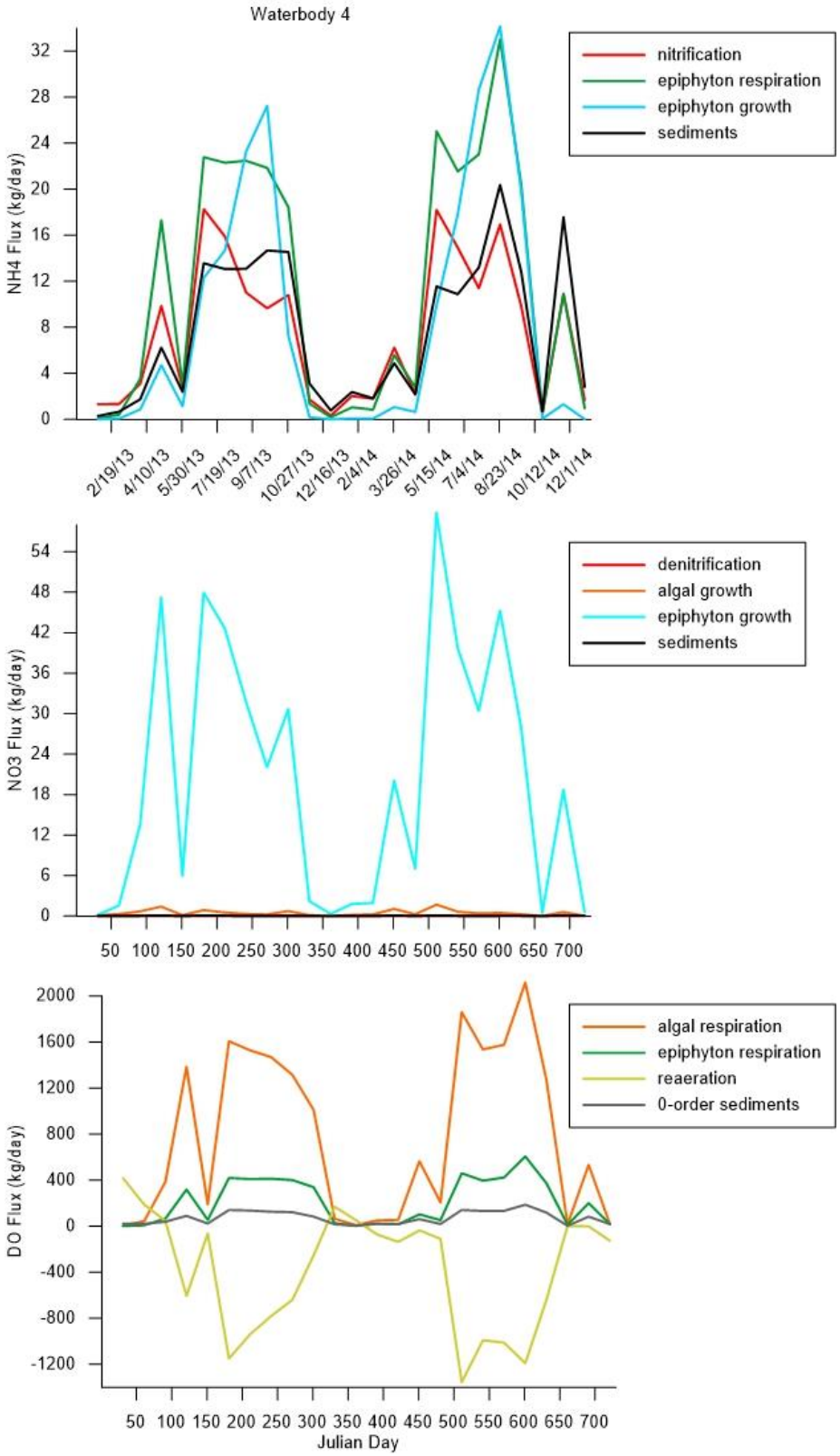

Figure 152. Dominant model-predicted NH4, NO3, and DO fluxes in waterbody 4

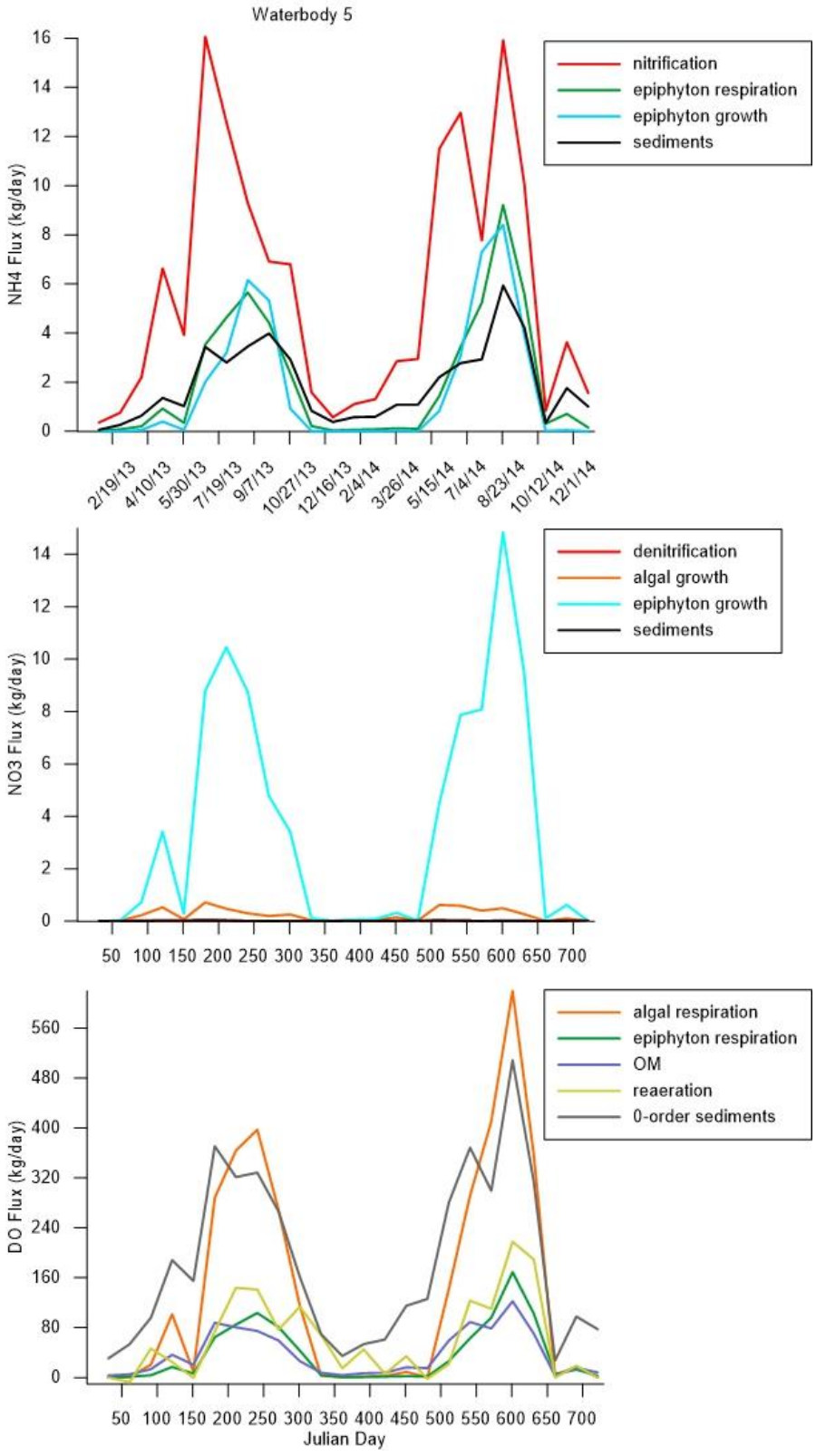

Figure 153. Dominant model-predicted NH4, NO3, and DO fluxes in waterbody 5

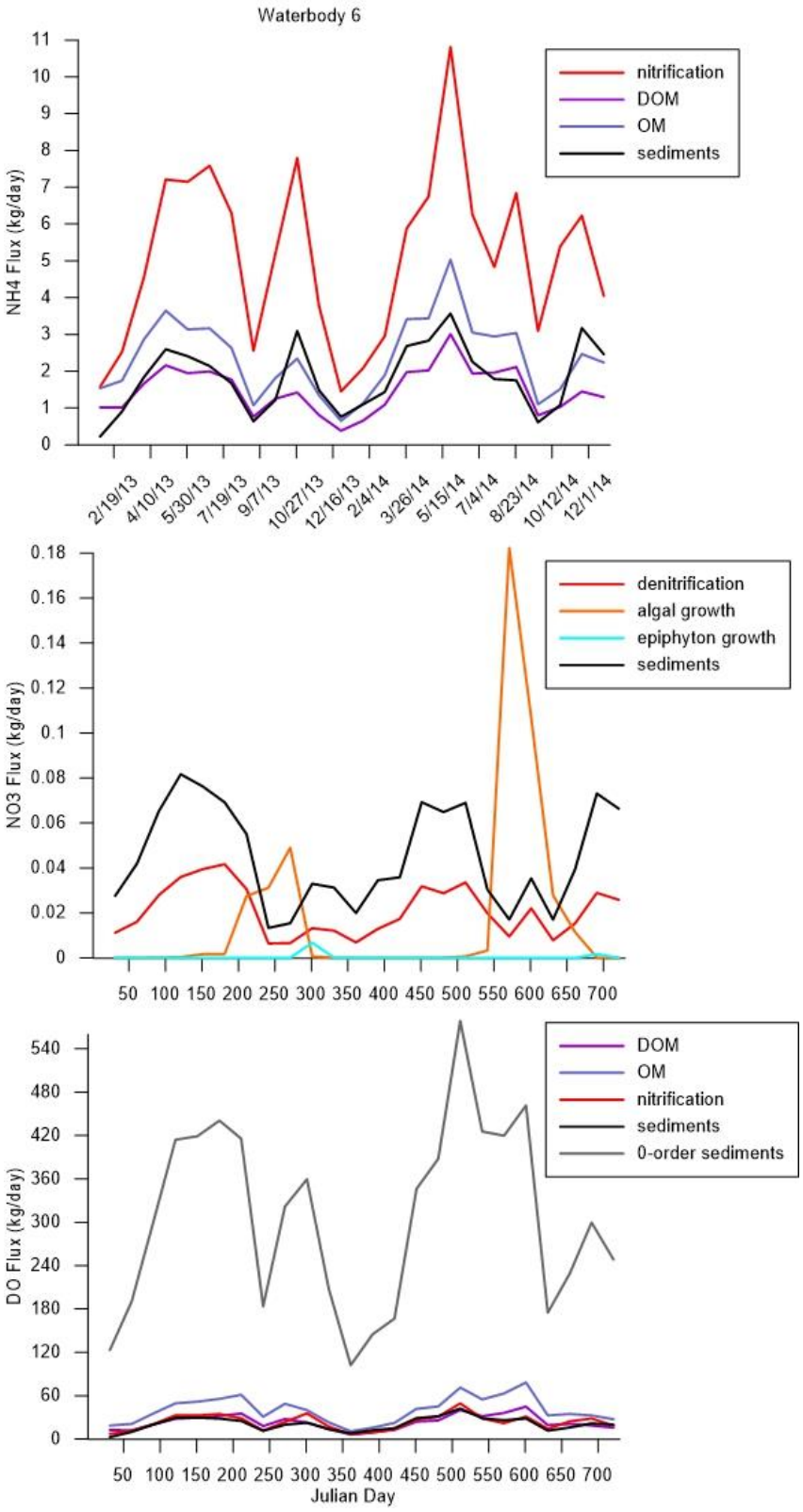

Figure 154. Dominant model-predicted NH4, NO3, and DO fluxes in waterbody 6

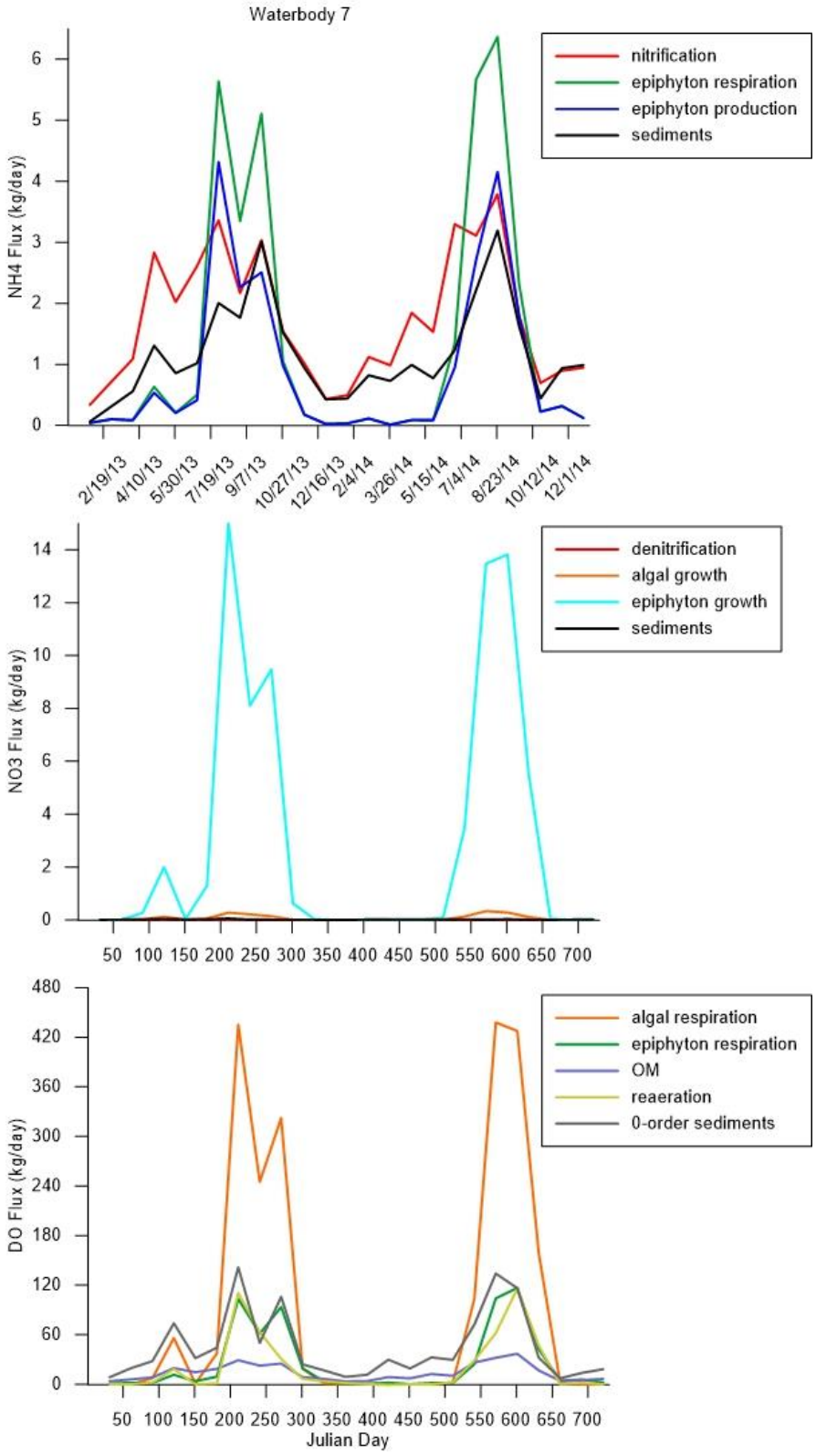

Figure 155. Dominant model-predicted NH4, NO3, and DO fluxes in waterbody 7

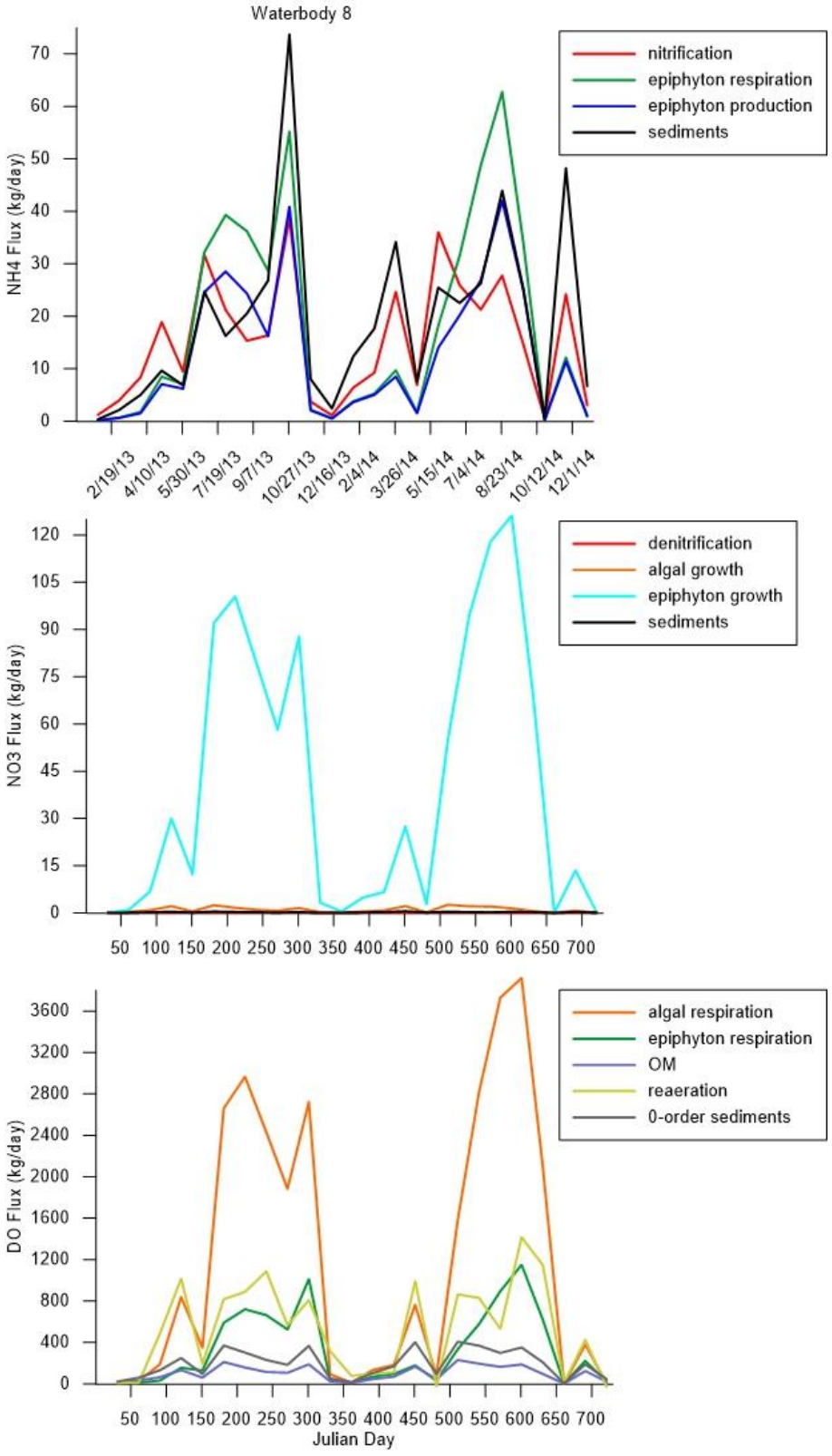

Figure 156. Dominant model-predicted NH4, NO3, and DO fluxes in waterbody 8

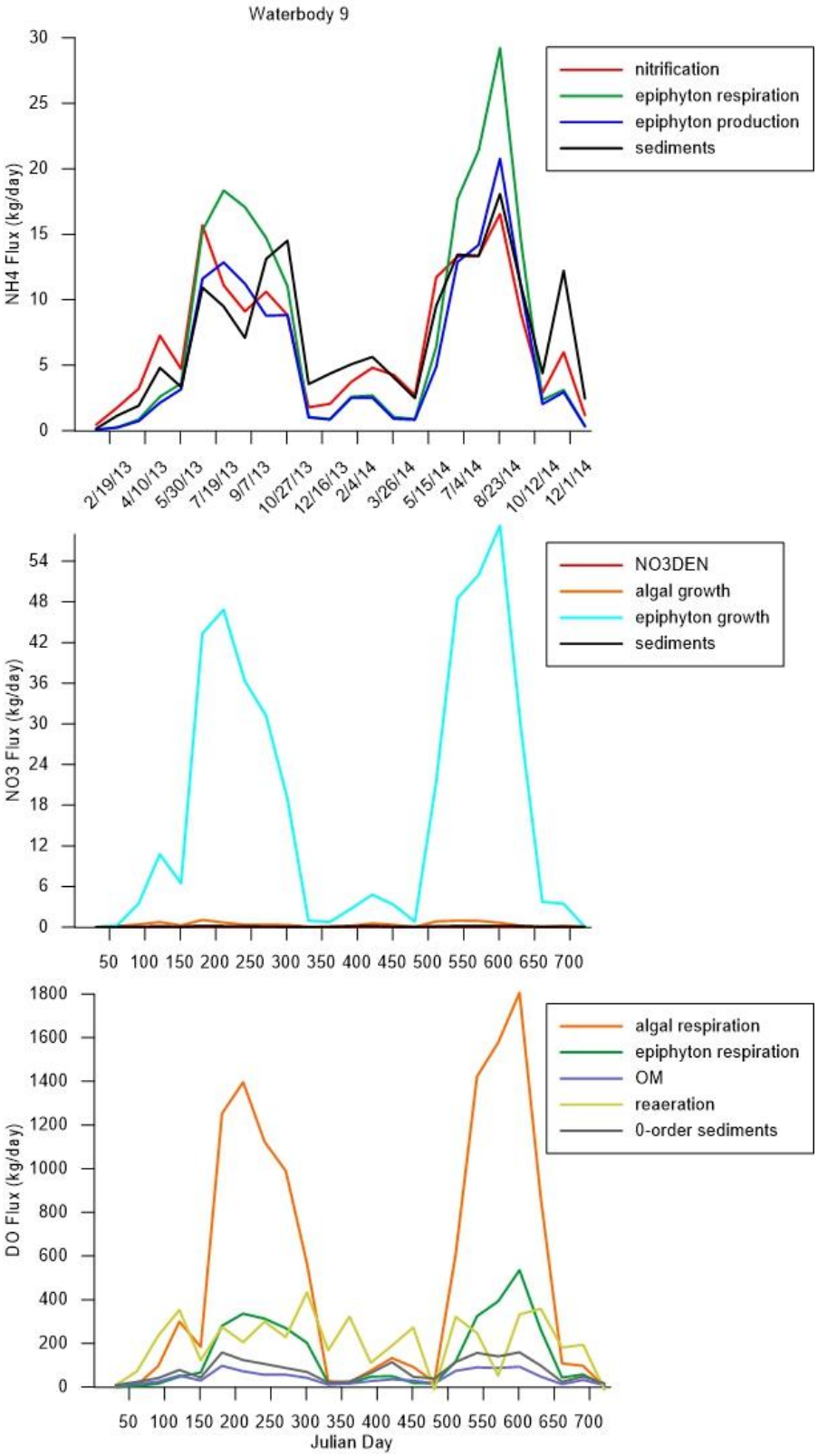

Figure 157. Dominant model-predicted NH4, NO3, and DO fluxes in waterbody 9

Algae, Epiphyton, & Zooplankton Kinetics

The model required many kinetic coefficients to describe algae, epiphyton, and zooplankton dynamics. Algal kinetics included maximum growth rate, maximum respiration rate, maximum excretion rate, maximum mortality

rate, settling rate, half-saturation for phosphorus limited growth, half-saturation for nitrogen limited growth, half-saturation for silica limited growth, and light saturation intensity at maximum photosynthesis rate (Cole and Wells, 2016). The algal temperature regime included temperature limits for growth and maximum growth and the fraction of algal growth at each temperature limit. Algal stoichiometry and initial condition concentrations were also input to the model. Similar kinetics, temperature regimes, and stoichiometry were also input for epiphyton and zooplankton.

Water quality calibration was sensitive to the dynamics of algae and periphyton/epiphyton because of their direct interactions with nutrients and dissolved oxygen. Nutrients decreased in the water column as a result of algae and epiphyton uptake during growth and increased as a result of algae and epiphyton respiration and mortality. DO increased in the water column during photosynthetic production, and decreased due to algae and epiphyton mortality as bacteria decayed the resulting organic matter. Correctly assessing the characteristics of algae, epiphyton, and zooplankton involved some trial-and-error. When these constituents created too much decaying biomass, the dissolved oxygen fell much lower than field data showed. When growth rates were too high and mortality rates were too low, the swings between peak and minimum dissolved oxygen and nutrients were too large.

No data exist for periphyton/epiphyton for the Chehalis River or the tributaries. Periphyton/epiphyton played an important role in model calibration, with uptake of nitrates and ammonia (with a preference for nitrates) during production and release of ammonia during respiration. Confirming the biomass of periphyton/epiphyton would assess whether the current water quality model is realistic.

Algae growth limitation by phosphorus from upstream of Pe Ell to upstream of the Newaukum River can be seen in Figure 158. Algae growth limitation by phosphorus from Route 6 Bridge to Porter can be seen Figure 159. Algae growth imitation by nitrogen from upstream of Pe Ell to upstream of the Newaukum River can be seen in Figure 160. Algae growth limitation by nitrogen from Route 6 Bridge to Porter can be seen in Figure 161. Algae growth limitation by light from upstream of Pe Ell to upstream of the Newaukum River can be seen in Figure 162. Algae growth limitation by light from Route 6 Bridge to Porter can be seen in Figure 163. Lower limitation values indicated more severe limitation.

Algal growth limitation from phosphorus and nitrogen became more important during summer months when light was plentiful. Similarly, algal limitation from light was more important during winter months when solar radiation decreased and cloud cover increased.

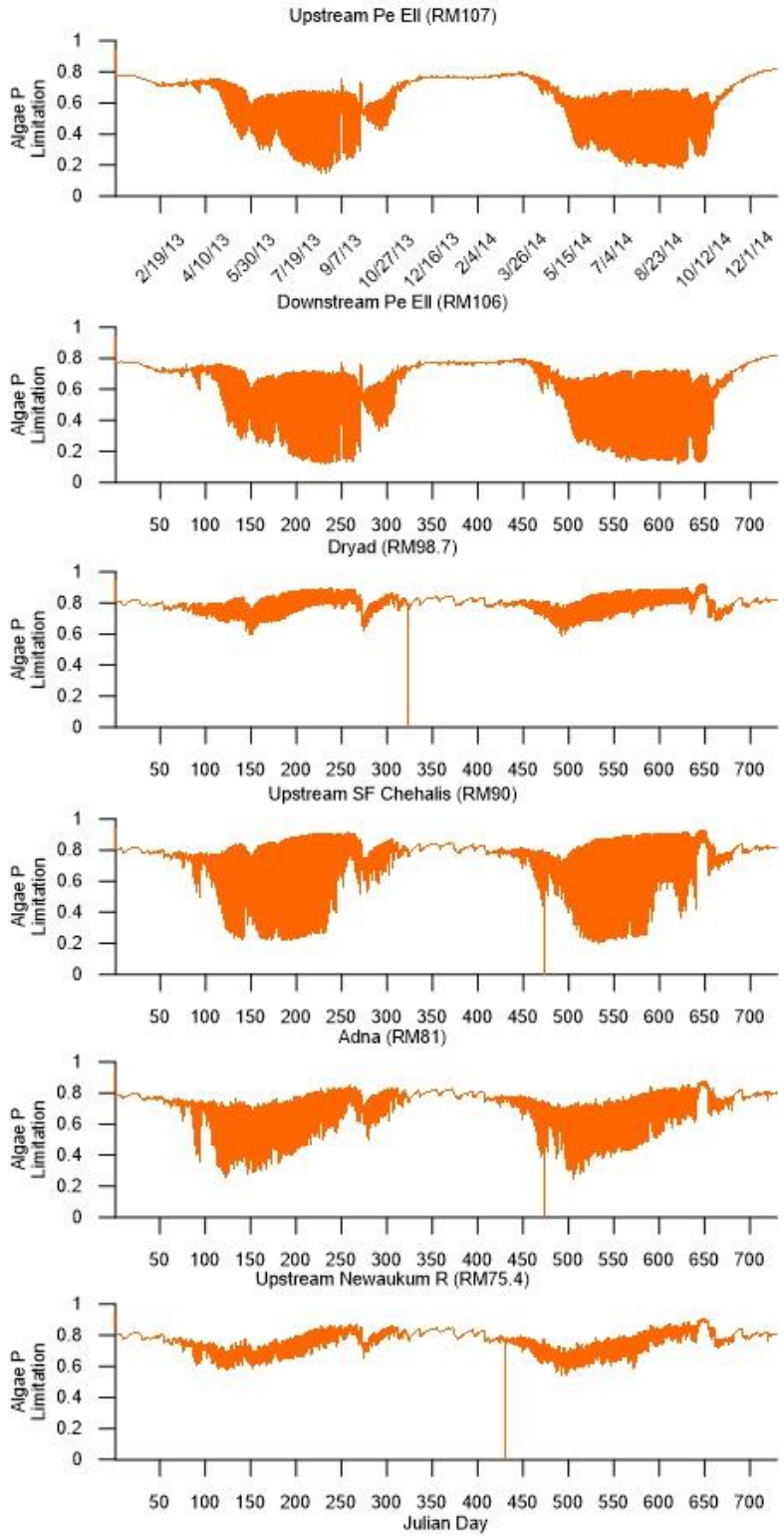

Figure 158. Algae growth limitation by phosphorus predicted by the model at upstream of Pe Ell, downstream of Pe Ell, Dryad, upstream of South Fork Chehalis River, Adna, and upstream of Newaukum River

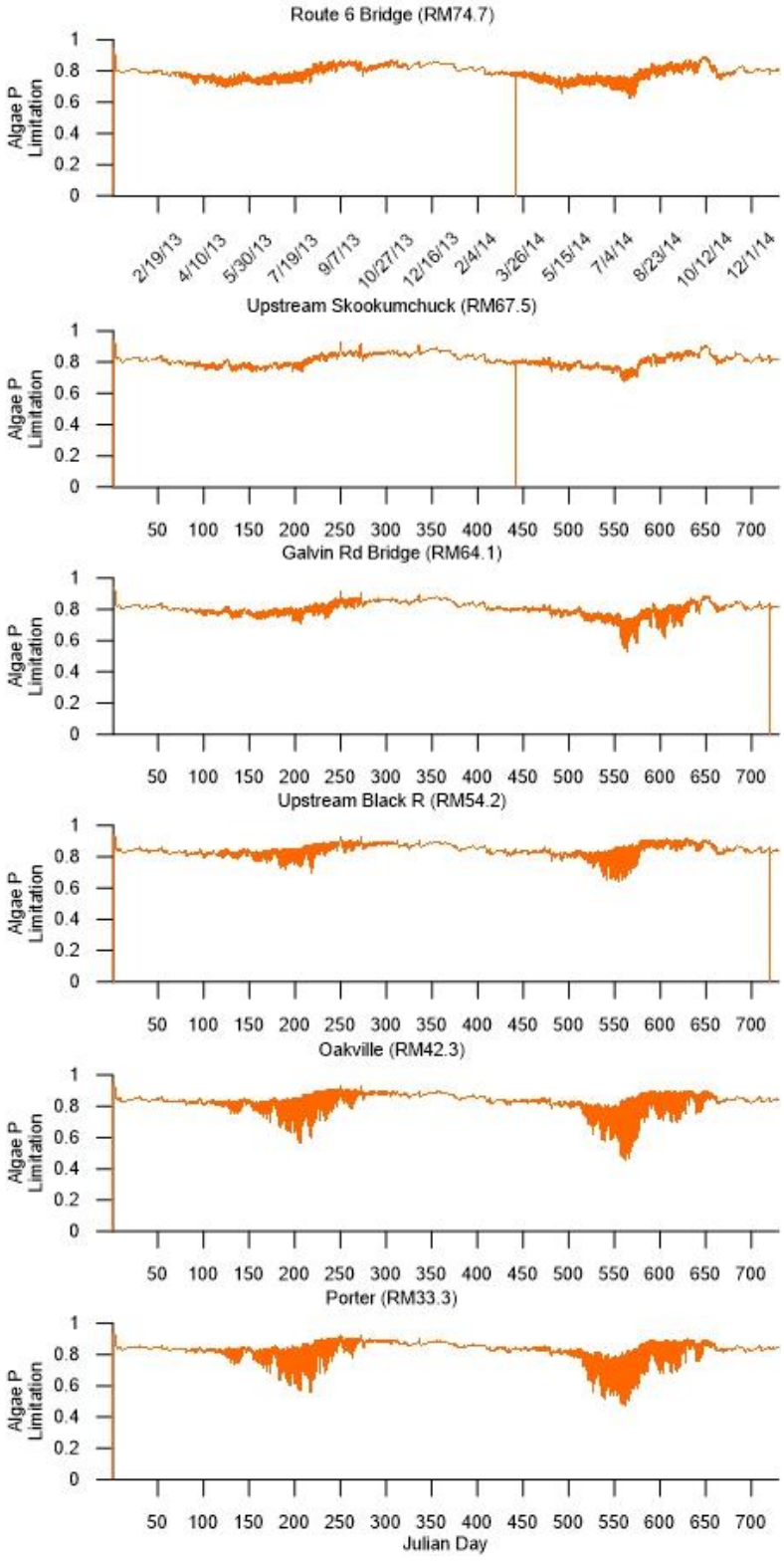

Figure 159. Algae growth limitation by phosphorus predicted by the model at Route 6 Bridge, upstream of Skookumchuck River, Galvin Road Bridge, upstream of Black River, Oakville, and Porter

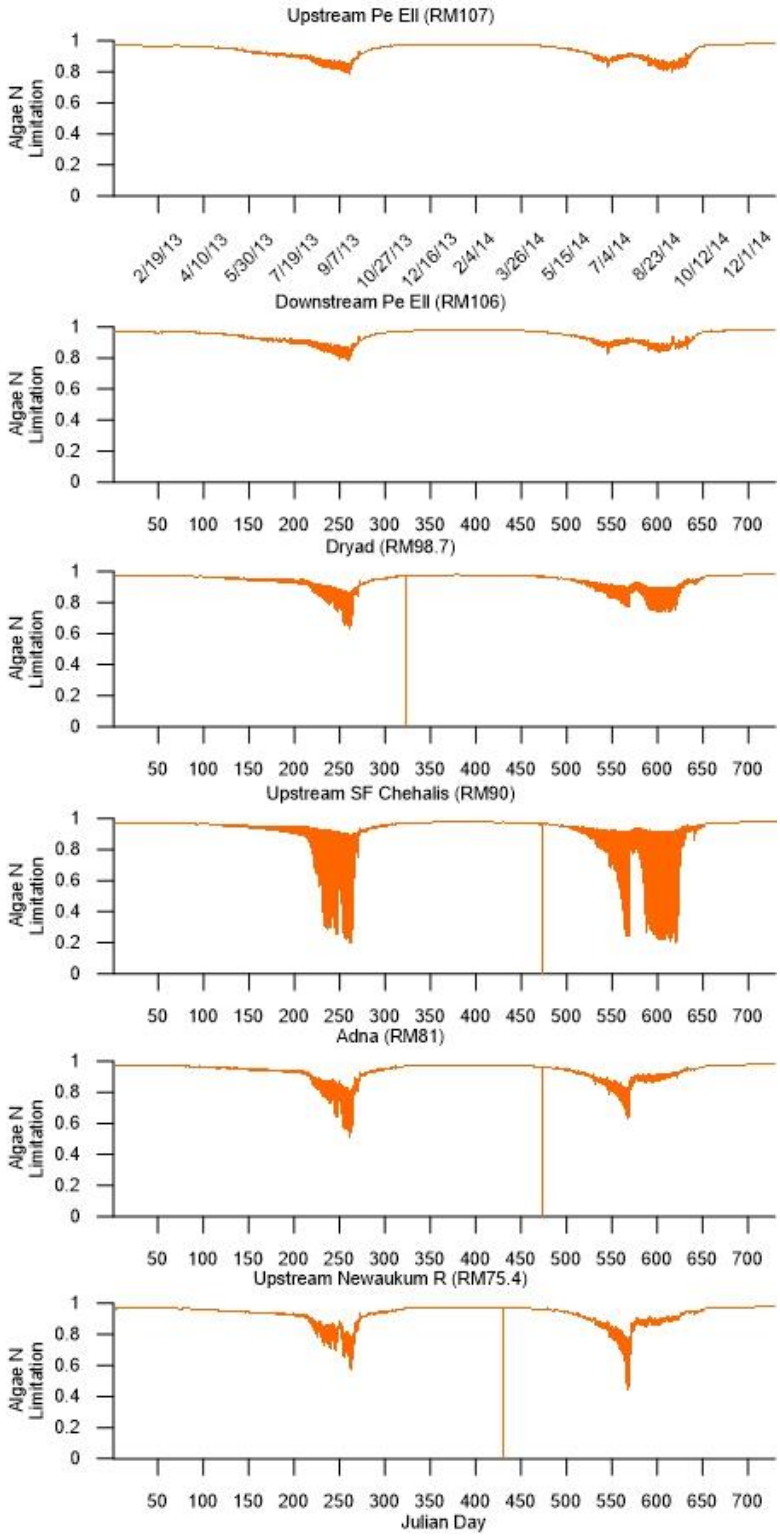

Figure 160. Algae growth limitation by nitrogen predicted by the model at upstream of Pe Ell, downstream of Pe Ell, Dryad, upstream of South Fork Chehalis River, Adna, and upstream of Newaukum River

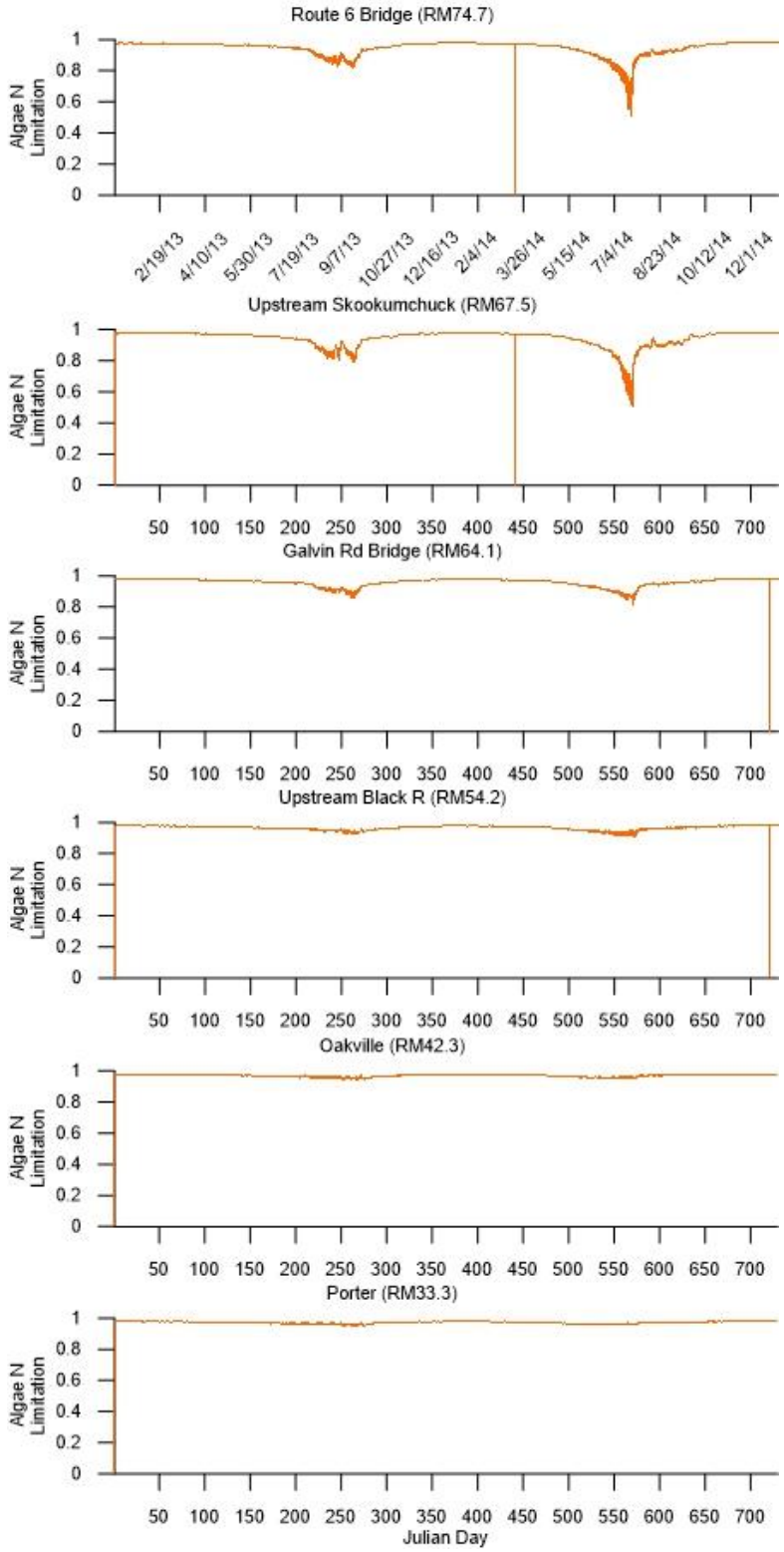

Figure 161. Algae growth limitation by nitrogen predicted by the model at Route 6 Bridge, upstream of Skookumchuck River, Galvin Road Bridge, upstream of Black River, Oakville, and Porter

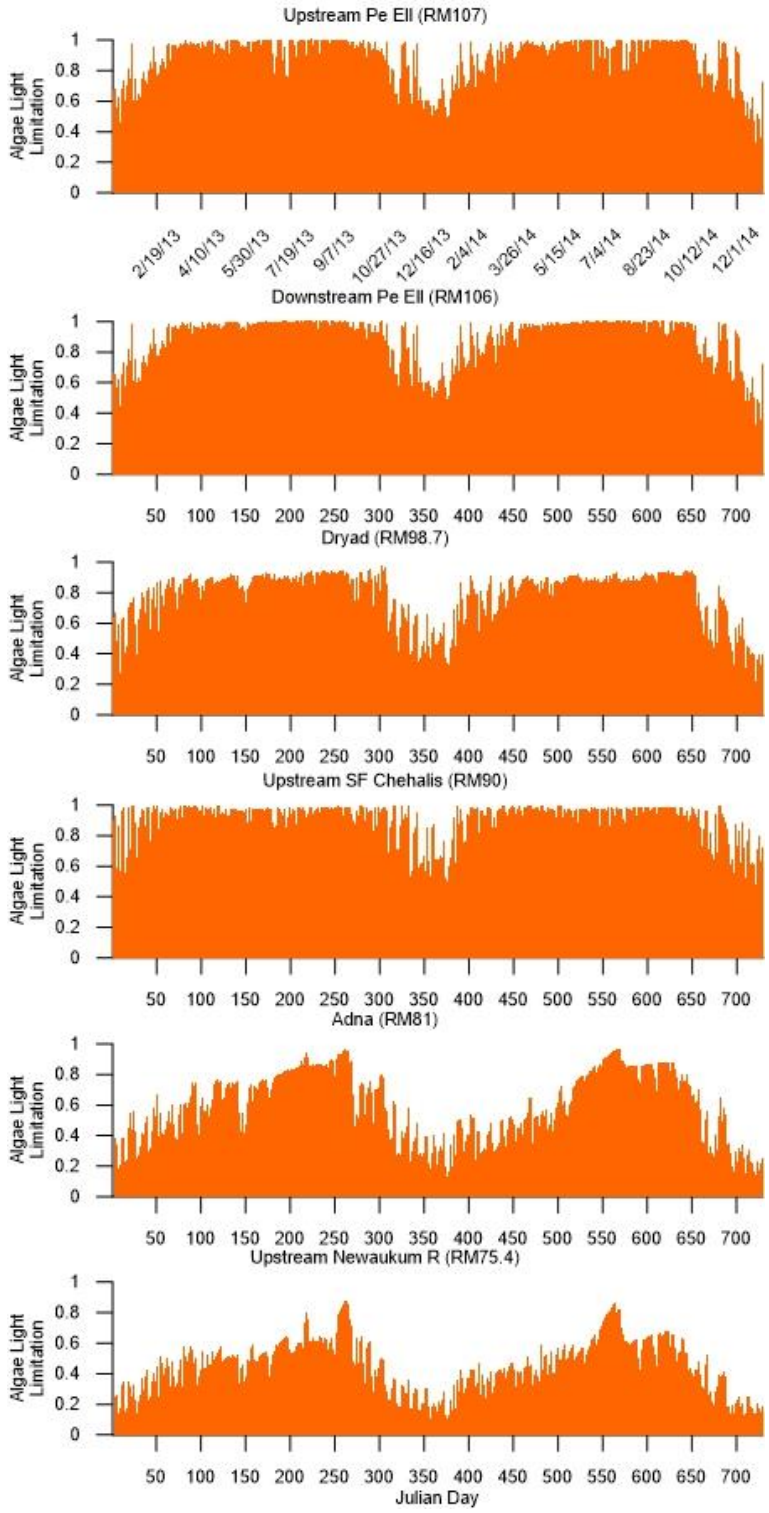

Figure 162. Algae growth limitation by light predicted by the model at upstream of Pe Ell, downstream of Pe Ell, Dryad, upstream of South Fork Chehalis River, Adna, and upstream of Newaukum River

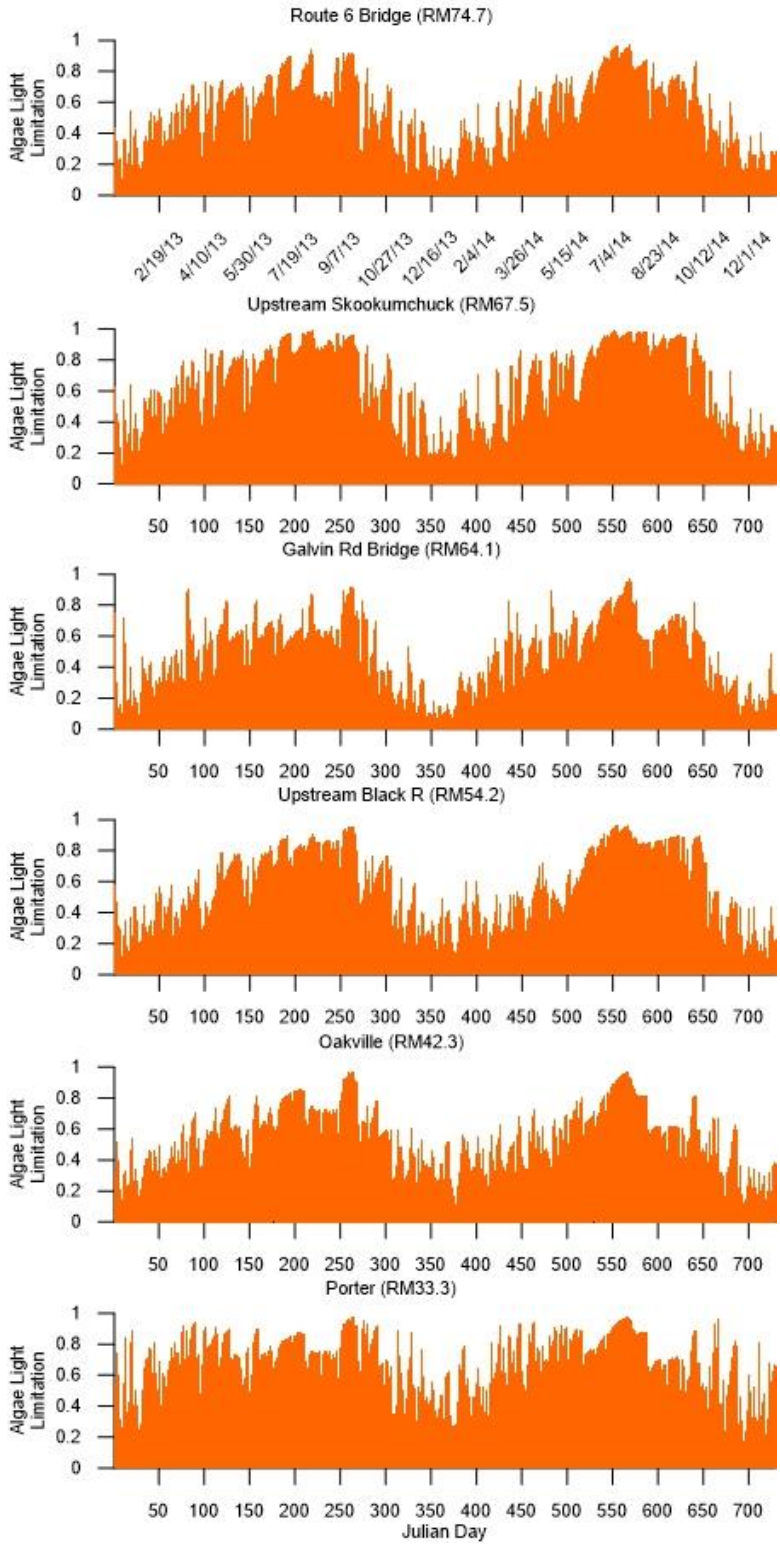

Figure 163. Algae growth limitation by light predicted by the model at Route 6 Bridge, upstream of Skookumchuck River, Galvin Road Bridge, upstream of Black River, Oakville, and Porter

Sediments

Sediment oxygen dynamics were important in the pool area where DO decreased near the channel bottom. Data for oxygen exchanges at the sediments were unavailable, so zero-order sediment oxygen demand (SOD) values were estimated for each segment. While generally SOD values are between 0.1 and 1 O_2 m^2 day^{-1}, they can

sometimes be higher (Cole and Wells, 2016). These values vary depending on sediment characteristics and algal production (Cole and Wells, 2016). SOD values in the pool were set to 1.9 g/m^2/day at 20^{o}C and SOD values upstream and downstream of the pool were set to 0.3 g/m^2/day. These values were important for matching DO values near the bottom of the channel that are seen in vertical profile data from the pool reach.

Large sediment fluxes in the upper waterbodies indicated sediments played a large role in ammonia predictions, due to the settling of particulate organic matter (POM) from wastewater treatment plants. First-order sediment decay was employed in the model. The rate of organic matter settling to the sediments (POMS) and the rate of BOD settling to the sediments (CBODS) were important for DO and nutrient calibration. Increased settling of organic matter to sediments increased oxygen demand as these organics decayed. Settling of organic matter to the sediments was also important for ammonia in the upper reaches. Particulate organic matter and BOD from the Pe Ell wastewater treatment plant settled in the sediments and decayed ammonia back into the water column, resulting in ammonia concentrations greater than seen in field data. By reducing POMS and CBODS, the particulates from the treatment plant were able to travel further downstream before settling.

The rate of particulate organic matter decay of the sediments (SEDK) was also available for adjustment, as it is possible that decay of organic matter in sediments may not be the same as in the water column. Decreasing SEDK indicated the sediments are more refractory in nature and decay more slowly. This helped with nutrient calibration. Burial of organics essentially locks the organics in the sediments as they settle and makes them unavailable to decay into the water column or take up oxygen. Increasing the rate of sediment burial of particulate organics (SEDBR) helped to reduce the concentration of nutrients released back into the water column during organic decay. This was especially important for ammonia.

Reaeration

The model requires the user to specify a reaeration regime for each waterbody. Each equation corresponds to a set of coefficients that help to describe how DO enters and leaves the water. For the upper waterbodies and lower model waterbodies, river reaeration equations dependent upon stream velocity were used that promoted higher reaeration exchanges. For the middle waterbodies where lake-like conditions exist, and reaeration is controlled by wind speed, lake reaeration equations were used. The lake formulations generally decreased reaeration in the pool area and allowed DO produced by photosynthesis to accumulate. Sometimes, when reaeration was too low, the model predicted DO levels that were too high. By reassessing the reaeration regime applied to each waterbody, DO was improved.

Comments About Model Predictions

Some data used for calibration could not be explained from known nutrient sources. For example, mainstem Chehalis River ammonia values were approximately 0.02 mg/L upstream of the Skookumchuck River and upstream of the Newaukum River. However, between these locations at Adna, the ammonia concentrations increased to approximately 0.15 mg/L. With no other data reflecting this increase in ammonia, it was not possible to calibrate the model to replicate the elevated ammonia values seen at Adna.

TKN is the sum of NH3 and organic matter as nitrogen. Since model predictions reasonably match mainstem NH3 data, the error in TKN predicts may be more closely related to errors in organic matter estimations.

PO4 was sensitive to periphyton/epiphyton characteristics. Further information about periphyton/epiphyton in the system would likely improve PO4 calibration.

Similar to ammonia data, sudden increases or decreases in mainstem constituent data that were not reflected elsewhere in available data were difficult for model predictions reproduce. For example, chlorophyll a increased to approximately 5 µg/L at the upstream of Skookumchuck River station around Julian day 200. The neighboring upstream and downstream monitoring stations, however, had chlorophyll a concentrations of 1 µg/L or less. This

chlorophyll a increase was not seen in any other tributary data, so was not reflected in the model predictions. A similar increase in TP data was seen at the Oakville monitoring station around Julian day 200, and similarly was not reflected in model predictions.

Algae and periphyton/epiphyton alter the pH of the water because of their uptake of carbon dioxide, which produces acidic species in the water column. However, pH is also a function of alkalinity, temperature, and total inorganic carbon. Single alkalinity data values on the Chehalis River were mentioned in some of the wastewater treatment plant fact sheets. These were not sufficient to provide alkalinity data for all of the tributaries entering the river. Because of the lack of data for alkalinity and total inorganic carbon, pH was not fully calibrated in this model.

Continuous Water Quality

The timing and magnitudes of model predictions were not always in agreement with field data, as seen in the continuous DO field data comparisons. Model DO diurnal variations were very sensitive to cloud cover. Improvements to meteorological data improved the model DO results. It was useful to view the cloud cover to aid calibration. The cloud cover values during the times continuous DO data were collected can be seen in Figure 164 for the waterbodies data were collected in. Additional cloud cover data would improve model predictions, especially since much of the cloud cover data were estimated based on solar radiation data and calculated theoretical clear sky solar radiation. As model improvements continue, investigations to improvements between model predictions and continuous field data will be explored.

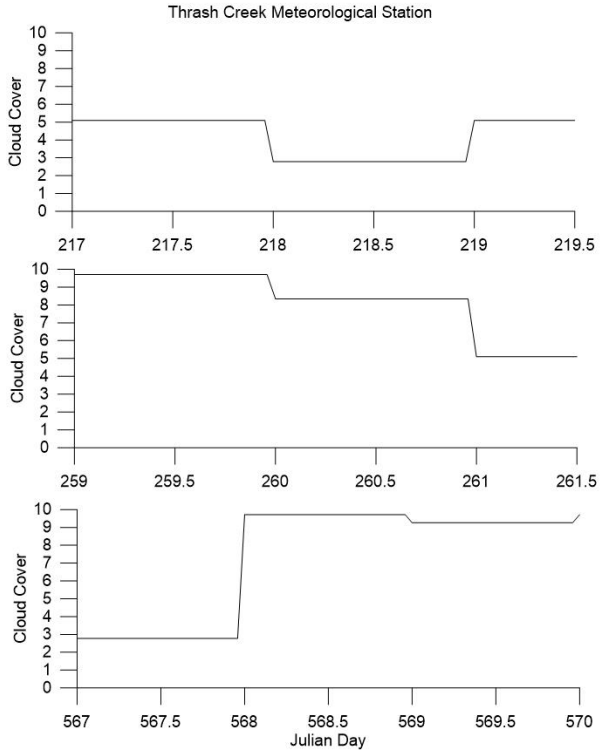

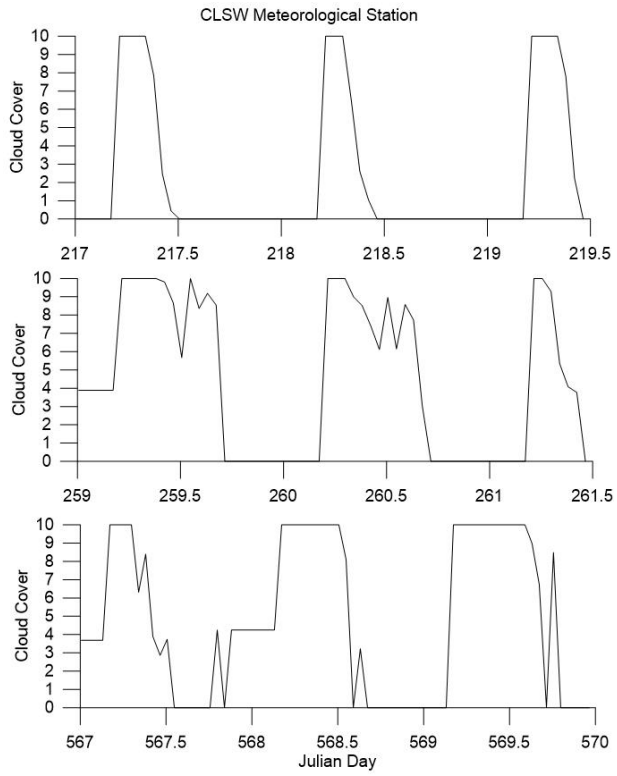

Figure 164. Cloud cover for Thrash Creek and CLSW during the times of continuous DO data collection (10 = fully cloudy and 0 = clear sky)

Vertical Profiles

Confirmation of locations of tributaries and monitoring stations in relation to the model grid would generally improve model results. Vertical profiles were especially sensitive to segment location, even when only off by one or two segments. Improvements to temperature vertical profiles is also important for DO profiles, as DO is a direct function of water temperature. Improvements to meteorological data could thus improve DO predictions.

Chehalis Reservoir Footprint Model

Water quality calibration data were not available in the domain of the footprint model. Model predictions at the dam site are plotted in Figure 165 through Figure 169. In order to help assess the accuracy of water quality predictions, data measured just upstream of the Pe Ell wastewater treatment plant, which is approximately 5 km downstream of the end of the model, were also plotted. Water quality parameters were consistent with those used in the Anchor QEA reservoir model and are plotted in Table 34.

Table 34. W2 Model Water Quality Parameters for footprint model.

Variable	Description	Units	Typical values*	Values
AX	Longitudinal eddy viscosity (for momentum dispersion)	m^2/sec	1	1

Variable	Description	Units	Typical values*	Values
DX	Longitudinal eddy diffusivity (for dispersion of heat and constituents)	m^2/sec	1	1
CBHE	Coefficient of bottom heat exchange	Wm^2/sec	0.30	0.30
TSED	Sediment (ground) temperature	°C		11.5
WSC	Wind sheltering coefficient		0.85	1-2
BETA	Fraction of incident solar radiation absorbed at the water surface		0.45	0.45
EXH20	Extinction for water	/m	0.25-0.45	0.25
AG1	Algal growth rate for group #1	/day	1-3	1.5
AM1	Algal mortality rate for group #1	/day		0.1
AE1	Algal excretion rate for group #1	/day	0.014-0.044	0.04
AR1	Algal dark respiration for group #1	/day	0.01-0.92	0.04
AS1	Algal settling rate for group #1	/day	0.02-1.00	0.1
ASAT1	Algae Saturation intensity at maximum photosynthetic rate for group #1	W/m^2	10-170	75
APOM1	Fraction of algal biomass lost by mortality to detritus for algae for group #1		0.8	0.8
AT1_1	Lower temperature for algal growth for group #1	°C		3
AT2_1	Lower temperature for maximum algal growth for group #1	°C		7
AT3_1	Upper temperature for maximum algal growth for group #1	°C		20
AT4_1	Upper temperature for algal growth for group #1	°C		30
AK1_1	Fraction of algal growth rate at AT1 for group #1		0.1	0.1
AK2_1	Fraction of maximum algal growth rate at AT2 for group #1		0.99	0.99
AK3_1	Fraction of maximum algal growth rate at AT3 for group #1		0.99	0.99

Variable	Description	Units	Typical values*	Values
AK4_1	Fraction of algal growth rate at AT4 for group #1		0.1	0.1
ALGP1	Stoichiometric equivalent between organic matter and phosphorus for algae group #1		0.005	0.005
ALGN1	Stoichiometric equivalent between organic matter and nitrogen for algae group #1		0.08	0.08
ALGC1	Stoichiometric equivalent between organic matter and carbon for algae group #1		0.4-0.5	0.45
AG2	Algal growth rate for group #2	/day	1-3	2
AM2	Algal mortality rate for group #2	/day		0.1
AE2	Algal excretion rate for group #2	/day	0.014-0.044	0.04
AR2	Algal dark respiration for group #2	/day	0.01-0.92	0.04
AS2	Algal settling rate for group #2	/day	0.02-1.00	0.1
ASAT2	Algae Saturation intensity at maximum photosynthetic rate for group #2	W/m^2	10-170	50
APOM2	Fraction of algal biomass lost by mortality to detritus for algae for group #2		0.8	0.8
AT1_2	Lower temperature for algal growth for group #2	^oC		7
AT2_2	Lower temperature for maximum algal growth for group #2	^oC		15
AT3_2	Upper temperature for maximum algal growth for group #2	^oC		30
AT4_2	Upper temperature for algal growth for group #2	^oC		35
AK1_2	Fraction of algal growth rate at AT1 for group #2		0.1	0.1
AK2_2	Fraction of maximum algal growth rate at AT2 for group #2		0.99	0.99
AK3_2	Fraction of maximum algal growth rate at AT3 for group #2		0.99	0.99
AK4_2	Fraction of algal growth rate at AT4 for group #2		0.1	0.1

Variable	Description	Units	Typical values*	Values
ALGP2	Stoichiometric equivalent between organic matter and phosphorus for algae group #2		0.005	0.005
ALGN2	Stoichiometric equivalent between organic matter and nitrogen for algae group #2		0.08	0.08
ALGC2	Stoichiometric equivalent between organic matter and carbon for algae group #2		0.4-0.5	0.45
LDOMDK	Labile DOM decay rate	/day	0.04-0.12	0.08
LRDDK	Labile to refractory decay rate	/day	0.001	0.01
RDOMDK	Maximum refractory decay rate	/day	0.001	0.001
LPOMDK	Labile Detritus decay rate	/day	0.04-0.1	0.005
POMS	Detritus settling rate	m/day	0.2-2	0.1
RPOMDK	Refractory detritus decay rate	/day	0.001	0.0005
OMT1	Lower temperature for organic matter decay	^oC	4	4
OMT2	Lower temperature for maximum organic matter decay	^oC	30	25
OMK1	Fraction of organic matter decay rate at OMT1		0.1	0.1
OMK2	Fraction of organic matter decay rate at OMT2		0.99	0.99
PO4R	Anaerobic sediment release rate of phosphorus as fraction of SOD			0.001
AHSP1	Algal half-saturation constant for phosphorus for group #1	g/m^3	0.002-0.01	0.003
AHSP2	Algal half-saturation constant for phosphorus for group #2	g/m^3	0.002-0.01	0.003
NH4DK	Ammonia decay rate (nitrification rate)	/day	0.001-1.3	0.12
AHSN1	Algal half-saturation constant for nitrogen for group #1	g/m^3	0.014	0.014
AHSN2	Algal half-saturation constant for nitrogen for group #2	g/m^3	0.014	0.014
NH4T1	Lower temperature for ammonia decay	^oC	5	5
NH4T2	Lower temperature for maximum ammonia decay	^oC	20	25
NH4K1	Fraction of nitrification rate at NH4T1		0.1	0.1

Variable	Description	Units	Typical values*	Values
NH4K2	Fraction of nitrification rate at NH4T2		0.99	0.99
NO3DK	Nitrate decay rate (denitrification rate)	/day	0.05-0.15	0.03
NO3T1	Lower temperature for nitrate decay	^{o}C	5	5
NO3T2	Lower temperature for maximum nitrate decay	^{o}C	20	25
NO3K1	Fraction of denitrification rate at NO3T1		0.1	0.1
NO3K2	Fraction of denitrification rate at NO3T2		0.99	0.99
O2NH4	Oxygen stoichiometric equivalent for ammonia decay		4.57	4.57
O2OM	Oxygen stoichiometric equivalent for organic matter decay		1.4	1.4
O2AR1	Oxygen stoichiometric equivalent for dark respiration for group #1		1.1	1.1
O2AR2	Oxygen stoichiometric equivalent for dark respiration for group #2		1.1	1.1
O2AG1	Oxygen stoichiometric equivalent for algal growth for group #1		1.4	1.4
O2AG2	Oxygen stoichiometric equivalent for algal growth for group #2		1.4	1.4
O2LIM	Dissolved oxygen concentration at which anaerobic processes begin	g/m^3	0.1	0.7
SEDK	First order sediment compartment decay rate	/day		0.02
SOD	Zeroth order sediment oxygen demand	$g/m^2/day$	0.3-6	0.1
SEDBR	Sediment burial rate	/day		0.01
* Cole and Wells (2016) **Galy-Lacaux et al. (1997)				

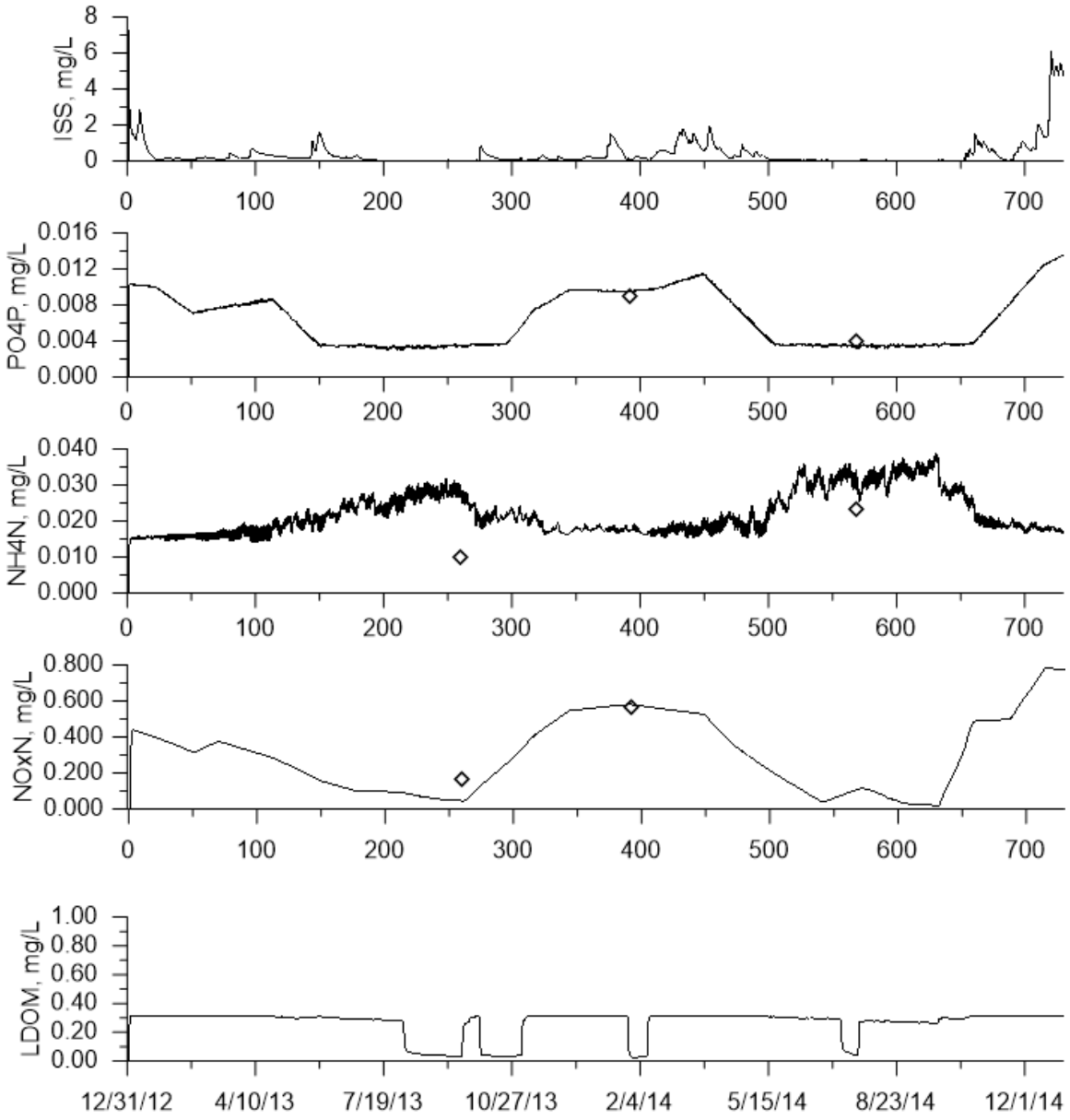

Figure 165. Water quality predictions at dam site (1). Data measured at station CHL-PEL-US, located approximately 5 km downstream of the dam site, are also plotted using diamond symbols.

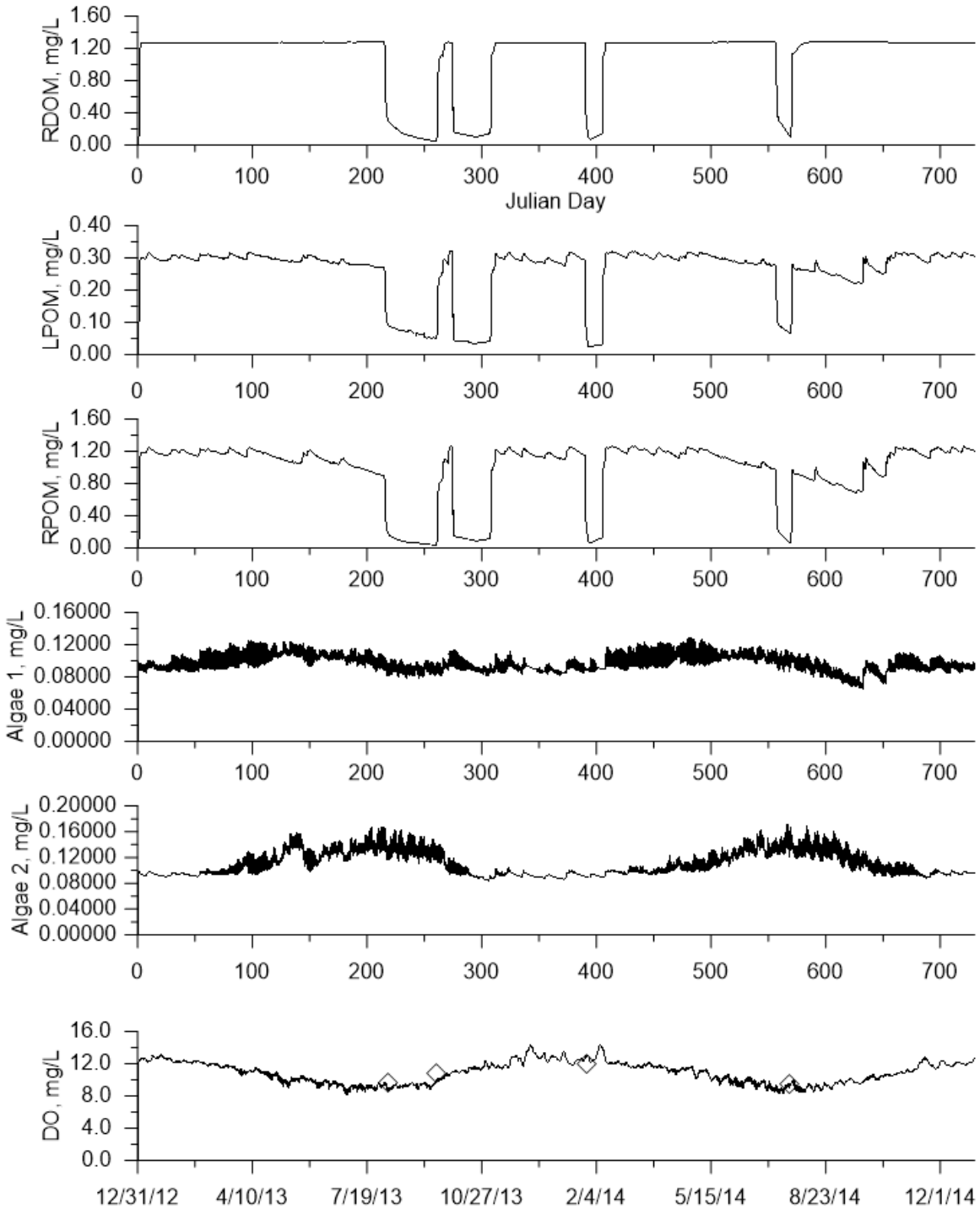

Figure 166. Water quality predictions at dam site (2). Data measured at station CHL-PEL-US, located approximately 5 km downstream of the dam site, are also plotted using diamond symbols.

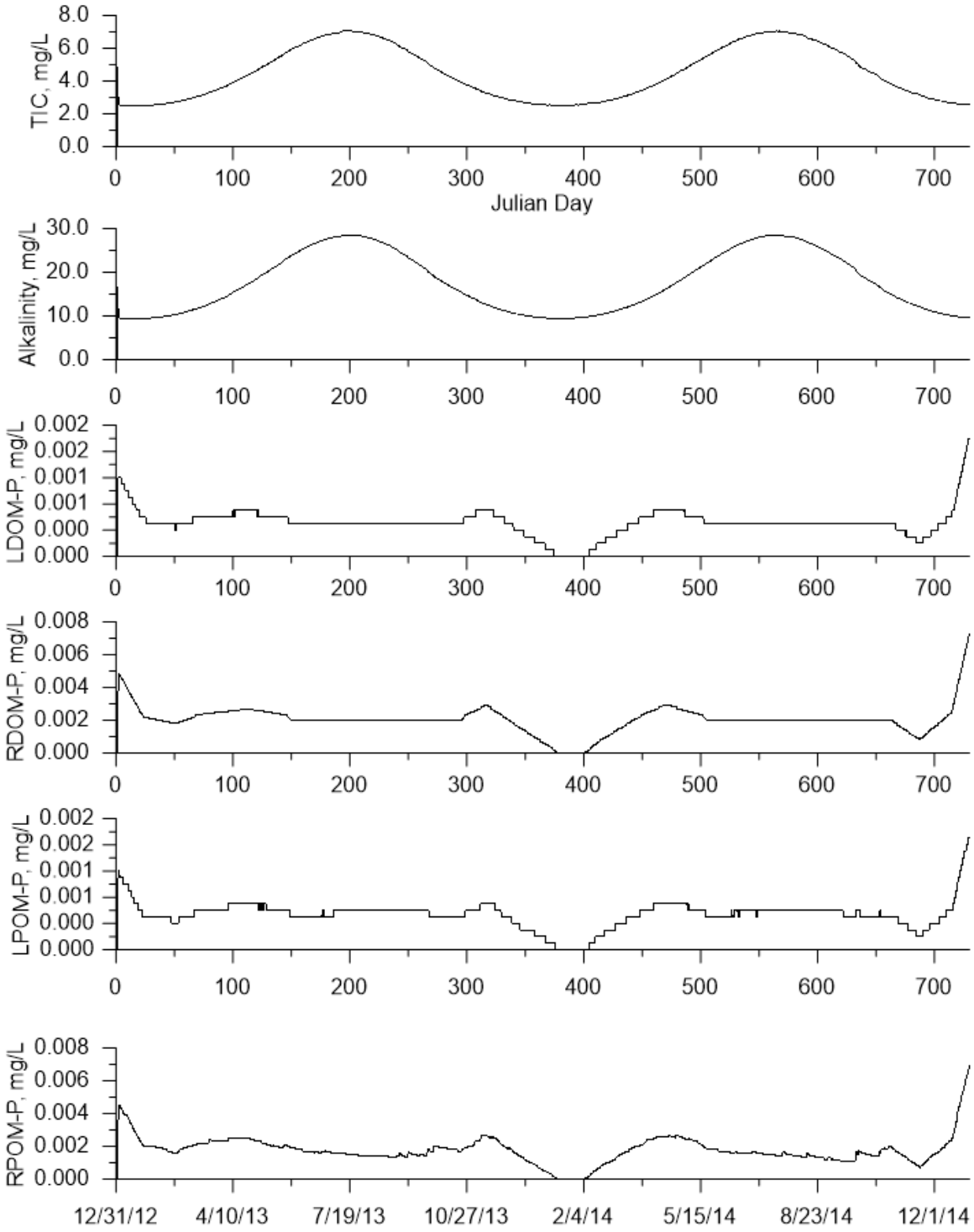

Figure 167. Water quality predictions at dam site (3).

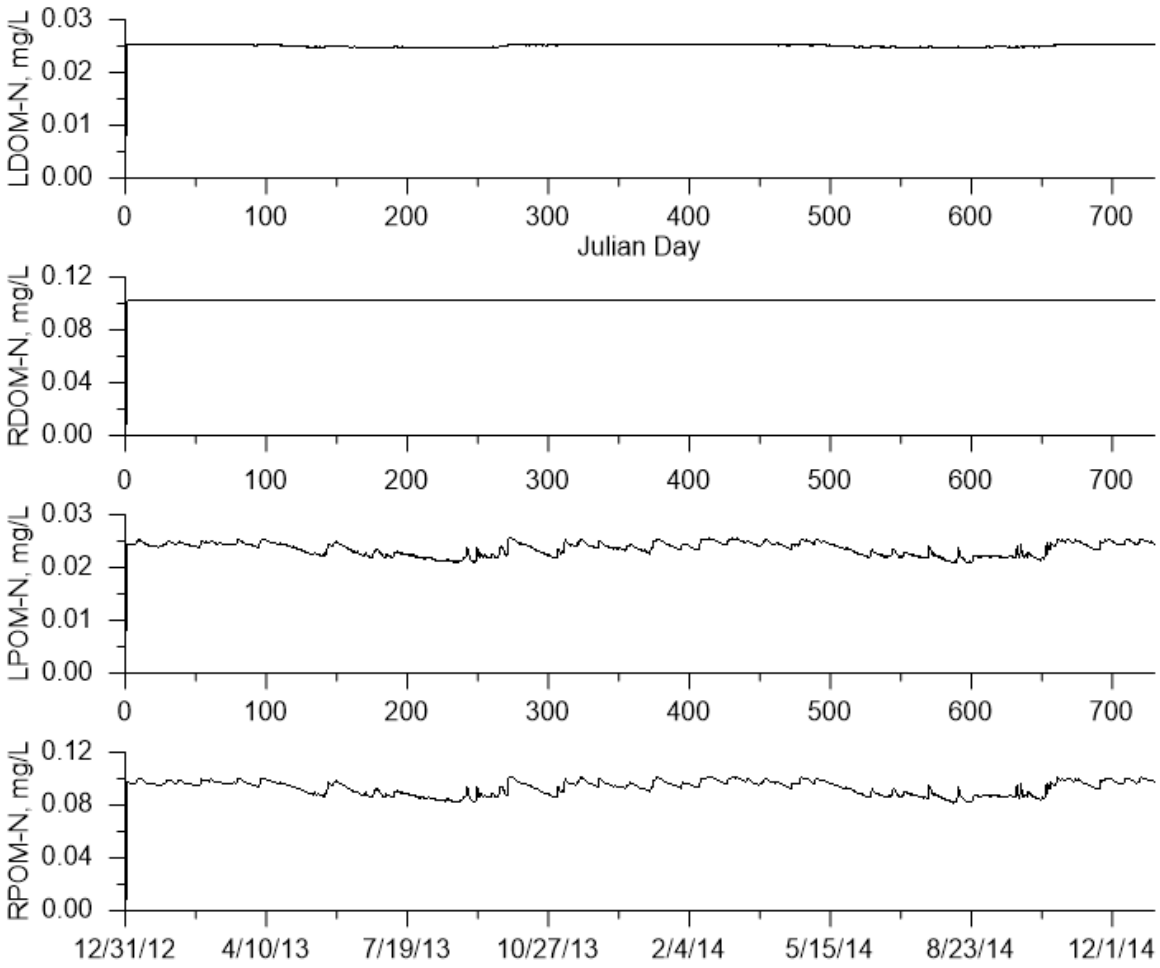

Figure 168. Water quality predictions at dam site (4).

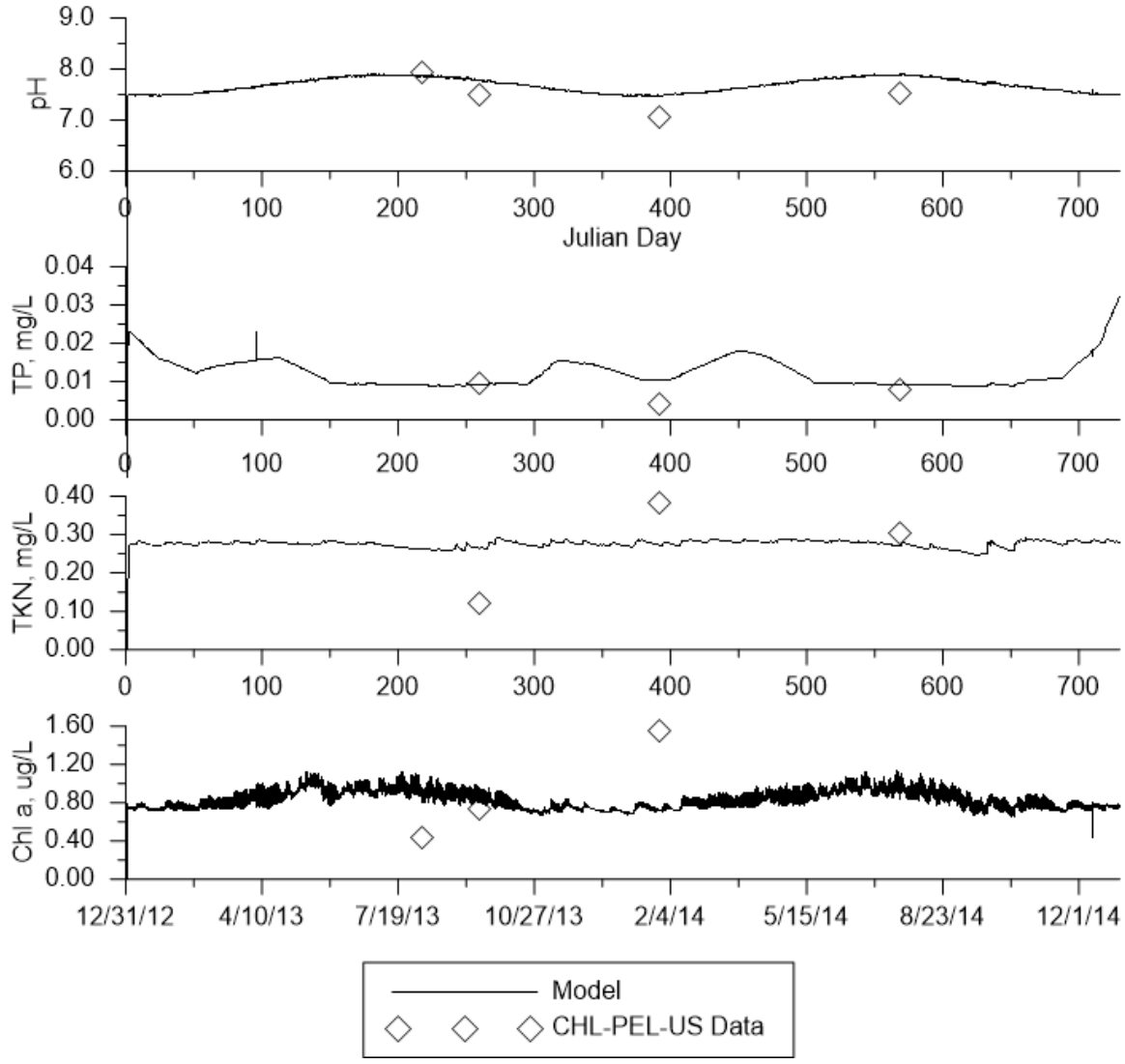

Figure 169. Water quality predictions at dam site (5). Data measured at station CHL-PEL-US, located approximately 5 km downstream of the dam site, are also plotted using diamond symbols.

Model Scenarios

Scenario Descriptions

Multiple scenarios were applied to the model inputs to simulate dam structure regimes for baseline conditions during 2013-2014 and future conditions. The results of these model simulations will allow for more informed management decisions and strategies in regards to dam implementation. Table 35 gives a list of the flood retention scenarios applied to the model.

Table 35. Chehalis River scenarios.

Scenario	Conditions	Reservoir Model (Simulated by Anchor QEQ)	Footprint Model (PSU)	Downstream Model (PSU)
Baseline	Current (2013-2014) and Future	Not Applicable	Yes	Yes

Scenario	Conditions	Reservoir Model (Simulated by Anchor QEQ)	Footprint Model (PSU)	Downstream Model (PSU)
FRFA Scenario 1	Current (2013-2014) and Future	Yes	Not Applicable	Yes
FRFA Scenario 2	Current (2013-2014) and Future	Yes	Not Applicable	Yes
FRO Summer – Riparian Shading	Current (2013-2014) and Future	Not Applicable	Yes	Yes
FRO Summer - No Shading	Current (2013-2014) and Future	Not Applicable	Yes	Yes
FRO – Dec 2007 Flood as Spring 2014	Current (2013-2014) and Future	Yes	Not Applicable	Yes
FRO – Dec 2007 Flood as Fall 2014	Current (2013-2014) and Future	Yes	Not Applicable	Yes
FRO – Jan 2009 Flood as Spring 2014	Current (2013-2014) and Future	Yes	Not Applicable	Yes
FRO – Jan 2009 Flood as Fall 2014	Current (2013-2014) and Future	Yes	Not Applicable	Yes

Flood Retention Only (FRO)

Flood Retention Only (FRO) is one of the dam management regimes. In this case the dam only operates during times when flooding is seen at Grand Mound, with Chehalis River flows greater than 38,800 cfs (Montgomery, 2016). This is approximately a 7-year flood with about 15% probability of occurrence (Montgomery, 2016). Dam outflow during these times would be reduced to 300 cfs. The inundation area for this scenario would have a median value of 187 acres, and could reach a maximum of 778 acres. The pool elevation for this scenario would have a median value of 513 feet, though could reach 520.4 feet at a maximum, which would result in a storage volume of 60,253 acre-feet (Montgomery, 2016).

Riparian shading for the FRO scenario was estimated using the vegetation management plan (Anchor QEQ,2016). Vegetation in the deciduous riparian shrubland area was assumed to be 2 m high and used a shade reduction factor of 0.5.

Flood Retention Flow Augmentation (FRFA)

Flood Retention Flow Augmentation (FRFA) is another dam management regime. Dam operations during flooding follow the same procedure as the FRO scenario. However, the dam would operate during other times as well. Minimum flow releases vary based on season. If the reservoir is not in a flooding operation state, inflows greater than 2,800 would be released. The downstream gage at Doty would be targeted to maintain a minimum flow of 5,000 cfs. Dam releases at a maximum of 15,000 cfs would result in flows at Doty of 23,000 cfs (Montgomery, 2016).

Within the FRFA regime, there are two sub-scenarios. FRFA scenario 1 includes lower dam outflows than FRFA scenario 2 during September and October, has less drawdown, and takes less time for the reservoir to refill during the winter season. Conversely, FRFA scenario 2 has higher dam outflows than FRFA scenario 1 during September and October, has more drawdown, and takes longer for the reservoir to refill during the winter season (Montgomery, 2016). FRFA scenario 1 has an elevation range of 598 to 683 feet; a storage volume range of 44,000

to 59,400 acre-feet, with a mean of 51,386 acre-feet; and an annual drawdown range of 9 to 29 feet. FRFA scenario 2 has an elevation range of 587 to 680 feet; a storage range of 36,800 to 121,700 acre-feet; a minimum storage range of 36,800 to 121,700 acre-feet, with a mean of 46,125 acre-feet; and an annual drawdown range of 8-40 feet (Montgomery, 2016).

Future Conditions

Current and potential future conditions for meteorological, flow, and temperature data were applied to each baseline and dam scenario. Modeling of future scenarios involved simulating one year. Anchor QEA used data made available by the University of Washington (Mauger, 2016) to develop meteorological input files for future climate scenarios. Flow multipliers for future climate scenarios were also provided by Anchor QEA (Hill, 2016), and are shown in Table 36. Tributary flows were multiplied by these values to simulate future flow conditions.

Table 36. Future conditions monthly flow multipliers (Hill, 2016).

Month	Flow Multiplier
January	1.129
February	1.085
March	0.994
April	0.938
May	0.889
June	0.851
July	0.817
August	0.785
September	0.813
October	1.055
November	1.058
December	1.145

As tributary temperatures were not made available for the future climate scenarios, these were assumed to increase by the same magnitude that air temperature increased. The difference in air temperature from baseline conditions to future climate conditions were added to tributary water temperatures from 2014.

Meteorological, flow, and temperature data were the only inputs to the model that were altered to simulate future conditions. All other model conditions and input data remained the same as for the baseline calibration simulations. Natural Conditions In order to simulate natural conditions on the Chehalis River, certain changes were made to model inputs. These changes were to input flow temperatures, some input flow constituents, and riparian shading. While additional changes to bathymetry, meteorological data, or other inputs would make for a more complete simulation of natural conditions, a simple first look was the aim.

Temperatures Inputs

Input temperatures were altered to simulate natural conditions using 2013-2014 data and temperature criteria. Any temperature value 10 ^{o}C or less remained the same. Temperature values greater than 10 ^{o}C within each time period a criteria applied were multiplied by a factor which ensured the largest temperature value fell at or below the applicable temperature criteria. For distributed flows, the criteria reach where the largest portion of the branch overlapped with was used for altering distributed flow temperatures. Wastewater treatment plants used input temperature data from the closest tributary with data available. Reaches and dates where various criteria applied are shown in Table 37 (Pickett, 2016). Figure 170 shows how the input temperatures were altered to simulate natural conditions for the upstream boundary, Elk Creek, South Fork Chehalis River, Newaukum River, Skookumchuck River, and Black River. Figure 171 shows how the input temperatures for distributed flows in branches 1, 2, 3, 4, 6, 9, and 10.

Table 37. Temperature criteria applicable to various reaches of the Chehalis River (Pickett, 2016)

	Temperature Criteria (degrees C)			
Time Period	Segments 321-191 RM 33.2-66.9	Segments 190-153 RM 66.9-75.2	Segments 152-89 RM 75.2-88.0	Segments 88-83 RM 88.0-90.2
Jan 1 - Feb 14	13.0	17.5	13.0	13.0
Feb 15 - May 15	13.0	17.5	13.0	13.0
May 16 - July 1	17.5	17.5	17.5	13.0
July 2 - Sept 14	17.5	17.5	17.5	17.5
Sept 15 - Sept 30	17.5	17.5	17.5	13.0
Oct 1 - Dec 31	13.0	17.5	13.0	13.0

RM 33.2 = Porter
RM 66.9 = Mouth of Skookumchuck River
RM 75.2 = Mouth of the Newaukum River
RM 88.0 = Mouth of South Fork Chehalis River
RM 90.2 = Upstream of Ceres Hill Road bridge, upstream of South Fork Chehalis River

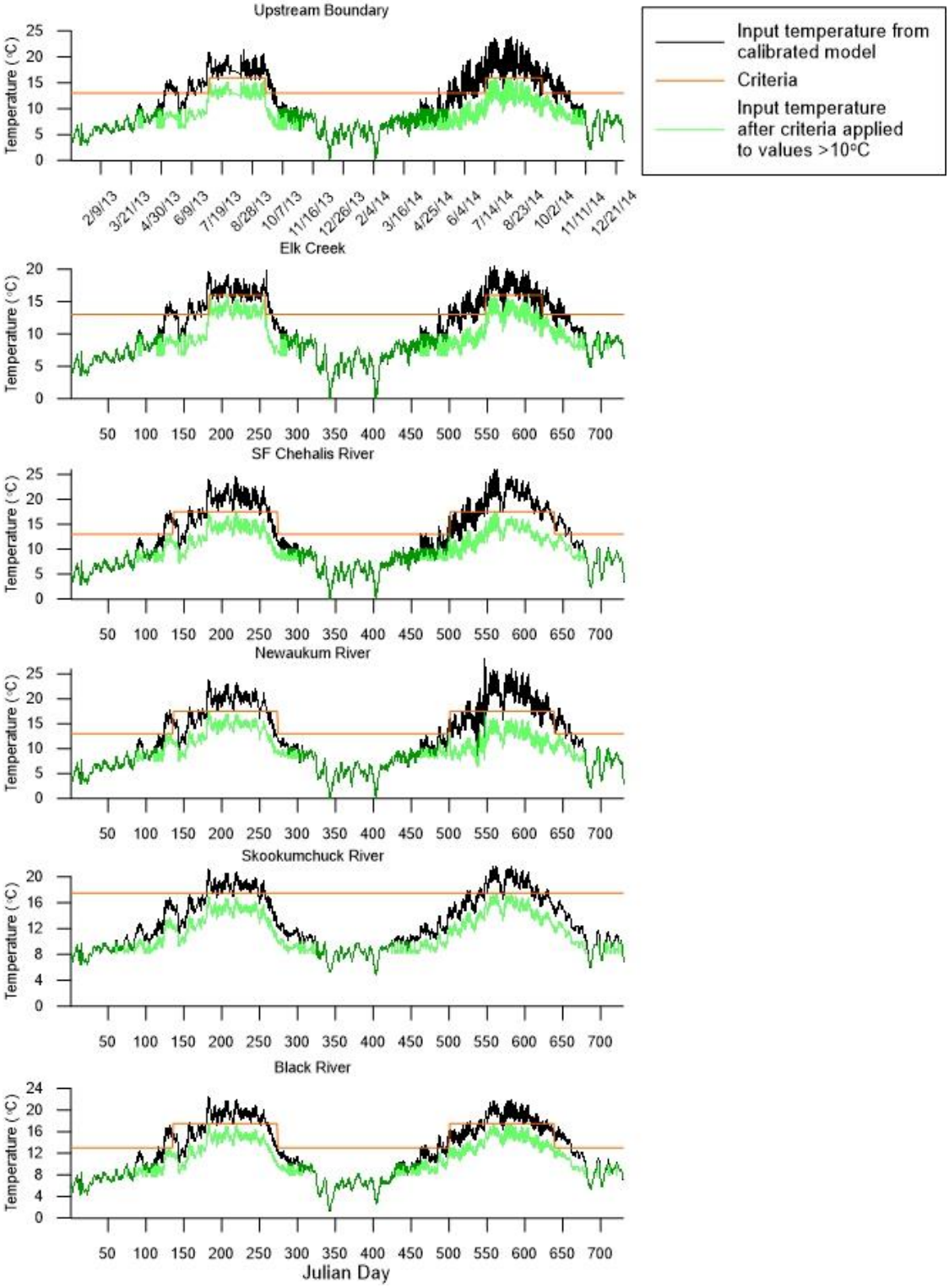

Figure 170. Temperature inputs simulating natural conditions for the upstream boundary, Elk Creek, South Fork Chehalis River, Newaukum river, Skookumchuck River, and Black River

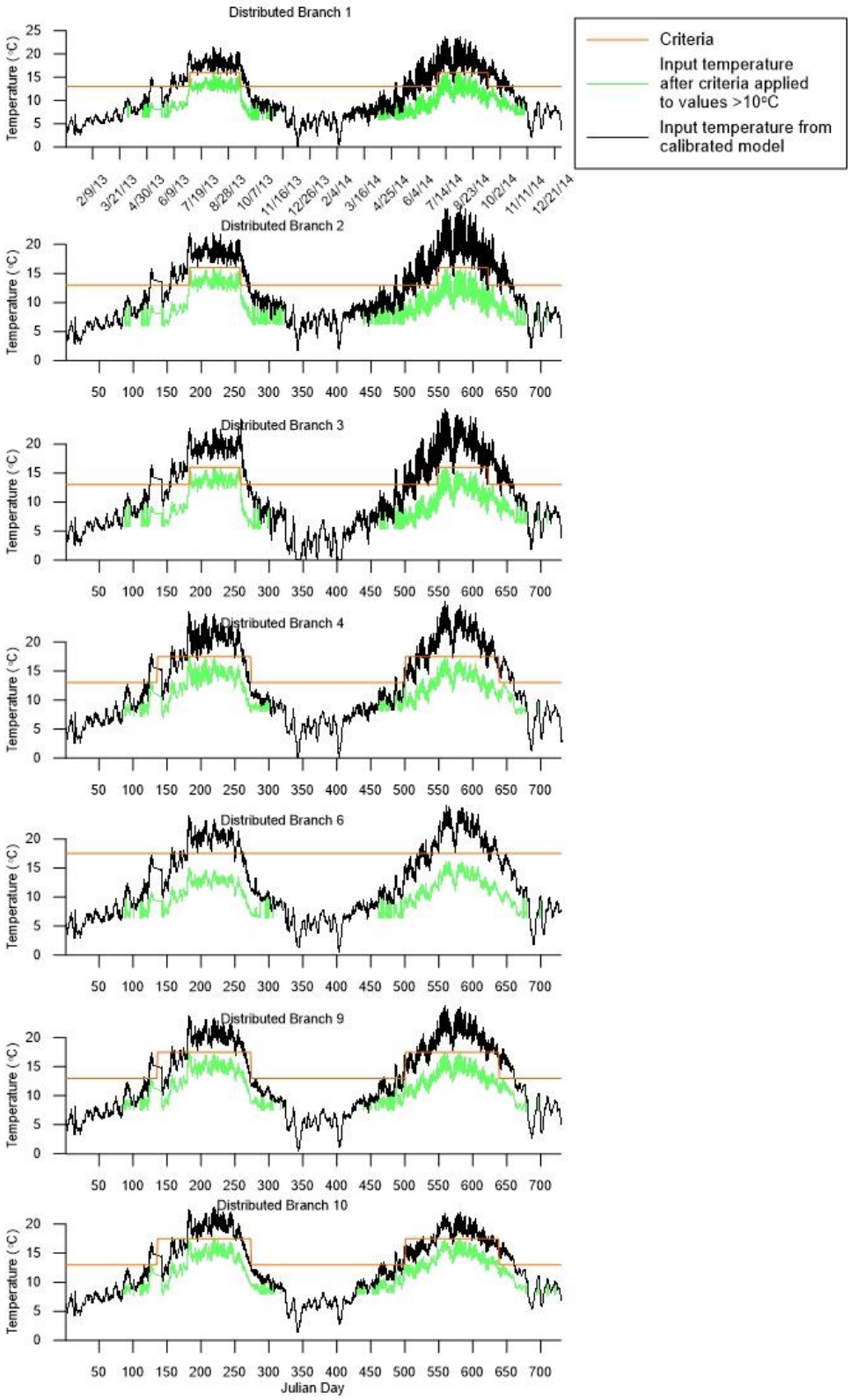

Figure 171. Temperature inputs simulating natural conditions for distributed flows in branches 1, 2, 3, 4, 6, 9, and 10

Constituent Inputs

Similar to temperature, DO criteria were available for various reaches of the Chehalis River. These criteria are shown in Table 38 (Pickett, 2016). DO values greater than criteria remained the same. When DO values were less than the criteria, the values were set to the criteria value to simulate natural conditions. DO values only dipped below the criteria for the upstream boundary, Elk Creek, and Lincoln Creek. Figure 172 shows the applicable criteria and how the input DO values were altered to simulate natural conditions for the upstream boundary, Elk Creek, and Lincoln Creek.

Table 38. Dissolved Oxygen criteria applicable to various reaches of the Chehalis River (Pickett, 2016)

	Dissolved Oxygen Criteria (mg/L)			
Time Period	Segments 321-197 RM 33.2-65.8	Segments 197-153 RM 65.8-75.2	Segments 152-83 RM 75.2-90.2	Segments 82-2 RM 90.2-118.4
Jan 1 to May 31	8.0	8.0	8.0	9.5
June 1 - Sept 15	8.0	5.0	8.0	9.5
Sept 16 - Dec 31	8.0	8.0	8.0	9.5

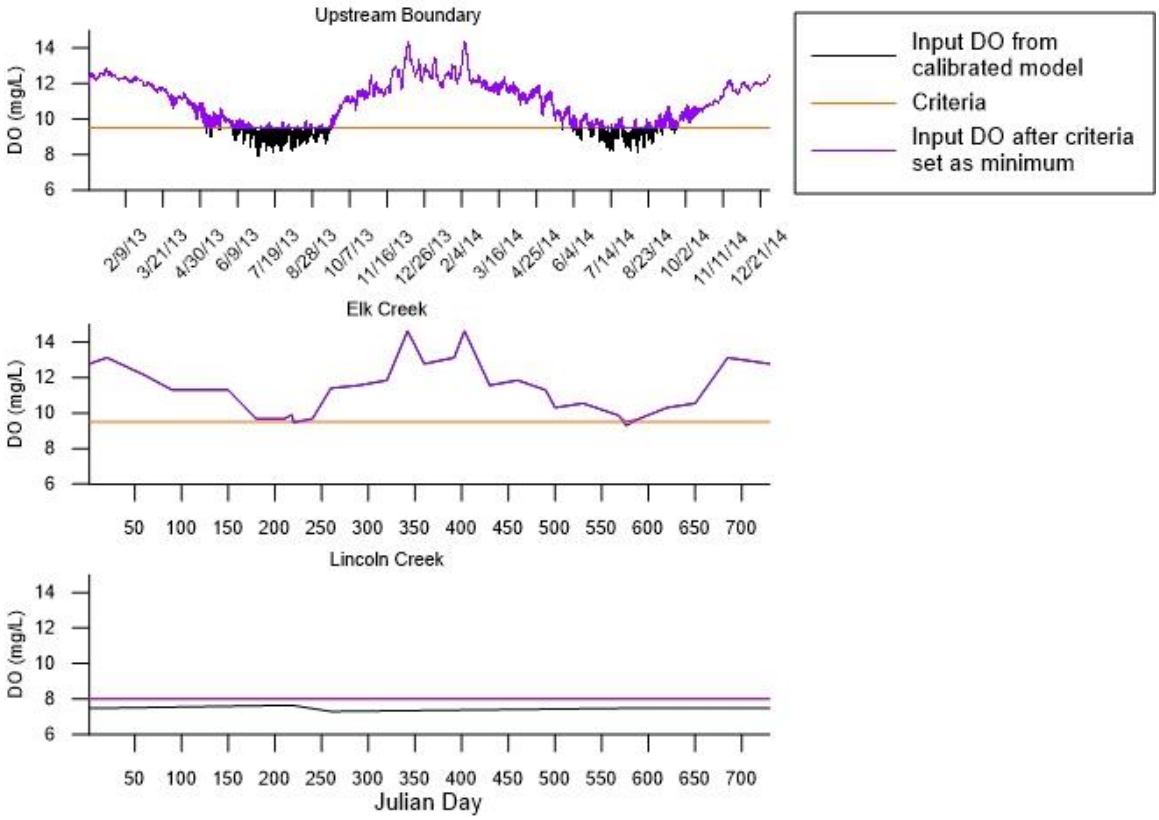

Figure 172. Dissolved Oxygen inputs simulating natural conditions for the upstream boundary, Elk Creek, and Lincoln Creek

Some other input constituents were altered to simulate natural conditions. Ammonia and nitrate were set at a maximum of 0.1 mg/L, while values below this remained the same as for calibration. Phosphate was set at a maximum of 0.005 mg/L, while values below this remained the same as for calibration. All input BOD values were set to zero. These changes were implemented for the upstream boundary, all tributary inputs, and all groundwater inputs. Wastewater treatment plants used input constituent values from the closest tributary with data. Additionally, all SOD values for all segments were set to 0.1.

Temperature Predictions

Downstream Model

Model predictions of daily maximum temperature of the baseline conditions, FRFA scenarios, and FRO scenarios upstream of Elk Creek are shown in Figure 173 and Figure 174 for current conditions and future conditions respectively. Predictions upstream of the S. F. Chehalis River are shown in Figure 175 and Figure 176 and predictions upstream of the Skookumchuck River are potted in Figure 177 and Figure 178.

The model predicted future climate conditions would increase water temperature for all scenarios. Temperature predictions were cooler for the FRFA scenarios than the baseline and FRO scenarios. However, differences in temperature predictions between the scenarios decreased moving downstream. Upstream of Elk Creek, temperatures differences between the baseline and FRO scenarios were small, whereas the FRFA scenarios could be more than 5° C cooler than the baseline in the summer. Differences between the baseline and FRFA scenarios upstream of the S. F. Chehalis River were approximately up to 3° C under current conditions and up to 5° C under future conditions. Upstream of the confluence with the Skookumchuck River, during the summer the FRFA scenario could be 1° C cooler than the baseline under current conditions and 2-3° C cooler under future conditions.

Temperature predictions of the flood scenarios for December 2007 and January 2009 are plotted in Figure 179 and Figure 180, respectively.

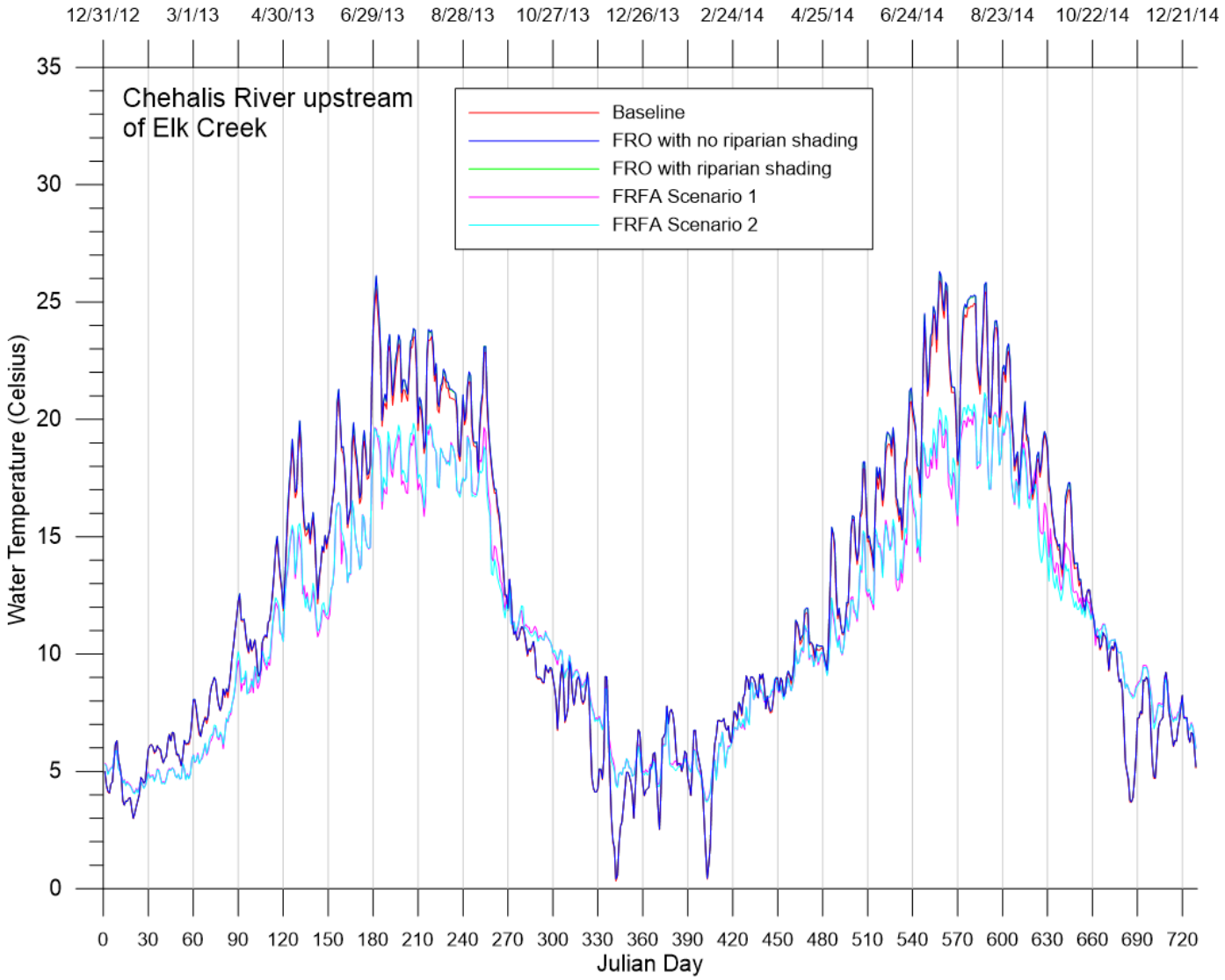

Figure 173. Downstream model daily maximum temperature predictions immediately upstream of the confluence with Elk Creek for current conditions baseline, FRO with no vegetative shading, and FRO with riparian shading, FRFA scenario 1, and FRFA scenario 2 simulations.

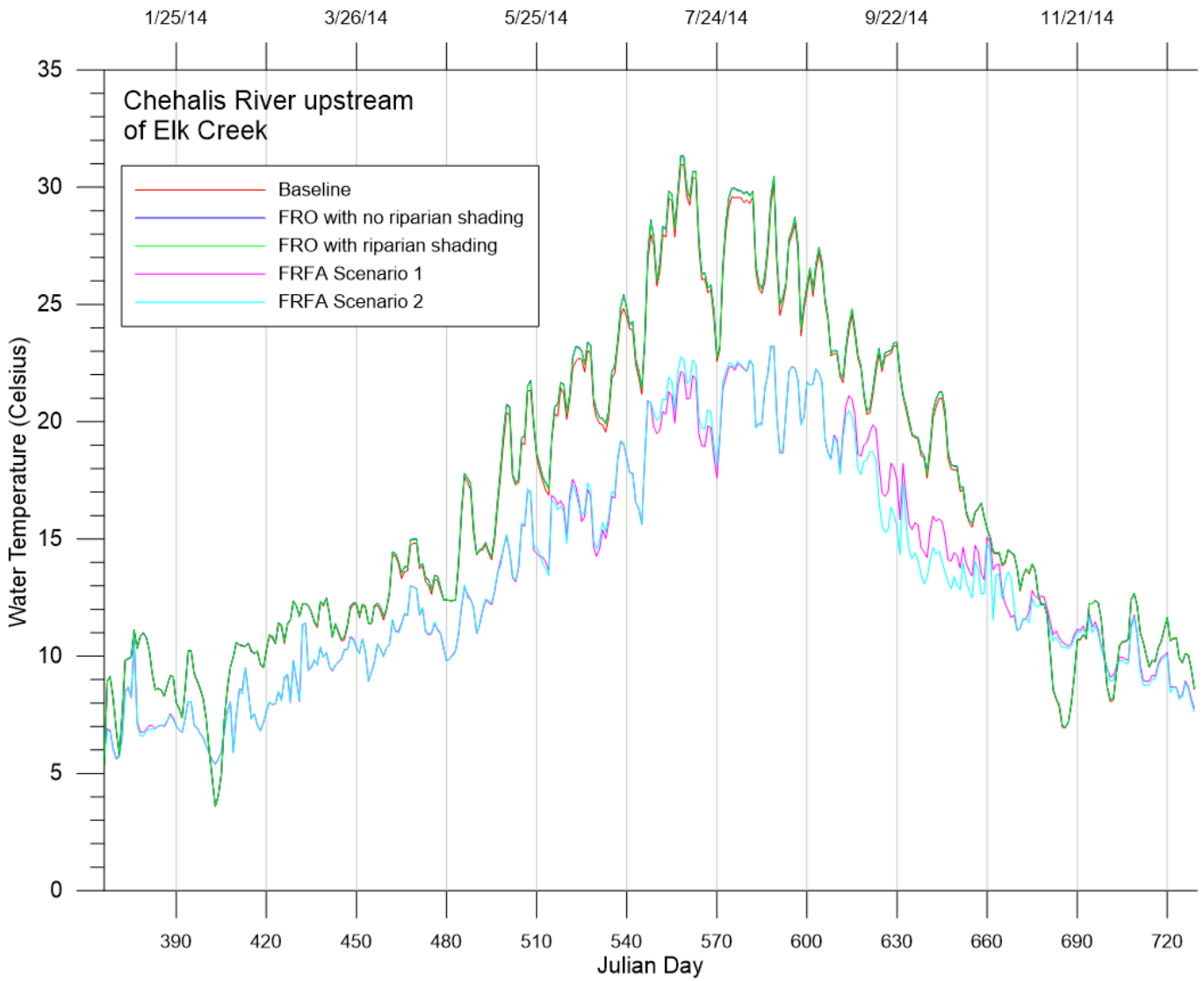

Figure 174. Downstream model daily maximum temperature predictions immediately upstream of the confluence with Elk Creek for future conditions baseline, FRO with no vegetative shading, and FRO with riparian shading, FRFA scenario 1, and FRFA scenario 2 simulations.

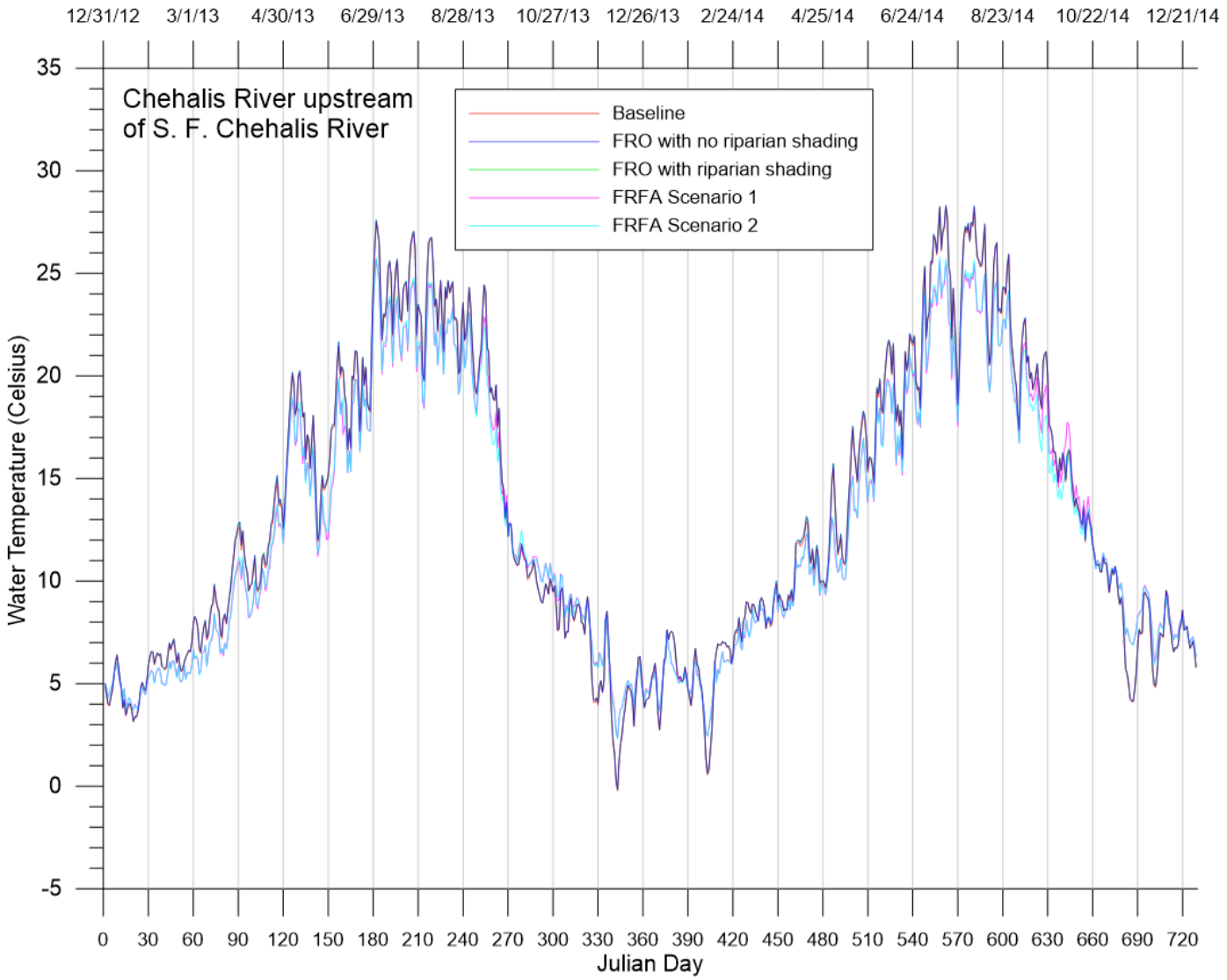

Figure 175. Downstream model daily maximum temperature predictions immediately upstream of the confluence with South Fork Chehalis River for current conditions baseline, FRO with no vegetative shading, and FRO with riparian shading, FRFA scenario 1, and FRFA scenario 2 simulations.

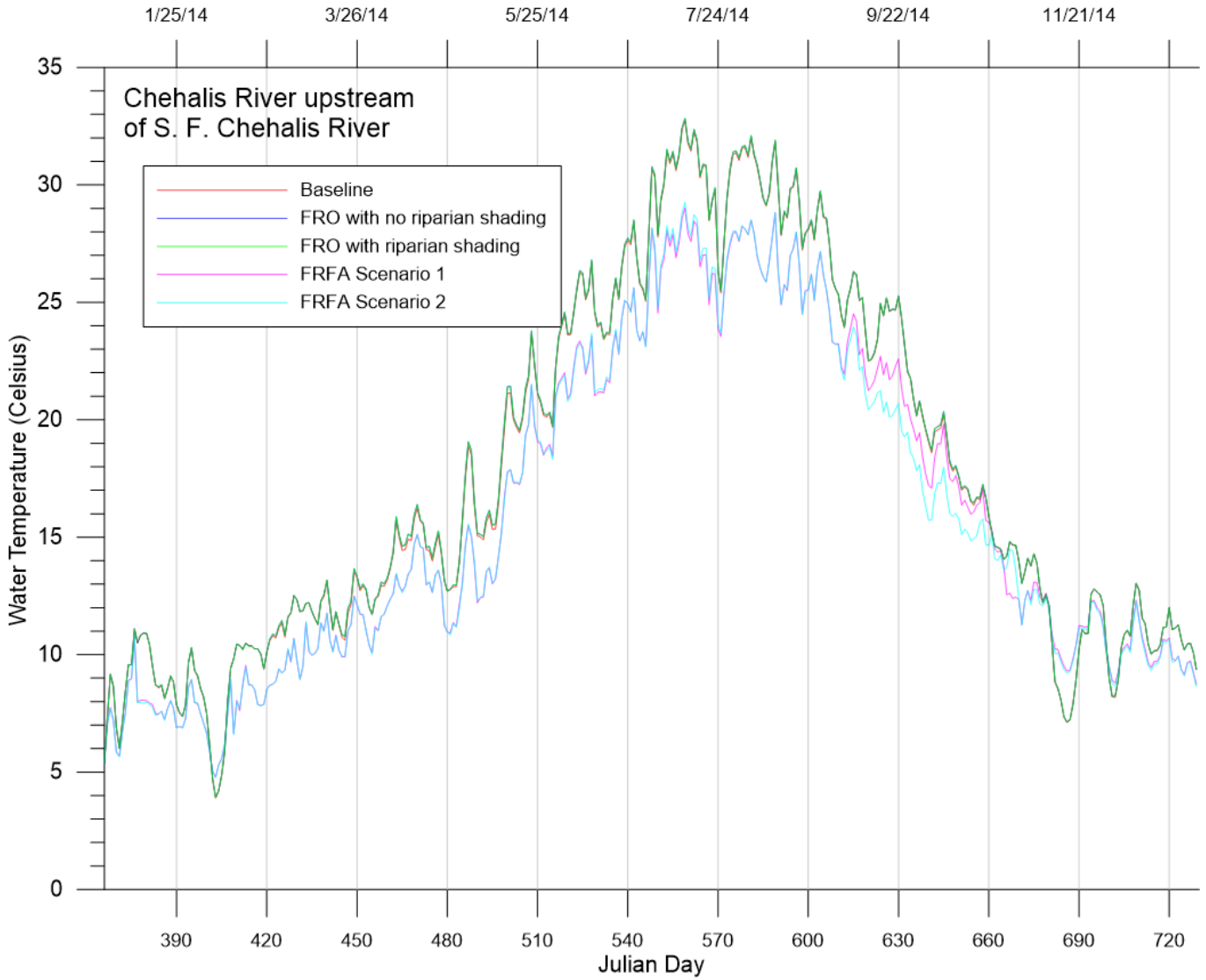

Figure 176. Downstream model daily maximum temperature predictions immediately upstream of the confluence with South Fork Chehalis River for future conditions baseline, FRO with no vegetative shading, and FRO with riparian shading, FRFA scenario 1, and FRFA scenario 2 simulations.

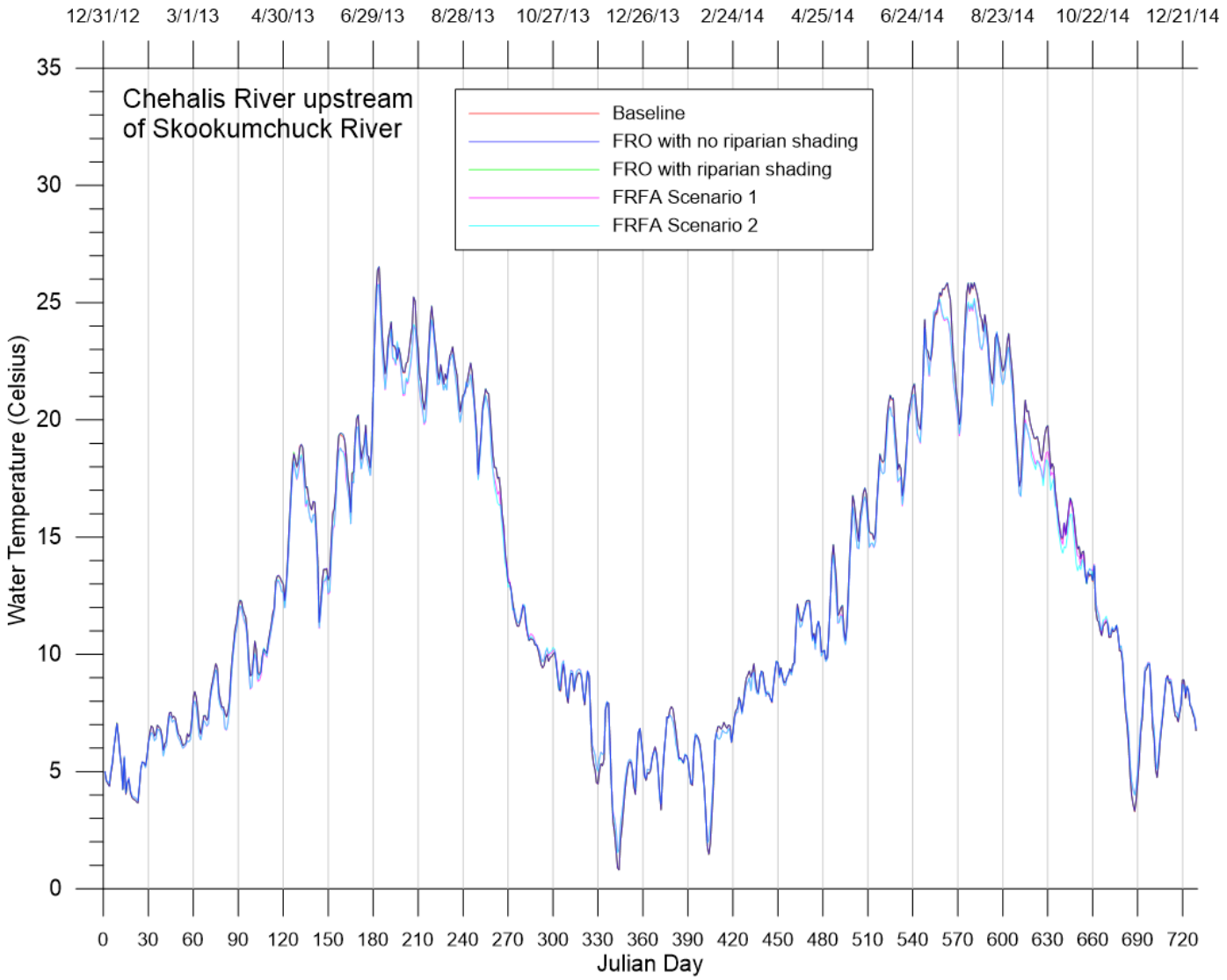

Figure 177. Downstream model daily maximum temperature predictions immediately upstream of the confluence with Skookumchuck River for current conditions baseline, FRO with no vegetative shading, and FRO with riparian shading, FRFA scenario 1, and FRFA scenario 2 simulations.

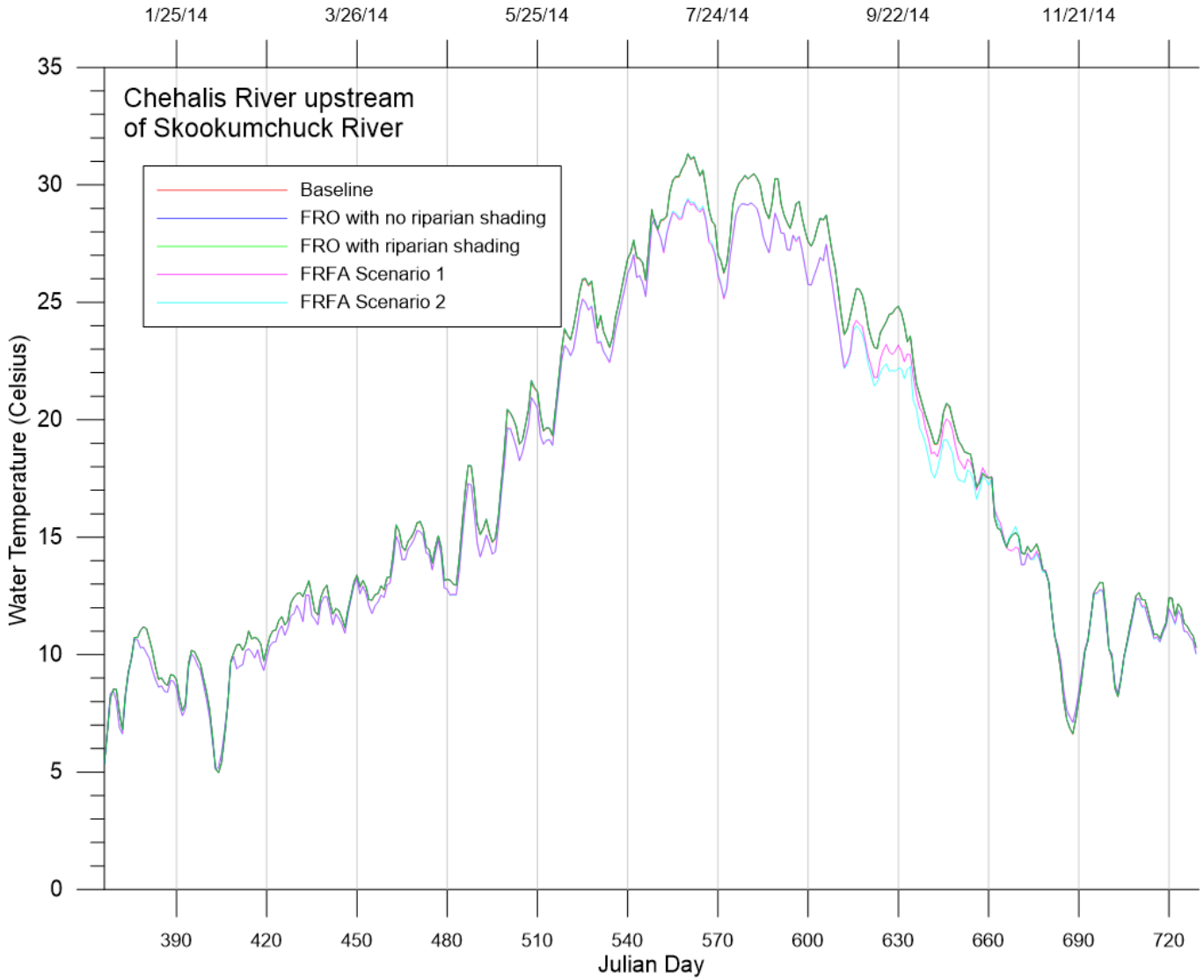

Figure 178. Downstream model daily maximum temperature predictions immediately upstream of the confluence with Skookumchuck River for future conditions baseline, FRO with no vegetative shading, and FRO with riparian shading, FRFA scenario 1, and FRFA scenario 2 simulations.

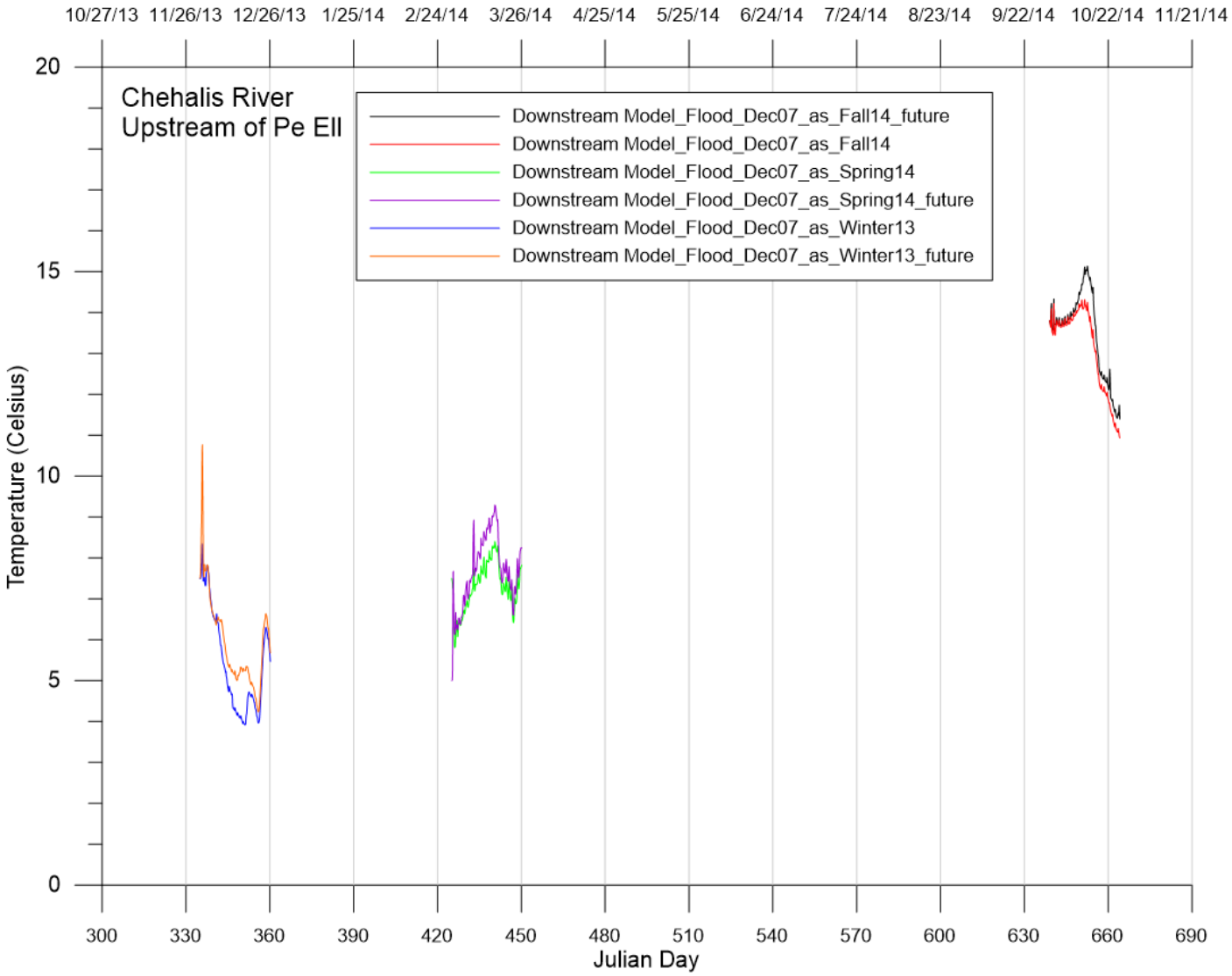

Figure 179. Temperature predictions of December 07 flood scenarios.

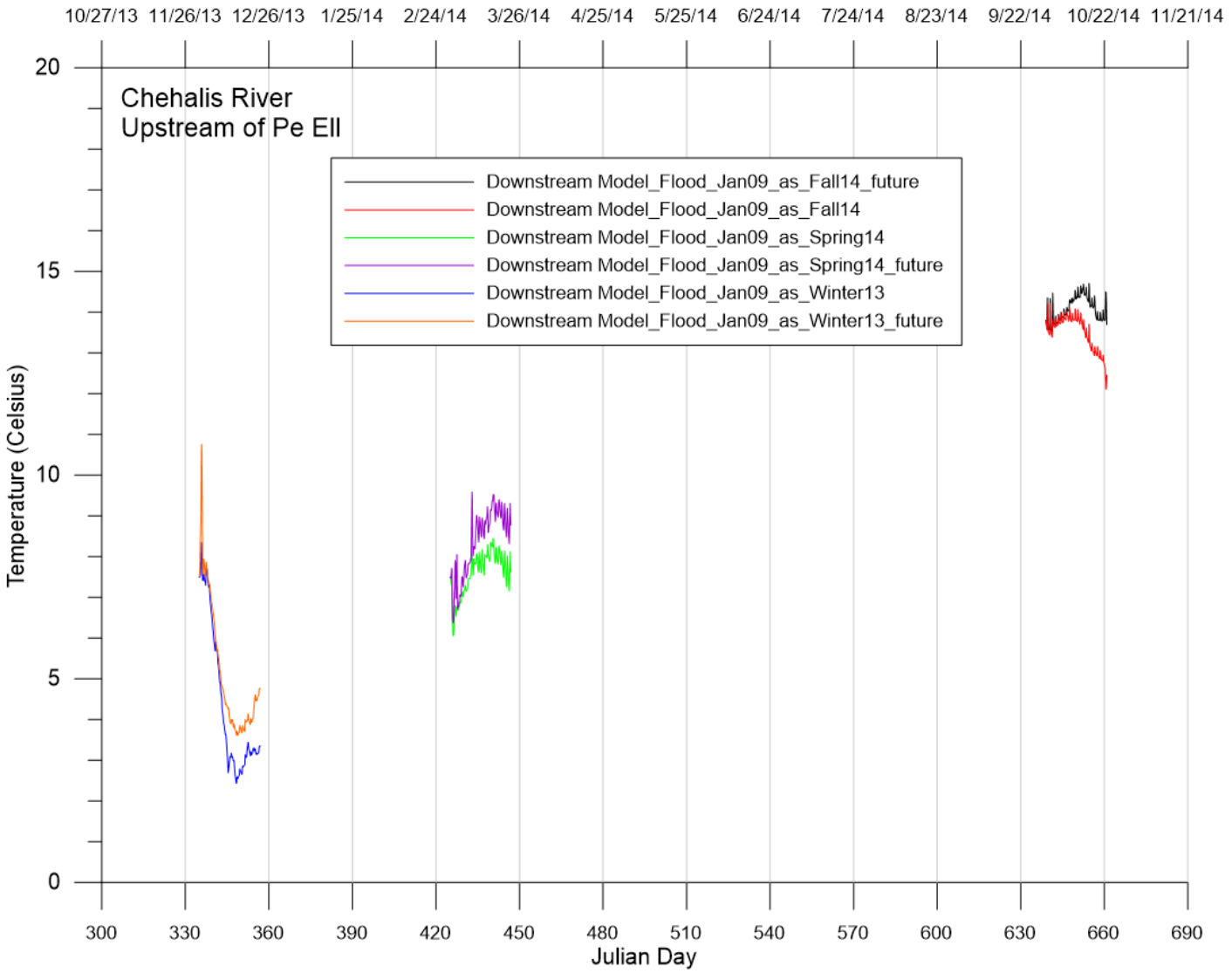

Figure 180. Temperature predictions of January 09 flood scenarios.

Footprint Model

Footprint model daily maximum temperature predictions at the proposed dam location for current and future conditions are plotted in Figure 181 and Figure 182, respectively. Daily maximum temperature were at least several degrees warmer under future conditions. Temperature differences between the FRO scenario with no riparian shading and the FRO with riparian shading were small. Daily maximum temperatures of the FRO scenarios could be up to 2-3° C warmer than the baseline scenarios during the summer.

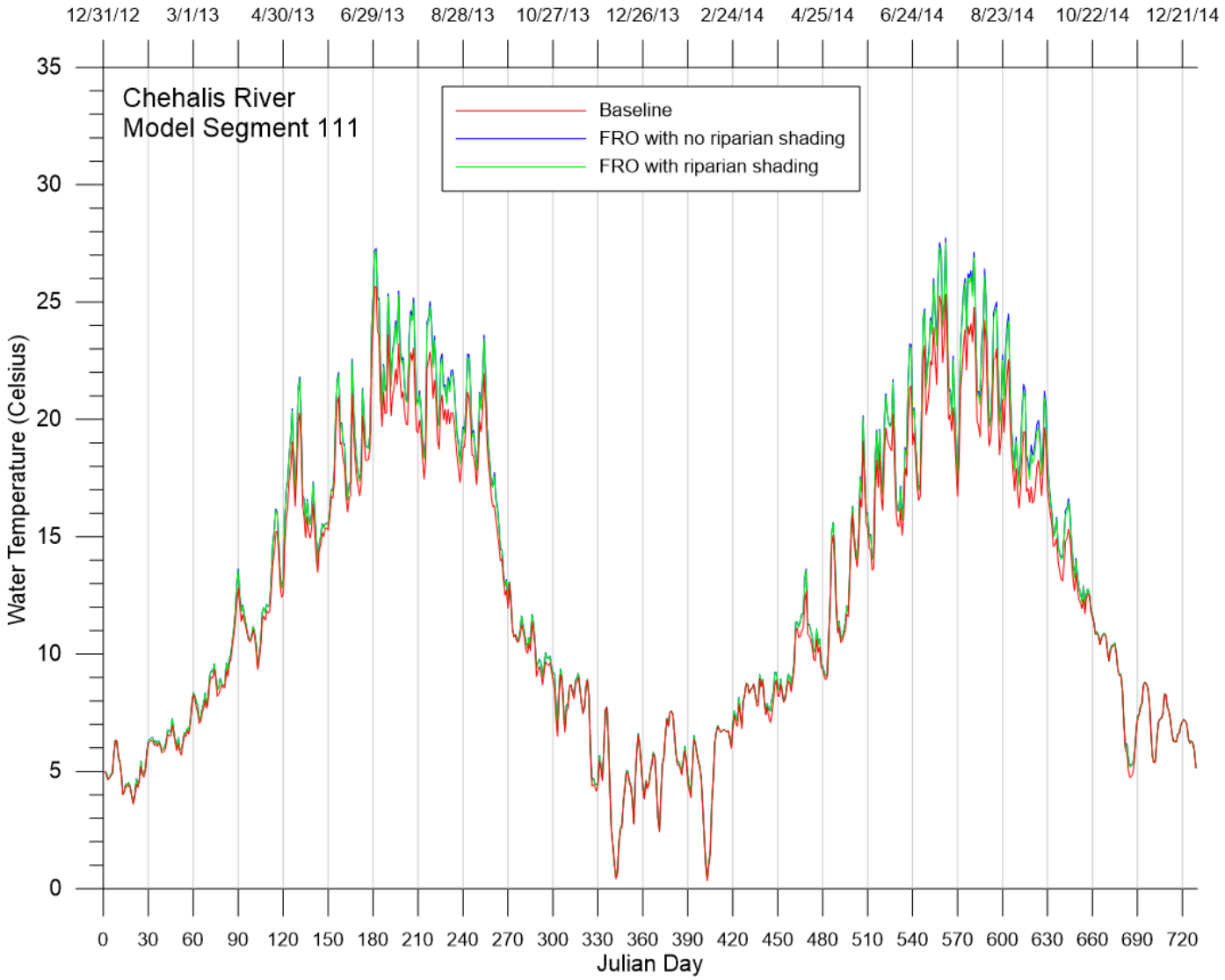

Figure 181. Footprint model daily maximum temperature predictions at the dam location for current conditions baseline, FRO with no vegetative shading, and FRO with riparian shading scenarios.

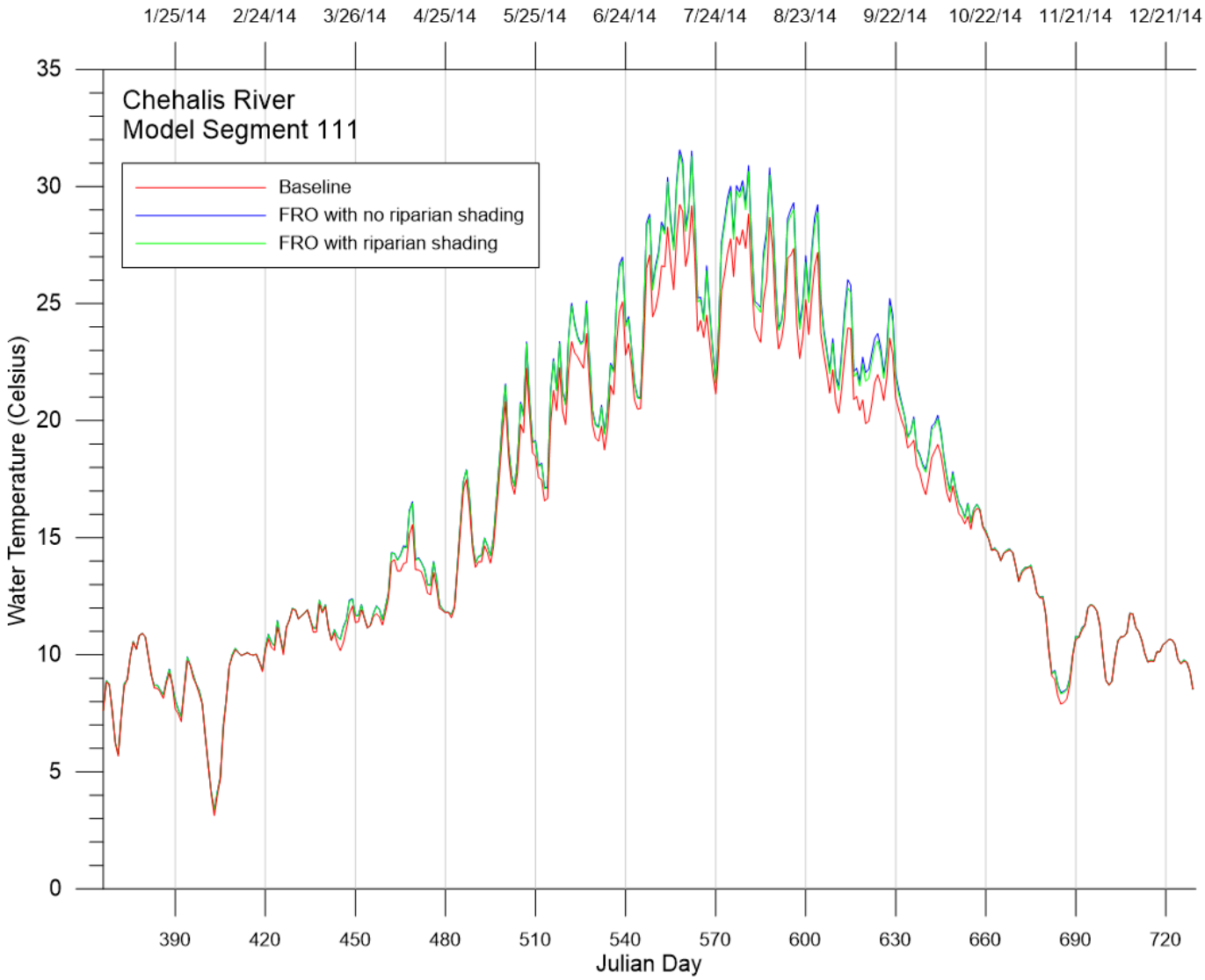

Figure 182. Footprint model daily maximum temperature predictions at the dam location for future conditions baseline, FRO with no vegetative shading, and FRO with riparian shading scenarios.

Water Quality Predictions

Downstream Model

DO and nutrients during summer months are discussed in this section. The warmer summer months are when river water quality and fish health and habitat are of the greatest concern. Updating the upstream boundary input constituents specific to each scenario would give more accurate water quality results.

Dissolved Oxygen

Scenario dissolved oxygen predictions are compared with the baseline for the confluence with the S. F. Chehalis River in Figure 183 through Figure 186. FRO scenario predictions were little different than the base predictions. FRFA scenario prediction were as much as 0.5 mg/l higher than the base scenario predictions because of higher possible DO saturation concentrations due to cooler water temperatures.

DO predictions upstream of the Skookumchuck River are shown in Figure 187 through Figure 190. FRO predictions differed little from the baseline at this location, but the FRFA scenario predictions was as much as 0.5 mg/l greater than the baseline during the summer of 2014.

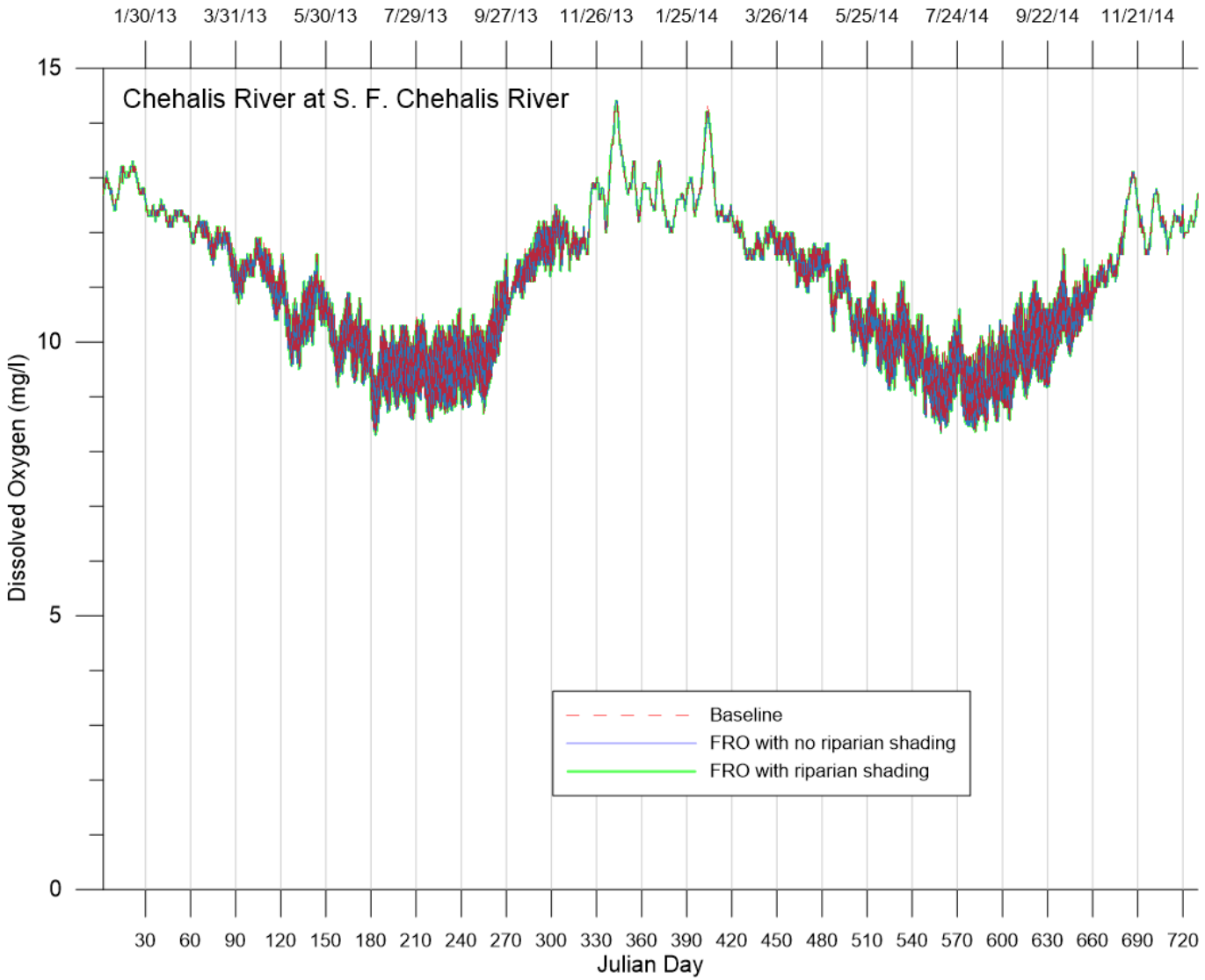

Figure 183. DO predictions at the confluence with South Fork Chehalis River for current conditions baseline, FRO with no vegetative shading, and FRO with riparian shading simulations.

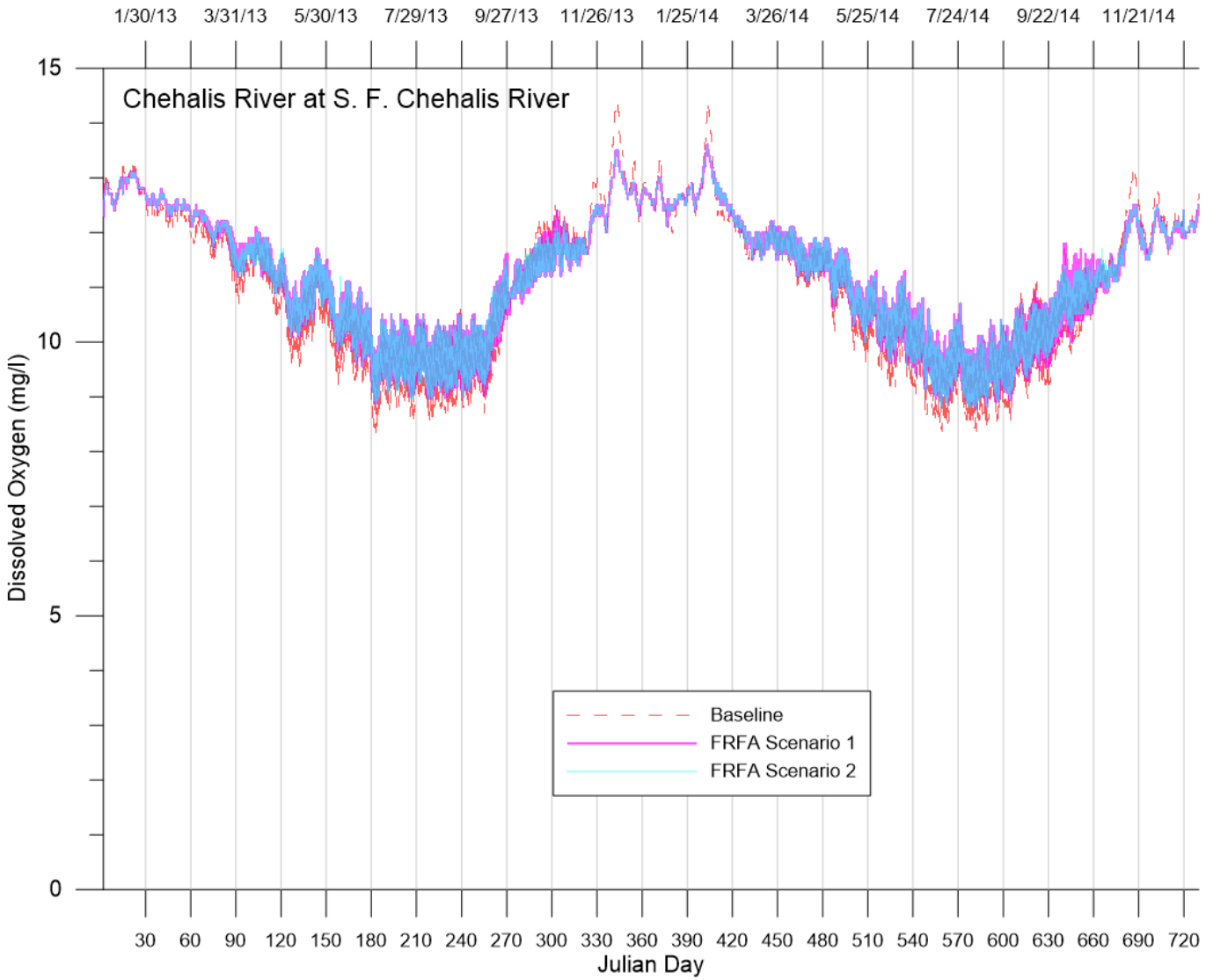

Figure 184. DO predictions at the confluence with South Fork Chehalis River for current conditions baseline, FRFA scenario 1, and FRFA scenario 2 simulations.

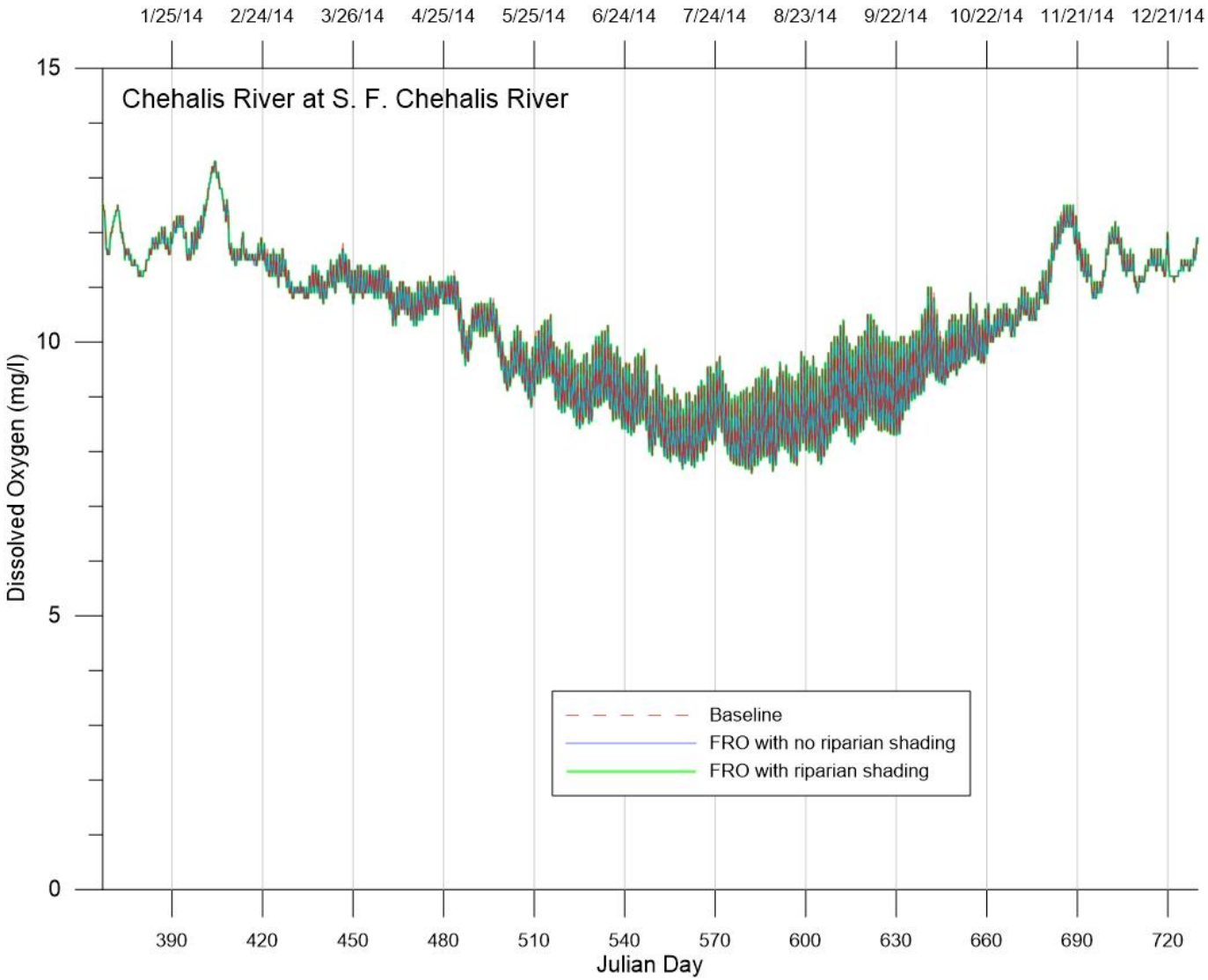

Figure 185. DO predictions at the confluence with South Fork Chehalis River for future conditions baseline, FRO with no vegetative shading, and FRO with riparian shading simulations.

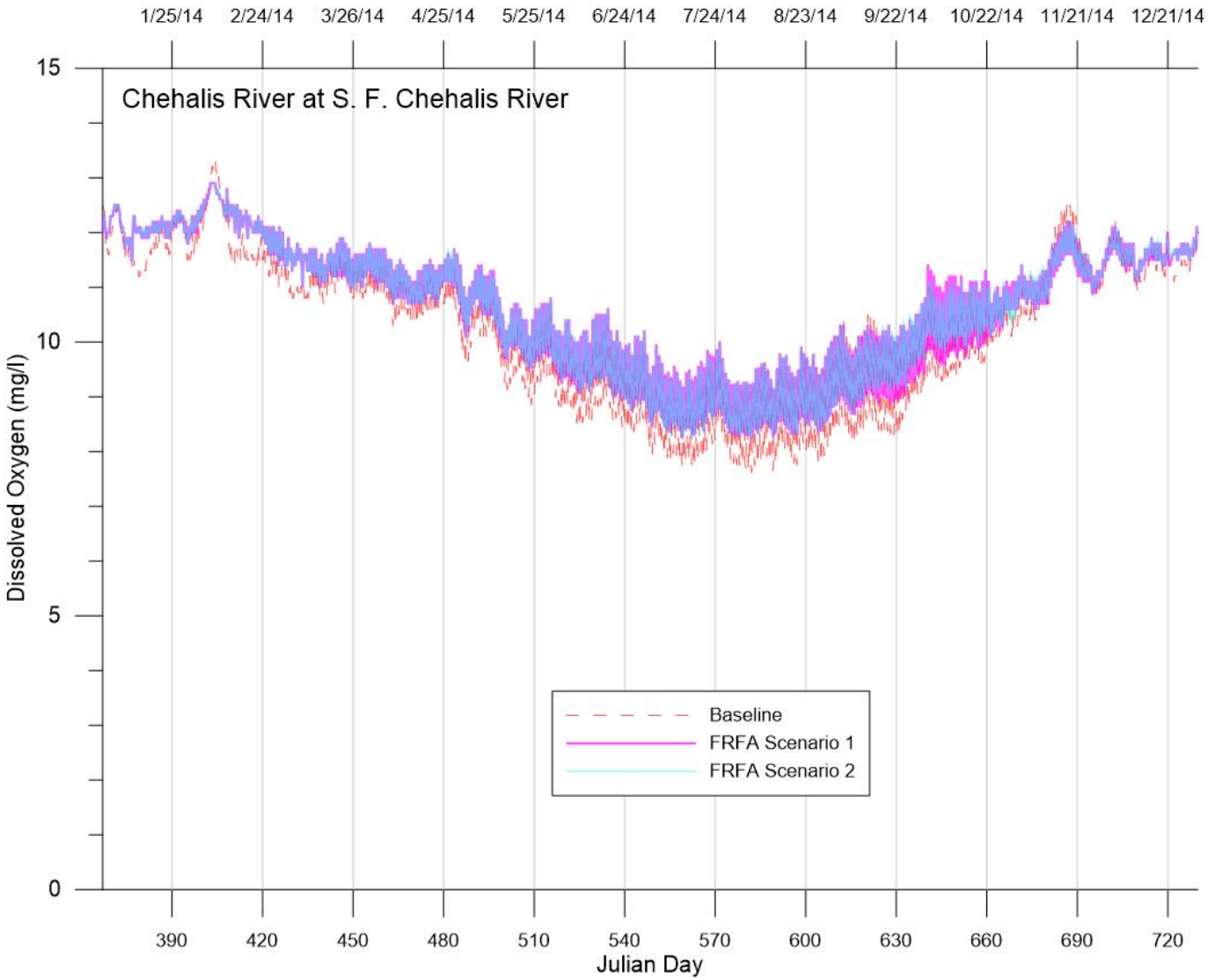

Figure 186. DO predictions at the confluence with South Fork Chehalis River for future conditions baseline, FRFA scenario 1, and FRFA scenario 2 simulations.

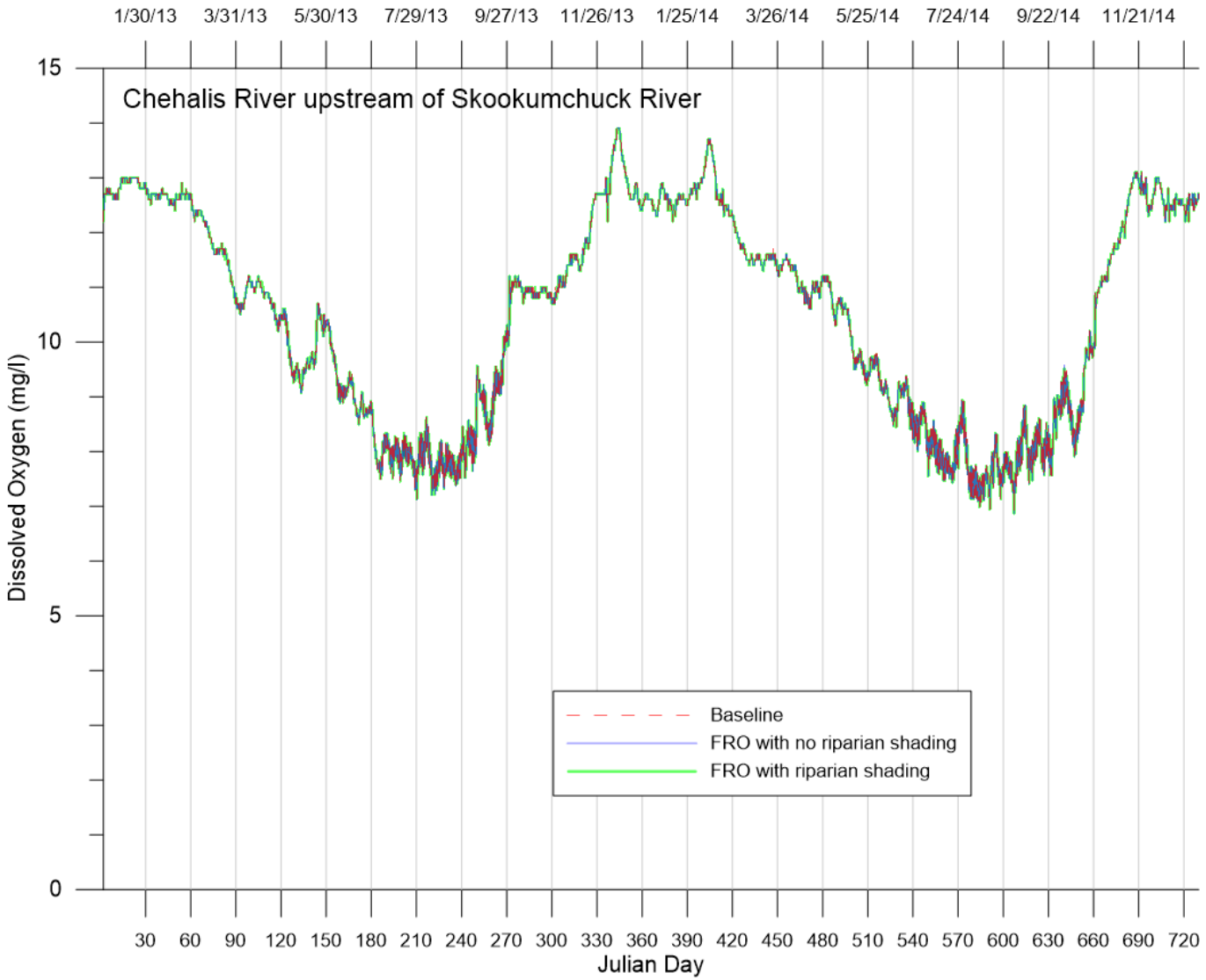

Figure 187. DO predictions upstream of the Skookumchuck River for current conditions baseline, FRO with no vegetative shading, and FRO with riparian shading simulations.

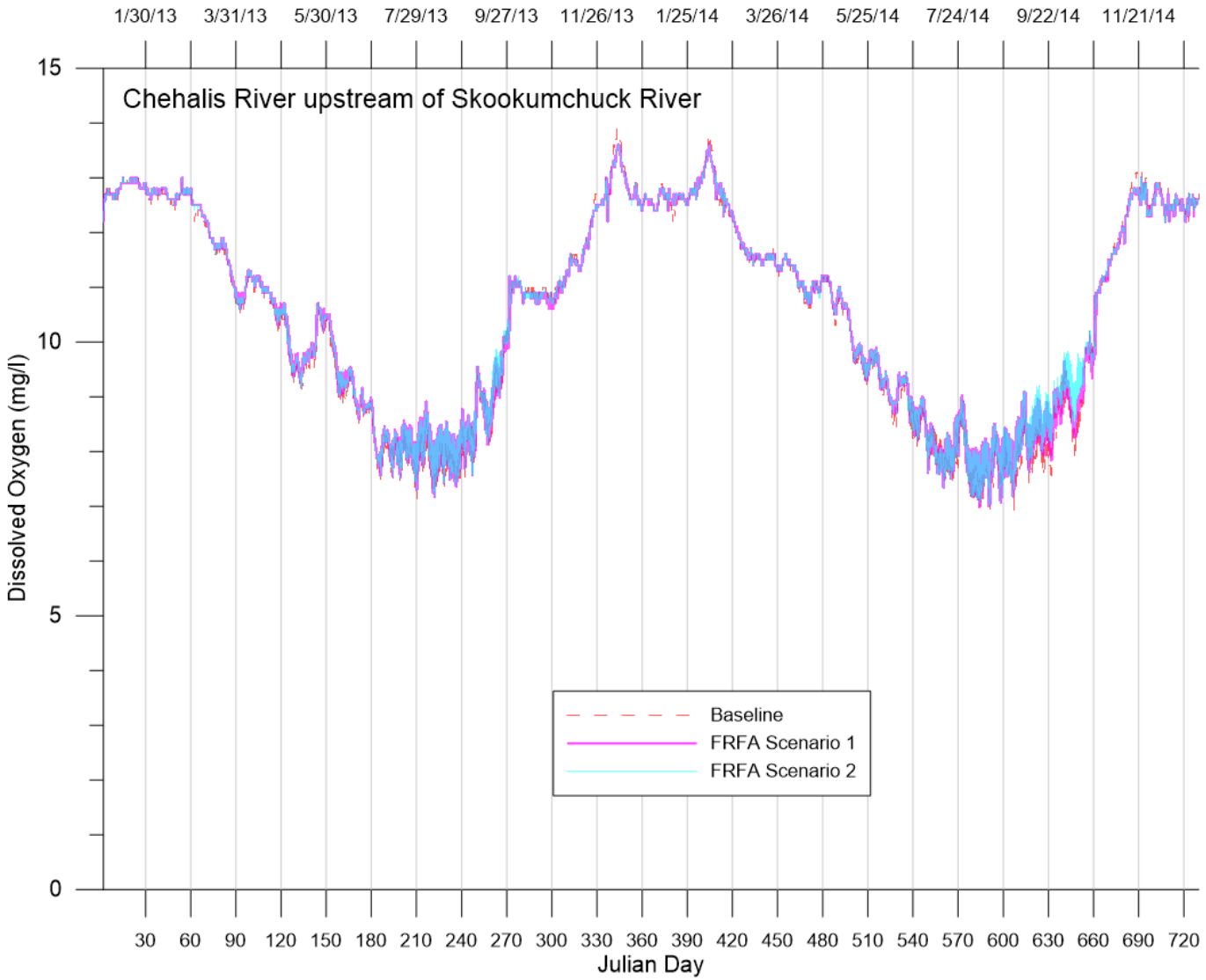

Figure 188. DO predictions upstream of the Skookumchuck River for current conditions baseline, FRFA scenario 1, and FRFA scenario 2 simulations.

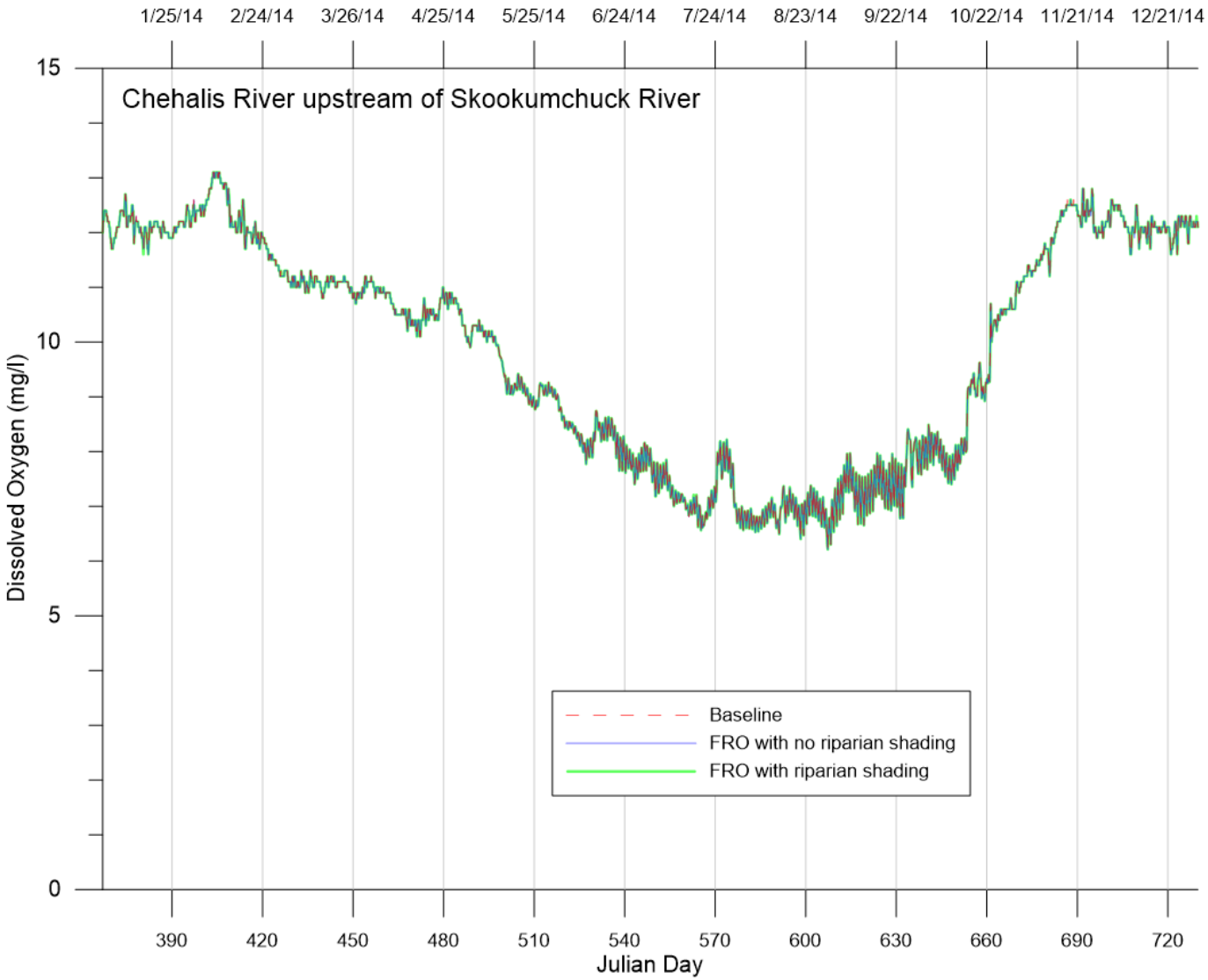

Figure 189. DO predictions downstream of the Skookumchuck River for future conditions baseline, FRO with no vegetative shading, and FRO with riparian shading simulations.

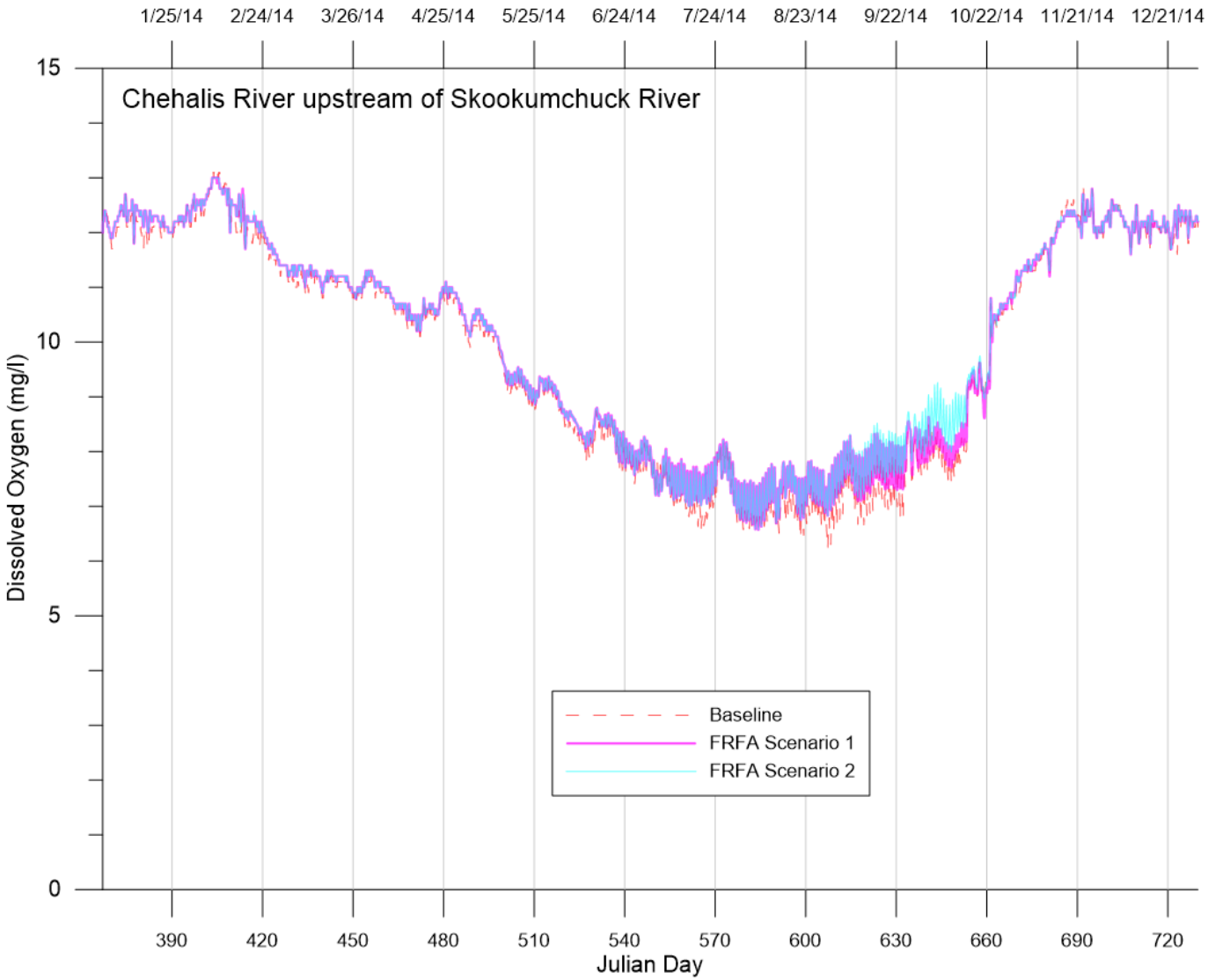

Figure 190. DO predictions downstream of the Skookumchuck River for future conditions baseline, FRFA scenario 1, and FRFA scenario 2 simulations.

Total Phosphorus

Figure 191 through Figure 194 show TP predictions for the scenarios at the confluence with the S. F. Chehalis River. TP for the FRO scenarios were close to baseline predictions. Because of lower concentrations released by the dam, FRFA scenarios TP prediction were less than the baseline predictions during the summer by as much as 15%.

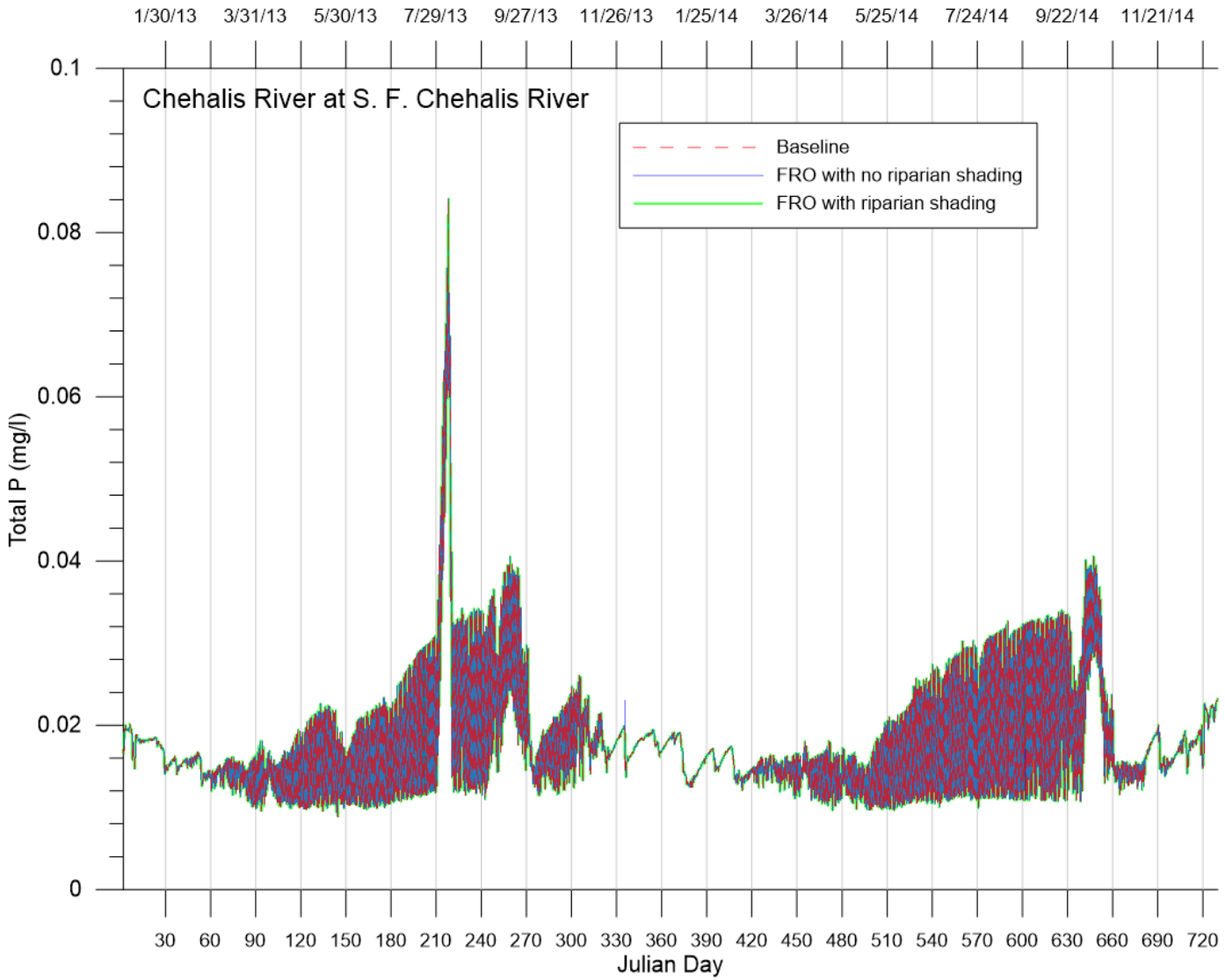

Figure 191. TP predictions at the confluence with South Fork Chehalis River for current conditions baseline, FRO with no vegetative shading, and FRO with riparian shading simulations.

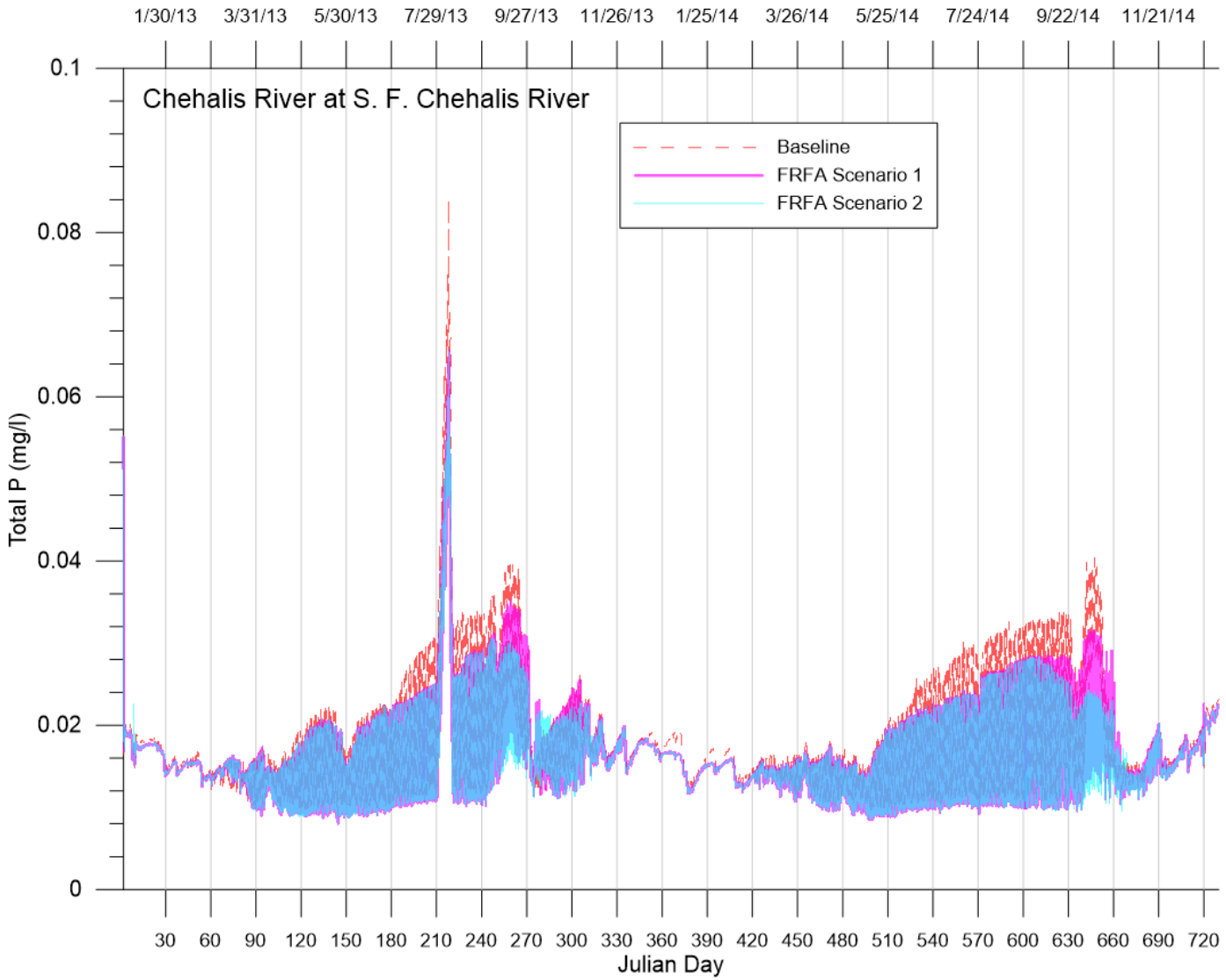

Figure 192. TP predictions at the confluence with South Fork Chehalis River for current conditions baseline, FRFA scenario 1, and FRFA scenario 2 simulations.

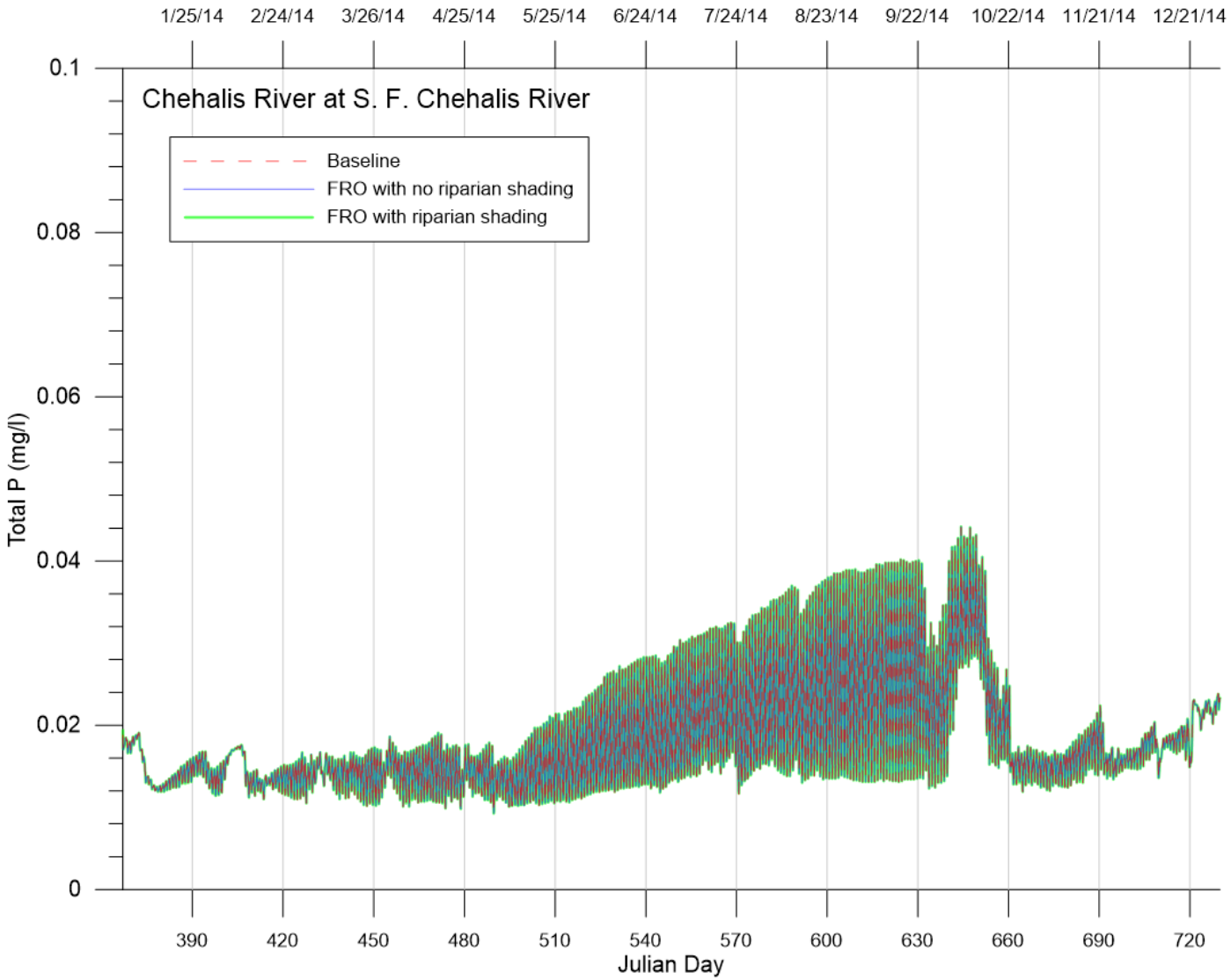

Figure 193. TP predictions at the confluence with South Fork Chehalis River for future conditions baseline, FRO with no vegetative shading, and FRO with riparian shading simulations.

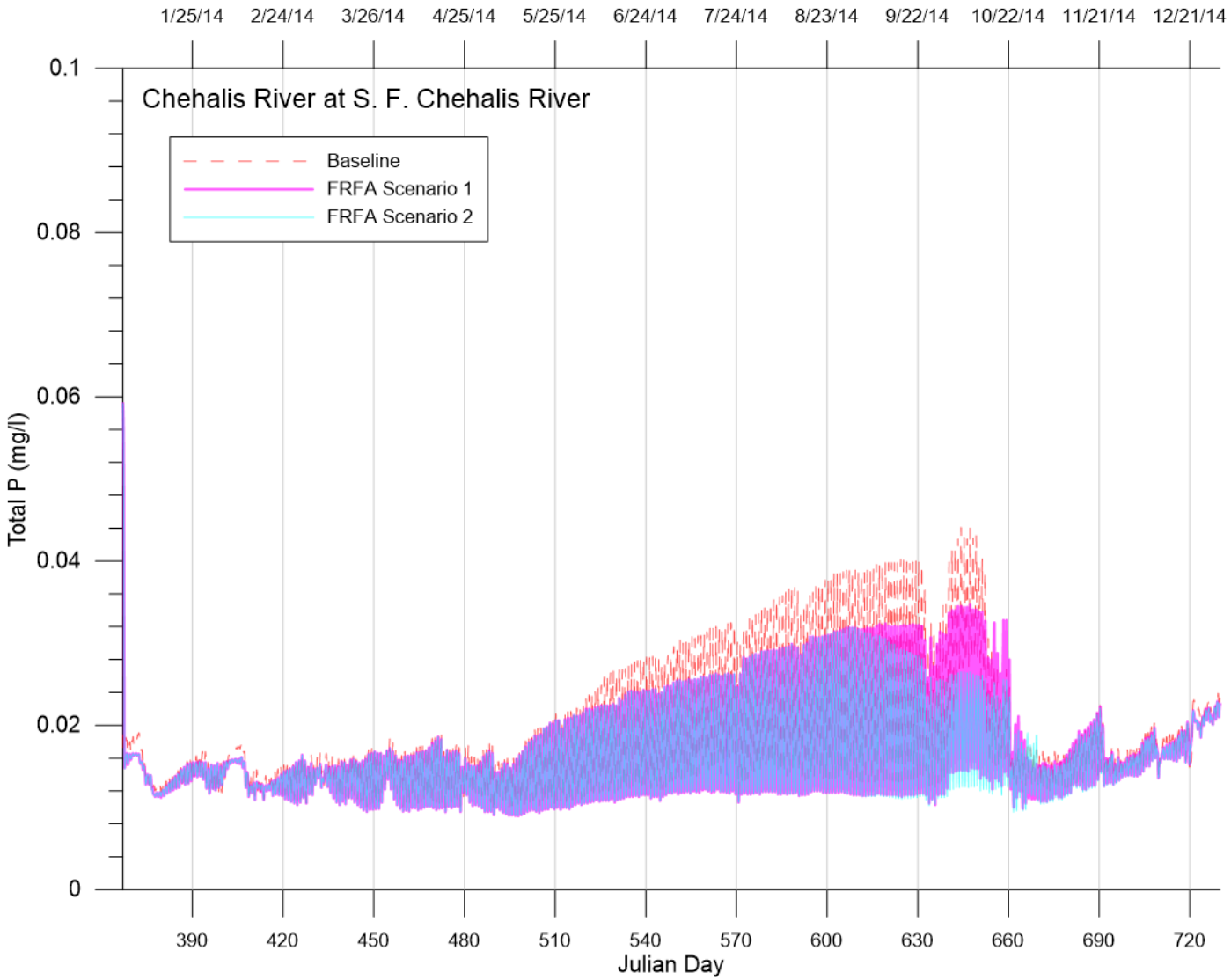

Figure 194. TP predictions at the confluence with South Fork Chehalis River for future conditions baseline, FRFA scenario 1, and FRFA scenario 2 simulations.

Total Nitrogen

TN predictions are shown in Figure 195 through Figure 198. Similarly to TP, baseline TN predictions were greater than the FRFA scenarios during the summer due to decreased loading in dam releases. There was little difference between FRO and baseline predictions.

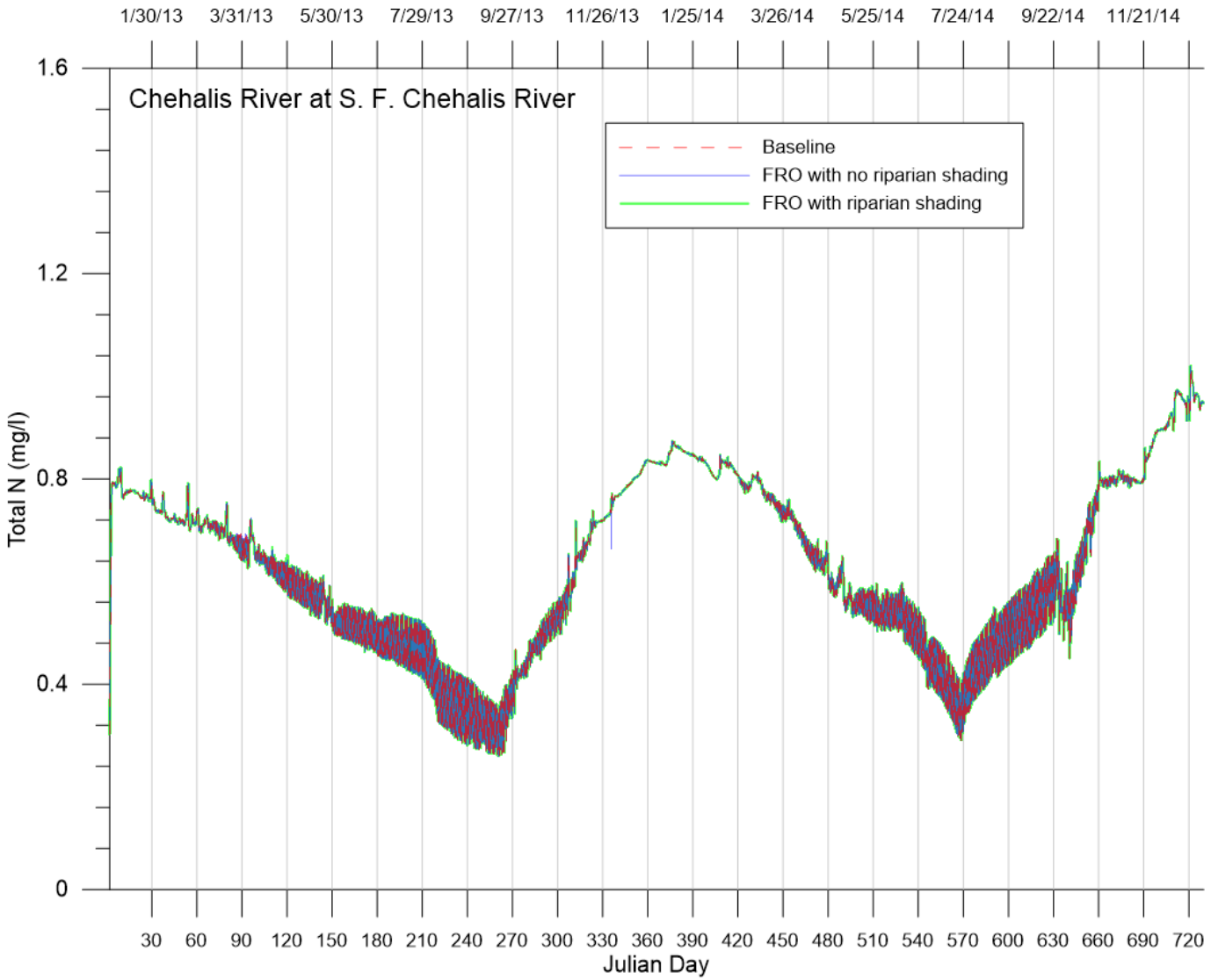

Figure 195. TN predictions at the confluence with South Fork Chehalis River for current conditions baseline, FRO with no vegetative shading, and FRO with riparian shading simulations.

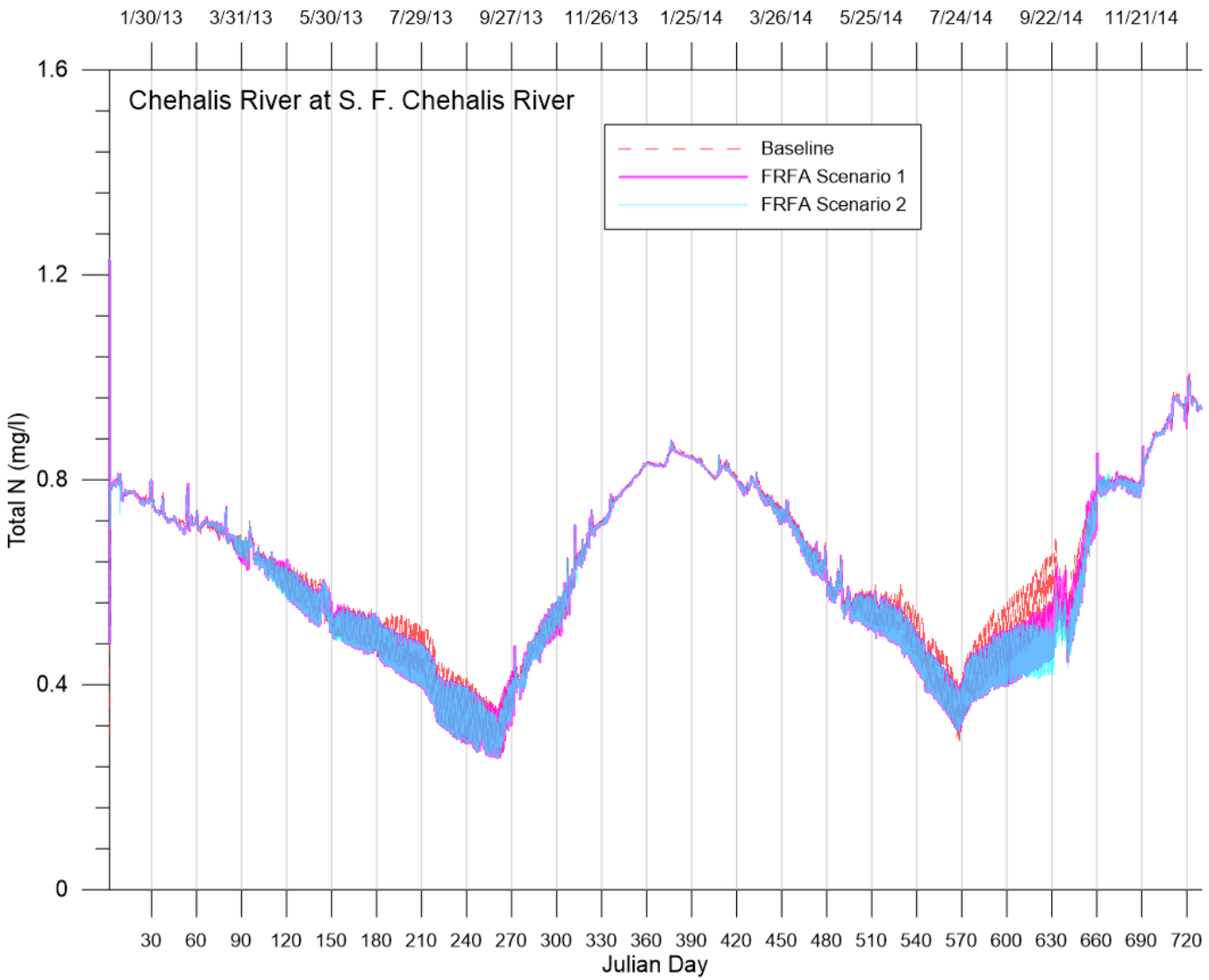

Figure 196. TN predictions at the confluence with South Fork Chehalis River for current conditions baseline, FRFA scenario 1, and FRFA scenario 2 simulations.

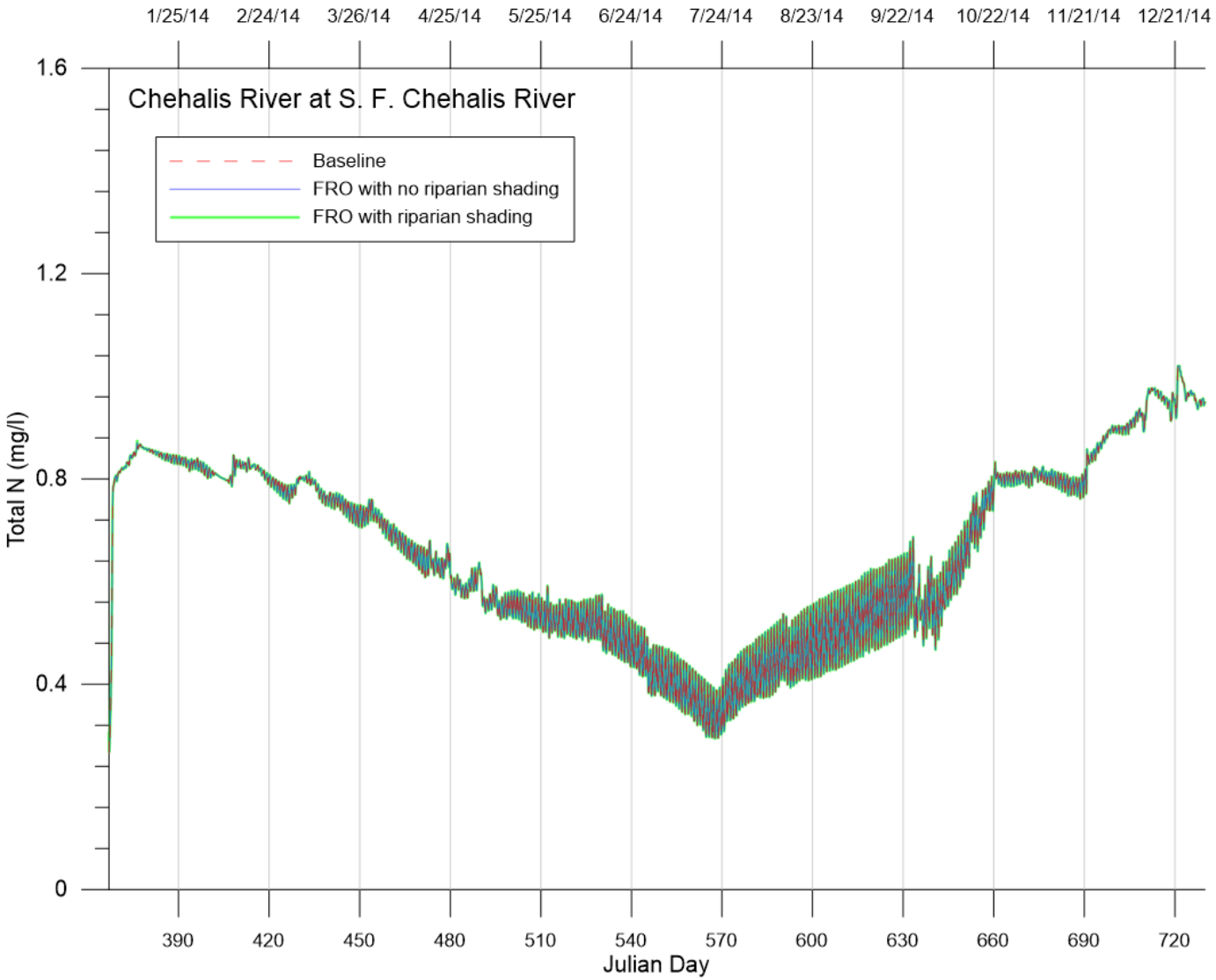

Figure 197. TN predictions at the confluence with South Fork Chehalis River for future conditions baseline, FRO with no vegetative shading, and FRO with riparian shading simulations.

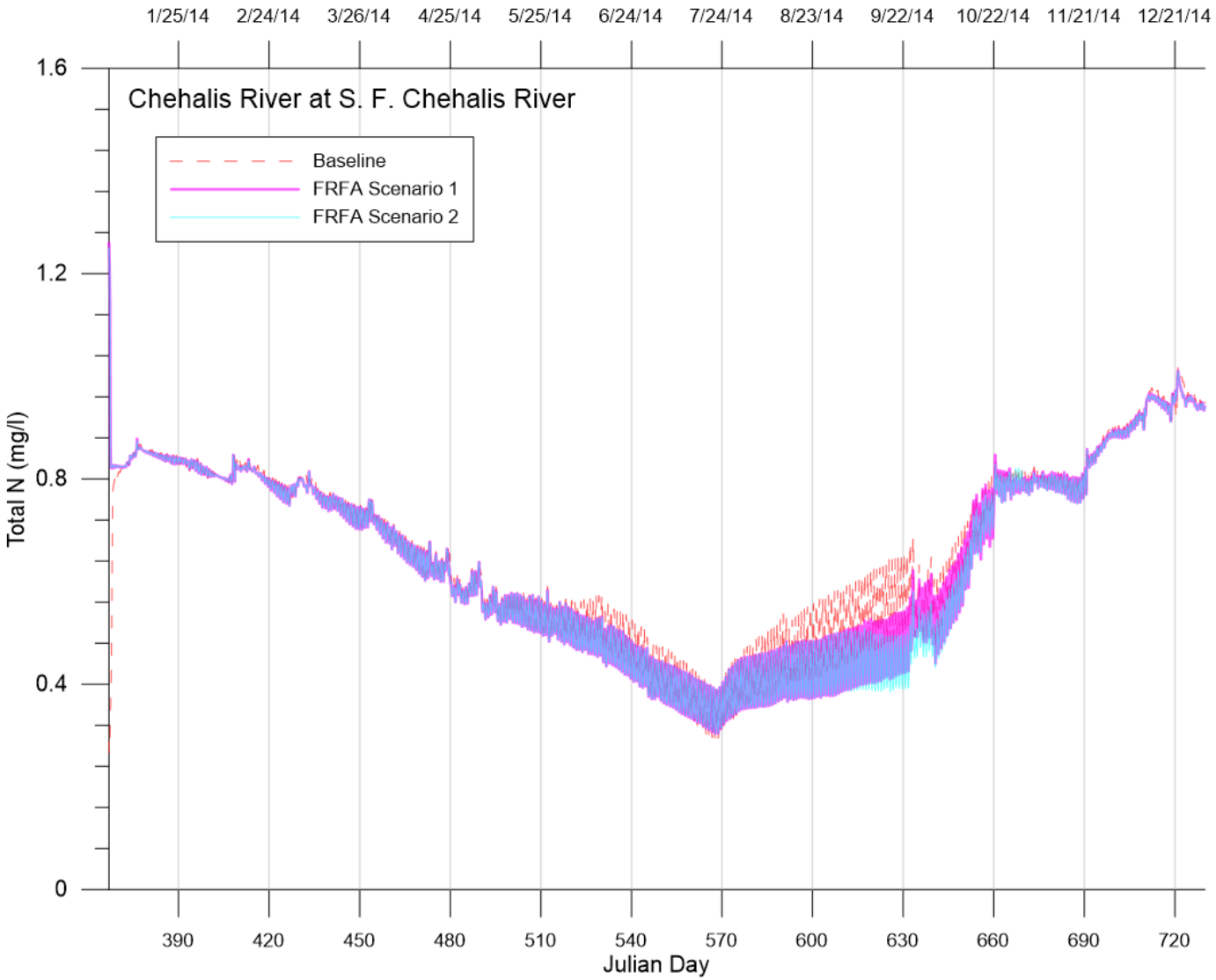

Figure 198. TN predictions at the confluence with South Fork Chehalis River for future conditions baseline, FRFA scenario 1, and FRFA scenario 2 simulations.

Chlorophyll a

Figure 199 through Figure 202 plot chlorophyll a predictions for the scenarios. FRFA chlorophyll a predictions were lower than the baseline due to lower algae concentrations released by the dam. Because there was little difference in nutrient availability, FRO and baseline predictions of chlorophyll a were similar.

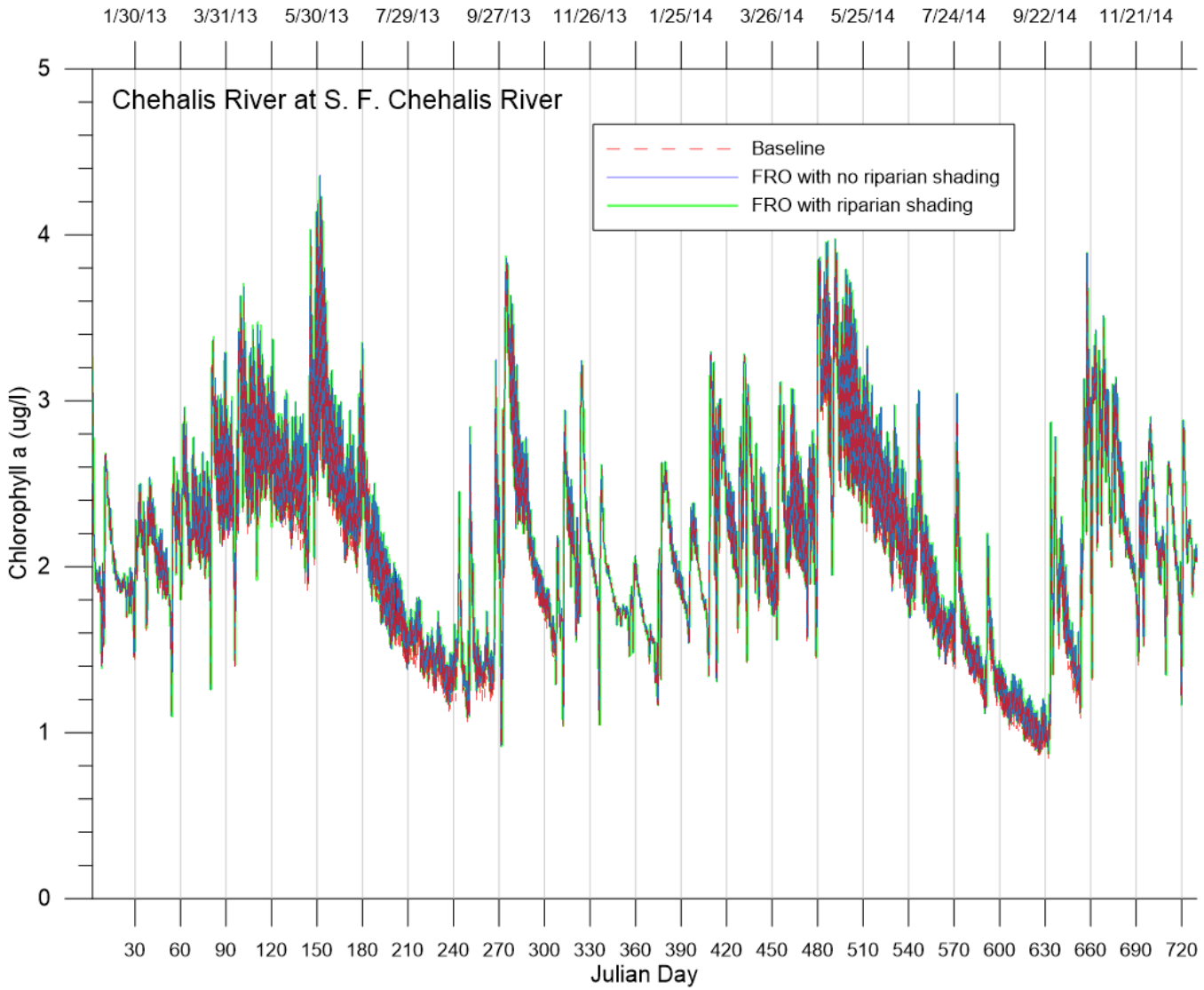

Figure 199. Chlorophyll a predictions at the confluence with South Fork Chehalis River for current conditions baseline, FRO with no vegetative shading, and FRO with riparian shading simulations.

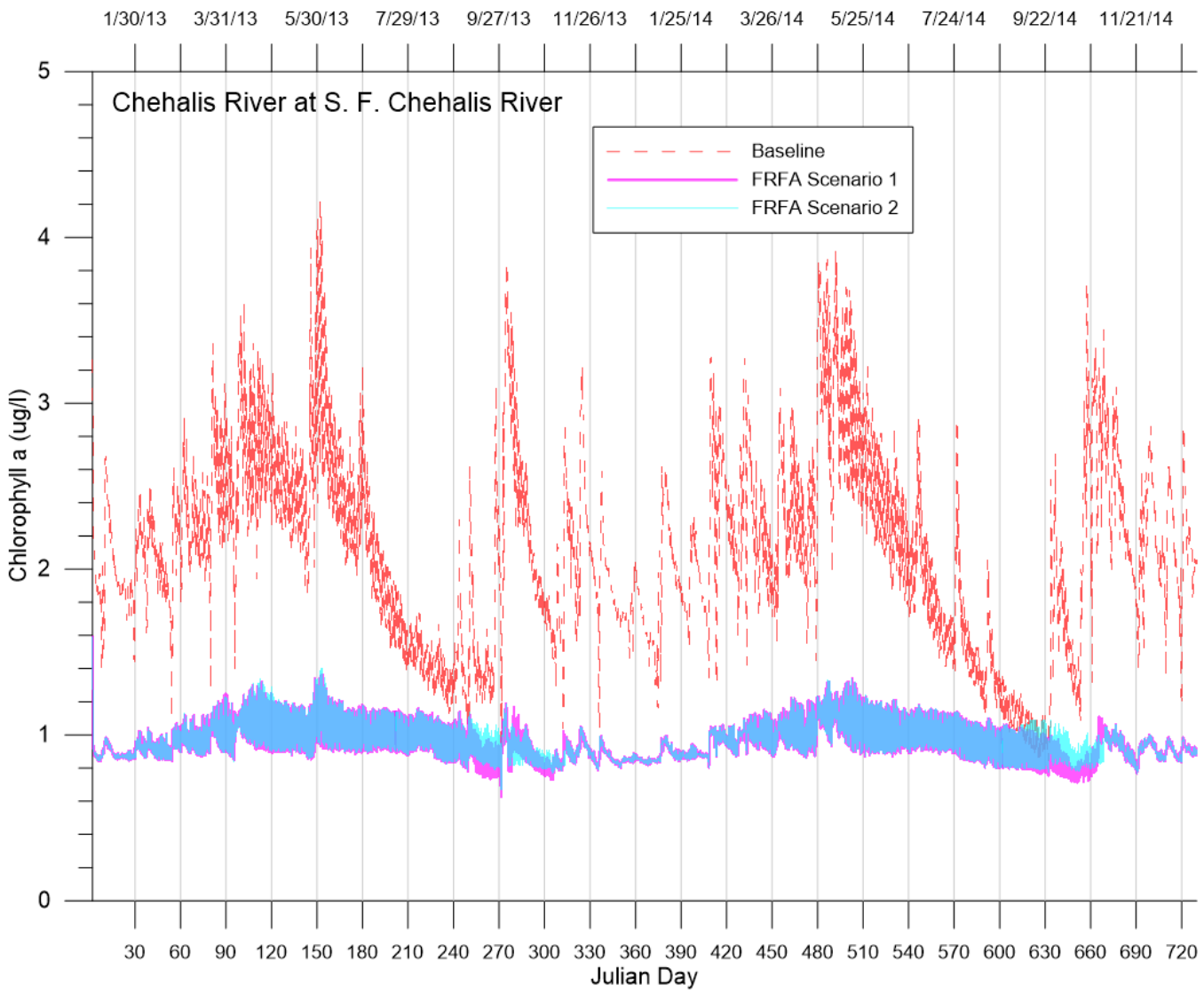

Figure 200. Chlorophyll a predictions at the confluence with South Fork Chehalis River for current conditions baseline, FRFA scenario 1, and FRFA scenario 2 simulations.

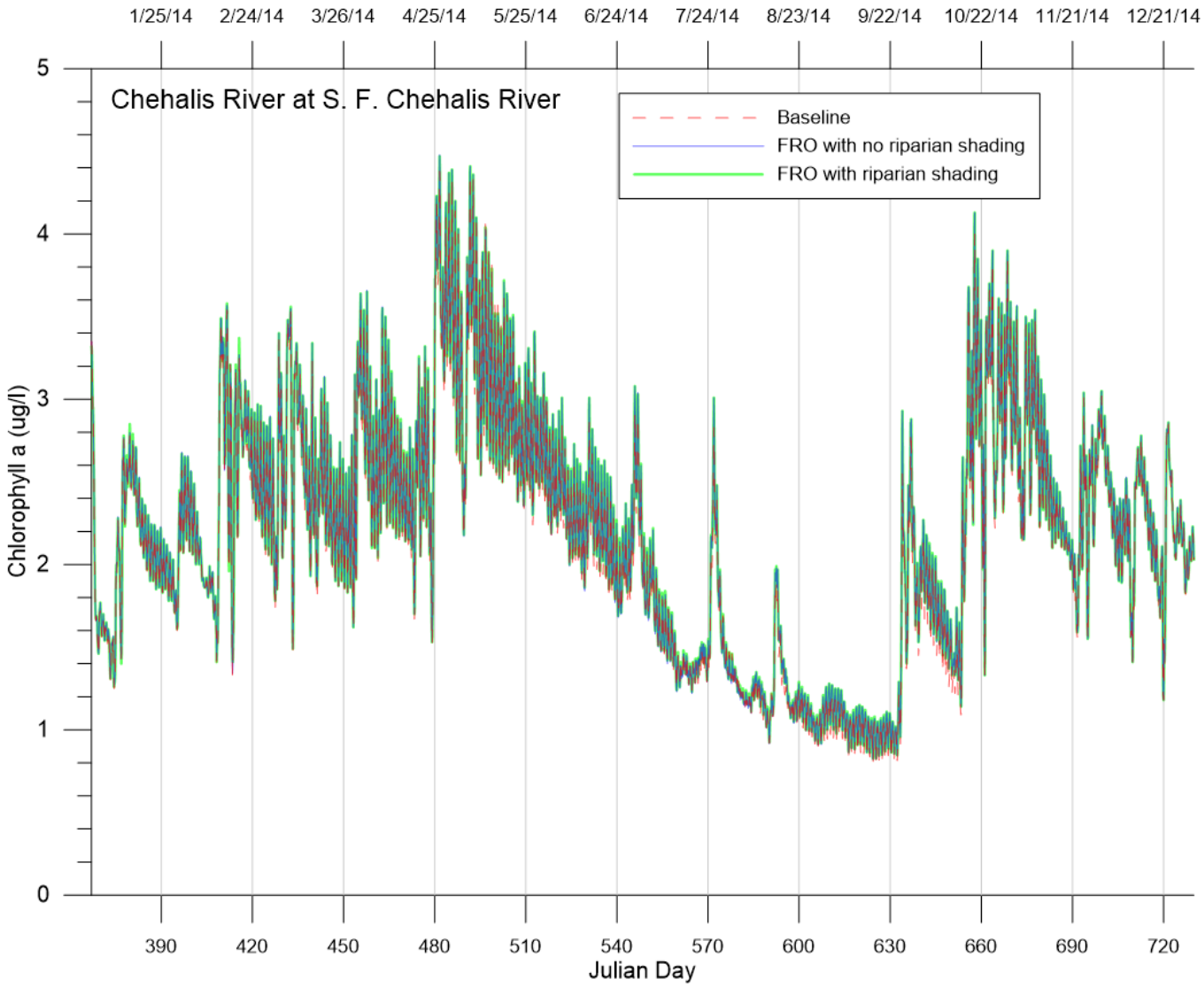

Figure 201. Chlorophyll a predictions at the confluence with South Fork Chehalis River for future conditions baseline, FRO with no vegetative shading, and FRO with riparian shading simulations.

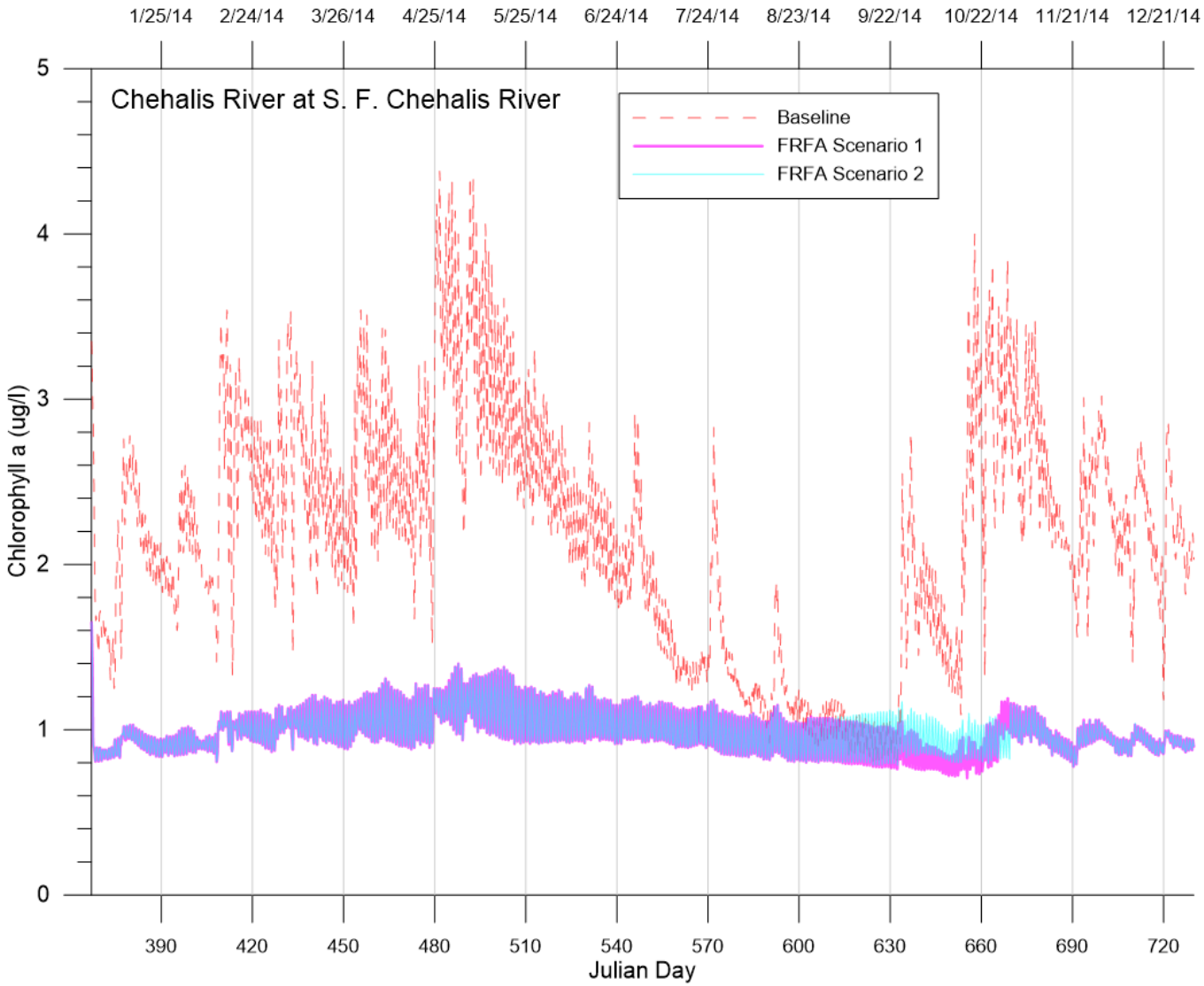

Figure 202. Chlorophyll a predictions at the confluence with South Fork Chehalis River for future conditions baseline, FRFA scenario 1, and FRFA scenario 2 simulations.

Footprint Model

Footprint model dissolved oxygen predictions at the proposed dam site for current and future conditions are plotted in Figure 203 and Figure 204, respectively. Differences in DO concentrations between baseline and the FRO scenarios were small, and mostly caused by lower saturation concentrations due to warmer temperatures. Total nitrogen and total phosphorus concentrations of the FRO scenarios relative to the baseline scenarios were unchanged (Figure 205 through Figure 208). Chlorophyll a predictions of the FRO scenarios were slightly higher because productivity increased due to the warmer water temperatures (Figure 209 and Figure 210).

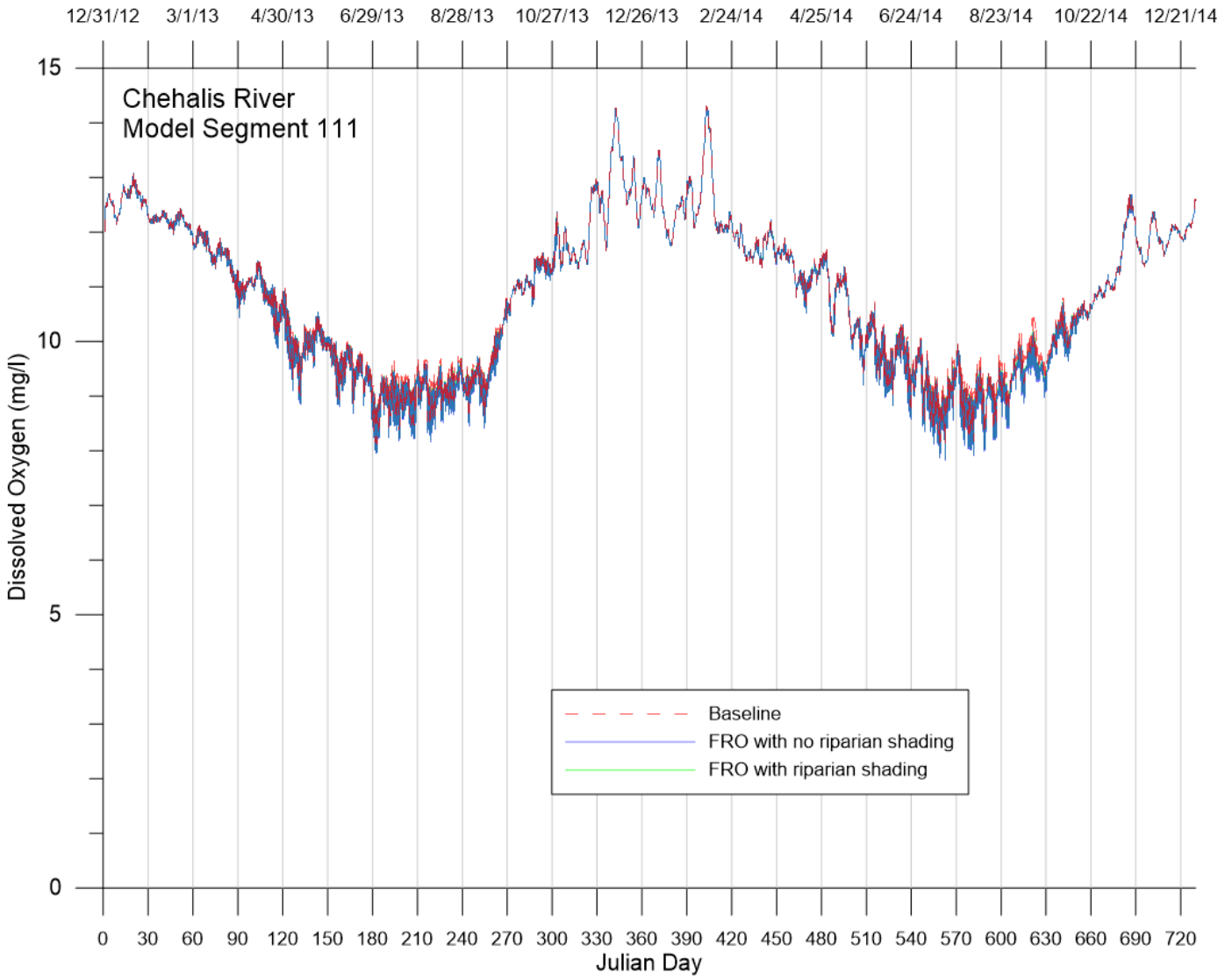

Figure 203. Footprint model dissolved Oxygen predictions for current conditions baseline and FRO scenarios.

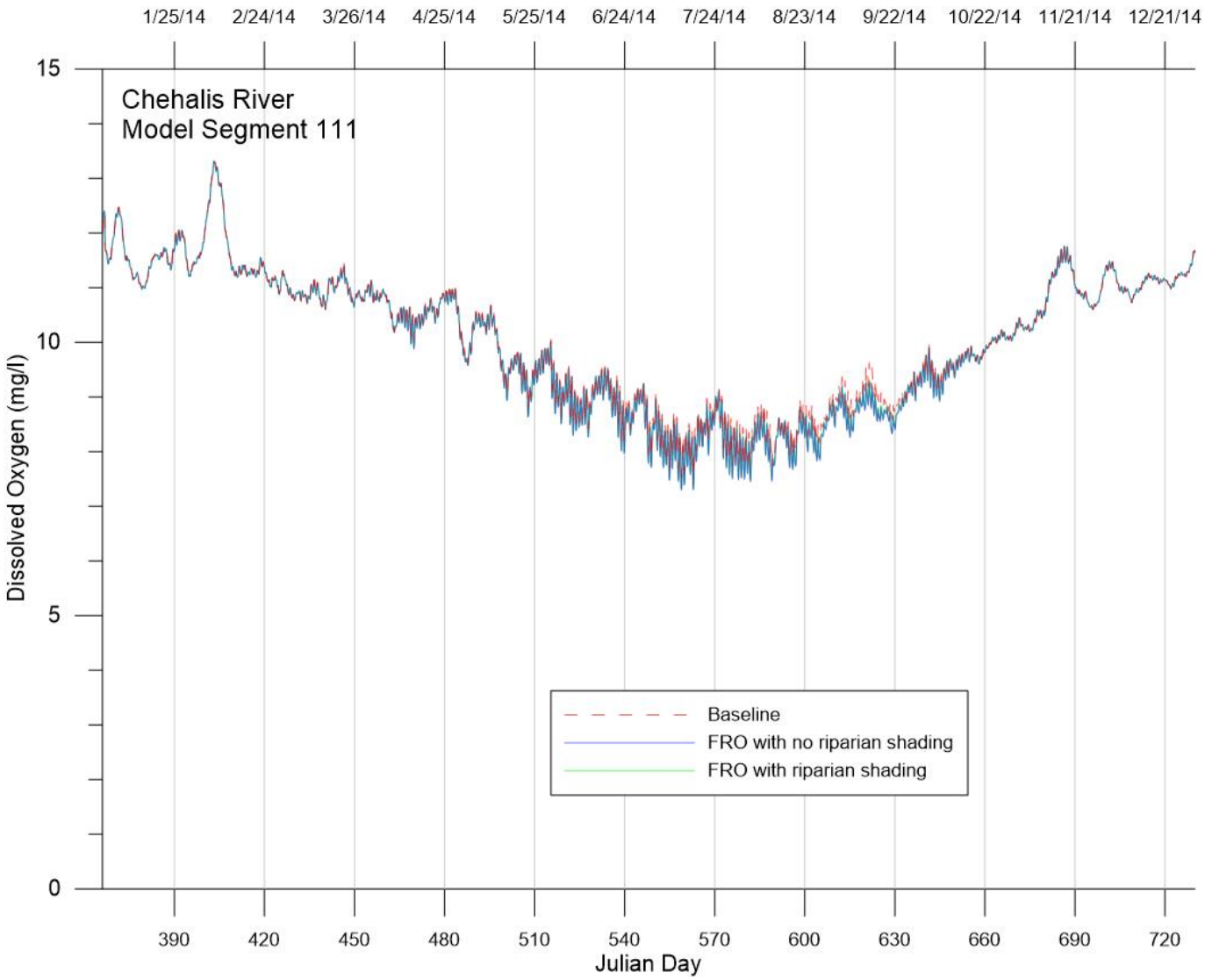

Figure 204. Footprint model dissolved oxygen predictions for future conditions baseline and FRO scenarios.

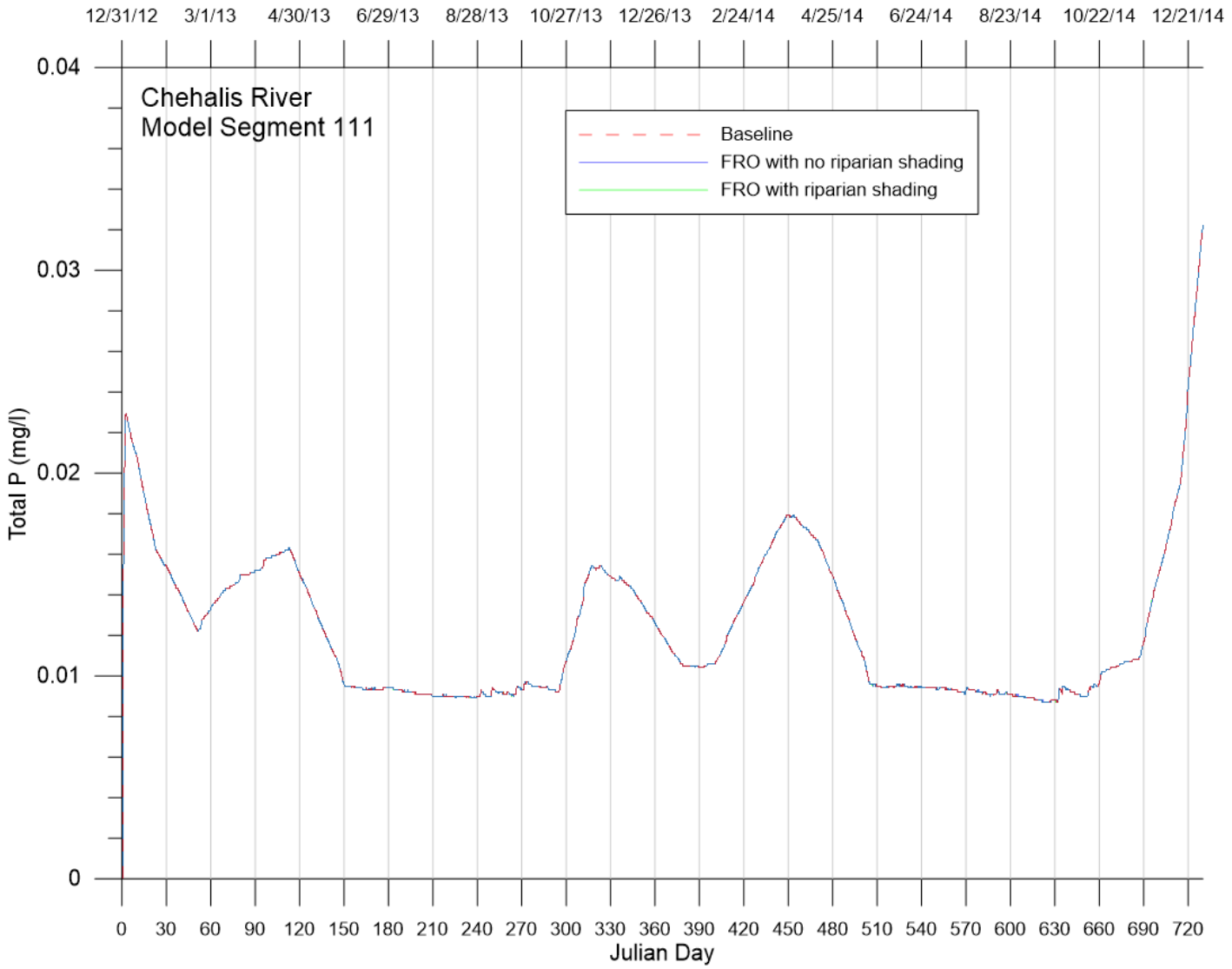

Figure 205. Footprint model TP predictions for current conditions baseline and FRO scenarios.

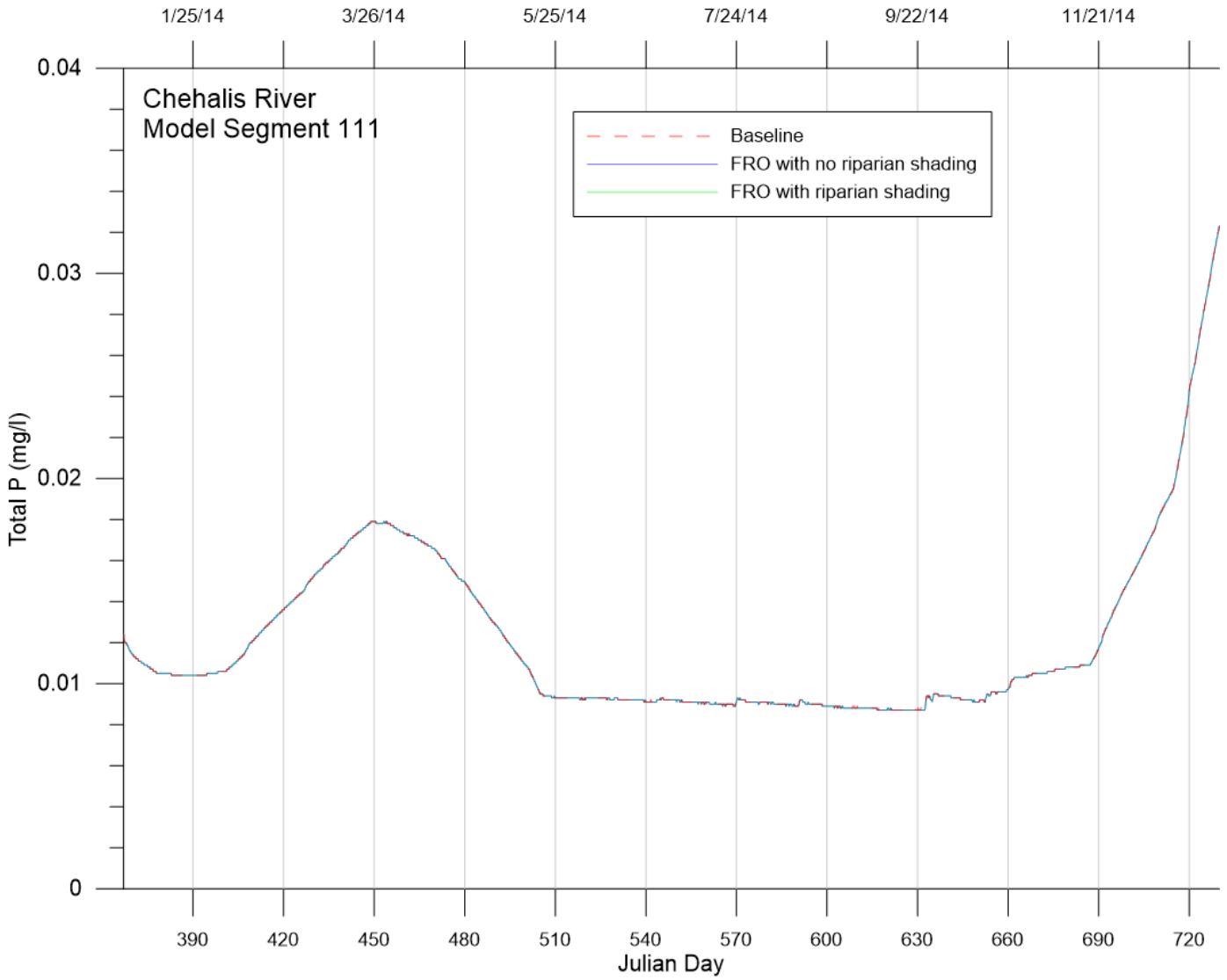

Figure 206. Footprint model TP predictions for future conditions baseline and FRO scenarios.

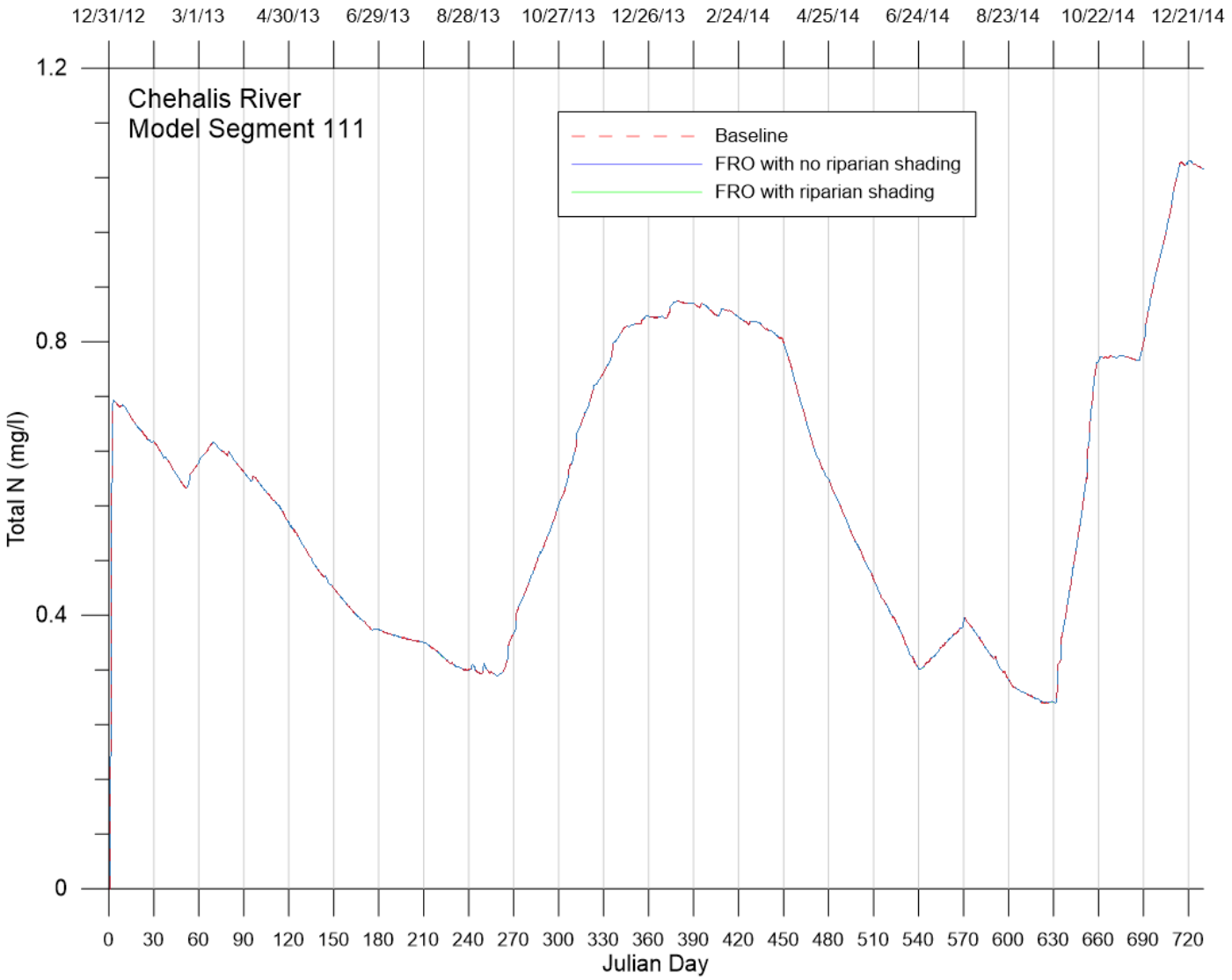

Figure 207. Footprint model TN predictions for current conditions baseline and FRO scenarios.

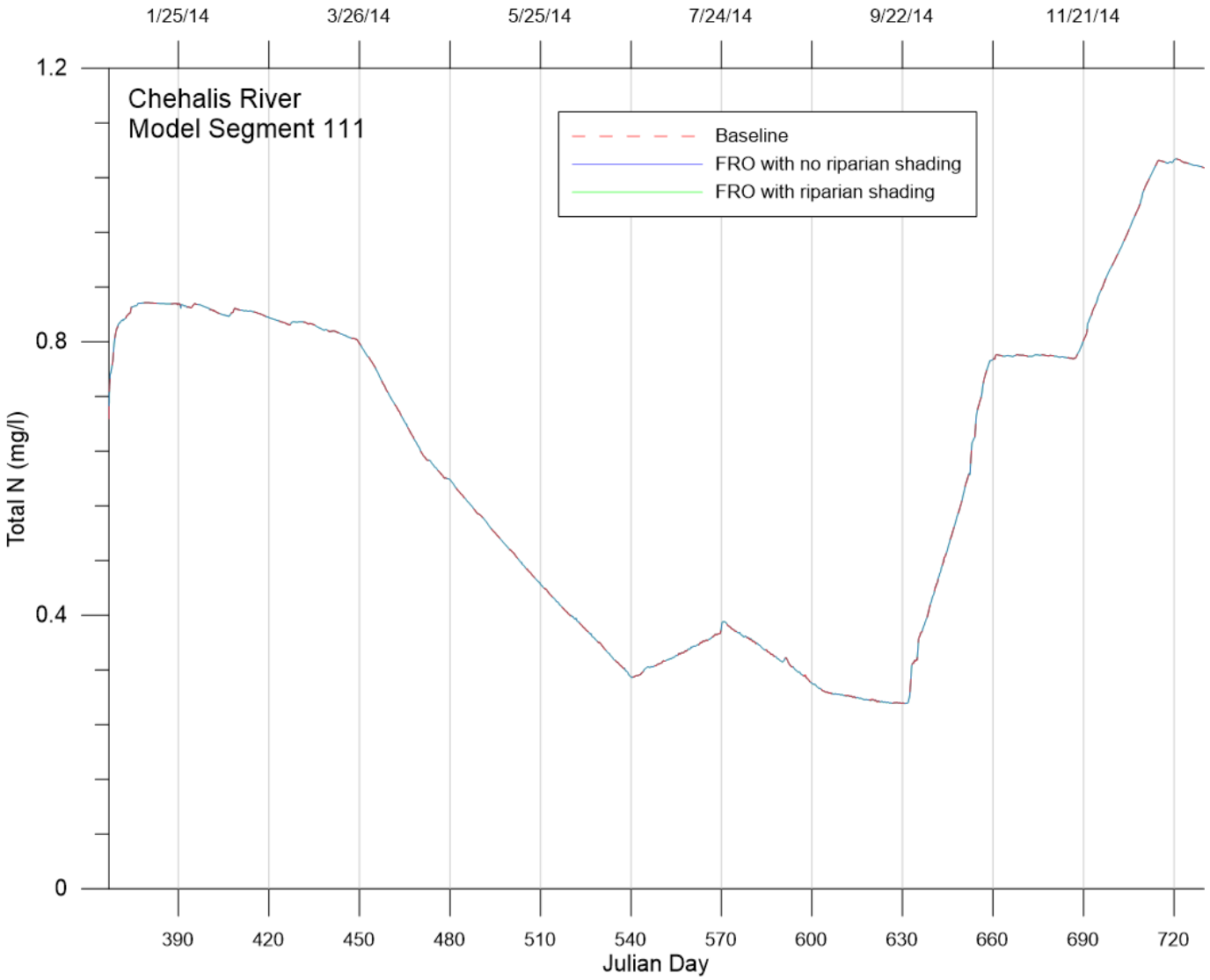

Figure 208. Footprint model TN predictions for future conditions baseline and FRO scenarios.

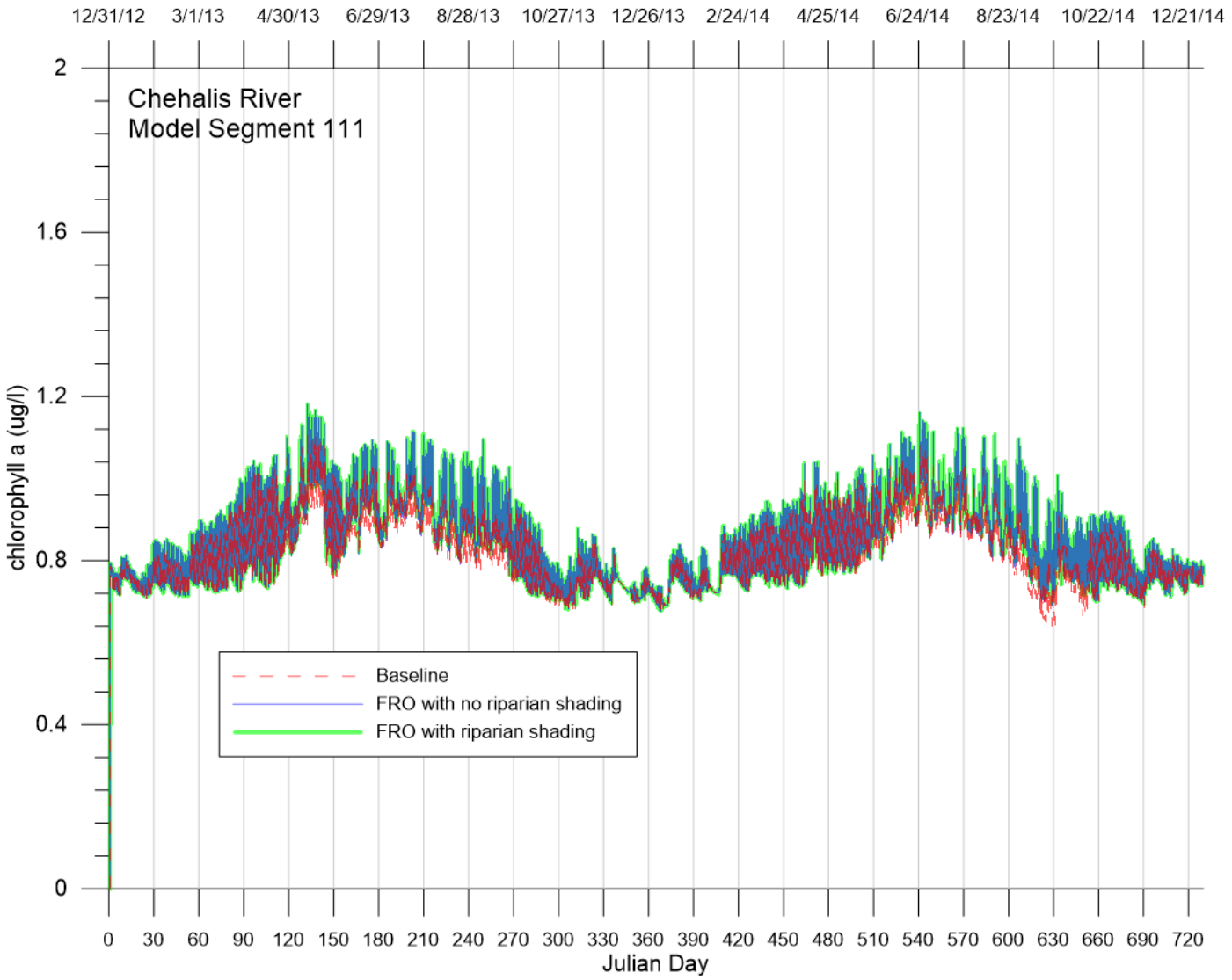

Figure 209. Footprint model chlorophyll a predictions for current conditions baseline and FRO scenarios.

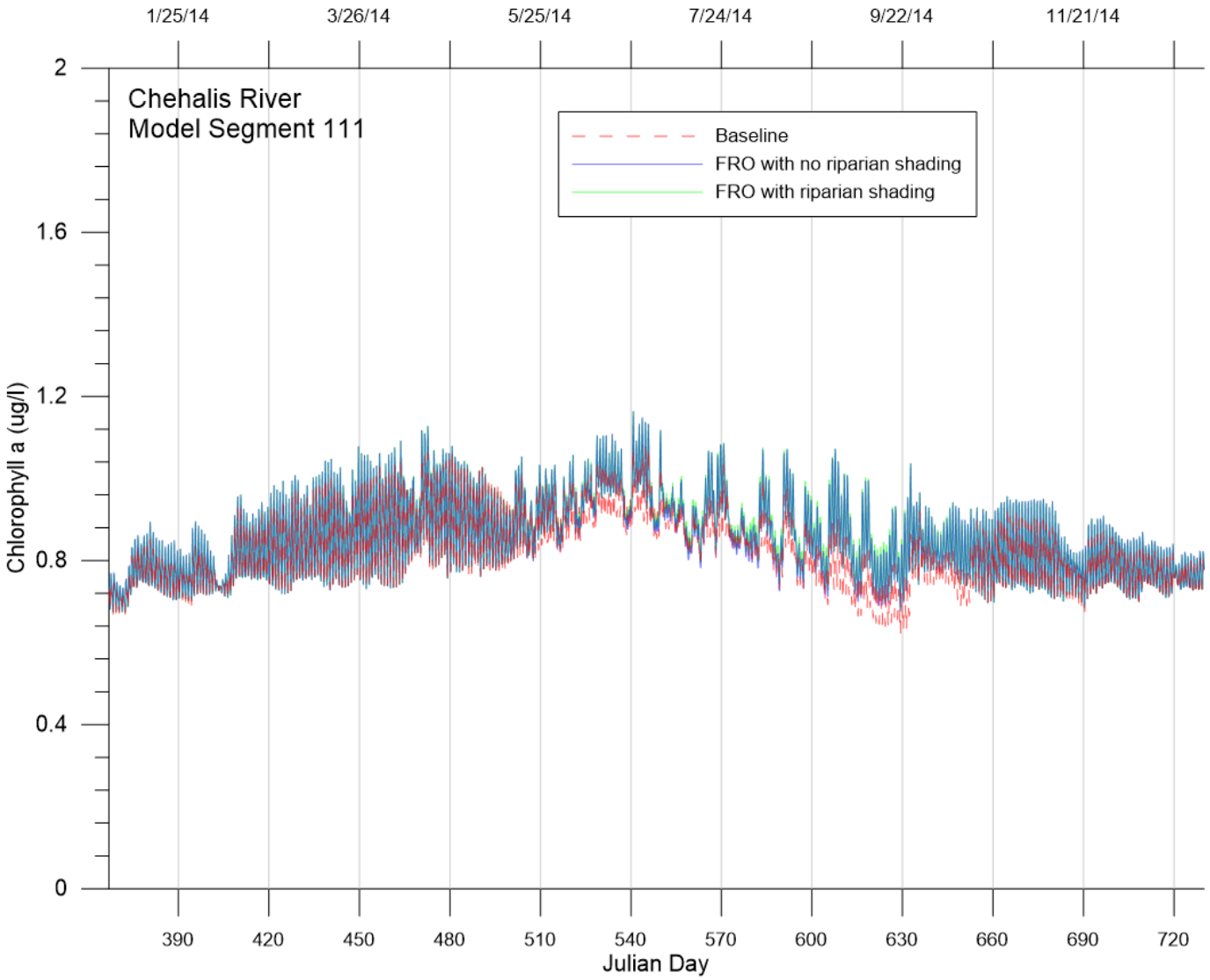

Figure 210. Footprint model chlorophyll a predictions for future conditions baseline and FRO scenarios.

Model Improvements

This section outlines methods in which the existing model could be improved.

Flow Data

More flow data are needed to reduce model uncertainty. Improved data regarding unmonitored withdrawals, rainfall overland flow, and groundwater interactions would increase understanding of how water is entering and leaving the system. Additional mainstem monitoring locations would allow for additional comparisons between model flow predictions and field data, allowing more certainty in model results. Additional mainstem monitoring would allow for more precise allocation of distributed flows throughout the model system. Many of the tributaries were completely unmonitored for flow. Monitoring these tributaries rather than estimating flows would be helpful for flow calibration.

Water Surface Elevation Datums

Datum verification for water surface elevations are necessary to improve model versus field data water level comparisons. Some of the locations with water surface elevation data had local datums that were not referenced to national standard datums, making it difficult to be sure the elevation data were referenced to the same datum as the model.

Temperature Data

Even though there were an abundance of temperature data in the Chehalis mainstem for 2013-2014, additional temperature monitoring would also be beneficial. Most of the temperature data sets did not span the entire model time period for the years 2013-2014. Many of the sites only had data for certain times in the year, for example only during the summer seasons. It would give a better understanding of the temperature dynamics if the data sets were more complete. Monitoring tributaries that had no temperature data, rather than estimating these values from another tributary, would also help improve temperature calibration.

Water Quality Data

More continuous water quality data for constituents such a dissolved oxygen, nutrients, algae, zooplankton, organic matter, etc. would be very beneficial. Much of the available water quality data for the mainstem Chehalis River and tributaries were data collected only at a couple times during the 2013-2014 calibration period. This made it difficult to distinguish specific seasonal and diurnal trends. Without additional data it is impossible to verify that some of these single point values were or weren't outliers. Some useful data were missing entirely. For example, periphyton/epiphyton behavior were shown to have important impacts on dissolved oxygen and nutrient results, but no data for periphyton/epiphyton was available.

The WWTPs had important impacts on many water quality constituents in the river. Many estimations and assumptions were required to fill data gaps for the WWTPs. Sometimes only monthly averages were available for certain constituents. Increased frequency of data collection would be useful for improving model predictions since these discharges have an important impact on the river.

PH is a function of algae and epiphyton characteristics, temperature, total inorganic carbon, and alkalinity. Properly calibrated values of pH were impossible to achieve because of the lack of alkalinity data. The few mainstem river values available were not sufficient to approximate for all the tributaries entering the system.

A confirmation of quality of data for some constituents would be useful in determining how well the model was calibrated. For example, confirming the abrupt increase and fall of ammonia between the monitoring stations upstream of the Skookumchuck River and upstream of the Newaukum River would be useful.

A description of the wastewater involved in land application as an alternative to river discharges during low flow summer months would be useful for characterizing the distributed flows. Currently, the distributed flows use constituent data from a nearby tributary, though the distributed flows may have distinct water quality characteristics.

Model Grid Confirmation

Confirmation of the model grid location, including segments, locations of tributaries and monitoring stations' locations would be useful to model calibration. River mile values and coordinates associated with various tributaries and monitoring stations came from multiple sources. Some monitoring stations did not have any river mile value attached to them and were estimated based on maps. A cohesive set of river mile values and coordinates for the various inputs and monitoring stations would allow for more precise calibration, especially for water surface elevation and vertical temperature and DO profile comparisons. These are very sensitive to segment location and sometimes gave very different results even when off by only a segment or two.

Meteorological Data

Improved meteorological data would be very useful for temperature and water quality calibration. Large meteorological data gaps often existed, as well as some data values outside a typical range for a given constituent. For example, while it is expected that specific days will have varied solar radiation values, the overall shape and magnitude of solar radiation over an entire year should be nearly the same from year to year. This was not true for any of the meteorological data sets in comparing solar radiation data sets for 2013 and 2014. Additionally, cloud cover data were only available from the Thrash Creek site near the upstream boundary, which is located at a higher elevation than the rest of the modeled system. Since cloud cover was seen to have a large impact on temperature calibration, a more complete view of the cloud cover throughout the basin would be useful. This would improve model vertical profile temperature results, and thus DO vertical profile predictions.

Bathymetry

In some cases, temperature was seen to be very sensitive to the bathymetry of the system, including segment widths and water depths. A more detailed look at specific segments, including comparing the model geometry to field data could improve model predictions. Having as accurate a grid as possible that most represents the real river system would allow for more accurate calibration of flow and depths, temperature, and water quality constituents. This is especially true in the pool areas where the model grid needs to reflect the pool volume accurately in order to reproduce travel times through the reaches. As a result, the model dye study travel times need to be verified by a field day study test to verify the model bathymetry.

Sediment Diagenesis Model

The current model uses both a zero order and first order sediment model. Even though the first order model is linked to sedimentation of organic matter, the zero order model is not. Hence, we recommend exploring the impact of the sediment diagenesis model on model predictions in the pool area.

Calibration to a Critical Low Flow Year

Calibration of the model to a critical low-flow year, such as 2015, would test the model during an extreme meteorological and hydrological year.

Summary

This report summarized the development of the Chehalis River mainstem model between the proposed dam site (river mile 108) and Porter (river mile 33.3) and the footprint stream model of the proposed unimpounded retention structure (river mile 108). The model was set-up from January 1, 2013 through December 31, 2014 and used as state variables velocities, water level, temperature, dissolved oxygen, algae, zooplankton, pH, organic matter and nutrients.

The mainstem model was composed of 10 branches of varying channel slope, 9 waterbodies, and 322 model segments of length approximately 400 m and vertical layer heights of 1 m. The footprint model included 13 branches, 13 waterbodies, model segments with lengths of 150 m, and layer heights of 0.5 m. Much of these data were available from river cross-sections used for a Chehalis HEC-RAS model.

Data collected for meteorological conditions, bathymetry, shading, flow, water level, groundwater characteristics, temperature, and many water quality constituents were used for input data to the model as well as for calibration by comparing model predictions versus field data. Many agencies provided these data, including Washington State Department of Ecology, Anchor QEA, USGS, Washington Department of Fish and Wildlife, Thurston County, wastewater treatment plant operators, RAWS, CRBFA, and NOAA.

The mainstem model was compared to field data at 3 locations: Doty, Grand Mound, and Porter gages. Distributed flows made it possible to take ungaged inflows and withdrawals into account. The model reproduced the hydrographs at these gage locations with typical absolute mean errors in flow from 0.57 to 7.5 m^3/s. The footprint model was compared to field data at Pe Ell gage and had a mean error of 1 m^3/s and an absolute mean flow error of 1.5 m^3/s.

Water surface elevations from model predictions and field data were compared at Doty, Adna, at Chehalis WWTP, Centralia, Grand Mound, Rochester, and Porter, with absolute mean errors from 0.29 to 0.93 m. Resolving uncertainty with the datums of some of the field gages could improve these values.

The reservoir footprint stream model did not have calibration data except at the end of the reservoir reach for comparison. For this approximate comparison, the footprint model temperature errors were below 1^oC. The mainstem model had temperature comparisons at 27 locations. For most of these locations the temperature errors (absolute mean errors) were well below 1^oC and the mean errors were close to 0 ^oC.

Temperature results were compared to field data on the river at many locations ranging from near the upstream boundary to the downstream boundary. Absolute mean error values ranged between 0.26 and 1.2 ^oC. These could be improved as further improvements to boundary conditions and grid setup are explored. Vertical profiles of temperatures predicted by the model compared to field data could also improve as cloud cover and bathymetry adjustments are investigated.

Multiple water quality constituents were calibrated through comparisons of model predictions and field data. This process was made more difficult due to a lack of water quality constituent field data for the mainstem Chehalis River, as well as the many tributaries. Hence, many estimations and approximations were made for model inputs. Due to lack of alkalinity data, pH could not be fully calibrated in the model. However, many constituents had good agreement between model predictions and field data, such as dissolved oxygen, nitrates, total phosphorus, and total suspended solids. Additional water quality data would allow for better model results. Improved temperature predictions would also improve water quality predictions, for example DO vertical profiles would be improved as vertical temperature profiles improve.

Scenarios were developed for these models evaluating the impact of the new reservoir on water quality downstream. In addition, the impacts of climate change were assessed. Temperature impacts of the scenarios were run with the full mainstem Chehalis model.

Multiple scenarios were applied to simulate potential dam implementation and operation strategies in order to assess their effects on water quality on the Chehalis River. Future climate conditions were also applied to the baseline model and dam scenarios.

Footprint model daily maximum temperatures were at least several degrees warmer under future conditions. The temperature differences between the FRO scenario with no riparian shading and the FRO with riparian shading were small. The daily maximum temperatures of the FRO scenarios could be up to 2-3° C warmer than the baseline scenarios during the summer.

The downstream model predicted future climate conditions would increase water temperature for all scenarios. Temperature predictions were cooler for the FRFA scenarios than the baseline and FRO scenarios. However, differences in temperature predictions between the scenarios decreased moving downstream. Just upstream of Elk Creek, temperatures differences between the baseline and FRO scenarios were small, whereas the FRFA scenarios could be more than 5° C cooler than the baseline in the summer. Differences between the baseline and FRFA scenarios upstream of the S. F. Chehalis River were approximately up to 3° C under current conditions and up to 5° C under future conditions. Upstream of the confluence with the Skookumchuck River, during the summer the FRFA scenario could be 1° C cooler than the baseline under current conditions and 2-3° C cooler under future conditions.

At the dam site differences in DO concentrations between baseline and the FRO scenarios were small, and mostly caused by lower saturation concentrations resulting from warmer temperatures. Total nitrogen and total phosphorus concentrations of the FRO scenarios relative to the baseline scenarios were unchanged. Chlorophyll a predictions of the FRO scenarios were slightly higher because increased productivity due to the warmer water temperatures.

Downstream of the dam site DO concentrations were generally higher for the FRFA dam scenarios than the baseline and FRO scenarios due to colder water temperatures. Chlorophyll a predictions of the FRFA scenarios were significantly lower the baseline due to lower algae concentrations in dam releases. TP and TN concentrations were also slightly lower for the FRFA scenarios relative to the baseline scenario due to decreased concentrations in dam releases. Predictions of DO, chlorophyll a, TP and TN for the FRO scenarios differed little from baseline concentrations.

These results have important implications for fish health and habitat, especially during critical warm summer months when the river is prone to violating water quality standards.

References

Anchor QEA, LLC. 2011. “Appendix A Draft Hydrologic and Hydraulic Modeling Report Chehalis River Fish Study”. Prepared for Chehalis River Basin Flood Authority, Chehalis, WA. November, 2011.

Anchor QEA. 2014. “Water Quality Studies – Chehalis Basin Strategy: Reducing Flood Damage and Enhancing Aquatic Species”. Prepared for Washington State Office of Financial Management. September, 2014.

Anchor QEA. 2016. “Draft Chehalis River Basin Strategy Technical Memorandum: Proposed Flood Retention Facility Pre-construction Vegetation Management Plan”. May 13, 2016.

Bilhimer, Dustin. 2015. “Chehalis Basin Strategy WQ Technical Tasks”. Water Quality Program, Washington Department of Ecology, Olympia, WA. September 22, 2015.

Bilhimer, Dustin. 2016. Personal communication, Washington Department of Ecology, Olympia, WA.

Bowman, Clint. 2016. Personal communication, Washington Department of Ecology, Olympia, WA.

Breckner, Michelle. 2016. Personal communication, Desert Research Institude Western Regional Climate Center, Reno, NV.

Brown and Caldwell. 2016. “Engineering Report”. Prepared for National Frozed Foods Corp. January 29, 2016.

Chehalis River Basin Flood Authority. 2016. Thrash Creek Station Data 2013-214.

Cole, T. and Wells, S. 2016. “CE-QUAL-W2: A Two-Dimensional, Laterally Averaged, Hydrodynamic and Water Quality Model, Version 4.0 User Manual”, Department of Civil and Environmental Engineering, Portland State University, Portland, OR.

Darigold Wastewater Treatment Plant. 2016a. Chehalis River Upstream Darigold WWTP Station Data 2013-2014, Site ID 41. Chehalis, WA.

Darigold Wastewater Treatment Plant. 2016b. Chehalis River Downstream Darigold WWTP Station Data 2013-2014, Site ID 40. Chehalis, WA.

Ely, D.M., Frasl, K.E., Marshall, C.A., and Reed, F. 2008. “Seepage Investigation for Selected River Reaches in the Chehalis River Basin, Washington”. U.S. Geological Survey Scientific Investigation Report 2008-5180, 12 p.

Epp, V. 2016. Personal communication, Washington Department of Ecology, Olympia Wa.

Erickson, Denis. 1993. “Chehalis River TMDL, Ground Water Reconnaissance and Estimated Inflows”. Washington Department of Ecology, Olympia, WA. Interdepartmental Correspondence. June 29, 1993.

Garrigues, R. S., Sinclair, K., and Tooley, J. 1998. “Chehalis River Watershed Surficial Aquifer Characterization”. Environmental Assessment Program, Watershed Ecology Section, Washington Department of Ecology, Olympia, WA. December, 1998.

Gendaszek, A.S. 2011. “Hydrogeologic Framework and Groundwater/Surface-Water Interactions of the Chehalis River Basin, Southwestern Washington”. U.S. Geological Survey Scientific Investigations Report 2011-5160, 42 p.

Hillock, J. 2016. Personal communication, Pe Ell, WA.

Merrill, A., Stillwater Sciences. 2014. “Riparian Shade along Lower Chehalis River”, prepared for Anchor QEA.

National Oceanic and Atmospheric Administration (NOAA). 2015. Chehalis-Centralia Airport Station, Site ID KCLS. Website: https://www.ncdc.noaa.gov/data-access/quick-links#dsi-3505

National Pollutant Discharge Elimination System (NPDES). 2011. “Fact Sheet for NPDES Permit WA0020982 City of Centralia”. Environmental Protection Agency.

National Pollutant Discharge Elimination System (NPDES). 2012. “Fact Sheet for NPDES Permit WA0021105 City of Chehalis Water Reclamation Facility”. Environmental Protection Agency.

National Pollutant Discharge Elimination System (NPDES). 2010. “Fact Sheet for NPDES Permit WA0037478 Facility Name Darigold, Inc. Chehalis Plant”. Environmental Protection Agency.

National Pollutant Discharge Elimination System (NPDES). 2003a. “Fact Sheet for NPDES Permit WA0042099 Grand Mound Wastewater Treatment Plant ”. Environmental Protection Agency.

National Pollutant Discharge Elimination System (NPDES). 2003b. “Fact Sheet for NPDES Permit WA0020192 Town of Pe Ell”. Environmental Protection Agency.

Patching, K. 2016. Personal communication, Thurston County Public Works, Olympia, WA.

Phelps, J. 2016. Personal communication, Pe Ell, WA.

Pickett, Paul. 2016. Personal communication, Olympia, WA.

Pitz, C.F., Sinclair, K.A., and Oestreich, A.J. 2005. “Hydrology and Quality of Groundwater in the Centralia-Chehalis Area Surficial Aquifer”. Groundwater Assessment Program, Washington Department of Ecology, Olympia, WA. December, 2005.

Remote Automated Weather Station (RAWS). 2014. Chehalis Washington Station Data 2013-2014, Site ID CLSW1; Huckleberry Ridge Station Data 2013-2014, Site ID HKFW1; and Minot Peak Station Data 2013-2014, Site ID MIPW1.

Stumm, W. and Morgan, J. 1981. Aquatic Chemistry, Wiley-Interscience, New York.

Thurston County, Streamflow Monitoring Data. 2014. Scatter Creek Station Data 2013-2014, Site ID 55a. Website: http://www.co.thurston.wa.us/monitoring/flow/flow-scatter.html

U.S. Geological Survey. 2016a. Chehalis River near Adna, WA Station Data 2013-2014, Site ID 12021800. Website: http://waterdata.usgs.gov/wa/nwis/uv?site_no=12021800

U.S. Geological Survey. 2016b. Chehalis River near Doty, WA Station Data 2013-2014, Site ID 12020000. Website: http://waterdata.usgs.gov/nwis/uv?12020000

U.S. Geological Survey. 2016c. Chehalis River at Chehalis WWTP, WA Station Data 2013-2014, Site ID 12025100. Website: http://waterdata.usgs.gov/wa/nwis/uv?site_no=12025100

U.S. Geological Survey. 2016d. Chehalis River at Centralia, WA Station Data 2013-2014, Site ID 12025500. Website: http://waterdata.usgs.gov/wa/nwis/uv?site_no=12025500

U.S. Geological Survey. 2016e. Chehalis River near Grand Mound, WA Station Data 2013-2014, Site ID 12027500. Website: http://waterdata.usgs.gov/nwis/uv?site_no=12027500

U.S. Geological Survey. 2016f. Chehalis River above Mahaffey Creek Station Data 2013-2014, Site ID 12019310. Website: http://waterdata.usgs.gov/nwis/uv?site_no=12019310

U.S. Geological Survey. 2016g. Chehalis River at Porter, WA Station Data 2013-2014, Site ID 12031000. Website: http://waterdata.usgs.gov/nwis/uv?site_no=12031000

U.S. Geological Survey. 2016h. Chehalis River at Porter, WA Station Data 2013-2014, Site ID 12031000. Website: http://waterdata.usgs.gov/nwis/uv?site_no=12031000

U.S. Geological Survey. 2016i. Chehalis River near Rochester, WA Station Data 2013-2014, Site ID 12028060. Website: http://waterdata.usgs.gov/wa/nwis/uv?site_no=12028060

U.S. Geological Survey. 2016j. Newaukum River near Chehalis, WA Station Data 2013-2014, Site ID 12025000. Website: http://waterdata.usgs.gov/nwis/uv/?site_no=12025000&agency_cd=USGS

U.S. Geological Survey. 2016k. Skookumchuck River near Bucoda, WA Station Data 2013-2014, Site ID 12026400. Website: http://waterdata.usgs.gov/wa/nwis/uv/?site_no=12026400&PARAmeter_cd=00060,00065

U.S. Geological Survey. 2016l. South Fork Chehalis River near Wildwood, WA Station Data 2013-2014, Site ID 12020800. Website: http://waterdata.usgs.gov/wa/nwis/uv/?site_no=12020800&PARAmeter_cd=00060,00065

U.S. Geological Survey. 2016m. ”StreamStats Version 3.0: WA”. Website: http://streamstatsags.cr.usgs.gov/v3_beta/viewer.htm?stabbr=WA

Washington Department of Ecology (WADOE). 2016a. Centralia STP Data 2013-2014, NPDES Permit No. WA0020982. Water Quality Permitting and Reporting Information System (PARIS).

Washington Department of Ecology (WADOE). 2016b. Chehalis STP Data 2013-2014, NPDES Permit No. WA0021105. Water Quality Permitting and Reporting Information System (PARIS).

Washington Department of Ecology (WADOE). 2016c. Darigold, Inc. STP Data 2013-2014, NPDES Permit No. WA0037478. Water Quality Permitting and Reporting Information System (PARIS).

Washington Department of Ecology (WADOE). 2016d. Pe Ell STP Data 2013-2014, NPDES Permit No. WA0020192. Water Quality Permitting and Reporting Information System (PARIS).

Washington Department of Ecology (WADOE). 2016e. Grand Mound STP Data 2013-2014, NPDES Permit No. WA0042099. Water Quality Permitting and Reporting Information System (PARIS).

Washington Department of Ecology (WADOE), River and Stream Water Quality Monitoring. 2016f. Black River at Hwy 12 Station Data 2013-2014, Site ID 23E060. Website: https://fortress.wa.gov/ecy/eap/riverwq/station.asp?sta=23E060

Washington Department of Ecology (WADOE), River and Stream Water Quality Monitoring. 2016g. Chehalis River at Dryad Station Data 2013-2014, Site ID 23A160. Website: https://fortress.wa.gov/ecy/eap/riverwq/station.asp?sta=23A160

Washington Department of Ecology (WADOE), River and Stream Water Quality Monitoring. 2016h. Chehalis River at Porter Station Data 2013-2014, Site ID 23A070. Website: https://fortress.wa.gov/ecy/eap/riverwq/station.asp?tab=continuous_oxy&sta=23A070

Washington Department of Ecology (WADOE), River and Stream Water Quality Monitoring. 2016i. Salzer Creek at Airport Road Station Data 2013-2014, Site ID 23H060. Website: https://fortress.wa.gov/ecy/eap/flows/station.asp?sta=23H060

Washington Department of Fish and Wildlife (WDFW). 2014. Chehalis Mainstem Station Data 2013-2014. Site IDs 3-UCH, 4-UCH, 11-UCH, 13-CH, 15-CH, 16-CH, 17-CH, 18-CH, 19-CH, 21-CH, 22-CH, 23-CH, NEW-1.

WEST Consultants, Inc. 2011. “Chehalis Basin Ecosystem Restoration General Investigation Study Baseline Hydrology and Hydraulics Modeling”. Prepared for the U.S. Army Corps of Engineers, Seattle, WA. November 30, 2011.

Zentner, G. 2016. Personal communication, Washington Department of Ecology, Olympia, WA.